Editing sustainable (and circular) polymers from CO_2 and renewables

Thesis submitted by Fabiana SIRAGUSA

in fulfilment of the requirements of the Doctorate Degree in Science

Academic year 2022-2023

Supervisor: Doctor Christophe DETREMBLEUR
Co-supervisor: Professor Gwilherm EVANO

Thesis jury :

Prof. Christine JEROME (Université de Liège, President)
Dr. Christophe DETREMBLEUR (Université de Liège, Supervisor)
Prof. Gwilherm EVANO (Université libre de Bruxelles, Co-supervisor)
Prof. Yves GEERTS (Université libre de Bruxelles, Secretary)
Prof. Karin ODELIUS (KTH Royal Institute of Technology)
Prof. Jean-François GOHY (Université catholique de Louvain)
Prof. Richard HOOGENBOOM (Universiteit Gent)

Summary

Among all materials, plastics have become one of the most important products of our daily life. Thanks to their ease of production and processing, low cost and customizable properties, plastics are indeed found in pretty much all sectors with applications, for example, in packaging, automotive, pharmaceutical industries or for electrical and electronical devices. However, they are mainly produced from petroleum and contaminate the environment when not properly recycled, which leads to the environmental disaster that we all know. The utilization of carbon dioxide (CO_2) as a substitute to petroleum is expected to limit our dependency to this depleting fossil resource and to avoid to be dramatically affected by the associated geopolitical issues that we are currently facing. CO_2 is indeed available at large quantities and low cost, and it might contribute to a more sustainable plastic sector by enabling the on-site production of plastics. To reach this ambitious goal, efficient transformations operating under mild conditions and producing limited waste have to be developed, and end-of-life scenarios of the new polymers have to be considered.

In this perspective, the aim of this PhD thesis is to merge innovative CO_2 transformations with bio-based molecules to produce functional polymers under mild conditions. This work was carried out in the framework of the Excellence of Science (EoS) “BIOFACT” project that deals with the transformation of lignin into high-value chemicals and polymers, starting with the very challenging selective depolymerization of lignin. My contribution to this project was to develop innovative routes to copolymerize a variety of lignin- (or sugar)-based diols or diamines with novel highly reactive CO_2-based cyclic carbonates with the objective to produce non-phosgene-based polycarbonates (with diols) and non-isocyanate-based polyurethanes (with diamines) at room temperature. The influence of the structure of the amine/alcohol and reaction conditions on the polymer structure and its thermal properties was investigated. With the aim of circular economy in mind, special attention was also devoted to the exploration of end-of-life options for the CO_2-based polymers by investigating chemical degradations *via* solvolysis or *via* novel approaches of polymers skeletal-editing.

This work was financed by the Fonds National de la Recherche Scientifique (F.R.S.-FNRS) and the Fonds Wetenschappelijk Onderzoek – Vlaanderen (FWO) in the frame of the EOS project n°O019618F (ID EOS: 30902231).

Résumé

Parmi tous les matériaux, les plastiques sont parmi les produits les plus importants de notre vie quotidienne. Grâce à leur facilité de production et de transformation, leur faible coût et leurs propriétés personnalisables, les plastiques se retrouvent en effet dans pratiquement tous les secteurs d'applications, par exemple, dans l'emballage, l'automobile, l'industrie pharmaceutique ou pour les appareils électriques et électroniques. Cependant, ils sont principalement produits à partir de pétrole et contaminent l'environnement lorsqu'ils ne sont pas correctement recyclés, ce qui conduit à la catastrophe environnementale que nous connaissons tous. L'utilisation du dioxyde de carbone (CO_2) comme substitut au pétrole devrait limiter notre dépendance à cette ressource fossile et éviter d'être affectés par les problèmes géopolitiques associés auxquels nous sommes actuellement confrontés. Le CO_2 est en effet disponible en grandes quantités et à faible coût, et il pourrait contribuer à un secteur du plastique plus durable en permettant la production sur site de plastiques. Pour atteindre cet objectif ambitieux, des transformations efficaces opérant dans des conditions douces et produisant peu de déchets doivent être développées, et des scénarios de fin de vie des nouveaux polymères doivent être envisagés.

L'objectif de cette thèse est de fusionner des transformations innovantes du CO_2 avec des molécules biosourcées pour produire des polymères fonctionnels dans des conditions douces. Ce travail a été réalisé dans le cadre du projet Excellence of Science (EoS) "BIOFACT" qui traite de la transformation de la lignine en produits chimiques et polymères, en commençant par la dépolymérisation sélective de la lignine. Ma contribution à ce projet est de développer des voies innovantes pour copolymériser une variété de diols ou de diamines issue de lignine (ou de sucre) avec de nouveaux carbonates cycliques hautement réactifs produits à partir de CO_2. Le but final est de donner accès à des polycarbonates sans phosgène ou des polyuréthanes non isocyanates à température ambiante. L'influence de la structure de l'amine/alcool et des conditions de réaction sur la structure du polymère et ses propriétés thermiques sont étudiées. Dans l'optique d'une économie circulaire, une attention particulière est également consacrée à l'exploration des options de fin de vie de certains de ces polymères en étudiant les dégradations chimiques via la solvolyse ou via de nouvelles approches d'édition du squelette des polymères.

Ce travail a été financé par le Fonds National de la Recherche Scientifique (F.R.S.-FNRS) et le Fonds Wetenschappelijk Onderzoek – Vlaanderen (FWO) dans le cadre du projet EOS n°O019618F (ID EOS : 30902231).

Acknowledgements

Looking back on these four years I can see how much I have grown up professionally and how much this experience has enriched me. During this time, I met a lot of people that inspired, pushed, encouraged and challenged me.

I would like to thank the members of jury: Prof. Yves Geerts, Prof. Karin Odelius, Prof. Jean-Francois Gohy and Prof. Richard Hogenboom to have accepted to read and review my thesis.

I especially thank Prof. Christine Jerome for welcoming me at the CERM and have been so kind and supportive. You convey love to people and the nice vibe in the lab is the reflection of that.

I thank my co-supervisor, Prof. Gwilherm Evano, for your guidance and for having follow me in these years.

I would like to express my deepest gratitude to my supervisor Dr. Christophe Detrembleur for giving me the opportunity to start a project that I loved. Working with you has contributed immensely to my growth. Thank you for believing in me, always encouraging me to work hard, and helping me to reach my goals. You always pushed to give the best of me and go further on my limits. You are a great inspiration and I learned a lot from you. Even if I always say "t'es chiant" and you desperate me when you speak about your recipes full of garlic, I enjoyed a lot with you, at work and outside. You are one of the reasons why I didn't hesitate to decide to stay a little bit longer in the CERM family. Thank you for being such a kind and caring mentor.

I specially thank Bruno for everything! Since the first day, you supported me and guided me, I learned a lot by your suggestions and knowledge. You are behind of everything and the CERM is lucky to have you in the team. You became a good friend and you made easier being far from my family, making me smile, when I was sad, and quiet when I was stressed. I have a special attachment to you and I hope to have shown it often enough. You are a gem! Coccole (waiting for the third one)!

I thank Dr. Antoine Debuigne and Dr. Philipe Lecomte for your suggestions and your guidance during my thesis. I thank Raphael Riva and Abdel for your company during the time spent together.
When I think about CERM, I automatically think about Val, Greg, Sophie, Martine and Charlotte. You are the CERM and without you this lab would not be the same. I thank Sophie to have been always there to listen, support, encourage me. Thank you for all the funny and crazy moments passed together. You are special and I care a lot about you! I thank Greg-Grey to have been patient for all the boring kinetics and questions, you have been always professional. You are essential and your experience enriched me. I thank Martine and Charlotte for your kindness towards me. It made such a positive impact! I thank in particular Val, you helped me a lot in the lab and you gave a big contribution to this thesis. You are amazing, sunny, funny. You transmit joy. You are my joy.

I want to thank a lot Jeremie (cerises), Luca, Mylan, Malihe, Pascal, Zoe, Maxime B., Maude, Lionel, Anna, Oscar, Florent, Francois, Marco, Maxime H., Hamid, Pierre, Philip, Antoine for all the nice moments passed together.

A particular thank goes to Thomas, my student, my office mate and specially my best friend. These years would not have been the same without you and you were essential for the progression of this work. We are an awesome team, the dream team. You showed me every day what can I do if I believe more in myself. You encouraged me that I can reach my objectives. You were there in the happy and bad moments. You were there, always. Words cannot describe the affection that I have for you, but you know that! You are a gift! Happy to have met you.

I want to thank my friends Cecilia, Arianna, Kevin, Matthieu, Andrea, Annaelle to have become my reference point in Belgium. We passed a lot of nice moments together and every time was precious for me. Thanks a lot.

Dietro ai miei successi c'è sempre stata la mia famiglia. Bruno, Mamma e Papà, voi siete stati sempre pronti a supportarmi e incoraggiarmi, e la lontananza non vi ha impedito di essere presenti. Siete stati la ragione per cui ho sempre cercato di dare il meglio di me e spero di non avervi mai deluso. I vostri sacrifici non sono stati inutili e questo lavoro è il risultato. Ringrazio Clara per avermi pensata sempre nonostante la lontananza e per avermi dato la gioia di diventare zia.

Last but not least, I thank Xavier. I thank you firstly because you are the reason why I started this amazing experience. You are the reason why I moved in Belgium and started a scary adventure that I would never succeed without you. You encouraged and supported me in these years, with love and patience. This achievement is thanks to you. This work is for you. I love you.

I dedicate my thesis to my beloved
grandfathers Giusto and Vito

Table of content

List of abbreviations

5CC	Five membered cyclic carbonate
αCC	4,4-Dimethyl-5-methylene-1,3-dioxolan-2-one
BPA-PC	Bisphenol A polycarbonate
Bis(αCC)	Bis(α-alkylidene cyclic carbonate)s
CHC	Cyclohexene carbonate
DBU	1,8-Diazabicyclo[5.4.0]undec-7-ene
DFT	Density functional theory
DMAc	Dimethylacetamide
DMC	Dimethyl carbonate
DMF	Dimethylformamide
DMSO	Dimethylsulfoxide
DNP	2,4-Dinitrophenolate
DPC	Diphenyl carbonate
DSC	Differential scanning calorimetry
HAc	Acetic acid
HRMS	High-resolution mass spectrometry
M_n	Number average molecular weight
M_w	Weight average molecular weight
NaHMDS	Sodium bis(trimethylsilyl)amide
NIPU	Non-isocyanate polyurethanes
NMR	Nuclear magnetic resonance
PET	Polyethylene terephtalate
PCL	Poly(caprolactone)
PCs	Poly(carbonate)s
PEG	Poly(ethyleneglicole)

POxa	Poly(oxazolidinone)s
P^{t}BuDHBC	Poly(*tert*-butyl 3,4-dihydroxybutyrate)
PUs	Poly(urethane)s
ROCOP	Ring-opening copolymerization
ROP	Ring-opening polymerization
SEC	Size exclusion chromatography
TBD	1,5,7-Triazabicyclo[4.4.0]dec-5-ene
T_g	Glass transition temperature
TGA	Thermal gravimetric analysis
THF	Tetrahydrofuraan
T_m	Melting temperature
TMB	1,3,5-Trimetoxybenzene
TMC	Trimethylene carbonate
WAXS	Wide angle X ray scattering
XRD	X-ray diffraction

Chapter I

The advent of recyclable CO_2-based polycarbonates

Table of contents

1. Introduction

Over the last century, the massive utilization of low cost commodity plastics has brought revolutionary progresses in our modern life. Their easy customizable properties permitted their emergence for multiple purposes in very distinct fields including the automotive, packaging, pharmaceutical, electrical, electronical and building sectors.[1,2] Despite their remarkable lightweight, flexibility, strength and durability, most of synthetic polymers lack of degradability by biological or abiotic means in landfills or the marine environment. Their persistency is now turning their initial magic into a major global ecological crisis. Moreover, most of the plastics are still produced from fossil resources making their carbon footprint dramatic. Recent predictions have highlighted a tripling of the actual plastics consumption at the horizon 2050. To abate the plastic pollution and decarbonize this industry, the European Commission recently adopted a vision specifying guidelines to rethink the fabrication and facilitate the recycling of plastics.[3] On the path to circularity and sustainability, one key measure encourages the utilization of biorenewable chemicals and gaseous effluents to create new low carbon footprint polymers with thermo-mechanical performances analogues to existing ones. In this context, waste CO_2 is expected to become a cornerstone to fundamentally reinvent the fabrication of plastics.[4] A recent prospective study highlighted a brilliant future for these materials with a 25 fold volume increase representing ~ 25% of the market share at the horizon 2050. As second obligation, these new engineered plastics should display enhanced intrinsic mechanical or chemical recycling ability. If the revalorization/recycling of end-of-life plastics is mandatory to prevent the relegation of waste materials in the environment, it remains a huge bottleneck.[5,6] Mechanical recycling often produces low performance 'downcycled' materials; such raw materials may need extensive additivation in order to be re-incorporated in consumer products.[7] Chemical re- and upcycling can offer a more diverse spectrum of end-of-life reuse scenarios, either yielding the original monomers to refabricate the same plastic with virgin-like material properties in a close-loop approach, or producing building blocks for innovative, intrinsically circular materials (open-loop recycling).[8–13] But, the inherent microstructure of (commodity) polymers with stable covalent carbon-carbon bonds still makes challenging their low-temperature selective chemical deconstruction. To date, only polymers containing C–O or C–N heteroatom linkages show sufficient lability and can be depolymerized through solvolytic approaches by employing nucleophiles or water or via thermal reversion into the native monomers or new chemicals.[14–16] Herein, we review the state-of-the-art in the recycling of CO_2-based polycarbonates that belong to an important family of polymers that will be studied in this PhD thesis. Fundamentals of the direct enchainment of CO_2 into polymer chains or the polymerization by well-established tools of prefabricated CO_2-based monomers will be briefly

described, yet setting the foundations to the discussions of the most relevant degradation/recycling pathways of these various polymers.

2. Few generalities on polycarbonates

Polycarbonates are polymers with easy customizable mechanical and thermal properties that vary from low thermal stability, poor mechanical properties and high susceptibility to hydrolysis/(bio)degradation for aliphatic PCs,[17] to transparency, high impact resistance, high rigidity and good thermal stability for aromatic PCs. Today, PCs are key components of electronic, optical and biomedical devices, construction materials, cars manufacturing, Li-ion batteries… The progresses in catalyst design are now permitting the synthesis of PCs directly from CO_2 via ring-opening copolymerization (ROCOP) with epoxides or alternatively by ring-opening polymerization (ROP) of cyclic carbonates, which may in turn be synthesized using CO_2. In addition to these (co)polymerization processes, a more traditional synthetic pathway consists in the polycondensation between diols and CO_2-sourced acyclic carbonates.[1,18–21] Some of these synthetic approaches are reaching now the industrial maturity. For example, CO_2-sourced poly(propylene carbonate) of M_n up to 100,000 g/mol containing 43 wt% of CO_2 content is viewed as a green alternative to polyethylene, yet serving as disposable packaging and mulching films that are compostable and biodegradable upon burial in soil.[22] Low viscous hydroxytelechelic poly(carbonates-*co*-ether)s, also named polyols such as Cardyon®, are now utilized to manufacture polyurethanes for flooring and foam applications.[23] Asahi Kasei Chemicals produces diphenyl carbonate from CO_2 that further serves in the production of bisphenol A polycarbonate via polycondensation at the scale of 1000 tons/year.[24]

3. ROCOP polycarbonates

3.1 *Fundamentals of CO_2/epoxide ROCOP*.

The ROCOP of CO_2 with propylene oxide was pioneered by Inoue who utilized a water/diethylzinc catalytic system to produce poly(propylene carbonate).[25] This seminal work gave momentum to flourishing catalytic breakthroughs in ROCOP that are summarized in multiple comprehensive reviews to which the reader is invited to read.[1,26–28] Conceptually, the polymerization manifold responds to a well-established coordination–insertion mechanism involving first the activation of the epoxide by a Lewis acid selected among $B(alk)_3$, trivalent Co, Cr, Al or divalent Zn metal centers complexed by Salen, Salphen, β-diimidate, bimetallic macrocyclic phenolates, amino triphenolate… ligands (Figure 1).[29–39] Then, the resulting activated epoxy monomer undergoes a ring-opening via nucleophilic attack by a Lewis base acting as nucleophile to form an alkoxide-metal intermediate. The subsequent insertion of carbon dioxide into this intermediate creates a metal carbonate species prone to propagation

by consecutive incorporation of epoxide units and CO_2 in an alternating fashion within the growing anionic chains (Scheme 1). The polymerization is terminated by adding a protic source furnishing polycarbonates with a hydroxyl chain end. The selection of the catalyst is of critical importance to control the microstructure of the polycarbonates. During the chain growth process, ether linkages may be formed by successive enchainment of epoxide molecules instead of alternated epoxide-CO_2 insertion. A second major impediment to the selective production of PCs by ROCOP of epoxides and CO_2 lies in the ease of the backbiting process from the free anionic growing PC chain, yet resulting in the formation of cyclic carbonate as co-product.

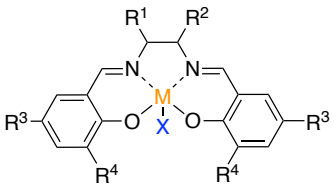

(1) Metal-salen/salphen

(1a) M = Cr (III), X = Cl
$R^1 = R^2$ = Ar or cyclohexyl
$R^3 = R^4$ = *t*Bu

(1b) M = Al (III), X = Cl
$R^1 = R^2 = R^3 = R^4$ = H

(1c) M = Co (III), X = OAc or Cl
$R^1 = R^2$ = Ar or cyclohexyl
R^3 = Br or *t*Bu R^4 = *t*Bu

(1d) M = Zn (II), X = Cl
$R^1 = R^2$ = Ar
R^3 = H R^4 = *t*Bu

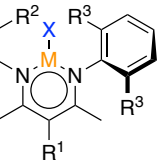

(2) Metal-β-diiminate

M = Zn
X = OMe **(2a, 2b)**, OAc **(2c),** O*i*Pr or $N(SiMe_3)_2$
R^1 = H **(2a, 2c)** or CN **(2b)**
R^2 = Et **(2a, 2b)** or *i*Pr **(2c)**
R^3 = Et **(2a)** or *i*Pr **(2b, 2c)**

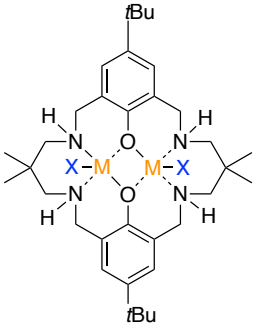

(3) Bimetallic macrocyclic phenolates

(3a) M = Zn (II), X = OAc

(3b) M = Fe (III), X = Cl

(3c) M = Mg (II), X = OAc or Br or O_2CCF_3

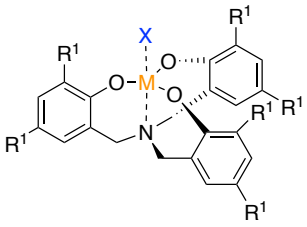

(4) Amino triphenolate

(4a) M = Al (III), X = THF or dimeric species
R^1 = H, Me, *t*Bu or Cl

(4b) M = Fe (III), X = THF or dimeric species
R^1 = H, Me, *t*Bu or Ar

Figure 1. Metal complexes used as catalysts for the copolymerization of epoxide with CO_2.

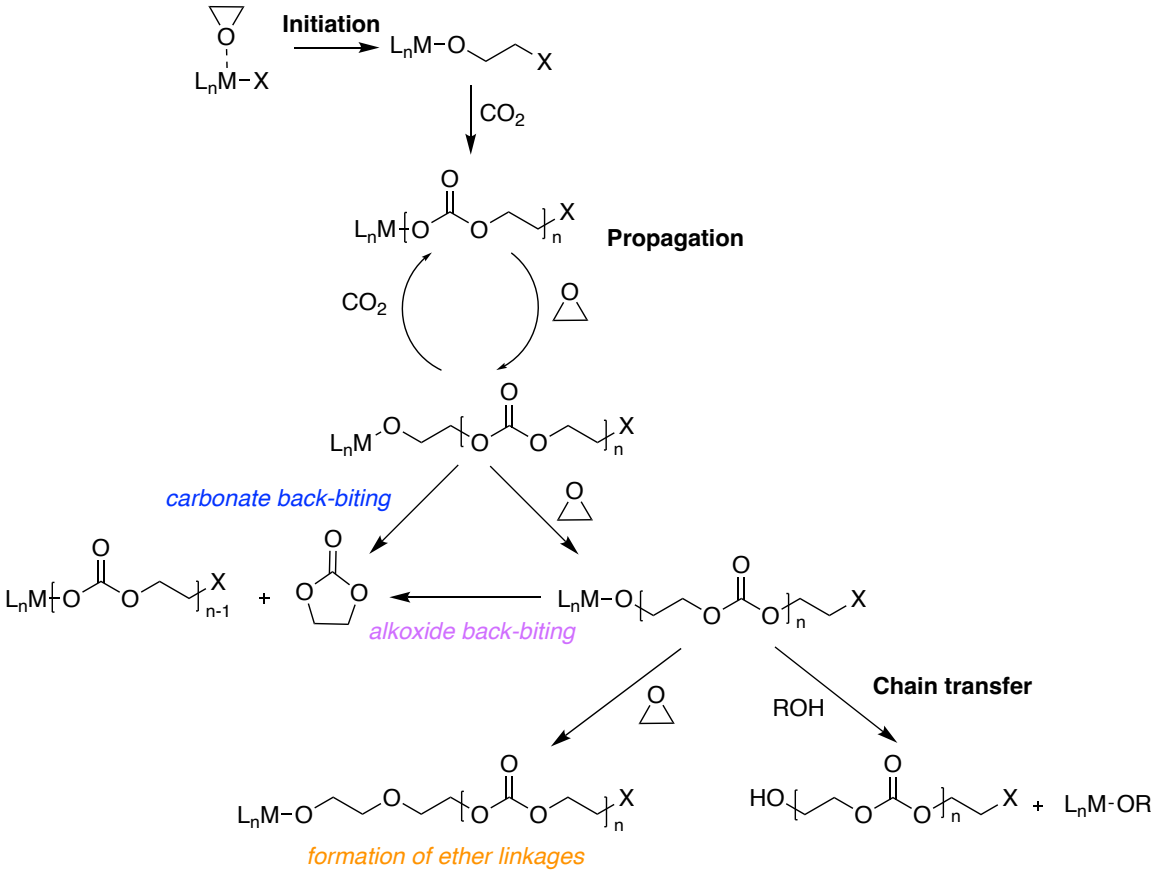

Scheme 1. General mechanism of synthesis of PCs by ROCOP of epoxide with CO_2.

ROCOP polycarbonates degrades via two main scenarios, either via their thermal (decarboxylative) reversion into added value chemicals or offspring monomers, or through solvolysis/hydrogenolysis processes.

3.2 *Thermal tail-to-head reversion of ROCOP PCs*.

The construction/deconstruction loop of ROCOP PCs is mainly governed by the polymer energetics with a major influence of the ceiling temperature below/above which the polymer chains grow/depolymerize[4,10,40]. Following the deprotonation of the OH chain-ends, aliphatic CO_2-based polycarbonates depolymerize into 5-membered cyclic carbonates. The process responds to the unzipping of the resulting anionic chains in a backbiting fashion leading to a steady curtailing in the PC molar masses while maintaining a low dispersity. To illustrate this concept, Darensbourg reported on the thermal anaerobic decomposition of series of aliphatic ROCOP polycarbonates derived from epoxides bearing both electron donating or electron withdrawing substituents, i.e. styrene oxide, epichlorohydrin and propylene oxide.[41] By employing a strong nitrogen base like 1,8-diazabicyclo[5.4.0]undec-7-ene (DBU), a rapid and complete depolymerization of poly(styrene carbonate) to styrene carbonate was accomplished at 22 °C in less than an hour. By switching to tetrabutylammonium salts with an azide counter-

anion ($^{n}Bu_4NN_3$), the same polymer was decomposed in less than 10 min at 70 °C, while its reversion to styrene carbonate was strongly slowed down with Cl anion or even not observed with bromide (Scheme 2). This reflects the vital role of the basicity of the anions or the base in the aliphatic PC deconstruction which endwise scission was initiated by the chain-end deprotonation. Similarly, the deconstruction of poly(CO_2-*alt*-epichlorohydrin) and poly(propylene carbonate) promoted by $^{n}Bu_4NN_3$ furnished exclusively and quantitatively the corresponding 5-membered cyclic carbonates. The depolymerization activation energies, obtained through kinetic studies, were found to increase in the order poly(styrene carbonate) (46.7 kJ/mol) < poly(CO_2-*alt*-epichlorohydrin) (76.2 kJ/mol) < poly(propylene carbonate) (80.5 kJ/mol).[41]

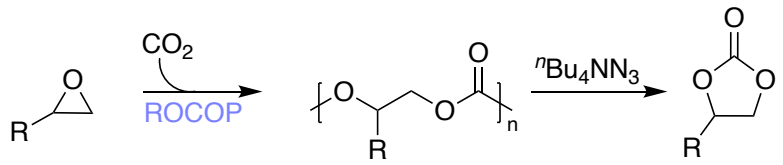

R = Me, CH_2Cl, Ph

Scheme 2. Synthesis of PCs by ROCOP of CO_2 with substituted-epoxides and their thermal degradation into 5-membered cyclic carbonates.

Through computational studies, Darensbourg highlighted that the metal-free backbiting reaction of aliphatic PCs, promoted by a free anionic polycarbonate chain-end, was inhibited by bulky groups at the methine carbon of the polymer microstructure, however it was accelerated by resonance stabilization.[42] The thermal reversion of aliphatic PCs into cyclic carbonates was strongly retarded in the presence of a binary catalyst (a combination of a base ($^{n}Bu_4NN_3$) and a (Salen)CrCl complex). This presumably arose from the binding of the anionic copolymer to the coordinatively unsaturated metal center. Unfortunately, despite the emergence of new generations of ROCOP catalysts displaying a high degree of stereo- and regioselectivity, the construction of aliphatic PCs from terminal epoxides and CO_2 that are free of any defects is still challenging. Importantly, the ether linkages act as termination nodes stopping the PCs unzipping, thus preventing the complete deconstruction of the chains.

Unlike aliphatic PCs, the ROCOP of CO_2 with (geometrically constrained) epoxides fused with cyclopentene, indene, cyclohexene, limonene or cycloheptene rings provided alicyclic PCs which thermal deconstruction features and products selectivity were governed by the judicious choice of the catalyst, the size of the alicyclic ring and/or the operative conditions. At the exception of poly(indene carbonate) (synthetized by ROCOP of **1**, Scheme 3)[43] that depolymerized into the corresponding *cis*-cyclic indene carbonate (Scheme 3, pathway *i*) , PCs derived from CO_2 and epoxides fused with a 5-membered alicyclic ring such as cyclopentene[44] or *O*- and *N*-heteroepoxide (*N*-aryl pyrrolidine oxide)[45,46] reverted preferentially into the parent

epoxide (**2** and **3** respectively) and CO_2 via a decarboxylative ring closure depolymerization pathway (Scheme 3, pathway *i'*). This is exemplified by the depolymerization of poly(cyclopentene carbonate). Aided by DFT calculations, Darensbourg demonstrated that the backbiting of these PCs to the epoxide monomer possessed a free energy barrier 6.6 kcal mol^{-1} lower than the one of the *trans*-cyclopentene carbonate (Scheme 3, pathway *ii*), claimed by the author as the kinetic product. Moreover, this latest is 19.9 kcal mol^{-1}, higher in enthalpy than its *cis*-boat conformer.[44] Therefore, the *trans*-conformation of cyclopentene carbonate is highly unstable due to the strain energy of the two five-membered fused rings and this product should not be observed upon depolymerization. This correlates with the depolymerization experiments. Bases such as $^{n}Bu_4NN_3$ and DBU were found ineffective in deconstructing poly(cyclopentene carbonate). Employing the stronger, non-nucleophilic base sodium bis(trimethylsily)amide (NaHMDS) enabled the slow reversion of the chains into cyclopentene oxide and *cis*-cyclopentene carbonate in a nearly equimolar ratio after 300 h at 110 °C (polymer degradation of 30%).[44] Extending the degradation time to 60 days changed the product distribution, with the formation of the cyclic carbonate specie being favored. The *in-situ* release of CO_2 creates an environment that not only changed the product selectivity but also slowed down the depolymerization rate, as confirmed by control depolymerization experiments driven under 0.7 bar. When reproducing the same experiment under reduced pressure, the PC deconstruction was enhanced with a polymer deconstruction yield of ~ 50% in 70 h, yet furnishing cyclopentene oxide (**3**) as the major product. It was assumed that cyclohexene oxide (**4**) arose from alkoxide endwise backbiting, whereas the *cis*-cyclic carbonate scaffold resulted from backbiting by a carbonate chain end. Unlike aliphatic ROCOP PCs, the metal-assisted depolymerization process accelerated the polymer deconstruction with a product distribution favoring the parent alicyclic epoxide monomer. Using a dual (Salen)Cr(II)Cl/$^{n}Bu_4NN_3$ catalytic system for 30 h at 110 °C, 86% of poly(cyclopentene carbonate) were reverted into cyclopentene oxide with a selectivity of 92%. With (Salen)Cr(III)Cl/bis(triphenylphosphine)iminium azide ($PPNN_3$), the PC was fully degraded in 40 min via pyrolysis at 200 °C, yet delivering cyclopentene oxide with a 94% selectivity.[47] Rather similar in concept was the loop synthesis of defect-free PCs of M_n up to 27,000 g/mol from CO_2 and 1-benzyl- or alkyl-oxycarbonyl-3,4-epoxy pyrrolidine driven by dinuclear Cr(III)-complex/PPNX or (Salen)Co(III)Cl/PPNX system (PPN=bis(triphenylphosphine)iminium) (with X = NO_3^- or 2,4-dinitrophenoxide) at 25-80 °C. This PC was quantitatively recycled at 100-110 °C (in solution) or via vacuum thermolysis at 200°C into the offspring epoxide by a ON/OFF reversible temperature switch.[46,48] If the formation of alicyclic carbonates with two fused five-membered rings in a *trans* conformation is energetically unfavorable due to the ring strain (as observed for poly(cyclopentene carbonate), such conformers became the competitive degradation products when reducing the ring strain via an increase of the fused alicyclic ring

size. These *trans* scaffolds might be revalorized as monomers for ROP polymerization (see section 4). Moreover, the judicious choice of the catalyst and operative conditions also allowed for controlling the PC degradation into the native epoxide and CO_2, or into the *trans*-alicyclic carbonate. These features are illustrated for the depolymerization of poly(cyclohexene carbonate) which endwise scission (Scheme 3, pathway *i'*) initiated by a (Salen)Cr(III)Cl/$PPNN_3$ catalytic system provided exclusively and quantitatively cyclohexene oxide (**4**) in bulk conditions at 200 °C in 20 min under static vacuum.[47] In contrast, *trans*-cyclohexene carbonate was selectively and quantitatively produced in solution at 110 °C after 170 h when $PPNN_3$ was replaced by $^{n}Bu_4NN_3$ (Scheme 3, pathway *ii*).[41] Similarly, Buchard recently applied a dinuclar Mg(II) complexes promoting the depolymerization of poly(cyclohexene carbonate) into the native epoxide (**4**) at 120 °C in 24 h with a high degree of selectivity (92-98%) while the mononuclear counterpart catalyst was less efficient and selectively furnished the *trans*-cyclohexene carbonate (Scheme 3, pathway *ii*).[49] Very recently the utilization of a homogeneous dinuclear methyl zinc catalyst $(BDI\text{-}ZnMe)_2$ gave access to poly(cyclohexene carbonate) by ROCOP of *meso*-cyclohexene oxide (**4**) with CO_2. In the presence of traces of water, the catalyst was converted into heterogeneous multi-nuclear zinc catalyst $(BDI\text{-}(ZnMe_2 \bullet 0.1H_2O))_n$, which selectively degraded the polymer into the starting monomers in 9 hours at 150 °C (Scheme 3, pathway *i'*).[50]

Trans-cyclohexadiene and *trans*-cycloheptene carbonates were identified as the sole degradation products of the corresponding ROCOP poly(hexadiene carbonate) and poly(cycloheptene carbonate) (Scheme 3, pathway *ii*, from compound **5** and **6**) when depolymerizations were assisted by the strong base NaHMDS and/or (Salen)Cr(III)Cl/ $^{n}Bu_4NN_3$ at 110 °C in solution.[51,52] Beside, biorenewable limonene oxide (LO) (**7**) was copolymerized at r.t. with CO_2 using β-diiminate (BDI) zinc catalyst to produce poly(limonene carbonate) with exclusive carbonate linkages. This PC reverted back exclusively in 5 h to LO, even under 40 bar of CO_2, at 110 °C when catalyzed by the strong base 1,5,7-triazabicyclo[4.4.0]dec-5-ene (TBD).[53] Detailed mechanistic studies showed a dominating endwise degradation of the chains through decarboxylative ring closure. Meanwhile, TBD catalyzed competitive intra- and intermolecular transcarbonation reactions between the alkoxide chain ends and the PC skeleton. This created “dead” polymers strands which only degraded slowly when involved in new transcarbonation reactions.

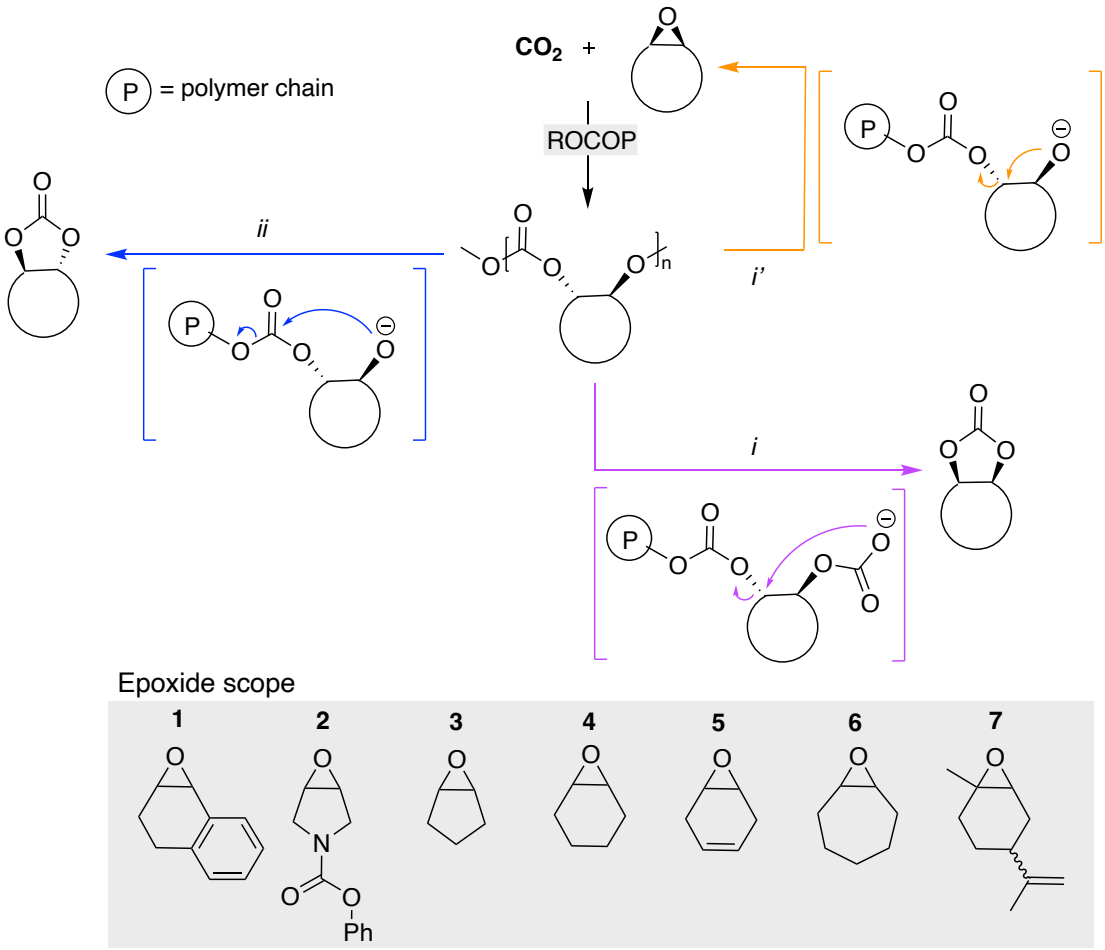

Scheme 3. Polycarbonate synthesis by ROCOP of various alicyclic epoxides with CO_2 and their depolymerization pathways.

3.3 *Hydrogenation of PCs*.

Recycling end-of-life ROCOP polycarbonates by metal-catalyzed hydrogenation offers an indirect route to convert CO_2 into methanol with the co-production of vicinal diols. This hydrogenative depolymerization scenario is illustrated for poly(propylene carbonate) of M_n up to 100,000 g/mol. Various noble or earth abundant metal complexes derived from Ru, Mn, Zn or Fe ligated by PNP or PNN pincer ligands were engineered and used in combination or without additional bases (KO^{t}Bu, KH) to promote the PC hydrogenation at 110-160 °C, in 16 to 50 h, under 45-50 bar of H_2 (Scheme 4).

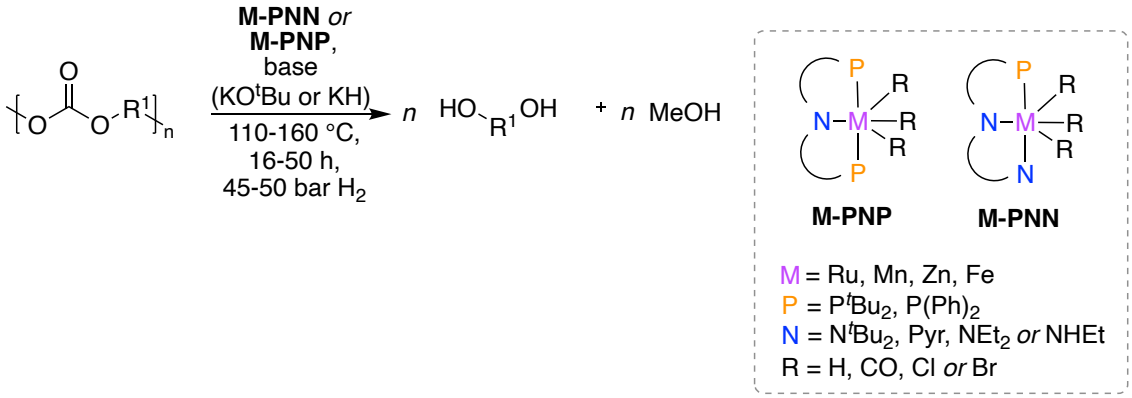

Scheme 4. Metal-PNP or PNN catalyzed hydrogenation of PCs.

As reported by Ding et al., the catalytic activity of Ru-PNP complexes for the hydrogenative depolymerization of poly(propylene carbonate) furnished methanol and propylene glycol with yields >99%.[54] Alike Ru systems, M_n complexes furnished propylene glycol and methanol but with lower yields of 91 % and 84 %, respectively.[55,56] By using KH as a base, the product selectivity was affected with side reactions delivering propylene carbonate by-product (30%) (Scheme 5), that was assumed to come from the competitive thermal reversion of the PC by unzipping or the carbonylation of the vicinal propylene glycol by the polymer chains.[56] Recent catalytic discoveries have enabled improving the hydrogenation process of poly(propylene carbonate), yet quantitatively delivering methanol and propylene glycol under mild conditions using an efficient Fe pincer complex that operated without requiring a base.[57]

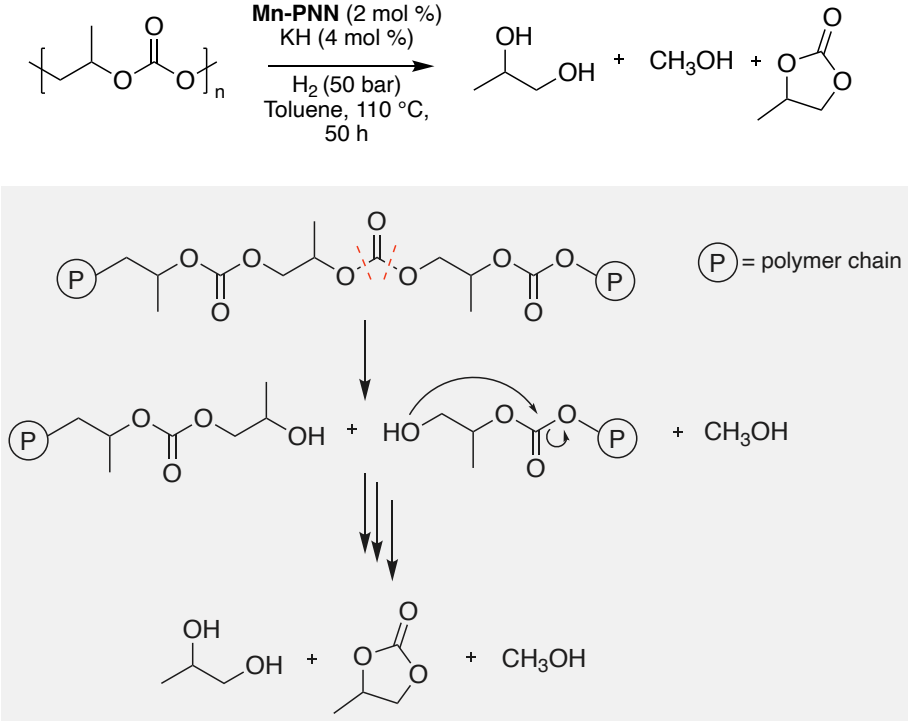

Scheme 5. Hydrogenative depolymerization of poly(propylene carbonate).

The overall deconstruction mechanism of PCs chains proceeded via domino hydrogenation events (Scheme 6).[55] Following the creation of a 16 electrons metal complex upon addition of a base, the heterolytic cleavage of H_2 enables the hydrogenation of the catalytic species via hydride addition onto the metal center as well as the protonation of the ligand. In a second step, the catalyst promotes the reduction of the carbonyl moiety of the PCs via transfer of the hydride to the sp^2 atom of the substrate. This creates two strains being end-capped either by a formate or an alcohol. Then, the formate species is involved in a novel hydrogenation event producing an alcohol terminated chain and formaldehyde. Formaldehyde is finally reduced into methanol co-product. The repetition of the depolymerization process at each carbonate linkage leads ultimately to the formation of the vicinal diol and methanol.

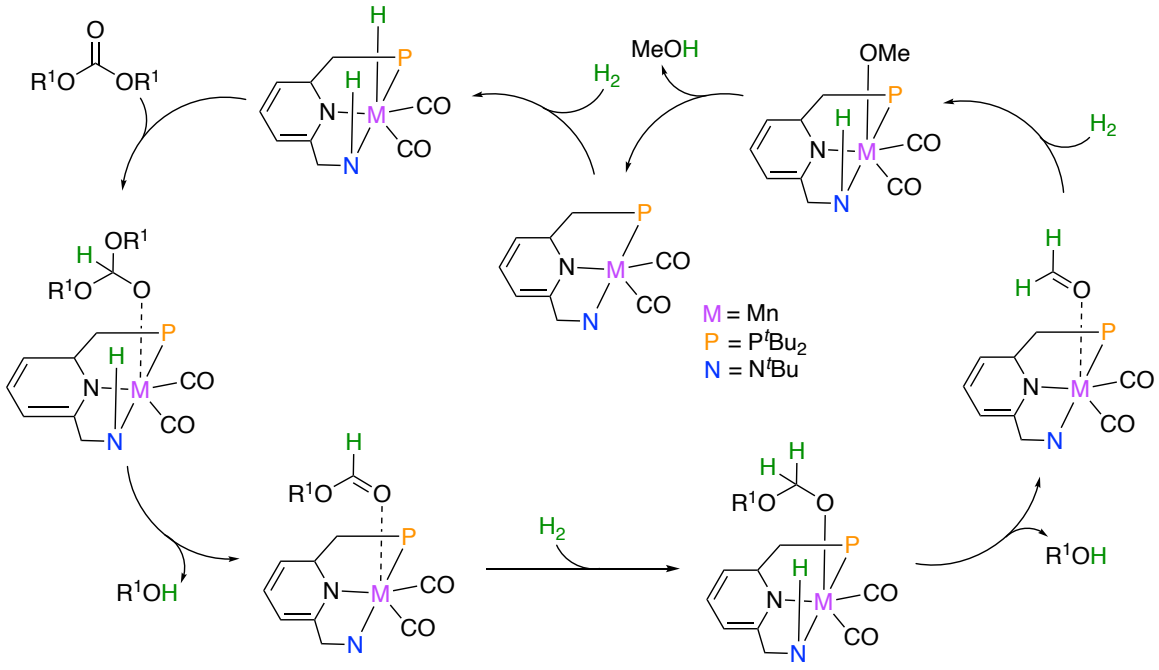

Scheme 6. Deconstruction mechanism of PCs via metal-PNN catalyzed hydrogenation.

3.4 *Solvolysis of ROCOP PCs*

Curiously, despite being one of the simplest mean to degrade O-C(O)-O containing polymers, the hydrolysis of ROCOP PCs has been rarely reported. Grinstaff created a library of novel hydrolysable aliphatic PCs from structurally diverse alkyl glycidate and glycidyl ester type oxyranyl monomers and CO_2.[58] PCs of M_n of 5,900 – 10,600 g/mol were synthesized under 15 bar of CO_2 and cobalt Salen complex at 25 °C (Scheme 7). The orientation of the ester linkage within the monomer dictated the polymerization features, glycidyl ester type epoxides being more reactive due to the low steric congestion and the suppression of the electron withdrawing effect of the carbonyl moiety. Hydrolytic cleavage in a 3/1 v/v THF/water solution of the ethyl glycidate poly(carbonate)s (PEAc), viewed as the degradable version of commercial poly(acrylate)s, furnished glyceric acid with co-production of ethanol and CO_2. The glycidyl

ester counterpart (PGC-E) degraded into glycerol concomitantly with acetic acid and CO_2. Both PCs showed appreciable degradation rates that were controlled by the pH. At low pH value of 5, both PCs display $t_{1/2}$ above 35 days, while the glycidyl ester polycarbonate showed a fast degradation rate with $t_{1/2}$ of only 2 days at pH = 9. Comparative studies also highlighted the easier degradation ability of the glycidyl ester PC than the constitutional isomeric glycidate materials.

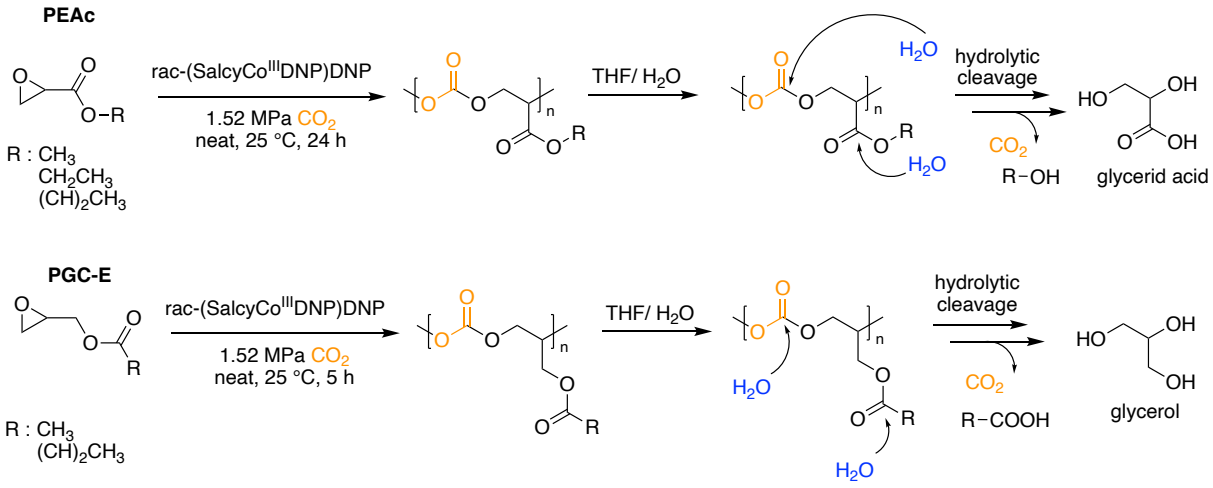

Scheme 7. Synthesis and degradation of PEAc and PGC-E.

Methanolysis of poly(1,2-propylene carbonate) was recently investigated by Enthaler. By using a cheap $Zn(OAc)_2$ or NaOAc catalyst, the depolymerization at 160 °C under microwave generated 1,2-propanediol and dimethyl carbonate after 10 min (Scheme 8).[59]

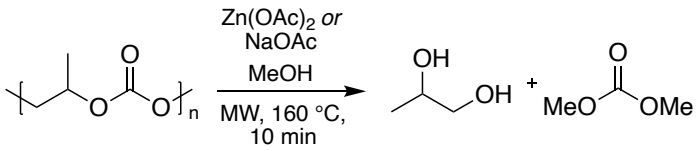

Scheme 8. Methanolysis of poly(1,2-propylene carbonate).

3.5 *Self-immolative PCs*

Self-immolative polymers refer to materials prone to end-to-head degradation upon cleavage of their backbones or end-caps. They differentiate from degradable polymers by their ability to amplify a response to an external stimulus, yet translating a single cleavage event into the total deconstruction of the chains via cascade events into new chemicals. Notably, such features have propelled self-immolative aliphatic polycarbonates as attractive materials for biomedical and pharmaceutical applications.[17] In the continuation of his previous works, Grinstaff designed series of PCs of controlled tacticity showing self-immolation properties. Racemic benzyl glycidate and benzyl glycidyl ester, i.e. oxiranyl monomers bearing respectively protected carboxylic acid and alcohol moieties, were copolymerized with 15 bar of CO_2 at 25

°C using racemic cobalt Salen complex with 2,4-dinitrophenolate (DNP) axial ligand, yet furnishing atactic PCs.[60] Applying a similar polymerization procedure to the *R*-enantiomers in the presence of (chiral) Salen cobalt complexes provided the chiral isotactic version of the polymers.[61] All PCs were characterized by M_n of 14,000 to 41,000 g/mol with 99% carbonate linkage selectivity and high regioregularity with a head-to-tail connectivity > 92-97%. Deprotection of the carboxylic acid or alcohol by hydrogenolysis provided poly(glyceric acid carbonate) (Scheme 9a) a degradable mimetic of poly(acrylic acid) and poly(1,2-glycerol carbonate) (Scheme 9b), a degradable substitute to poly(1,3-glycerol carbonate). Poly(glyceric acid carbonate) remained stable for month in the dry state, however unlike poly(acrylic acid), degraded in 26 days in water. Remarkably, by dissolving the PC in a buffer solution at pH = 8.4, the polymer readily self-immolated in 8 h with formation of O-carboxyanhydride structures that resulted from an intramolecular cyclization of the carboxylate moiety onto the adjacent carbonate linkage. Beside, by simple thermal treatment at 37 °C, poly(1,2-glycerol carbonate) spontaneously self-degraded ($t_{1/2}$ = 2-3 days) to produce the thermodynamically stable glycerol carbonate through repetitive intramolecular cyclizations, in line with Frey's similar work.[62]

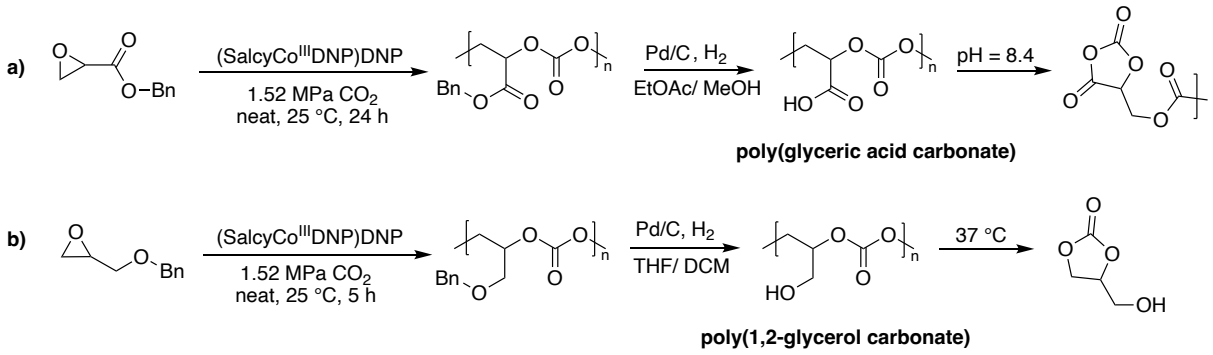

Scheme 9. Synthesis and hydrogenolysis of poly(benzyl glycidate carbonate)s and poly(benzyl 1,2-glycerol carbonate)s to form poly(glyceric acid carbonate) and poly(1,2-glycerol carbonate).

Similar strategy has been embraced by Darensbourg for the chemical depolymerization of acetyl-capped poly(*tert*-butyl 3,4-dihydroxybutyrate carbonate) (P^{t}BuDHBC).[63] The polymer was obtained by cobalt salen complex catalyzed ROCOP of racemic-*tert*-butyl 3,4-epoxybutanoate and CO_2, following a deprotection by trifluoroacetic acid (TFA) and subsequent deprotonation with K_2CO_3 in MeOH. Dissolving the polymer in water (pH = 8) at 37 °C promoted the full degradation into β-hydroxy-γ-butyrolactone and 3,4-dihydroxybutytrate (Scheme 10).

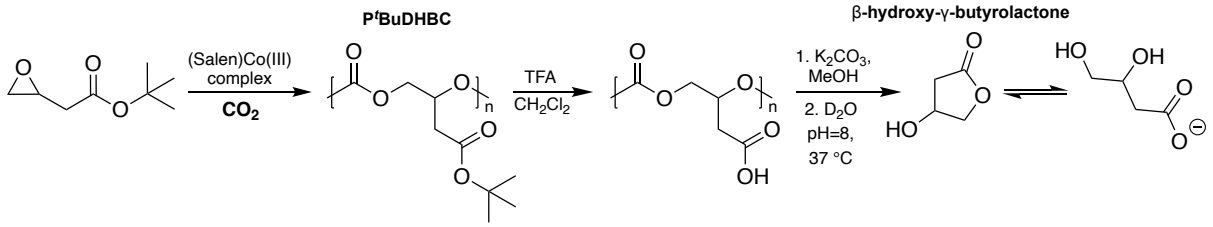

Scheme 10. Synthesis and degradation of poly(*tert*-butyl 3,4-dihydroxybutyrate carbonate).

4. ROP Polycarbonates

4.1 *Access to CO_2-sourced cyclic carbonates and fundamentals of their ROP*

The last decade has seen the emergence of non-reductive coupling methods of CO_2 to afford cyclic carbonates, yet potentially serving as monomers for the construction of aliphatic polycarbonates via ionic, coordination-insertion, enzymatic or dual chain-end-monomer activation ROP mechanisms, as extensively reviewed elsewhere.[1,17,64] The well-established [3+2] coupling of CO_2 with epoxide provides a large portfolio of five-membered cyclic carbonates (5CCs) under very attractive process conditions.[21,29,65–68] These heterocycles with small ring strain are stable and their ring-opening polymerization is thermodynamically disfavored and typically accompanied by the elimination of CO_2 to deliver poly(ether-carbonate)s (Scheme 11a).[64] The in-chain ether linkage defects are suppressed by polymerizing five-membered cyclic carbonates fused in the *trans*-fashion to a six-membered ring (*trans*-cyclohexene carbonate (CHC)) (Scheme 11b). Such alicyclic carbonates, produced for instance by thermal reversion of CO_2-sourced poly(cyclohexene carbonate) (see section 3.2), dispose of sufficient ring-strain to deliver the aliphatic polycarbonates without decarboxylation upon anionic[69] or coordination-insertion[32,70] ROP conditions. For example, the ^{t}BuOK-initiated anionic polymerization of *trans*-cyclohexene carbonate produced the corresponding PC of M_n = 11,000 g/mol with > 99% carbonate linkages. For this system, the associated thermodynamics ($\Delta H°_{polym}$ = −23 kJ mol^{-1} and $\Delta S°_{polym}$ = −63 Jmol^{-1}K^{-1}) compare favorably with those reported for the easy polymerizable trimethylene carbonate (TMC).[69]

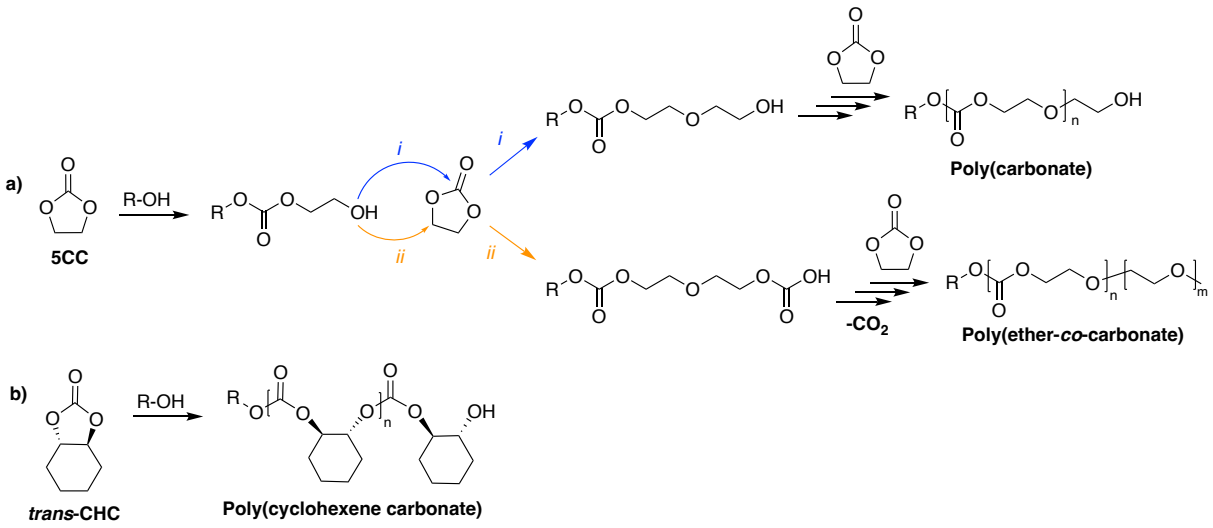

Scheme 11. Effect of the structure of cyclic carbonate for the introduction of in-chain defects.

The ROP of six-membered cyclic carbonates such as trimethylene carbonate (TMC) is by far less challenging and known for a century.[71,72] (Functional) TMC and even larger ring carbonates are accessible from CO_2 and ubiquitous alcohol substrates such as homoallylic alcohol[73] or 1,*n*-diols (with *n* = 2-4).[21,74–77] Despite these synthetic pathways required stochiometric amount of base, sacrificial reagents or desiccant such as halide salts, alkyl halides, tosyl chloride or cyanopyridines, a broad array of differently functionalized six-to-eight-membered cyclic carbonates were produced in 45−85% yield. Some of them were successfully polymerized using dual organocatalysts consisting in a combination of a superbase (DBU, TBD) and a (thio)urea cocatalyst, yet furnishing (substituted) PCs in 1 to 36 h with predictable M_n = 1,250 - 12,300 g/mol (Scheme 12).[78]

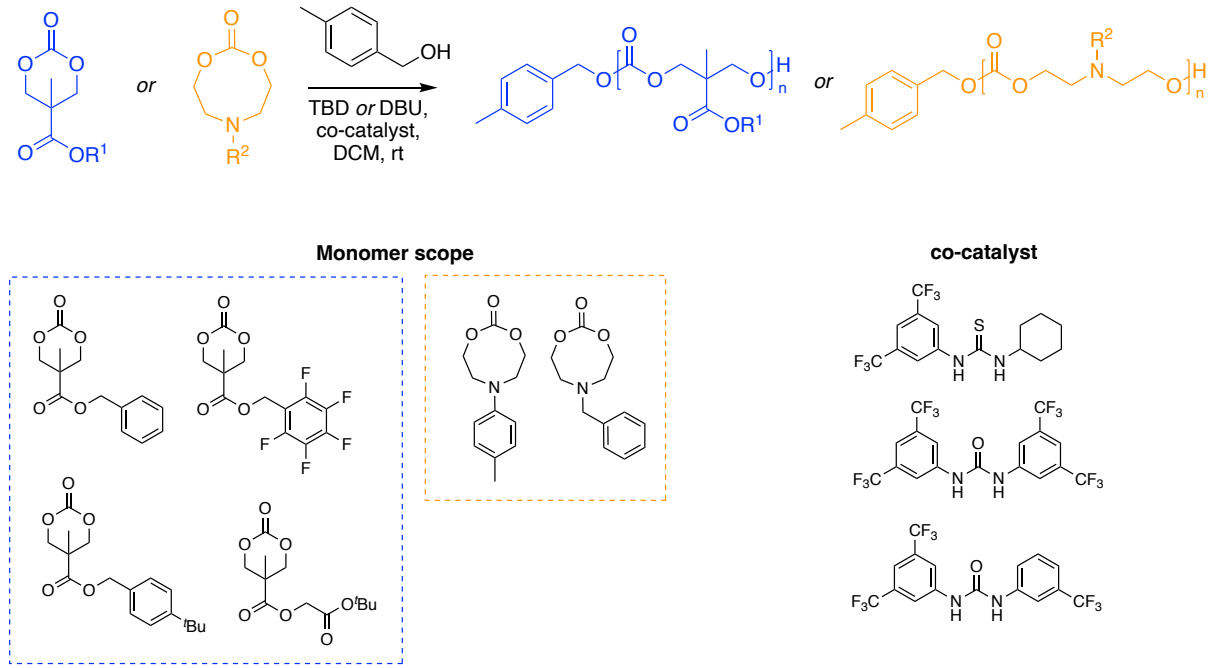

Scheme 12. The ROP of six and eight-membered cyclic carbonates.

Another relevant example by Buchard exploited a CO_2-sourced cyclic carbonate fused with a *D*-mannose unit in a *trans* configuration to deliver regioregular PCs (M_n up to 33,000 g/mol) at ambient temperature by TBD controlled ring-opening polymerization (Scheme 13).[79]

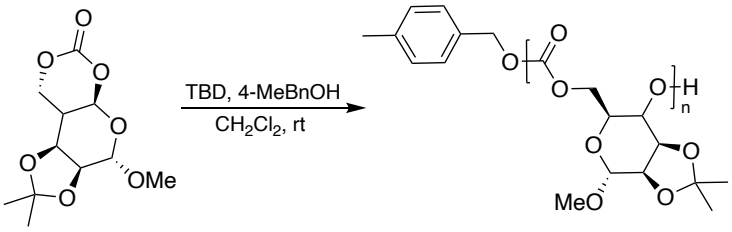

Scheme 13. ROP of CO_2- and *D*-mannose-sourced cyclic carbonate.

The catalytic ring expansion of (substituted) oxetanes with CO_2 is another mean to access TMC and functional analogues.[80–87] As the six-membered cyclic carbonate is thermodynamically less stable than the resulting PC, affording high cyclic *vs* linear co-product is strongly dependent on the catalyst and operating conditions (Scheme 14). Various metal complexes including (Salen)CoCl[88,89] or $VO(acac)_2$ /onium salts[82], Al(III)- and Fe(III)-based amino-(triphenolate)s[80,90,91] and dual organocatalysts such as alkyl boranes/onium or phosphonium halide,[85] ammonium acetate/I_2 [81] were reported for such transformation. Selectivity for TMC > 85-99 % was generally achieved at low CO_2 pressure and low temperature. As illustrated by Coulembier for the ammonium acetate/I_2 catalytic system[81], the energetic barriers for TMC *vs* poly(TMC) formation by oxetane/CO_2 coupling was estimated to 36.9 kJ/mol *vs* 49.9 kJ/mol. This sufficient 13 kJ/mol difference in energetic barrier suggested a thermally controllable product selectivity, the formation of TMC being favored at low temperature while poly(TMC) was produced at higher temperature (generally > 75-100°C). Besides, increasing the steric congestion of the oxetane improved the selectivity towards the cyclic carbonate formation.[89,92] Despite the ROP of the so-produced six-membered heterocycles was not reported, additional contributions highlighted the formation of poly(TMC) from CO_2 and oxetanes through the enchainment of *in-situ* formed TMC by using DBU/I_2 [87] or $^{n}Bu_4NI$/fluoroalcohols dual catalysts.[93] Aided by DFT studies, the CO_2/oxetane ROCOP mechanism was excluded due to unfavorable polymerization energetics. The formation of the resulting PC with M_n < 10,000 g/mol and the presence of low (or no) ether linkage defects were attributed to the *in-situ* formation of TMC followed in a domino fashion by its ROP. Recently, Kleij discovered that β-epoxy alcohols with an *anti*-configuration delivered hydroxy-functional densely substituted bicyclic 6-membered carbonates upon direct coupling with CO_2 (Scheme 15).[94] This breakthrough concept employed a binary catalysis involving an Al(III) aminotriphenolate complex and *N,N*-Diisopropylethylamine (DIPEA) as nitrogen base additive and operated at low CO_2 pressure of 10 bar in 22 h at 100 °C.

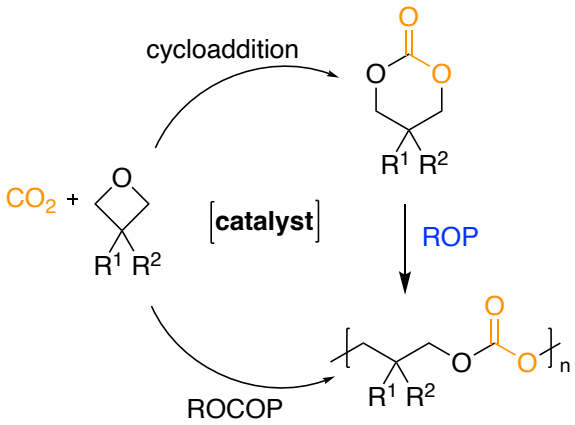

Scheme 14. Synthesis of poly(TMC) from CO_2 and oxetanes.

Diversification of the substrate scope furnished a portfolio of new scaffolds with yields of 44 to 91%. One representative bicyclic carbonate heterocycle and its *O*-protected version by a silyl group were subjected to ROP using TBD as catalyst at r.t., yet providing respectively oligomers of low M_n = 1,700 g/mol (for R=H) or short PCs chains with M_n = 8,600 g/mol in 20 h (for R = $SiMe_3$) (Scheme 15).

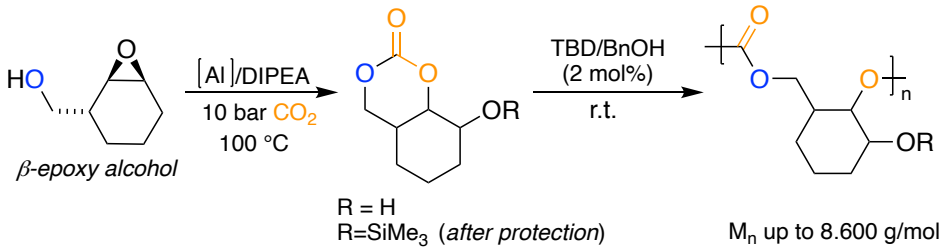

Scheme 15. ROP of β-epoxy alcohols derived six-membered cyclic carbonates.

Larger ring-strained carbonates were also prone to ROP. To the best of our knowledge, only one example from Zhu focused on the synthesis of 7-membered cyclic carbonates fused in a *trans*-fashion with a cyclohexyl or cyclohexadiene ring by carbonylation of *trans*-cyclohexane-1,2-diyldimethanol or *trans*-cyclohexadiene-1,2-diyldimethanol (Scheme 16).[95]

Thanks to the high ring strain, this new class of highly reactive monomer polymerized in the presence an yttrium alkyl complex ligated by tetradentate aminobisphenolate chelatant. The ROP was expedient in toluene and approached 100 % monomer conversion within 30 seconds, furnishing PCs with M_n up to 673,000 g/mol (Scheme 16). In the continuation of his work on the carbonylation of diols by CO_2,[96] Hedrick reported series of 8-membered heterocycles furnishing PC of M_n = 1,250 – 7,500 g/mol in 1.5 – 24 h at r.t. using appropriate (binary) organocatalysts (Scheme 12).[78]

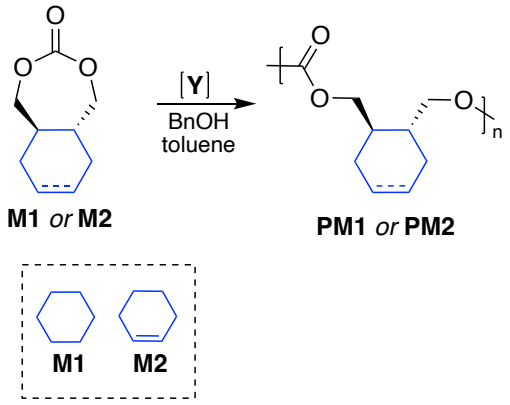

Scheme 16. ROP of seven-membered trans-cyclohexane or cyclohexadiene cyclic carbonate.

4.2 *Thermal tail-to-head reversion of ROP PCs*

Examples of thermal reversion of CO_2-derived ROP PCs into repolymerizable scaffolds remain rare. The close loop recycling of CO_2-sourced PCs made by ROP is illustrated by Coates with isotactic poly(cyclohexene oxide) with hydroxyl end caps.[32] The endwise thermal unzipping of this PC was promoted by NaHMDS base at 250 °C and delivered the corresponding enantiopure 5-membered cyclic carbonate fused in a *trans* configuration with a cyclohexene ring, i.e. (*S,S*)-2,2-cyclohexene carbonate (Scheme 17). This monomer was repolymerized following a ROP scenario into isotactic poly(cyclohexene carbonate) using ethyl zinc isopropoxide as a catalyst at 50 °C for 16 h. Rather similar in concept is the depolymerization of poly(5-methyl-5-benzyloxymethyl-1,3-dioxan-2-one), a functional version of poly(TMC) with benzyloxymethyl moieties pending along the main skeleton (Scheme 18).[92] This CO_2-sourced PC reverted by a backbiting pathway into the corresponding six-membered cyclic carbonate (5-methoxymethyl-5-methyl-1,3-dioxan-2-one) in the presence of (salen)Cr(III)chloride complexes and $^{n}Bu_4NN_3$ additive, at 110 °C in 16 h. Under argon atmosphere, the depolymerization was slow, delivering the heterocycle with a yield of 30 % in 200 h, while the depolymerization was strongly retarded, even inhibited, under 7 bar of CO_2. Despite their close loop recycling was not illustrated, the ROP of cyclic carbonates of similar structure was demonstrated in the presence of a $Ti(^{i}OPr)_4$ catalyst at 210 °C, yet potentially completing the virtuous polymer-to-monomer-to-polymer cycle.[97]

As illustrated below, 7-membered cyclic carbonates containing *trans*-cyclohexyl-fused rings afforded high molar mass PCs that followed complete depolymerization at room temperature into new cyclic dimers by simple use of MeOK (Scheme 19). These polymers degraded in a stereoselective manner at high selectivity and yield into enantiomerically pure (*R,R,S,S*) cyclic carbonate dimers identified as the stable thermodynamic configuration.

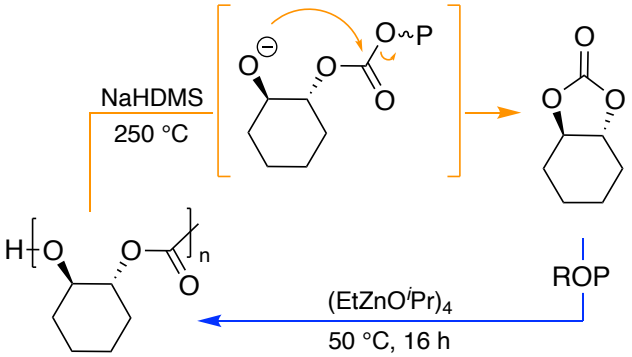

Scheme 17. Thermal reversion of CO_2-derived ROP PCs into repolymerizable cyclohexene carbonates.

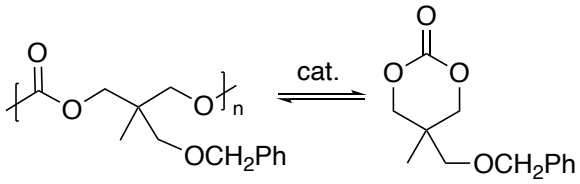

Scheme 18. Depolymerization of poly(3-benzyloxymethyl-3-methyloxetane carbonate) into six-membered cyclic carbonate.

As oligomer intermediates were identified during the process, and by analogy with Odelius' contribution on the ROP of similar macrocycles and their polymer-to-monomer regeneration (Scheme 19), it was supposed that an *in-situ* transesterification depolymerization mechanism governed the deconstruction of the chains.[98] By simple temperature switch to 150 °C, the new dimeric macrocyclic carbonates reentered the polymerization loop through anionic ROP (using MeOK or ^{t}BuOK as a base), yet reforming PCs with microstructure identical to the native material, but of significant lower molar mass (M_n < 7,600 g/mol)(Scheme 19).[95]

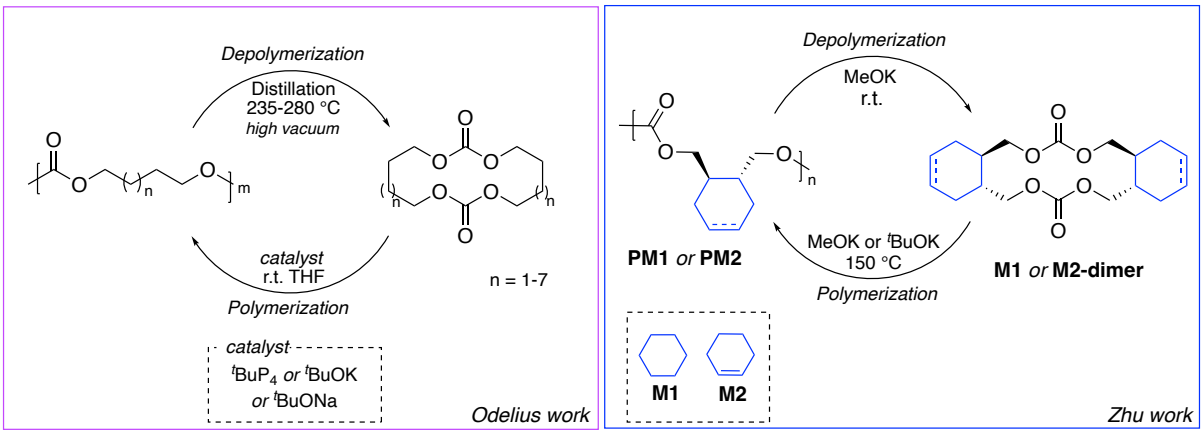

Scheme 19. Depolymerization of poly(*trans*-cyclohexane or cyclohexadiene)carbonates into macrocyclic carbonates.

4.3 *Solvolysis of ROP PCs*

Beside their thermal reversion to the *trans*-cyclohexene carbonate, isotactic poly(cyclohexene carbonate) was quantitatively degraded by hydrolysis into *trans*-1,2-cyclohexanol and CO_2 by using a NaOH/MeOH mixture (Scheme 20). To the best of our knowledge, the hydrolytic degradation of CO_2-based poly(cyclohexene carbonate) was applied to polymers synthetized by ROCOP. However, considering the polymeric structure, it should be possible to extend such methodology to poly(cyclohexene carbonate) and other CO_2-sourced ROP polymers.[99–101] One also underline that poly(trimethylene carbonate) and functional analogues are now easily accessible by ROP of CO_2-sourced monomers. Thanks to their easy tunable degradation properties and biocompatibility, these aliphatic PCs are widely explored for biomedical use for drug delivery, tissue regeneration or the design of vascular grafts. Despite not being the topic of the review, one invites the reader to refer to the excellent review of Dove illustrating all the degradation pathways of such materials via hydrolysis, oxidation, in-vivo/enzymatic deconstruction.[17]

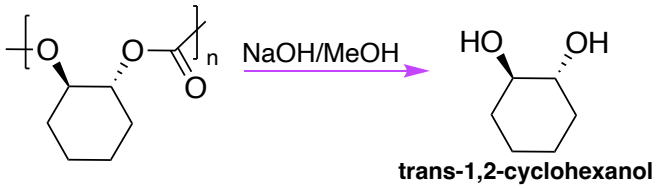

Scheme 20. Solvolysis of poly(cyclohexene carbonate).

5. Step-growth copolymerization (SGP) PCs

5.1 *Fundamentals of CO_2-sourced PCs by SGP*

The direct copolymerization of CO_2 and diols is an appealing but challenging method to fabricate PCs, while avoiding using toxic phosgene. The condensation of CO_2 and diols leads to water by-product formation which removal is mandatory to construct PCs chains with reasonable molar masses.[102,103] The most relevant contribution in this research area was reported by Tamura and coworkers who described first direct copolymerization of CO_2 with a wide scope of 1,*x*-diols (*x* > 4) by using CeO_2 heterogeneous catalyst and 2-cyanopyridine as desiccant (Scheme 21).[102] Such approach furnishes only oligomers (M_n up to 1,650 g/mol) as a result of various side reactions. The concomitant hydration of the cyanopyridine in presence of the cerium catalyst leads to the formation of the corresponding amide that interferes in the chain growth process. Its reaction with diol chain-ends provides the corresponding ester with release of NH_3 further causing the ammonolysis of the carbonate linkages and consequently, the PCs chain scission.[103] The formation of ester chain ends was slightly minimized by switching from cyanopyridine to 2-furonitrile as dehydrating agent, yet leading to polymers with

slightly higher molar masses (M_n up to 5,000 g/mol). Different dehydrating agent/processes (e.g. membranes, molecular sieves, chemical agents) were also explored, but with moderate success to fabricate PCs of higher molar masses.[104,105]

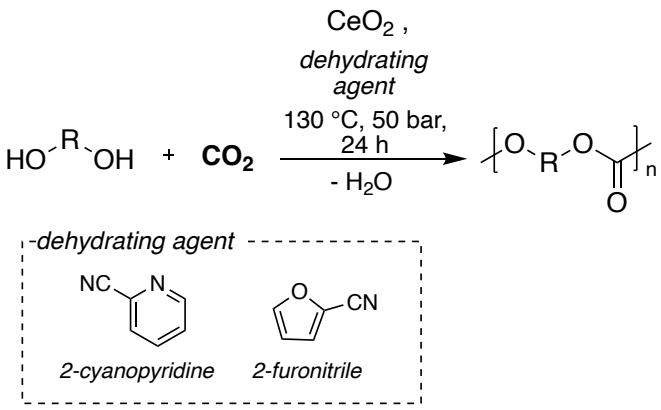

Scheme 21. Direct polymerization of CO_2 and diols by polycondensation.

The step-growth copolymerization (SGP) between diols and a carbonyl source (such as phosgene) is a well-established methodology to deliver high molar masses PCs with diverse microstructures and side-chain functionalities. [1] Alternative synthetic pathways to produce PCs were developed by using ecofriendly CO_2-derived precursors such as dimethyl- (DMC) or diphenyl- (DPC) carbonates. The polycondensation of CO_2-sourced acyclic aliphatic or aromatic carbonates with diols is a common synthetic strategy that permits to access a large palette of PCs with tunable properties. First, oligocarbonates of low molar mass were produced via transcarbonation reaction at moderate temperature (80-140 °C). The chain-extension was then performed under high vacuum and at temperature (150-300 °C) to remove the methanol (for DMC) or phenol (for DPC) that was released and favor the chains growth (Scheme 22).

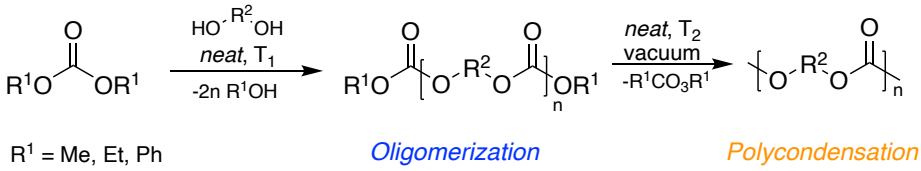

Scheme 22. Polycondensation of acyclic carbonates and diols.

Due to their outstanding thermo-mechanical properties, aromatic PCs are largely exploited in a plethora of applications. The industrial production of aromatic PCs follows phosgenation of bisphenol A (BPA) (Scheme 23, pathway *i*). However, the phosgene process presents non-negligible safety issues which pushed the scientists to replace it by diphenyl carbonate (DPC). The first non-phosgene process from CO_2 has been developed by Asahi and Kasei group reporting a two-step procedure of polycondensation between DPC as carbonyl source and BPA to furnish BPA-PCs (Scheme 23, pathway *ii*).[106,107]

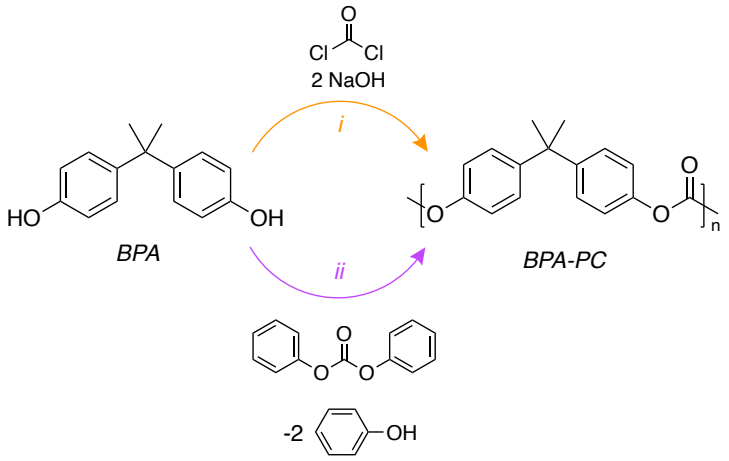

Scheme 23. Synthetic pathways for BPA-PC.

In 2017, our group pioneered a versatile and appealing conceptual approach to produce PCs from novel CO_2-based monomers, i.e. bis(α-alkylidene carbonate)s (bisαCCs) and diols (e.g. 1,4-butanediol) through organocatalyzed step-growth copolymerization under mild reaction conditions (Scheme 24a). The presence of the exovinylene group enhances the reactivity of these 5-membered cyclic carbonates, including against alcohols, and their organocatalyzed ring-opening is regio-selective as the result of the keto-enol tautomerism. Defect-free poly(*oxo*-carbonate)s were thus easily obtained with M_n up to 25,000 g/mol at room temperature.[108] The scope of the polymers was extended to poly(ethylene glycol) (PEG) diols to produce poly(carbonate-*co*-ether)s of M_n up to 60,000 g/mol of potential interest as solid electrolytes for battery applications.[109] Novel poly(cyclic carbonate-*co*-thioether)s were also accessible by the organocatalyzed copolymerization of bisαCCs with dithiols at r.t.[110,111] Similarly, Schaub et al. designed recently new bisαCCs from the tricomponent reaction between 1,4-butynediol, epoxides and CO_2, and successfully tailored poly(*oxo*-carbonates) by polyaddition with 1,4-butanediol. However, low molar masses PCs (M_n < 3,000 g/mol) were obtained (Scheme 24b).[112]

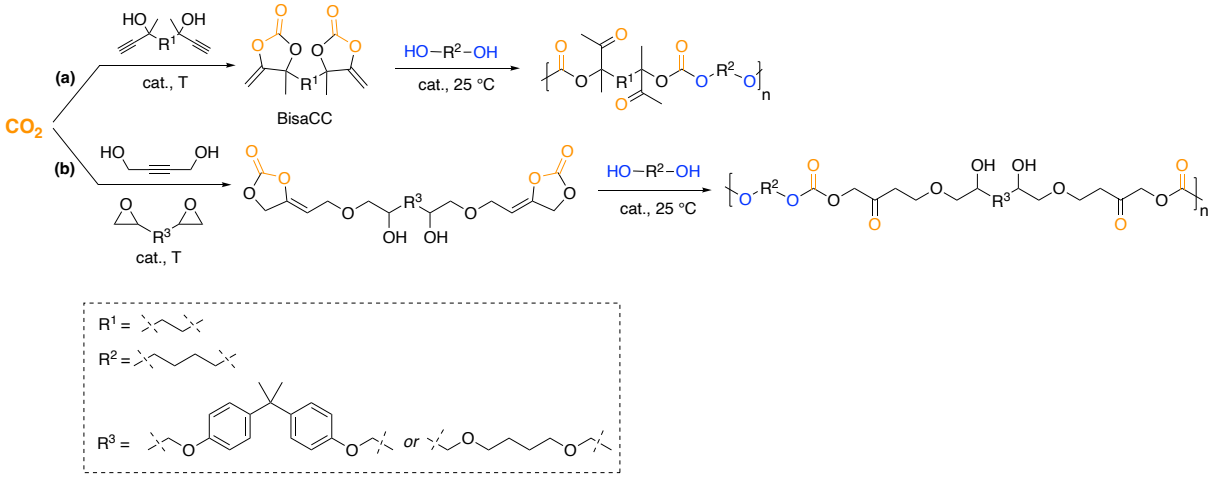

Scheme 24. Synthesis of PCs by step-growth copolymerization of bisαCCs with diols.

5.2 *Chemical degradation of SGP PCs*

During the last decade, a strong effort has been exerted on the BPA-PC depolymerization. Thanks to the presence of the carbonyl moieties within the chain, the BPA-PC backbone is prone to easy cleavage by suitable reagents. Using adapted catalysts, BPA-PC can be deconstructed by hydrolysis, alcoholysis or aminolysis, further releasing the native BPA monomer and some useful co-products such as (a)cyclic carbonates, urea, carbamates or methanol (Scheme 25).[113–122] In addition, the catalyzed hydrogenative depolymerization was investigated by using metal-complex catalysts and permitted to recover BPA as well as methanol.[57] The BPA-PC degradation was largely described in dedicated reviews.[123]

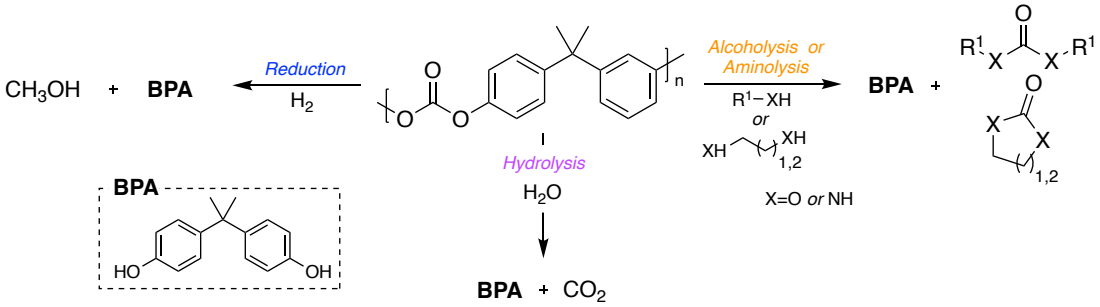

Scheme 25. Chemical degradation of BPA-PC.

6. Conclusions

Synthetic plastics have become ubiquitous and versatile materials in our modern life. Notwithstanding their considerable presence, *non*-treated plastic wastes lead to *non*-negligible ecological and biological-health issues, but also to economical damages due to the loss of potential resources. The fossil origin of plastics also makes their carbon footprint dramatic. Pushed by environmental incentives and legal obligations from the European Commission, there is now an urgent need to reinvent the fabrication of plastics, ideally by exploiting raw biochemicals and waste effluents such as CO_2, while making them more easily degradable/recyclable. This introduction illustrates where scientists are shifting their gaze for the development of more sustainable plastic materials using raw CO_2. In particular, it summarizes briefly the most relevant synthetic approaches for the production of polycarbonates and highlights their emerging end-of-life scenario. Thanks to catalytic breakthrough discoveries, there is now an impressive body of knowledge on how to construct and control the PCs microstructure via the R(OC)OP approaches, yet imparting desired properties often guided by the need of the final application. Their thermal *tail-to-head* reversion is multi-factors dependent (ceiling temperature, catalytic system, the presence of defects within the main skeleton,…) and provides either the native monomers or (macro)cyclic carbonate products. Aliphatic ROCOP PCs undergo fast and facile base promoted deconstruction by endwise unzipping to deliver exclusively 5-membered cyclic carbonates. Generally, ROCOP PCs derived from (geometrically constrained) epoxides fused with aliphatic ring necessitate binary catalysts composed of a strong base and a Salen complex to deconstruct slowly the chains even under high thermal conditions. PCs derived from CO_2 and epoxides fused with 5-membered ring such as cyclopentene revert preferentially into the parent epoxide and CO_2 through decarboxylative ring closure depolymerization. The release of CO_2 enables to accommodate the strain-induced distortions in these fused systems, minimizing the energy of the two five-membered fused rings. Besides, the formation of alicyclic carbonates with a *trans* conformation becomes energetically favorable when i) reducing the ring strain via an increase of the fused alicyclic ring size (6- or 7-membered rings) and/or ii) driving the chains depolymerization under CO_2 atmosphere, so limiting/preventing the formation of the corresponding fused epoxide by decarboxylative ring closure depolymerization.

The close loop recycling of CO_2-sourced PCs made by ROP has been rarely illustrated. Hydroxyl terminated PCs derived from 5-membered alicyclic carbonates or 6-membered rings revert via *tail-to-head* backbiting above their ceiling temperatures (T > 200-250 °C) into the native cyclic monomers in the presence of appropriate base (NaHMDS) or dual catalyst systems (e.g. azide salt/Salen complex). Beside, ROP PCs derived from 7-membered cyclic carbonates degrades at r.t. using MeOK in a stereoselective manner at high selectivity and

yield into enantiopure cyclic carbonate dimers. Their polymer-to-monomer regeneration is governed by an *in-situ* transesterification depolymerization mechanism.

The chemical degradation of PCs via hydrolysis, solvolysis or hydrogenolysis is more versatile as it is virtually adaptable to all types of PCs, whatever their origin and microstructures. All approaches require appropriate catalysts and thermal activation, yet leading to the total deconstruction of the chains with concomitant formation of mixture of diols and CO_2 (hydrolysis), (a)cyclic carbonates and ureas (solvolysis) or methanol (hydrogenolysis).

Finally, designing PCs that are intrinsically degradable on demand is an alternative way to overcome the accumulation of plastic waste. Such concept is illustrated for ROCOP PCs designed from oxiranyl monomers bearing protected carboxylic acid and alcohol moieties in which the introduction of a protected active group along the chain skeleton permits to trigger depolymerization upon deprotection. The chain degradation is initiated *via* an intramolecular cyclization, leading to the formation of cyclic compounds such as O-carboxyanhydride, glycerol carbonate or β-hydroxy-γ-butyrolactone.

Depolymerizing PCs into high-value-added products that can be upcycled is a new direction for a more sustainable plastic development. It is noteworthy that almost all current recycling/upcycling strategies focus on RO(CO)P made PCs, with only few studies exploring the chemical degradation of PCs made by SGP. Due to the increasing interest in SGP PCs, this brings to light that research is still needed for their sustainable design while considering that they should be degradable and recyclable.

References

(1) Grignard, B.; Gennen, S.; Jérôme, C.; Kleij, A. W.; Detrembleur, C. Advances in the Use of CO_2 as a Renewable Feedstock for the Synthesis of Polymers. *Chem. Soc. Rev.* **2019**, *48*, 4466–4514. https://doi.org/10.1039/c9cs00047j.

(2) PlascticsEurope. *Plastics-the Facts 2021 An Analysis of European Plastics Production, Demand and Waste Data*.

(3) European Commission. *A New Circular Economy Action Plan For a Cleaner and More Competitive Europe*; 2020.

(4) Dabral, S.; Schaub, T. The Use of Carbon Dioxide (CO_2) as a Building Block in Organic Synthesis from an Industrial Perspective. *Adv. Synth. Catal.* **2019**, *361*, 223–246. https://doi.org/10.1002/adsc.201801215.

(5) Zheng, J.; Suh, S. Strategies to Reduce the Global Carbon Footprint of Plastics. *Nat. Clim. Chang.* **2019**, *9*, 374–378. https://doi.org/10.1038/s41558-019-0459-z.

(6) García, J. M. Catalyst: Design Challenges for the Future of Plastics Recycling. *Chem* **2016**, *1*, 813–819. https://doi.org/10.1126/science.aad1694.

(7) Ignatyev, I. A.; Thielemans, W.; Van der Beke, B. Recycling of Polymers: A Review. *ChemSusChem* **2014**, *7*, 1579–1593. https://doi.org/10.1002/cssc.201300898.

(8) Jehanno, C.; Alty, J. W.; Roosen, M.; de Meester, S.; Dove, A. P.; Chen, E. Y. X.; Leibfarth, F. A.; Sardon, H. Critical Advances and Future Opportunities in Upcycling Commodity Polymers. *Nature* **2022**, *603*, 803–814. https://doi.org/10.1038/s41586-021-04350-0.

(9) Fagnani, D. E.; Tami, J. L.; Copley, G.; Clemons, M. N.; Getzler, Y. D. Y. L.; McNeil, A. J. 100th Anniversary of Macromolecular Science Viewpoint: Redefining Sustainable Polymers. *ACS Macro Lett.* **2021**, *10* , 41–53. https://doi.org/10.1021/acsmacrolett.0c00789.

(10) Coates, G. W.; Getzler, Y. D. Y. L. Chemical Recycling to Monomer for an Ideal, Circular Polymer Economy. *Nat. Rev. Mater.* **2020**, *5* , 501–516. https://doi.org/10.1038/s41578-020-0190-4.

(11) Vollmer, I.; Jenks, M. J. F.; Roelands, M. C. P.; White, R. J.; van Harmelen, T.; de Wild, P.; van der Laan, G. P.; Meirer, F.; Keurentjes, J. T. F.; Weckhuysen, B. M. Beyond Mechanical Recycling: Giving New Life to Plastic Waste. *Angew. Chem. Int. Ed.* **2020**, *59*, 15402–15423. https://doi.org/10.1002/anie.201915651.

(12) Roy, P. S.; Garnier, G.; Allais, F.; Saito, K. Strategic Approach Towards Plastic Waste Valorization: Challenges and Promising Chemical Upcycling Possibilities. *ChemSusChem* **2021**, *14*, 1–22. https://doi.org/10.1002/cssc.202100904.

(13) Sardon, H.; Dove, A. P. Plastics Recycling with a Difference: A Novel Plastic with Useful Properties Can Easily Be Recycled Again and Again. *Science* **2018**, *360*, 380–381. https://doi.org/10.1126/science.aat4997.

(14) Chen, H.; Wan, K.; Zhang, Y.; Wang, Y. Waste to Wealth: Chemical Recycling and Chemical Upcycling of Waste Plastics for a Great Future. *ChemSusChem* **2021**, *14*, 4123–4136. https://doi.org/10.1002/cssc.202100652.

(15) Worch, J. C.; Dove, A. P. 100th Anniversary of Macromolecular Science Viewpoint: Toward Catalytic Chemical Recycling of Waste (and Future) Plastics. *ACS Macro Lett.* **2020**, 1494–1506. https://doi.org/10.1021/acsmacrolett.0c00582.

(16) Ellis, L. D.; Rorrer, N. A.; Sullivan, K. P.; Otto, M.; McGeehan, J. E.; Román-Leshkov, Y.; Wierckx, N.; Beckham, G. T. Chemical and Biological Catalysis for Plastics Recycling and Upcycling. *Nat. Catal.* **2021**, *4*, 539–556. https://doi.org/10.1038/s41929-021-00648-4.

(17) Yu, W.; Maynard, E.; Chiaradia, V.; Arno, M. C.; Dove, A. P. Aliphatic Polycarbonates from Cyclic Carbonate Monomers and Their Application as Biomaterials. *Chem. Rev.* **2021**. https://doi.org/10.1021/acs.chemrev.0c00883.

(18) Zhang, X.; Fevre, M.; Jones, G. O.; Waymouth, R. M. Catalysis as an Enabling Science for Sustainable Polymers. *Chem. Rev.* **2018**, *118*, 839–885. https://doi.org/10.1021/acs.chemrev.7b00329.

(19) Bobbink, F. D.; van Muyden, A. P.; Dyson, P. J. En Route to CO_2 -Containing Renewable Materials: Catalytic Synthesis of Polycarbonates and Non-Isocyanate Polyhydroxyurethanes Derived from Cyclic Carbonates. *Chem. Commun.* **2019**, *55*, 1360–1373. https://doi.org/10.1039/c8cc07907b.

(20) Huang, J.; Worch, J. C.; Dove, A. P.; Coulembier, O. Update and Challenges in Carbon Dioxide-Based Polycarbonate Synthesis. *ChemSusChem* **2020**, *13*, 469–487. https://doi.org/10.1002/cssc.201902719.

(21) Brege, A.; Grignard, B.; Méreau, R.; Detrembleur, C.; Jerome, C.; Tassaing, T. En Route to CO_2-Based (a)Cyclic Carbonates and Polycarbonates from Alcohols Substrates by Direct and Indirect Approaches. *Catalysts* **2022**, *12*, 124. https://doi.org/10.3390/catal12020124.

(22) Cao, H.; Wang, X. Carbon Dioxide Copolymers: Emerging Sustainable Materials for Versatile Applications. *SusMat.* **2021**, *1*, 88–104. https://doi.org/10.1002/sus2.2.

(23) Covestro. Cardyon®: Sustainable Polyol with up to 20% CO_2 by Covestro. *Covestro AG*. 2022.

(24) Fukuoka, S.; Kawamura, M.; Komiya, K.; Tojo, M.; Hachiya, H.; Hasegawa, K.; Aminaka, M.; Okamoto, H.; Fukawa, I.; Konno, S. A Novel Non-Phosgene Polycarbonate Production Process Using by-product CO_2 as Starting Material. *Green Chem.* **2003**, *5*, 497–507. https://doi.org/10.1039/B304963A.

(25) Inoue, S.; Koinuma, H.; Tsuruta, T. Copolymerization of Carbon Dioxide and Epoxide. *J. Polym. Sci. B* **1969**, *7*, 287–292. https://doi.org/https://doi.org/10.1002/pol.1969.110070408.

(26) Taherimehr, M.; Pescarmona, P. P. Green Polycarbonates Prepared by the Copolymerization of CO2 with Epoxides. *J. Appl. Polym. Sci.* **2014**, *131*, 1–17. https://doi.org/10.1002/app.41141.

(27) Paul, S.; Zhu, Y.; Romain, C.; Brooks, R.; Saini, P. K.; Williams, C. K. Ring-Opening Copolymerization (ROCOP): Synthesis and Properties of Polyesters and Polycarbonates. *Chem. Commun.* **2015**, *51*, 6459–6479. https://doi.org/10.1039/c4cc10113h.

(28) Plajer, A. J.; Williams, C. K. Heterocycle/Heteroallene Ring-Opening Copolymerization: Selective Catalysis Delivering Alternating Copolymers. *Angew. Chem. Int. Ed.* **2022**, *61*, e202104495. https://doi.org/10.1002/anie.202104495.

(29) Kamphuis, A. J.; Picchioni, F.; Pescarmona, P. P. CO_2-Fixation into Cyclic and Polymeric Carbonates: Principles and Applications. *Green Chem.* **2019**, *21*, 406–448. https://doi.org/10.1039/c8gc03086c.

(30) Bhat, G. A.; Darensbourg, D. J. Progress in the Catalytic Reactions of CO_2 and Epoxides to Selectively Provide Cyclic or Polymeric Carbonates. *Green Chem.* **2022**, *24*, 5007–5034. https://doi.org/10.1039/d2gc01422j.

(31) Diallo, A. K.; Kirillov, E.; Slawinski, M.; Brusson, J. M.; Guillaume, S. M.; Carpentier, J. F. Syndioselective Ring-Opening Polymerization and Copolymerization of Trans-1,4-Cyclohexadiene Carbonate Mediated by Achiral Metal- and Organo-Catalysts. *Polym. Chem.* **2015**, *6*, 1961–1971. https://doi.org/10.1039/c4py01713g.

(32) Ellis, W. C.; Jung, Y.; Mulzer, M.; di Girolamo, R.; Lobkovsky, E. B.; Coates, G. W. Copolymerization of CO_2 and Meso Epoxides Using Enantioselective β-Diiminate Catalysts: A Route to Highly Isotactic Polycarbonates. *Chem. Sci.* **2014**, *5*, 4004–4011. https://doi.org/10.1039/c4sc01686f.

(33) Cui, S.; Qin, Y.; Li, Y. Sustainable Approach for the Synthesis of Biopolycarbonates from Carbon Dioxide and Soybean Oil. *ACS Sustain. Chem. Eng.* **2017**, *5*, 9014–9022. https://doi.org/10.1021/acssuschemeng.7b01819.

(34) Kember, M. R.; Buchard, A.; Williams, C. K. Catalysts for Co2/Epoxide Copolymerisation. *Chem. Commun.* **2011**, *47*, 141–163. https://doi.org/10.1039/c0cc02207a.

(35) Cheng, M.; Darling, N. A.; Lobkovsky, E. B.; Coates, G. W. Enantiomerically-Enriched Organic Reagents via Polymer Synthesis: Enantioselective Copolymerization of Cycloalkene Oxides and CO_2 Using Homogeneous, Zinc-Based Catalysts. *Chem. Commun.* **2000**, 2007–2008. https://doi.org/10.1039/b005537i.

(36) Darensbourg, D. J.; Chung, W. C.; Wilson, S. J. Catalytic Coupling of Cyclopentene Oxide and CO_2 Utilizing Bifunctional (Salen)Co(III) and (Salen)Cr(III) Catalysts: Comparative Processes Involving Binary (Salen)Cr(III) Analogs. *ACS Catal.* **2013**, *3*, 3050–3057. https://doi.org/10.1021/cs4008667.

(37) Sobrino, S.; Navarro, M.; Fernández-Baeza, J.; Sánchez-Barba, L. F.; Lara-Sánchez, A.; Garcés, A.; Castro-Osma, J. A.; Rodríguez, A. M. Effcient Production of Poly(Cyclohexene Carbonate) via ROCOP of Cyclohexene Oxide and CO_2 Mediated by NNO-Scorpionate Zinc Complexes. *Polymers* **2020**, *12*, 2148. https://doi.org/10.3390/POLYM12092148.

(38) Shao, H.; Reddi, Y.; Cramer, C. J. Modeling the Mechanism of CO_2/Cyclohexene Oxide Copolymerization Catalyzed by Chiral Zinc β-Diiminates: Factors Affecting Reactivity and Isotacticity. *ACS Catal.* **2020**, *10*, 8870–8879. https://doi.org/10.1021/acscatal.0c02299.

(39) Kember, M. R.; Knight, P. D.; Reung, P. T. R.; Williams, C. K. Highly Active Dizinc Catalyst for the Copolymerization of Carbon Dioxide and Cyclohexene Oxide at One Atmosphere Pressure. *Angew. Chem. Int. Ed.* **2009**, *48*, 931–933. https://doi.org/10.1002/anie.200803896.

(40) Darensbourg, D. J.; Yeung, A. D. Thermodynamics of the Carbon Dioxide-Epoxide Copolymerization and Kinetics of the Metal-Free Degradation: A Computational Study. *Macromolecules* **2013**, *46*, 83–95. https://doi.org/10.1021/ma3021823.

(41) Darensbourg, D. J.; Wei, S. H. Depolymerization of Polycarbonates Derived from Carbon Dioxide and Epoxides to Provide Cyclic Carbonates. A Kinetic Study. *Macromolecules* **2012**, *45*, 5916–5922. https://doi.org/10.1021/ma301110c.

(42) Wu, G. P.; Wei, S. H.; Lu, X. B.; Ren, W. M.; Darensbourg, D. J. Highly Selective Synthesis of CO_2 Copolymer from Styrene Oxide. *Macromolecules* **2010**, *43*, 9202–9204. https://doi.org/10.1021/ma1021456.

(43) Darensbourg, D. J.; Wei, S. H.; Wilson, S. J. Depolymerization of Poly(Indene Carbonate). A Unique Degradation Pathway. *Macromolecules* **2013**, *46*, 3228–3233. https://doi.org/10.1021/ma400441m.

(44) Darensbourg, D. J.; Wei, S. H.; Yeung, A. D.; Ellis, W. C. An Efficient Method of Depolymerization of Poly(Cyclopentene Carbonate) to Its Comonomers: Cyclopentene Oxide and Carbon Dioxide. *Macromolecules* **2013**, *46*, 5850–5855. https://doi.org/10.1021/ma401286x.

(45) Liu, Y.; Zhou, H.; Guo, J. Z.; Ren, W. M.; Lu, X. B. Completely Recyclable Monomers and Polycarbonate: Approach to Sustainable Polymers. *Angew. Chem. Int. Ed.* **2017**, *56*, 4862–4866. https://doi.org/10.1002/anie.201701438.

(46) Yu, Y.; Fang, L. M.; Liu, Y.; Lu, X. B. Chemical Synthesis of CO_2-Based Polymers with Enhanced Thermal Stability and Unexpected Recyclability from Biosourced Monomers. *ACS Catal.* **2021**, *11*, 8349–8357. https://doi.org/10.1021/acscatal.1c01376.

(47) Yu, Y.; Gao, B.; Liu, Y.; Lu, X. Efficient and Selective Chemical Recycling of CO_2 -Based Alicyclic Polycarbonates via Catalytic Pyrolysis. *Angew. Chem. Int. Ed.* **2022**, *61*, e202204492. https://doi.org/10.1002/anie.202204492.

(48) Liu, Y.; Zhou, H.; Guo, J.-Z.; Ren, W.-M.; Lu, X.-B. Completely Recyclable Monomers and Polycarbonate: Approach to Sustainable Polymers. *Angew. Chem. Int. Ed.* **2017**, *56*, 4862–4866. https://doi.org/10.1002/ange.201701438.

(49) Singer, F. N.; Deacy, A. C.; McGuire, T. M.; Williams, C. K.; Buchard, A. Chemical Recycling of Poly(Cyclohexene Carbonate) Using a Di-MgII Catalyst. *Angew. Chem. Int. Ed.* **2022**, *61*, e202201785. https://doi.org/10.1002/anie.202201785.

(50) Liao, X.; Cui, F.-C.; He, J.-H.; Ren, W.-M.; Lu, X.-B.; Zhang, Y.-T. A Sustainable Approach for the Synthesis of Recyclable Cyclic CO_2 -Based Polycarbonates. *Chem. Sci.* **2022**, *13*, 6283–6290. https://doi.org/10.1039/d2sc01387h.

(51) Liu, Y.; Fang, L.-M.; Ren, B.-H.; Lu, X.-B. Asymmetric Alternating Copolymerization of CO_2 with Meso-Epoxides: Ring Size Effects of Epoxides on Reactivity, Enantioselectivity, Crystallization, and Degradation. *Macromolecules* **2020**, *53*, 2912–2918. https://doi.org/10.1021/acs.macromol.9b02407.

(52) Darensbourg, D. J.; Chung, W. C.; Arp, C. J.; Tsai, F. Te; Kyran, S. J. Copolymerization and Cycloaddition Products Derived from Coupling Reactions of 1,2-Epoxy-4-Cyclohexene and Carbon Dioxide. Postpolymerization Functionalization via Thiol-Ene Click Reactions. *Macromolecules* **2014**, *47*, 7347–7353. https://doi.org/10.1021/ma501781k.

(53) Li, C.; Sablong, R. J.; van Benthem, R. A. T. M.; Koning, C. E. Unique Base-Initiated Depolymerization of Limonene-Derived Polycarbonates. *ACS Macro Lett.* **2017**, *6*, 684–688. https://doi.org/10.1021/acsmacrolett.7b00310.

(54) Han, Z.; Rong, L.; Wu, J.; Zhang, L.; Wang, Z.; Ding, K. Catalytic Hydrogenation of Cyclic Carbonates: A Practical Approach from CO_2 and Epoxides to Methanol and Diols. *Angew. Chem. Int. Ed.* **2012**, *51*, 13041–13045. https://doi.org/10.1002/ange.201207781.

(55) Zubar, V.; Lebedev, Y.; Azofra, L. M.; Cavallo, L.; El-Sepelgy, O.; Rueping, M. Hydrogenation of CO_2 -Derived Carbonates and Polycarbonates to Methanol and Diols by Metal-Ligand Cooperative Manganese Catalysis. *Angew. Chem. Int. Ed.* **2018**, *57*, 13439–13443. https://doi.org/10.1002/ange.201805630.

(56) Kumar, A.; Janes, T.; Espinosa-Jalapa, N. A.; Milstein, D. Manganese Catalyzed Hydrogenation of Organic Carbonates to Methanol and Alcohols. *Angew. Chem. Int. Ed.* **2018**, *57*, 12076–12080. https://doi.org/10.1002/ange.201806289.

(57) Alberti, C.; Fedorenko, E.; Enthaler, S. Hydrogenative Depolymerization of End-of-Life Polycarbonates by an Iron Pincer Complex. *ChemistryOpen* **2020**, *9*, 818–821. https://doi.org/10.1002/open.202000161.

(58) Beharaj, A.; Ekladious, I.; Grinstaff, M. W. Poly(Alkyl Glycidate Carbonate)s as Degradable Pressure-Sensitive Adhesives. *Angew. Chem. Int. Ed.* **2019**, *58*, 1–6. https://doi.org/10.1002/ange.201811894.

(59) Alberti, C.; Rijono, D.; Wehrmeister, M.; Cheung, E.; Enthaler, S. Depolymerization of Poly(1,2-Propylene Carbonate) via Ring Closing Depolymerization and Methanolysis. *ChemistrySelect* **2022**, *7*, e202104004. https://doi.org/10.1002/slct.202104004.

(60) Zhang, H.; Grinstaff, M. W. Synthesis of Atactic and Isotactic Poly(1,2-Glycerol Carbonate)s: Degradable Polymers for Biomedical and Pharmaceutical Applications. *J. Am. Chem. Soc.* **2013**, *135*, 6806–6809. https://doi.org/10.1021/ja402558m.

(61) Zhang, H.; Lin, X.; Chin, S.; Grinstaff, M. W. Synthesis and Characterization of Poly(Glyceric Acid Carbonate): A Degradable Analogue of Poly(Acrylic Acid). *J. Am. Chem. Soc.* **2015**, *137*, 12660–12666. https://doi.org/10.1021/jacs.5b07911.

(62) Geschwind, J.; Frey, H. Poly(1,2-Glycerol Carbonate): A Fundamental Polymer Structure Synthesized from CO_2 and Glycidyl Ethers. *Macromolecules* **2013**, *46*, 3280–3287. https://doi.org/10.1021/ma400090m.

(63) Tsai, F. te; Wang, Y.; Darensbourg, D. J. Environmentally Benign CO_2-Based Copolymers: Degradable Polycarbonates Derived from Dihydroxybutyric Acid and Their Platinum-Polymer Conjugates. *J. Am. Chem. Soc.* **2016**, *138*, 4626–4633. https://doi.org/10.1021/jacs.6b01327.

(64) Abdel Baki, Z.; Dib, H.; Sahin, T. Overview: Polycarbonates via Ring-Opening Polymerization, Differences between Six- and Five-Membered Cyclic Carbonates: Inspiration for Green Alternatives. *Polymers* **2022**, *14*, 2031. https://doi.org/10.3390/polym14102031.

(65) Alves, M.; Grignard, B.; Mereau, R.; Jerome, C.; Tassaing, T.; Detrembleur, C. Organocatalyzed Coupling of Carbon Dioxide with Epoxides for the Synthesis of Cyclic Carbonates: Catalyst Design and Mechanistic Studies. *Catal. Sci. Technol.* **2017**, *7*, 2651–2684. https://doi.org/10.1039/c7cy00438a.

(66) Pescarmona, P. P.; Taherimehr, M. Challenges in the Catalytic Synthesis of Cyclic and Polymeric Carbonates from Epoxides and CO_2. *Catal. Sci. Technol.* **2012**, *2*, 2169–2187. https://doi.org/10.1039/c2cy20365k.

(67) Cokoja, M.; Wilhelm, M. E.; Anthofer, M. H.; Herrmann, W. A.; Kühn, F. E. Synthesis of Cyclic Carbonates from Epoxides and Carbon Dioxide by Using Organocatalysts. *ChemSusChem* **2015**, *8*, 2436–2454. https://doi.org/10.1002/cssc.201500161.

(68) Guo, L.; Lamb, K. J.; North, M. Recent Developments in Organocatalysed Transformations of Epoxides and Carbon Dioxide into Cyclic Carbonates. *Green Chem.* **2021**, *23*, 77–118. https://doi.org/10.1039/d0gc03465g.

(69) Tezuka, K.; Komatsu, K.; Haba, O. The Anionic Ring-Opening Polymerization of Five-Membered Cyclic Carbonates Fused to the Cyclohexane Ring. *Polym. J.* **2013**, *45*, 1183–1187. https://doi.org/10.1038/pj.2013.50.

(70) Guerin, W.; Diallo, A. K.; Kirilov, E.; Helou, M.; Slawinski, M.; Brusson, J. M.; Carpentier, J. F.; Guillaume, S. M. Enantiopure Isotactic PCHC Synthesized by Ring-Opening Polymerization of Cyclohexene Carbonate. *Macromolecules* **2014**, *47*, 4230–4235. https://doi.org/10.1021/ma5009397.

(71) Carothers, W. H.; Natta, F. J. van. Studies on Polymerization and Ring Formation. Glycol Esters of Carbonic Acid. *J. Am. Chem. Soc.* **1930**, *52*, 314–326. https://doi.org/10.1021/ja01364a045.

(72) Abdel Baki, Z.; Dib, H.; Sahin, T. Overview: Polycarbonates via Ring-Opening Polymerization, Differences between Six- and Five-Membered Cyclic Carbonates: Inspiration for Green Alternatives. *Polymers* **2022**, *14*, 2031. https://doi.org/10.3390/polym14102031.

(73) Cardillo, G.; Orena, M.; Porzi, G.; Sandri, S. A New Regio- and Stereo-Selective Functionalization of Allylic and Homoallylic Alcohols. *J. Chem. Soc. Chem. Commun.* **1981**, 465–466. https://doi.org/10.1039/C39810000465.

(74) Honda, M.; Tamura, M.; Nakao, K.; Suzuki, K.; Nakagawa, Y.; Tomishige, K. Direct Cyclic Carbonate Synthesis from CO_2 and Diol over Carboxylation/Hydration Cascade Catalyst of CeO_2 with 2-Cyanopyridine. *ACS Catal.* **2014**, *4*, 1893–1896. https://doi.org/10.1021/cs500301d.

(75) McGuire, T. M.; López-Vidal, E. M.; Gregory, G. L.; Buchard, A. Synthesis of 5- to 8-Membered Cyclic Carbonates from Diols and CO_2: A One-Step, Atmospheric Pressure and Ambient Temperature Procedure. *J. CO2 Util.* **2018**, *27*, 283–288. https://doi.org/10.1016/j.jcou.2018.08.009.

(76) Bobbink, F. D.; Gruszka, W.; Hulla, M.; Das, S.; Dyson, P. J. Synthesis of Cyclic Carbonates from Diols and CO_2 Catalyzed by Carbenes. *Chem. Commun.* **2016**, *52*, 10787–10790. https://doi.org/10.1039/c6cc05730f.

(77) Brege, A.; Méreau, R.; McGehee, K.; Grignard, B.; Detrembleur, C.; Jerome, C.; Tassaing, T. The Coupling of CO_2 with Diols Promoted by Organic Dual Systems: Towards Products Divergence via Benchmarking of the Performance Metrics. *J. CO2 Util.* **2020**, *38*, 88–98. https://doi.org/10.1016/j.jcou.2020.01.003.

(78) Hedrick, J. L.; Piunova, V.; Park, N. H.; Erdmann, T.; Arrechea, P. L. Simple and Efficient Synthesis of Functionalized Cyclic Carbonate Monomers Using Carbon Dioxide. *ACS Macro Lett.* **2022**, *11*, 368–375. https://doi.org/10.1021/acsmacrolett.2c00060.

(79) Gregory, G. L.; Jenisch, L. M.; Charles, B.; Kociok-Köhn, G.; Buchard, A. Polymers from Sugars and CO_2: Synthesis and Polymerization of a d-Mannose-Based Cyclic Carbonate. *Macromolecules* **2016**, *49*, 7165–7169. https://doi.org/10.1021/acs.macromol.6b01492.

(80) Rintjema, J.; Guo, W.; Martin, E.; Escudero-Adán, E. C.; Kleij, A. W. Highly Chemoselective Catalytic Coupling of Substituted Oxetanes and Carbon Dioxide. *Chem. Eur. J.* **2015**, *21*, 10754–10762. https://doi.org/10.1002/chem.201501576.

(81) Huang, J.; Jehanno, C.; Worch, J. C.; Ruipérez, F.; Sardon, H.; Dove, A. P.; Coulembier, O. Selective Organocatalytic Preparation of Trimethylene Carbonate from Oxetane and Carbon Dioxide. *ACS Catal.* **2020**, *10*, 5399–5404. https://doi.org/10.1021/acscatal.0c00689.

(82) Darensbourg, D. J.; Horn, A.; Moncada, A. I. A Facile Catalytic Synthesis of Trimethylene Carbonate from Trimethylene Oxide and Carbon Dioxide. *Green Chem.* **2010**, *12*, 1376–1379. https://doi.org/10.1039/c0gc00136h.

(83) Fujiwara, M.; Baba, A.; Matsuda, H. The Cycloaddition of Heterocumulenes to Oxetanes in the Presence of Catalytic Amounts of Tetraphenylstibonium Iodide. *J. Heterocycl. Chem.* **1989**, *26*, 1659–1663. https://doi.org/https://doi.org/10.1002/jhet.5570260628.

(84) Darensbourg, D. J.; Moncada, A. I. Tuning the Selectivity of the Oxetane and CO_2 Coupling Process Catalyzed by (Salen)CrCl/ n-Bu4NX: Cyclic Carbonate Formation vs Aliphatic Polycarbonate Production. *Macromolecules* **2010**, *43*, 5996–6003. https://doi.org/10.1021/ma100896x.

(85) Zhang, C. J.; Wu, S. Q.; Boopathi, S.; Zhang, X. H.; Hong, X.; Gnanou, Y.; Feng, X. S. Versatility of Boron-Mediated Coupling Reaction of Oxetanes and Epoxides with CO_2: Selective Synthesis of Cyclic Carbonates or Linear Polycarbonates. *ACS Sustain. Chem. Eng.* **2020**, *8*, 13056–13063. https://doi.org/10.1021/acssuschemeng.0c04768.

(86) Tran, D. K.; Rashad, A. Z.; Darensbourg, D. J.; Wooley, K. L. Sustainable Synthesis of CO_2-Derived Polycarbonates from d-Xylose. *Polym. Chem.* **2021**, *12*, 5271–5278. https://doi.org/10.1039/d1py00784j.

(87) Huang, J.; de Winter, J.; Dove, A. P.; Coulembier, O. Metal-Free Synthesis of Poly(Trimethylene Carbonate) by Efficient Valorization of Carbon Dioxide. *Green Chem.* **2019**, *21*, 472–477. https://doi.org/10.1039/c8gc03607a.

(88) Darensbourg, D. J.; Moncada, A. I. (Salen)Co(II)/n-Bu 4NX Catalysts for the Coupling of CO_2 and Oxetane: Selectivity for Cyclic Carbonate Formation in the Production of Poly-(Trimethylene Carbonate). *Macromolecules* **2009**, *42*, 4063–4070. https://doi.org/10.1021/ma9002006.

(89) Darensbourg, D. J.; Moncada, A. I.; Choi, W.; Reibenspies, J. H. Mechanistic Studies of the Copolymerization Reaction of Oxetane and Carbon Dioxide to Provide Aliphatic Polycarbonates Catalyzed by (Salen)CrX Complexes. *J. Am. Chem. Soc.* **2008**, *130*, 6523–6533. https://doi.org/10.1021/ja800302c.

(90) Whiteoak, C. J.; Martin, E.; Belmonte, M. M.; Benet-Buchholz, J.; Kleij, A. W. An Efficient Iron Catalyst for the Synthesis of Five- and Six-Membered Organic Carbonates under Mild Conditions. *Adv. Synth. Catal.* **2012**, *354*, 469–476. https://doi.org/10.1002/adsc.201100752.

(91) Whiteoak, C. J.; Kielland, N.; Laserna, V.; Escudero-Adán, E. C.; Martin, E.; Kleij, A. W. A Powerful Aluminum Catalyst for the Synthesis of Highly Functional Organic Carbonates. *J. Am. Chem. Soc.* **2013**, *135*, 1228–1231. https://doi.org/10.1021/ja311053h.

(92) Darensbourg, D. J.; Moncada, A. I.; Wei, S. H. Aliphatic Polycarbonates Produced from the Coupling of Carbon Dioxide and Oxetanes and Their Depolymerization via Cyclic Carbonate Formation. *Macromolecules* **2011**, *44*, 2568–2576. https://doi.org/10.1021/ma2002323.

(93) Alves, M.; Grignard, B.; Boyaval, A.; Méreau, R.; de Winter, J.; Gerbaux, P.; Detrembleur, C.; Tassaing, T.; Jérôme, C. Organocatalytic Coupling of CO_2 with Oxetane. *ChemSusChem* **2017**, *10*, 1128–1138. https://doi.org/10.1002/cssc.201601185.

(94) Qiao, C.; Shi, W.; Brandolese, A.; Benet-Buchholz, J.; Escudero-Adán, E. C.; Kleij, A. W. A Novel Catalytic Route to Polymerizable Bicyclic Cyclic Carbonate Monomers from Carbon Dioxide. *Angew. Chem. Int. Ed.* **2022**, *31*, e202205053. https://doi.org/10.1002/anie.202205053.

(95) Zhang, W.; Dai, J.; Wu, Y. C.; Chen, J. X.; Shan, S. Y.; Cai, Z.; Zhu, J. B. Highly Reactive Cyclic Carbonates with a Fused Ring toward Functionalizable and Recyclable Polycarbonates. *ACS Macro Lett.* **2022**, *11*, 173–178. https://doi.org/10.1021/acsmacrolett.1c00653.

(96) Tan, E. W. P.; Hedrick, J. L.; Arrechea, P. L.; Erdmann, T.; Kiyek, V.; Lottier, S.; Yang, Y. Y.; Park, N. H. Overcoming Barriers in Polycarbonate Synthesis: A Streamlined Approach for the Synthesis of Cyclic Carbonate Monomers. *Macromolecules* **2021**, *54*, 1767–1774. https://doi.org/10.1021/acs.macromol.0c02880.

(97) Yang, J.; Hao, Q.; Liu, X.; Ba, C.; Cao, A. Novel Biodegradable Aliphatic Poly(Butylene Succinate-Co-Cyclic Carbonates)s with Functionalizable Carbonate Building Blocks. 1. Chemical Synthesis and Their Structural and Physical Characterization. *Biomacromolecules* **2004**, *5*, 209–218. https://doi.org/10.1021/bm0343242.

(98) Huang, J.; Olsén, P.; Svensson Grape, E.; Inge, A. K.; Odelius, K. Simple Approach to Macrocyclic Carbonates with Fast Polymerization Rates and Their Polymer-to-Monomer Regeneration. *Macromolecules* **2022**, *55*, 608–614. https://doi.org/10.1021/acs.macromol.1c02225.

(99) Liu, Y.; Wang, M.; Ren, W. M.; Xu, Y. C.; Lu, X. B. Crystalline Hetero-Stereocomplexed Polycarbonates Produced from Amorphous Opposite Enantiomers Having Different Chemical Structures. *Angew. Chem. Int. Ed.* **2015**, *54*, 7042–7046. https://doi.org/10.1002/anie.201501417.

(100) Nozaki, K.; Nakano, K.; Hiyama, T. Optically Active Polycarbonates: Asymmetric Alternating Copolymerization of Cyclohexene Oxide and Carbon Dioxide. *J. Am. Chem. Soc.* **1999**, *121*, 11008–11009. https://doi.org/10.1021/ja992433b.

(101) Hua, Y. Z.; Lu, L. J.; Huang, P. J.; Wei, D. H.; Tang, M. S.; Wang, M. C.; Chang, J. B. Highly Enantioselective Catalytic System for Asymmetric Copolymerization of Carbon Dioxide and Cyclohexene Oxide. *Chem. Eur. J.* **2014**, *20*, 12394–12398. https://doi.org/10.1002/chem.201403088.

(102) Tamura, M.; Ito, K.; Honda, M.; Nakagawa, Y.; Sugimoto, H.; Tomishige, K. Direct Copolymerization of CO_2 and Diols. *Sci. Rep.* **2016**, *6*, 1–9. https://doi.org/10.1038/srep24038.

(103) Gu, Y.; Matsuda, K.; Nakayama, A.; Tamura, M.; Nakagawa, Y.; Tomishige, K. Direct Synthesis of Alternating Polycarbonates from CO_2 and Diols by Using a Catalyst System of CeO_2 and 2-Furonitrile. *ACS Sustain. Chem. Eng.* **2019**, *7*, 6304–6315. https://doi.org/10.1021/acssuschemeng.8b06870.

(104) Gong, Z. J.; Li, Y. R.; Wu, H. L.; Lin, S. D.; Yu, W. Y. Direct Copolymerization of Carbon Dioxide and 1,4-Butanediol Enhanced by Ceria Nanorod Catalyst. *Appl. Catal. B* **2020**, *265*, 118524–118536. https://doi.org/10.1016/j.apcatb.2019.118524.

(105) Gu, Y.; Tamura, M.; Nakagawa, Y.; Nakao, K.; Suzuki, K.; Tomishige, K. Direct Synthesis of Polycarbonate Diols from Atmospheric Flow CO_2 and Diols without Using Dehydrating Agents. *Green Chem.* **2021**, *23*, 5786–5796. https://doi.org/10.1039/d1gc01172c.

(106) Fukuoka, S.; Kawamura, M.; Komiya, K.; Tojo, M.; Hachiya, H.; Hasegawa, K.; Aminaka, M.; Okamoto, H.; Fukawa, I.; Konno, S. A Novel Non-Phosgene Polycarbonate Production Process Using by-Product CO_2 as Starting Material. *Green Chem.* **2003**, *5*, 497–507. https://doi.org/10.1039/B304963A.

(107) Fukuoka, S.; Fukawa, I.; Adachi, T.; Fujita, H.; Sugiyama, N.; Sawa, T. Industrialization and Expansion of Green Sustainable Chemical Process: A Review of Non-Phosgene Polycarbonate from CO_2. *Org. Process Res. Dev.* **2019**, *23*, 145–169. https://doi.org/10.1021/acs.oprd.8b00391.

(108) Gennen, S.; Grignard, B.; Tassaing, T.; Jérôme, C.; Detrembleur, C. CO_2 -Sourced α-Alkylidene Cyclic Carbonates: A Step Forward in the Quest for Functional Regioregular Poly(Urethane)s and Poly(Carbonate)s. *Angew. Chem. Int. Ed.* **2017**, *56*, 10394–10398. https://doi.org/10.1002/anie.201704467.

(109) Ouhib, F.; Meabe, L.; Mahmoud, A.; Eshraghi, N.; Grignard, B.; Thomassin, J.-M.; Aqil, A.; Boschini, F.; Jérôme, C.; Mecerreyes, D.; Detrembleur, C. CO_2 -Sourced Polycarbonates as Solid Electrolytes for Room Temperature Operating Lithium Batteries. *J. Mater. Chem. A* **2019**, *7*, 9844–9853. https://doi.org/10.1039/C9TA01564G.

(110) Ouhib, F.; Grignard, B.; van den Broeck, E.; Luxen, A.; Robeyns, K.; van Speybroeck, V.; Jerome, C.; Detrembleur, C. A Switchable Domino Process for the Construction of Novel CO_2 -Sourced Sulfur-Containing Building Blocks and Polymers. *Angew. Chem. Int. Ed.* **2019**, *58*, 11768–11773. https://doi.org/10.1002/anie.201905969.

(111) Ouhib, F.; Meabe, L.; Mahmoud, A.; Grignard, B.; Thomassin, J.-M.; Boschini, F.; Zhu, H.; Forsyth, M.; Mecerreyes, D.; Detrembleur, C. Influence of the Cyclic versus Linear Carbonate Segments in the Properties and Performance of CO_2 -Sourced Polymer Electrolytes for Lithium Batteries. *ACS Appl. Polym. Mater.* **2020**, *2*, 922–931. https://doi.org/10.1021/acsapm.9b01130.

(112) Dabral, S.; Licht, U.; Rudolf, P.; Bollmann, G.; Hashmi, A. S. K.; Schaub, T. Synthesis and Polymerisation of α-Alkylidene Cyclic Carbonates from Carbon Dioxide, Epoxides and the Primary Propargylic Alcohol 1,4-Butynediol. *Green Chem.* **2020**, *22*, 1553–1558. https://doi.org/10.1039/c9gc04320a.

(113) Hata, S.; Goto, H.; Yamada, E.; Oku, A. Chemical Conversion of Poly(Carbonate) to 1,3-Dimethyl-2-Imidazolidinone (DMI) and Bisphenol A: A Practical Approach to the Chemical Recycling of Plastic Wastes. *Polymer* **2002**, *43*, 2109–2116. https://doi.org/10.1016/S0032-3861(01)00800-X.

(114) Jehanno, C.; Demarteau, J.; Mantione, D.; Arno, M. C.; Ruipérez, F.; Hedrick, J. L.; Dove, A. P.; Sardon, H. Synthesis of Functionalized Cyclic Carbonates through Commodity Polymer Upcycling. *ACS Macro Lett.* **2020**, *9*, 443–447. https://doi.org/10.1021/acsmacrolett.0c00164.

(115) Iannone, F.; Casiello, M.; Monopoli, A.; Cotugno, P.; Sportelli, M. C.; Picca, R. A.; Cioffi, N.; Dell'Anna, M. M.; Nacci, A. Ionic Liquids/ZnO Nanoparticles as Recyclable Catalyst for Polycarbonate Depolymerization. *J. Mol. Catal. A Chem.* **2017**, *426*, 107–116. https://doi.org/10.1016/j.molcata.2016.11.006.

(116) Wu, C. H.; Chen, L. Y.; Jeng, R. J.; Dai, S. A. 100% Atom-Economy Efficiency of Recycling Polycarbonate into Versatile Intermediates. *ACS Sustain. Chem. Eng.* **2018**, *6*, 8964–8975. https://doi.org/10.1021/acssuschemeng.8b01326.

(117) Wang, Z.; Yang, R.; Xu, G.; Liu, T.; Wang, Q. Chemical Upcycling of Poly(Bisphenol A Carbonate) Plastic Catalyzed by ZnX2 via an Amino-Alcoholysis Strategy. *ACS Sustain. Chem. Eng.* **2022**, *10*, 4529–4537. https://doi.org/10.1021/acssuschemeng.1c08408.

(118) Singh, S.; Lei, Y.; Schober, A. Direct Extraction of Carbonyl from Waste Polycarbonate with Amines under Environmentally Friendly Conditions: Scope of Waste Polycarbonate as a Carbonylating Agent in Organic Synthesis. *RSC Adv.* **2015**, *5*, 3454–3460. https://doi.org/10.1039/c4ra14319a.

(119) Liu, Y.; Lu, X. B. Chemical Recycling to Monomers: Industrial Bisphenol-A-Polycarbonates to Novel Aliphatic Polycarbonate Materials. *J. Polym. Sci.* **2022**, 1–13. https://doi.org/10.1002/pol.20220118.

(120) Quaranta, E.; Sgherza, D.; Tartaro, G. Depolymerization of Poly(Bisphenol A Carbonate) under Mild Conditions by Solvent-Free Alcoholysis Catalyzed by 1,8-Diazabicyclo[5.4.0]Undec-7-Ene as a Recyclable Organocatalyst: A Route to Chemical Recycling of Waste Polycarbonate. *Green Chem.* **2017**, *19*, 5422–5434. https://doi.org/10.1039/c7gc02063e.

(121) Do, T.; Baral, E. R.; Kim, J. G. Chemical Recycling of Poly(Bisphenol A Carbonate): 1,5,7-Triazabicyclo[4.4.0]-Dec-5-Ene Catalyzed Alcoholysis for Highly Efficient Bisphenol A and Organic Carbonate Recovery. *Polymer* **2018**, *143*, 106–114. https://doi.org/10.1016/j.polymer.2018.04.015.

(122) Quaranta, E.; Minischetti, C. C.; Tartaro, G. Chemical Recycling of Poly(Bisphenol A Carbonate) by Glycolysis under 1,8-Diazabicyclo[5.4.0]Undec-7-Ene Catalysis. *ACS Omega* **2018**, *3*, 7261–7268. https://doi.org/10.1021/acsomega.8b01123.

(123) Kim, J. G. Chemical Recycling of Poly(Bisphenol A Carbonate). *Polym. Chem.* **2020**, *11*, 4830–4849. https://doi.org/10.1039/c9py01927h.

Aim of the thesis

Polycarbonates (PCs) and polyurethanes (PUs) are major classes of polymers synthetized on multi-tons scales and broadly used nowadays due to their easily customizable properties. The use of toxic and hazardous phosgene and/or isocyanates to produce PCs and PUs is however a major issue and motivated the search for greener and safer alternatives. Merging carbon dioxide (CO_2) as a sustainable, non-toxic, cheap and broadly available C1-feedstock with bio-based nucleophiles (alcohols or amines) to produce polymers provided a substantial incentive to produce materials with lower environmental impact. Several synthetic routes have indeed been explored for the synthesis of PCs and PUs by employing CO_2 directly as comonomer or as a carbon source to produce polymerizable building-blocks.

Recently, our research group was the first to report the utilization of CO_2-sourced bis (exovinylene cyclic carbonate)s (bisαCCs) for the preparation of novel regioregular non-phosgene-based polycarbonates (PCs) and non-isocyanate-based polyurethanes (NIPUs) by step-growth copolymerization with diols (for PCs) or diamines (for NIPUs). Thanks to the presence of the exocyclic C=C double bond, the ring-opening by the nucleophile was facile at 25 °C in the absence (with diamines) or presence (with diols) of DBU as an organocatalyst. With diols, poly(*oxo*-carbonate)s were produced. With primary diamines, poly(hydroxy-oxazolidinone)s were obtained, whereas poly(*oxo*-urethane)s were formed with secondary diamines. Although the proof of concept was published by our group prior to my PhD thesis, only limited examples were published and the pros/cons of this technology were still to be investigated.

In the frame of the EOS project, the aim of my thesis was to implement the synthesis of novel sustainable poly(*oxo*-carbonate)s and poly(hydroxy-oxazolidinone)s by the step-growth copolymerization of bisαCCs with a variety of bio-based diamines and diols derived, mainly derived from lignin and sugars. Thanks to the highly oxygenated polymeric network of lignin, its chemical depolymerization yields interesting diols and diamines that could be utilized as comonomers in our processes. A large scope of substrates and reaction conditions will be investigated in order to design polymers of diversified structures and properties. An additional goal of my research is to explore various end-of-life options for the new CO_2-based polymers, mainly by chemical degradation into attractive building blocks.

In the first chapter we summarized the advent of recyclable CO_2-sourced polycarbonates. After a brief description on the main methods to produce these polymers, a special attention was paid to the end-of-use perspectives for their recyclability or biodegradability, with the aim to highlight where more research is needed.

In Chapter II, we investigate the scope of the organocatalyzed step-growth copolymerization of bisαCCs with bio-based diols into poly(*oxo*-carbonate)s. Model reactions are first carried out on small molecules in order to understand the structural influence of the alcohols and the polymerization temperature on the rate of the cyclic carbonate ring-opening and the product selectivity. Based on these studies, a series of regio-regular poly(*oxo*-carbonate)s could be prepared from sugar- or lignin- derived diols at 25 °C. Finally, the effect of the microstructures of the poly(*oxo*-carbonate)s on their thermal properties is evaluated.

In Chapter III, the chemical degradation of some of these regioregular poly(*oxo*-carbonate)s is investigated. As the ketone are electrophilic than the carboxyl group of the carbonate linkages, we hypothesize that the ketones might facilitate energy efficient polymer aminolysis at room temperature under catalyst-free conditions. This facile deconstruction method permits to recycle the bio-mass derived diols and to produce *N*-substituted bis(oxazolidinone)s that might be repurposed into recyclable polymers.

In Chapter IV, we report the edition of new step-growth polymers (poly(carbonate-urea)s or poly(carbonate-amide)s) from waste CO_2 and upcycled commodity plastics. We demonstrate that the unprotected in-chain urea or secondary amide functionalities of the polymers can trigger their degradation via cascade ring-closing events upon a thermal switch in the presence of an organic base as the catalyst. Ultimately, we explore the selective depolymerization of these polymers from plastic mixtures composed of commodity polyethylene terephthalate or polycaprolactone. The goal is to offer new options for recycling plastics waste mixtures while delivering high value-added chemicals.

In Chapter V, we describe the synthesis and the characterization of novel poly(oxazolidinone)s by step-growth polymerization of CO_2-sourced bisαCCs with various primary diamines. With the objective to study the influence of the reaction conditions on the structure and macromolecular parameters of the polymers and to optimize the reaction conditions, model reactions on small molecules are first performed. Then, a variety of CO_2- and lignin-derived poly(hydroxy-oxazolidinone)s is synthesized and fully characterized. We also consider the dehydration of the poly(hydroxy-oxazolidinone)s as a tool to produce a novel class of poly(oxazolidinone)s with exocyclic vinylene functionality, i.e. poly(alkylidene oxazolidinone)s.

Chapter II

Access to bio-renewable and CO_2-based polycarbonates from exovinylene cyclic carbonates

Fabiana Siragusa, Elias Van Den Broeck, Connie Ocando, Alejandro J. Müller, Gilles De Smet, Bert U.W. Maes, Julien De Winter, Veronique Van Speybroeck, Bruno Grignard,* Christophe Detrembleur**

Reference: *ACS Sustainable Chem. Eng. 2021, 9, 4, 1714–1728.*

https://doi.org/10.1021/acssuschemeng.0c07683

Author contributions: F.S., C.D. and B.G. designed and planned the project. F.S. synthesized and characterized all polymers and carried out all the model reactions. E.V.B. and V.V.S. carried out DFT modelling. C.O. ad A.M. characterized the polymers by Flash DSC and XRD analyses. G.D.S. and B.M characterized the model compounds by HRMS. J.D.W. carried out MALDI mass analysis. F.S. wrote the manuscript with contributions from all co-authors.

ABSTRACT

We investigate the scope of the organocatalyzed step-growth copolymerization of CO_2-sourced exovinylene bicyclic carbonates with bio-based diols into polycarbonates. Series of regio-regular poly(*oxo*-carbonate)s were prepared from sugar- (1,4-butanediol, isosorbide) or lignin-derived (1,4-benzenedimethanol, 1,4-cyclohexanediol) diols at 25 °C with 1,8-diazabicyclo[5.4.0]undec-7-ene (DBU) as catalyst, and their defect-free structure was confirmed by NMR studies. Their DSC and WAXS showed that most of them were able to crystallize. When the polymerizations were carried out at 80 °C, some structural defects were introduced within the polycarbonate chains, which limited the polymer molar mass. Model reactions were carried out to understand the influence of the structure of the alcohols, the temperature (25 or 80 °C) and the use of DBU on the rate of the alcoholysis of the cyclic carbonate and on the products/linkages selectivity. A full mechanistic understanding was given by means of static and dynamic based DFT calculations showing the determining role of DBU on the stability of the intermediates and its important role in the rate-determining steps is revealed. Furthermore, the origin of the side reactions observed at 80 °C was discussed and rationalized by DFT modelling. As an impressive diversity of bio-based diols is accessible at large scale and low cost, this process of valorization of carbon dioxide opens new perspectives in the sustainable production of bioplastics under mild conditions.

Introduction

Polycarbonates (PCs) are widely used in the automotive industry and in the electric/electronic or the construction sectors. Their unique features derived from their excellent physical properties such as high thermal stability and impact resistance combined with their excellent transparency make them suitable for organic glasses, optical fibers, resistant packaging, etc.[1,2] PCs are industrially manufactured by phosgenation of diols. The corrosive and highly toxic phosgene combined with the quest for polymers with reduced carbon footprint pushed the scientific community and the industries to engineer novel synthetic pathways for this important polymer family.[3,4] Amongst the numerous processes currently investigated for producing PCs, merging carbon dioxide (CO_2) as a safe and renewable substitute to phosgene with bio-based diols appeared as a promising and appealing approach for greener PCs.[5–7] Indeed, the recent developments in biorefineries (e.g. lignin fractionations and sugar fermentation techniques) have contributed to diversify the range of bio-based alcohols and polyols that can be exploited for the production of more sustainable materials.[8,9] Although the direct copolymerization of (bio-based) diols with CO_2 is highly attractive for the preparation of PCs by an alternative phosgene-free route, this process currently remains very challenging due to the difficult removal of water during the polycondensation (Scheme 1a). The rare examples showed that only low molar mass PCs (M_n < 5,000 g/mol) were collected by using a high loading of metal oxides[10] or organocatalyst/desiccant dual systems at high temperatures, with a limited substrate scope.[6] Another attractive approach to merge CO_2 and diols for the production of a larger range of PCs consists in the melt polycondensation of acyclic dialkyl- (e.g. dimethyl carbonate) or diaryl-carbonates (e.g. diphenyl carbonate) with diols. The dialkyl-/diaryl-carbonates were prepared by the dehydrative coupling of CO_2 with the corresponding alcohols (Scheme 1b). The polycondensation is often carried out in a multistage process involving the fabrication of oligomers at moderate temperature (T = 80 - 120 °C) followed by applying a high vacuum at higher temperature (T > 200 °C) to remove the volatile by-products (methanol or phenol) pushing the reaction towards the formation of polymers of higher molar mass.[11–14] Recently, our group pioneered the exploitation of a novel family of CO_2-based monomers (bis(α-alkylidene carbonate)s, bisαCCs) for the facile construction of PCs by the organocatalyzed step-growth copolymerization with diols under mild reaction conditions (Scheme 1c).[15,16] The presence of an exovinylene group on the 5-membered cyclic carbonate moiety significantly enhanced its reactivity with alcohols and controlled the regio-selective ring-opening producing regio-regular functional PCs (poly(*oxo*-carbonate)s) at room temperature up to reasonable molar masses (M_n = 17,000 g/mol). These novel monomers were produced by the zinc iodide catalyzed carboxylative coupling of CO_2 to bis(propargylic alcohol)s. BisαCCs were also able to copolymerize with amines to produce new polyurethanes[15,17,18] or

with thiols to provide novel sulfur-containing polymers, i.e. polythiocarbonates and poly(cyclic carbonate-*co*-thioether)s.[19] Although this family of CO_2-sourced monomers was highlighted by BASF[20] as promising building blocks for the preparation of CO_2-based polymers, their utilization for PC synthesis is still in its infancy. In 2019, we exploited bisαCCs for chain extending poly(ethylene glycol) (PEG) diols and producing poly(carbonate-*co*-ether)s that found promising application as solid electrolytes in Li-ion batteries.[16] The same concept adapted to a mixture of PEG diol and a dithiol enabled to produce new poly(carbonate-*co*-(thio)ether)s containing both linear and cyclic carbonate linkages within the polymer backbone, that demonstrated some utility for battery applications.[21] Very recently, Schaub et al. designed new bisαCCs from 1,4-butynediol, epoxides and CO_2, and successfully tailored low molar mass poly(β-*oxo*-carbonates) by polyaddition with 1,4-butanediol (Scheme 1d).[22] *In-situ* formed bis(αCC)s could also be polymerized by an organocatalyzed cascade reaction between a bispropargylic alcohol, CO_2 and a diol. However, only low molar mass polymers (M_n < 3,000 g/mol) were collected due to the occurrence of side-reactions.[23] Hitherto, only linear aliphatic primary diols (i.e. 1,4-butanediol or PEG diol) were copolymerized with pre-formed bisαCCs until reasonable molar masses whereas the reactivity of bisαCCs towards biorenewable alcohols of different chemical structures remains unknown. Understanding the copolymerization features while identifying the limitations of the bisαCCs chemistry are key features to enlarge the scope of PCs that could be produced by this appealing process.

In this work, we demonstrate that combining bisαCCs with various bio-based diols derived from sugar[24–26] or lignin[8,9] diversifies the range of regio-regular PCs that can be produced (Scheme 1c). We investigate the influence of the alcohol structure (i.e. (cyclo)aliphatic or aromatic) and the temperature on the polymerization features, the PC microstructure and molar mass, and on their thermal properties. Kinetic studies carried out on model compounds combined with modeling also enable us to understand the formation of some unexpected linkages in the polymer chain. This study demonstrates that a large scope of functional CO_2 and bio-sourced polymers with a high bio-renewable content can be easily produced by this new process, potentially enlarging the application range of PCs.

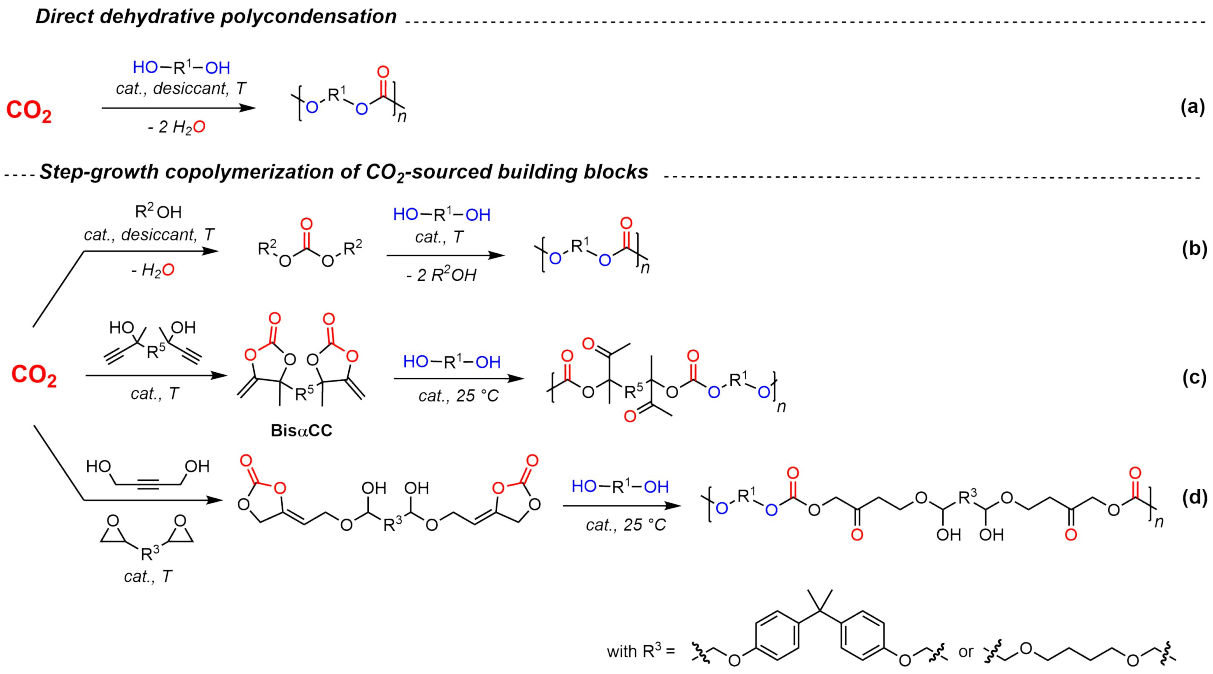

Scheme 1: Synthesis of polycarbonates by copolymerization of diols with CO_2 or CO_2-sourced building blocks: (a) direct dehydrative polycondensation of diols with CO_2; (b) melt polycondensation of acyclic carbonates, prepared by the dehydrative coupling of CO_2 with alcohols, with diols; (c) organocatalyzed step-growth copolymerization of CO_2-sourced exovinylene bicyclic carbonates with bio-based diols; (d) step-growth copolymerization of bisαCCs, obtained from epoxides, CO_2 and 1,4-butynediol.

Results and discussion

Prior considering the polymerizations, we first carried out a series of reactions on model compounds. The objective of these studies was to probe the reactivity of the α-alkylidene cyclic carbonate group with alcohols of various structures that mimic bio-based alcohols that will be used later in polymerization (Scheme 2). The main goal was to identify the optimal conditions for high yields and selectivity, and to investigate the influence of the temperature on the process. Although the temperature was expected to accelerate the reactions, it might also promote some side reactions that have to be identified as they might have an impact on the polymer microstructure and molar masses. These model reactions are therefore of prime importance for understanding the polymerization processes that will then be studied.

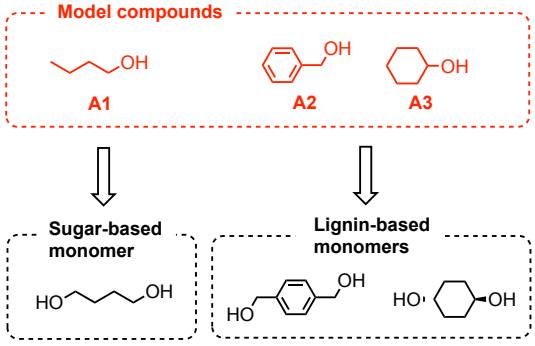

Scheme 2: Model compounds that mimic the structure of sugar- and lignin-based monomers.

Alcoholysis of exovinylene cyclic carbonate via model reactions

4,4-Dimethyl-5-methylene-1,3-dioxolan-2-one (**αCC**, Figure 1a) was selected as the model cyclic carbonate and was synthetized by the quantitative carboxylative coupling of CO_2 to 2-methyl-3-butyn-2-ol catalyzed by tetrabutyl ammonium phenolate.[27] Three alcohols, 1-butanol (**A1**), cyclohexanol (**A2**) and benzylalcohol (**A3**) were selected based on their structural similarities with sugar or lignin-based diols (Scheme 2) that will be involved later in the polymerizations. Butanol was also used as a benchmark for the sake of comparison with the two other alcohols.

The reactions were first realized at 25 °C under stoichiometric conditions using dry DMSO as solvent. These stoichiometric conditions between **αCC** and the alcohol were selected to fit the conditions required for a step-growth polymerization that will be implemented later. As expected, no alcoholysis of **αCC** was observed even after 24 h for all alcohols in the absence of catalyst. The addition of 1,5-diazabicyclo(5.4.0)undec-7-ene (DBU) (5 mol% compared to **αCC**) was then considered as it was previously shown to catalyze the ring-opening of α-alkylidene cyclic carbonates with primary aliphatic alcohols.[15] Under these conditions, the *oxo*-carbonate adducts were selectively and quantitatively formed (> 99% yield) after 24 h of reaction (Figure 1a). The rates of the ring-opening by the different alcohols were determined by ^{1}H-NMR analysis (Figure S1-S3) and the results are presented in Figure 1b. Primary alcohols butanol **A1** and benzyl alcohol **A3** displayed similar reactivities with an **αCC** conversion of 78% and 69% in 2 h, respectively (Figure 1). The secondary alcohol **A2** presented a lower reactivity with a αCC conversion of 15% after 2 h. The lower reactivity of cyclohexanol was assigned to the steric hindrance around the alcohol group.

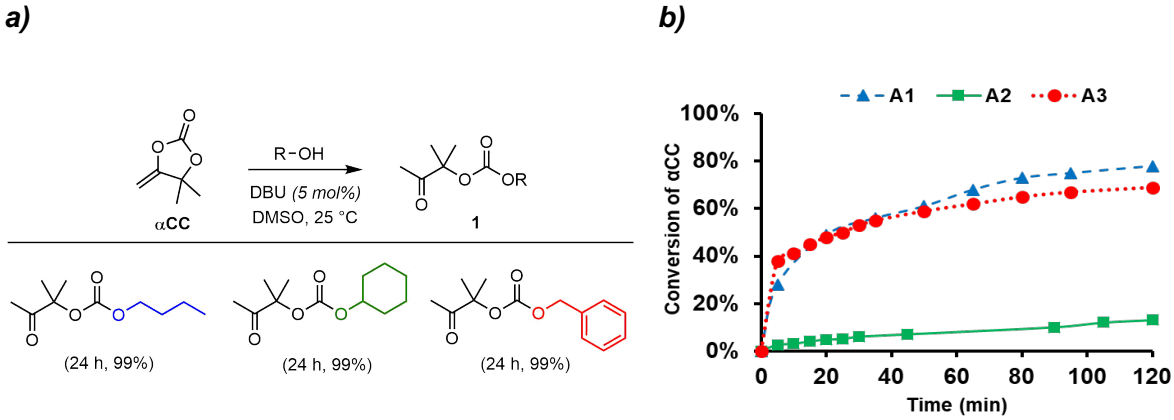

Figure 1. DBU-catalyzed alcoholysis of **αCC** with 1-butanol **A1**, cyclohexanol **A2** or benzyl alcohol **A3** at 25 °C. a) reaction scheme and products yields after 24 h; b) conversion of **αCC** *vs* time. Conditions: αCC (4 mmol), alcohol (4 mmol), DBU (0.2 mmol) in dry DMSO (1 mL) at 25 °C under nitrogen atmosphere.

We then considered the reactions at a higher temperature (80 °C) in order to accelerate the conversion of **αCC** (Table 1; Figure S4 - S6 in Supporting Information). With **A1** and **A3**, **αCC** was selectively and almost quantitatively (> 98%) converted into their corresponding *oxo*-carbonate **1** in a very short period of time, 15 min (Table 1, entries 1 and 9). The secondary alcohol **A2** still reacted slowly but faster compared to the same reaction carried out at 25 °C (**αCC** conversion of 59% in 15 min at 80 °C; Table 1, entry 5). When the reaction time was extended further when using **A2**, the corresponding *oxo*-carbonate **1** was selectively and quantitatively produced with no side product being identified even after 48 h at 80 °C. Importantly, despite the **αCC** ring-opening was complete with **A3** after 15 min at 80 °C, maintaining this temperature for a longer period of time (up to 48 h) was detrimental to the selectivity of the reaction. Indeed, trace amounts of tetrasubstituted ethylene carbonate **2**, dibenzyl carbonate **3** and hydroxyketone **4** were observed after 2 h. Moreover, the content of these side products increased substantially with the reaction time to reach 38% of **2**, 10% of **3** and 12% of **4** after 48 h. The yield in the *oxo*-carbonate **1** was thus decreased to 40% while it was 99% after 15 min of reaction with **A3**. No side product was noted for the reaction of **αCC** with **A1**, even after 48 h at 80 °C. Note that the NMR structural identification of the products **1**-**4** was confirmed by comparison of the GC-MS analysis of the crude reaction mixture (**A3** + **αCC** with DBU for 48 h at 80 °C) (Figure S7-S11) with those of their commercially available or isolated reference samples (Figure S12-S16).

These observations suggested that the side products observed for the reaction of **αCC** with **A3** were formed by rearrangement of the *oxo*-carbonate **1**. In order to give some clues to this hypothesis, this *oxo*-carbonate **1** was purified, isolated, solubilized in DMSO and added by DBU (5 mol%) in the presence or not of **A3** (0.5 eq. *vs* **1**). Table 2 shows the results. In the two cases, the *oxo*-carbonate **1** was converted into the tetrasubstituted ethylene carbonate **2** as the major product, and into dibenzyl carbonate **3** and hydroxyketone **4** as the minor ones. The conversion of **1** increased with the reaction time, with a faster reaction noted in the presence of benzyl alcohol **A3**. Therefore, these experiments demonstrate that the formation of products **2**, **3** and **4** originated from a rearrangement of **1**, and was accelerated by the addition of benzyl alcohol. The origin of these side products is of prime importance because these side reactions are expected to affect the polymer molar mass and microstructure. A deep mechanistic investigation has therefore been performed in the next section.

Table 1. Alcoholysis of exovinylene cyclic carbonate with 1-butanol **A1**, cyclohexanol **A2** and benzyl alcohol **A3** at 80 °C.

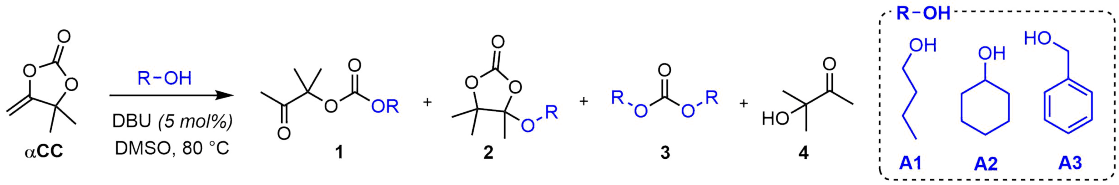

Entry	R-OH	Time	Conv. αCC [%]	Yield 1 [%][a]	Yield 2 [%][a]	Yield 3 [%][a]	Yield 4 [%][a]
1	A1	15 min	98	98	0	0	0
2		2 h	>99	>99	0	0	0
3		24 h	>99	>99	0	0	0
4		48 h	>99	>99	0	0	0
5	A2	15 min	59	59	0	0	0
6		2 h	89	89	0	0	0
7		24 h	>99	>99	0	0	0
8		48 h	>99	>99	0	0	0
9	A3	15 min	>99	>99	0	0	0
10		2 h	>99	94	3	2	1
11		24 h	>99	56	25	8	11
12		48 h	> 99	40	38	10	12

[a] Yield determined by ^{1}H-NMR spectroscopy on the crude product.
Conditions: αCC (4 mmol), alcohol (4 mmol), DBU (0.2 mmol) in dry DMSO (1 mL) at 80 °C under nitrogen atmosphere.

Table 2. Rearrangement of *oxo*-carbonate **1** (prepared from **αCC** and **A3**) at 80 °C in the presence or not of additional **A3**.

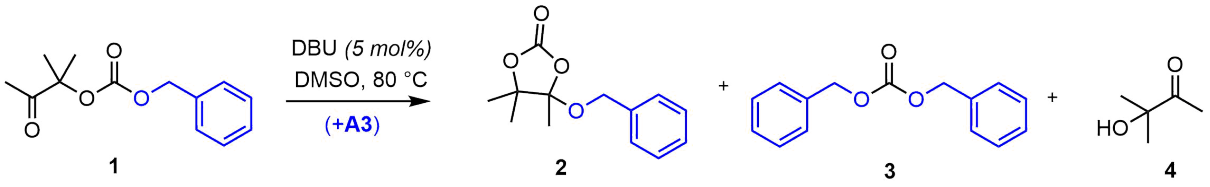

Entry	R-OH	Time	Conv.1 [%]	Yield 2 [%][a]	Yield 3 [%][a]	Yield 4 [%][a]
1	No	6h	21	62	19	19
2		24 h	42	58	19	23
3[b]	A3	6 h	70	72	16	12
4[b]		24 h	88	60	23	17

[a] Yield determined by ^{1}H-NMR spectroscopy on the crude product. [b] Reaction conducted in the presence of **A3** (0.5 eq. *vs* **1**). Conditions: *oxo*-carbonate 1 (4.06 mmol), DBU (0.203 mmol) in dry DMSO (1 mL) at 80 °C under nitrogen atmosphere.

Mechanistic insight into the alcoholysis of exovinylene cyclic carbonate

Tetrasubstituted ethylene carbonates were identified by Costa et al. when **αCC** was generated *in-situ* by the reaction of a propargylic alcohol with CO_2 in the presence of allyl alcohol or phenol catalyzed by superbases (7-Methyl-1,5,7-triazabicyclo[4.4.0]dec-5-ene (MTBD) or 1,5,7-Triazabicyclo[4.4.0]dec-5-ene (TBD)) at 100 °C.[28] These side products were also observed by He et al. for similar reactions when phenol or allyl alcohol was substituted by benzyl alcohol in the presence of a silver salt (Ag_2CO_3/PPh_3) catalyst.[29] Although it was suggested that they might be formed by tautomerization of *oxo*-carbonate **1** and/or the addition of the alcohol to the unsaturated double bond of **αCC**, the authors refrained to propose any reaction mechanism.

Our experimental results presented in Table 1 indicate that only benzyl alcohol (**A3**) is able to form some tetrasubstituted ethylene carbonate **2** while butanol (**A1**) and cyclohexanol (**A2**) only furnished the corresponding *oxo*-carbonates **1**, at least under the investigated conditions. In order to gain insight into the origin of this reaction and to understand the importance of the structure of the alcohol on the reaction selectivity, Density Functional Theory (DFT) based on static and molecular dynamics simulations were performed (see Supporting Information).

One may suggest that the formation of the tetrasubstituted ethylene carbonate **2** is following a similar reaction pathway than for the addition of thiols to **αCC**[19]: fast reversible formation of the *oxo*-carbonate **1** by the DBU-catalyzed ring opening of **αCC** by benzyl alcohol (Scheme 3: Pathway 1, see Supporting Information) with the concomitant slow and irreversible addition of

the alcohol to the disubstituted C=C double bond forming tetrasubstituted ethylene carbonate **2** (Scheme 3: Pathway 2, see Supporting Information). However, our theoretical calculations are suggesting an alternative more favorable pathway for the formation of **2** starting from *oxo*-carbonate **1** (Scheme 3: Pathways 1 and 3). This latter compound **1** reacts with benzyl alcohol (**A3**) that is also liberated through the reversible reaction from the carbonate. In these calculations, we accounted for the DBU catalyst and the solvent environment, implicitly in the static simulations and explicitly for all intermediates in the MD simulations, respectively. The stability of the various intermediates at operating conditions, and thus the formation of **int 3** and **int 7**, are more thoroughly discussed in Supporting Informations.

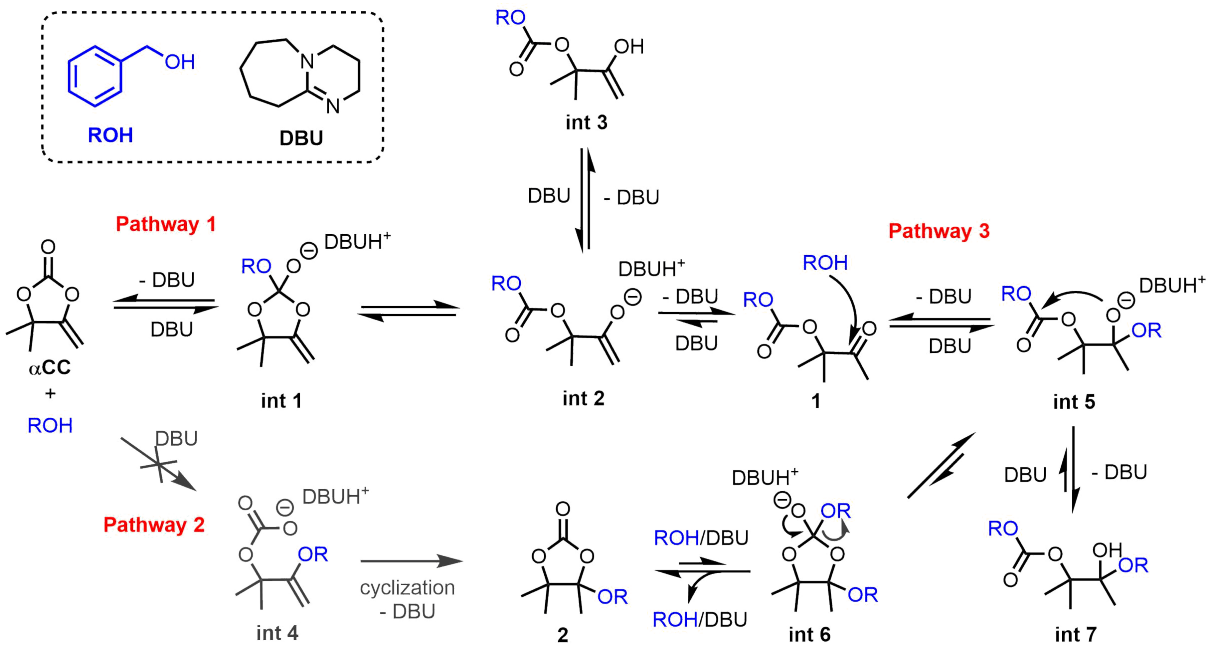

Scheme 3. Mechanism of formation of the tetrasubstituted ethylene carbonate **2** by addition of benzyl alcohol to **αCC**.

The free energy profile of the reaction (Pathways 1 and 3) is shown in Scheme 4. A key feature is the acidic strength of the alcohols with their pKa values that are sufficiently high to disfavor the formation of the corresponding salt (alkoxide). Instead, the alcohol and DBU are forming a strong hydrogen-bonded complex (Figure S19), which is facilitating the subsequent reactions. Regular MD simulations of the reactant complex confirm this as they show that this hydrogen-bonded complex, and not the corresponding salt, dominates the reactant region. Furthermore, salt formation is not observed in any of the static calculations.

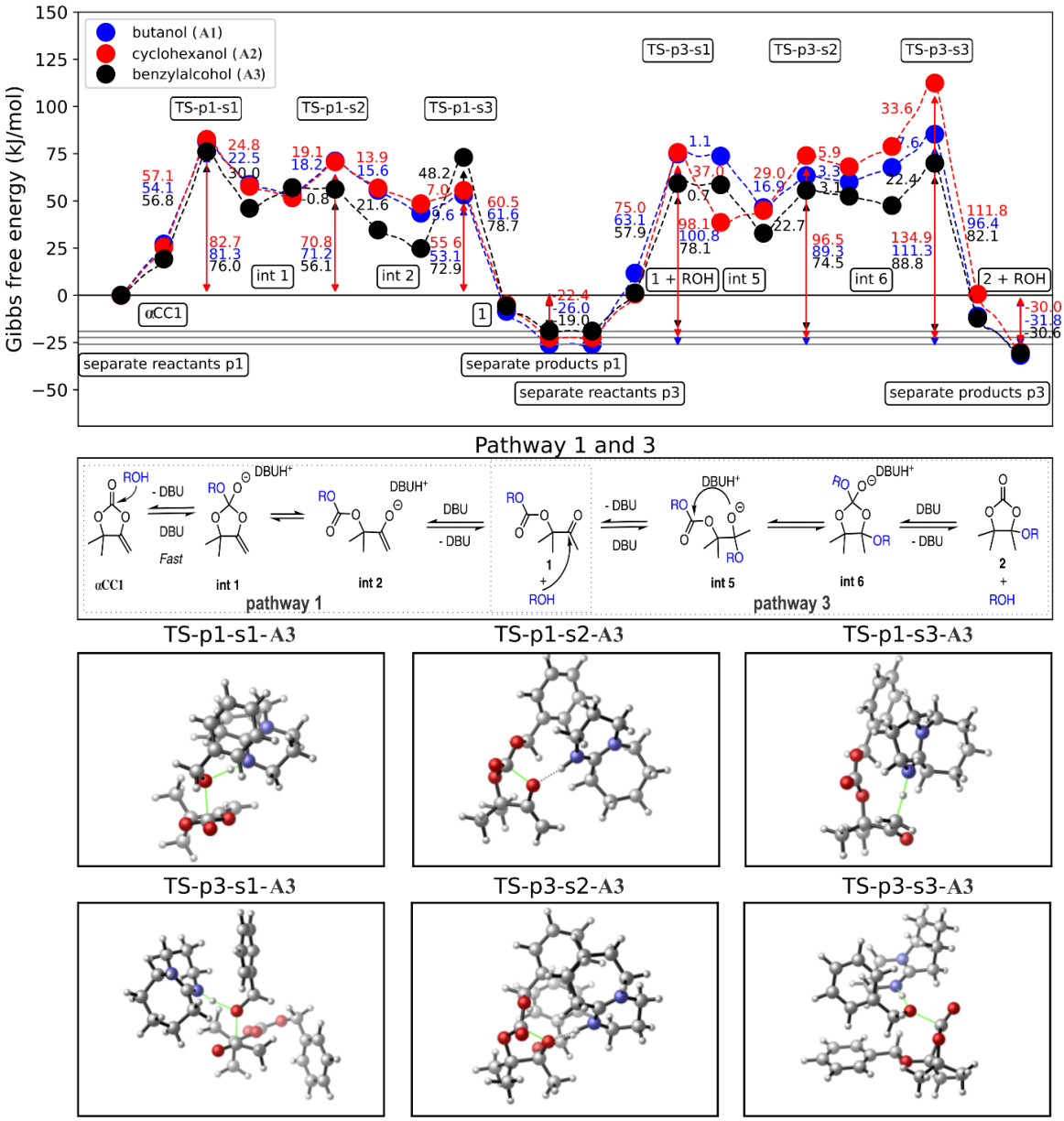

Scheme 4. Gibbs free energy profile with the corresponding reaction scheme and transition state structures for pathway 1 (p1) with formation of *oxo*-carbonate **1**, and pathway 3 (p3) with formation of tetrasubstituted ethylene carbonate **2**. The separate reactants for p3 are rescaled to the separate product of p1. Green bonds in the TS figures indicate bonds which are broken or formed. Energies in kJ·mol^{-1}. (ωB97-XD/6-311++G**, iefpcm(ϵ=46.826), 298 K, 1atm)

As shown in Scheme 4, the rate-limiting step for the formation of the *oxo*-carbonate **1** is the nucleophilic addition of the alcohol to the carbonate carbonyl of **αCC** (TS-p1-s1) with apparent activation energies of 76.0, 81.3 and 82.7 kJ·mol^{-1} for benzyl alcohol **A3**, butanol **A1** and cyclohexanol **A2**, respectively (in correspondence to the experiments). This mechanism is triggered by the formation of a catalyst-alcohol ion-pair complex with immediate (rate-limiting) attack of the alcohol on the neighbouring **αCC**. Based on the relative differences of the activation energies for the different alcohols, which are < 10 kJ·mol^{-1}, the *oxo*-carbonate **1** formation should occur for all alcohols used, which is confirmed experimentally (Table 1). The

reverse apparent reaction barriers amount to 91.9, 79.1 and 78.0 kJ·mol^{-1} for **A1**, **A3** and **A2** respectively. Reverse activation energies are hence within the same order of magnitude as the forward one which suggests the reversibility of this pathway.

Noteworthy is the presence of π-cation and π-induced dipole interactions between the catalyst DBU-H$^+$ and benzyl alcohol **A3**, which is (obviously) not present for **A1** and **A2** (Scheme 4 and Figure 2a and 2b). These interactions substantially lower the activation barrier for the formation of **int 2** (or hence for the reverse reaction) and have a strong stabilizing effect on this intermediate in contrast to the stability of **int 2** for **A1** and **A2** (Scheme 4). To illustrate this, non-covalent interaction plots are shown in Figures 2a and 2b which indicate that **int 2** is indeed much more stable due to the presence of stabilizing interactions between the benzylic moiety and DBU-H$^+$ which are completely absent for butanol (and cyclohexanol) featuring aliphatic chains. Additionally, for benzyl alcohol a (spontaneous) equilibrium reaction is observed between **int 2** and **int 3**, this can hence directly influence the equilibria in which **int 2** is involved (Supporting Information, Figure S21 simulation 1 and simulation 2). An increased stability of **int 1** and **int 2**, induced by interactions between the benzylic group and the DBU-H$^+$, and the extra equilibria between **int 2** and **int 3** can directly influence reaction kinetics for both the forward and reverse pathways (and hence the subsequent formation of tetrasubstituted ethylene carbonate **2**) which is not possible for **A1** and **A2**.

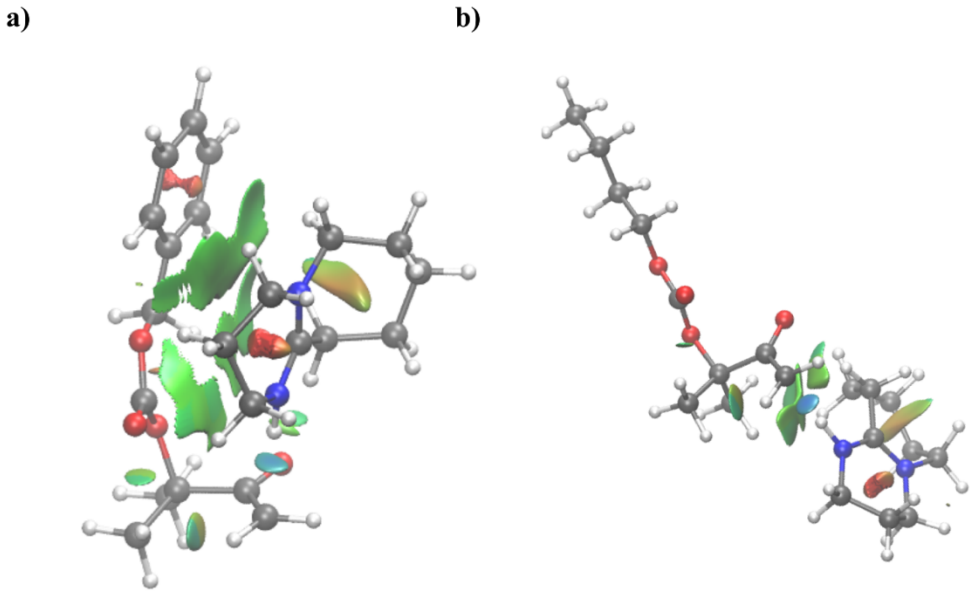

Figure 2. Non-covalent interaction plots for **int 2** with a) benzyl alcohol b) butanol as the used alcohol. Green surfaces indicate weak VdW interactions, blue surfaces indicate strong stabilizing interaction (e.g. hydrogen bonding) and red surfaces indicate repulsive/destabilizing interactions.

Subsequently, as postulated by Lu et al.,[30] tetrasubstituted ethylene carbonate **2** can be formed through Pathway 3 by a nucleophilic attack of a second alcohol molecule on the ketone of the

formed *oxo*-carbonate **1**. This leads to the formation of **int 5** (Scheme 4 and Scheme 3, Pathway 3) which is yet again the rate-determining step for this pathway. In contrast to Pathway 1, we do observe significant differences for the rate-determining step of Pathway 3 (> 10 kJ·mol^{-1}) in line with the experimental results. Apparent activation energies for Pathway 3, with respect to the separate reactants of Pathway 3, are 78.1, 100.8 and 98.1 kJ·mol^{-1} for **A3**, **A1** and **A2**, respectively. These barrier heights are in sharp contrast to the previously proposed Pathway 2 (Supporting Information, Scheme S2) as they are lowered by more than 50 kJ·mol^{-1}, showing that this new proposal is much more feasible. Furthermore, the trends are, for Pathway 3, in line with the experimental observations which is not the case for Pathway 2 (Supporting Information, *vide infra*), i.e., formation of tetrasubstituted ethylene carbonate is observed only for **A3**.

Intermediate stability is, similar to Pathway 1, increased for benzyl alcohol which can also be attributed to the induced π-type interactions. **Int 6**, is clearly a meta-stable state which is prone to ring opening resulting in the formation of **int 5**. This meta-stability is also observed during the corresponding MD simulations (Supporting Information, Figures S23). Scheme 4 further indicates that the tetrasubstituted ethylene carbonate **2** is thermodynamically favored and that the reverse reaction barrier is drastically higher than for Pathway 1 shifting the equilibrium in favor of **2**. Additionally, it is noted throughout the static and dynamic simulations that the DBU positioning is highly determining for the stability (Figure 2, see Supporting Information Pathways 1 and 3).

To elaborate on the differences for the different alcohols, rate-constants are calculated for the rate-limiting steps, the results are presented in Table 3. Both for pathway 1 and 3, benzyl alcohol **A3** has increased rate constants compared to butanol **A1** and cyclohexanol **A2**, especially for the latter pathway a substantial increase is observed, i.e. 4 orders of magnitude with respect to **A1** and **A2**. More interesting to compare are the ratios of the rate-constants which give an indication for the preference of each system to proceed along a certain pathway in case all reactants are present, i.e. *oxo*-carbonate **1** formation has already occurred. For benzyl alcohol both pathways are almost equally likely, in contrast to butanol and cyclohexanol which show a large preference (up to 3 orders of magnitude) for pathway 1. This can hence explain why, assuming reversibility of pathway 1 is feasible for all alcohols, no tetrasubstituted ethylene carbonate is observed for either butanol and cyclohexanol.

Table 3. Reaction rates for the rate-determining steps of pathway 1 and 3 ($k_{1,p1}$ and $k_{1,p3}$, $M^{-2}\cdot s^{-1}$). Rate-constants are calculated with respect to the separate reactants or products. (ωB97-XD/6-311++G**, iefpcm(ϵ=46.826), 298 K, 1 atm)

Alcohol	$k_{1,pathway1}$	$k_{1,pathway\ 3}$	$k_{1,p\ pathway1}/k_{1,\ pathway3}$
benzyl alcohol (A3)	$3{,}05\cdot10^{-1}$	$1{,}28\cdot10^{-1}$	2,4
butanol (A1)	$3{,}58\cdot10^{-2}$	$1{,}37\cdot10^{-5}$	2607,2
cyclohexanol (A2)	$2{,}03\cdot10^{-2}$	$3{,}98\cdot10^{-5}$	510,3

As illustrated in Scheme 5, the side products **3** and **4** observed for the model reaction reported in Table 1 for **A3** can reasonably be obtained by the DBU promoted transcarbonation of product **1** with benzyl alcohol as the α-hydroxyketone is a good leaving group, as also suggested by He et al.[29] In accordance with this, **3** and **4** are indeed formed in almost identical amounts. Assuming reactivity similar to pathway 1 for the different alcohols, the transcarbonation route is expected to proceed more easily for benzyl alcohol than for the aliphatic alcohols **A1** and **A2**.

Calculation of Parr functions enabled to elaborate on the difference in chemoselectivity of the alcohol attack on *oxo*-carbonate **1**, i.e. its preferential addition to the ketone (C=O) (to form the tetrasubstituted ethylene carbonate **2**) or carbonate ((O)C=O) group (to form **3** and **4**)(Supporting Information, Scheme S5). They showed that the formation of tetrasubstituted ethylene carbonate **2** is preferential over the transcarbonation route as the C=O is more electrophilic than the carbonate site and therefore more prone to nucleophilic attack. This chemoselectivity is in line with the experimental results presented in Table 1.

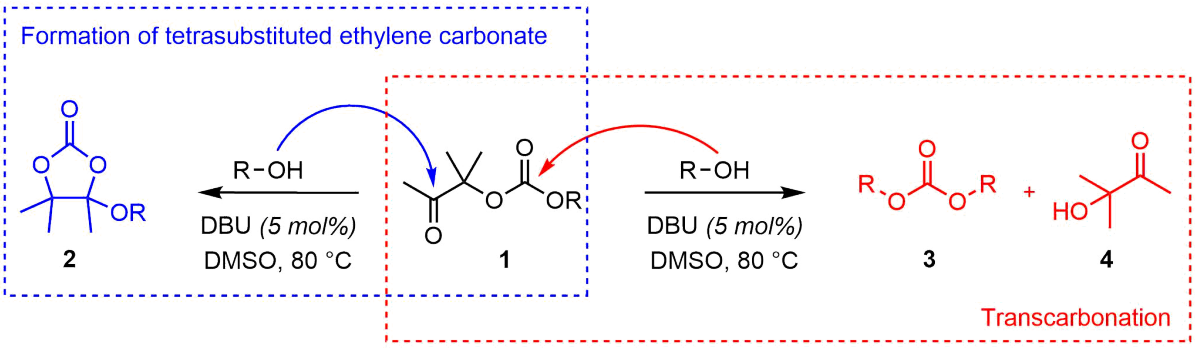

Scheme 5. Chemoselectivity in the DBU-catalyzed addition of alcohol to *oxo*-carbonate.

From these modelling studies, it therefore appears that the formation of tetrasubstituted ethylene carbonate **2** proceeds through a nucleophilic attack of the alcohol on the formed *oxo*-carbonate **1** (Scheme 2). This route explains the experimental observations and the difference

of reactivity for the three different alcohols. Additionally, it is found that the DBU catalyst is affecting the intermediate stability. On one hand, it forms a strong hydrogen-bonded complex with the alcohol. On the other hand, for the specific combination of benzyl alcohol **A3** and DBU, it is shown that π-type interactions (e.g. cation-π, π-π and π-induced dipole interactions) enable extra stabilization of the various intermediates, which potentially increase reaction rates. Finally, reactivity descriptors show the preference of the ketone group over carbonate towards nucleophilic attack, which explains the observed difference in yield for the tetrasubstituted ethylene carbonate **2** and the products **3** and **4** that results from the transcarbonation route.

Synthesis of poly(oxo-carbonate)s by polyaddition of bis(α-alkylidene cyclic carbonate)s with biosourced diols

A series of novel poly(β-*oxo*-carbonate)s was prepared by the polyaddition of two different CO_2-sourced bis(α-alkylidene cyclic carbonate) (bisαCC), i.e. meso-4,4'-(ethane-1,2-diyl)bis(4-methyl-5-methylene-1,3-dioxolan-2-one) (**C1**) and 1,9-dimethylene-2,4,10,12-tetraoxodispiro[4.2.4^8.2^5]tetradecane-3,11-dione (**C2**) with equimolar amount of sugar- (1,4-butanediol **S1** or isosorbide **S2**) or lignin-derived (1,4-benzenedimethanol **L1** or *trans*-1,4-cyclohexanediol **L2**) diols (Scheme 6, Table 4). **S1** was here used as a benchmark diol.

Polymerizations at 25 °C. First, all copolymerizations were carried out at 25 °C by using DBU as organocatalyst (5 mol% compared to **C1** or **C2**) in dry DMSO (C = 0.78 M). For all polycarbonate synthetized, the ^{1}H-NMR spectroscopy showed a full monomer consumption after 24 h. The copolymerization of *meso*-bisαCC C1 and 1,4-butanediol (**S1**) or isosorbide (**S2**) was homogeneous during the reaction and gave poly(*oxo*-carbonate)s **C1S1** and **C1S2** with weight average molar mass (M_w) of 26,700 g/mol and 9,300 g/mol, respectively (Table 4, entries 1 and 2, Figure S24). Their characterizations by ^{1}H- and ^{13}C-NMR spectroscopy gave clear insights into the formation of regioregular *oxo*-carbonate linkages and the absence of polymers defects (Figure 3). The ^{1}H-NMR spectra highlighted the typical resonances of the methylene of **C1S1** (δ = 4.10 ppm) or the methine of **C1S2** (δ = 5.01 ppm) adjacent to the *oxo*-carbonate linkages as well as signals at δ = 2.10-2.14 ppm from the methyl group of the pendent ketone moiety. The formation of the *oxo*-carbonate linkages was further confirmed by the ^{13}C-NMR resonances typical of the *oxo* and carbonate groups at δ = 206.0 - 206.5 ppm and δ =152.9 - 153.6 ppm, respectively. Changing *meso*-bisαCC **C1** for *spiro*-bisαCC **C2** gave two new polymers, **C2S1** and **C2S2**, with different solubility behaviors (Table 4, entries 5 and 6). While **C2S2** displayed a M_w of 10,000 g/mol that remained soluble in DMSO during the course of the polymerization, **C2S1** precipitated during its formation and was found insoluble in all common organic solvents making the determination of its molar mass by SEC analysis

impossible. ^{1}H- and ^{13}C-NMR spectra of **C2S2** gave the typical signatures of a regioregular poly(*oxo*-carbonate) (Figure 3). The microstructure of **C2S1** was elucidated by solid state ^{13}C-NMR spectroscopy that confirmed the formation of the polycarbonate by the presence of the ketone and carbonate signals at δ = 207.3 ppm and δ = 154.4 ppm, respectively (Figure S25).

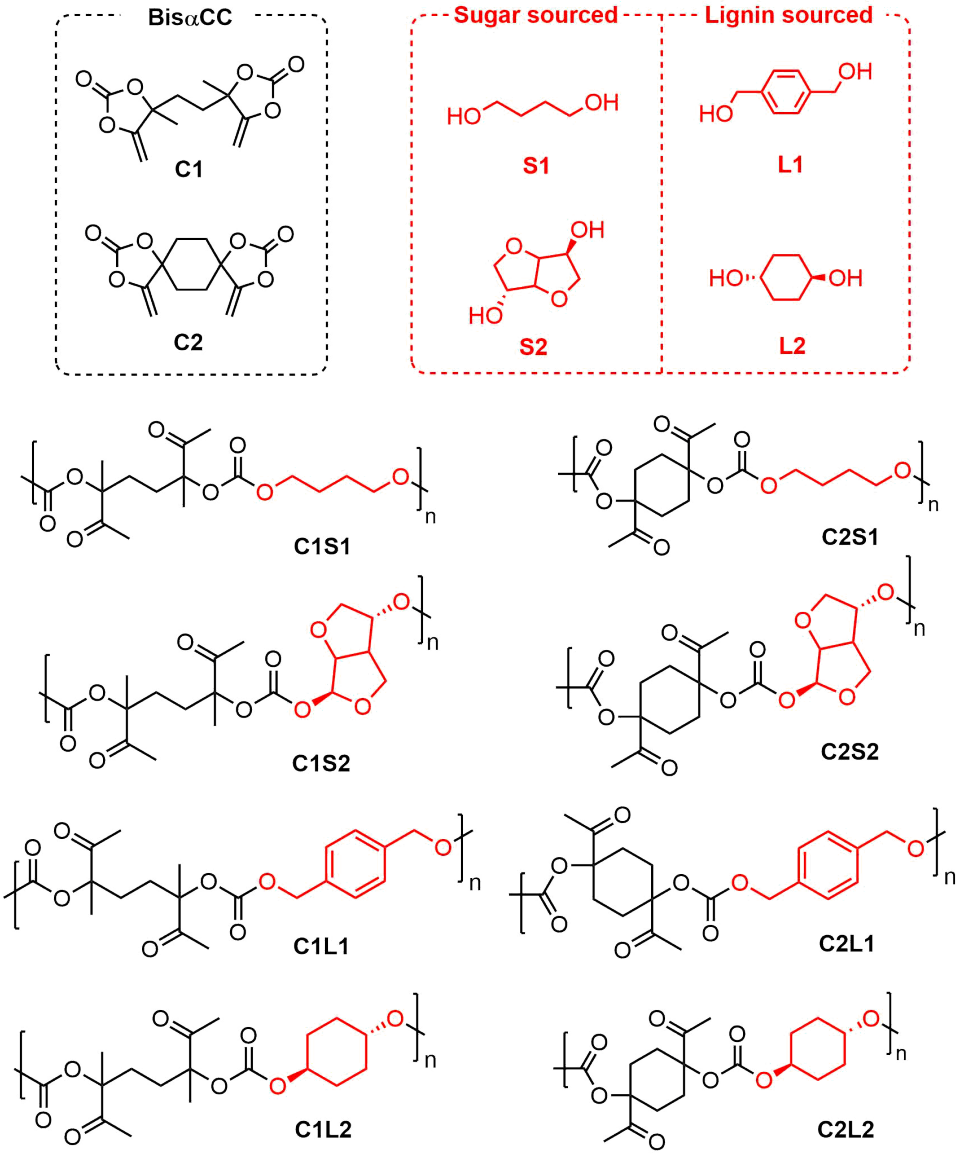

Scheme 6. Scope of poly(*oxo*-carbonate)s synthetized by organocatalyzed step-growth copolymerization of CO_2-sourced bisαCCs with bio-based diols.

The scope of poly(*oxo*-carbonate)s was extended to the copolymerization of **C1** or **C2** with the lignin-derived diols **L1** and **L2** (Table 4, entries 3, 4, 7 and 8). Initially, the medium was homogeneous but the four polycarbonates precipitated during their formation in DMSO. After 24 h, the polymers were isolated by filtration and found to be insoluble in the solvent used for SEC (DMF/LiBr or THF). However, **C1L1** and **C1L2** were found soluble in $CHCl_3$ and their molecular parameters were thus determined by SEC in $CHCl_3$. SEC analysis provided M_w of 13,600 g/mol for **C1L1** and 9,400 g/mol for **C1L2** (Figure S26). Their ^{1}H- and ^{13}C-NMR spectra

confirmed the formation of the corresponding regioregular poly(*oxo*-carbonate)s (Figure 3). As **C2L1** and **C2L2** were insoluble to many common organic solvents ($CHCl_3$, THF, DMF, DMSO), their structural characterization was only possible by solid state ^{13}C-NMR spectroscopy. Both **C2L1** and **C2L2** displayed the microstructure of a poly(*oxo*-carbonate) (Figure S27).

Table 4. Poly(*oxo*-carbonate)s synthetized by DBU-catalyzed step-growth copolymerization of bisαCCs with various diols at 25 °C: molecular characteristics and thermal properties.

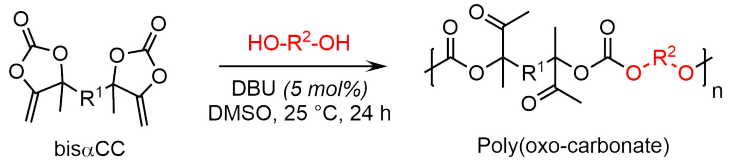

Entry	Polymer	M_n (g/mol)[a]	M_w (g/mol)[a]	Đ[a]	$T_{deg.10\%}$ (°C)[c]	T_g/T_m (°C)	X_c, (%)[h] at RT
1	C1S1	13400	26700	1.99	265	41/60 [d]	10
2	C1S2	4500	9300	2.06	256	88/-- [f]	0
3	C1L1	6000[b]	13600[b]	2.24[b]	216	71/84[d]	8
4	C1L2	6000[b]	9400[b]	1.57[b]	257	95/119[d]	8
5	C2S1	--[g]	--[g]	--[g]	255	97/253[e]	46
6	C2S2	6800	10000	1.47	253	153/174 [d]	0
7	C2L1	--[g]	--[g]	-- [g]	239	104/282[e]	25
8	C2L2	-- [g]	-- [g]	--[g]	271	--/343 [e]	36

Conditions: bisαCC (3.93 mmol), alcohol (3.93 mmol), DBU (0.196 mmol) in dry DMSO (5 mL) at 25 °C under nitrogen atmosphere for 24 h.[a]Determined by SEC in DMF/LiBr. [b]Determined by SEC in $CHCl_3$. [c]Determined by TGA analysis at 10 % of weight loss. [d]Determined by flash DSC analysis. The reported values of T_m were taken from the heating runs at 5000 K/s and after cooling the sample at 0.1 K/s. The reported values of T_g were taken from the heating runs at 1000 K/s and after cooling the sample at 4000 K/s. [e] Determined by flash DSC analysis. The reported values of T_m and T_g were taken from the first scan at heating rate of 20000 K/s (to avoid degradation); The T_m values can be a mix between degradation and melting. [f]Determined by DSC analysis. [g]The polymer is insoluble in common organic solvents ($CHCl_3$, THF, DMF or DMSO). [h] Degree of crystallinity of the powder from synthesis. The software Origin was employed to deconvolute WAXS patterns into amorphous and crystalline contributions, obtaining the degree of crystallinity by dividing the area under a crystalline peak by the total area under the diffractogram.

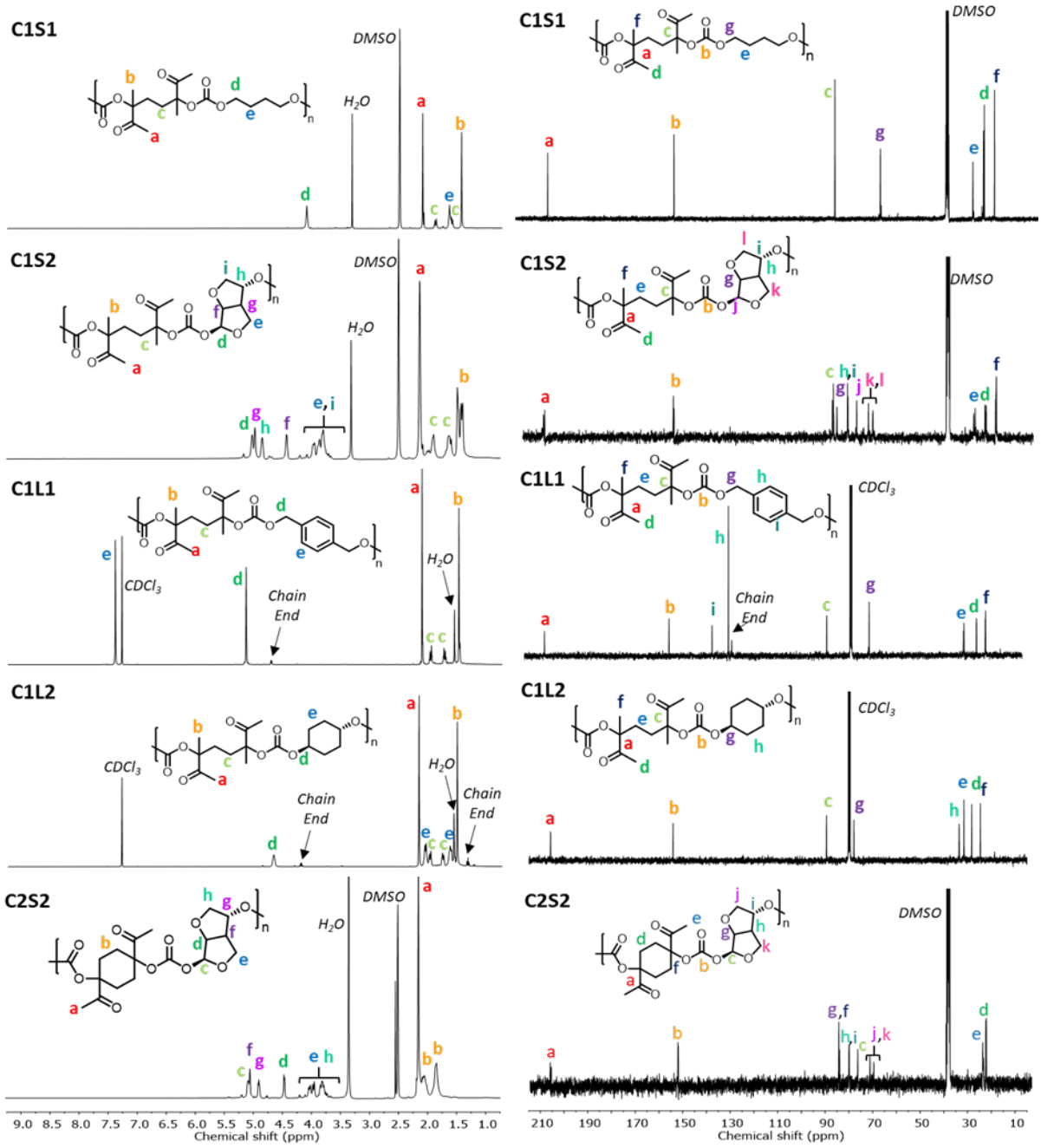

Figure 3. ^{1}H- and ^{13}C-NMR characterizations of poly(*oxo*-carbonate)s **C1S1** and **C1S2** (in DMSO-d_6), **C1L1** and **C1L2** (in $CDCl_3$) and **C2S2** (in DMSO-d_6).

To attest for the microstructure of the polymers and get further insights on the nature of the chain-ends, the poly(*oxo*-carbonate) **C1S1** was selected for characterization by mass spectrometry (Figure 4). At first sight, a difference of 344 amu between each signal in the **C1S1** distributions confirms the presence of the corresponding *oxo*-carbonate units within the polymers. Although the mass parameters (M_n or M_w) could not be determined due to the high molar mass dispersity, the structural information also reveals that linear chains coexist with cyclic species (macrocyclic chains). The presence of the macrocycles may arise from the end-

to-end cyclization of the growing chains as often observed in step-growth polymerizations.[31,32] **C1S1** displayed two types of chains with different end-groups. The most intense population is attributed to a linear poly(*oxo*-carbonate) terminated with butanediol units. The second linear distribution is associated with poly(*oxo*-carbonate) end-capped at one extremity by a hydroxyketone (e.g. *m/z* 3439.5), which may originate from the hydrolysis of the exovinylene chain-end upon MALDI characterization. It is also important to note that the cyclic species are mainly detected at low molecular weights and are probably over estimated.

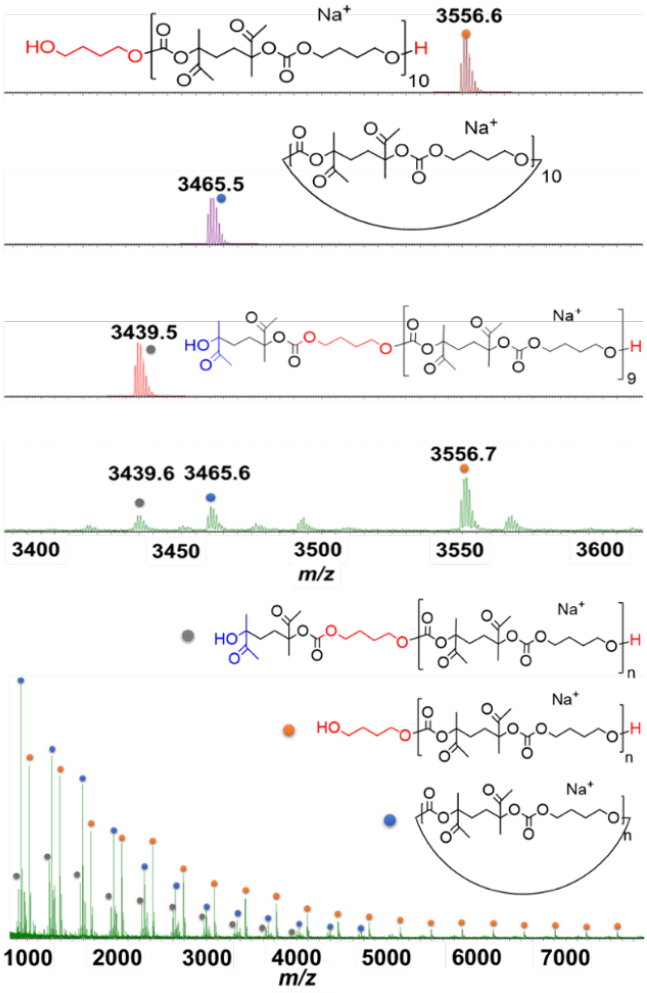

Figure 4. MALDI mass spectrum recorded for **C1S1**, bottom part of the figure corresponds to the experimental mass spectrum while the upper part is a magnification the m/Z area between 3,400 and 3,600 g/mol with comparison between the experimental mass spectrum and the theoretical isotopic model.

Polymerizations at 80 °C. In order to accelerate the polymerizations and tentatively target PCs of higher molar masses, the polymerizations were carried out at 80 °C. For these studies, only *meso*-bisαCC **C1** was considered as it provided (at 25 °C) polymers that were soluble in common organic solvents, and that could be characterized by liquid state NMR spectroscopy and SEC analysis. For the sake of comparison, all experimental conditions were identical to the previous polymerizations, except for the temperature (80 °C *vs.* 25 °C), and results are compared in Table 5. As determined by ^{1}H-NMR spectroscopy for all polycarbonate synthetized, **C1** was totally consumed after 24 h. When **C1** was copolymerized with **S1** or **L2**, polymers with *oxo*-carbonates linkages were obtained (Table 5, entries 1 and 3). No tetrasubstituted ethylene carbonate-type linkages were evidenced by ^{1}H-NMR spectroscopy, at least within the detection limits of the technique (Figure S28-S29 and S30-S31). These observations matched with our model reactions between **αCC** and **A1** or **A2** realized at 80 °C that did not reveal the formation of a 5-membered cyclic carbonate. Surprisingly, both **C1S1** and **C1L2** displayed significantly lower M_w compared to those measured for the same polymer produced at 25 °C. Indeed, **C1S1** prepared at 80 °C presented a M_w of 7,000 g/mol at 80 °C (*vs* 26,700 g/mol at 25 °C) and **C1L2** a M_w of 7,500 g/mol (*vs* 9,400 g/mol at 25 °C) (entries 1 and 3, Table 5) (Figures S32 and S33). The transcarbonation reaction between the hydroxyl chain ends of the growing polymers and the *oxo*-carbonate linkages (that was favored at high temperature as demonstrated on the model reactions) were assumed to be responsible for the lower molar masses observed at 80 °C (Scheme 7). This side reaction left a polymer chain end-capped by an unreactive hydroxyketone and a polymer chain bearing a new carbonate linkage. The presence of the hydroxyketone chain-end was suggested by the presence of new singlets in the ^{1}H-NMR spectra of **C1S1** or **C1L2** at 2.22 ppm (characteristic of a methyl attached to an *oxo* group) and 1.30 ppm. The presence of a shoulder at 4.07 ppm (for **C1S1**) or 4.46 ppm (for **C1L2**) in the signals typical of the methylene or methine adjacent to the *oxo*-carbonate moieties attested the new carbonate linkage resulting from this transcarbonation reaction. By comparison of the relative intensities of the peaks at 2.22 ppm and 2.10 ppm, one quantified the level of the carbonate defect to 4% for **C1S1** and 6% for **C1L2**.

The occurrence of the transcarbonation side reaction on the polymer molar mass was further illustrated by carrying out three identical polymerizations of **C1** with **S1** at 80 °C and by stopping them at different periods of time (1 h, 6 h and 24 h). Results are presented in Table S4 (Supporting Information). It comes out that the comonomers were rapidly consumed at the early stage of the reaction, giving the formation of a polymer of moderate molar mass (M_w = 10,000 g/mol after 1 h). However, with the reaction time, the polymer molar mass was decreased to 5,800 g/mol after 24 h due to the occurrence of the transcarbonation reaction. This polymer molar mass is also illustrated in Figure S34 with the SEC chromatograms that

shifted towards the lower molar mass values with the reaction time. The transcarbonation was however slow and long reaction times were needed to observe the structural defects on the polymer.

When **C1** was copolymerized with **L1**, a polymer with a low M_w of 3,500 g/mol (*vs* 13,600 g/mol at 25 °C) was synthetized after 24 h (Table 5, entry 2, Figure S35). Here also, polycarbonates terminated by the hydroxyketone moiety and bearing some carbonate defects originating from the transcarbonation reaction were observed at a content of 8%. In contrast to the two previous examples, one also noticed the formation of additional 5-membered cyclic carbonate linkages within the polymer microstructure with a content of 12% as determined by ^{1}H-NMR spectroscopy (Figure S36), in accordance with the model reactions with benzylalcohol. Indeed, new methylene and methyl resonances of a tetrasubstituted ethylene carbonate unit were detected at 4.50, 1.63 and 1.45 ppm. The formation of these cyclic carbonate moieties was further corroborated by ^{13}C-NMR spectroscopy by a new carbonyl signal at 145.0 ppm, two quaternary carbons at 82.3 ppm and 108.2 ppm as well as two methyl peaks attached to the carbonate cycle at 23.1 and 26.0 ppm (Figure S37).

Conclusively, structural defects were generated within the PC backbone when polymerizations were carried out at 80 °C, at least for long reaction times. They resulted from a slow transcarbonation reaction that furnished carbonate defect linkages and end-capped hydroxyketone PCs. In some cases (with 1,4-benzenedimethanol), an additional side reaction occurred by the slow addition of the alcohol to the C=C double bond of bisαCC forming a cyclic carbonate linkage, in line with the observations made on the model reactions.

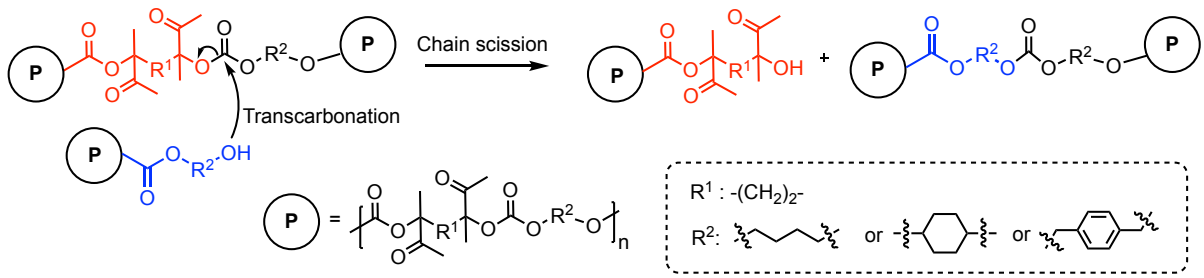

Scheme 7. Transcarbonation reaction between the hydroxyl chain ends of the growing polymers and the *oxo*-carbonate linkages

Table 5. Comparison of the structure of the carbonate linkages and macromolecular characteristics of the PCs prepared by DBU-catalyzed copolymerization of bisαCCs with diols at 25 and 80 °C in dry DMSO.

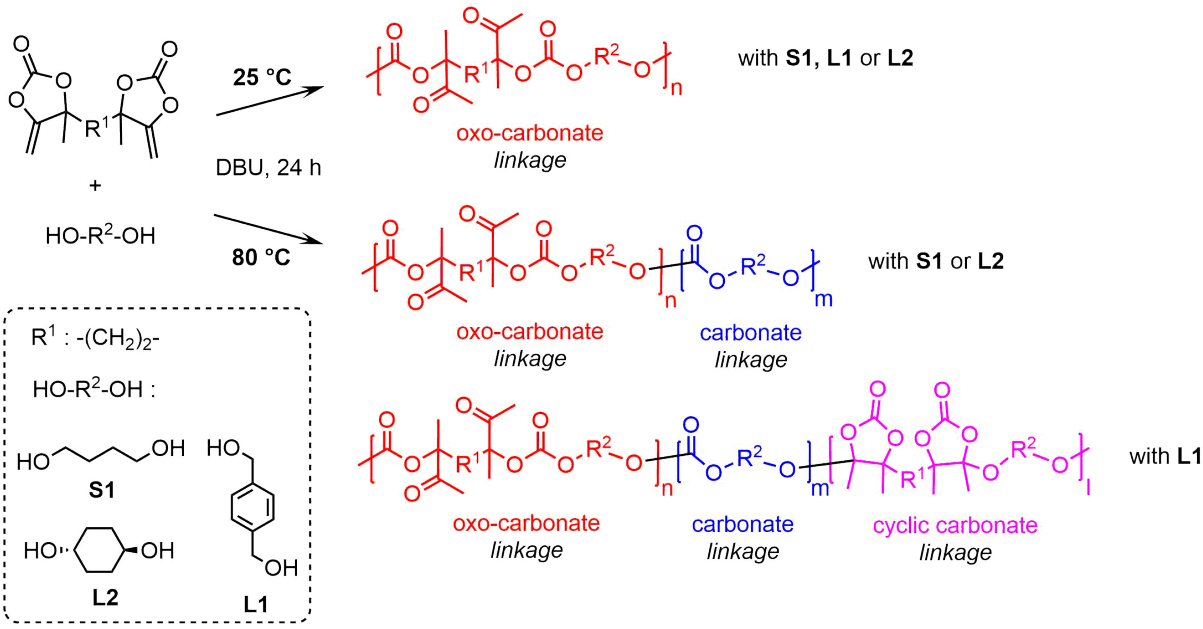

Entry	Polymer	T (°C)	*oxo*-carbonate linkage (%)	cyclic carbonate linkage (%)	carbonate linkage (%)	M_n (g/mol)[a]	M_w (g/mol)[a]	$Đ$[a]
1	C1S1	25	100	0	0	13,400	26,700	1.99
		80	96	0	4	3,800	7,000	1.84
2	C1L1	25	100	0	0	6,000[b]	13,600[b]	2.24[b]
		80	80	12	8	1,900[b]	3,500[b]	1.83[b]
3	C1L2	25	100	0	0	6,000[b]	9,400[b]	1.57[b]
		80	94	0	6	3,300[b]	7,500[b]	2.25[b]

Conditions: bisαCC (3.93 mmol), alcohol (3.93 mmol), DBU (0.196 mmol) in dry DMSO (5 mL) at 25 °C or 80 °C, under nitrogen atmosphere. Conversion bisαCC >99%

[a] Determined by SEC in DMF/LiBr. [b] Determined by SEC in $CHCl_3$.

Thermal properties of poly(oxo-carbonate)s.

The thermal properties of all defect-free poly(*oxo*-carbonate)s prepared at 25 °C were evaluated by thermogravimetric analysis (TGA) and (flash) dynamic scanning calorimetry (DSC) which results are summarized in Table 4 The thermal degradation profiles of PCs are illustrated in Figure S38. The four polymers **C1S1**, **C1S2**, **C2S1** and **C2S2** displayed moderate thermal stabilities with decomposition temperatures at 10% weight loss, $T_{d10\%}$, between 255 °C and 265 °C. Copolymers made from **L2** showed thermal stability in the same range of temperature with $T_{d10\%}$ of 257 °C and 271 °C respectively for **C1L2** and **C2L2**. Changing the aliphatic diols by the aromatic diol **L1** led to polymers **C1L1** and **C2L1** with lower thermal stability as attested by $T_{d10\%}$ of 216 °C and 239 °C. PCs containing the aromatic group were also leaving some char at 600 °C (6 wt% for **C1L1** and 14 wt% for **C2L1**), whereas all other aliphatic PCs were almost completely decomposed at this temperature.

Remarkably, all poly(*oxo*-carbonate)s reported in Table 4 were able to crystallize (except for sample **C1S2** that remained amorphous) as indicated by the reported melting point values. The glass transition temperature (T_g) and melting temperature (T_m) of the semicrystalline PCs were determined by standard DSC and Fast Scanning Chip Calorimetry (Flash DSC). Flash DSC was employed to quench semi-crystalline samples employing cooling rates of 4,000 ºC/s. In this way the fastest crystallizing samples were either quenched to the amorphous state or their crystallinities were substantially reduced. The T_g could therefore easily be determined during a subsequent heating scan. When the melting point of the sample was higher than 200 ºC, the Flash DSC was used to heat the sample at 20,000 ºC/s to avoid degradation as much as possible and still detect the melting endotherm.

From the copolymer series illustrated in Table 4, **C1S2** made from *meso*-BisαCC and isosorbide was amorphous with only a T_g at 88 °C (Figure S39). All the other samples were semi-crystalline and their T_g and T_m values are reported in Table 4 (Figure S40-S46). Based on their chemical structures illustrated in Scheme 6, a close correlation was found between high values of T_g/T_m transitions and the chain rigidity in most cases, as expected.

Figure 5 shows the WAXS diffractograms of selected samples. The presence of well-defined diffraction peaks confirmed the semi-crystalline character of the samples and their degree of crystallinity was calculated by dividing the area of the crystalline peaks (previously separated to the amorphous region by an approximate calculation of the amorphous contribution, see Supporting Information). Crystallinity values varied from 8% for the less crystalline **C1L2** sample to 46% for the most crystalline **C2S1** sample (entries 4 and 5, Table 4). The crystalline structure of the novel poly(*oxo*-carbonate)s prepared here is unknown, so we cannot assign the reflections to the crystallographic planes that originate them. Establishing the crystalline

structure of the polymers is however beyond the scope of the present paper. Nevertheless, judging by the changes in diffraction angles and their corresponding distances (Supporting Information, Table S5) the polymers all crystallized in different types of unit cells, as their chemical structure varies significantly from one another and hence in molecular chain packing within their respective crystalline structures.

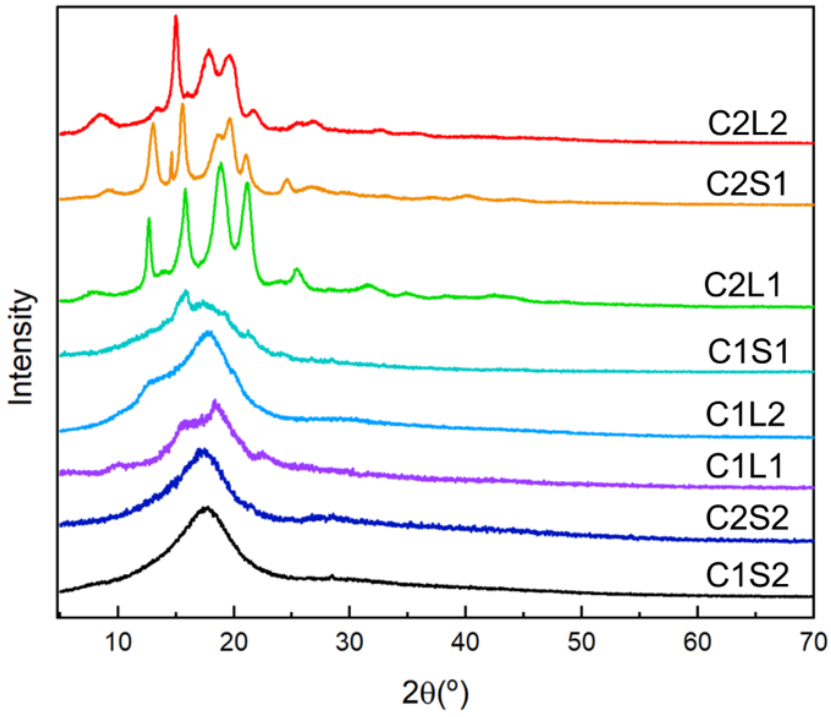

Figure 5. WAXS patterns taken at room temperature of poly(*oxo*-carbonate)s.

Conclusion

The emergence of CO_2-sourced exovinylene bicyclic carbonates (bisαCCs) in polymer science prompted us to investigate the scope and limitations of their organocatalyzed step-growth copolymerization with bio-renewable diols into polycarbonates (PCs). Model reactions were first carried out on small molecules in order to understand the structural influence of the alcohols, the temperature (25 or 80 °C) and the use of an organocatalyst (1,8-Diazabicyclo[5.4.0]undec-7-ene; DBU) on the rate of the cyclic carbonate ring-opening and the product selectivity. Based on these studies, a series of regioregular and defect-free poly(*oxo*-carbonate)s of different structures and reasonable molar masses (M_w up to 26,700 g/mol) were prepared at 25 °C by using sugar- (1,4-butanediol, isosorbide) or lignin-derived (1,4-benzenedimethanol, 1,4-cyclohexanediol) diols and two different CO_2-sourced bis(αCCs). By performing the polymerizations at 80 °C, structural defects were however introduced within the poly(*oxo*-carbonate) chains, i.e. a second type of carbonate linkage was originating from transcarbonation reactions in all cases. When 1,4-benzenedimethanol was used, an additional side reaction was noted and provided tetrasubstituted ethylene carbonate linkages. These side reactions observed at 80 °C limited the polymer molar mass for long reaction times. The mechanism of formation of these side reactions was considered by DFT modelling on model compounds. It was found that the tetrasubstituted ethylene carbonate linkage proceeded through a nucleophilic attack of the alcohol on the ketone group of the formed *oxo*-carbonate, inducing cyclization. Importantly, the DBU catalyst influenced the intermediate stability. It formed a strong hydrogen-bonded complex with the alcohol and, for the specific combination of benzyl alcohol (a model compound of 1,4-benzenedimethanol) and DBU, π-type interactions (e.g. cation-π, π-π and π-induced dipole interactions) were noted and enabled extra stabilization of the various intermediates which potentially increased the reaction rates. Finally, reactivity descriptors enabled to explain the observed difference in yield for the tetrasubstituted ethylene carbonate linkage and the linear carbonate (originating from transcarbonation).

Finally, the thermal properties of the poly(*oxo*-carbonate)s designed at 25 °C were evaluated by thermogravimetric (TGA) and (flash) differential scanning calorimetry (DSC) experiments. Depending on their microstructures, poly(*oxo*-carbonate)s presented a degradation temperature between 216 °C and 271 °C. With the exception of one poly(*oxo*-carbonate) made from isosorbide that was amorphous with a glass transition temperature (T_g) of 88 °C, all the other polycarbonates were semi-crystalline with a melting temperature (T_m) ranging from 60 to 343 °C. Preliminary wide-angle X-ray scattering (WAXS) studies confirmed the ability of these PCs to crystallize.

This work highlights the potential of this process for the facile preparation of polycarbonates using diols and carbon dioxide as bioresources under mild reaction conditions, and shows how the polymer linkages can be modified by the experimental conditions. The fraction of bio-renewables (CO_2 + diol) incorporated in the polymers is high (50-60 wt%), attesting for the importance of the process for the more sustainable production of plastics. The level of sustainability of these materials might be further increased by proposing greener routes to producing bisαCCs. Indeed, their current synthesis uses petro-based diones (1,4-cyclohexanone or 2,5-hexanedione in this work) and Grignard's reagent (ethynyl magnesium bromide) to preparing the propargylic alcohols needed for coupling to CO_2. Bio-based approaches might consist of starting from 1,4-cyclohexanone[33] prepared from succinic acid or from 2,5-hexanedione[34,35] obtained by hydrolysis of sugar-derived 2,5-dimethylfuran. Grignard's reagents will still have to be used, however bispropargylic alcohols might be easily obtained from calcium carbide as the acetylene source.[36,37]

Experimental section

Materials

Benzyl alcohol (99%). 1-butanol (98%) and cyclohexanol were purchased from Sigma-Aldrich. 1,4-butanediol (99%), 1,4-cyclohexanediol (99%), *trans*-1,4-cyclohexanediol were supplied by Fluorochem. while 1,8-diazabicyclo[5.4.0]undec-7-ene (DBU 99%) and 1,4-benzenedimethanol (99%) were purchased from TCI. 4,4-dimethyl-5-methylene-1,3-dioxolan-2-one (αCC), 4.4'-(ethane-1.2-diyl)bis(4-methyl-5-methylene-1.3-dioxolan-2-one (**C1**) and 1,9-dimethylene-2,4,10,12-tetraoxodispiro[4.2.4^8.2^5]tetradecane-3,11-dione (**C2**) and tetrabutylammonium phenolate were synthetized as reported elsewhere by our group.[15,19,27] All solid reagents were dried before use with azeotropic distillations in toluene. All the solvents were dried overnight on activated 3 Å molecular sieves. All the reactions were performed under inert atmosphere of N_2.

Characterization methods

Nuclear magnetic resonance (NMR) spectroscopy. ^{1}H NMR analyses were performed on Bruker 400 MHz spectrometers in DMSO or $CDCl_3$ at 25 °C in the Fourier transform mode. 16 or 64 scans for a ^{1}H spectra and 512 or 2048 scans for ^{13}C spectra were recorded. Cross-polarization magic angle spinning (CP-MAS) solid state ^{13}C NMR spectra were collected using a Bruker Avance DSX-400 instrument. Samples were packed in 4 mm zirconia rotors and spun at 10 kHz.

Gas chromatography-mass spectrometry (GC-MS). Samples were prepared by taking 100 µL of the compound mixture and diluting in acetone. The sample was filtered over a syringe filter and further diluted to a concentration of 10^{-4} - 10^{-5} M. 3 µL of the samples were injected. The

apparatus used was an Agilent Technologies 7890 A GC System coupled to an Agilent Technologies 5975 C inert MSD with triple-axis detector. As column an Optima 725820.30 30 m × 250 µm × 0.25 µm was selected. Carrier gas was helium. The following oven program was used: 50 °C for 3 min then 10 °C/min to 300 °C followed by 300 °C for 5 min. The front inlet was heated at 200 °C. Mass was scanned from 50 to 450 amu.

Size exclusion chromatography (SEC). Number-average and weight-average molecular weights and molecular weight dispersity (Mw/Mn) values of polymers were determined by size exclusion chromatography (SEC) in dimethylformamide (DMF) and in chloroform ($CHCl_3$). The SEC in DMF contained LiBr (0.025 M) and were conducted at 55 °C (flow rate: 1 mL/min) with a Waters chromatograph equipped with three columns (Waters Styragel PSS gram 1000 Å (×2), 30 Å), dual λ absorbance detector (Waters 2487) and a refractive index detector (Waters 2414). The SEC in chloroform were conducted at 35 ºC at a flow rate of 1 $cm^3 \cdot min^{-1}$, using an isocratic pump (VE 1122, Viscotek) a set of two PLgel 5 µm MIXED-C ultra-high efficiency column and a Shodex SE 61 differential refractive index detector as well as a variable wavelength UV detector (Spectra 100, Spectra-Physics). A volume of 100 µL of sample solution in chloroform (concentration 0.3 % w/v) was injected. Polystyrene standards (Polymer Laboratories) with narrow molecular weight distributions were used to generate a calibration curve.

Positive-ion Matrix assisted LASER Desorption/Ionization-Mass Spectrometry (MALDI-MS) experiments were performed using a Waters QToF Premier mass spectrometer equipped with a Nd:YAG laser operating at 355 nm (third harmonic) with a maximum output of 65 µJ delivered to the sample in 2.2 ns pulses at 50 Hz repeating rate. Time-of-flight mass analysis was performed in the reflectron mode at a resolution of about 10k (m/z 569). All samples were analyzed using trans-2-[3-(4-tert-butylphenyl)-2-methylprop-2-enylidene]malononitrile (DCTB) as a matrix. Polymer samples were dissolved in $CHCl_3$ to obtain $1mg \cdot mL^{-1}$ solution. Additionally, 40 µL of $2mg.mL^{-1}$ NaI solution in acetonitrile was added to the polymer solution.

Thermogravimetric analysis (TGA) was performed on a TGA2 instrument from Mettler Toledo. Around 5 mg of sample was heated at 20°C/min until 600°C under N_2 atmosphere (20 mL/min).

Differential scanning calorimetry (DSC) was performed on a DSC Q2000 differential calorimeter (TA Instruments). All the experiments were performed under ultrapure nitrogen flow. Samples of 5–8 mg were used and placed in sealed aluminium pans. The samples were first heated at a rate of 10 °C min^{-1} from 25 °C to 150 °C. Subsequently, the samples were cooled down to -80° C at a rate of 10 °C min^{-1} and then heated to 230 C at 10 °C min^{-1}. The last heating cycle was used for the determination of the T_g.

Flash differential scanning calorimetry (FDSC) was performed on a Flash DSC2+ instrument from Mettler Toledo, equipped with a Huber TC-100 intracooler. The cooling rate employed was−4000K/s, and the heating rates were 1,000 K/s, 5,000 K/s and 20,000 K/s. Applying a very fast cooling rate (−4,000 K/s), most samples were quenched to the amorphous state (or their crystallinity was greatly reduced), thereby facilitating the detection of their glass transition upon subsequent heating at 1,000 K/s. Second, the use of fast heating rates permits to avoid cold crystallization of the samples. For the detection of the melting temperature, a cooling rate of −0.1 K/s was also employed in order to induce crystallization of the samples at −80°C from the melted state before the subsequent heating scan at 5,000 K/s. The polymers with higher values of T_m were evaluated at a heating rate of 20,000 K/s to avoid the degradation of the sample. Before each experiment, the sensor was conditioned and calibrated. A flow of nitrogen gas was applied to perform the measurements under an inert atmosphere, maintaining an 80 mL/min flow rate. For a good contact between the sample and sensor, a fluorinated oil was casted over the sensor and then the sample was loaded. This oil doesn't show thermal transitions in the temperature range under study. The samples were analyzed in a range from −80 to 200 °C or 350°C, depending of the thermal degradation temperature of each polymer determined by TGA. The reported values of T_g and T_m were taken from the heating runs. As the mass employed in fast chip calorimeter experiments is so small, the results are assumed to be independent of sample mass. The STARe software was used to analyze the data.

WAXS X-ray powder diffraction patterns were collected by using a Philips X'pert PRO automatic diffractometer operating at 40 kV and 40 mA, in theta-theta configuration, secondary monochromator with Cu-Ka radiation (λ = 1.5418 Å) and a PIXcel solid state detector (active length in 2θ 3.347º). Data were collected from 5 to 70° 2θ, step size 0.026º and time per step of 150s at RT. 1º fixed soller slit and divergence slit giving a constant volume of sample illumination were used.

General procedure for model reaction of αCC with alcohols

All model reactions were conducted at 25 °C with equimolar ratio of αCC and nucleophile in dry DMSO (C = 4 mol/L) under N_2 atmosphere. Kinetics were monitored by ^{1}H NMR spectroscopy following the representative procedure for the αCC –alcohol reaction: αCC (4 mmol 1 eq.) and alcohol (4 mmol 1 eq.) were added in a reaction tube with 1 mL of dry DMSO and 5 mol% DBU (0.2 mmol) compared to αCC. Samples were taken after different time intervals and analyzed by ^{1}H NMR spectroscopy to determine the αCC conversion.

General procedure for the synthesis poly(β-*oxo*-carbonate)s

Representative procedure for the synthesis of polycarbonates: C1 (3.93 mmol, 1 g) and 1.4-benzenedimethanol (3.93 mmol, 0.542 g) were added in a flask and dry DMSO (5 mL) and

DBU (0.196 mmol, 0.03 mL) were added under nitrogen at room temperature (25 °C). The reaction medium was then stirred at 25°C for 24h. At the end of the reaction, an aliquot was withdrawn to determine the conversion of the monomers by ^{1}H-NMR spectroscopy. The polymer was purified by precipitation in methanol/water (1:1). The polymer was then dried under vacuum at 25°C for 48 h and analyzed by ^{1}H- and ^{13}C- NMR spectroscopy and SEC. The same procedure was carried out for the other polymers.

References

(1) Kyriacos, D. *Polycarbonates*; Elsevier Ltd, 2017. https://doi.org/10.1016/B978-0-323-35824-8.00017-7.

(2) Fukuoka, S.; Tojo, M.; Hachiya, H.; Aminaka, M.; Hasegawa, K. Green and Sustainable Chemistry in Practice : Development and Industrialization of a Novel Process for Polycarbonate Production from CO_2 without Using Phosgene. *Polym. J.* 2007, *39* (2), 91–114. https://doi.org/10.1295/polymj.PJ2006140.

(3) Kim, W. B.; Joshi, U. A.; Lee, J. S. Making Polycarbonates without Employing Phosgene: An Overview on Catalytic Chemistry of Intermediate and Precursor Syntheses for Polycarbonate. *Ind. Eng. Chem. Res.* 2004, *43* (9), 1897–1914. https://doi.org/10.1021/ie034004z.

(4) Fukuoka, S.; Fukawa, I.; Adachi, T.; Fujita, H.; Sugiyama, N.; Sawa, T. Industrialization and Expansion of Green Sustainable Chemical Process: A Review of Non-Phosgene Polycarbonate from CO_2. *Org. Process Res. Dev.* 2019, *23* (2), 145–169. https://doi.org/10.1021/acs.oprd.8b00391.

(5) Grignard, B.; Gennen, S.; Jérôme, C.; Kleij, A. W.; Detrembleur, C. Advances in the Use of CO_2 as a Renewable Feedstock for the Synthesis of Polymers. *Chem. Soc. Rev.* 2019, *48*, 4466–4514. https://doi.org/10.1039/c9cs00047j.

(6) Tamura, M.; Ito, K.; Honda, M.; Nakagawa, Y.; Sugimoto, H.; Tomishige, K. Direct Copolymerization of CO_2 and Diols. *Sci. Rep.* 2016, *6*, 1–9. https://doi.org/10.1038/srep24038.

(7) Huang, J.; Worch, J. C.; Dove, A. P.; Coulembier, O. Update and Challenges in Carbon Dioxide-Based Polycarbonate Synthesis. *ChemSusChem* 2020, *13* (3), 469–487. https://doi.org/10.1002/cssc.201902719.

(8) Schutyser, W.; Renders, T.; Van Den Bosch, S.; Koelewijn, S. F.; Beckham, G. T.; Sels, B. F. Chemicals from Lignin: An Interplay of Lignocellulose Fractionation, Depolymerisation, and Upgrading. *Chem. Soc. Rev.* 2018, *47* (3), 852–908. https://doi.org/10.1039/c7cs00566k.

(9) Sun, Z.; Fridrich, B.; De Santi, A.; Elangovan, S.; Barta, K. Bright Side of Lignin Depolymerization: Toward New Platform Chemicals. *Chem. Rev.* 2018, *118* (2), 614–678. https://doi.org/10.1021/acs.chemrev.7b00588.

(10) Gong, Z. J.; Li, Y. R.; Wu, H. L.; Lin, S. D.; Yu, W. Y. Direct Copolymerization of Carbon Dioxide and 1,4-Butanediol Enhanced by Ceria Nanorod Catalyst. *Appl. Catal. B Environ.* 2020, *265* (September 2019), 118524–118536. https://doi.org/10.1016/j.apcatb.2019.118524.

(11) Zhaozhong, J.; Chen, L.; Wenchun, X.; Gross, R. A. Controlled Lipase-Catalyzed Synthesis of Poly(Hexamethylene Carbonate). *Macromolecules* 2007, *40* (22), 7934–7943. https://doi.org/10.1021/ma070665m.

(12) Meabe, L.; Lago, N.; Rubatat, L.; Li, C.; Müller, A. J.; Sardon, H.; Armand, M.; Mecerreyes, D. Polycondensation as a Versatile Synthetic Route to Aliphatic Polycarbonates for Solid Polymer Electrolytes. *Electrochim. Acta* 2017, *237*, 259–266. https://doi.org/10.1016/j.electacta.2017.03.217.

(13) Sun, J.; Kuckling, D. Synthesis of High-Molecular-Weight Aliphatic Polycarbonates by Organo-Catalysis. *Polym. Chem.* 2016, *7* (8), 1642–1649. https://doi.org/10.1039/c5py01843a.

(14) Naik, P. U.; Refes, K.; Sadaka, F.; Brachais, C. H.; Boni, G.; Couvercelle, J. P.; Picquet, M.; Plasseraud, L. Organo-Catalyzed Synthesis of Aliphatic Polycarbonates in Solvent-Free Conditions. *Polym. Chem.* 2012, *3* (6), 1475–1480. https://doi.org/10.1039/c2py20056b.

(15) Gennen, S.; Grignard, B.; Tassaing, T.; Jérôme, C.; Detrembleur, C. CO_2 -Sourced α-Alkylidene Cyclic Carbonates: A Step Forward in the Quest for Functional Regioregular Poly(Urethane)s and Poly(Carbonate)S. *Angew. Chem. Int. Ed.* 2017, *56* (35), 10394–10398. https://doi.org/10.1002/anie.201704467.

(16) Ouhib, F.; Meabe, L.; Mahmoud, A.; Eshraghi, N.; Grignard, B.; Thomassin, J.-M.; Aqil, A.; Boschini, F.; Jérôme, C.; Mecerreyes, D.; Detrembleur, C. CO_2 -Sourced Polycarbonates as Solid Electrolytes for Room Temperature Operating Lithium Batteries. *J. Mater. Chem. A* 2019, *7* (16), 9844–9853. https://doi.org/10.1039/C9TA01564G.

(17) Gennen, S.; Grignard, B.; Jérôme, C.; Detrembleur, C. CO_2-Sourced Non-Isocyanate Poly(Urethane)s with PH-Sensitive Imine Linkages. *Adv. Synth. Catal.* 2019, *361* (2), 355–365. https://doi.org/10.1002/adsc.201801230.

(18) Habets, T.; Siragusa, F.; Grignard, B.; Detrembleur, C. Advancing the Synthesis of Isocyanate-Free Poly(Oxazolidones)s: Scope and Limitations. *Macromolecules* 2020, *53* (15), 6396–6408. https://doi.org/10.1021/acs.macromol.0c01231.

(19) Ouhib, F.; Grignard, B.; Van Den Broeck, E.; Luxen, A.; Robeyns, K.; Van Speybroeck, V.; Jerome, C.; Detrembleur, C. A Switchable Domino Process for the Construction of Novel CO_2 -Sourced Sulfur-Containing Building Blocks and Polymers. *Angew. Chem. Int. Ed.* 2019, *58* (34), 11768–11773. https://doi.org/10.1002/anie.201905969.

(20) Dabral, S.; Schaub, T. The Use of Carbon Dioxide (CO_2) as a Building Block in Organic Synthesis from an Industrial Perspective. *Adv. Synth. Catal.* 2019, *361* (2), 223–246. https://doi.org/10.1002/adsc.201801215.

(21) Ouhib, F.; Meabe, L.; Mahmoud, A.; Grignard, B.; Thomassin, J.-M.; Boschini, F.; Zhu, H.; Forsyth, M.; Mecerreyes, D.; Detrembleur, C. Influence of the Cyclic versus Linear Carbonate Segments in the Properties and Performance of CO_2 -Sourced Polymer Electrolytes for Lithium Batteries. *ACS Appl. Polym. Mater.* 2020, *2* (2), 922–931. https://doi.org/10.1021/acsapm.9b01130.

(22) Dabral, S.; Licht, U.; Rudolf, P.; Bollmann, G.; Hashmi, A. S. K.; Schaub, T. Synthesis and Polymerisation of α-Alkylidene Cyclic Carbonates from Carbon Dioxide, Epoxides and the Primary Propargylic Alcohol 1,4-Butynediol. *Green Chem.* 2020, *22*, 1553–1558. https://doi.org/10.1039/c9gc04320a.

(23) Tounzoua, C. N.; Grignard, B.; Brege, A.; Jerome, C.; Tassaing, T.; Mereau, R.; Detrembleur, C. A Catalytic Domino Approach toward Oxo-Alkyl Carbonates and Polycarbonates from CO_2 , Propargylic Alcohols, and (Mono- and Di-)Alcohols. *ACS Sustain. Chem. Eng.* 2020, *8*, 9698–9710. https://doi.org/10.1021/acssuschemeng.0c01787.

(24) Kricheldorf, H. R. “Sugar Diols” as Building Blocks of Polycondensates. *J. Macromol. Sci. C* 1997, *37* (4), 599–631. https://doi.org/10.1080/15321799708009650.

(25) Yu, Y.; Pang, C.; Jiang, X.; Yang, Z.; Ma, J.; Gao, H. Copolycarbonates Based on a Bicyclic Diol Derived from Citric Acid and Flexible 1,4-Cyclohexanedimethanol: From Synthesis to Properties. *ACS Macro Lett.* 2019, *8* (4), 454–459. https://doi.org/10.1021/acsmacrolett.9b00184.

(26) Burgard, A.; Burk, M. J.; Osterhout, R.; Dien, S. Van; Yim, H. ScienceDirect Development of a Commercial Scale Process for Production of 1 , 4-Butanediol from Sugar. *Curr. Opin. Biotech. 42*, 118–125. https://doi.org/10.1016/j.copbio.2016.04.016.

(27) Grignard, B.; Ngassamtounzoua, C.; Gennen, S.; Gilbert, B.; Méreau, R.; Jerome, C.; Tassaing, T.; Detrembleur, C. Boosting the Catalytic Performance of Organic Salts for the Fast and Selective Synthesis of α-Alkylidene Cyclic Carbonates from Carbon Dioxide and Propargylic Alcohols. *ChemCatChem* 2018, *10* (12), 2584–2592. https://doi.org/10.1002/cctc.201800063.

(28) Ca’, N. Della; Gabriele, B.; Ruffolo, G.; Veltri, L.; Zanetta, T.; Costa, M. Effective Guanidine-Catalyzed Synthesis of Carbonate and Carbamate Derivatives from Propargyl Alcohols in Supercritical Carbon Dioxide. *Adv. Synth. Catal.* 2011, *353* (1), 133–146. https://doi.org/10.1002/adsc.201000607.

(29) Zhou, Z.-H.; Song, Q.-W.; Xie, J.-N.; Ma, R.; He, L.-N. Silver(I)-Catalyzed Three-Component Reaction of Propargylic Alcohols, Carbon Dioxide and Monohydric Alcohols: Thermodynamically Feasible Access to β-Oxopropyl Carbonates. *Chem. Asian J.* 2016, *11* (14), 2065–2071. https://doi.org/10.1002/asia.201600600.

(30) Zhou, H.; Zhang, H.; Mu, S.; Zhang, W. Z.; Ren, W. M.; Lu, X. B. Highly Regio- And Stereoselective Synthesis of Cyclic Carbonates from Biomass-Derived Polyols: Via Organocatalytic Cascade Reaction. *Green Chem.* 2019, *21* (23), 6335–6341. https://doi.org/10.1039/c9gc03013a.

(31) Kricheldorf, H. R. Cyclic Polymers : Synthetic Strategies and Physical Properties. 2010, *48* (September 2009), 251–284. https://doi.org/10.1002/POLA.

(32) Josse, T.; Winter, J. De; Gerbaux, P.; Coulembier, O. Cyclic Polymers by Ring-Closure Strategies Angewandte. *Angew. Chem. Int. Ed.* 2016, *55* (45), 13944–13958. https://doi.org/10.1002/anie.201601677.

(33) Arnold T. Nielsen and Wayne R. Carpenter. 1,4-Cyclohexanedione. *Org. Synth.* 1965, *45* (September), 25. https://doi.org/10.15227/orgsyn.045.0025.

(34) Nikbin, N.; Caratzoulas, S.; Vlachos, D. G. On the Brønsted Acid-Catalyzed Homogeneous Hydrolysis of Furans. *ChemSusChem* 2013, *6* (11), 2066–2068. https://doi.org/10.1002/cssc.201300432.

(35) Li, Y.; Lv, G.; Wang, Y.; Deng, T.; Wang, Y.; Hou, X.; Yang, Y. Synthesis of 2,5-Hexanedione from Biomass Resources Using a Highly Efficient Biphasic System. *ChemistrySelect* 2016, *6*, 1252–1255. https://doi.org/10.1002/slct.201600280.

(36) Hosseini, A.; Seidel, D.; Miska, A.; Schreiner, P. R. Fluoride-Assisted Activation of Calcium Carbide: A Simple Method for the Ethynylation of Aldehydes and Ketones. *Org. Lett.* 2015, *17* (11), 2808–2811. https://doi.org/10.1021/acs.orglett.5b01219.

(37) Sum, Y. N.; Yu, D.; Zhang, Y. Synthesis of Acetylenic Alcohols with Calcium Carbide as the Acetylene Source. *Green Chem.* 2013, *15* (10), 2718–2721. https://doi.org/10.1039/c3gc41269e.

Supporting Informations

Kinetic studies of model reactions of αCC with alcohols

The αCC conversion was estimated by comparison of the relative intensities of the peaks associated to olefinic protons at 4.60 and 4.77 ppm and the peak of the methyl group in α-position of the ketone at 2.05 ppm according to the equation:

$$Conv. = 1 - \left(\frac{\frac{(I4.60 + I4.77)}{2}}{\frac{(I4.60 + I4.77)}{2} + \frac{I2.05}{3}} \right) \qquad \text{(Eq. 1)}$$

Model reactions between αCC and alcohols at 25 °C monitored by ^{1}H NMR spectroscopy

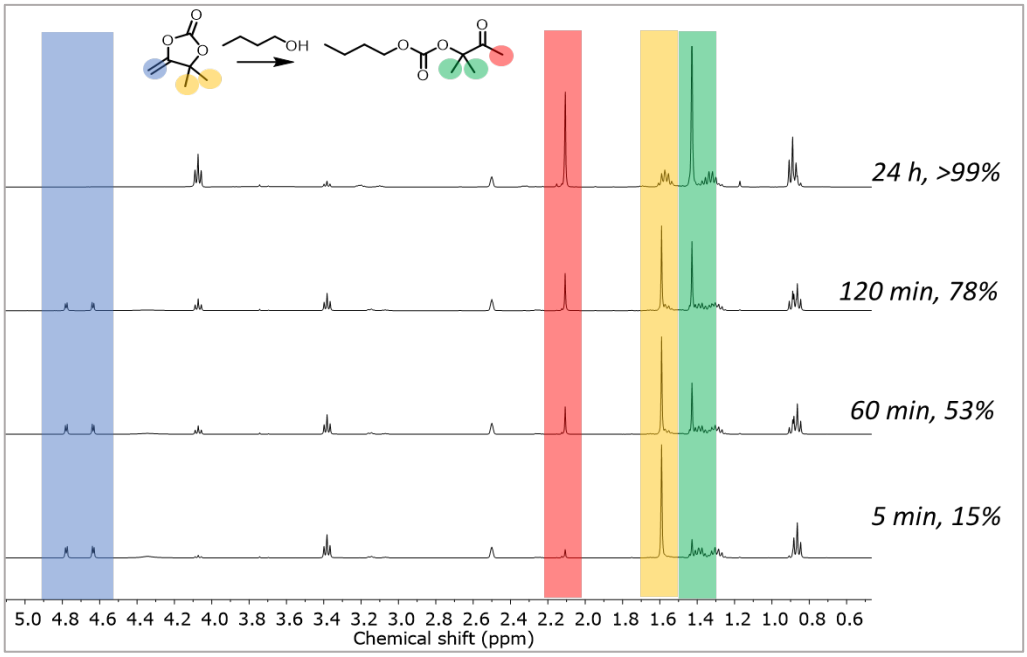

Figure S1. ^{1}H-NMR (in DMSO-d_6) monitoring of the reaction of **αCC** with **A1**, at 25 °C, catalyzed by DBU (5 mol%).

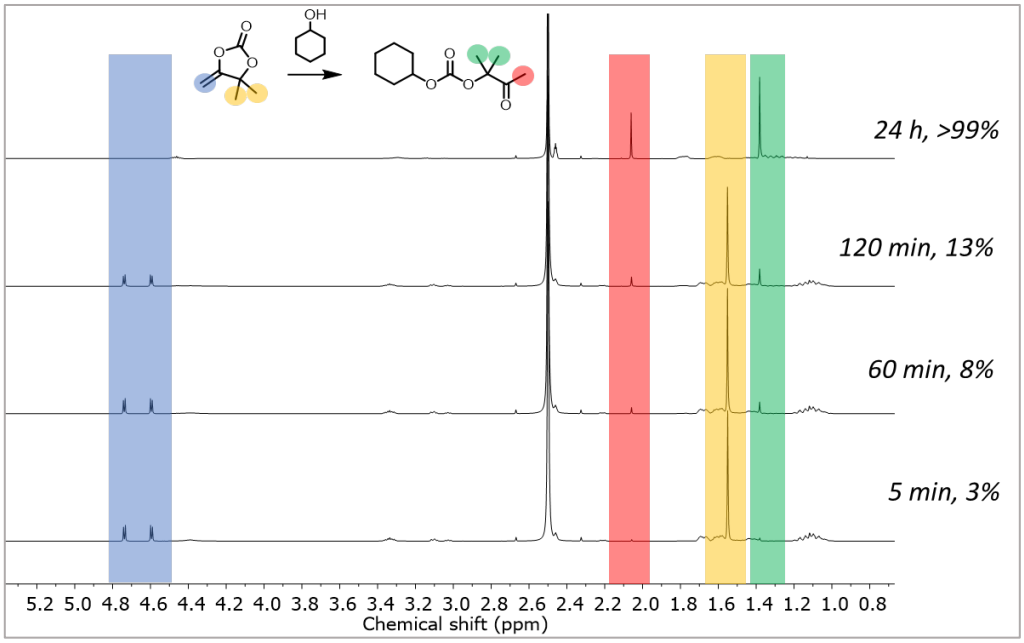

Figure S2. ^{1}H-NMR (in DMSO-d_6) monitoring of the reaction of **αCC** with **A2**, at 25 °C, catalyzed by DBU (5 mol%).

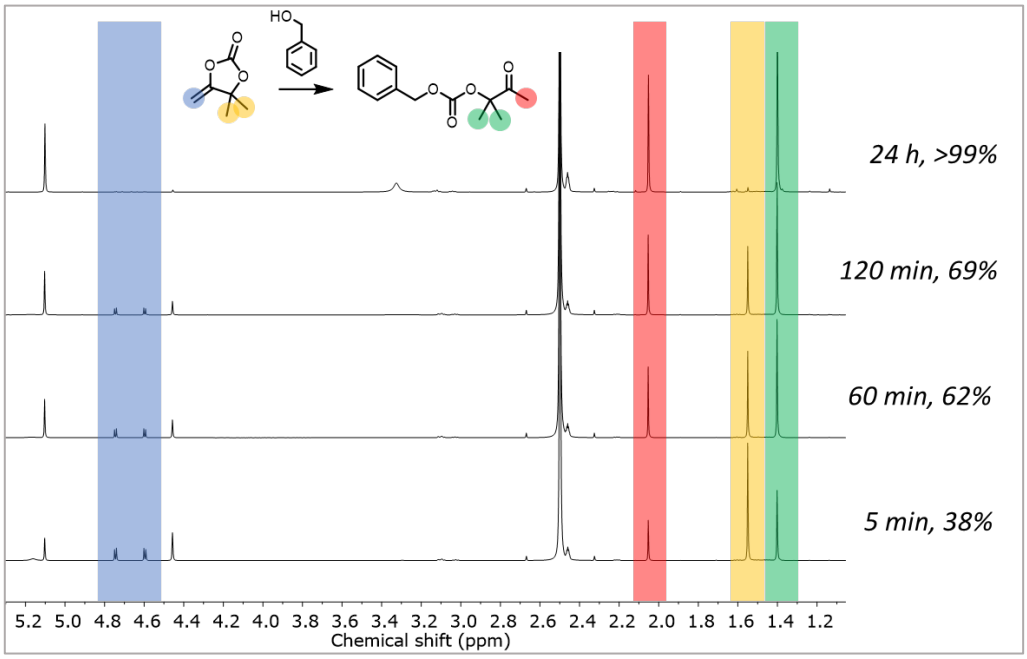

Figure S3. ^{1}H-NMR (in DMSO-d_6) monitoring of the reaction of **αCC** with **A3**, at 25 °C, catalyzed by DBU (5 mol%).

Model reactions between αCC and alcohols at 80 °C monitored by ^{1}H NMR spectroscopy

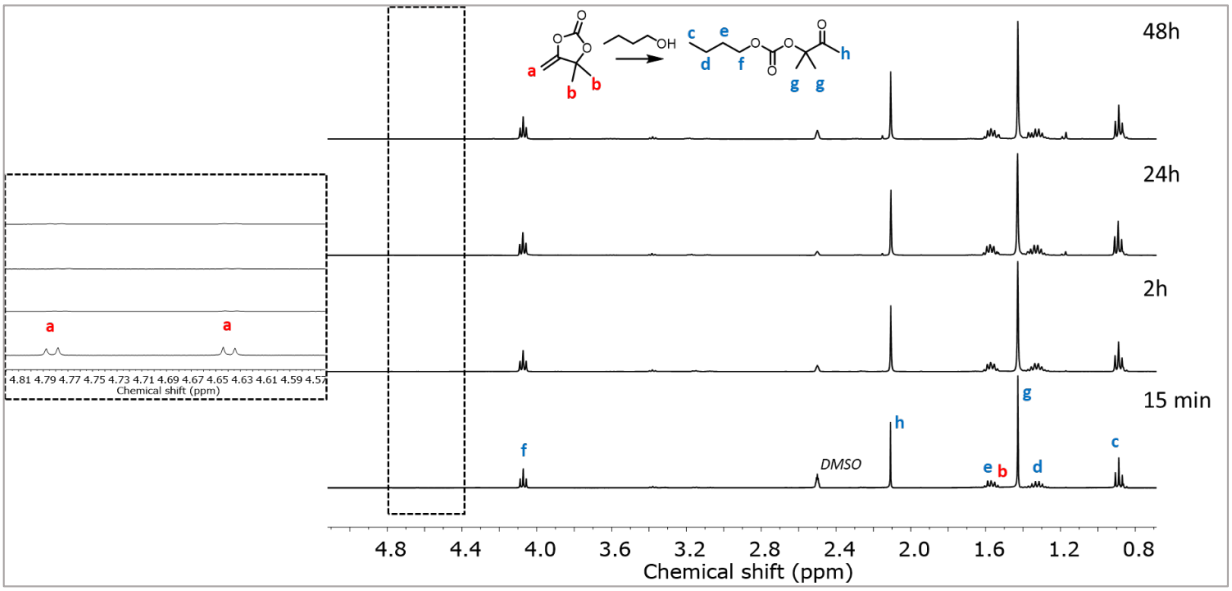

Figure S4. ^{1}H-NMR (in DMSO-d_6) monitoring of the reaction of **αCC** with **A1**, at 80 °C, catalyzed by DBU (5 mol%).

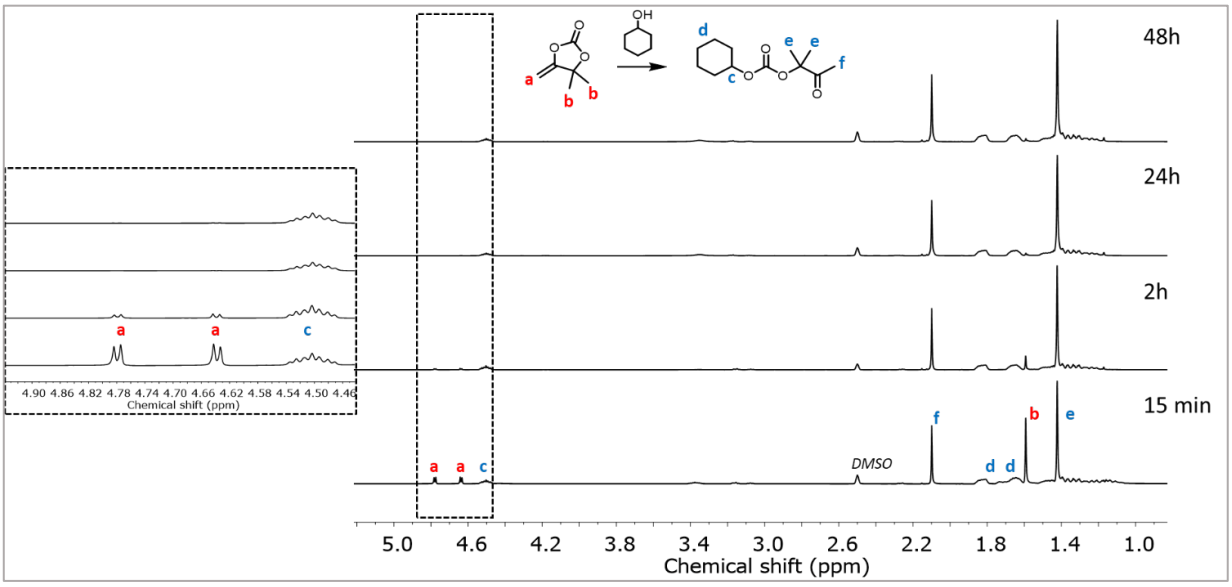

Figure S5. ^{1}H-NMR (in DMSO-d_6) monitoring of the reaction of **αCC** with **A2**, at 80 °C, catalyzed by DBU (5 mol%).

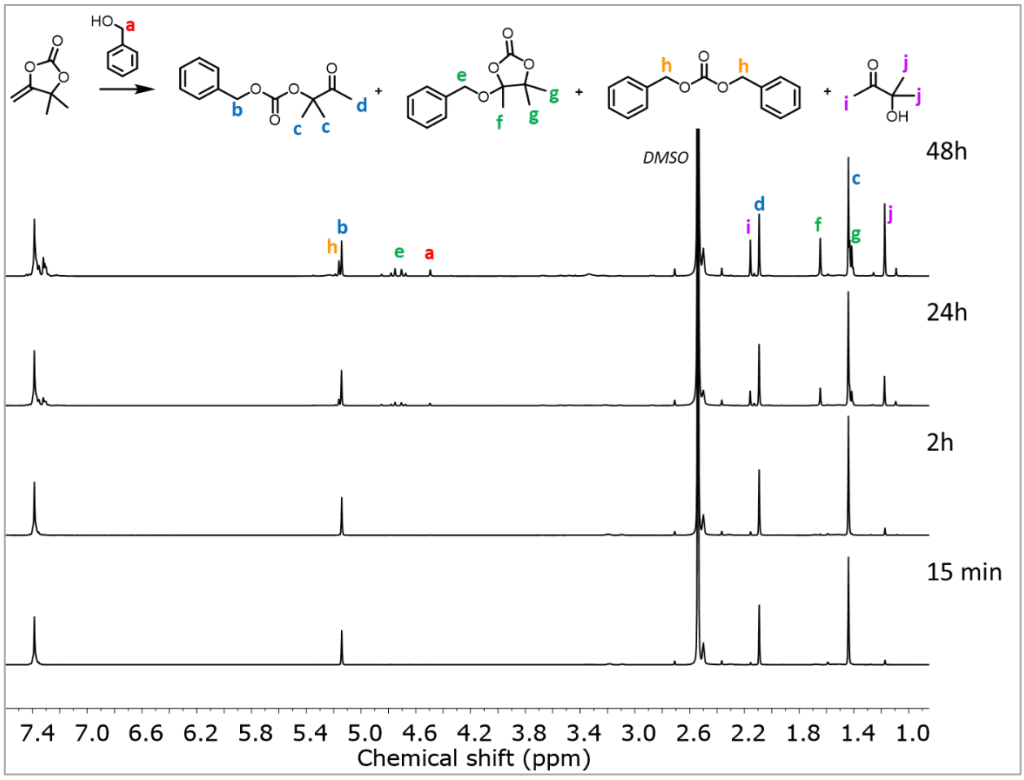

Figure S6. ^{1}H-NMR (in DMSO-d_6) monitoring of the reaction of **αCC** with **A3**, at 80 °C, catalyzed by DBU (5 mol%).

GC-FID-MS analysis

GC-FID-MS analysis of alcoholysis of αCC with benzyl alcohol (A3) at 80°C

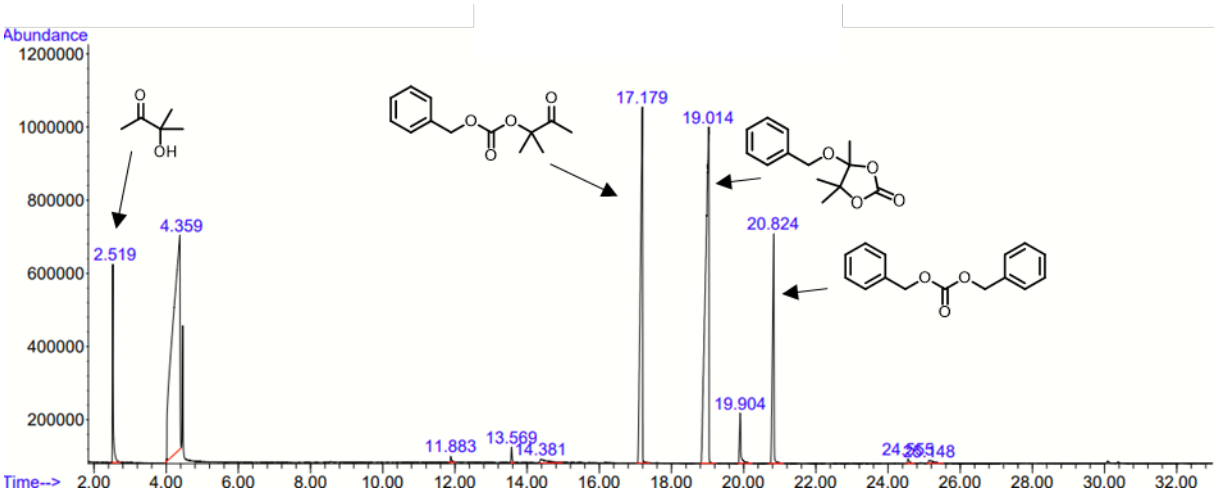

Figure S7. GC-FID analysis of the crude reaction mixture for the reaction of **αCC** with **A3** at 80 °C for 48 h.

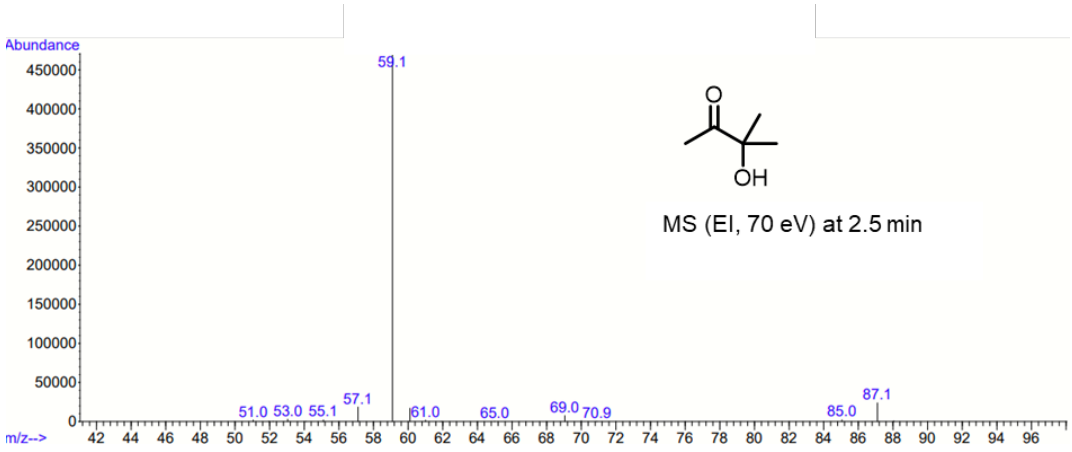

Figure S8. Mass spectrum of the compound eluting at 2.5 min: 3-hydroxy-3-methylbutan-2-one (**4**).

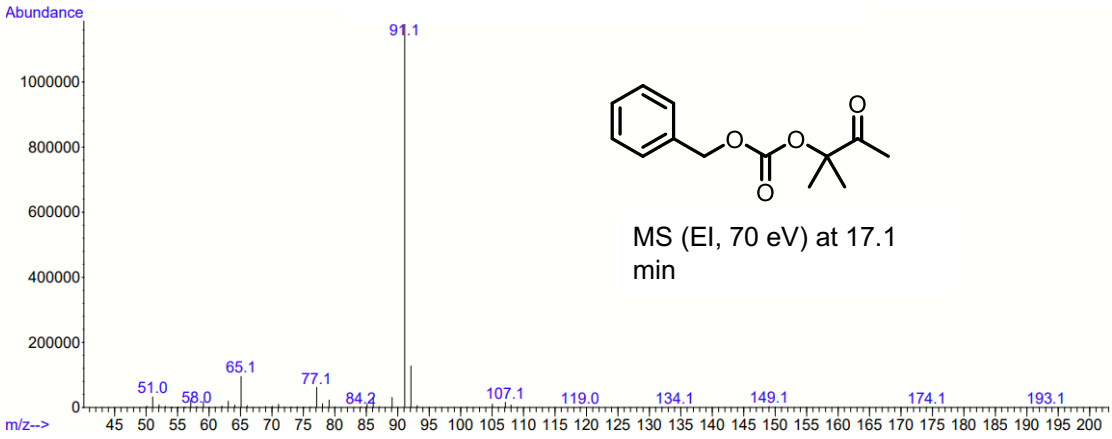

Figure S9. Mass spectrum of the compound eluting at 17.1 min: benzyl (2-methyl-3-oxobutan-2-yl) carbonate (**1**).

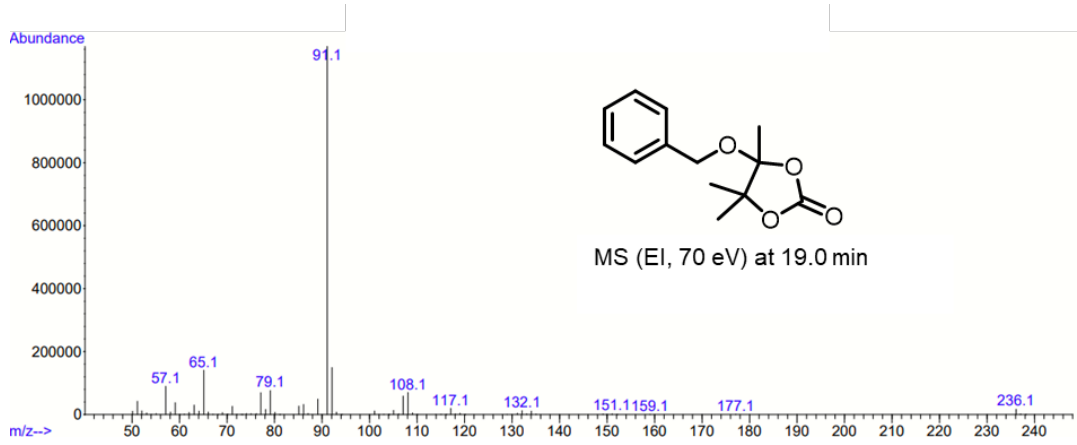

Figure S10. Mass spectrum of the compound eluting at 19.0 min: 4-(benzyloxy)-4,5,5-trimethyl-1,3-dioxolan-2-one (**2**).

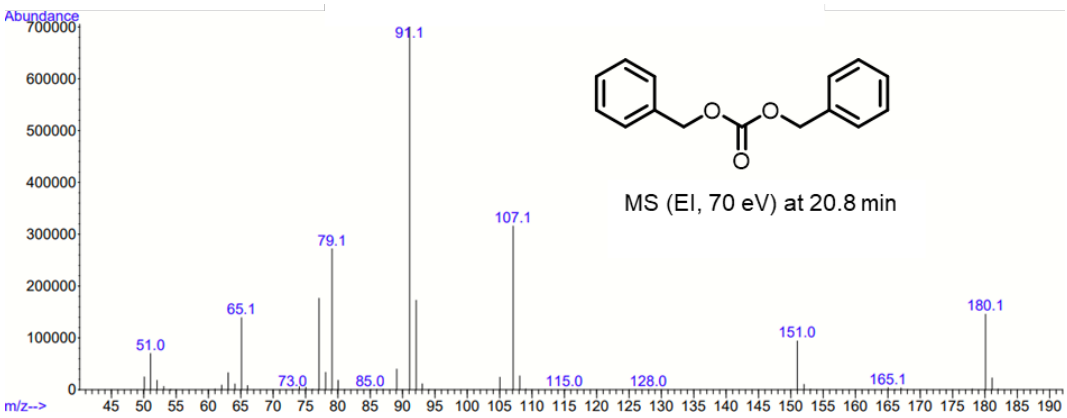

Figure S11. Mass spectrum of the compound eluting at 20.8 min: dibenzyl carbonate (**3**).

MS reference spectra

Reference spectra were obtained from commercially available or synthetized molecules.

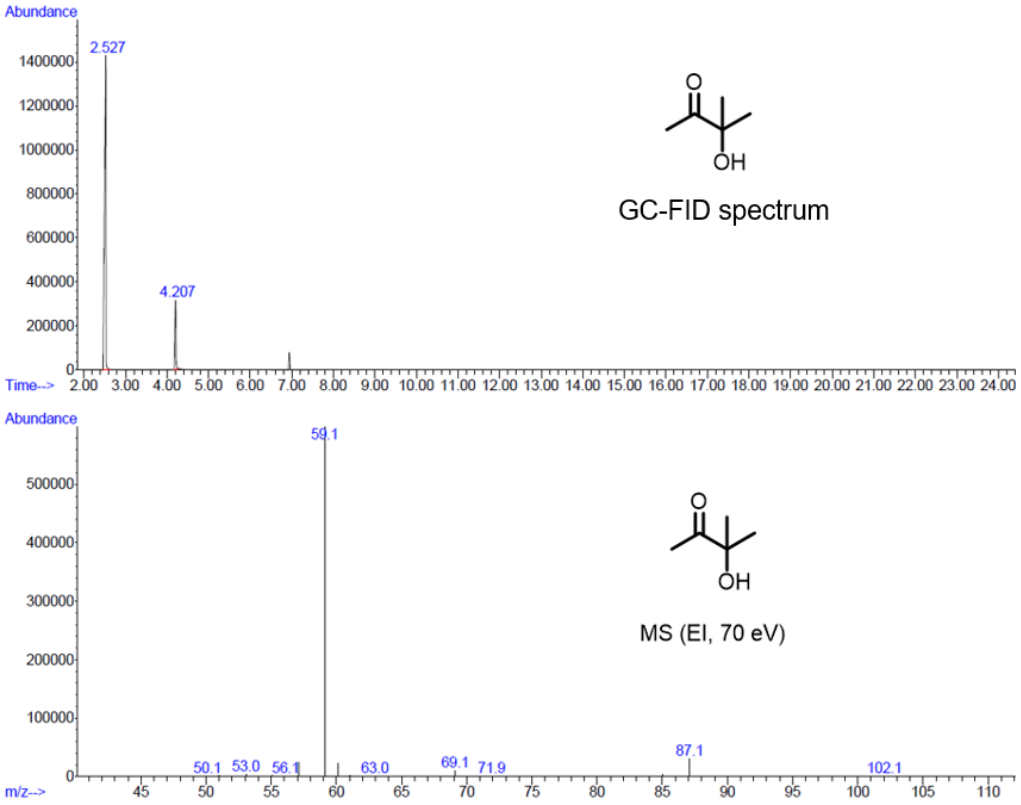

Figure S12. 3-Hydroxy-3-methylbutan-2-one (**4**) GC-FID and MS spectra. The compound elutes at 2.5 min (M=102.1).

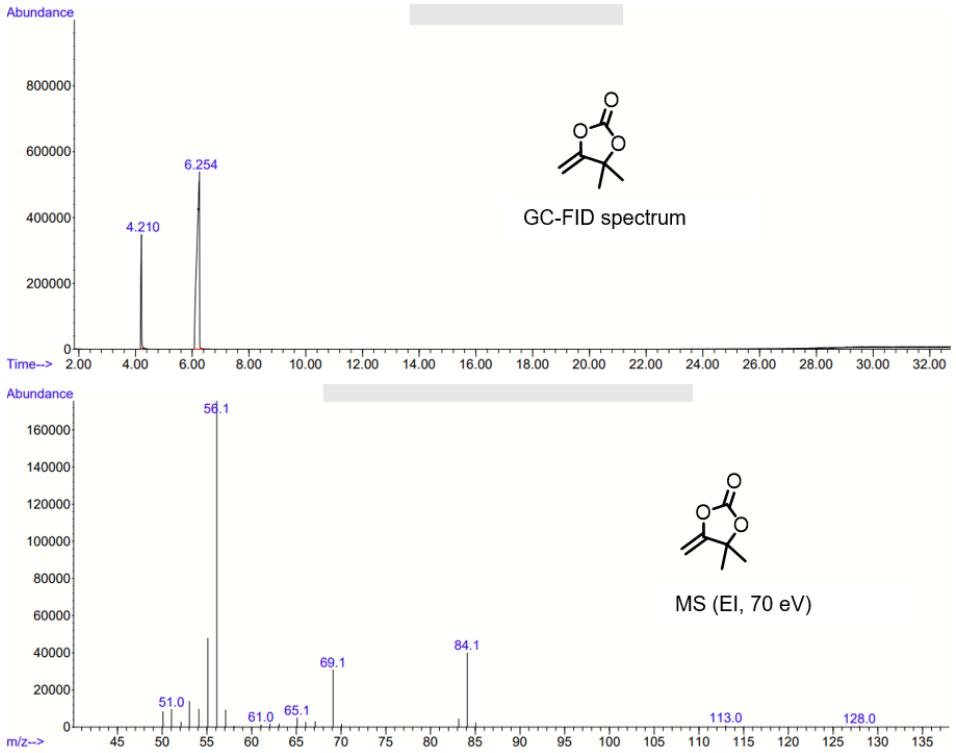

Figure S13. 4,4-Dimethyl-5-methylene-1,3-dioxolan-2-one (αCC) GC-FID and MS spectra. The compound elutes at 6.2 min (M=128.0).

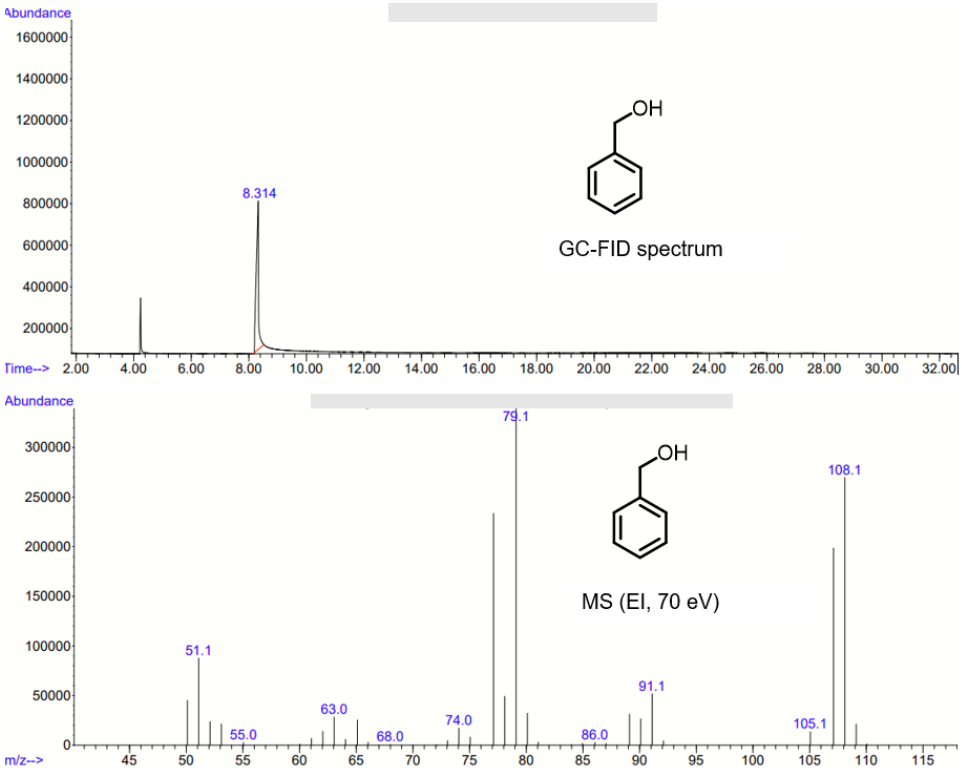

Figure S14. Benzyl alcohol (**A3**) GC-FID and MS spectra. The compound elutes at 8.3 min (M=108.1). The mass spectrum is in accordance with literature.[1]

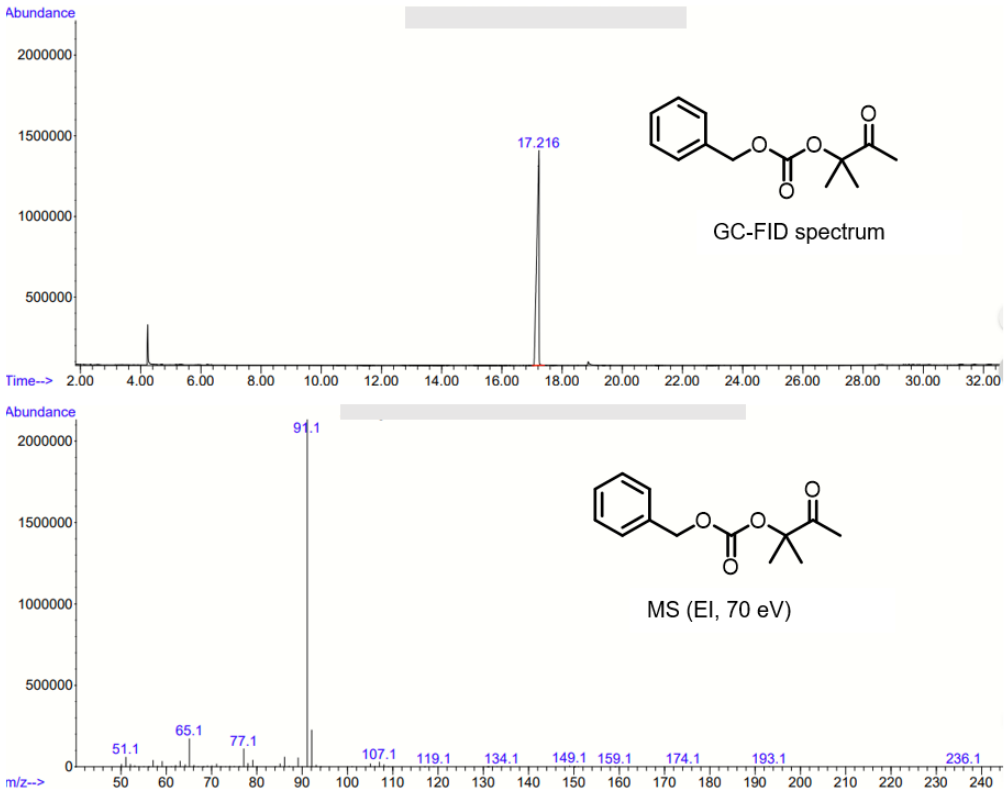

Figure S15. Benzyl (2-methyl-3-oxobutan-2-yl) carbonate (**1**) GC-FID and MS spectra. The compound elutes at 17.2 min (M=236.1).

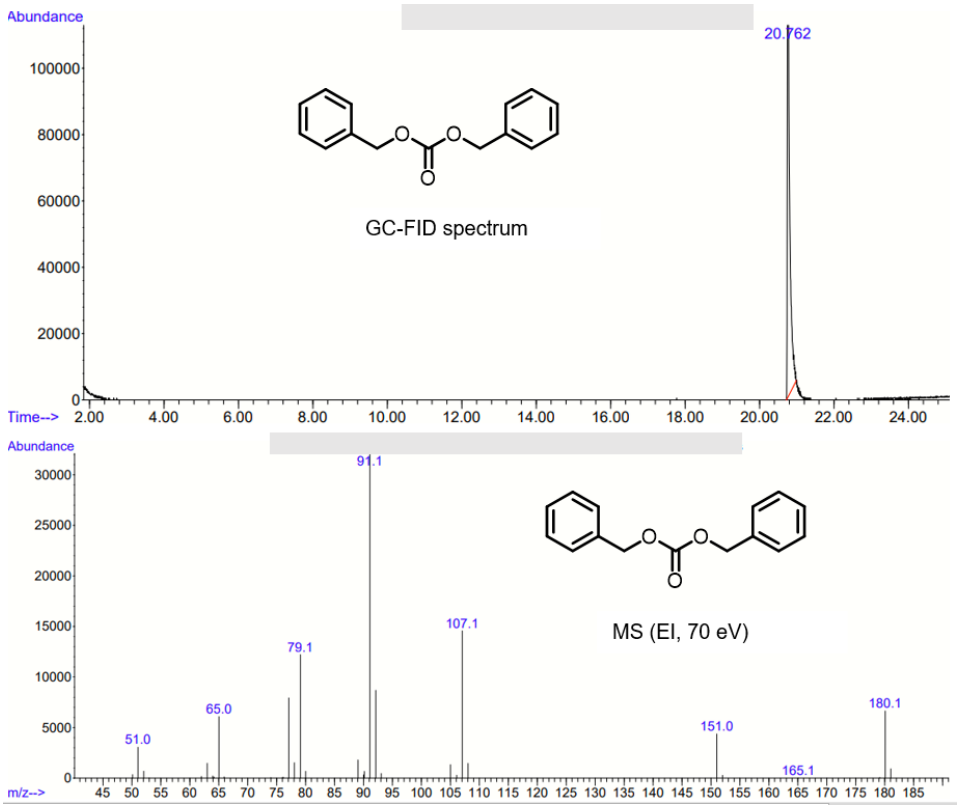

Figure S16. Dibenzyl carbonate (**3**) GC-FID and MS spectra. The compound elutes at 20.8 min (M=180.1). The mass spectrum is in accordance with literature.[2]

DFT calculations

Methodology

Static density functional theory calculations

The ωB97X-D functional is used for all geometry optimizations and transition state (TS) searches. This is a hybrid functional which accounts for non-covalent interactions through an adjusted Grimme D2 dispersion scheme. It is used in combination with triple-ζ basis set adding polarization and diffuse functions to accurately describe TSs and anionic species (6-311++G(d,p)).[3] Furthermore, this functional has shown to give reliable results for medium sized organic molecules and was recently reviewed as one of the hybrid functionals to use in atomistic calculations by Mardirossian et al.[4] Transition-, reactant- and product states are identified by means of a frequency analysis which results in a single negative frequency for a TS and all positive frequencies for reactant - and product states. Additionally intrinsic reaction coordinate (IRC) calculations are performed to assess the correctness of the transition state and obtain corresponding pre- and post-reactive complexes which were then further optimized.[5–8] The solvent , dimethylsulfoxide (DMSO), is accounted for by means of an implicit solvent model: the integral equation formalism variant of the polarized continuum model (IEF-PCM).[9] All calculations are performed with the Gaussian 16 package.[10] A conformational analysis has been performed for all reactant -, product - and transition states, only the most favorable conformations are shown and discussed in this work. Pre- and post-reactive complexes were only optimized starting from the IRC results and were hence not further conformationally analyzed. Reported apparent - and intrinsic barrier heights are with respect to the separate reactants of the pathway and with respect to the pre-reactive complex of the elementary step, respectively.

Reaction kinetics: rate constants (k)

Rate constants k(T) are calculated by using the Eyring-Polanyi equation (see Eq. 2):

$$k(T) = \kappa(T)\frac{k_B T}{h}(c^0)^{1-m}e^{\left(\frac{-\Delta G^{\ddagger}}{RT}\right)} \qquad (Eq.\ 2)$$

Where, κ(T) is the transmission coefficient by convention taken as unity, k_B is the Boltzmann constant ($1.380658.10^{-23}$ J·K^{-1}), R is the universal gas constant (8,314 J·mol^{-1}·K^{-1}), T is the temperature (298 K), h is Planck's constant ($6{,}6260755\cdot10^{-34}$ J·s), c^0 is the standard concentration (1 mol·L^{-1} (M)), m is the molecularity of the reaction and $\Delta G^{\ddagger}$ is the Gibbs free activation energy between the TS and the reactants. Remark that this ignores tunneling effects, more accurate descriptions exist but are beyond the scope of this work, the reader is referred to a review by Truhlar and coworkers).[11] Only multi-molecular reaction rates are presented (with respect to the separate reactants).

Reactivity indices: Parr functions

In order to analyze the chemoselectivity of the nucleophilic attack of the alcohol on *oxo*-carbonate **1** (see Main manuscript) the Parr functions P(r), proposed by Domingo et al, are calculated.[12,13] They are given by the following two equations:

$$P^{-}(r) = \rho_s^{rc}(r) \qquad (Eq.\ 3)$$
$$P^{+}(r) = \rho_s^{ra}(r) \qquad (Eq.\ 4)$$

Where ρ_s^{rc} is the atomic spin density (ASD) at the r atom of the radical cation of the *oxo*-carbonate and ρ_s^{ra} is the ASD at the r atom of the radical anion of the *oxo*-carbonate. The ASD, which are here equal to the Mulliken spin densities, then provide the local electrophilicity $P^{+}(r)$ and the local nucleophilicity $P^{-}(r)$ Parr functions of the neutral molecule. In a review by Domingo et al. it is illustrated that Parr functions are superior to condensed fukui functions for predicting local reactivity for polar reactions.[14]

Non-covalent interactions visualization

The influence of DBU on intermediate stability through intermolecular interactions is analyzed using the Non-covalent interaction (NCI) plot tool, NCIPLOT.[15,16] This plotting tool visualizes non-covalent interactions based on the reduced gradient s and the electron density ρ(r). Furthermore, it allows us to distinguish between weak Van der Waals interactions, strong stabilizing interaction (e.g. hydrogen bonds) and destabilizing interactions (e.g. repulsive interactions) based on the sign of second eigenvalue (λ_2) of the electron-density Hessian and the value of ρ(r). Based on a the graph of s vs. sign(λ_2)ρ(r) a cut-off is chosen to visualize a specific range of interactions, here 0.06 is chosen for the electron density and 0.3 for the reduced gradient. Recently, this tool was successfully applied for the analysis of non-covalent interactions, more specifically cation-π interactions, in the cationic-ring opening polymerization of 2-alkyl-2-oxazoline by one of the co-authors.[17] For more information concerning this tool the reader is referred to the aforementioned literature.

Molecular dynamics

To assess intermediate stability and gain valuable insights into the activity of DBU, regular molecular dynamics (MD) simulations at the DFT level are performed accounting for the solvent environment explicitly (Figure S17). Both benzyl alcohol and butanol are considered because it is expected that cyclohexanol will have a similar behavior as butanol as both are aliphatic alcohols which are fully saturated. All simulations are performed at operating conditions, i.e. 1 atm and 25 °C.

System set-up

In order to construct a realistic solvent box in which the system under investigation is solvated by a single solvent layer of DMSO (<60 molecules), a force field calculation is performed in the isothermal-isobaric ensemble to produce a solvent box with a corresponding realistic density, which closely represents the experimental system. An initial configuration is constructed for the reactant structures with 60 DMSO molecules using Packmol.[18] The subsequent equilibration run is performed with the GPU accelerated OpenMM code in combination with the recently developed Parsley force field by the Open Force Field consortium (Parsley v1.0.0.).[19–21] Prior to this run it is checked whether the Parsley force field is able to reproduce the experimental density for a pure DMSO solvent box, which is the case. The temperature is controlled using a Langevin thermostat and the pressure is controlled using a Monte Carlo barostat implemented within the OpenMM software package. The resulting cubic solvent box dimension, which were then used in the ab intio NVT simulations, are 19.779 x 19.779 x 19.779 Å³ for benzyl alcohol (Figure S17) and 19.777 x 19.777 x 19.777 Å³ for butanol. For Pathway 3 no adjustments were made (apart from adding an extra alcohol molecule), however the influence on the resulting density and qualitative observations is expected to be negligible. Solvent boxes for production runs are then generated based on pre- and/or post-reactive complexes from the static calculations and 60 DMSO molecules accounting for the obtained box dimensions.

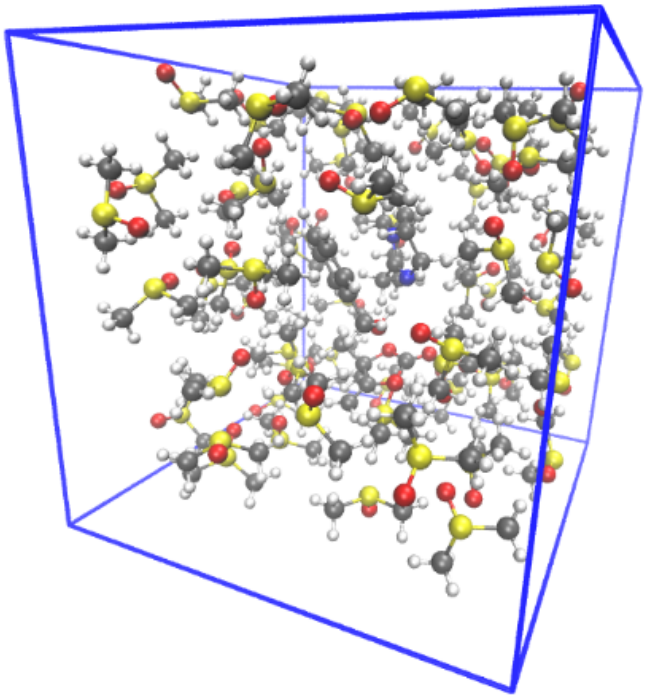

Figure S17. Initial solvent box configuration for benzyl alcohol, αCC1 and DBU with 60 DMSO molecules, created with Packmol. Periodic box is shown in blue with dimensions 19.779 x 19.779 x 19.779 Å³.

Ab initio molecular dynamics simulations

The molecular dynamics simulations, using the aforementioned box dimensions, are performed in the canonical (NVT) ensemble at 298 K using the CP2K software (CP2K 6.1).[22] The temperature is controlled using a Nosé-hoover thermostat.[23,24] To integrate the equations of motion a time step of 0.5 fs is used. The self-consistent field (SCF) convergence criterion was fixed at 10^{-5} Hartree. The BLYP functional is chosen for the energy calculations with inclusion of D3 dispersion corrections and the TZVP-GTH basis set.[25–27] This basis set combines both Gaussian basis function and plane waves, furthermore a screening was performed for an optimal associated cut off energy which amounted to 300 Ry and is used for all atoms.[25,28–31] Analysis of all trajectories is performed with MDTraj.[31] Equilibration runs are incorporated in the analysis as the meta-stable intermediates already rearranged during this phase. Depending on the stability of the analyzed intermediate, different starting structures were used to investigate the effect of the DBU positioning.

Computational results

Here we present the results from a thorough mechanistic study on the conversion of αCC1 with various alcohols in the presence of the bicyclic amidine base 1,8-diazabicyclo[5.4.0]undec-7-ene (DBU) catalyst. The DBU catalyst is accounted for in all reaction steps in which it can play an active role either through hydrogen bonding or by actively taking part as an acid-base catalyst. As mentioned previously, the solvent is accounted for implicitly in the static calculations and explicitly in the regular MD simulations. Important to note is the role of DBU throughout the simulations, DBU has an increased interest as a green, recyclable catalyst which can potentially be used both as a Lewis-base catalyst but also as a nucleophile in which it activates reactant species, mostly its activity is attributed to its capacity to act as a Lewis-base and stabilize different states through hydrogen bonding.[32–38] It is hence a multipurpose catalyst which is far from completely understood. Hence it is attempted to unravel its activity within this specific system.

Reactants

As mentioned in the Main manuscript, the alcohols remain in a neutral state due their corresponding pKa values, indicating the equilibrium is in favor of the neutral alcohol.

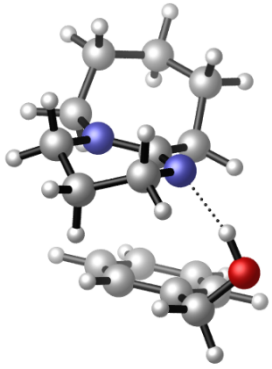

Figure S18. Optimized benzyl alcohol-catalyst complex. (ωB97-XD/6-311++G**, iefpcm(ϵ=46.826), 298 K)

This is on one hand seen throughout the static calculations because we were unable to identify a stable alkoxide both in pre-reactive complexes (see green bonds in TS-s1 of all located pathways, indicating that the bond is broken and hence the hydrogen-bonded complex is formed instead of the corresponding salt) nor in separate calculations optimizing the DBU-alcohol configuration (Figure S18). For all alcohols a distinct hydrogen-bond is observed between the alcohol and the DBU. Also the MD simulations of the reactants confirm that the alcohol indeed remains neutral (Figure S19). Furthermore, in line with the static calculations, a hydrogen-bonded complex prevails throughout the simulations for both butanol and benzyl alcohol which is shown by the short (< 2 Å) distance between the alcoholic hydrogen and DBU nitrogen. It can hence be concluded that the use of an aprotic solvent is key for this system because the DBU and alcohol will form a strong hydrogen-bonded complex which will facilitate subsequent reactions. This feature of the DBU-alcohol system (the instability of the alkoxide) is important to keep in mind as it rules out several mechanisms of which a few are shown below.

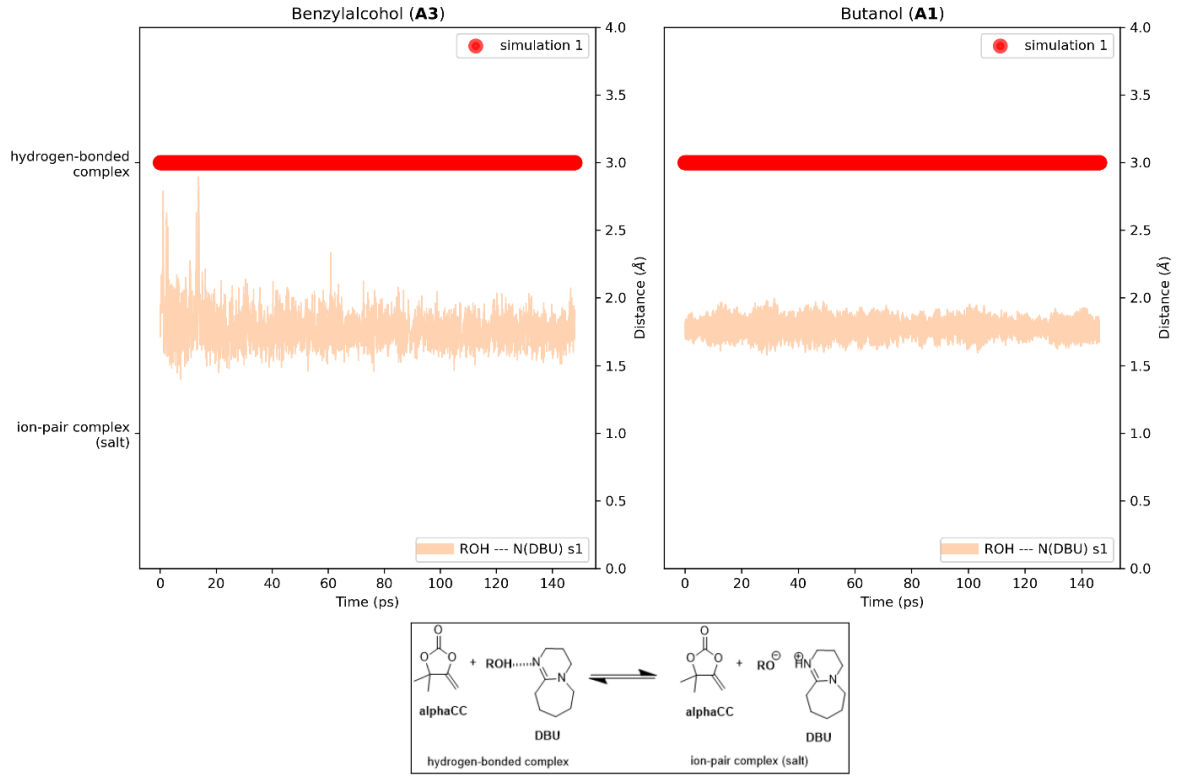

Figure S19. Evolution of the reactant complex in an explicit solvent simulation (y-axis left), and evolution of the hydrogen bond distance (y-axis right). Benzyl alcohol (**A3**) and butanol (**A1**). (BLYP-D3/TZVP-GTH, 60 DMSO molecules, 298 K, 1 atm).

Pathway 1

The minimal free energy profile for pathway 1, see *Main manuscript* Scheme 3, for benzyl alcohol, butanol and cyclohexanol is shown in Scheme S1. Here we will shortly highlight the different steps and features of the pathway however for a discussion on the energetics the reader is referred to the *Main manuscript*.

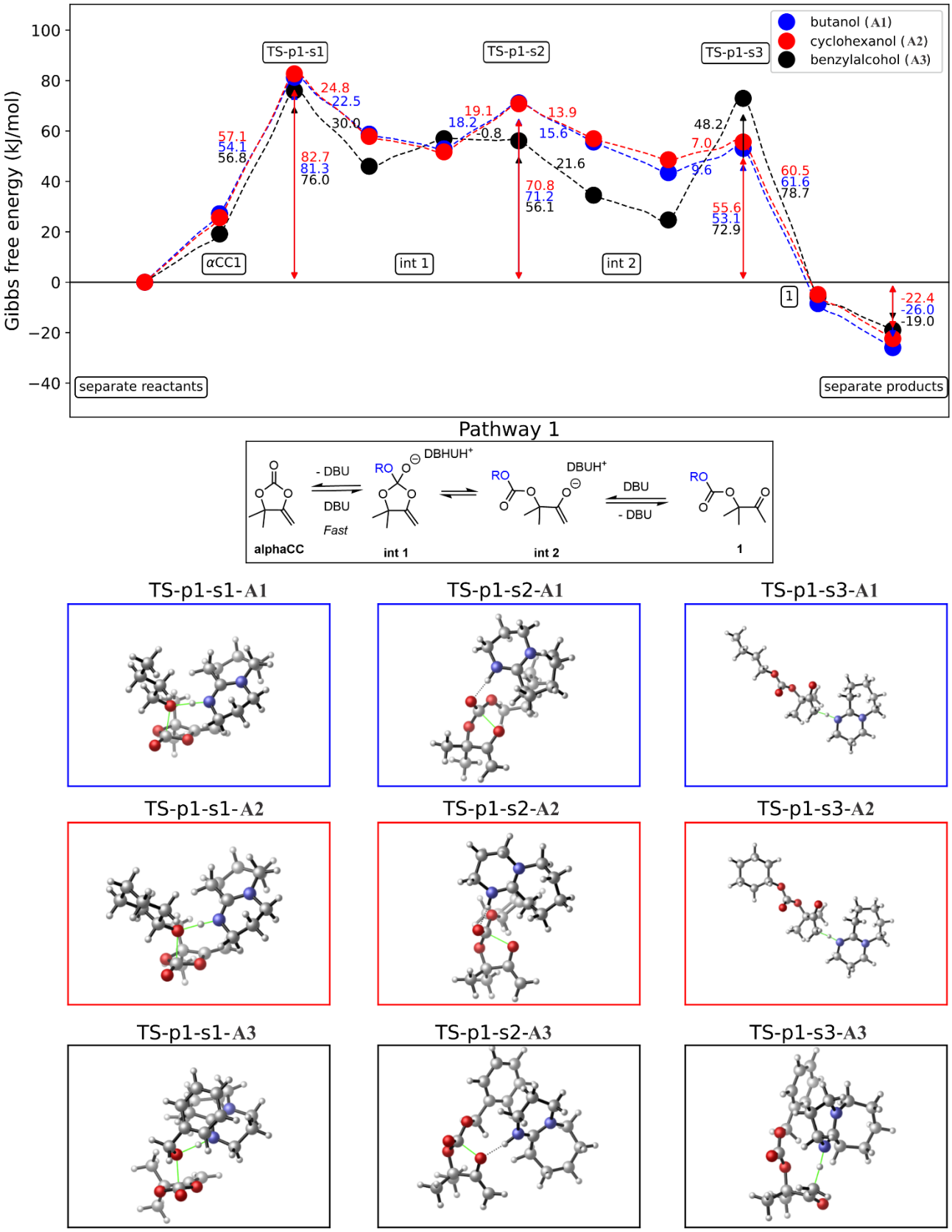

Scheme S1. Gibbs free energy profile with the corresponding reaction scheme and transition state structures for pathway 1 (p1), with formation of *oxo*-carbonate **1**. Green bonds in the TS figures indicate bonds which are broken or formed. Arrows indicate Gibbs free energy differences with respect to the separate reactants displayed next to them. Energies in kJ·mol^{-1}. (ωB97-XD/6-311++G**, iefpcm(ε=46.826), 298 K, 1 atm).

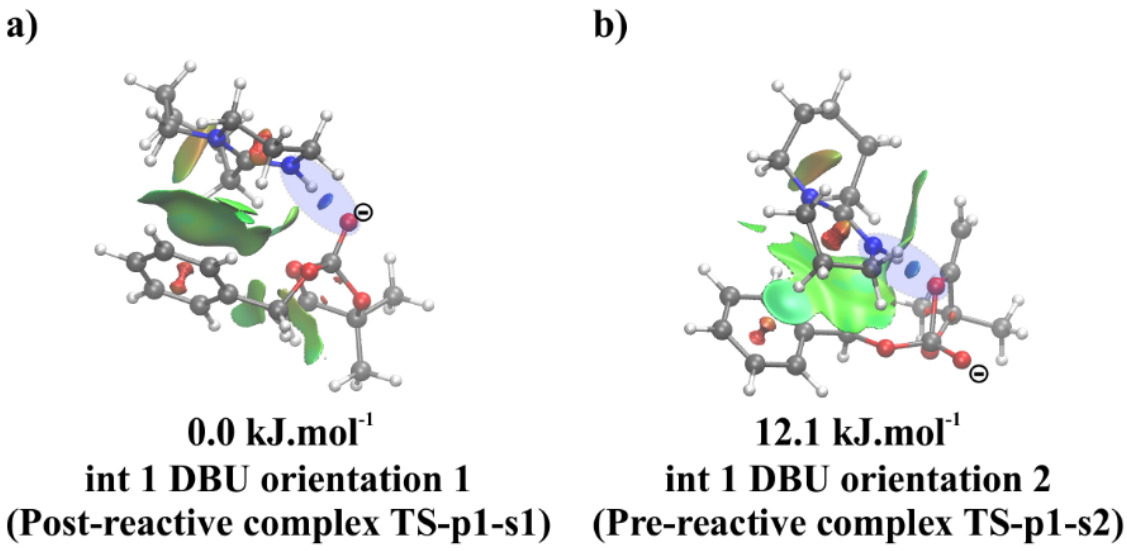

Figure S20. Nci-plots for 2 different conformations of int 1 for benzyl alcohol DBU-oxygen coordination is highlighted by the blue ellipse. a) DBU-H^+ is coordinated to the oxyanion; b) DBU-H^+ is coordinated to the oxygen atom which is the oxyanion in **int 2**.

In the first step a nucleophilic attack occurs of the alcohol forming **int 1**. Remark that deprotonation of the alcohol occurs in a concerted fashion here (indicated by the green bonds in TS-p1-s1) meaning that the pre-reactive complex of step 1 is the neutral DBU and alcohol, not the alkoxide and DBU-H^+. Remarkable is the relatively high difference between post- and pre-reactive complexes for the subsequent steps. Despite representing the same molecular state, relative free energies differ significantly due to the positioning of the DBU-H^+ with respect to the side chain, hence the used alcohol, and the oxyanion. This is illustrated in Figure S20, which indicates that depending on the DBU-H^+ positioning (with which moiety it is forming a hydrogen bond) stability can be altered. In case of benzyl alcohol, we can see that the pre-reactive complex of step 2 will spontaneously rearrange towards **int 2**. This highlights an important feature of the DBU catalyst and of **int 1**, i.e. hydrogen bonding with DBU-H^+ can increase (or decrease) intermediate stability (remark that one could also refer to this bond as an ionic bond). This concept is further illustrated through MD simulations of **int 1** for benzyl alcohol (**A3**), see Figure S21 (left) simulation 2 and simulation 3 (remark that different starting configurations are used in each simulation, in this case for **int 1**).

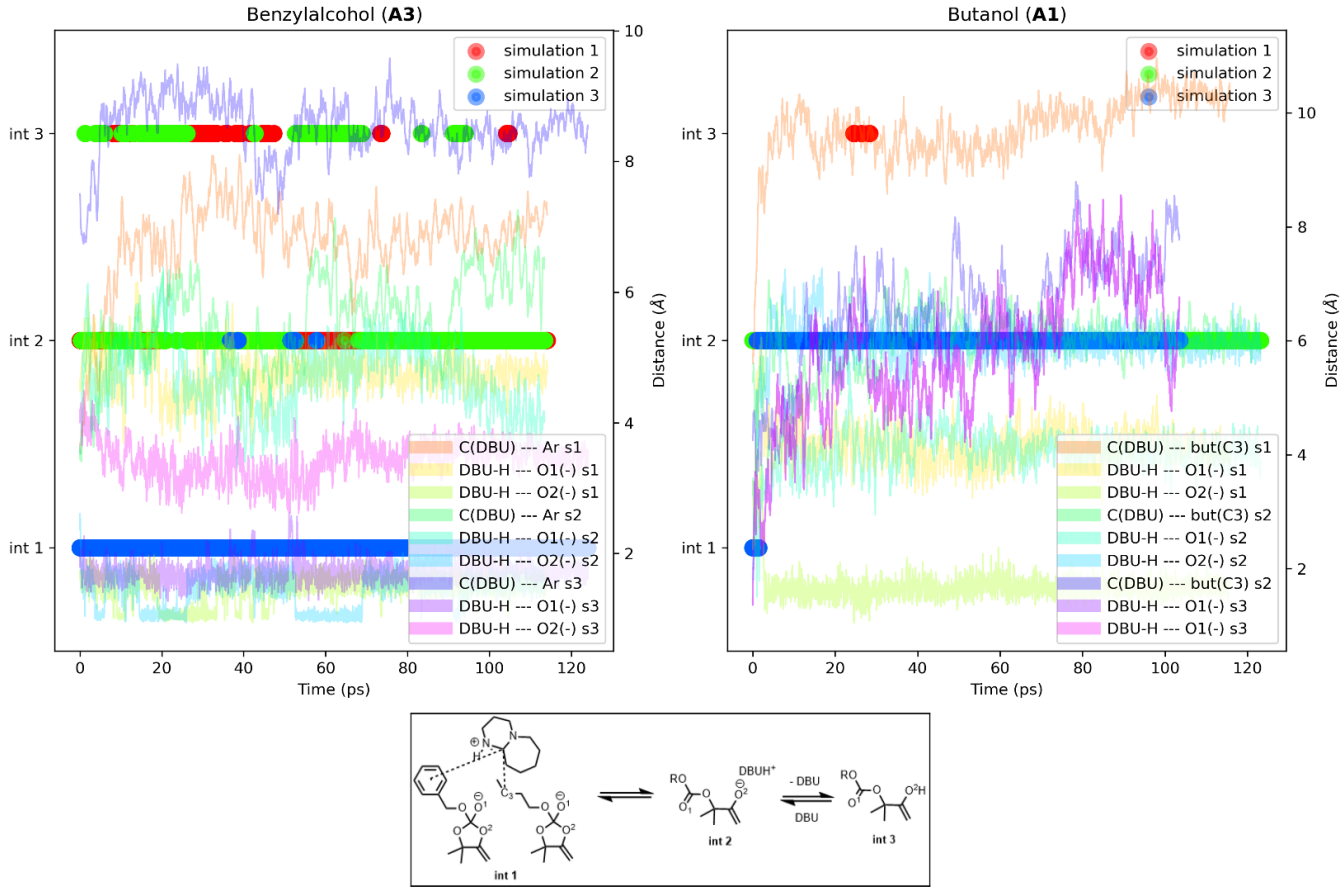

Figure S21. Evolution of different starting configurations for the intermediates of pathway 1 in explicit solvent simulations for benzyl alcohol (**A3)** and butanol (**A1**). (BLYP-D3/TZVP-GTH, 60 DMSO molecules, 298 K, 1 atm).

Both simulations 2 and 3 start from different conformation of **int 1** with DBU-H$^+$ but for simulation 2 ring opening occurs which does not for simulation 3 (showing close coordination of DBU-H$^+$ towards O^1). This thus confirms that DBU, or the hydrogen bond between DBU-H$^+$ and the intermediate, can greatly affect intermediate stability. Simulaton 1 starts from **int 2** and is in equilibrium with **int 3**. For butanol, all simulations start from different starting configurations of int 1 and all resulted in ring opening of **int 1**, no starting conformations were found which resulted in the formation of stable **int 1** (see Figure S21 (right)). However based on the static approach we assume this intermadiate is also formed.

Subsequent ring opening with formation of **int 2** can hence be triggered by a change in hydrogen-bonding pattern between DBU and **int 1**. **Int 2** is clearly more stable for benzyl alcohol than for butanol and cyclohexanol because of the presence of these π-type interactions (cation-π and π induced dipole, Figure S20) which are present for both **int 1** and **int 2**, see Figure S20 and Figure 2 in the *Main manuscript*. Furthermore, it is seen in the MD simulation for benzyl alcohol that **int 2** is in equilibrium with **int 3**, this is however not observed for butanol. To elaborate on this difference, **int 3** is calculated statically for both the pre-reactive complex of step 3 for benzyl alcohol and butanol, see Table S1. Remarkably they indicate that for

butanol equilibrium is shifted towards **int 3** (in contrast to **int 2**). The fact this is not observed in the MD simulations indicates that the formation of **int 3** is higher activated than for benzyl alcohol. The results for benzyl alcohol are in line with the MD results because **int 2** is favored in this case, this reaction however occurs spontaneously during the MD results pointing to a lower activation energy which most probably is again because of the π-type interactions lowering the activation barrier. Remark that here no thorough conformational analysis is performed on the pre-reactive complex.

Table S1. Relative stabilities of **int 2** and **3** for benzyl alcohol and butanol. ΔG° = G(**int 3**) – G(**int 2**). Free energie difference in $kJ \cdot mol^{-1}$. (ωB97-XD/6-311++G**, iefpcm(ϵ=46.826), 298 K, 1 atm).

Alcohol	ΔG^0
Benzyl alcohol	10.5
Butanol	-19.6

Formation of *oxo*-carbonate **1** is then caused by a proton-transfer reaction between DBU-H^+ and the negatively charged carbon atom (which is in conjugation with the oxyanion). With respect to αCC1 the formation of **1** is thermodynamically favored. Based on the forward and backward activation barriers and the relative difference between the separate reactants and products we can assume that this reaction is an equilibrium reaction.

In summary for pathway 1, a reversible nucleophilic addition occurs for the different alcohols under investigation. The DBU catalyst has a distinct influence on the intermediate stability through hydrogen bonding and specifically for benzyl alcohol (**A3**) also through π-type interactions. Furthermore, MD simulations reveal formation of **int 3**.

Pathway 2

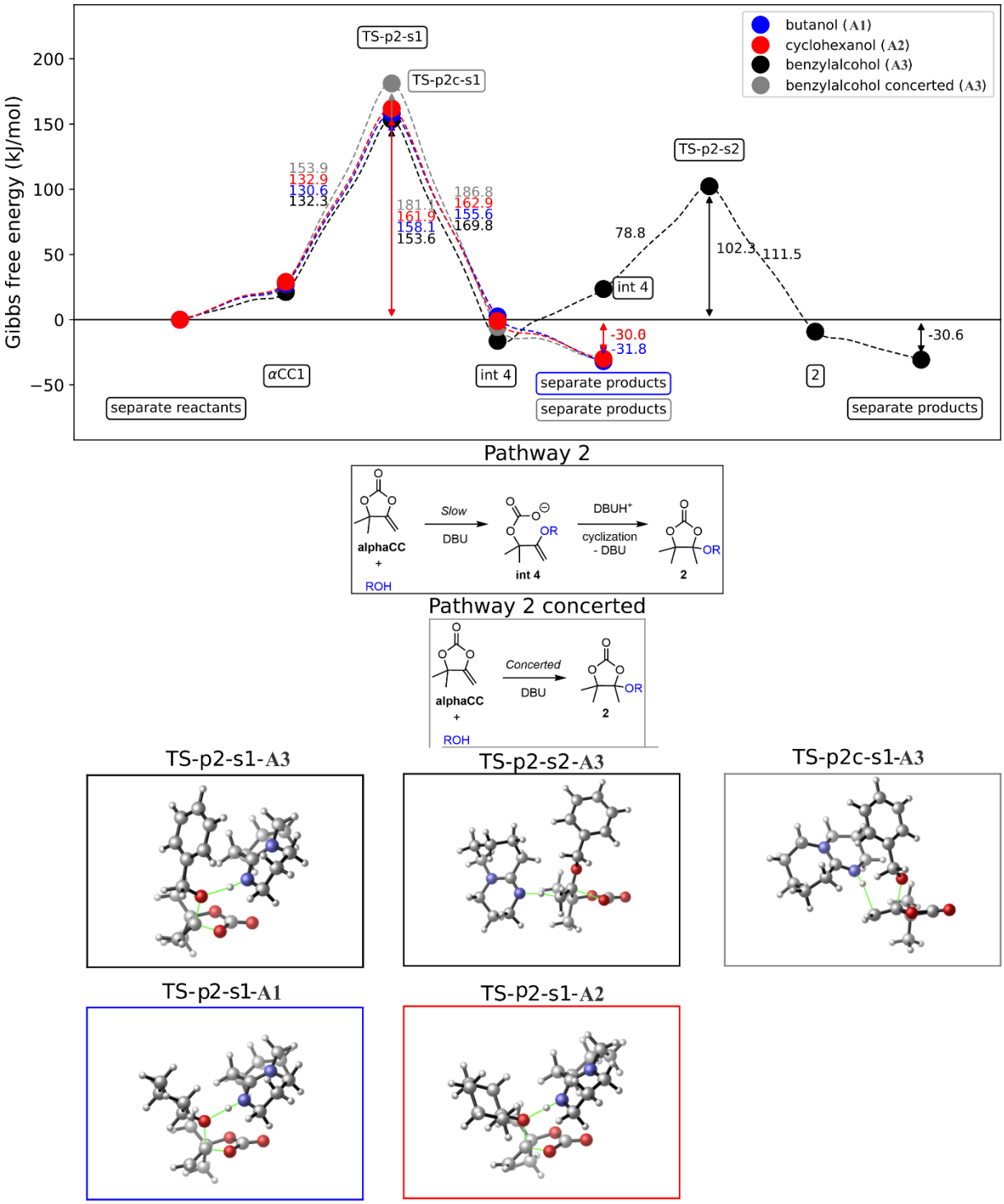

Scheme S2. Gibbs free energy profile with the corresponding reaction scheme and transition state structures for the stepwise mechanism of pathway 2 (p2) and the concerted one (p2c), with formation of tetrasubstituted ethylene carbonate **2**. Green bonds in the TS figures indicate bonds which are broken or formed. Arrows indicate Gibbs free energy differences with respect to the separate reactants displayed next to them. Energies in kJ·mol^{-1}. (ωB97-XD/6-311++G**, iefpcm(ε=46.826), 298 K, 1 atm)

In accordance to our previous theoretical work regarding the use of thiols instead of alcohol, we have investigated the tetrasubstituted ethylene carbonate formation pathway for the alcohols under investigation.[39] Again, two mechanisms are found for this pathway, a concerted one and a stepwise one.

The results are shown in Scheme S2. Remark that step 2 is not modelled for butanol and cyclohexanol because this pathway is deemed unfeasible based on the highly activated first step. Furthermore, an alternative, more feasible pathway is found (Pathway 3, *vide infra*). The rate-limiting step for this pathway, is again the nucleophilic addition of the alcohol (with 'simultaneous' proton transfer). However, as we can see from both apparent and intrinsic activation energies, the different alcohols show no significant differences for this step. Furthermore, the barrier heights are rather high especially when we compare these to Pathway 3 which represents a new proposal for the formation of **2**. We are hence unable to explain the experimental results based on pathway 2, however pathway 3 is able to explain the formation of tetrasubstituted ethylene carbonate **2** and will be discussed in the following section.

The concerted mechanism for benzyl alcohol is even more unfeasible as the apparent barrier height is increased by almost 20 $kJ \cdot mol^{-1}$. Alternatively, one could also form tetrasubstituted ethylene carbonate **2** via the mechanism shown in Scheme S3. However, taking the observations into account for the reactants species we can assume that formation of the alkoxide is not possible for the systems under investigation and it would immediately react towards **2** which is thus equal to the concerted reaction mechanism shown in Scheme S2.

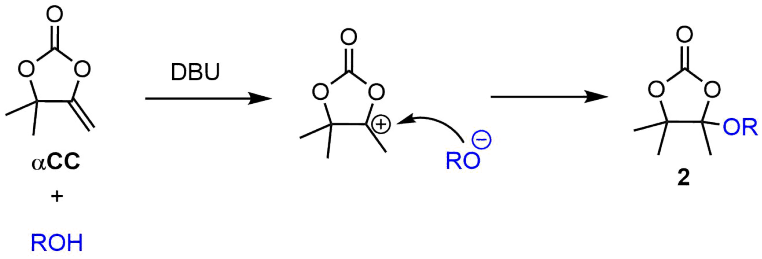

Scheme S3. Stepwise alternative for the formation of tetrasubstituted ethylene carbonate 2.

For completeness, intermediate stability is assessed at operating conditions for benzyl alcohol, see Figure S22. **Int 4** remains stable throughout the simulation with a strong hydrogen bond present between the oxyanion and DBU-H^+ in simulation 2. For simulation 1 the DBU diffuses away slightly, but **int 4** remains stable nonetheless.

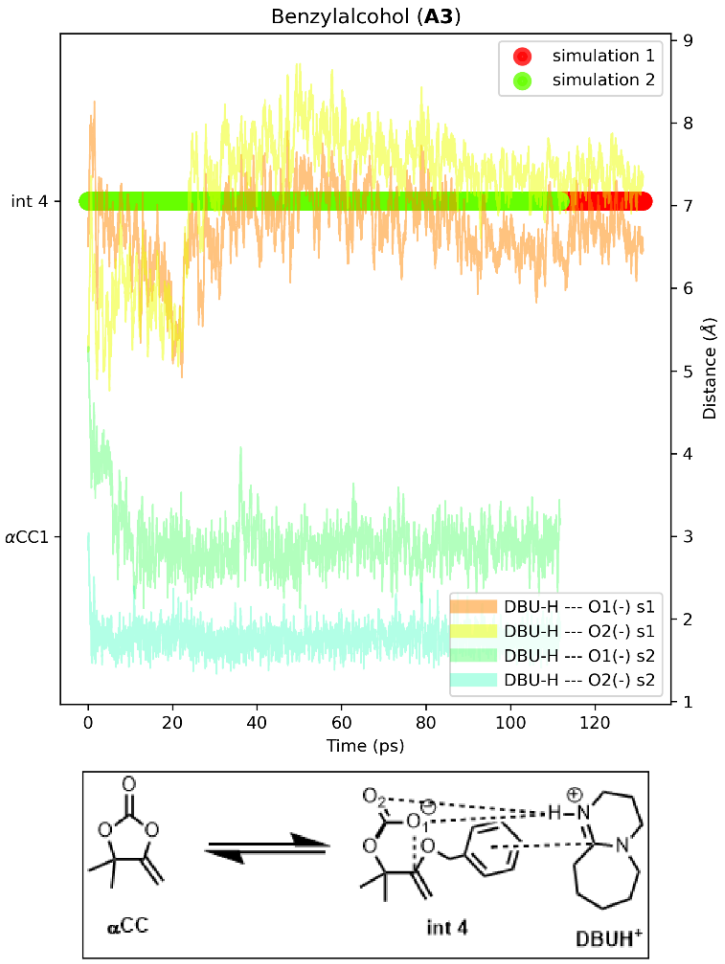

Figure S22. Evolution of different starting configurations for the intermediates of pathway 2 in explicit solvent simulations for benzyl alcohol (**A3)** and butanol (**A1**). (BLYP-D3/TZVP-GTH, 60 DMSO molecules, 298 K, 1 atm).

Pathway 3

In search for a new tetrasubstituted ethylene carbonate **2** formation route we present here an alternative pathway. This pathway is much more feasible than Pathway 2 as apparent barrier heights are drastically decreased and experimental observations can be explained. The results are shown in Scheme S4. This pathway is also thoroughly discussed in the *Main manuscript.*

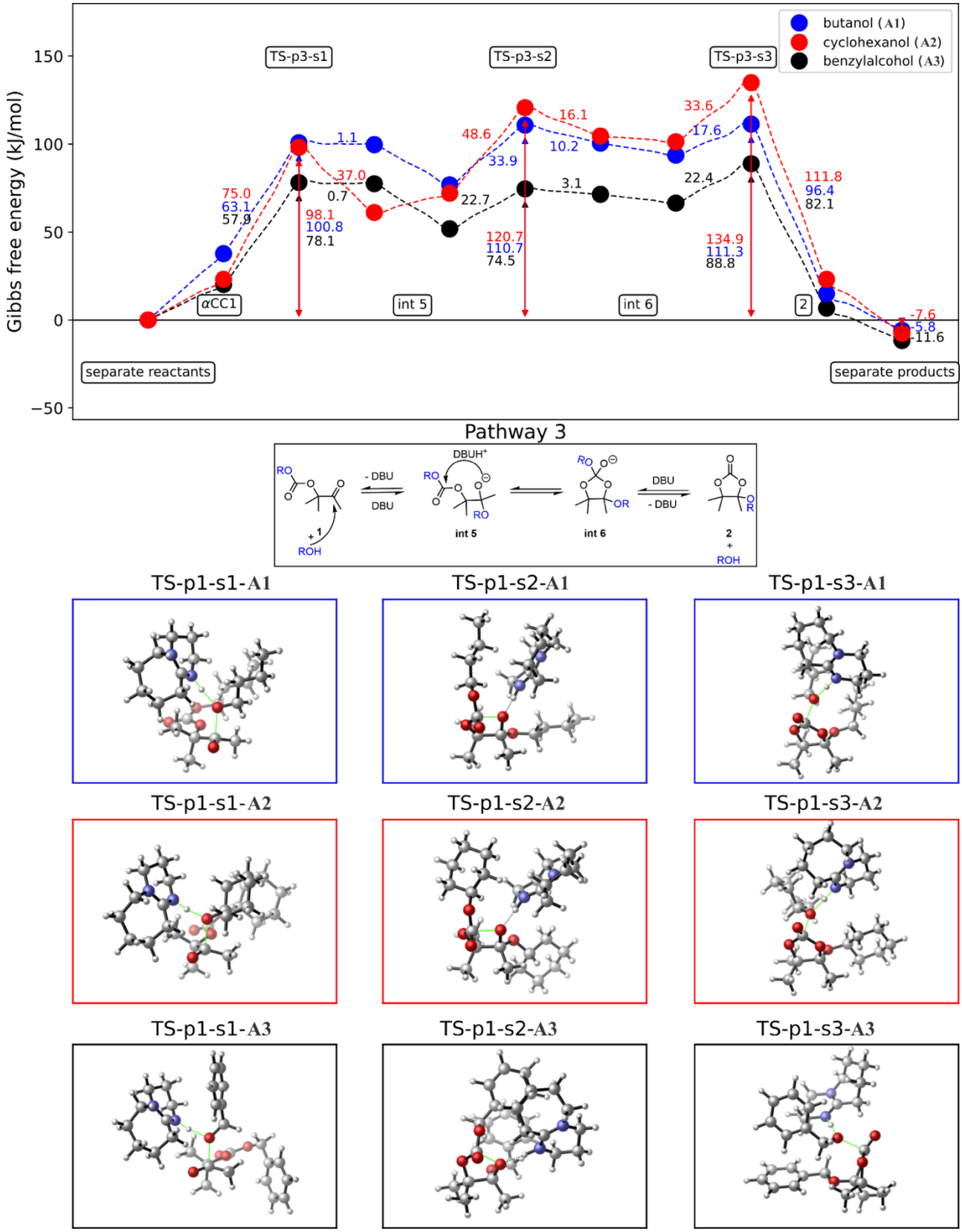

Scheme S4. Gibbs free energy profile with the corresponding reaction scheme and transition state structures for pathway 3 (p3), with formation of tetrasubstituted ethylene carbonate **2** starting from *oxo*-carbonate **1** and an extra alcohol molecule. Green bonds in the TS figures indicate bonds which are broken or formed. Arrows indicate Gibbs free energy differences with respect to the separate reactants displayed next to them. Energies in kJ·mol^{-1}. (ωB97-XD/6-311++G**, iefpcm(ϵ=46.826), 298 K, 1 atm)

Similar to Pathway 1 and 2, the nucleophilic attack of the alcohol is the rate-determining step for this pathway with formation of **int 5**. In contrast to pathway 2, here we start from the previously formed *oxo*-carbonate **1** instead of **αCC**. As equimolar ratios are used, the attacking alcohol originates from its liberation through the reverse pathway 1, which is an equilibrium reaction. Subsequently ring closure occurs with formation of **int 6**. This intermediate appears to be a meta-stable state as the reverse barrier heights are rather low, especially for benzyl alcohol. This is confirmed in the regular MD simulation, see Figure S23. Here one can see that the simulations starting from different configurations for **int 6**, i.e. simulation 2 and 3 for benzyl alcohol (**A3**) and simulation 1 and 2 for butanol (**A1**), spontaneously rearrange towards **int 5** and subsequently to **int 7** which is similar to the observation made for **int 1** for pathway 1 (see Figure S21 simulation 2). Starting from **int 5**, i.e. simulation 1, this is also true. However, **int 7** is not formed in the static approach and we can hence assume that formation of this intermediate at operating conditions can affect the equilibria between **1** and **int 5**. To verify that **int 7** is more stable than **int 5**, the relative stability is calculated which is shown in Table S2. This indeed agrees with what is seen at operating condition during the MD simulations because the equilibrium lies strongly in favor of **int 7**. Similar observations are made for butanol, see Figure S23 and Table S2.

Subsequently the alcohol moiety is expelled from **int 6** with formation of the corresponding tetrasubstituted ethylene carbonate **2** and alcohol. These are slightly more stable than the reactants which should hence favor its formation.

Table S2. relative stabilities of **int 5** and **int 7** for benzyl alcohol and butanol. **Int 7** is formed from a conformationally optimized **int 5** configuration. $\Delta G° = G(\text{int 7}) - G(\text{int 5})$. Free energy difference in $kJ.mol^{-1}$. (ωB97-XD/6-311++G**, iefpcm(ε=46.826), 298 K, 1 atm)

Alcohol	ΔG^0
Benzyl alcohol	-11.7
Butanol	-17.3

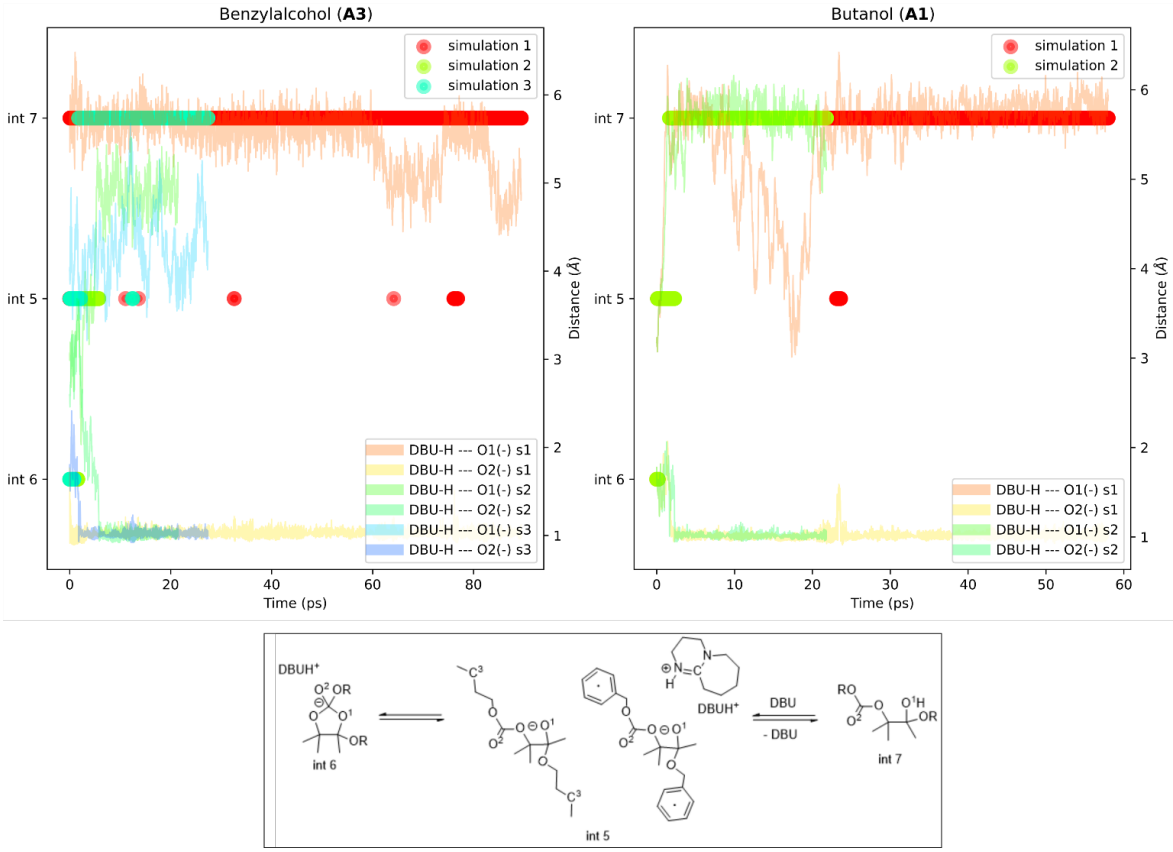

Figure S23. Evolution of different starting configurations for the intermediates of pathway 3 in explicit solvent simulations for benzyl alcohol (**A3)** and butanol (**A1**). (BLYP-D3/TZVP-GTH, 60 DMSO molecules, 298 K, 1 atm)

Chemoselectivity of the DBU-catalyzed addition of alcohol to *oxo*-carbonate.

To elaborate on the difference in chemoselectivity of the alcohol attack on *oxo*-carbonate **1**, i.e. its preferential addition to the ketone (C=O) or carbonate ((O)C=O) group (Scheme S5), Parr functions are calculated with $P^+(\mathbf{r})$ representing the local electrophilicity and $P^-(\mathbf{r})$ the local nucleophilicity of the neutral molecule (see Section 3.1.3).

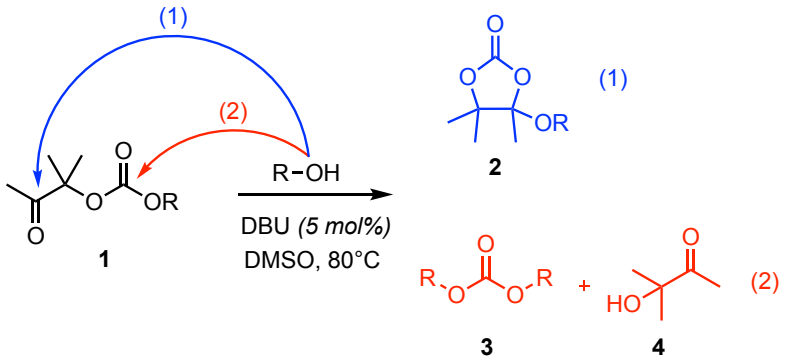

Scheme S5. The two possible DBU-catalyzed addition modes for the alcohol to *oxo*-carbonate.

The highest value of $P^+(\mathbf{r})$ represents the most probable site to be attacked by the nucleophile, i.e. the used alcohol. The results are shown in Table S3 and indicate, based on $P^+(\mathbf{r})$, that the C=O site is the most electrophilic one and hence most favored in the attack by the nucleophile,

in line with the experiments. This illustrates that, in case pathway 3 is accessible for the system (Scheme 3, *Main manuscript*), the formation of tetrasubstituted ethylene carbonate **2** is preferential over the transcarbonation route.

Table S3. Electrophilic (P^+(**r**)) and nucleophilic (P^-(r)) Parr functions for the two carbonyl carbon atoms of the respective *oxo*-carbonates.

oxo-carbonate	atom	P^+(r)	P^-(r)
benzyl alcohol (**A3**)	(O)C=O	-0,0166	0,0060
	C=O	0,0010	0,0001
butanol (**A1**)	(O)C=O	0,2771	-0,0031
	C=O	2,5253	-0,0576
cyclohexanol (**A2**)	(O)C=O	0,2583	-0,0038
	C=O	2,5025	-0,0580

For the Optimized Cartesian Coordinates, please, refer back to the article:
ACS Sustainable Chem. Eng. ***2021****, 9, 4, 1714–1728****.***

Characterizations of poly(β-*oxo*-carbonate)s

C1S1 (Table 4, entry 1). ^{1}H NMR (400 MHz, DMSO): δ = 4.10 ppm (m. 4H), δ = 2.10 ppm (s. 6H), δ = 1.89-1.59 ppm (m. 4H), δ = 1.65 ppm (m. 4H), δ = 1.44 ppm (s. 6H).
^{13}C NMR (400 MHz, DMSO): δ = 206.0 ppm, δ = 153.6 ppm, δ = 86.7 ppm, δ = 67.8 ppm, δ = 29.3 ppm, δ = 24.9 ppm, δ = 24.5 ppm, δ = 20.3 ppm.
C1S2 (Table 4, entry 2). ^{1}H NMR (400 MHz, DMSO): δ = 5.01 ppm (s. 1H), δ = 4.97 ppm (s. 1H), δ = 4.84 ppm (m. 1H), δ = 4.44 ppm (m. 1H), δ = 3.98-3.80 ppm (m. 4H), δ = 2.14 ppm (s. 6H), δ = 1.79-1.48 ppm (m. 4H), δ = 1.46-1.42ppm (m. 6H).
^{13}C NMR (400 MHz, DMSO): δ = 206.5 ppm, δ = 152.9 ppm, δ = 87.5 ppm, δ = 87.4 ppm, δ = 85.6 ppm, δ = 81.1 ppm, δ = 77.5 ppm, δ = 72.7 ppm, δ = 70.9 ppm, δ = 25.6 ppm, δ = 24.7 ppm, δ = 20.4 ppm.
C1L1 (Table 4, entry 3). ^{1}H NMR (400 MHz, $CDCl_3$): δ = 7.37 ppm (s. 4H), δ = 5.13 ppm (s. 4H), δ = 2.10 ppm (s. 6H), δ = 1.94-1.73 ppm (m. 4H), δ = 1.47 ppm (s. 6H).
^{13}C NMR (400 MHz, $CDCl_3$): δ = 205.7 ppm, δ = 153.3 ppm, δ = 135.2 ppm, δ = 128.4 ppm, δ =126.9 ppm, δ = 86.9 ppm, δ = 69.1 ppm, δ = 29.3 ppm, δ = 23.9 ppm, δ = 20.1 ppm.
C1L2 (Table 4, entry 4). ^{1}H NMR (400 MHz, $CDCl_3$): δ = 4.65 ppm (s. 2H), δ = 2.15 ppm (s. 6H), δ = 2.04-1.62 ppm (m. 8H), δ = 1.95-1.75 ppm (m. 4H), δ = 1.50 ppm (s. 6H).
^{13}C NMR (400 MHz, $CDCl_3$): δ = 205.8 ppm, δ = 152.9 ppm, δ = 86.6 ppm, δ =74.8 ppm, δ = 29.3 ppm, δ = 27.3 ppm, δ = 23.9 ppm, δ = 20.2 ppm.
C2S1 (Table 4, entry 5). ^{13}C CP-MAS NMR (10 kHz): δ = 207.3 ppm, δ = 154.4 ppm, δ = 86.6 ppm, δ = 69.9 ppm, δ = 28.7 ppm, δ = 28.7 ppm, δ = 24.2 ppm.
C2S2 (Table 4, entry 6). ^{1}H NMR (400 MHz, DMSO): δ = 5.07 ppm (s. 1H), δ = 5.04 ppm (s. 1H), δ = 4.89 ppm (m. 1H), δ = 4.46 ppm (m. 1H), δ = 4.03-3.80 ppm (m. 4H), δ = 2.15 ppm (s. 6H), δ = 2.04-1.84 ppm (m. 8H).
^{13}C NMR (400 MHz, DMSO): δ = 205.2 ppm, δ = 151.9 ppm, δ = 98.8 ppm, δ = 84.6 ppm δ = 80.4 ppm, δ = 76.7 ppm, δ = 71.6 ppm, δ = 70.0 ppm, δ = 24.5 ppm, δ = 23.2 ppm.
C2L1 (Table 4, entry 7). ^{13}C CP-MAS NMR (10 kHz): δ = 206.5 ppm, δ = 154.4 ppm, δ = 134.5, δ = 126.1, δ = 86.81 ppm, δ = 70.8 ppm, δ = 28.2 ppm, δ = 24.9 ppm.
C2L2 (Table 4, entry 8). ^{13}C CP-MAS NMR (10 kHz): δ = 205.0 ppm, δ = 154.0 ppm, δ = 86.4, δ = 76.9, δ = 29.6 ppm, δ = 23.3 ppm.

Characterizations of purified poly(*oxo*-carbonate)s from sugar-based diols synthetized at 25 °C

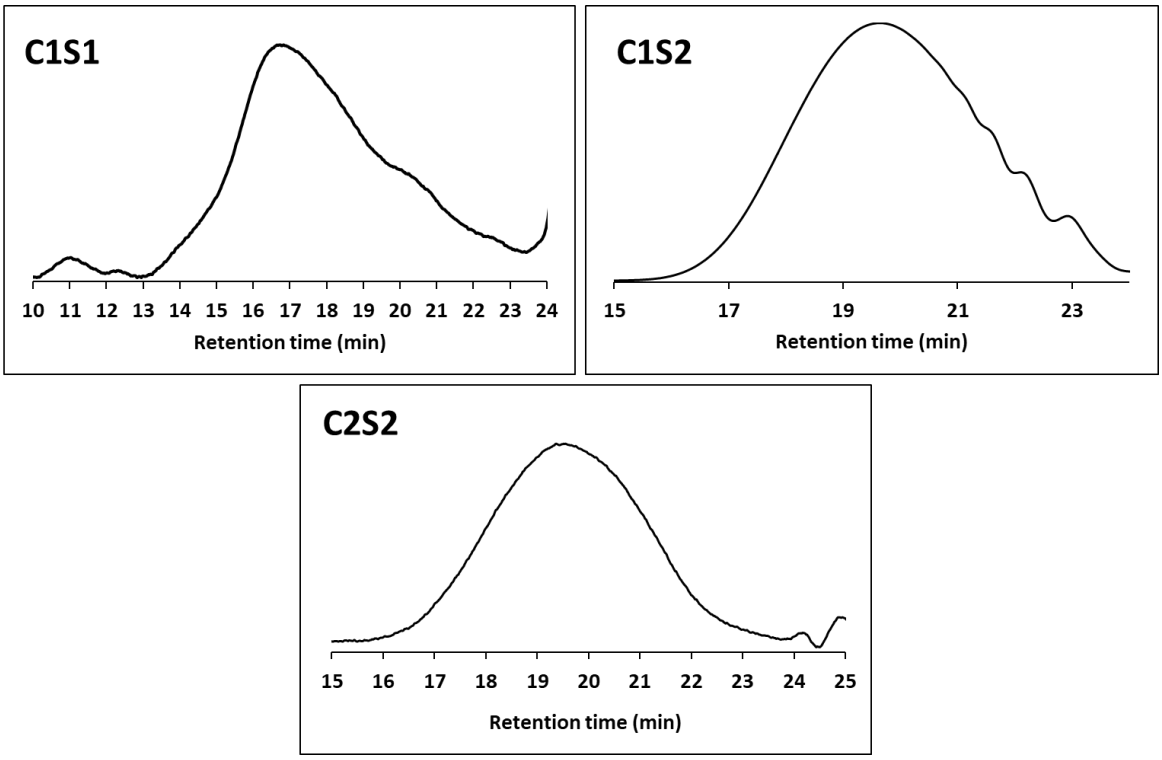

Figure S24. SEC chromatograms in DMF of purified **C1S1**, **C1S2** and **C2S2**.

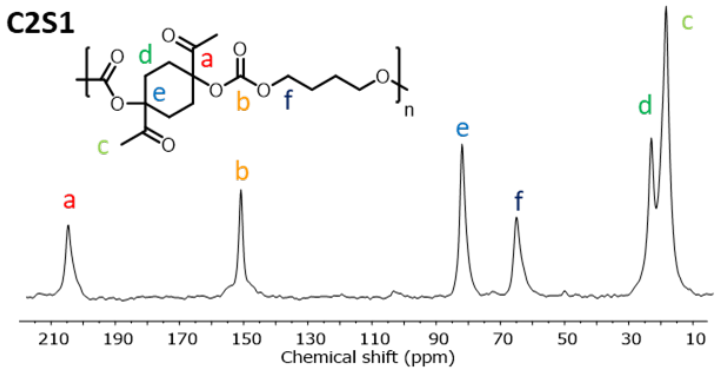

Figure S25. ^{13}C CP-MAS NMR spectra of purified **C2S1**.

Characterizations of purified poly(*oxo*-carbonate)s from lignin-based diols synthetized at 25 °C

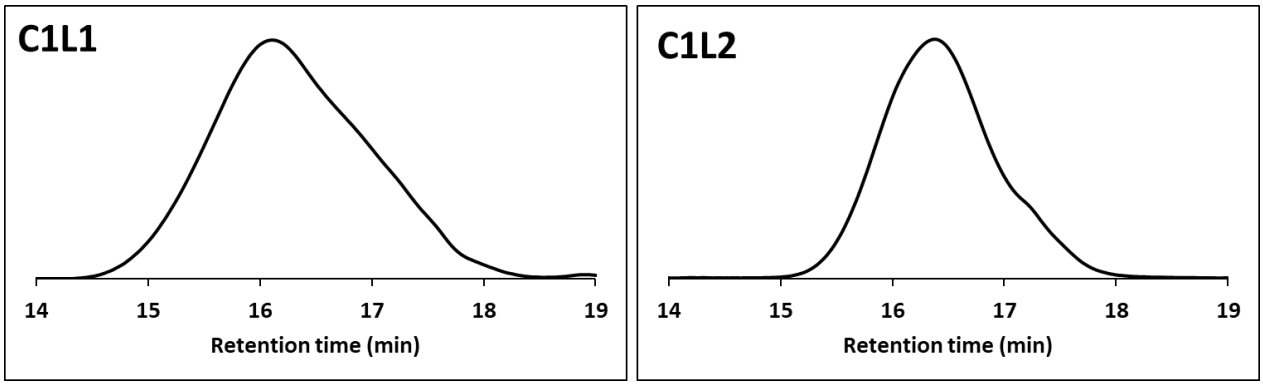

Figure S26. SEC chromatograms in $CHCl_3$ of purified **C1L1** and **C1L2**.

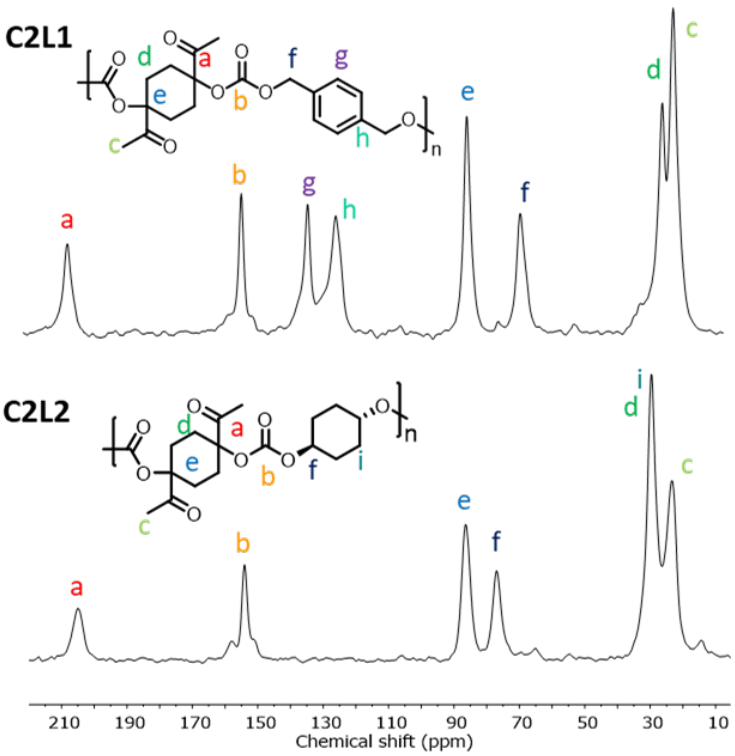

Figure S27. ^{13}C CP-MAS NMR spectra of purified **C2L1** and **C2L2**.

Synthesis and characterization of poly(*oxo*-carbonate)s synthetized at 80 °C

The synthesis of PCs at 80 °C follows the same procedure for the synthesis of PCs at 25 °C. At the end of the reaction, an aliquot was withdrawn to determine the conversion of the monomers and to analyze the polymers by ^{1}H- and ^{13}C- NMR spectroscopy and SEC.

SEC chromatograms and ^{1}H and ^{13}C-NMR spectra of C1S1 and C1L2 synthetized at 80 °C

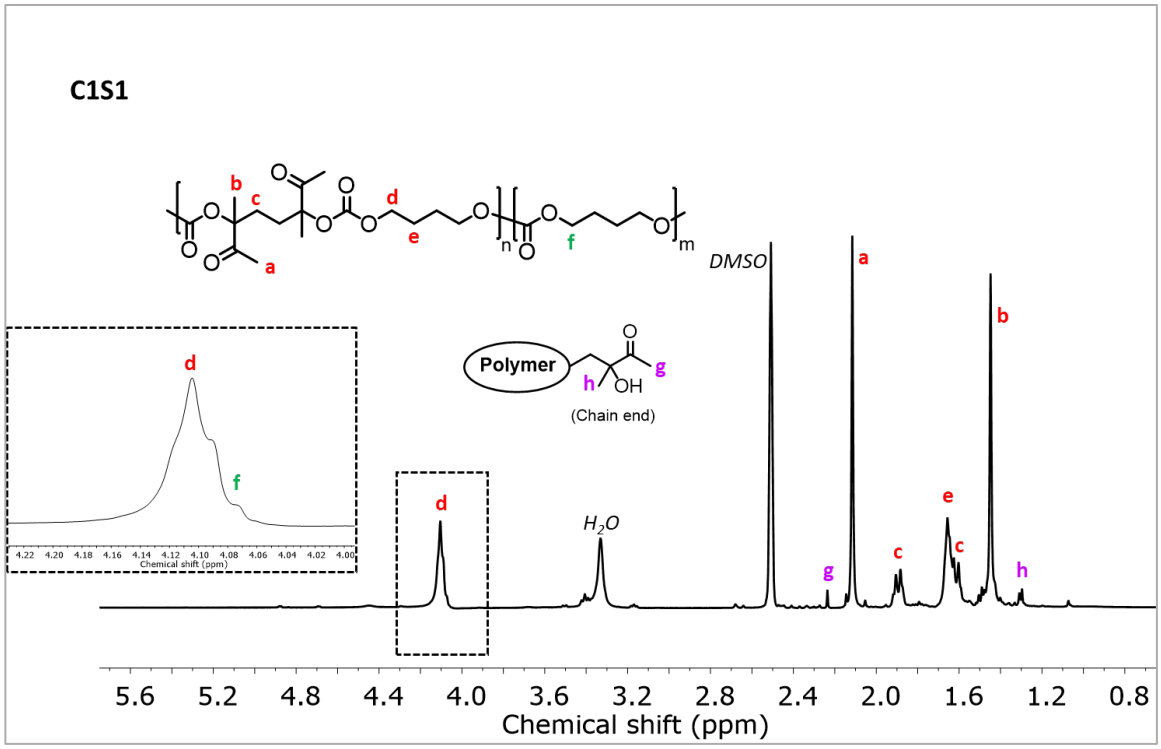

Figure S28. ^{1}H-NMR spectrum in DMSO-d_6 of **C1S1** synthetized at 80 °C.

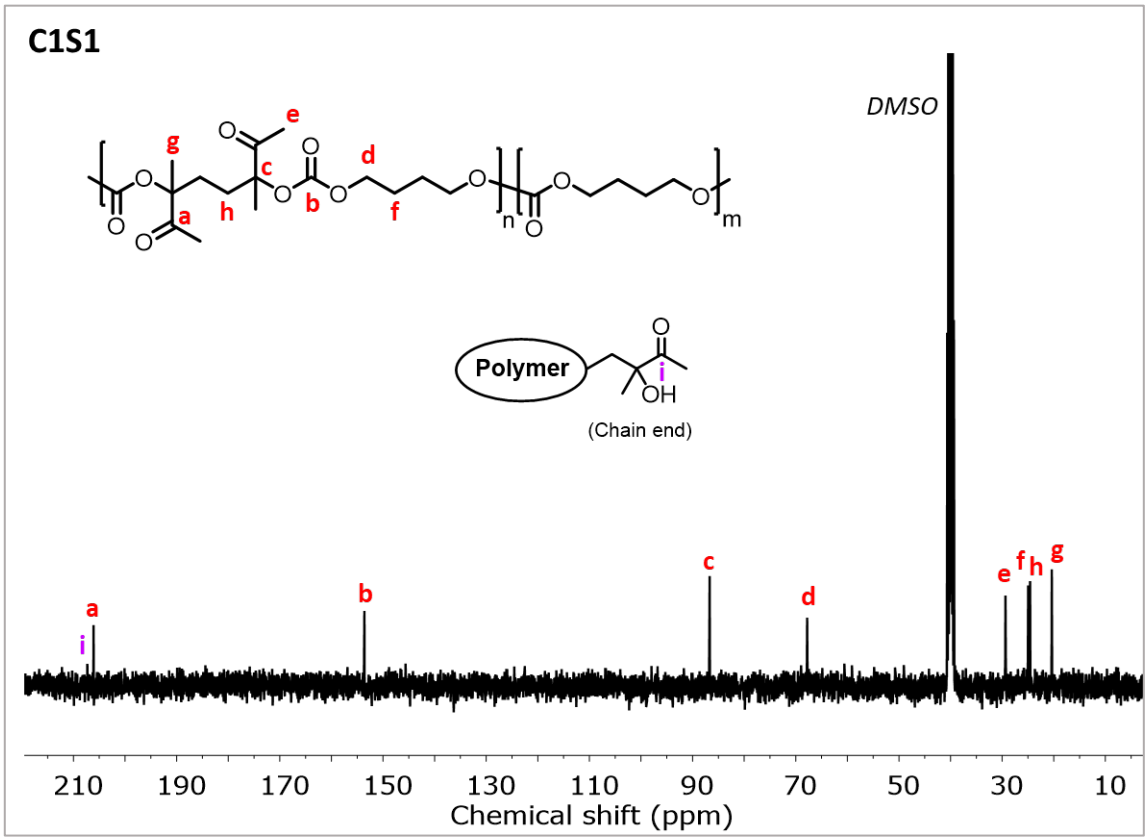

Figure S29.[13]C-NMR spectrum in DMSO-d_6 of **C1S1** synthetized at 80 °C.

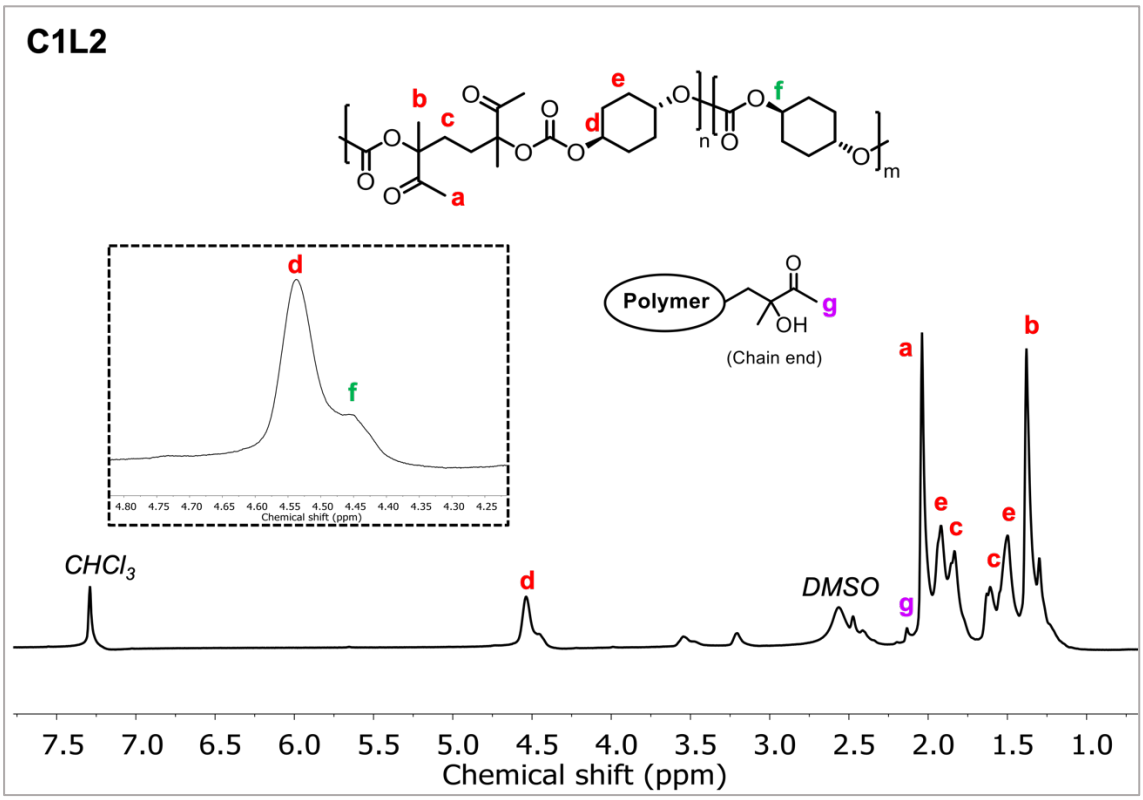

Figure S30. [1]H-NMR spectrum in $CDCl_3$ of **C1L2** synthetized at 80 °C.

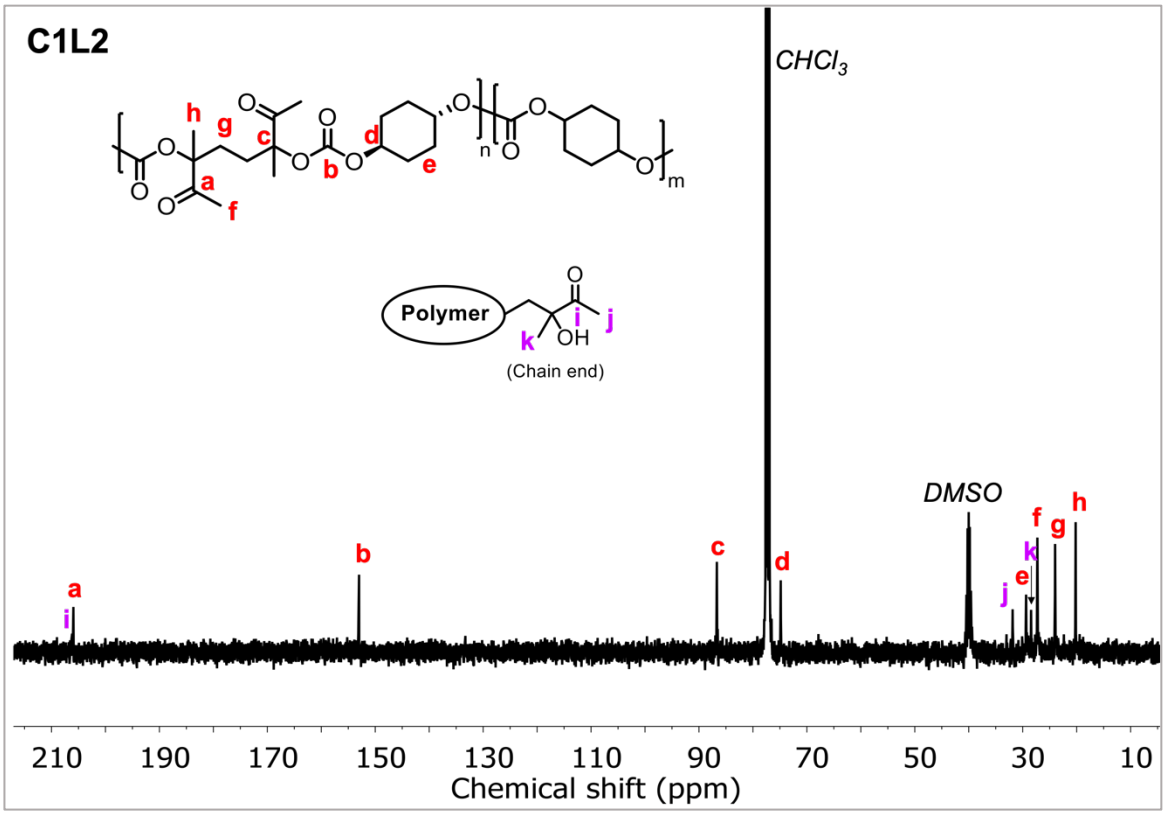

Figure S31. ^{13}C-NMR spectrum in $CDCl_3$ of **C1L2** synthetized at 80 °C.

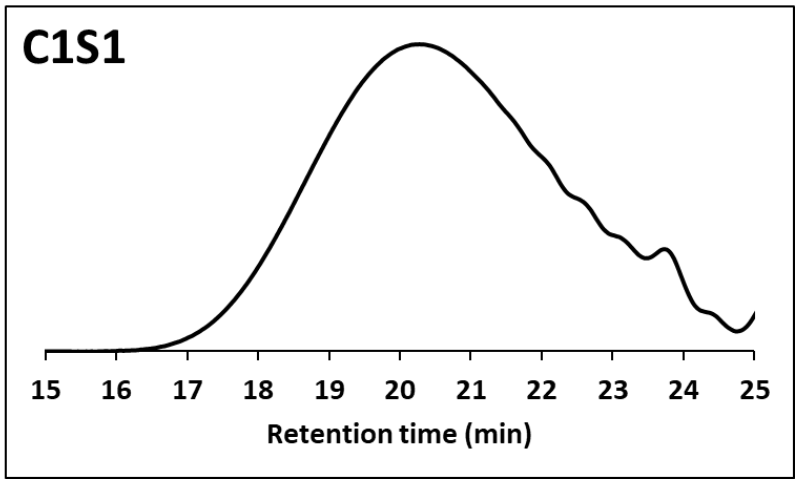

Figure S32. SEC chromatogram in DMF of **C1S1** synthetized at 80 °C.

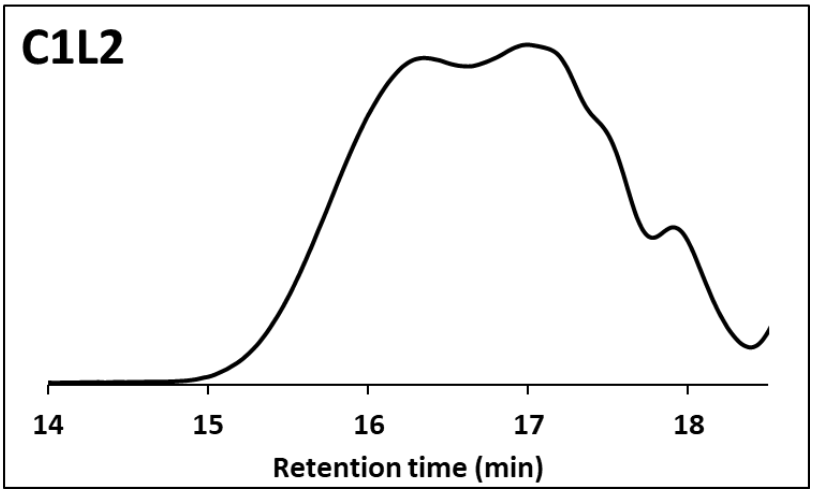

Figure S33. SEC chromatogram in $CHCl_3$ of **C1L2** synthetized at 80 °C.

Table S4. Polymerization of C1S1 at 80°C at different periods of time.

Entry	Time	Conv.C1 [%]	*oxo*-carbonate linkage (%)	cyclic carbonate linkage (%)	carbonate linkage (%)	M_n (g/mol)[a]	M_w (g/mol)[a]	$Đ$[a]
1	1 h	> 99	100	0	0	6,400	10,000	1.57
2	6 h	> 99	98	0	2	6,000	9,400	1.54
3	24 h	> 99	93	0	7	4,200	5,800	1.36

Conditions: bisαCC1 (3.93 mmol), Butanediol (3.93 mmol), DBU (0.196 mmol) in dry DMSO (5 mL) at 80 °C, under nitrogen atmosphere.
[a] Determined by SEC in DMF/LiBr.

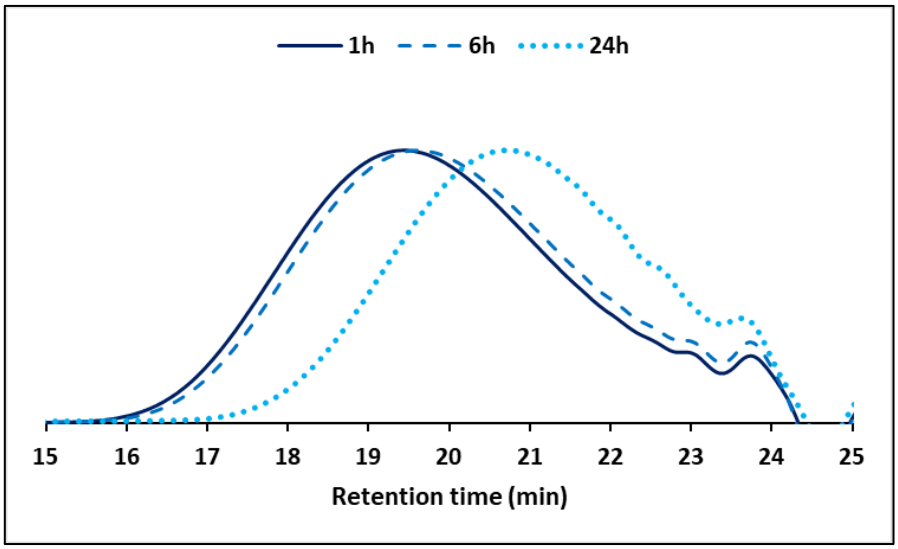

Figure S34. SEC chromatograms of polymerization of **C1S1** at 80°C at different periods of time.

SEC chromatogram and ^{1}H and ^{13}C-NMR spectra of C1L1 synthetized at 80 °C

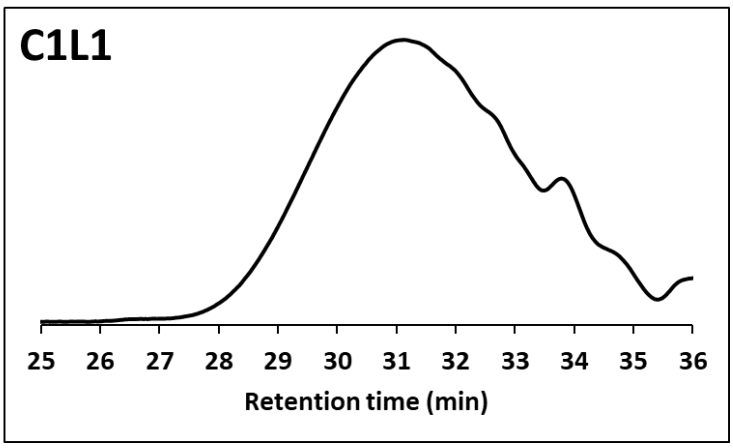

Figure S35. SEC chromatograms in $CHCl_3$ of **C1L1** synthetized at 80 °C.

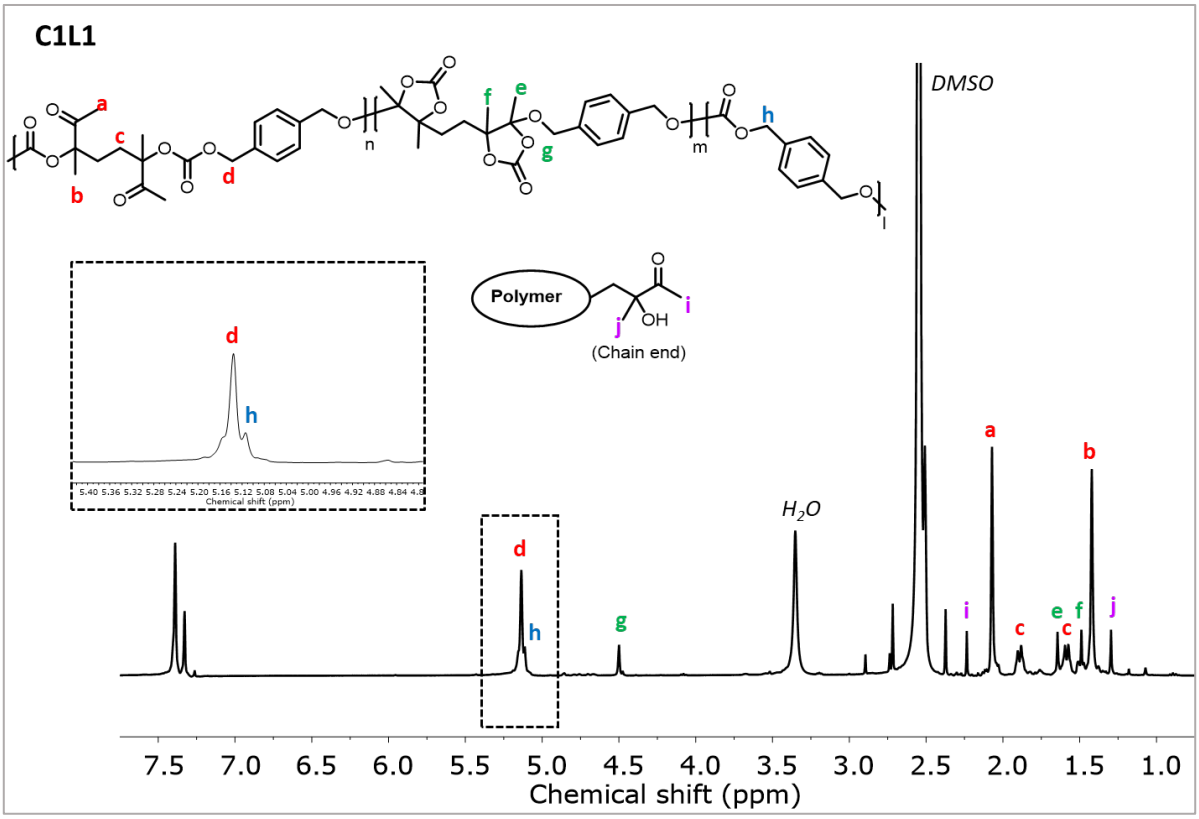

Figure S36. ^{1}H-NMR spectrum in $CDCl_3$ of **C1L1** synthetized at 80 °C.

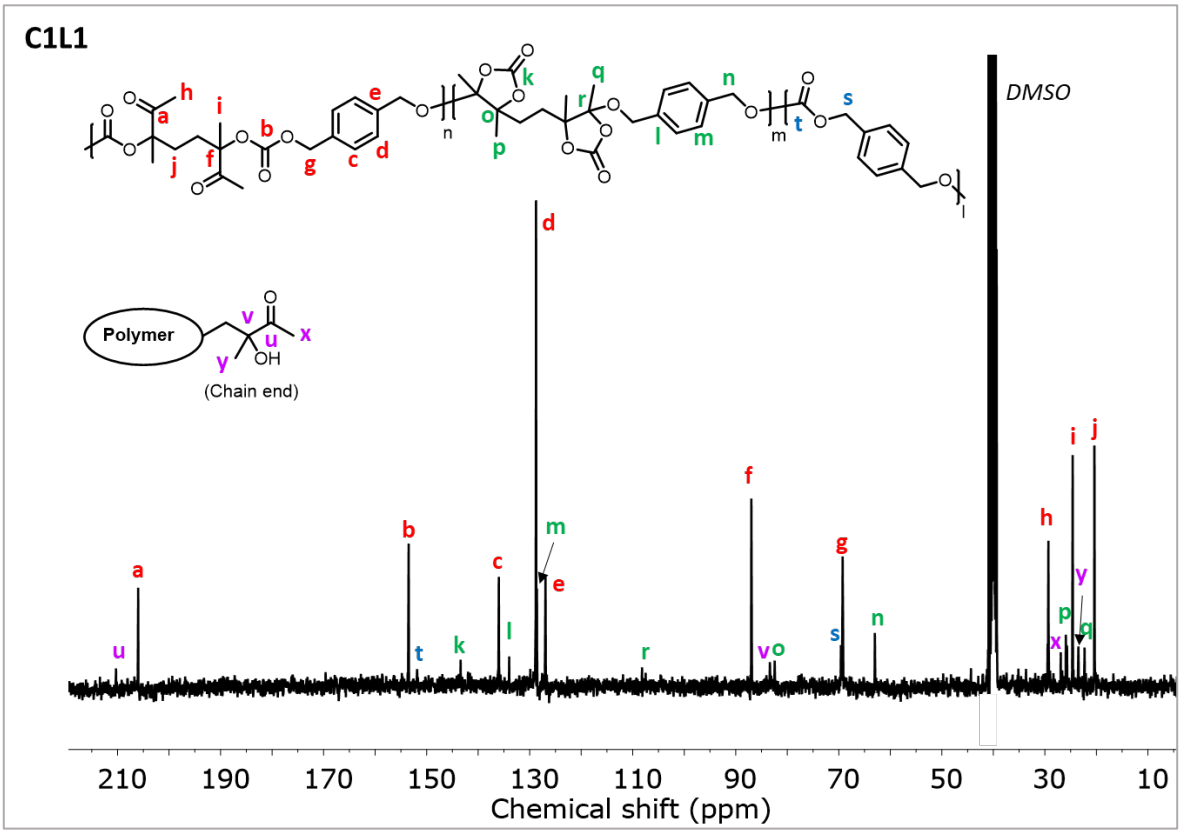

Figure S37. ^{13}C-NMR spectrum in $CDCl_3$ of **C1L1** synthetized at 80 °C.

Thermal analysis of poly(*oxo*-carbonate)s

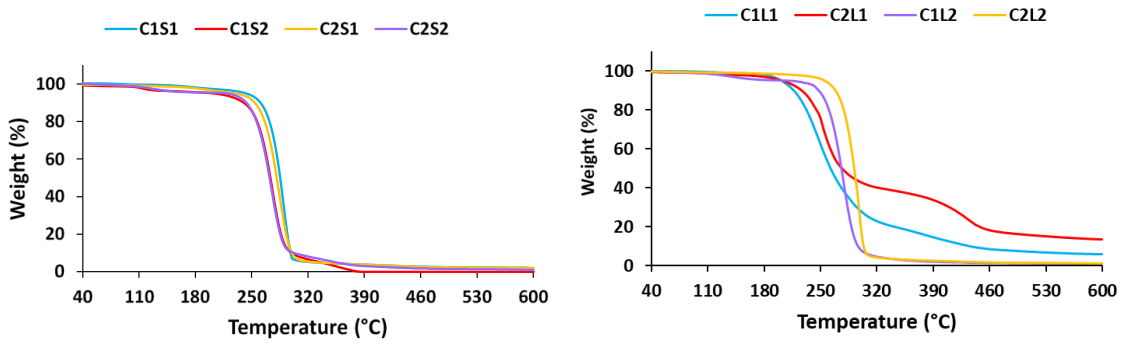

Figure S38: Thermal degradation curves of poly(*oxo*-carbonate)s derived from bisαCCs (**C1** and **C2**) and the bio-based diols **S1**, **S2**, **L1** and **L2**. TGA analyses were realized under N_2 flow at a heating rate of 20 °C/min.

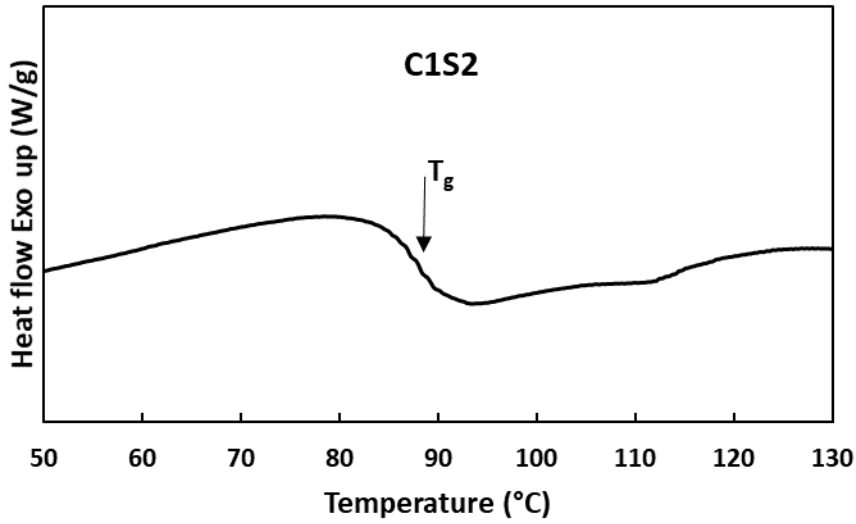

Figure S39*:* DSC heating curve of **C1S2**.

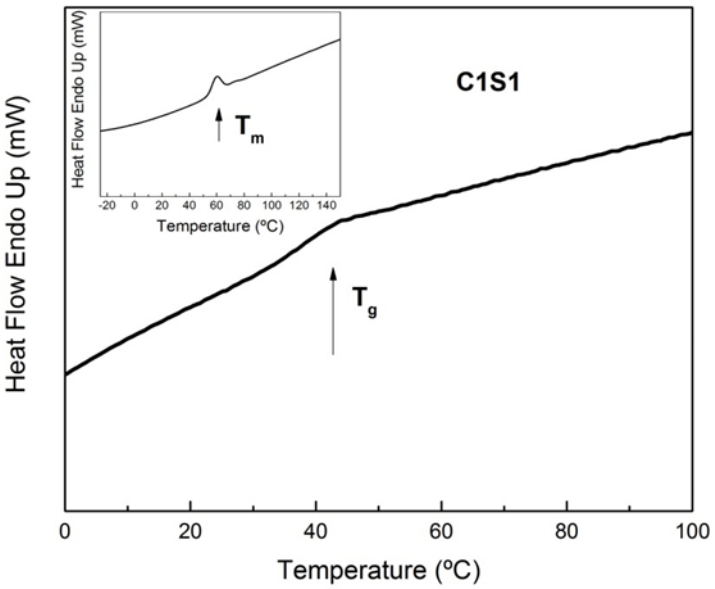

Figure S40. FSC heating curve for **C1S1** obtained at 1,000 K/s after cooling at -4,000 °C/s. The inset is the heating scan at 5,000 °C/s after cooling at -0.1 °C/s.

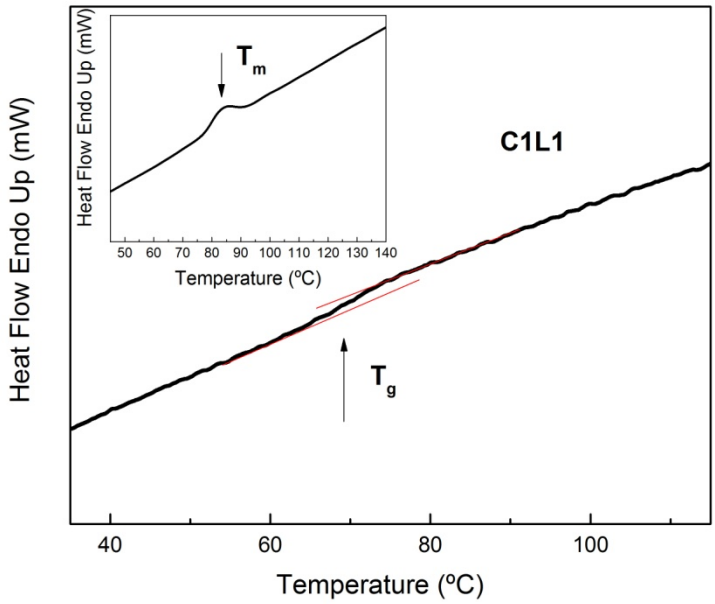

Figure S41. FSC heating curve for **C1L1** obtained at 1,000 K/s after cooling at -4,000 °C/s. The inset is the heating scan at 5,000 °C/s after cooling at -0.1 °C/s.

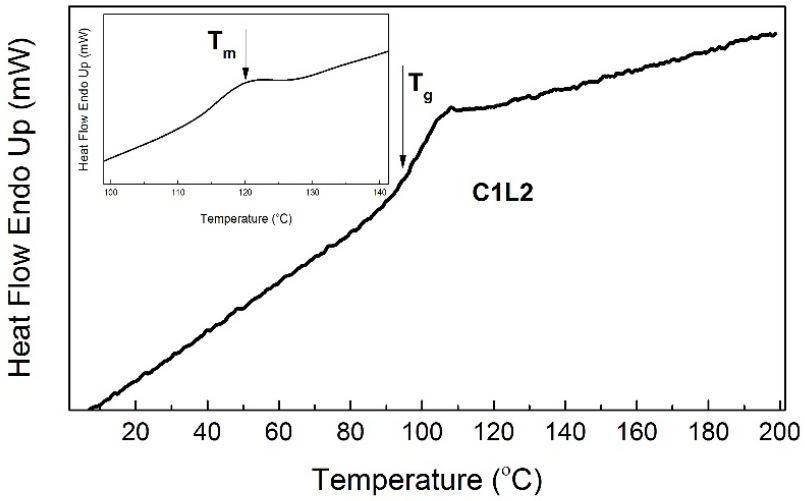

Figure S42. FSC heating curve for **C1L2** obtained at 1,000 K/s after cooling at -4,000 °C/s. The inset is the heating scan at 5,000 °C/s after cooling at -0.1 °C/s.

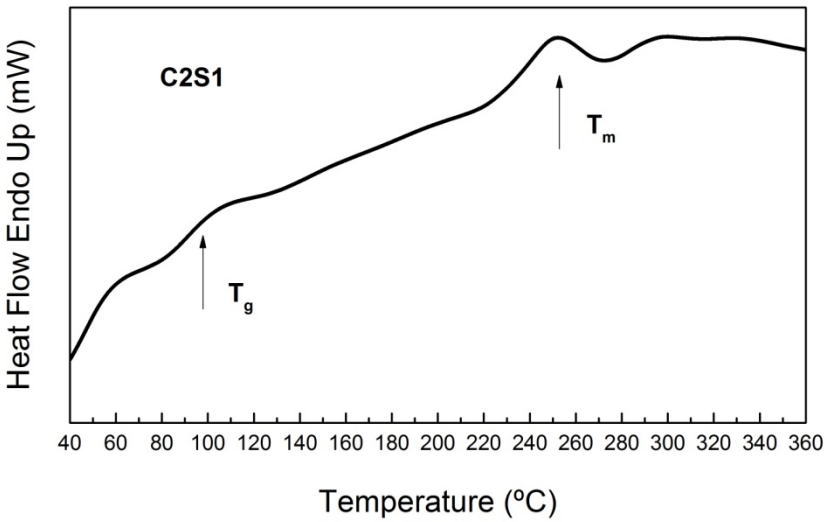

Figure S43. FSC heating curve for **C2S1** obtained at 20,000 K/s.

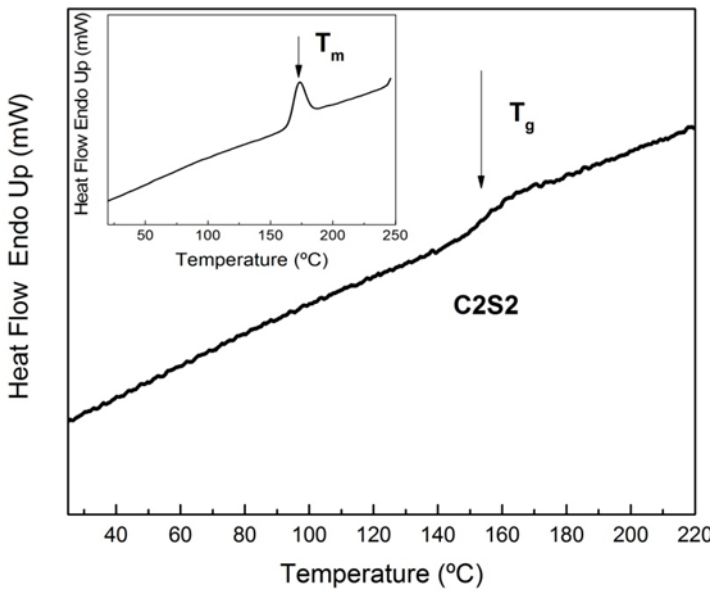

Figure S44. FSC heating curve for **C2S2** obtained at 1,000 K/s after cooling at -4,000 °C/s. The inset is the heating scan at 5,000 °C/s after cooling at -0.1 °C/s.

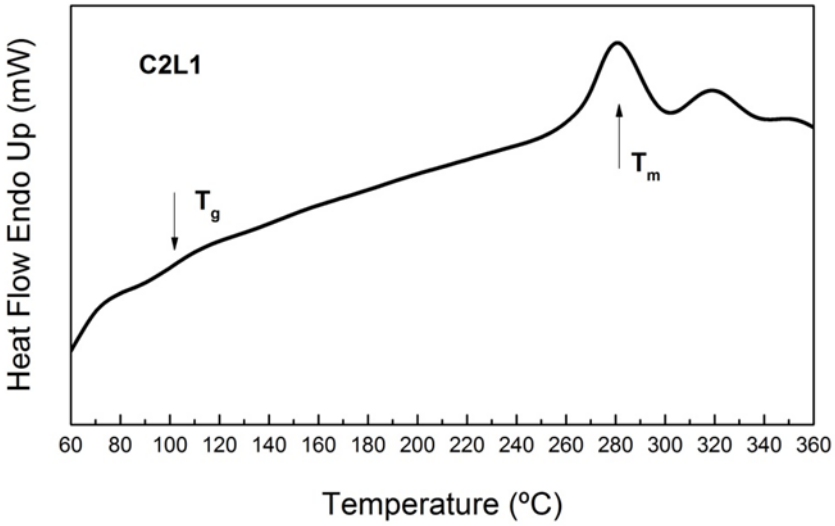

Figure S45. FSC heating curve for **C2L1** obtained at 20,000 K/s.

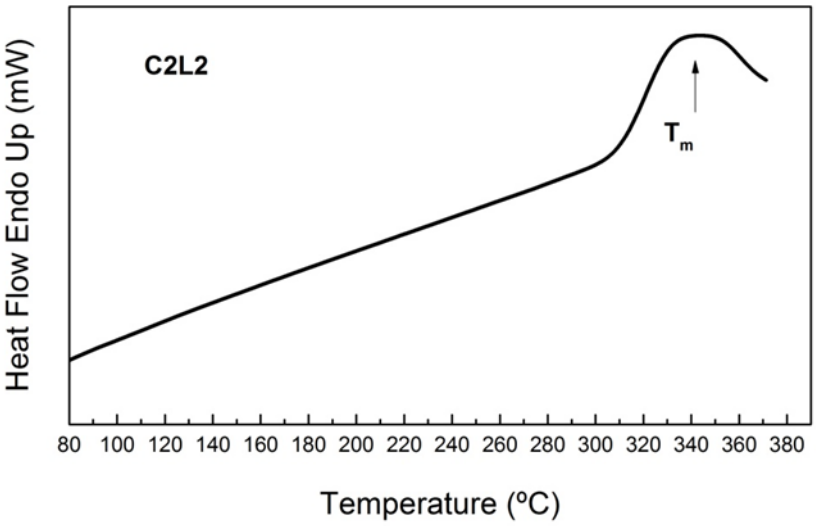

Figure S46. FSC heating curve for **C2L2** obtained at 20,000 K/s.

Table S5*:* Bragg´s law parameters (2θ and d spacings) calculated for polycarbonates synthetized at 25 °C.

C2L1		C2S1		C2L2		C1S1		C1L1		C1L2	
2θ (º)	**d(Å)**	**2θ (º)**	**d(Å)**	**2θ (º)**	**d(Å)**	**2θ (º)**	**d(Å)**	**2θ (º)**	**d(Å)**	**2θ (º)**	**d(Å)**
7.87	11.23	9.19	9.62	8.47	10.44	15.85	5.59	10.13	8.73	12.82	6.91
12.66	6.99	13.02	6.80	13.34	6.64	17.34	5.11	15.72	5.64		
15.82	5.60	14.63	6.05	14.99	5.91	19.18	4.63	18.43	4.81		
18.88	4.70	18.65	4.76	15.98	5.55	21.23	4.18	22.49	3.95		
21.19	4.19	19.64	4.52	17.80	4.98	24.13	3.69				
23.96	3.71	21.03	4.22	19.62	4.52						
25.47	3.50	24.57	3.62	21.63	4.11						
31.61	2.83	26.77	3.33	25.57	3.48						
34.86	2.57	40.13	2.25	26.84	3.32						
38.26	2.35	44.39	2.04	32.74	2.74						
42.70	2.12										
48.63	1.87										

References

(1) Ford, L.; Atefi, F.; Singer, R. D.; Scammells, P. J. Grignard Reactions in Pyridinium and Phosphonium Ionic Liquids. *European J. Org. Chem.* **2011**, *2011* (5), 942–950. https://doi.org/10.1002/ejoc.201001468.

(2) Fiorani, G.; Selva, M. Synthesis of Dibenzyl Carbonate: Towards a Sustainable Catalytic Approach. *RSC Adv.* **2014**, *4* (4), 1929–1937. https://doi.org/10.1039/c3ra42904k.

(3) Chai, J. Da; Head-Gordon, M. Long-Range Corrected Hybrid Density Functionals with Damped Atom-Atom Dispersion Corrections. *Phys. Chem. Chem. Phys.* **2008**, *10* (44), 6615–6620. https://doi.org/10.1039/b810189b.

(4) Mardirossian, N.; Head-Gordon, M. Thirty Years of Density Functional Theory in Computational Chemistry: An Overview and Extensive Assessment of 200 Density Functionals. *Mol. Phys.* **2017**, *115* (19), 2315–2372. https://doi.org/10.1080/00268976.2017.1333644.

(5) Fukui, K. The Path of Chemical Reactions - The IRC Approach. *Acc. Chem. Res.* **1981**, *14* (12), 363–368. https://doi.org/10.1021/ar00072a001.

(6) Dykstra, C. E.; Frenking, G.; Kim, K. S.; Scuseria, G. E. *Theory and Applications of Computational Chemistry*; **2005**, 1-7.

(7) Hratchian, H. P.; Schlegel, H. B. Accurate Reaction Paths Using a Hessian Based Predictor-Corrector Integrator. *J. Chem. Phys.* **2004**, *120* (21), 9918–9924. https://doi.org/10.1063/1.1724823.

(8) Hratchian, H. P.; Schlegel, H. B. Using Hessian Updating to Increase the Efficiency of a Hessian Based Predictor-Corrector Reaction Path Following Method. *J. Chem. Theory Comput.* **2005**, *1* (1), 61–69. https://doi.org/10.1021/ct0499783.

(9) Tomasi, J.; Mennucci, B.; Cammi, R. Quantum Mechanical Continuum Solvation Models. *Chem. Rev.* **2005**, *105* (8), 2999–3093. https://doi.org/10.1021/cr9904009.

(10) Frisch, M. J.; Trucks, G. W.; Schlegel, H. B.; Scuseria, G. E.; Robb, M. A.; Cheeseman, J. R.; Scalmani, G.; Barone, V.; Petersson, G. A.; Nakatsuji, H.; Li, X.; Caricato, M.; Marenich, A. V; Bloino, J.; Janesko, B. G.; Gomperts, R.; Mennucci, B.; Hratchian, H. P. Gaussian 16. *Gaussian, Inc.* Wallingford CT 2016.

(11) Bao, J. L.; Truhlar, D. G. Variational Transition State Theory : Theoretical Framework and Recent Developments. *Chem. Soc. Rev.* **2017**, *46*, 7548–7596. https://doi.org/10.1039/c7cs00602k.

(12) Domingo, L. R.; Pérez, P.; Sáez, J. A. Understanding the Local Reactivity in Polar Organic Reactions through Electrophilic and Nucleophilic Parr Functions. *RSC Adv.* **2013**, *3* (5), 1486–1494. https://doi.org/10.1039/C2RA22886F.

(13) Chamorro, E.; Pérez, P.; Domingo, L. R. On the Nature of Parr Functions to Predict the Most Reactive Sites along Organic Polar Reactions. *Chem. Phys. Lett.* **2013**, *582*, 141–143. https://doi.org/https://doi.org/10.1016/j.cplett.2013.07.020.

(14) Domingo, L. R.; Ríos-gutiérrez, M.; Pérez, P. Applications of the Conceptual Density Functional Theory Indices to Organic Chemistry Reactivity. *Molecules* **2016**, *21*, 748–770. https://doi.org/10.3390/molecules21060748.

(15) Contreras-García, J.; Johnson, E. R.; Keinan, S.; Chaudret, R.; Piquemal, J.-P.; Beratan, D. N.; Yang, W. NCIPLOT: A Program for Plotting Non-Covalent Interaction Regions. *J. Chem. Theory Comput.* **2011**, *7* (3), 625–632. https://doi.org/10.1021/ct100641a.

(16) Alonso, M.; Woller, T.; Martín-martínez, F. J.; Contreras-garcía, J.; Geerlings, P.; Proft, F. De. Understanding the Fundamental Role of p / p , s / s , and s / p Dispersion Interactions in Shaping Carbon-Based Materials. **2014**, *20* (Scheme 1), 4931–4941. https://doi.org/10.1002/chem.201400107.

(17) Van Den Broeck, E.; Verbraeken, B.; Dedecker, K.; Cnudde, P.; Vanduyfhuys, L.; Verstraelen, T.; Van Hecke, K.; Jerca, V. V.; Catak, S.; Hoogenboom, R.; Van Speybroeck, V. Cation−π Interactions Accelerate the Living Cationic Ring-Opening Polymerization of Unsaturated 2-Alkyl-2-Oxazolines. *Macromolecules* **2020**, *53* (10), 3832–3846. https://doi.org/10.1021/acs.macromol.0c00865.

(18) Martínez, L.; Andrade, R.; Birgin, E. G.; Martínez, J. M. PACKMOL: A Package for Building Initial Configurations for Molecular Dynamics Simulations. *J. Comput. Chem.* **2009**, *30* (13), 2157–2164. https://doi.org/10.1002/jcc.21224.

(19) Qiu, Y.; Smith, D. G. A.; Boothroyd, S.; Wagner, J.; Bannan, C. C.; Gokey, T.; Jang, H.; Lim, V. T.; Lucas, X.; Tjanaka, B.; Shirts, M. R.; Gilson, M. K.; Chodera, J. D.; Bayly, C. I.; Mobley, D. L.; Wang, L.-P. Openforcefield/Openforcefields: Version 1.0.0 “Parsley.” *openforcefield/openforcefields*. Zenodo 2019.

(20) Mobley, D. L.; Bannan, C. C.; Rizzi, A.; Bayly, C. I.; John, D.; Lim, V. T.; Lim, N. M.; Beauchamp, K. A.; Slochower, D. R.; Shirts, M. R.; Gilson, M. K.; Eastman, P. K. Perception. **2019**, *14* (11), 6076–6092. https://doi.org/10.1021/acs.jctc.8b00640.Escaping.

(21) Eastman, P.; Swails, J.; Chodera, J. D.; McGibbon, R. T.; Zhao, Y.; Beauchamp, K. A.; Wang, L.-P.; Simmonett, A. C.; Harrigan, M. P.; Stern, C. D.; Wiewiora, R. P.; Brooks, B. R.; Pande, V. S. OpenMM 7: Rapid Development of High Performance Algorithms for Molecular Dynamics. *PLOS Comput. Biol.* **2017**, *13* (7), 1–17.

(22) VandeVondele, J.; Krack, M.; Mohamed, F.; Parrinello, M.; Chassaing, T.; Hutter, J. Quickstep: Fast and Accurate Density Functional Calculations Using a Mixed Gaussian and Plane Waves Approach. *Comput. Phys. Commun.* **2005**, *167* (2), 103–128. https://doi.org/https://doi.org/10.1016/j.cpc.2004.12.014.

(23) Nosé, S. A Molecular Dynamics Method for Simulations in the Canonical Ensemble. *Mol. Phys.* **1984**, *52* (2), 255–268. https://doi.org/10.1080/00268978400101201.

(24) Martyna, G. J.; Klein, M. L.; Tuckerman, M. Nosé – Hoover Chains : The Canonical Ensemble via Continuous Dynamics. *J. Chem. Phys.* **1998**, *97* (April 1992), 2635–2643.

(25) Grimme, S.; Antony, J.; Ehrlich, S.; Krieg, H. A Consistent and Accurate Ab Initio Parametrization of Density Functional Dispersion Correction (DFT-D) for the 94 Elements H-Pu. *J. Chem. Phys.* **2010**, *132* (15), 154104–154118. https://doi.org/10.1063/1.3382344.

(26) Grimme, S. Supramolecular Binding Thermodynamics by Dispersion-Corrected Density Functional Theory. *Chem. Eur. J.* **2012**, *18* (32), 9955–9964. https://doi.org/10.1002/chem.201200497.

(27) Hutter, J.; Iannuzzi, M.; Schiffmann, F.; VandeVondele, J. Cp2k: Atomistic Simulations of Condensed Matter Systems. *WIREs Comput. Mol. Sci.* **2014**, *4* (1), 15–25. https://doi.org/10.1002/wcms.1159.

(28) Becke, A. D. Density-Functional Exchange-Energy Approximation with Correct Asymptotic Behavior. *Phys. Rev. A* **1988**, *38* (6), 3098–3100. https://doi.org/10.1103/PhysRevA.38.3098.

(29) Lee, C.; Yang, W.; Parr, R. G. Development of the Colle-Salvetti Correlation-Energy Formula into a Functional of the Electron Density. *Phys. Rev. B* **1988**, *37* (2), 785–789. https://doi.org/10.1103/PhysRevB.37.785.

(30) Lippert, G.; Hutter, J.; Parrinello, M. TheGaussianAndAugmented-Plane-. *Theor. Chem. Acc.* **1999**, *103*, 124–140. https://doi.org/10.1007/s002149900042.

(31) Lippert, G.; Hutter, J.; Parrinello, M. A Hybrid Gaussian and Plane Wave Density Functional Scheme. *Mol. Phys.* **1997**, *92* (3), 477–488. https://doi.org/10.1080/002689797170220.

(32) Li, X.; Wei, D.; Li, Z. Theoretical Study on DBU-Catalyzed Insertion of Isatins into Aryl Difluoronitromethyl Ketones: A Case for Predicting Chemoselectivity Using Electrophilic Parr Function. *ACS Omega* **2017**, *2* (10), 7029–7038. https://doi.org/10.1021/acsomega.7b00907.

(33) Alves, M.; Méreau, R.; Grignard, B.; Detrembleur, C.; Jérôme, C.; Tassaing, T. DFT Investigation of the Reaction Mechanism for the Guanidine Catalysed Ring-Opening of Cyclic Carbonates by Aromatic and Alkyl-Amines. *RSC Adv.* **2017**, *7* (31), 18993–19001. https://doi.org/10.1039/C7RA00220C.

(34) Coady, D. J.; Fukushima, K.; Horn, H. W.; Rice, J. E.; Hedrick, J. L. Catalytic Insights into Acid/Base Conjugates: Highly Selective Bifunctional Catalysts for the Ring-Opening Polymerization of Lactide. *Chem. Commun.* **2011**, *47* (11), 3105–3107. https://doi.org/10.1039/C0CC03987J.

(35) Wang, B.; Luo, Z.; Elageed, E. H. M.; Wu, S.; Zhang, Y.; Wu, X.; Xia, F.; Zhang, G.; Gao, G. DBU and DBU-Derived Ionic Liquid Synergistic Catalysts for the Conversion of Carbon Dioxide/Carbon

Disulfide to 3-Aryl-2-Oxazolidinones/[1,3]Dithiolan-2-Ylidenephenyl- Amine. *ChemCatChem* **2016**, *8* (4), 830–838. https://doi.org/10.1002/cctc.201500928.

(36) Morri, A. K.; Thummala, Y.; Doddi, V. R. The Dual Role of 1,8-Diazabicyclo[5.4.0]Undec-7-Ene (DBU) in the Synthesis of Terminal Aryl- and Styryl-Acetylenes via Umpolung Reactivity. *Org. Lett.* **2015**, *17* (18), 4640–4643. https://doi.org/10.1021/acs.orglett.5b02398.

(37) Zhu, L.; Yuan, H.-Y.; Zhang, J. Mechanistic Investigation-Inspired Activation Mode of DBU and the Function of the α-Diazo Group in the Reaction of the α-Amino Ketone Compound and EDA: [DBU-H]+-DMF-H2O and α-Diazo as Strong N-Terminal Nucleophiles. *Org. Chem. Front.* **2019**, *6* (15), 2678–2686. https://doi.org/10.1039/C9QO00602H.

(38) Fanjul-Mosteirín, N.; Jehanno, C.; Ruipérez, F.; Sardon, H.; Dove, A. P. Rational Study of DBU Salts for the CO2 Insertion into Epoxides for the Synthesis of Cyclic Carbonates. *ACS Sustain. Chem. Eng.* **2019**, *7* (12), 10633–10640. https://doi.org/10.1021/acssuschemeng.9b01300.

(39) Ouhib, F.; Grignard, B.; Van Den Broeck, E.; Luxen, A.; Robeyns, K.; Van Speybroeck, V.; Jerome, C.; Detrembleur, C. A Switchable Domino Process for the Construction of Novel CO2 -Sourced Sulfur-Containing Building Blocks and Polymers. *Angew. Chem. Int. Ed.* **2019**, *58* (34), 11768–11773. https://doi.org/10.1002/anie.201905969.

Chapter III

A catalyst-free approach for the degradation of bio- and CO_2-sourced polycarbonates: a step toward a circular plastic economy

Fabiana Siragusa, Thomas Habets, Raphael Méreau, Gwilherm Evano, Bruno Grignard, Christophe Detrembleur**

Reference: *ACS Sustainable Chem. Eng. 2022, 10, 8863–8875.*

https://doi.org/10.1021/acs.macromol.2c00696

Author contributions: F.S., C.D., B.G. and G.E. designed and planned the project. F.S. synthesized and characterized all polymers and carried out all the model reactions. T.H. and R.M. carried out DFT modelling. F.S. wrote the manuscript with contributions from all co-authors.

ABSTRACT

Designing easily degradable polymers has become a new challenge to overcome the post-consumer plastic waste accumulation in the environment. Polycarbonates are important polymers that can be chemically recycled, however most often their degradation requires high temperatures and/or the use of catalysts. In this work, we report the facile chemical recycling of regioregular polycarbonates prepared by the organocatalyzed copolymerization of CO_2-sourced exovinylene biscyclic carbonates (BisαCC) with diols derived from biomass. These polymers, thanks to their pending ketone groups, are rapidly (< 30 min) and totally deconstructed into the parent diol and a bis(oxazolidinone) by catalyst-free aminolysis at 25 °C. By using 3-propanolamine for the aminolysis, a hydroxy-functionalized bis(oxazolidinone) is recovered, that can be copolymerized with BisαCC to yield a polymer alternating carbonate and oxazolidinone linkages. Importantly, the same bis(oxazolidinone) scaffold is recovered as the main product by aminolysis of this copolymer, offering a close-loop recycling scenario for this polymer. This work illustrates that these polycarbonates are prone to facile and complete aminolysis under mild and catalyst-free conditions, but can also be exploited to prepare new building blocks for the synthesis of novel degradable polymers. The mechanism of formation of these heterocycles is studied by model reactions and rationalized by DFT calculations.

Introduction

Following a century of innovation, commodity polymers have reshaped our modern life-style and quality by entering into numerous everyday consumers goods. However, their long-term accumulation in nature and oceans coupled to the lack of viable end-of-life recycling scenario - generally limited to single use - turned their magic into an environmental disaster.[1–3] This prompted the scientists to develop new approaches to recycle or upcycle plastics.[4–9] While polyolefins or vinyl-type polymers are difficult to depolymerize by chemical pathways due to strong C-C bonds constituting their main chain backbone, step-growth polymers with in chain C-O or C-N linkages (such as polyesters, polycarbonates, polyurethanes) offer multiple chemical depolymerization opportunities.[10,11] In this context, solvolysis are now privileged to regenerate the initial monomers (for close-loop recycling) or to develop new value-added chemicals (for open-loop recycling).[12–16] This is typically exemplified with representative bisphenol A polycarbonate that was extensively depolymerized into the native bisphenol A via hydrolysis, or into mixtures of bisphenol A and carbonylated products ((a)cyclic carbonates, oxazolidinones or ureas) by alcoholysis or aminolysis (Scheme 1A).[17–21] However, most of these depolymerization pathways are generally slow and/or necessitate high temperatures (> 90 °C), and use thermally stable (1,5,7-triazabicyclo[4.4.0]dec-5-ene and methanesulfonic acid (TBD:MSA) salts or ionic liquids)[22–25] or sophisticated (ZnO nanoparticles/$^{n}Bu_4NCl$)[26] catalysts, or cyclic amidine and guanidine bases (TBD or DBU)[27–29] to deliver degradation products with high yields. Further optimization of the depolymerization processes by combining catalyst innovations with the development of creative energy efficient protocols still remains under-developed. To tackle this issue, the eco-conception of new plastics designed to be intrinsically and chemically fully recyclable under mild operative conditions is gaining momentum.

In the last years, our group pioneered the fabrication of a new class of (semicrystalline) polycarbonates (poly(*oxo*-carbonate)) by the room temperature polyaddition of CO_2-sourced bis (exovinylene cyclic carbonate)s and diols, some of them having already shown promising utilization as solid electrolytes for Li-ion batteries.[30–34] Despite both monomers found a CO_2 and bio-renewable origin, the end-of-life recycling scenario of these polymers is unknown and has to be evaluated to meet the sustainability goals of our modern society. These polycarbonates structurally differ from their conventional analogues by the presence of additional ketone moieties within or pending along the main skeleton. The pending ketones at the β-position of the carbonate units already endowed polymers with a slow catalytic (organobase, 20 mol%) and thermal (T = 40 °C) degradation ability by using unstable hydroperoxides.[35]

Herein, as the ketone groups display higher electrophilicity than the carbonyl group of the carbonate linkages, we hypothesized that the ketones might facilitate energy efficient polymer

aminolysis at room temperature under catalyst-free conditions. By the chemo-selective addition of a primary amine to the ketone, it is possible not only to completely degrade the PCs, but also to recycle the derived diols monomers and to upcycle *N*-substituted bis(oxazolidinones), which may be repurposed for biomedical, commodity or engineering applications, or used as building blocks for organic synthesis (Scheme 1B). The so-proposed depolymerization approach is first proven in concept on model primary amines and *oxo*-alkyl carbonate scaffolds prior extension to the polymer degradation. By a smart selection of the amine, we will also demonstrate that a new polymerizable oxazolidinone scaffold is obtained with a high yield, which can re-enter the fabrication loop of circular polymers virtually infinitely recyclable.

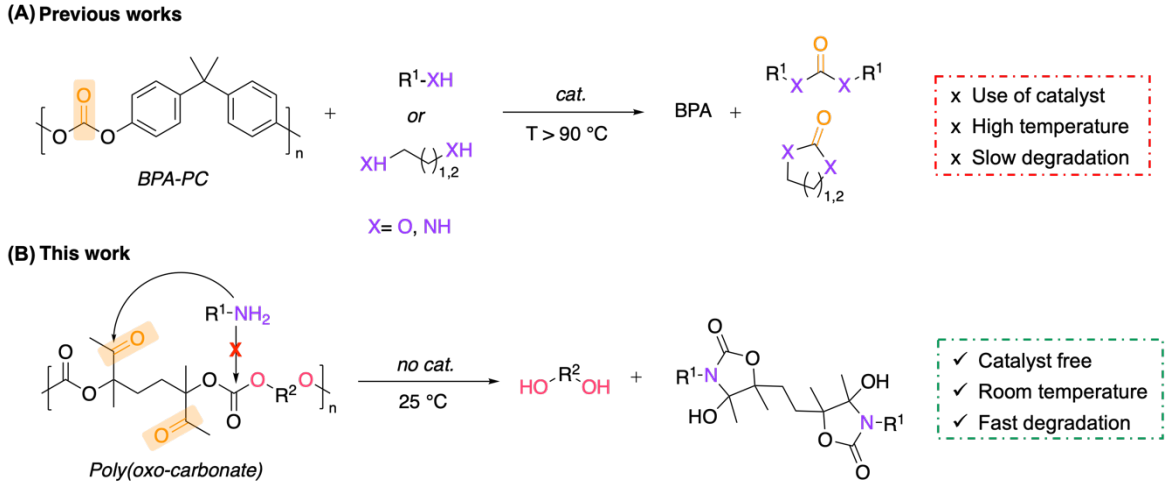

Scheme 1. A) Chemical degradation by alcoholysis and aminolysis of BPA-PC and B) Poly(*oxo*-carbonate)s aminolysis.

Results and Discussion

Model study on representative organic scaffolds. The reactivity of model *oxo*-carbonates - mimicking the repetitive units of poly(*oxo*-carbonate)s – with primary amines was first investigated to get insights into the kinetics of the process and facilitate the identification of the degradation products. To do so, we first synthetized three oxo-alkyl carbonates (Figure 1, products **O1-3)** by alcoholysis of 4,4-dimethyl-5-methylene-1,3-dioxolan-2-one (αCC) with 1-butanol (**O1**), benzyl alcohol (**O2**) and cyclohexanol (**O3**) following a previously reported procedure (Scheme S1 and Figures S1-S3). Then, the aminolysis of the *oxo*-carbonate with propylamine **A1** (3 eq.) and without catalyst, in THF and at room temperature (25 °C) was evaluated. The reaction was monitored by ^{1}H-NMR analysis for 24 h after quenching each aliquot with formic acid to neutralize the unreacted amine (Figure 1A-C and Figures S4-S7). **O1** and **O2** displayed rather high reactivity toward propyl amine with respective consumptions

of 79 % and 88 % after 1 h whereas no conversion was observed for **O3**. After 24 h, the *oxo*-carbonates **O1** and **O2** were totally consumed (> 99 %) (Figure 1B-C), while 70% of **O3** was transformed due to the steric hindrance brought by the secondary alcohol (Figure 1C). All the aminolyses furnished the corresponding alcohol **1**, hydroxy-oxazolidinone **2** and an imine **3**, with no other side product (Figure 1A and 1C). When the reactions with **O1** and **O2** are considered, the selectivity for **2** and **3** is 72-75 % and 28-25 %, respectively, and is rather constant with the reaction time (Figure S8).

Afterwards, we decided to perform the aminolysis of **O1** by using amines with increased steric hindrance and, hence, decreased nucleophilicity,[37] i.e benzyl amine **A2** and cyclohexyl amine **A3** (Figures S9-S10). By changing **A1** for **A2**, the reaction rate was strongly decreased, with a **O1** conversion of only 52 % after 24 h. However, the selectivity for **2** and **3** was not significantly affected (78 % for **2** and 22 % for **3**). Lastly, **A3** appeared, logically, much less reactive as attested by a low **O1** conversion of 15 % after the same period of time. Moreover, the use of the sterically congested cyclohexyl amine is detrimental to the product selectivity as it increased the formation of the by-product **3** up to 40 %. The formed hydroxy-oxazolidinones were separated and recovered by extraction in diethyl ether. Their structure was confirmed by ^{1}H- and ^{13}C-NMR analyses and high-resolution mass spectrometry (HRMS) (Figures S11-S16).

For a deep understanding of the aminolysis process, a mechanistic investigation was performed in the next section.

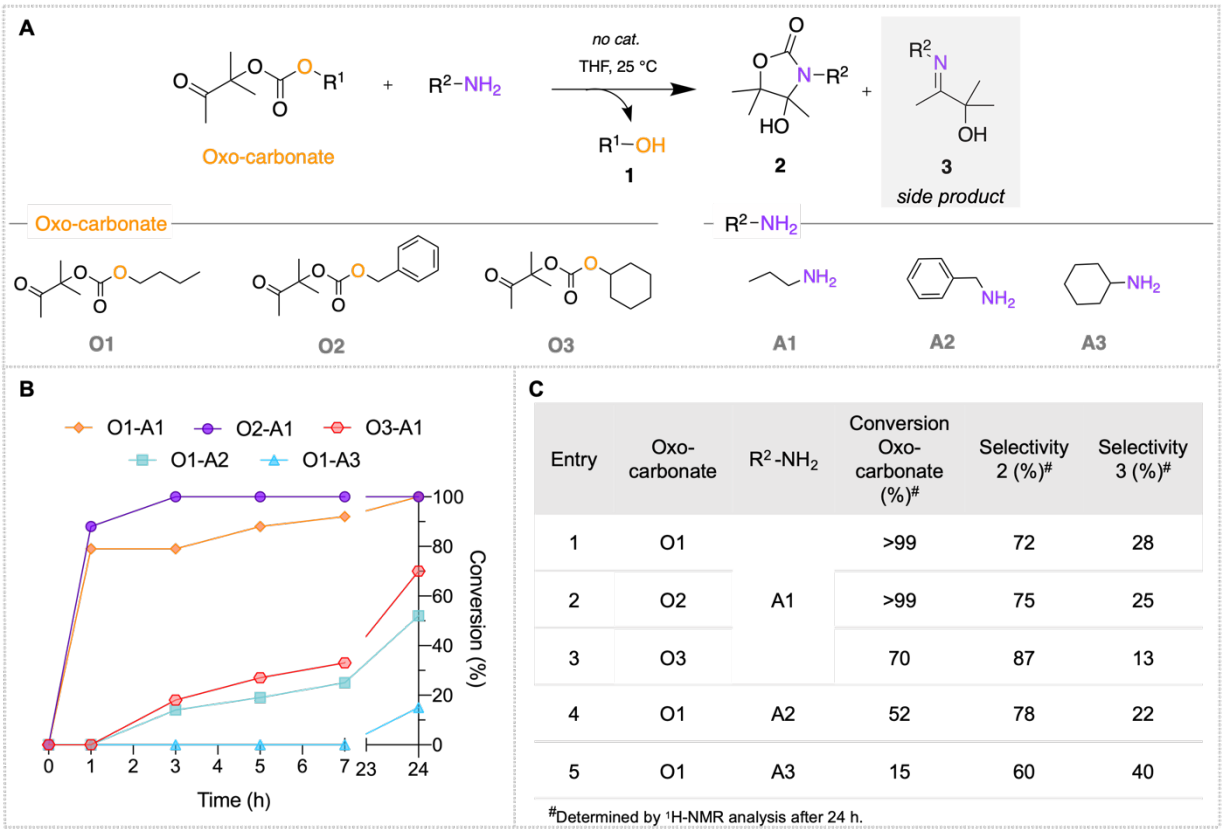

Entry	Oxo-carbonate	R^2-NH_2	Conversion Oxo-carbonate (%)#	Selectivity 2 (%)#	Selectivity 3 (%)#
1	O1	A1	>99	72	28
2	O2		>99	75	25
3	O3		70	87	13
4	O1	A2	52	78	22
5	O1	A3	15	60	40

#Determined by ^{1}H-NMR analysis after 24 h.

Figure 1. A) Catalyst-free aminolysis of *oxo*-carbonates with propyl amine **A1**, benzyl amine **A2** and cyclohexyl amine **A3** (3 eq. compared the *oxo*-carbonate) at 25 °C in THF (C = 2 M); B) conversion of *oxo*-carbonates *vs* time; C) conversion of *oxo*-carbonates and selectivity in the formed products after 24 h.

Mechanistic insight. As postulated in our previous work, the *oxo*-carbonate presents two electrophilic sites, the ketone and the carbonate groups.[30] We might therefore expect the aminolysis to occur on both sites (Scheme 2). An attack of the amine to the carbonate might release two different products depending on which side the C-O bond of the carbonate is broken (Scheme 2A). As no carbamate was observed in the reaction medium under our operating conditions (Scheme S2), we therefore assumed that the attack to the carbonate may only release the alcohol leaving group and the *oxo*-urethane (**int 1**), which can further undergo cyclization into the experimentally observed hydroxy-oxazolidinone **2**. The other possible pathway is the attack of the amine to the ketone, i.e. the most electrophilic site as previously supported by the Parr function calculations.[30] Similarly to the preferential attack of the ketone by an alcohol that delivered a hemiacetal, the addition of the amine was expected to furnish a hemiaminal species (**int 2**). In this scenario, both the secondary amine and alcohol groups of **int 2** might then play the role of the nucleophile to attack the carbonate group to form the oxazolidinone **2** or the cyclic carbonate **int 3**, respectively.

To shed light on the energetics and intermediates forming the oxazolidinone **2** and the by-product **3**, density functional theory (DFT) calculations were performed at the ωB97-XD/6-

311++G(d,p) level of theory. Calculations were performed on the model *oxo*-carbonate from butanol **O1** and with propylamine **A1**. Detailed energy profiles are provided in Scheme 2 and supporting discussions are available in supporting information.

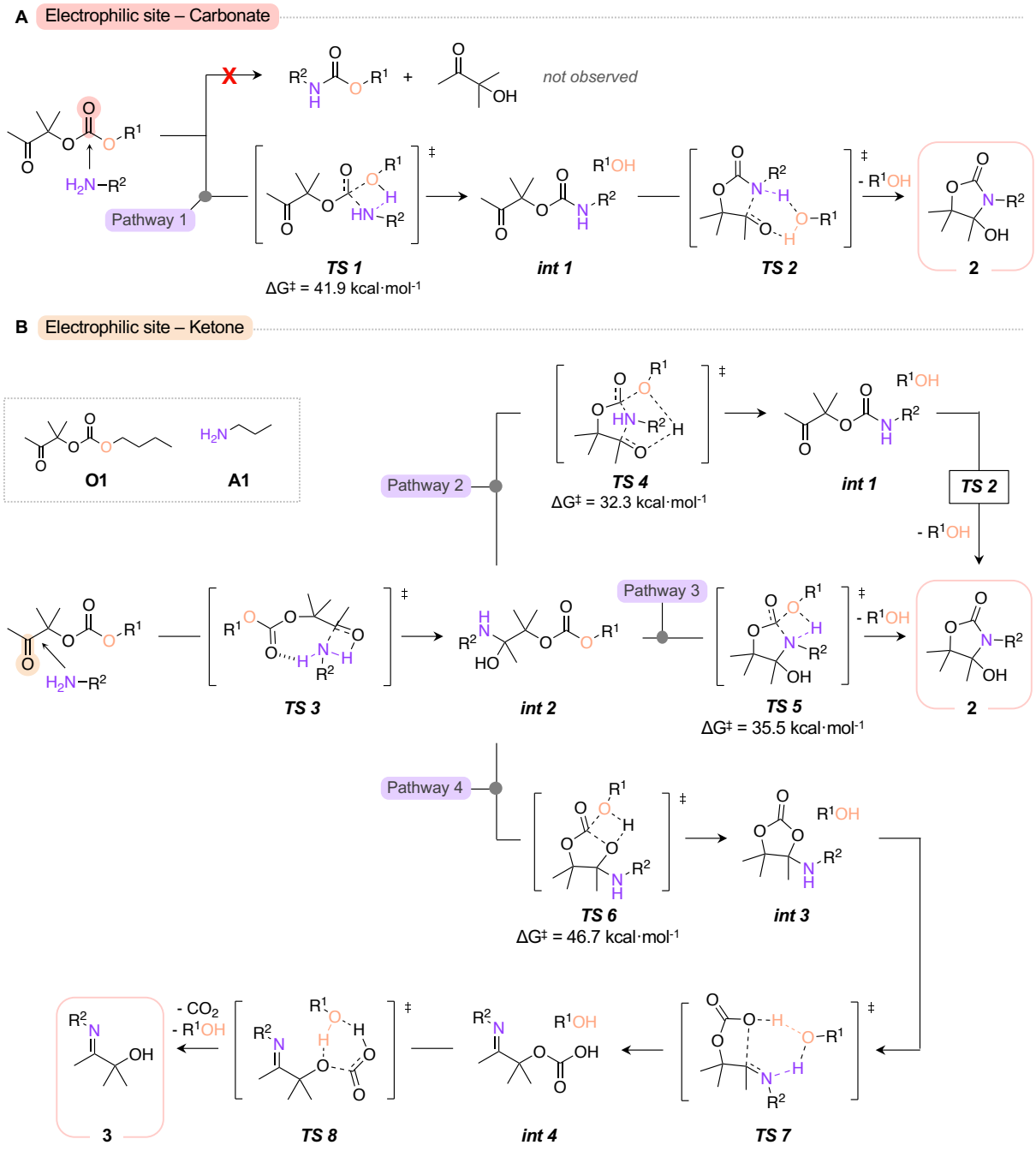

Scheme 2. Mechanism of *oxo*-carbonate **O1** aminolysis with **A1** and formation of products **2** and **3** through the four different pathways. Schematic transition state structures are given for each reaction step and the Gibbs free energy differences (expressed in kcal·mol^{-1}) are given for the rate-determining steps (ωB97-XD/6-311++G(d,p)).

First, the aminolysis of the carbonate toward the oxazolidinone product **2** was envisaged (pathway 1; Scheme 2A, Figure S17). The nucleophilic attack of the amine to the carbonate provided the *oxo*-urethane **int 1** by direct hydrogen transfer from the amine to the leaving alcohol. This first step accounts for the rate-determining step of the reaction with an energy barrier of 41.9 kcal·mol^{-1} (Figure S17). The *oxo*-urethane **int 1** then undergoes an intramolecular cyclization to form **2**.

The calculations of aminolysis to ketone moiety demonstrated that the *oxo*-carbonate leads to the product **2** by two other possible pathways. Pathway 2 (Scheme 2B) consists first in the attack of the ketone by the amine to form a hemiaminal intermediate **int 2** (Figures S18 and S19). The second step, which is the rate-determining step, is the addition of the hemiaminal secondary amine to the carbonate with proton transfer from the hemiaminal alcohol to the leaving alcohol. The original C-N bond is broken to form a new carbamate bond (Scheme 2B and Figure S20 ***TS 4***), resulting in the *oxo*-urethane **int 1** with an energy barrier of 32.3 kcal·mol^{-1}. The third step of this pathway consists in the cyclization into **2**, same as happening in pathway 1. Pathway 3 (Scheme 2B, Figure S21) begins with the formation of **int 2** however, unlike pathway 2, the secondary amine attacks the carbonate function with direct proton transfer from the amine to the leaving alcohol (Figure S22), forming **2**. The second step is the rate-determining step with an energy barrier of 35.5 kcal·mol^{-1}. Both pathways 2 and 3 have close energy barriers which are way lower than pathway 1 (9.6 kcal·mol^{-1} less for pathway 2 and 6.4 kcal·mol^{-1} for pathway 3).

Although both pathways 1 and 2 proceed through the formation of **int 1**, this species was not experimentally observed by NMR during any of the reaction kinetics. This is in contrast with experimental results from our previous study where *oxo*-urethane species (**int 1**) were observed during the reaction of αCC and different amines. This effect might be explained by the fact that the cyclization reaction into **2** was highly favored in the presence of the released alcohol, which could act as proton shuttle between the nitrogen and the pendent ketone. The energy barrier of the cyclization has been calculated to be of 23.0 kcal·mol^{-1} for the most stable transition state (Figures S17 and S19), which is very low compared to the rate-determining steps of both pathways and consequently makes this cyclization step expeditive.

The formation of **2** is highly exergonic with an energy of the separate products of -13.2 kcal·mol^{-1} compared to the starting reactants. Importantly, when hydrogen bonding between **2** and the released alcohol is considered, this value was decreased to -29.1 and -19.7 kcal·mol^{-1} for pathways 2 and 3, respectively (Figure S19 and S21). The formation of **int 1** in pathway 2 was also providing a strongly bonded complex with the released alcohol displaying a relative energy of -17.8 kcal·mol^{-1}. These reactions thus have very high reverse energy barriers (43.1 kcal·mol^{-1} for pathway 2 and 48.5 kcal·mol^{-1} for pathway 3), attesting the irreversible character of these routes.

The formation of imine **3** can be rationalized through the pathway 4 from **int 2** (Scheme 2B), achieving a ring-closing step by the nucleophilic attack of the alcohol to the carbonate with direct proton transfer to the leaving alcohol (Figures S23 and S24). This path leads to a five-membered cyclic carbonate intermediate **int 3** via an activation barrier of 46.7 kcal·mol^{-1}. The cyclic carbonate with the secondary amine pending group was however never observed during the reaction kinetics. In fact, calculations show that this intermediate is prone to ring-open with formation of a C=N double bond, thus affording **int 4**. The intermediate then undergoes decarboxylation to furnish the imine **3**. Same as in pathways 1 and 2 where **int 1** cyclization was assisted by the released alcohol, the most stable transition state was found with the butanol acting as proton relay (for both ***TS 7*** and ***TS 8***). This route might as well be irreversible as the reverse activation barrier accounts for 55.6 kcal·mol^{-1} (8.9 kcal·mol^{-1} higher than the forward reaction) and with the concomitant release of CO_2 from the reaction medium.

As pathway 4 has depicted a large energy barrier for the formation of **3** compared to pathways 2 and 3 (> 10 kcal·mol^{-1}), one could expect the exclusive formation of **2**. However, a selectivity of 72% in **2** was obtained after 24 h of reaction with 3 equivalents of **A1** compared to **O1**. Although precedent calculations are helpful to rationalize the formation of the products and to get an insight of the favored pathways, they do not take into account numerous neighboring compounds that may participate in the process. However, calculations involving a large number of extra molecules is out of the scope of this paper. In an attempt to rationalize the formation of **3** in non-negligible amounts, the rate-determining step of the reaction was modelized using an extra amine molecule. A first experiment using butanol (released during the reaction) does not lead to any change in the activation energy, even when it was used in a proton shuttle configuration (Figure S25). This is expected as no change in selectivity is observed during the reaction kinetics (Figures S5-S10). However, using an extra amine drastically decreases the energy barrier of the reaction. The most stable isolated path consists in using the amine as proton relay in a two-step manner. In this scenario, the energy barrier decreased from 46.7 to 26.0 kcal·mol^{-1} (Scheme 3). The first step of the reaction involves the formation of a tetrahedral intermediate **int 2'** stabilized by hydrogen bonds and the second step relies in the hydrogen transfer toward the leaving alcohol (Scheme 3). From these calculations, using an excess of amines is therefore expected to decrease the selectivity in **2**. To verify this hypothesis, we compared the rate and the selectivity of the aminolysis of **O1** for different contents of amine **A1** (1, 3 and 15 equivalents of **A1** *vs* the *oxo*-carbonate). Results are summarized in Figure 2A, 2B and 2C. As expected, by increasing the content of amine, the **O1** conversion was strongly raised from 10 % with 1 eq. amine after 3 h of reaction, to 79 and 100% with 3 and 15 eq. amine, respectively. In line with the calculations, the increase of the amine content from 1 to 3 eq. decreased the selectivity in **2** from 85% to 72%, in favor of

the formation of the imine by-product **3**. The decrease of selectivity in **2** was less pronounced when further increasing the amine excess from 3 (72% of **2**) to 15 eq. (68% of **2**). Similarly to our previous observations, the selectivity of the three reactions is rather constant over the whole reaction time.

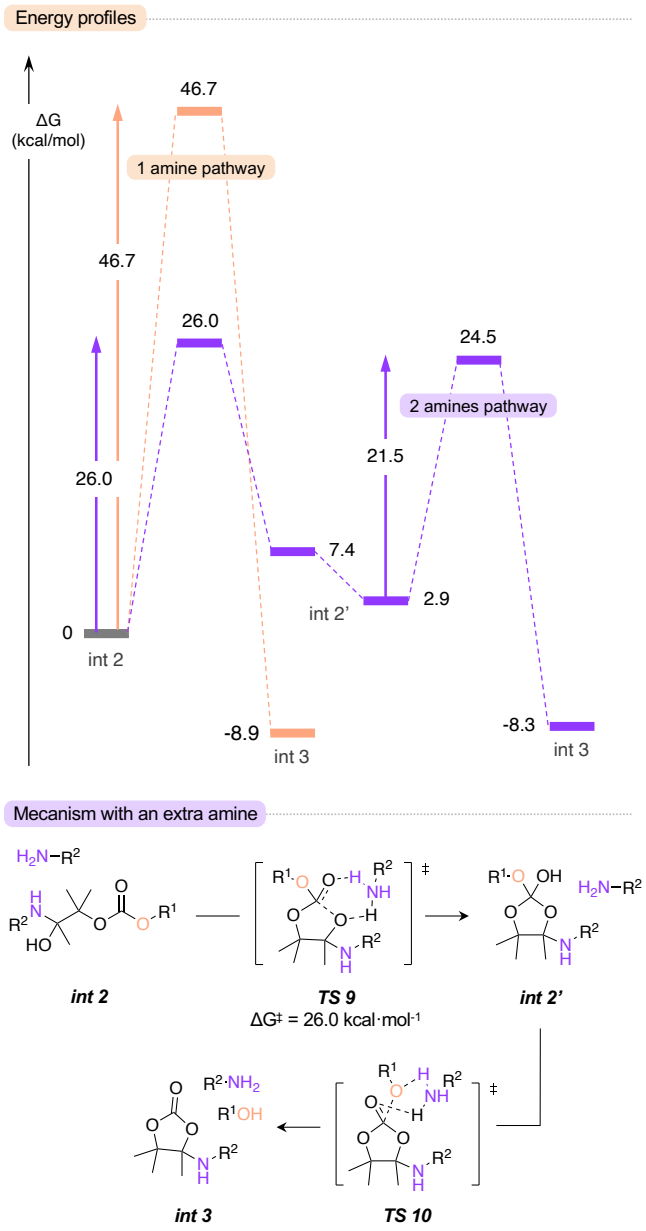

Scheme 3. Gibbs free energy profile for the reaction from **int 2** to **int 3** in pathway 4 without and with the presence of an extra amine molecule. Corresponding reaction scheme and schematic transition state structures are given for the two-step pathway involving an extra amine molecule. Gibbs free energy differences are expressed in kcal·mol^{-1} (ωB97-XD/6-311++G(d,p)).

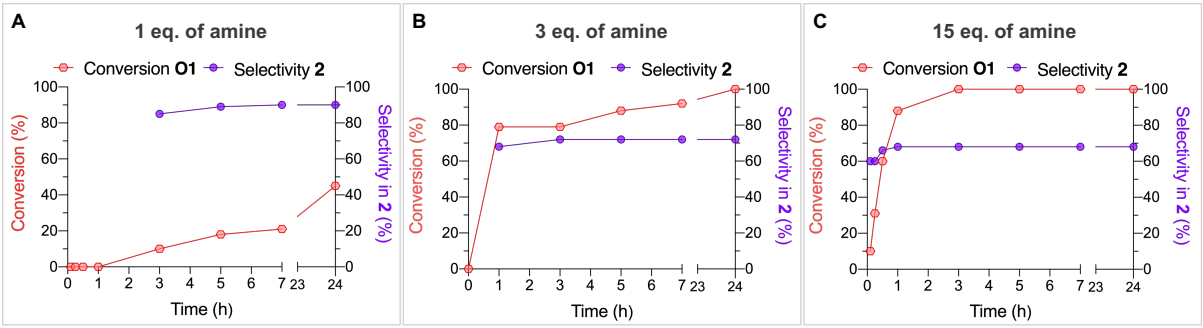

Figure 2. Influence of amine content (**A1**) at A) 1 eq., B) 3 eq., C) 15 eq. *vs* the oxo-carbonate on the **O1** conversion and selectivity in product **2** for the catalyst-free aminolysis of *oxo*-carbonate **O1**.

These modeling studies confirm the higher ketone reactivity toward nucleophiles than the carbonate in *oxo*-carbonate compounds. The formation of a hemiaminal intermediate (**int 2**) after aminolysis of the ketone was a common step for pathways 2-4. Although following different routes, both pathways 2 and 3 lead to the formation of the hydroxy-oxazolidinone product **2** with similar energy barriers. The formation of the imine **3** was rationalized through pathway 4 passing through a five-membered cyclic carbonate intermediate (**int 3**). The energy barrier for this reaction was rather high compared to the other pathways, in line with the selectivity experimentally obtained. As the activation energy for the rate-determining step is strongly decreased when involving an extra amine in the mechanism, we hypothesized that selectivity toward **2** might be improved by diminishing the amine loading in the reaction medium. This was experimentally verified by monitoring the aminolysis of **O1** with 1 equivalent of **A1** as discussed above and illustrated in Figures 2A-B. High selectivity in **2** of 90% was obtained in the presence of 1 eq. of amine (Figure 2A), compared to 72% with 3 eq. after 24 h of reaction (Figure 2B).

Aminolysis of poly(oxo-carbonate)s. Capitalizing on the model reactions, the degradation experiments were extended to poly(*oxo*-carbonate)s. To do so, three polymers of different microstructures were synthetized by step-growth copolymerization of the CO_2-sourced bis-exovinylene cyclic carbonate (**BisαCC**) with 1,4-butanediol (**PC1**), 1,4-benzenedimethanol (**PC2**) or 1,4-cyclohexanediol (**PC3**) at 25 °C with DBU as organocatalyst (5 mol% *vs* BisαCC) following a procedure previously described by our group (Scheme 4, Figures S26-S31).[30]

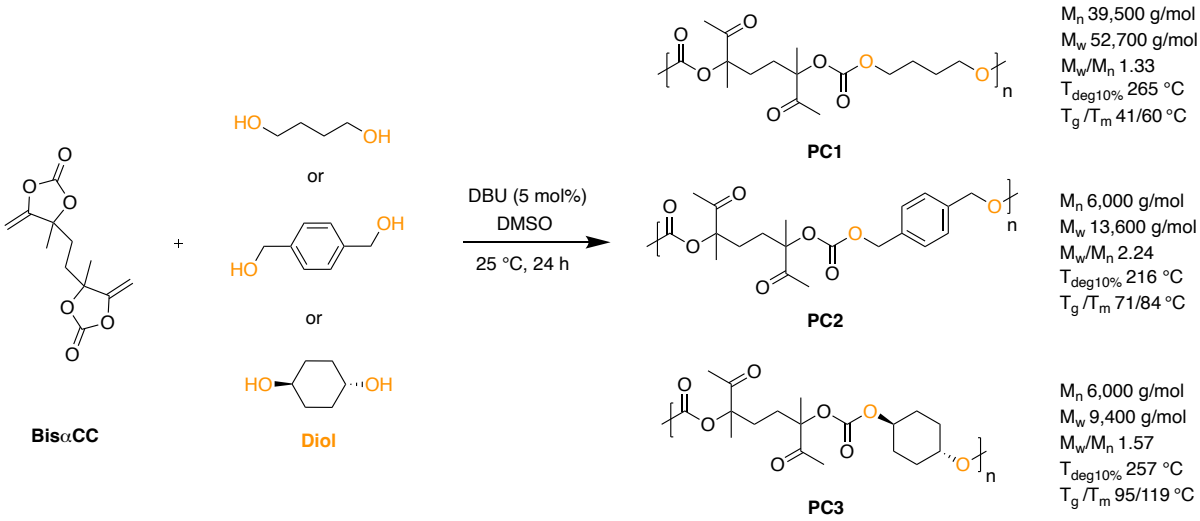

Scheme 4. Synthesis of **PC1**, **PC2** and **PC3** by step-growth copolymerization, and their molecular characteristics and thermal properties. The thermal properties of the polymers were determined and reported in our previous work.[30]

Afterwards, propylamine (the most efficient amine tested for the model reactions) was selected for the aminolysis of the poly(*oxo*-carbonate)s. **PC1** was first depolymerized at room temperature using propylamine **A1** (3 eq. *vs* each ketone moiety of the polymeric repeating unit) in THF (Figure 3A). The **PC1** degradation was monitored by ^{1}H-NMR spectroscopy (to determine the degradation percentage and identify the degradation products) and SEC analysis (to follow the change in the molar mass of the polymer chains) (Figures 3B, 3C and 3D) (for the complete kinetic overlay spectra and identification products see Figures S32 and S33 in the supporting information section). Interestingly, 89 % of **PC1** was already degraded in 1 h. This was highlighted by ^{1}H-NMR spectroscopy, with the significant decrease of the signal intensity of the methyl adjacent to the ketone moiety at δ = 2.10 ppm (Figure 3D) and the concomitant appearance of new signals at 3.03 ppm and 3.22 ppm typical of methylene group in alpha position to the nitrogen atom of oxazolidinone and imine moieties, respectively. Besides, the **PC1** molar mass (M_n) dropped from 39,500 g/mol to 1,600 g/mol in 1 h (Figures 3B and 3C) which attested for the chain degradation. The **PC1** aminolysis was then extended to 24 h to ensure the total polymer deconstruction (> 99 %) into 1,4-butanediol **1a** (isolated yield = 85 %) and bis(hydroxy-oxazolidinone) **2a** (isolated yield = 56 %) (Figures S34 and S35). Alike the model reactions, imine containing scaffolds side products were observed as well (17 % of the total composition). However, attempts to isolate these side products by chromatography were unsuccessful due to their poor chemical stability.

To minimize the formation of the imine side-products, a degradative experiment of **PC1** was carried out at a lower temperature, i.e. 6 °C. Under this condition, the polymer deconstruction was significantly slowed down, however already reaching 90 % after 24 h. Nevertheless, the alcohol/oxazolidinone/imine molar composition remained almost unchanged (50/38/12

compared to 50/33/17 at 25 °C) (Figure S36). It is important to note that the previous DFT modelling evidenced that a second amine acting as a proton relay in the degradation mechanism diminished by ~2 the activation energy of the rate determining step of the imine formation (Scheme 3). Therefore, as shown in the model reaction (Figure 2B and 2C), the use of an excess of amine is detrimental for the products selectivity. Therefore, **PC1** was deconstructed at 25 °C in THF using only 1 eq. of **A1** *vs* each ketone moiety of the polymeric repeating unit. Remarkably and similarly to the model reaction (Figure 2A), the formation of the imine side products was found very low as attested by the alcohol/oxazolidinone/imine molar composition of 50/45/5 (Figure S37). Despite the product selectivity was improved, decreasing the amine content slowed down the **PC1** degradation rate that reached 70 % in 24 h (Figure S37) and 86% after 48 h (Figure S38).

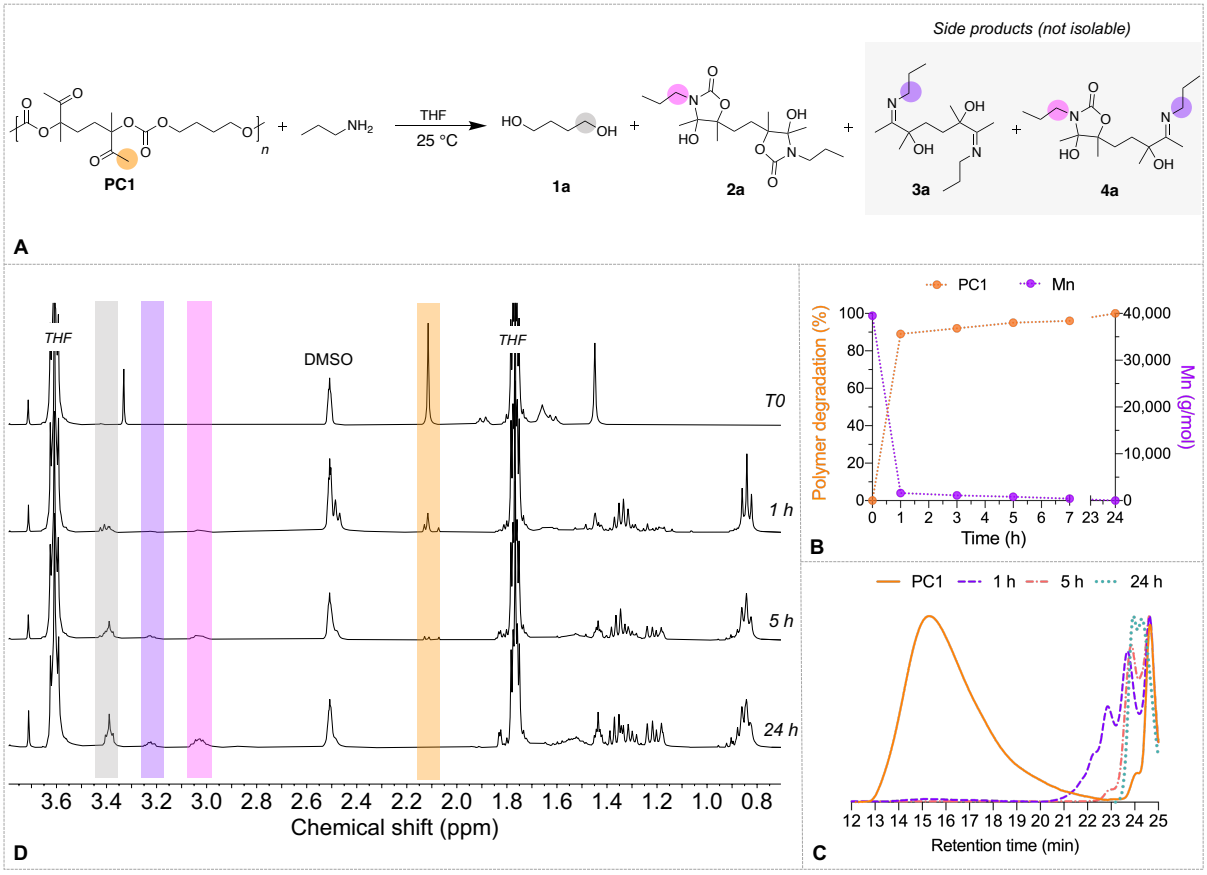

Figure 3. A) Room temperature aminolysis of **PC1** and degradation products; B) time evolution of the **PC1** degradation (via ^{1}H-NMR spectroscopy using 1,3,5-Trimethoxybenzene as internal standard) and the **PC1** M_n (determined by SEC); C) time evolution of the SEC profiles of **PC1** (using DMF/LiBr as eluent); D) kinetics of degradation of **PC1** followed by ^{1}H-NMR (in DMSO-d_6). Note that T0 was recorded before adding propylamine, since this last one is very reactive.

Unfortunately, applying a similar degradation protocol to **PC2** and **PC3** was impossible as both polymers were insoluble in THF. Consequently, we evaluated the possibility to degrade the three poly(*oxo*-carbonate)s **PC1-3** by suspending them in **A1** used in large excess.

Remarkably, the polymers degradation was expeditious, with a total disassembly of **PC1-3** in less than 30 min at rt (Scheme 5, Figures S39-S41). Diols **1a-c** were recovered with isolated yields > 90% and product **2a** was collected at a lower yield of 25% due to the formation of the imine side products (50:50 imine/oxazolidinone molar ratio).

Alike the majority of step-growth copolymers, impediments to the **PC1-3** recycling by solvolysis lies on the formation of a mixture of products that needs separation for further valorization. Oxazolidinones are important organic synthons widely used in medicinal chemistry and organic synthesis.[38–45] However, the possible applications of bis(hydroxy-oxazolidinone) **2a** are unknown. In order to illustrate the versatility of the solvolysis process to provide useful building blocks, we replaced propylamine by propanolamine **A4.** This amine was expected to furnish a new bis(hydroxy-oxazolidinone) **2b** bearing two primary alcohols possibly suitable for repolymerization by the step-growth manifold (Scheme 6).

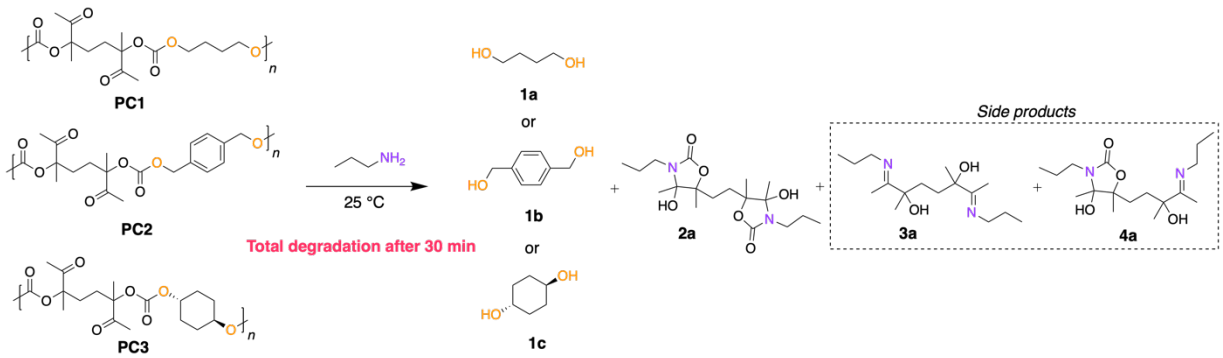

Scheme 5. PC1-3 aminolysis using propyl amine as solvent.

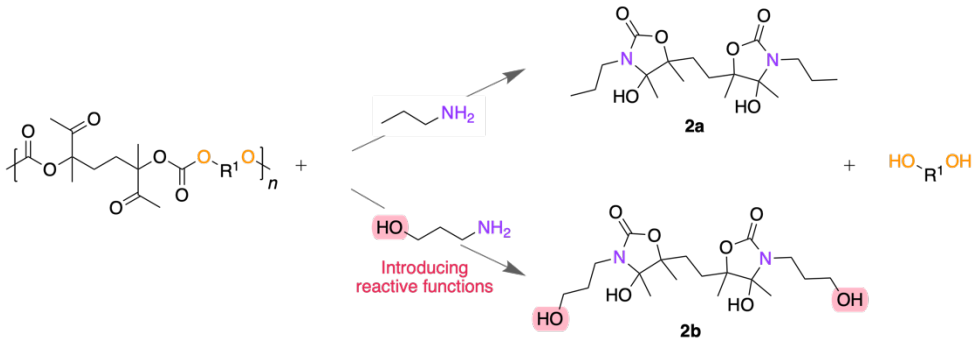

Scheme 6. Conceptualization of functionalized bis(hydroxy-oxazolidinone).

To validate the concept, the aminolysis of **PC1** by **A4** (3 eq. *vs* each ketone moiety of the polymeric repeating unit) was carried out at 25 °C in THF under catalyst-free conditions. After 1 h, 98% of **PC1** was already depolymerized (Figure S42), providing after 24 h the main products **1a** and **2b** with respective isolated yields of 92% and 65%. The structure of **2b** was

confirmed by high resolution mass spectrometry, ^{1}H- and ^{13}C-NMR analysis (Figures S43 and S44). The presence of imine by-products was also observed in the crude sample, yet not isolable.

We then investigated the use of **2b** as a comonomer for the step-growth copolymerization with BisαCC in the presence of DBU (5 mol% *vs* BisαCC), in DMSO, for 24 h at 25 °C (Figure 4A). The ^{1}H- and ^{13}C-NMR spectra of **PC4** (Figure 4B and Figure S45) confirmed the formation of a polymer alternating *oxo*-carbonate and hydroxy-oxazolidinone linkages. This was evidenced by the typical resonances of the two methyl groups of the *oxo*-carbonate fragments at δ = 1.44 ppm and δ = 2.12 ppm as well as the peak at δ= 4.11 ppm corresponding to the methylene group adjacent to the linear carbonate. Moreover, the presence of the methylene signal at δ = 3.17 ppm attested for the insertion of **2b** within the polymer chains. The copolymer microstructure was confirmed by ^{13}C-NMR via the presence of the ketone and carbonate groups at δ = 206.3 ppm and δ = 153.61 ppm, respectively, and the carbonyl resonance of the hydroxy-oxazolidinone group at δ = 156.9 ppm. The methylene signal at δ= 66.4 ppm supported the formation of the carbonate linkages by reaction of the two monomers. Remarkably, **2b** participated to the **PC4** construction by the chemoselective addition of the more reactive primary alcohols to the exovinylene cyclic carbonates, furnishing linear chains with M_w = 16,000 g/mol soluble in THF (Figure 4C). No crosslinked material was collected, further supporting that the tertiary alcohols were not involved in the reaction.

The thermal properties of **PC4** were then evaluated by thermogravimetric analysis (TGA) (Figure 4D) and modulated differential scanning calorimetry (mDSC) (Figure 4E). **PC4** was found thermally stable with a high decomposition temperature at 10% weight loss $T_{d10\%}$ of 242 °C, thus in the same range of the initial polycarbonate **PC1** (Scheme 4). The DSC analysis revealed the presence of two glass-transition temperatures (T_g) at 64 °C and 124 °C. This unusual thermal behavior was recently observed by our group for other types of poly(hydroxy-oxazolidinone)-containing copolymers, i.e. poly(thiocarbonate-*co*-hydroxy-oxazolidinone)s obtained by the terpolymerization of BisαCC with dithiols and diamines.[46] We hypothesized that the first T_g corresponds to the main glassy matrix, while the second T_g might be related to the presence of hydrogen bonding between the hydroxy-oxazolidinone linkages, leading to a minor glassy phase. Further investigations would however be needed to fully explain this unusual but reproducible thermal behavior, which is out of scope of this paper.

On the path to circularity, the poly(*oxo*-carbonate-*co*-hydroxy-oxazolidinone) **PC4** was recycled in a closed loop scenario by exploiting the pendent ketones, in a similar fashion than for the previous poly(*oxo*-carbonate)s (Figure 5). Indeed, by using 3 eq. of **A4** *vs* each ketone moiety of the polymeric repeating unit, in THF, at 25 °C, **PC4** was totally degraded after 24 h, furnishing **2b** with a high selectivity of 85 % (Figure S46). **PC4** was thus depolymerized into

the starting monomer mainly, that could be reused multiple times. Removing the imine by-product is however needed prior recycling. This can be easily achieved by flash chromatography on silica column using dichloromethane/acetone (50:50) mixture, that furnished **2b** with 72% isolated yield (see experimental section for details). This innovative approach follows the life cycle of poly(*oxo*-carbonate)s from their synthetic design, promoting the use of renewable feedstock by using lignin or sugar-based diols and CO_2-derived cyclic carbonates, to their degradation process.

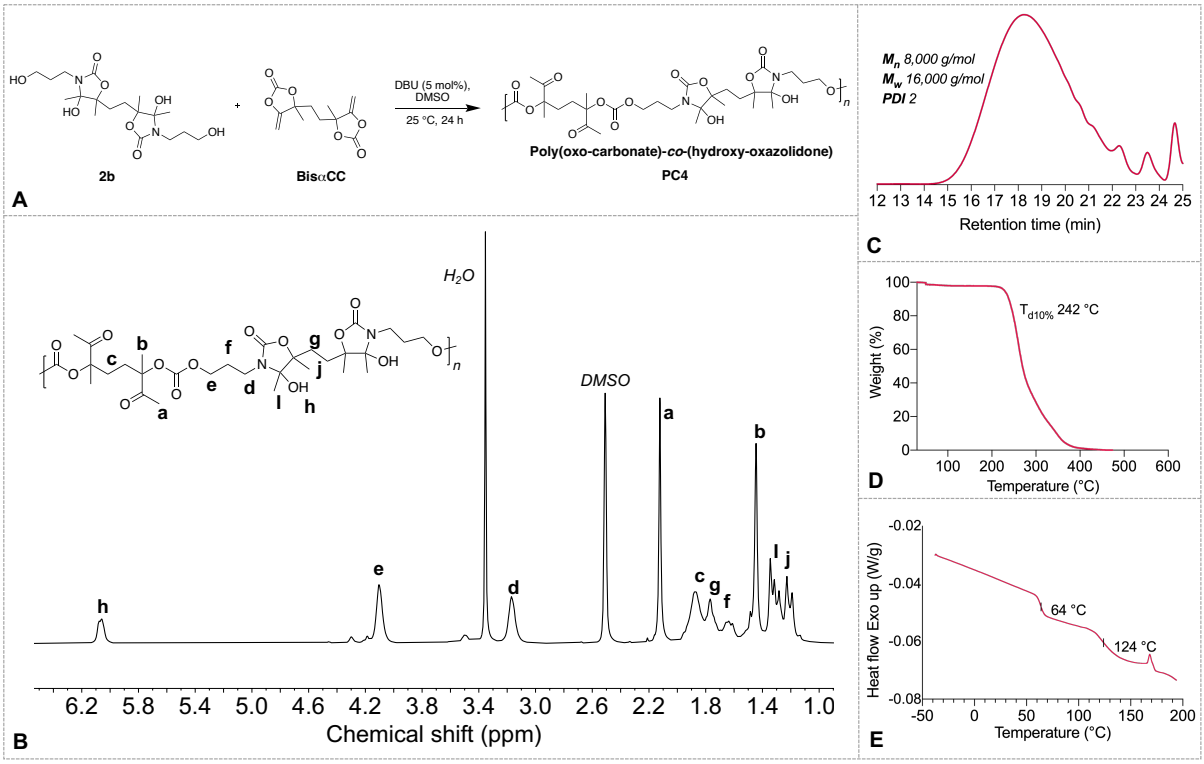

Figure 4. A) Synthesis of poly(*oxo*-carbonate-*co*-hydroxy-oxazolidinone) **PC4**; B) ^{1}H-NMR characterization of purified **PC4** (in DMSO-d_6); C) SEC of **PC4** recorded in DMF/LiBr; D) thermal degradation of **PC4**; E) differential scanning calorimetry analysis of **PC4** (T_g values are obtained from the second heating scan).

The efficient, selective and environmental-friendly chemical depolymerization process satisfied most of sustainable and desirable conditions (i.e. catalyst-free and mild reaction conditions, fast degradation) leading to value-added chemicals. These latter could be utilized to re-construct new polymeric materials that can be degraded into the starting monomers and reused in a close-loop scenario, minimizing the post-consumer plastic waste.

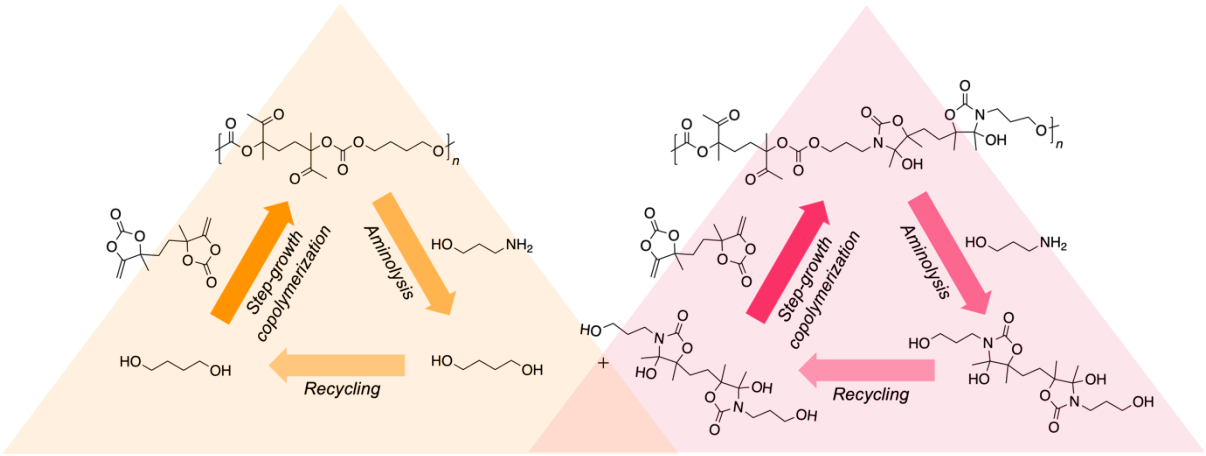

Figure 5. Closed-loop polymerization-depolymerization system.

Conclusion

Chemical depolymerization has become a worldwide challenge to convert plastic wastes into monomers or value-added products. By appropriate editing polycarbonates by step-growth copolymerization of bis(exovinylene cyclic carbonate)s with diols, the unique microstructural features of the polymers facilitate their rapid deconstruction by aminolysis at room temperature. The starting diols were recovered at high yields, together with bis(oxazolidinone) scaffolds and a small amount of imine by-products. Expeditive depolymerizations (complete in less than 30 min at rt) were also achieved when the polycarbonates were directly reacted in the amine used as solvent and reagent. Model reactions were carried out to understand the influence of the amine structure on the efficiency of the aminolysis and the selectivity of the reaction. DFT modeling evidenced the preferential attack of the amine to the more electrophilic ketone site rather than on the carbonate one, leading to an hemiaminal intermediate. The latter cyclized by the attack of its secondary amine to the carbonate and furnished the oxazolidinone scaffold after the release of alcohol.

Importantly, by selecting a functional amine (e.g. propanolamine), the facile and complete polycarbonate deconstruction was obtained at rt after 24 h, and a bis(oxazolidinone) bearing two primary alcohol groups was recovered at moderate isolated yield (65%), together with the starting diol (used for constructing the polycarbonate) at a high isolated yield of 92%. The functional bis(oxazolidinone) was upcycled by its step-growth copolymerization with a bis(exovinylene cyclic carbonate) to furnish a polymer alternating *oxo*-carbonate and oxazolidinone linkages at rt. The aminolysis of this polymer by the same amine furnished the starting bis(oxazolidinone) as the main degradation product, that can be involved in a closed loop scenario to prepare the same polymer.

Well-beyond demonstrating that poly(*oxo*-carbonate)s can be easily and rapidly depolymerized by aminolysis under mild conditions, we herein demonstrate that these polymers can also be exploited to produce new attractive building blocks by the appropriate choice of the amine used for aminolysis.

Experimental section

Materials.

4,4-dimethyl-5-methylene-1,3-dioxolan-2-one (αCC), 4,4'-(ethane-1.2-diyl)bis(4-methyl-5-methylene-1,3-dioxolan-2-one (BisαCC) were synthesized as reported elsewhere by our group.[31,36] Propylamine (99%) was purchased from Fluka. Benzyl alcohol (99%), 1-butanol (98%), cyclohexanol, 1,8-diazabicyclo[5.4.0]undec-7-ene (DBU 99%) and 3-amino-1-propanol (99%) were purchased from Sigma-Aldrich. 1,4-butanediol (99%), *trans*-1,4-cyclohexanediol (99%), were supplied by Fluorochem, while 1,4-benzenedimethanol (99%) was purchased from TCI. All the reactions were performed under inert atmosphere of N_2.

Characterization methods.

Nuclear magnetic resonance (NMR) spectroscopy. NMR analyses were performed on Bruker 400 MHz spectrometers in DMSO or $CDCl_3$ at 25 °C in the Fourier transform mode. 16 or 64 scans for a ^1H spectra and 512 or 2048 scans for ^{13}C spectra were recorded.

Size exclusion chromatography (SEC). Number-average and weight-average molecular weights and molecular weight dispersity (M_w/M_n) values of polymers were determined by size exclusion chromatography (SEC) in dimethylformamide (DMF) and in chloroform ($CHCl_3$). The SEC in DMF contained LiBr (0.025 M) and were conducted at 55 °C (flow rate: 1 mL/min) with a Waters chromatograph equipped with three columns (Waters Styragel PSS gram 1000 Å (×2), 30 Å), dual λ absorbance detector (Waters 2487) and a refractive index detector (Waters 2414). The SEC in chloroform were conducted at 35 ºC at a flow rate of 1 $cm^3 \cdot min^{-1}$, using an isocratic pump (VE 1122, Viscotek) a set of two PLgel 5 µm MIXED-C ultra-high efficiency column and a Shodex SE 61 differential refractive index detector as well as a variable wavelength UV detector (Spectra 100, Spectra-Physics). A volume of 100 µL of sample solution in chloroform (concentration 0.3 % w/v) was injected. Polystyrene standards (Polymer Laboratories) with narrow molecular weight distributions were used to generate a calibration curve.

High Resolution Mass Spectrometry (HRMS). High-resolution mass spectra in positive mode were recorded using a 6520 series quadrupole time-of-flight (Q-TOF) mass spectrometer (Agilent) fitted with a multimode ion source.

Thermogravimetric analysis (TGA) in the polymers were performed on a TGA2 instrument from Mettler Toledo. Around 5 mg of sample was heated at 20 °C/min until 600 °C under N_2 atmosphere (20 mL/min).

Modulated Differential scanning calorimetry (mDSC) analyses were performed on a DSC 250 differential calorimeter (TA Instruments). All the experiments were performed under ultrapure nitrogen flow. Samples of 2–5 mg were used and placed in sealed aluminum pans. The samples were first heated at a rate of 10 °C min^{-1} from 25 °C to 90 °C. Then, after an isotherm of 5 min at 90 °C, the samples were cooled down to -40 °C at a rate of 10 °C min^{-1}, followed by an isotherm of 5 min at -40 °C. Subsequently, modulate temperature segment was set with an amplitude of 2.00 °C for 60.0 seconds, followed by an isothermal of 5.0 min. The sample was heated at rate of 2.00 °C/min to 200.00 °C. The last heating cycle was used for the determination of the T_g.

Representative procedure for the synthesis of oxo-carbonates

αCC (4 mmol, 1 eq.) and alcohol (4 mmol, 1 eq.) were added in a reaction tube with dry DMF (1 mL) and DBU (0.2 mmol, 5 mol% compared to αCC). Samples were taken after 24 h and analyzed by ^{1}H-NMR spectroscopy to determine the αCC conversion. The *oxo*-carbonates were purified by extraction in the diethyl ether/water mixture. The organic phase was dried over magnesium sulfate, and dried under vacuum in order to remove the solvent.

Representative procedure for the degradation of oxo-carbonates and purification of hydroxy-oxazolidinones

O1 (0.81 g, 4 mmol) and propylamine (3 eq.) were added in a flask. All model reactions were conducted at 25 °C in THF (2 mL) under N_2 atmosphere. Samples were taken after different time intervals, adding formic acid to neutralize the amine, and analyzed by ^{1}H-NMR spectroscopy DMSO-d_6 to determine the *oxo*-carbonate conversion.

To recover the hydroxy-oxazolidinones, diethyl ether was added to the reaction crude and the organic phase was extracted with water (three times). The organic phase was dried over magnesium sulfate and the solvent was removed under vacuum. Then the hydroxy-oxazolidinones were recrystallized in cyclohexane/ethyl acetate 80:20 and let at -20 °C for 24 h. After filtration, the white solid collected was dried under vacuum for 24 h.

General procedure for the synthesis poly(oxo-carbonate)s

BisαCC (3.93 mmol, 1 g) and 1,4-butanediol (3.93 mmol, 0.358 g), dry DMSO (5 mL) and DBU (30 µL, 5 mol% *vs* BisαCC) were added to a flask at 25 °C. The reaction medium was then stirred for 24 h. At the end of the reaction, an aliquot was withdrawn to determine the conversion of the monomers by ^{1}H-NMR spectroscopy. The polymer was purified by precipitation in methanol/water (1:1) and then dried under vacuum at 25 °C for 24 h, and

characterized by ^{1}H-NMR spectroscopy and SEC. The same procedure was carried out for the other polymers.

Kinetics of polymer aminolysis in THF

In a typical procedure, in a glass tube were introduced 0.4 g of **PC1**, propylamine (3 eq. *vs* each ketone moiety of the polymeric repeating unit, 0.412 g) and dry THF (1.2 mL) under N_2 and adding 1,3,5-Trimethoxybenzene (TMB) as internal standard. The reaction was realized at 25 °C. The kinetic was monitored by ^{1}H-NMR spectroscopy in DMSO-d_6 and by SEC analysis. To separate **2a** from the reaction medium, THF was removed in the rotavapor and then, the crude medium was dissolved in a minimum volume of dichloromethane/acetone (50:50) and purified by flash chromatography on silica using the same solvent mixture as eluent (isolated yield = 56 %).

Polymer aminolysis using amine as solvent

Representative procedure for the degradation of polycarbonates: **PC1** (0.4 g) and propyl amine (3 mL) were added in a flask under N_2 atmosphere. The reaction medium was stirred at 25 °C for 30 min. Samples was analyzed by ^{1}H-NMR spectroscopy in DMSO-d_6 and SEC in DMF to determine the *oxo*-carbonate conversion. **PC2** and **PC3** are only soluble in $CHCl_3$ and the polymer degradation was determined by ^{1}H-NMR spectroscopy in $CDCl_3$.

To separate **2a** from the reaction medium, the excess of propyl amine was removed in the rotavapor and then, the crude medium was dissolved in a minimum volume of dichloromethane/acetone (50:50) and purified by flash chromatography on silica using the same solvent mixture as eluent.

The same procedure was carried out to separate **2a** from 1,4-cyclohexanediol for the **PC3** degradation. In case to separate **2a** from 1,4-benzenedimethanol for the **PC2** degradation, diethyl ether was first used as eluent in order to remove the alcohol; dichloromethane/methanol (50:50) was then used as eluent to isolate **2a**.

Procedure for the depolymerization of PC1 by propanolamine A4

PC1 (0.4 g), propanolamine (3 eq. *vs* each ketone moiety of the polymeric repeating unit, 0.524 g) and dry THF (1.2 mL) were added in a flask N_2 atmosphere, adding 1,3,5-Trimethoxybenzene (TMB) as internal standard. The reaction medium was stirred at 25 °C for 24 h. Samples was taken and analyzed by ^{1}H-NMR spectroscopy and SEC (in DMF/LiBr) to determine the *oxo*-carbonate conversion. The bis(hydroxy-oxazolidinone) **2b** was separated from the other products by flash chromatography on silica using as dichloromethane/acetone (50:50). (isolated yield = 65 %).

Synthesis of PC4

BisαCC (3.93 mmol, 1 g), **2b** (3.93 mmol, 1.590 g), dry DMSO (5 mL) and DBU (0.196 mmol, 0.03 mL) were added in a flask and let to react under N_2 atmosphere at 25 °C. The reaction medium was then stirred for 24 h. After 24 h, the reaction was deactivated by adding formic acid (0.045 mL) and an aliquot was withdrawn to determine the conversion of the monomers by ^{1}H-NMR spectroscopy. The polymer was purified by precipitation in water, followed by dissolution of the polymer in THF and dialysis in THF with a Spectra/Por dialysis membrane (pretreated RC tubing 1 kDa). **PC4** was then precipitated in diethyl ether and dried under vacuum at 25 °C for 48 h. The polymer was characterized by ^{1}H- and ^{13}C-NMR spectroscopy, SEC, TGA and DSC.

Procedure for PC4 depolymerization

PC4 (0.4 g), propanolamine (3 eq. *vs* each ketone moiety of the polymeric repeating unit, 0.274 g) **A4** and dry THF (1.2 mL) were added in a flask under N_2 atmosphere. The reaction medium was stirred at 25 °C for 24 h. Samples was taken and analyzed by ^{1}H-NMR spectroscopy to determine the *oxo*-carbonate conversion. The bis(hydroxy-oxazolidinone) **2b** was isolated with 72% yield by flash chromatography on silica using as dichloromethane/acetone (50:50), followed by solvent removing under vacuum.

References

(1) Helms, B. A.; Russell, T. P. Reaction: Polymer Chemistries Enabling Cradle-to-Cradle Life Cycles for Plastics. *Chem* **2016**, *1*, 816–818. https://doi.org/10.1016/j.chempr.2016.11.016.

(2) Geyer, R.; Jambeck, J. R.; Law, K. L. Production, Use, and Fate of All Plastics Ever Made. *Science Advances* **2017**, *3*, e1700782.

(3) Korley, L. T. J.; Epps, T. H.; Helms, B. A.; Ryan, A. J. Toward Polymer Upcycling-Adding Value and Tackling Circularity. *Science (1979)* **2021**, *373*, 66–69.

(4) Roy, P. S.; Garnier, G.; Allais, F.; Saito, K. Strategic Approach Towards Plastic Waste Valorization: Challenges and Promising Chemical Upcycling Possibilities. *ChemSusChem* **2021**, *14*, 1–22. https://doi.org/10.1002/cssc.202100904.

(5) Vollmer, I.; Jenks, M. J. F.; Roelands, M. C. P.; White, R. J.; van Harmelen, T.; de Wild, P.; van der Laan, G. P.; Meirer, F.; Keurentjes, J. T. F.; Weckhuysen, B. M. Beyond Mechanical Recycling: Giving New Life to Plastic Waste. *Angewandte Chemie - International Edition* **2020**, *59*, 15402–15423. https://doi.org/10.1002/anie.201915651.

(6) Garcia, J. M.; Robertson, M. L. The Future of Plastics Recycling. *Science (1979)* **2017**, *358*, 870–872. https://doi.org/10.1126/science.aaq0324.

(7) Sardon, H.; Dove, A. P. Plastics Recycling with a Difference: A Novel Plastic with Useful Properties Can Easily Be Recycled Again and Again. *Science (1979)* **2018**, *360*, 380–381. https://doi.org/10.1126/science.aat4997.

(8) Zheng, J.; Suh, S. Strategies to Reduce the Global Carbon Footprint of Plastics. *Nature Climate Change* **2019**, *9*, 374–378. https://doi.org/10.1038/s41558-019-0459-z.

(9) Coates, G. W.; Getzler, Y. D. Y. L. Chemical Recycling to Monomer for an Ideal, Circular Polymer Economy. *Nature Reviews Materials* **2020**, *5*, 501–516. https://doi.org/10.1038/s41578-020-0190-4.

(10) Jehanno, C.; Pérez-Madrigal, M. M.; Demarteau, J.; Sardon, H.; Dove, A. P. Organocatalysis for Depolymerisation. *Polymer Chemistry* **2019**, *10*, 172–186. https://doi.org/10.1039/c8py01284a.

(11) Ellis, L. D.; Rorrer, N. A.; Sullivan, K. P.; Otto, M.; McGeehan, J. E.; Román-Leshkov, Y.; Wierckx, N.; Beckham, G. T. Chemical and Biological Catalysis for Plastics Recycling and Upcycling. *Nature Catalysis* **2021**, *4*, 539–556. https://doi.org/10.1038/s41929-021-00648-4.

(12) Fagnani, D. E.; Tami, J. L.; Copley, G.; Clemons, M. N.; Getzler, Y. D. Y. L.; McNeil, A. J. 100th Anniversary of Macromolecular Science Viewpoint: Redefining Sustainable Polymers. *ACS Macro Letters* **2021**, *10*, 41–53. https://doi.org/10.1021/acsmacrolett.0c00789.

(13) Worch, J. C.; Dove, A. P. 100th Anniversary of Macromolecular Science Viewpoint: Toward Catalytic Chemical Recycling of Waste (and Future) Plastics. *ACS Macro Letters* **2020**, *9*, 1494–1506. https://doi.org/10.1021/acsmacrolett.0c00582.

(14) Hou, Q.; Zhen, M.; Qian, H.; Nie, Y.; Bai, X.; Xia, T.; Laiq Ur Rehman, M.; Li, Q.; Ju, M. Upcycling and Catalytic Degradation of Plastic Wastes. *Cell Reports Physical Science* **2021**, *2*, 100514. https://doi.org/10.1016/j.xcrp.2021.100514.

(15) Roland, C. D.; Moore, C. M.; Leal, J. H.; Semelsberger, T. A.; Snyder, C.; Kostal, J.; Sutton, A. D. Fully Recyclable Polycarbonates from Simple, Bio-Derived Building Blocks. *ACS Applied Polymer Materials* **2021**, *3*, 730–736. https://doi.org/10.1021/acsapm.0c01028.

(16) Kosloski-Oh, S. C.; Wood, Z. A.; Manjarrez, Y.; de Los Rios, J. P.; Fieser, M. E. Catalytic Methods for Chemical Recycling or Upcycling of Commercial Polymers. *Materials Horizons* **2021**, *8*, 1084–1129. https://doi.org/10.1039/d0mh01286f.

(17) Kim, J. G. Chemical Recycling of Poly(Bisphenol A Carbonate). *Polymer Chemistry* **2020**, *11*, 4830–4849. https://doi.org/10.1039/c9py01927h.

(18) Singh, R.; Shahi, S.; Geetanjali. Chemical Degradation of Poly(Bisphenol A Carbonate) Waste Materials: A Review. *ChemistrySelect* **2018**, *3*,11957–11962. https://doi.org/10.1002/slct.201802577.

(19) Hata, S.; Goto, H.; Yamada, E.; Oku, A. Chemical Conversion of Poly(Carbonate) to 1,3-Dimethyl-2-Imidazolidinone (DMI) and Bisphenol A: A Practical Approach to the Chemical Recycling of Plastic Wastes. *Polymer* **2002**, *43*, 2109–2116. https://doi.org/10.1016/S0032-3861(01)00800-X.

(20) Singh, S.; Lei, Y.; Schober, A. Direct Extraction of Carbonyl from Waste Polycarbonate with Amines under Environmentally Friendly Conditions: Scope of Waste Polycarbonate as a Carbonylating Agent in Organic Synthesis. *RSC Advances* **2015**, *5*, 3454–3460. https://doi.org/10.1039/c4ra14319a.

(21) Mormann, W.; Spitzer, D. Ammonolysis of Polycarbonates with (Supercritical) Ammonia: An Alternative for Chemical Recycling. *Advances in Polycarbonates* **2005**, *898*, 244–261. https://doi.org/10.1021/bk-2005-0898.ch018.

(22) Jehanno, C.; Demarteau, J.; Mantione, D.; Arno, M. C.; Ruipérez, F.; Hedrick, J. L.; Dove, A. P.; Sardon, H. Synthesis of Functionalized Cyclic Carbonates through Commodity Polymer Upcycling. *ACS Macro Letters* **2020**, *9*, 443–447. https://doi.org/10.1021/acsmacrolett.0c00164.

(23) Liu, F.; Li, L.; Yu, S.; Lv, Z.; Ge, X. Methanolysis of Polycarbonate Catalysed by Ionic Liquid [Bmim][Ac]. *Journal of Hazardous Materials* **2011**, *189*, 249–254. https://doi.org/10.1016/j.jhazmat.2011.02.032.

(24) Li, L.; Liu, F.; Li, Z.; Song, X.; Yu, S.; Liu, S. Hydrolysis of Polycarbonate Using Ionic Liquid [Bmim][Cl] as Solvent and Catalyst. *Fibers and Polymers* **2013**, *14*, 365–368. https://doi.org/10.1007/s12221-013-0365-3.

(25) Huang, W.; Wang, H.; Hu, W.; Yang, D.; Yu, S.; Liu, F.; Song, X. Degradation of Polycarbonate to Produce Bisphenol A Catalyzed by Imidazolium-Based DESs under Metal-and Solvent-Free Conditions. *RSC Advances* **2021**, *11*, 1595–1604. https://doi.org/10.1039/d0ra09215k.

(26) Iannone, F.; Casiello, M.; Monopoli, A.; Cotugno, P.; Sportelli, M. C.; Picca, R. A.; Cioffi, N.; Dell'Anna, M. M.; Nacci, A. Ionic Liquids/ZnO Nanoparticles as Recyclable Catalyst for Polycarbonate Depolymerization. *Journal of Molecular Catalysis A: Chemical* **2017**, *426*, 107–116. https://doi.org/10.1016/j.molcata.2016.11.006.

(27) Quaranta, E.; Sgherza, D.; Tartaro, G. Depolymerization of Poly(Bisphenol A Carbonate) under Mild Conditions by Solvent-Free Alcoholysis Catalyzed by 1,8-Diazabicyclo[5.4.0]Undec-7-Ene as a Recyclable Organocatalyst: A Route to Chemical Recycling of Waste Polycarbonate. *Green Chemistry* **2017**, *19*, 5422–5434. https://doi.org/10.1039/c7gc02063e.

(28) Do, T.; Baral, E. R.; Kim, J. G. Chemical Recycling of Poly(Bisphenol A Carbonate): 1,5,7-Triazabicyclo[4.4.0]-Dec-5-Ene Catalyzed Alcoholysis for Highly Efficient Bisphenol A and Organic Carbonate Recovery. *Polymer* **2018**, *143*, 106–114. https://doi.org/10.1016/j.polymer.2018.04.015.

(29) Quaranta, E.; Minischetti, C. C.; Tartaro, G. Chemical Recycling of Poly(Bisphenol A Carbonate) by Glycolysis under 1,8-Diazabicyclo[5.4.0]Undec-7-Ene Catalysis. *ACS Omega* **2018**, *3*, 7261–7268. https://doi.org/10.1021/acsomega.8b01123.

(30) Siragusa, F.; van den Broeck, E.; Ocando, C.; Müller, A. J.; de Smet, G.; Maes, B. U. W.; de Winter, J.; van Speybroeck, V.; Grignard, B.; Detrembleur, C. Access to Biorenewable and CO2-Based Polycarbonates from Exovinylene Cyclic Carbonates. *ACS Sustainable Chemistry and Engineering* **2021**, *9*, 1714–1728. https://doi.org/10.1021/acssuschemeng.0c07683.

(31) Gennen, S.; Grignard, B.; Tassaing, T.; Jérôme, C.; Detrembleur, C. CO2 -Sourced α-Alkylidene Cyclic Carbonates: A Step Forward in the Quest for Functional Regioregular Poly(Urethane)s and Poly(Carbonate)s. *Angewandte Chemie International Edition* **2017**, *56*, 10394–10398. https://doi.org/10.1002/anie.201704467.

(32) Ouhib, F.; Meabe, L.; Mahmoud, A.; Eshraghi, N.; Grignard, B.; Thomassin, J. M.; Aqil, A.; Boschini, F.; Jérôme, C.; Mecerreyes, D.; Detrembleur, C. CO2 -Sourced Polycarbonates as Solid Electrolytes for Room Temperature Operating Lithium Batteries. *Journal of Materials Chemistry A* **2019**, *7*, 9844–9853. https://doi.org/10.1039/c9ta01564g.

(33) Ouhib, F.; Meabe, L.; Mahmoud, A.; Grignard, B.; Thomassin, J.-M.; Boschini, F.; Zhu, H.; Forsyth, M.; Mecerreyes, D.; Detrembleur, C. Influence of the Cyclic versus Linear Carbonate Segments in the Properties and Performance of CO2 -Sourced Polymer Electrolytes for Lithium Batteries. *ACS Applied Polymer Materials* **2020**, *2*, 922–931. https://doi.org/10.1021/acsapm.9b01130.

(34) Ngassam Tounzoua, C.; Grignard, B.; Detrembleur, C. Exovinylene Cyclic Carbonates: Multifaceted CO2-Based Building Blocks for Modern Chemistry and Polymer Science. *Angewandte Chemie International Edition* **2022**, e202116066. https://doi.org/10.1002/anie.202116066.

(35) Zhang, Y. F.; Lai, W. M.; Xie, S.; Zhou, H.; Lu, X. B. Facile Synthesis, Structure and Properties of CO2-Sourced Poly(Thioether-: Co -Carbonate)s Containing Acetyl Pendants via Thio-Ene Click Polymerization. *Polymer Chemistry* **2022**, *13*, 201–208. https://doi.org/10.1039/d1py01477c.

(36) Tounzoua, C. N.; Grignard, B.; Brege, A.; Jerome, C.; Tassaing, T.; Mereau, R.; Detrembleur, C. A Catalytic Domino Approach toward Oxo-Alkyl Carbonates and Polycarbonates from CO2 , Propargylic Alcohols, and (Mono- and Di-)Alcohols. *ACS Sustainable Chemistry & Engineering* **2020**, *8*, 9698–9710. https://doi.org/10.1021/acssuschemeng.0c01787.

(37) Kanzian, T.; Nigst, T. A.; Maier, A.; Pichl, S.; Mayr, H. Nucleophilic Reactivities of Primary and Secondary Amines in Acetonitrile. *European Journal of Organic Chemistry* **2009**, 6379–6385. https://doi.org/10.1002/ejoc.200900925.

(38) Qiu, H.; Chen, X.; Zhang, J. Design, Synthesis and Application of a New Type of Bifunctional Le-Phos in Highly Enantioselective γ-Addition Reactions of N-Centered Nucleophiles to Allenoates. *Chemical Science* **2019**, *10*, 10510–10515. https://doi.org/10.1039/c9sc04073k.

(39) Hashimoto, T.; Nakatsu, H.; Yamamoto, K.; Maruoka, K. Chiral Brønsted Acid-Catalyzed Asymmetric Trisubstituted Aziridine Synthesis Using α-Diazoacyl Oxazolidinones. *J Am Chem Soc* **2011**, *133*, 9730–9733. https://doi.org/10.1021/ja203901h.

(40) Liu, H.; He, X.; Phillips, D.; Zhu, X.; Yang, K.; Lau, T.; Wu, B.; Xie, Y.; Nguyen, T. N.; Wang, X. Azacyclic Compounds as Inhibitors of Cannabinoid Receptor 1 and Their Preparation, Pharmaceutical Compositions and Use in the Treatment of CB1-Mediated Diseases. WO2008076754, 2008.

(41) Alder, C. M.; Baldwin, I. R.; Barton, N. P.; Campbell, A. J.; Champigny, A. C.; Harling, J. D.; Maxwell, A. C.; Simpson, J. K.; Smith, I. E. D.; Tame, C. J.; Wilson, C.; Woolven, J. M. Preparation of 2-[2-(Benzo- or Pyrido-)Thiazolylamino]-6-Aminopyridine Derivatives Useful in the Treatment of Respiratory, Allergic or Inflammatory Diseases. WO2011110575, 2011.

(42) Poindexter, G. S.; Owens, D. A.; Dolan, P. L.; Woo, E. The Use of 2-Oxazolidinones as Latent Aziridine Equivalents. 2. Aminoethylation of Aromatic Amines, Phenols, and Thiophenols. *The Journal of Organic Chemistry* **1992**, *57*, 6257–6265. https://doi.org/10.1021/jo00049a037.

(43) Chang, Z.; Huang, J.; Wang, S.; Chen, G.; Zhao, H.; Wang, R.; Zhao, D. Copper Catalyzed Late-Stage C(Sp3)-H Functionalization of Nitrogen Heterocycles. *Nature Communications* **2021**, *12*, 1–11. https://doi.org/10.1038/s41467-021-24671-y.

(44) Mittag, T.; Christensen, K. L.; Lindsay, K. B.; Nielsen, N. C.; Skrydstrup, T. Direct Entry to Peptidyl Ketones via SmI2-Mediated C−C Bond Formation with Readily Accessible N-Peptidyl Oxazolidinones. *The Journal of Organic Chemistry* **2008**, *73*, 1088–1092. https://doi.org/10.1021/jo702286b.

(45) Deng, B.-L.; Hartman, T. L.; Buckheit Robert W.; Pannecouque, C.; de Clercq, E.; Fanwick, P. E.; Cushman, M. Synthesis, Anti-HIV Activity, and Metabolic Stability of New Alkenyldiarylmethane HIV-1 Non-Nucleoside Reverse Transcriptase Inhibitors. *Journal of Medicinal Chemistry* **2005**, *48*, 6140–6155. https://doi.org/10.1021/jm050452s.

(46) Habets, T.; Siragusa, F.; Müller, A. J.; Grossman, Q.; Ruffoni, D.; Grignard, B.; Detrembleur, C. Facile Construction of Functional Poly(Monothiocarbonate) Copolymers under Mild Operating Conditions. *Polymer Chemistry* **2022**. https://doi.org/10.1039/D2PY00307D.

Supporting Informations

Characterization of *oxo*-carbonates

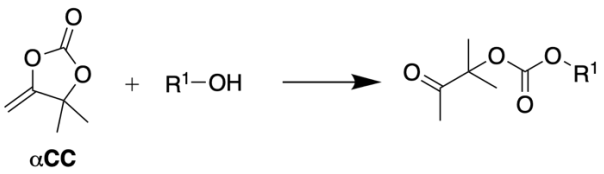

Scheme S1. Synthesis of *oxo*-carbonates.

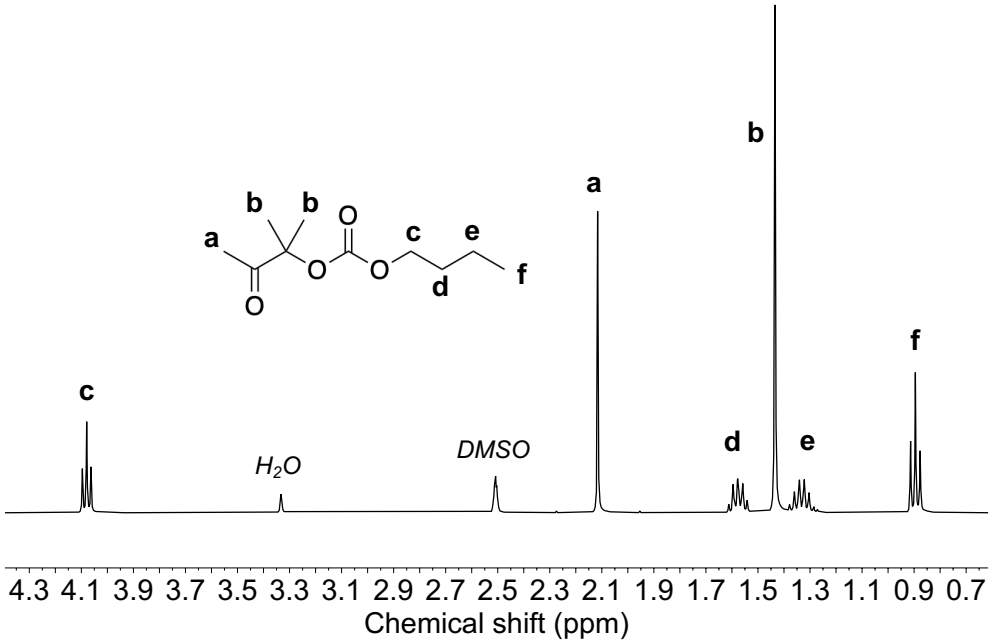

Figure S1. ^{1}H-NMR (in DMSO-d_6) of **O1** *oxo*-carbonate.

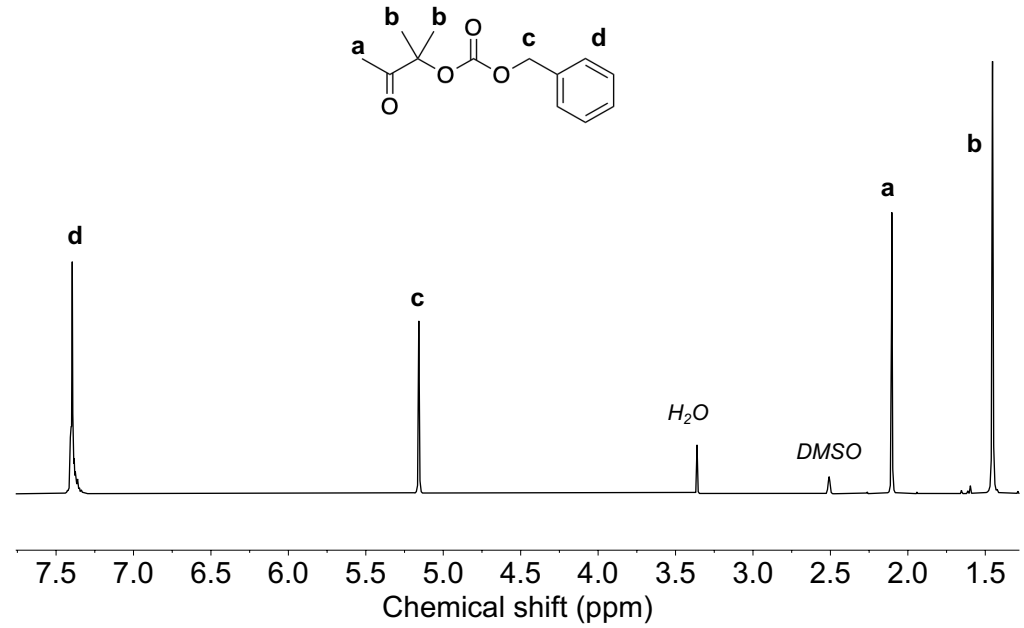

Figure S2. ^{1}H-NMR (in DMSO-d_6) of **O2** *oxo*-carbonate.

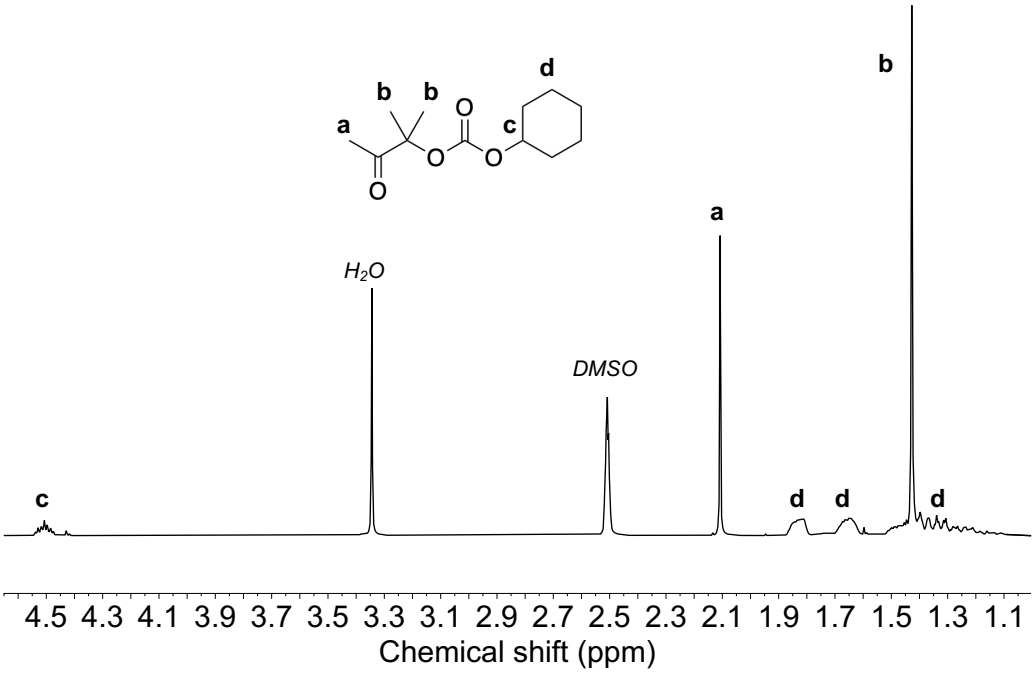

Figure S3. ^{1}H-NMR (in DMSO-d_6) of **O3** *oxo*-carbonate.

Model reactions

Kinetics model reactions

For each model reaction the oxo-carbonate conversion was determined by selecting and integrating the peak at 2.12 ppm of *oxo*-carbonate and the peak of released alcohol (for butanol at 3.38 ppm) following the equation 1:

$$Conv. = 1 - \left(\frac{I\left(\frac{2.12}{3}\right)}{I\left(\frac{2.12}{3}\right) + I\left(\frac{3.38}{2}\right)} \right) \qquad (Eq. 1)$$

Note that the determination of the selectivity was obtained by the integration of methyl (at δ= 1.23 ppm) of hydroxy-oxazolidinone and of the methyl (at δ= 2.15 ppm) of hydroxy-ketone formed by imine hydrolysis in acid media.

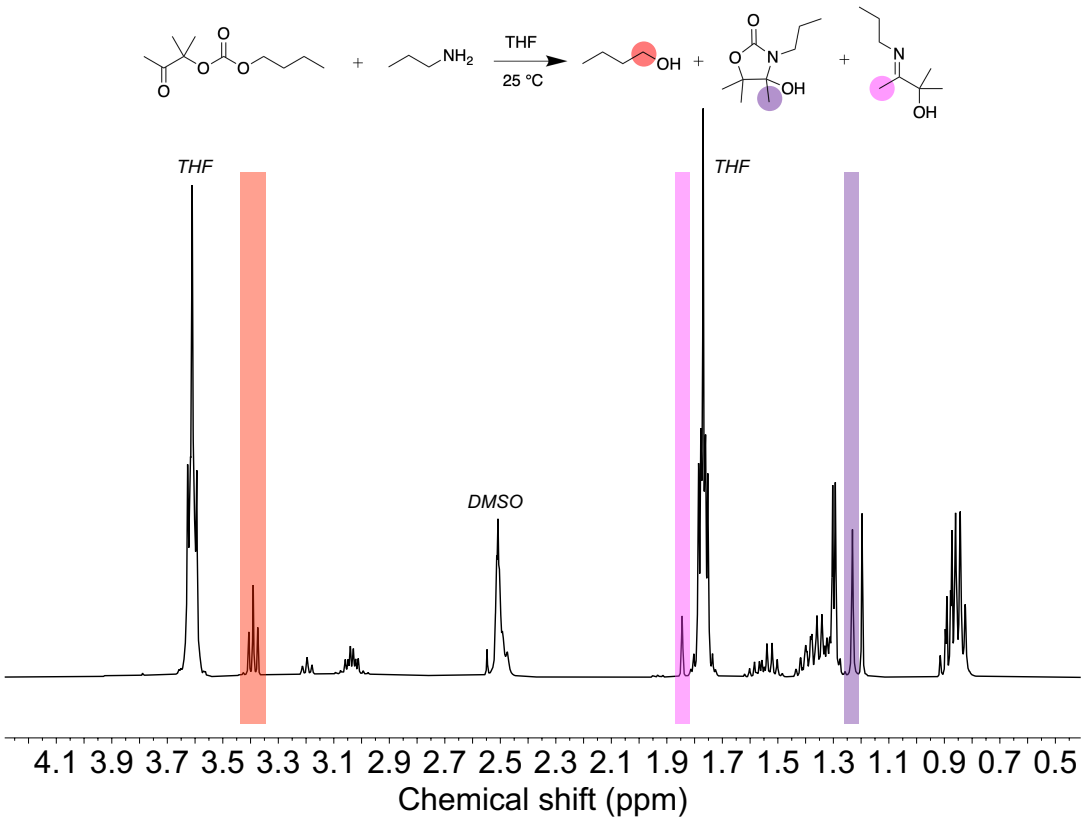

Figure S4. ^{1}H-NMR spectrum of *Oxo*-carbonate **O1** aminolysis with **A1** after 24 h without quenching with formic acid (in DMSO-d_6).

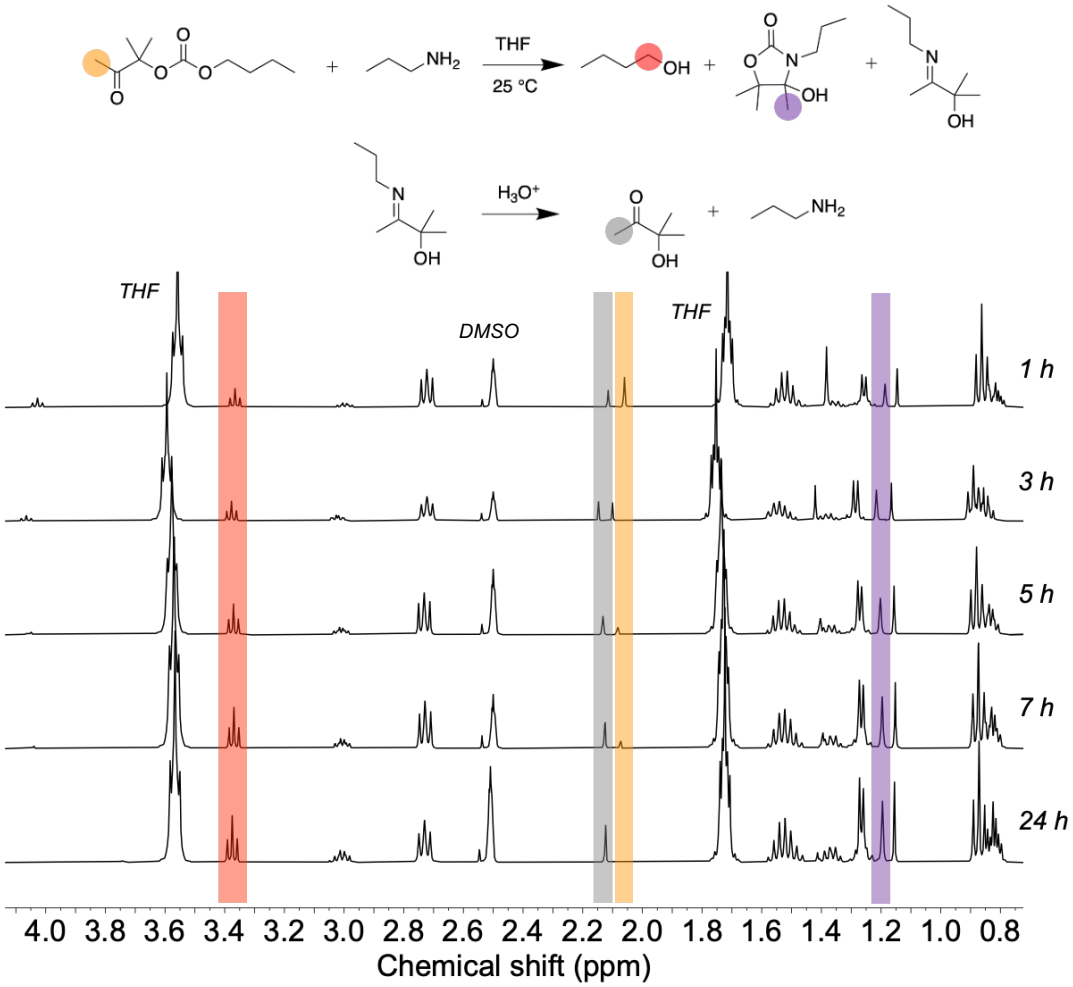

Figure S5. Overlay spectra of *Oxo*-carbonate **O1** aminolysis kinetic with **A1** followed by ^{1}H-NMR (in DMSO-d_6).

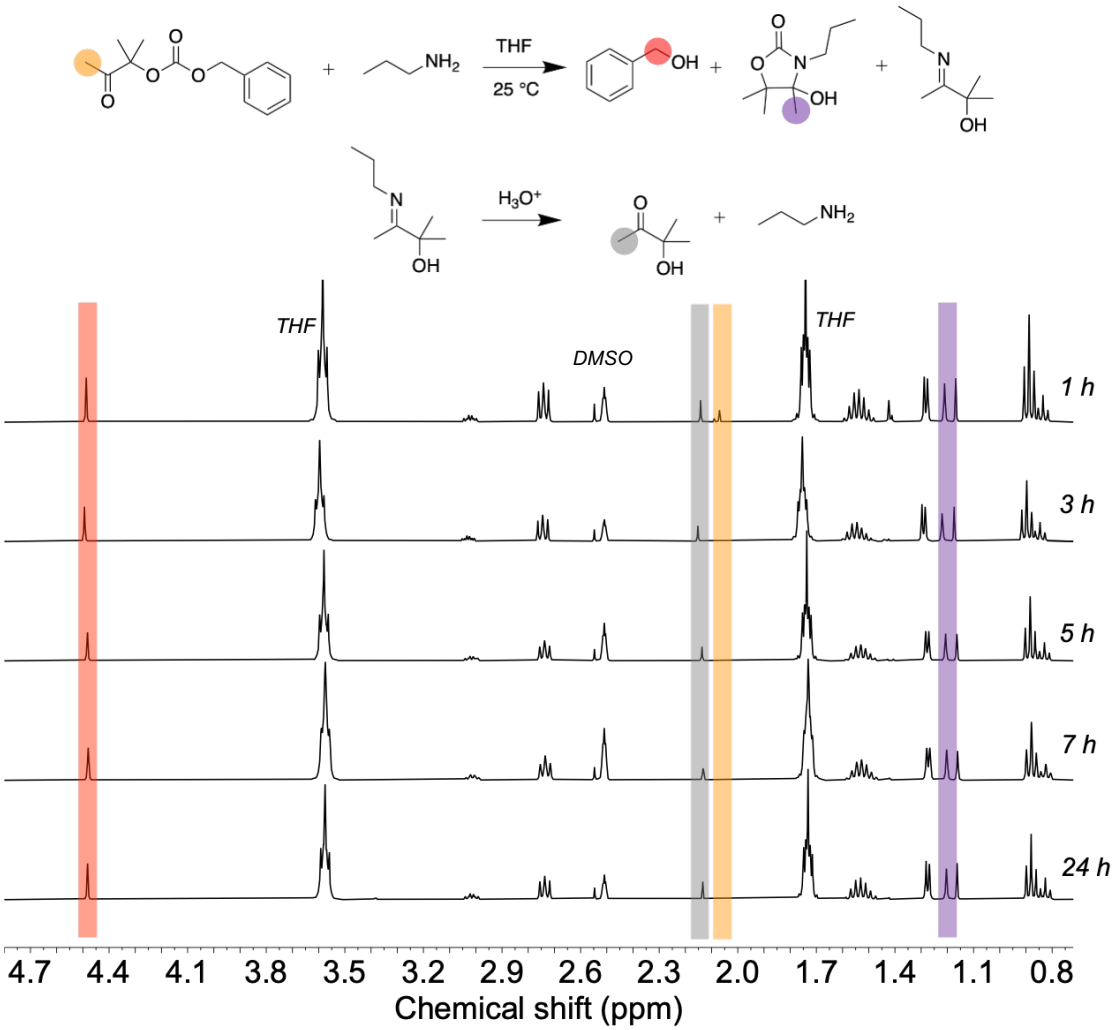

Figure S6. Overlay spectra of *Oxo*-carbonate **O2** kinetic aminolysis with **A1** followed by ^{1}H-NMR (in DMSO-d_6).

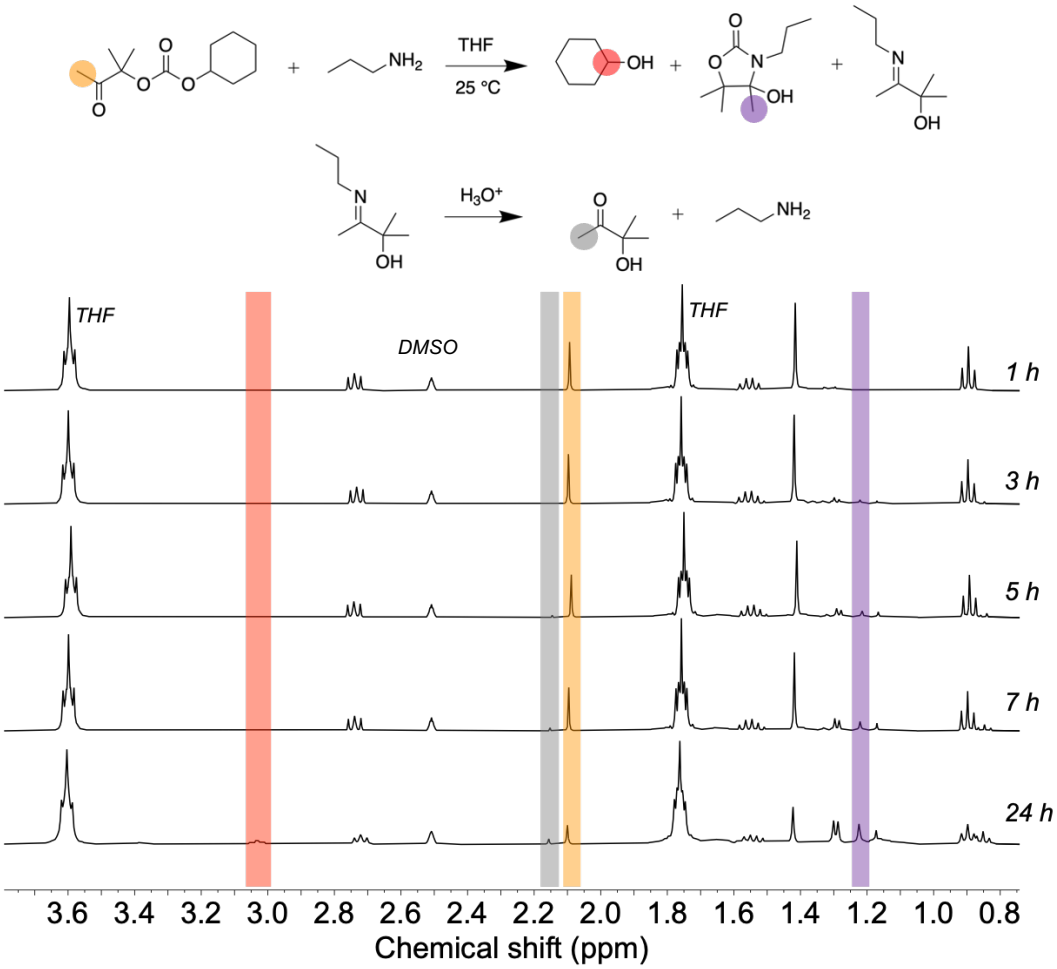

Figure S7. Overlay spectra of *Oxo*-carbonate **O3** aminolysis kinetic with **A1** followed by ^{1}H-NMR (in DMSO-d_6).

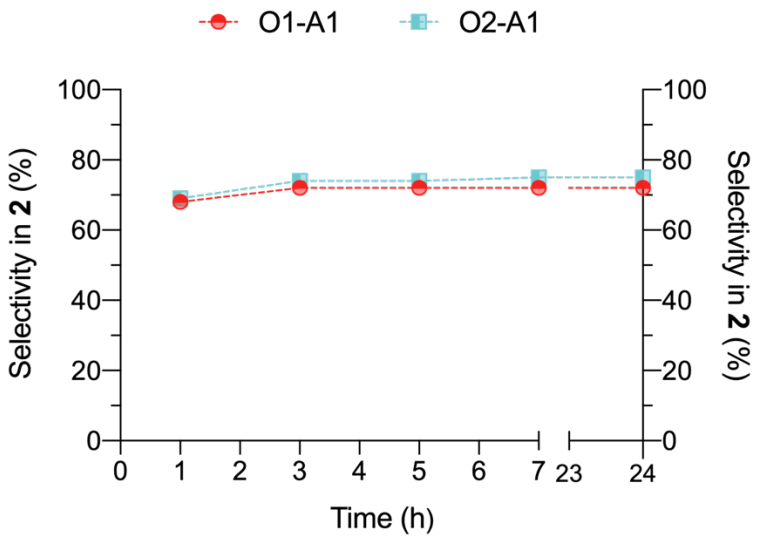

Figure S8. Selectivity in **2** *vs* time of catalyst-free aminolysis of oxo-carbonates **O1** and **O2** with propyl amine **A1** (3 eq. compared the ketone moiety) at 25 °C in THF (C = 2 M).

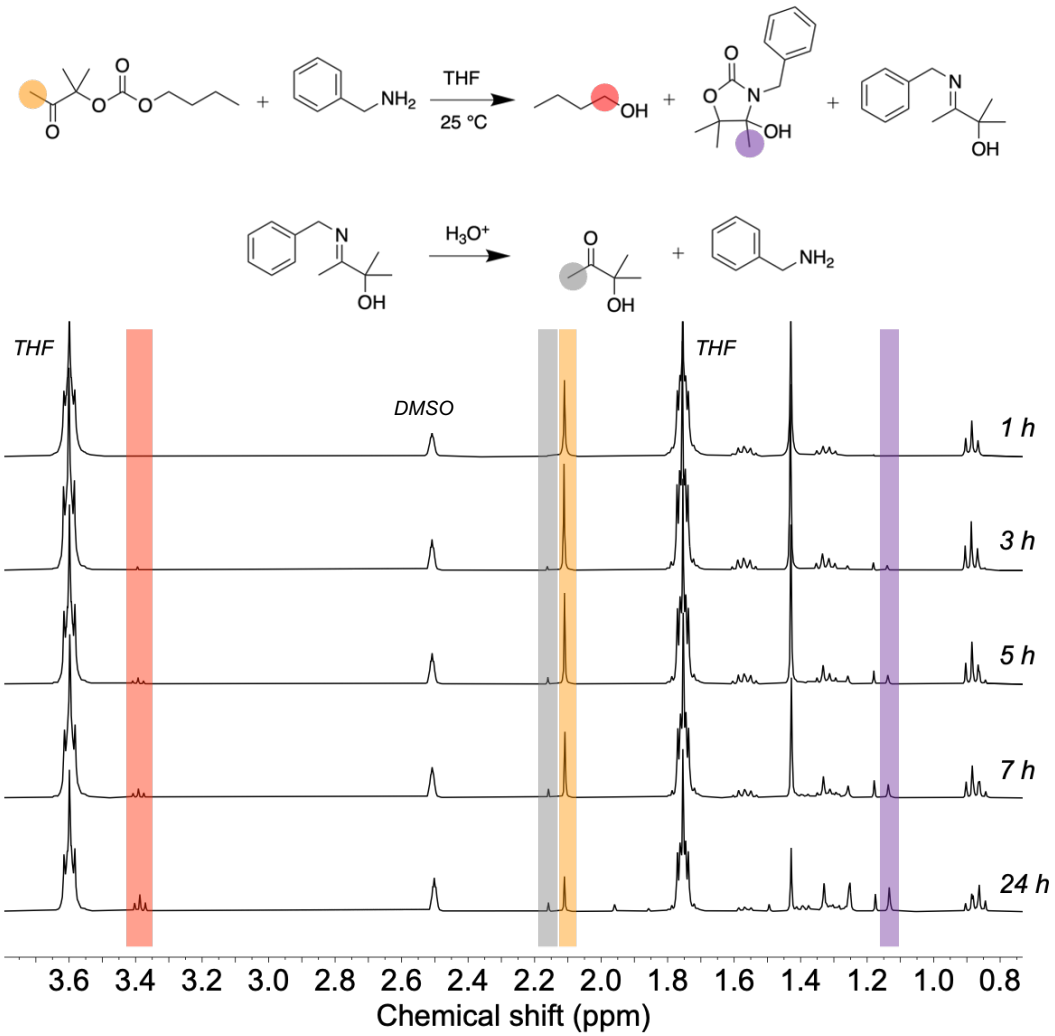

Figure S9. Overlay spectra of *Oxo*-carbonate **O1** aminolysis kinetic with **A2** followed by ^{1}H-NMR (in DMSO-d_6).

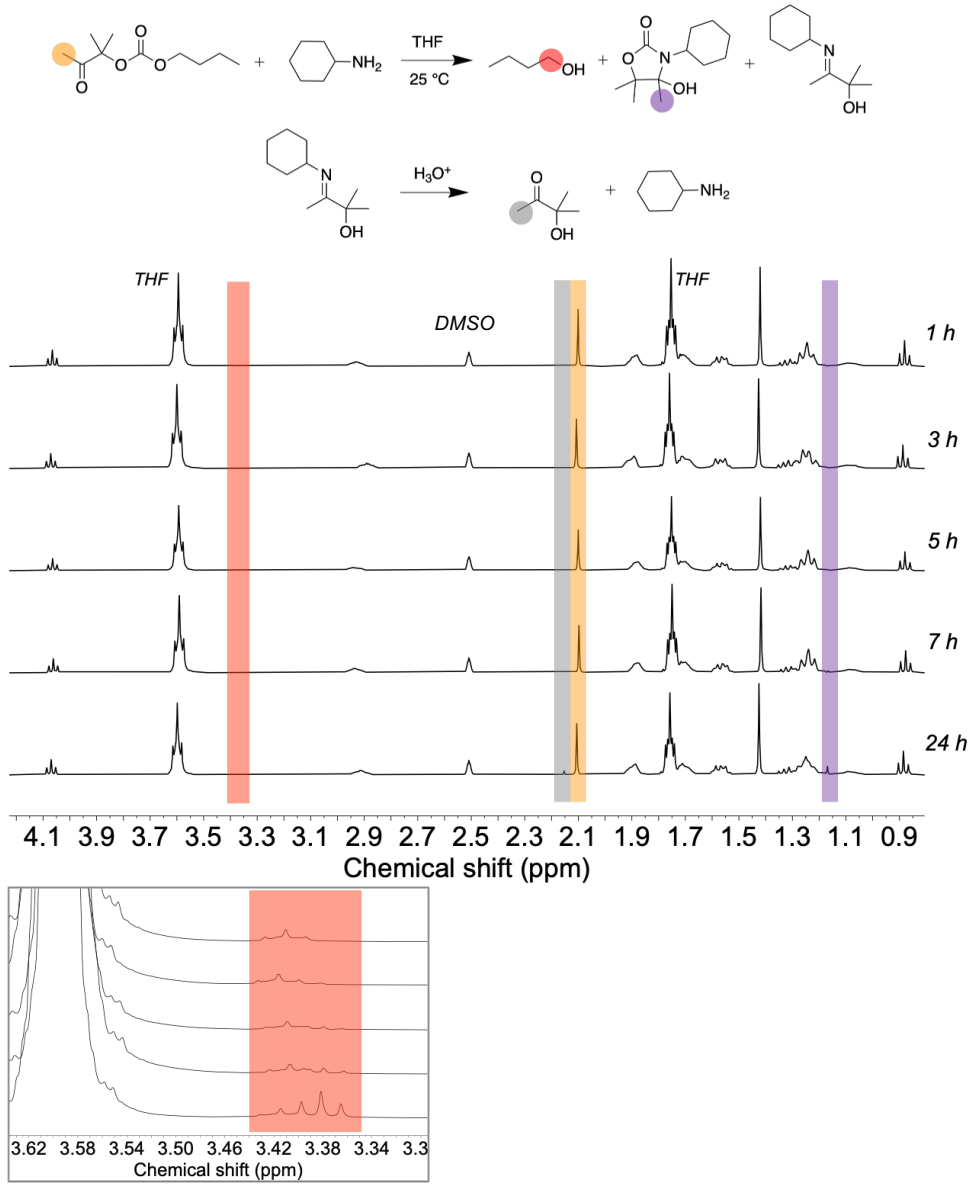

Figure S10. Overlay spectra of *Oxo*-carbonate **O1** aminolysis kinetic with **A3** followed by ^{1}H-NMR (in DMSO-d_6).

Characterization of hydroxy-oxazolidinones

4-hydroxy-4,5,5-trimethyl-3-propyloxazolidin-2-one

^{1}H NMR (400 MHz, DMSO-d_6): δ = 5.92 ppm (s, 1H), δ = 3.03 ppm (m, 2H), δ = 1.53 ppm (m, 2H), δ = 1.30 ppm (s, 3H), δ = 1.29 ppm (s, 3H), δ = 1.23 ppm (s, 3H), δ = 0.85 ppm (m, 3H).

^{13}C NMR (400 MHz, DMSO-d_6): δ = 156.9 ppm, δ = 89.7 ppm, δ = 84.5 ppm, δ = 41.6 ppm, δ = 25.1 ppm, δ = 22.8 ppm, δ = 21.0 ppm, δ = 11.8 ppm.

ESIHRMS m/z calcd for $C_9H_{17}NO_3$ $[M+H]^+$ 187,1208, found 188,1208.

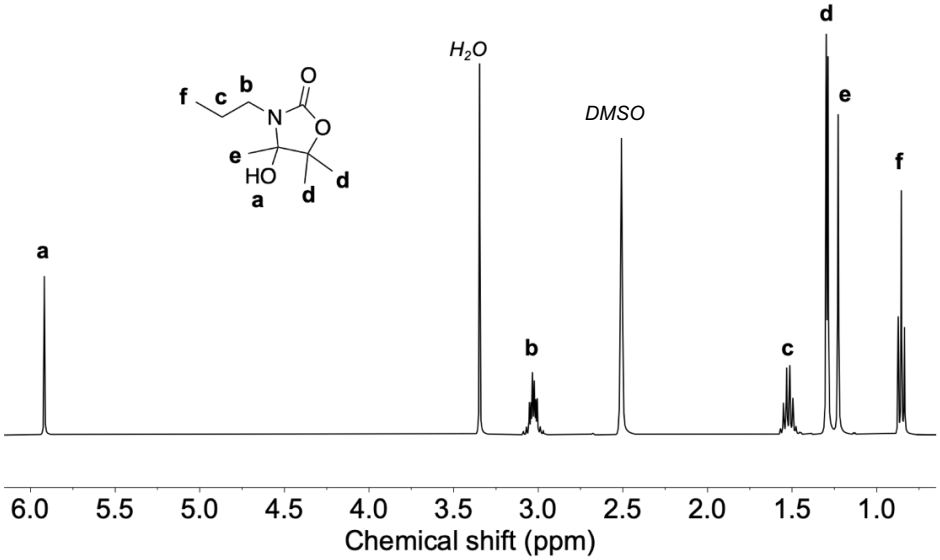

Figure S11. ^{1}H-NMR (in DMSO-d_6) of purified 4-hydroxy-4,5,5-trimethyl-3-propyloxazolidin-2-one.

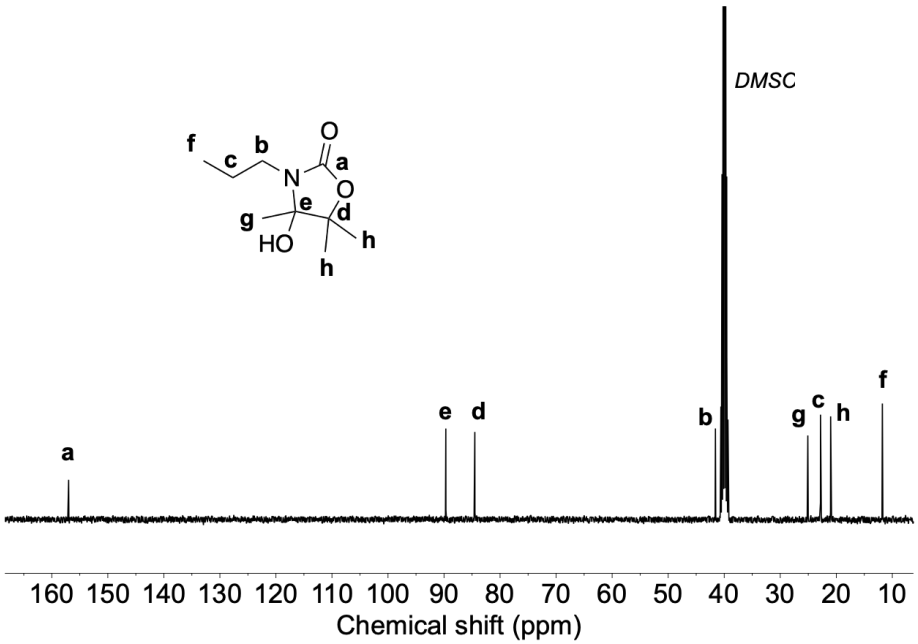

Figure S12. ^{13}C-NMR (in DMSO-d_6) of purified 4-hydroxy-4,5,5-trimethyl-3-propyloxazolidin-2-one.

3-benzyl-4-hydroxy-4,5,5-trimethyloxazolidin-2-one

^{1}H NMR (400 MHz, DMSO-d_6): δ = 7.31 ppm (m, 5H), δ = 6.16 ppm (s, 1H), δ = 4.42- 4.19 ppm (m, 2H), δ = 1.33 ppm (s, 3H), δ = 1.26 ppm (s, 3H), δ = 1.13 ppm (s, 3H).

^{13}C NMR (400 MHz, DMSO-d_6): δ = 157.5 ppm, δ = 139.4 ppm, δ = 128.9 ppm, δ = 127.3 ppm, δ = 89.9 ppm, δ = 84.9 ppm, δ = 43.1 ppm, δ = 25.2 ppm, δ = 21.2 ppm, δ = 20.9 ppm.

ESIHRMS m/z calcd for $C_{13}H_{17}NO_3$ $[M+H]^+$ 235,1281, found 236,1281.

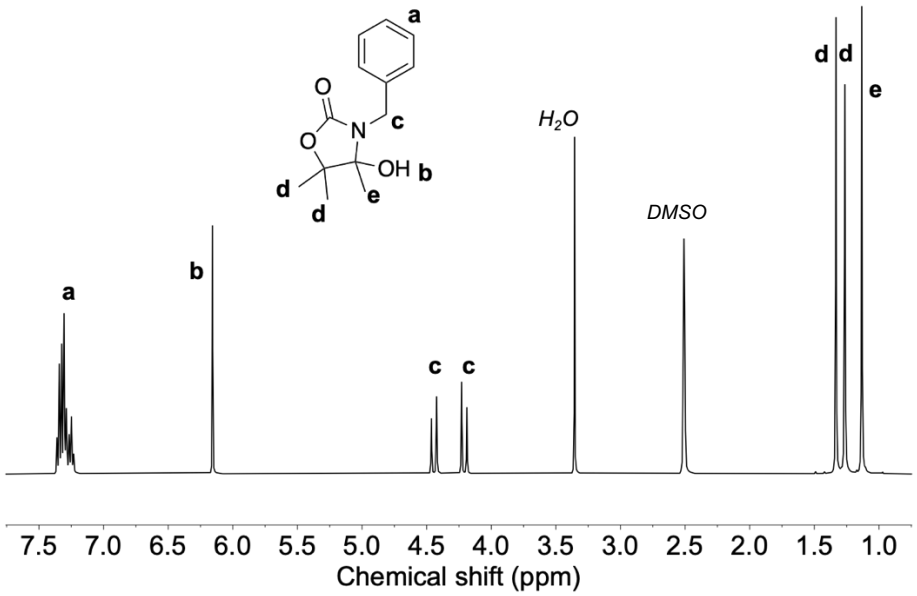

Figure S13. ^{1}H-NMR (in DMSO-d_6) of purified 3-benzyl-4-hydroxy-4,5,5-trimethyloxazolidin-2-one.

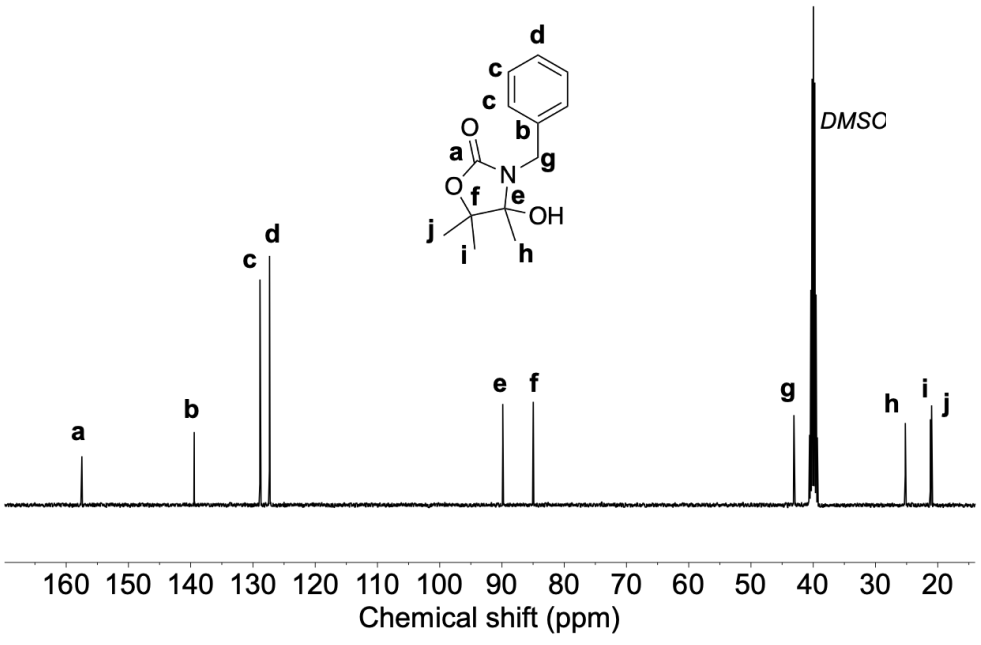

Figure S14. ^{13}C-NMR (in DMSO-d_6) of purified 3-benzyl-4-hydroxy-4,5,5-trimethyloxazolidin-2-one.

3-cyclohexyl-4-hydroxy-4,5,5-trimethyloxazolidin-2-one

^{1}H NMR (400 MHz, DMSO-d_6): δ = 5.87 ppm (s, 1H), δ = 3.04 ppm (m, 1H), δ = 2.03- 1.59 ppm (m, 8H), δ = 1.30 ppm (s, 3H), δ = 1.26 ppm (s, 3H), δ = 1.20 ppm (s, 3H), δ = 1.07 ppm (m, 2H).

^{13}C NMR (400 MHz, DMSO-d_6): δ = 155.1 ppm, δ = 90.5 ppm, δ = 83.8 ppm, δ = 51.4 ppm, δ = 30.7 ppm, δ = 26.2 ppm, δ = 25.5 ppm, δ = 24.9 ppm, δ = 21.2 ppm.

ESIHRMS m/z calcd for $C_{12}H_{21}NO_3$ $[M+H]^+$ 227,1521, found 228,1593.

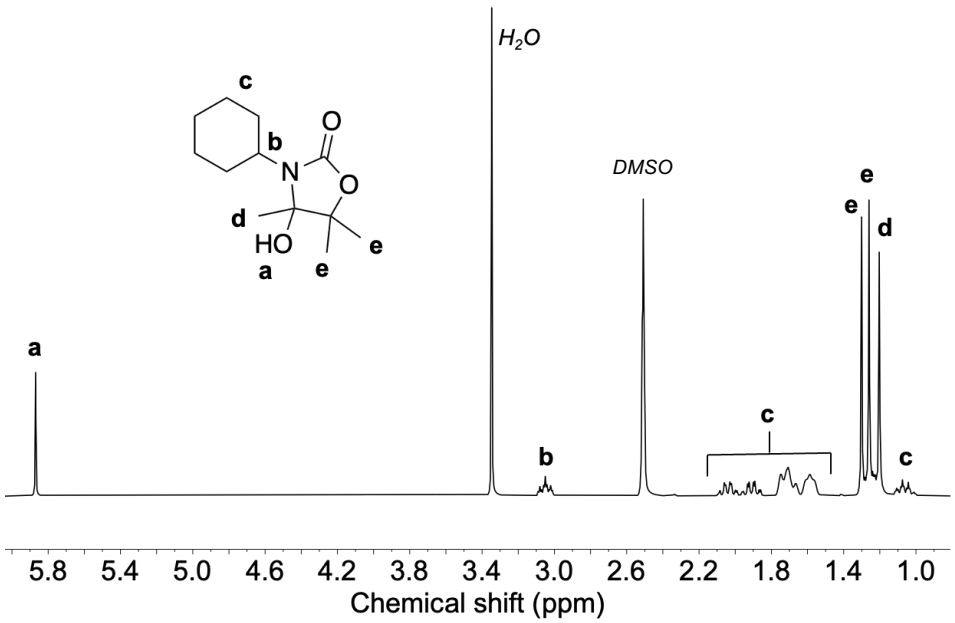

Figure S15. ^{1}H-NMR (in DMSO-d_6) of purified 3-cyclohexyl-4-hydroxy-4,5,5-trimethyloxazolidin-2-one.

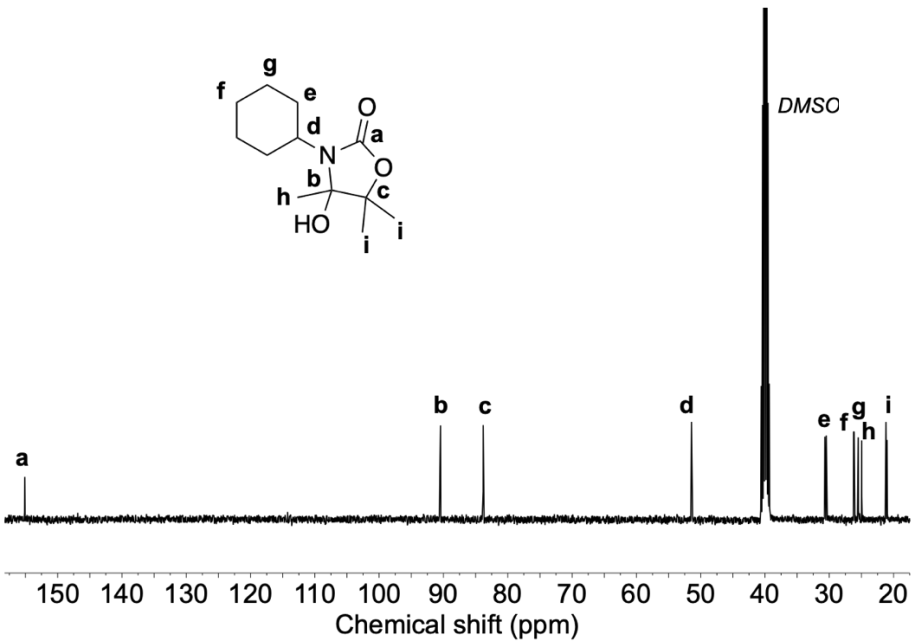

Figure S16. ^{13}C-NMR (in DMSO-d_6) of purified 3-cyclohexyl-4-hydroxy-4,5,5-trimethyloxazolidin-2-one.

Mechanistic insight of the aminolysis of *oxo*-carbonates

Raw DFT data can be accessed in the *Iochem BD* database through this DOI: 10.19061/iochem-bd-6-133.[1]

Methodology

Preliminary calculations of equilibrium structures were performed using a semi-empirical model (PM7)[2] to determine the most stable conformations. These semi-empirical calculations were performed using the MOPAC software.[3] The lowest energy structures obtained at the semi-empirical level were further investigated using the Density Functional Theory (DFT) method implemented in the Gaussian 16 package.[4] DFT calculations of geometries, energies and vibrational frequencies reported in this paper were carried out with the ωB97X-D functional[5] using the 6-311++G(d,p) basis set. All frequencies of each structure have also been calculated to verify the presence of a single imaginary frequency for transition states and the absence of imaginary frequency for ground states. The intrinsic reaction coordinate (IRC) method has been used to verify that the obtained transition states were effectively connected to the desired minima. A wide range of possible configurations and interactions have been modelled and the more stable of them are reported in this work. To consider entropic effects, the energies mentioned in this study correspond to the Gibbs free energy.

Results

The different studied reaction pathways were discussed in the main manuscript. A more detailed discussion is provided here with the corresponding Gibbs free energy profiles.

<u>Pathway 1 – Attack on the carbonate group</u>

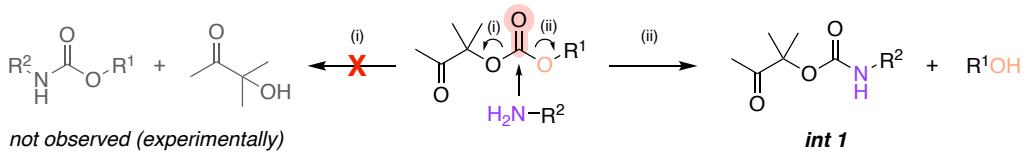

Scheme S2. Possible reaction products from the attack of the amine onto the carbonate group of the *oxo*-carbonate.

Pathway 1 concerns the attack of the amine onto the carbonate group of the *oxo*-carbonate. The attack on the carbonate can provide different products depending on which of the two C-O bond is broken. As only the hydroxy-oxazolidinone product **2** was observed experimentally, the pathway toward carbamate and hydroxyketone (Scheme S2-(i)) was not considered here. From the pre-reaction complex, a concerted attack of the amine onto the carbonate with direct proton transfer from the nitrogen to the released alcohol is achieved to form an *oxo*-urethane **int 1** (Scheme S2-(ii) and Figure S17). The second step is the intramolecular cyclization of **int**

1 by attack of the nitrogen (of the carbamate group) onto the ketone group to form the five-membered carbamate ring **2**. The rate-determining step of this route is the addition of the amine on the carbonate, with an energy barrier of 41.9 kcal·mol^{-1}. The second step, with an energy barrier of 23.0 kcal·mol^{-1}, is thoroughly discussed in the main manuscript.

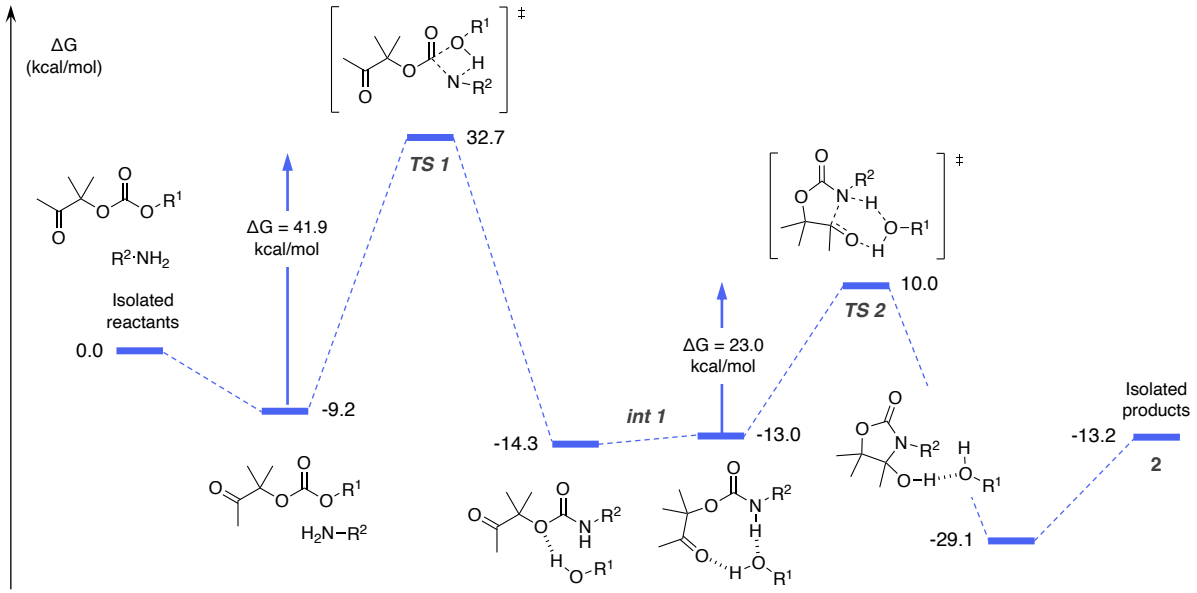

Figure S17. Gibbs free energy profile for the pathway 1 with respective geometries of transition states and intermediates.

Pathways 2-3-4 – Attack on the ketone group and formation of a hemiaminal intermediate

Pathways 2, 3, and 4 all rely on the attack of the amine onto the electrophilic ketone group of the *oxo*-carbonate. The first step, common to all routes, consists in the formation of a hemiaminal intermediate **int 2**. This occurs through a concerted attack of the amine on the ketone with direct proton transfer from the nitrogen to the oxygen of the ketone. The energy barrier of the transition state **TS 3** toward **int 2** is characterized by a rather low value of 28.1 kcal·mol^{-1}. This is explained by the stabilization of the structure through alkyl chains stacking between the reactants and a hydrogen bond between the amine and the sp2 oxygen of the carbonate (length of 2.01 Å, Figure S18-A). Once the hemiaminal **int 2** is formed, the same interactions lower its energy to -10.4 kcal·mol^{-1} compared to the separate reactants, although the hydrogen bond displays a higher distance between the two atoms (2.32 Å, Figure S18-B). The reverse energy barrier is calculated to be of 32.6 kcal·mol^{-1} which is very close to the forward direction (4.5 kcal·mol^{-1} of difference), thus highlighting the potential reversible character of this first step.

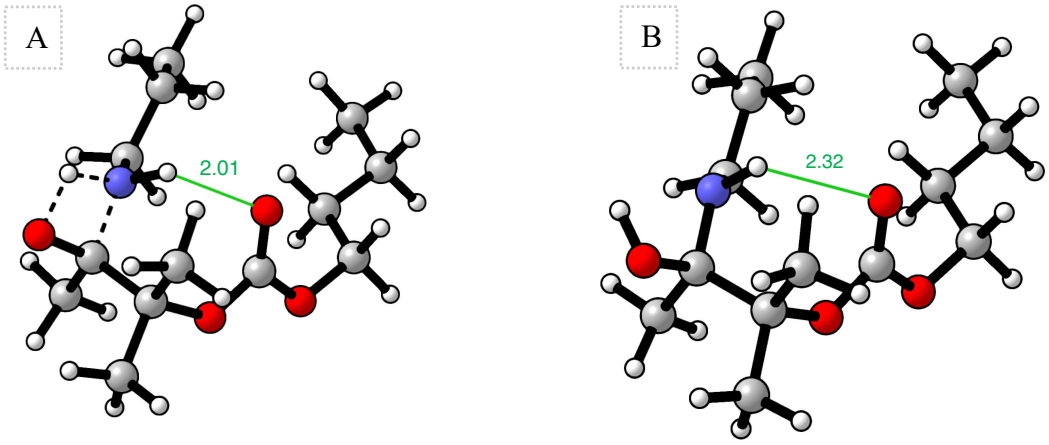

Figure S18.Geometries of (A) the transition state **TS 3** and (B) the post-reactive intermediate **int 2**. Dotted bonds in the TS structures indicate bonds which are broken or formed. Green bonds indicate hydrogen bonds. Distances are expressed in Å.

Pathway 2

In pathway 2, the second step begins from a complex stabilized by hydrogen bonding and favoring the positioning of the nitrogen toward the carbonate (Figure S19, **int 2**). As the attack of the nitrogen on the carbonate proceeds, the original C-N bond of the hemiaminal is broken to yield the new carbamate bond through a five-membered ring structure **TS 4** (Figure S19 and S20). Simultaneously, the hydrogen of the alcohol is transferred to the leaving alcohol to form a ketone group. The *oxo*-urethane **int 1** is obtained and can undergo intramolecular cyclization (as in pathway 1) to yield the hydroxy-oxazolidinone product **2**. The formation of **int 1** from the hemiaminal **int 2** is the rate-determining step of the reaction with an energy barrier of 32.3 kcal·mol^{-1}.

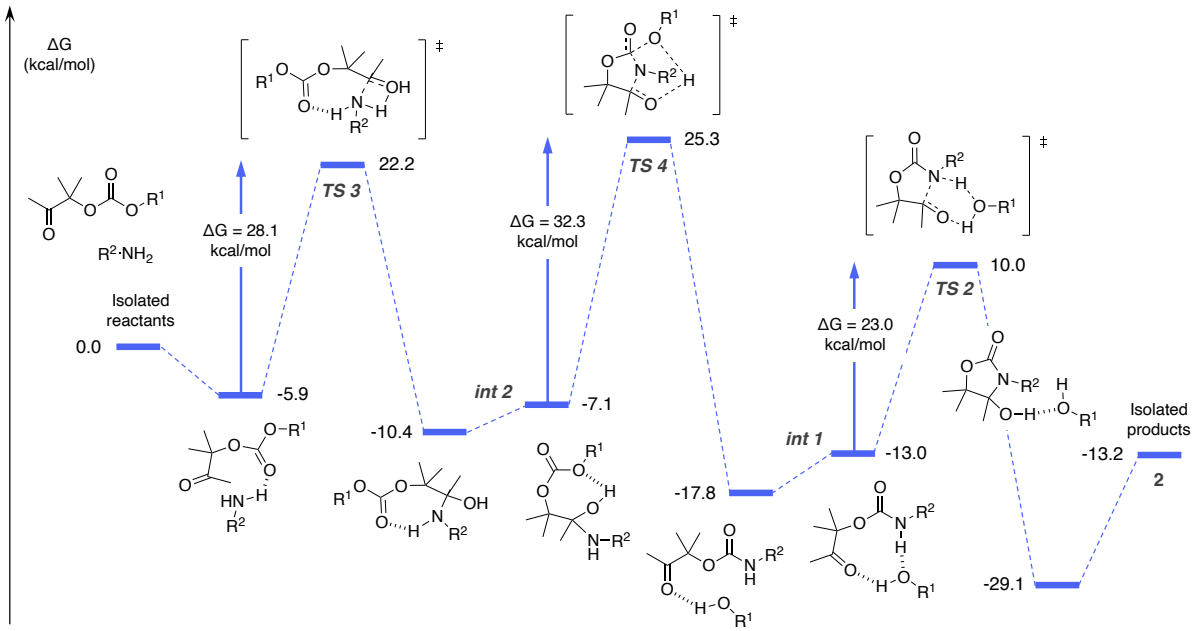

Figure S19. Gibbs free energy profile for the pathway 2 with respective geometries of transition states and intermediates.

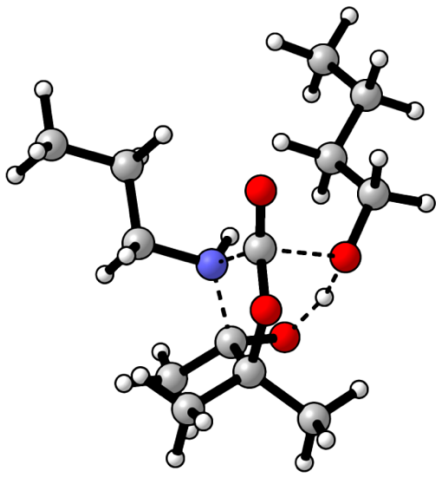

Figure S20. Geometry of the transition state **TS 4**. Dotted bonds in the TS structure indicate bonds which are broken or formed.

Pathway 3

Pathway 3 begins similarly to pathway 2 with a complex stabilized by hydrogen bonding and favoring the positioning of the nitrogen toward the carbonate (Figure S21, **int 2**). Then, the concerted attack of the secondary amine onto the carbonate with direct proton transfer from nitrogen to the leaving alcohol occurs to form the product **2** in a one-step manner (Figure S22). The energy barrier of this step, which is the rate-determining step of the reaction, is calculated to be 35.5 kcal·mol^{-1} (of the same order than pathway 2, with a difference in energy of 3.2 kcal·mol^{-1}).

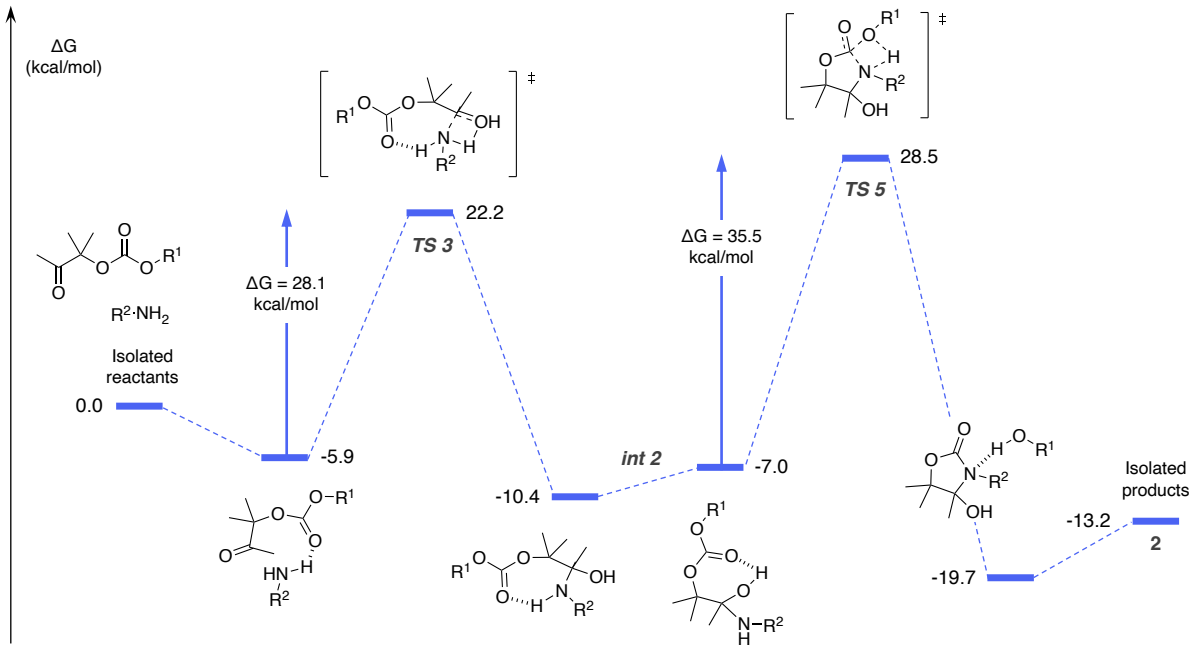

Figure S21. Gibbs free energy profile for the pathway 3 with respective geometries of transition states and intermediates.

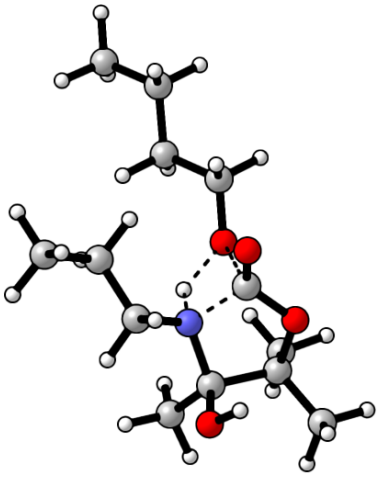

Figure S22. Geometry of the transition state **TS 5**. Dotted bonds in the TS structure indicate bonds which are broken or formed.

Pathway 4

Pathway 4 begins with a complex stabilized by hydrogen bonding and favoring the positioning of the oxygen atom toward the carbonate (Figure S23, **int 2**). From this intermediate, a tetrasubstituted cyclic carbonate intermediate **int 3** is formed through attack of the alcohol onto the carbonate with direct proton transfer to the leaving alcohol. The so-formed cyclic carbonate bearing a secondary amine is highly stabilized by hydrogen bonding (2.07 Å between hydrogen of NH and oxygen of OH; 2.28 Å between hydrogen of OH and oxygen of carbonyl group; Figure S24). The energy barrier of this step is 46.7 kcal·mol^{-1}. However, the reverse energy

barrier is increased to 55.6 kcal·mol^{-1} thanks to the high stabilization of the cyclic carbonate intermediate **int 3**. The ring is then spontaneously opened by assistance of the alcohol which plays the role of proton relay between the secondary amine proton and the carbonate group. The quaternary C-O bond is broken and an imine is subsequently obtained with an energy barrier of 28.6 kcal·mol^{-1}. The intermediate **int 4** can then undergo decarboxylation with the alcohol playing the role of proton relay. This step is even lower in energy, with an energy barrier of 21.8 kcal·mol^{-1}. The released alcohol plays a major role in this reaction as it permits to bypass transition states with highly strained 4-membered rings to let place to six-membered ring structures (**TS 7**, **TS 8**). The imine **3** is therefore formed with the release of the alcohol and CO_2.

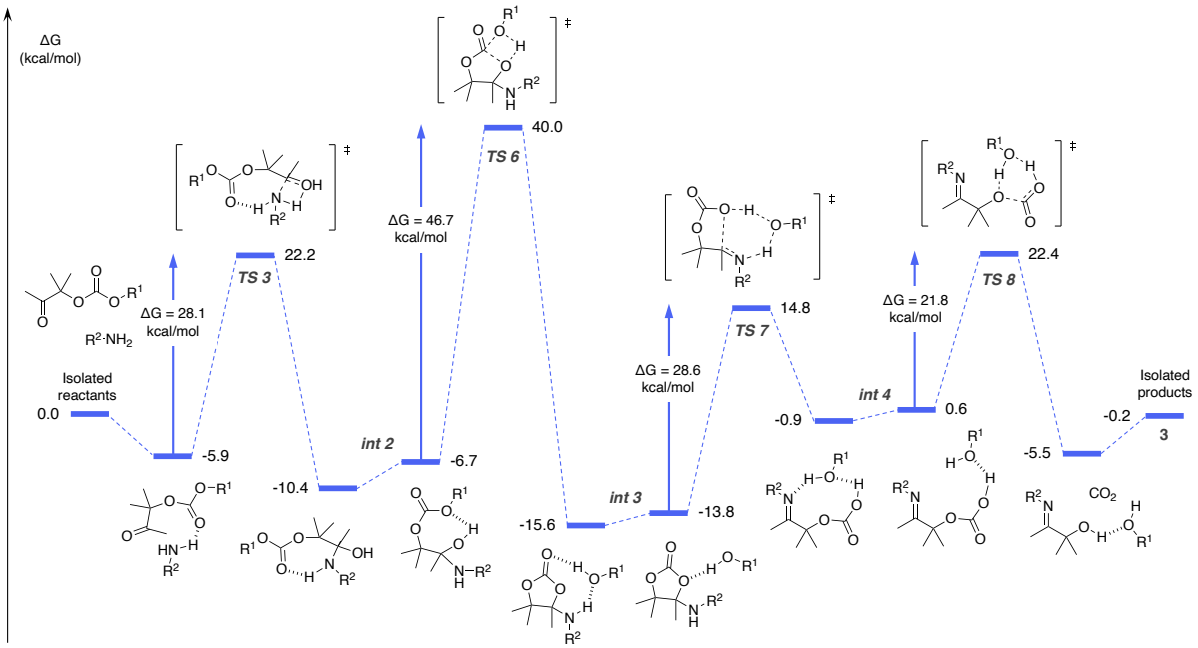

Figure S23. Gibbs free energy profile for the pathway 4 with respective geometries of transition states and intermediates.

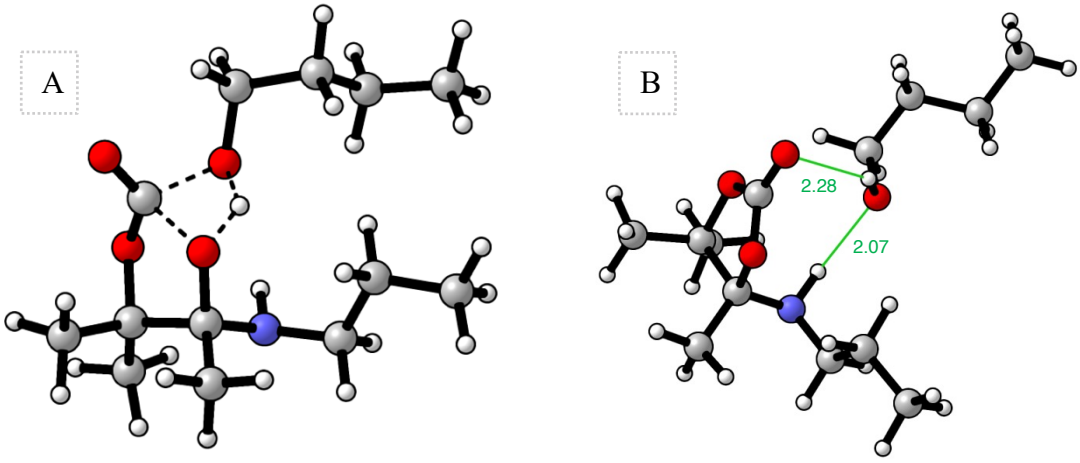

Figure S24. Geometries of (A) the transition state **TS 6** and (B) the post-reactive intermediate **int 3**. Dotted bonds in the TS structure indicate bonds which are broken or formed. Green bonds indicate hydrogen bonds. Distances are expressed in Å.

Pathway 4 – Alcohol as proton shuttle from **int 2** to **int 3**

Alcohols are prone to act as proton relays in many mechanisms and the same step was calculated using the model alcohol (butanol) as proton relay (**TS 11**). As shown in Figure S25, the energy barrier of the reaction is nearly the same in both cases, thus the use of an extra alcohol molecule in the mechanism does not favor the formation of **int 3**.

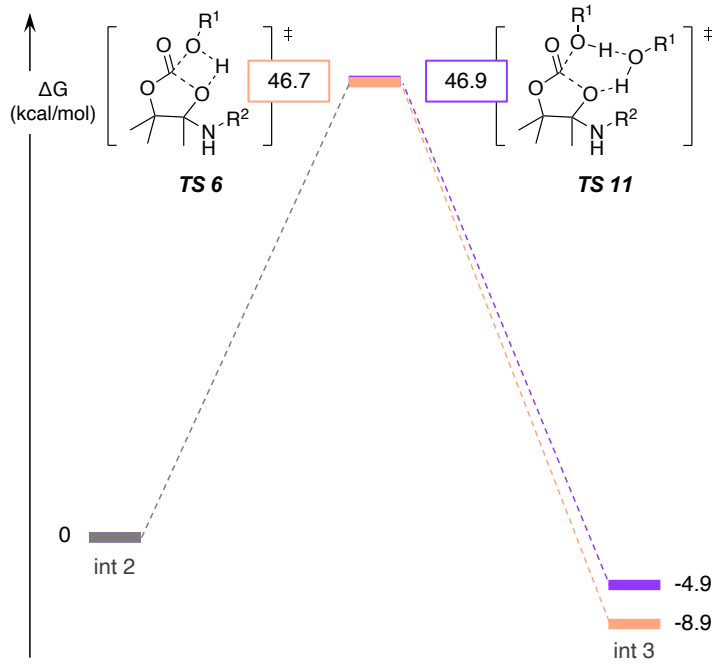

Figure S25. Gibbs free energy profile for the reaction from int 2 to int 3 in pathway 4 without (in orange) and with (in purple) the presence of an extra alcohol molecule. Gibbs free energy differences are expressed.

For the Optimized Cartesian Coordinates, please, refer back to the article:
ACS Sustainable Chem. Eng. 2022, 10, 8863–8875.

Characterization of poly(*oxo*-carbonate)s

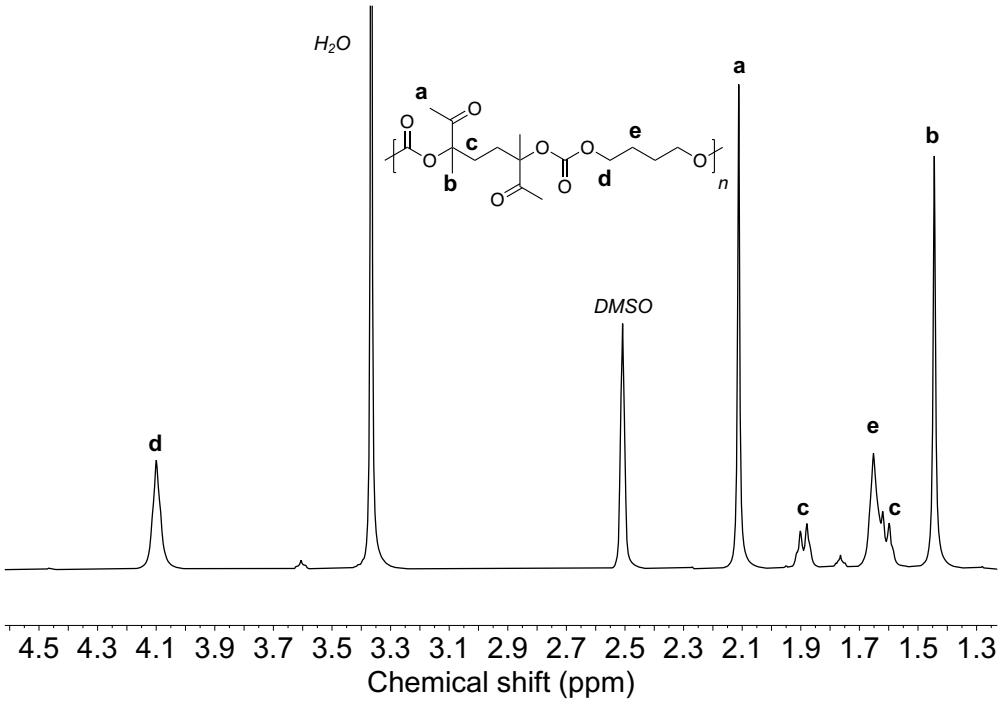

Figure S26. ^{1}H-NMR (in DMSO-d_6) spectrum of purified **PC1**.

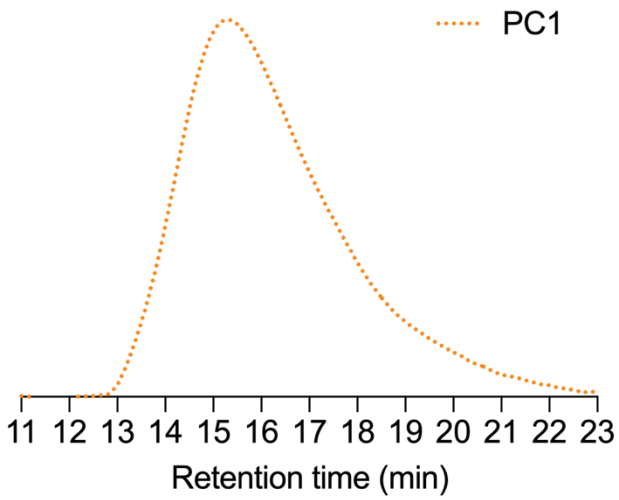

Figure S27. SEC chromatogram of purified **PC1** (in DMF/LiBr).

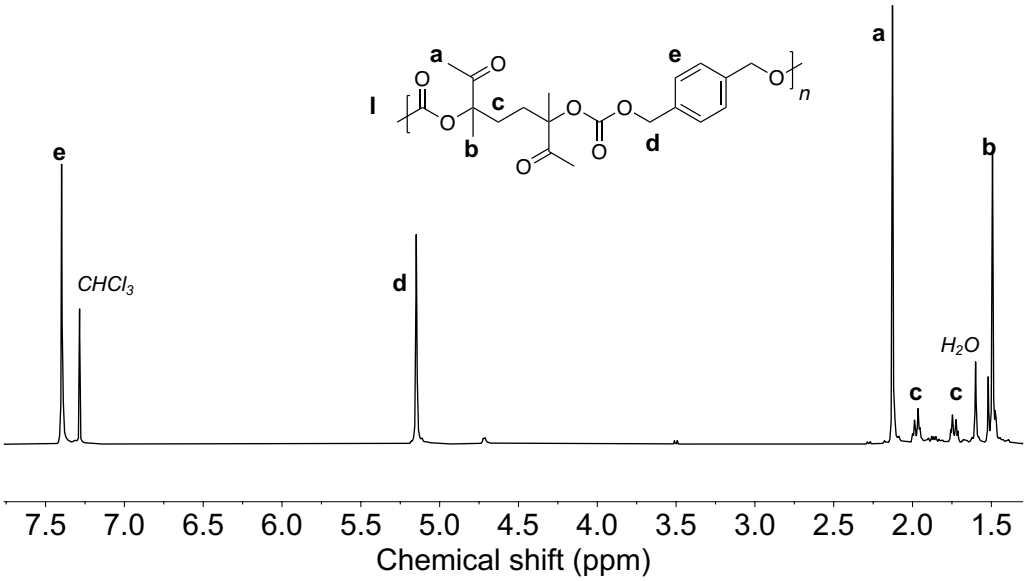

Figure S28. ^{1}H-NMR (in $CDCl_3$) spectrum of purified **PC2**.

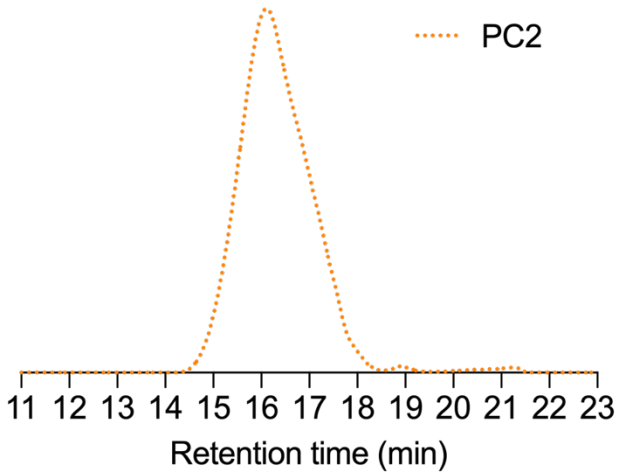

Figure S29. SEC chromatogram of purified **PC2** (in $CHCl_3$).

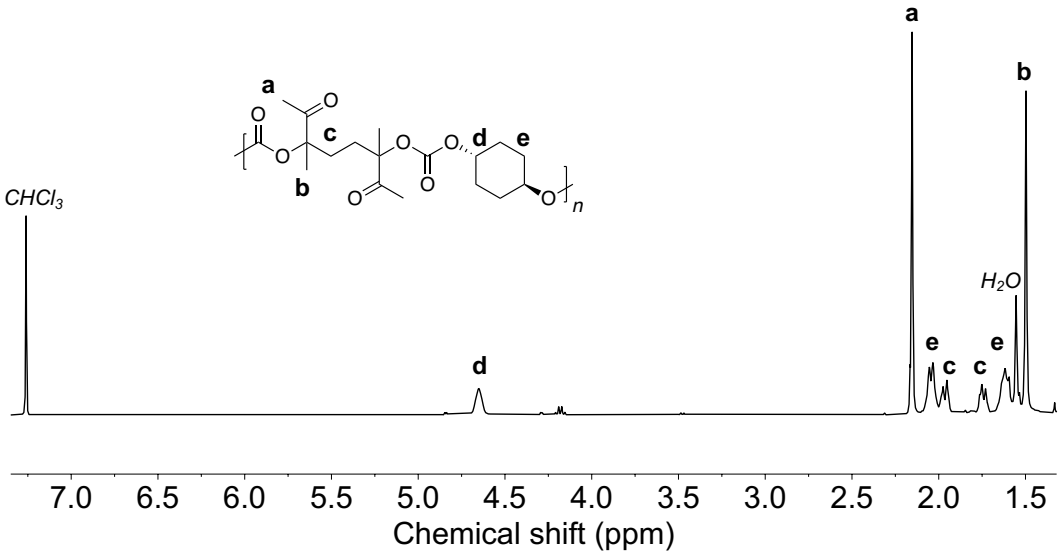

Figure S30. ^{1}H-NMR (in $CDCl_3$) spectrum of purified **PC3**.

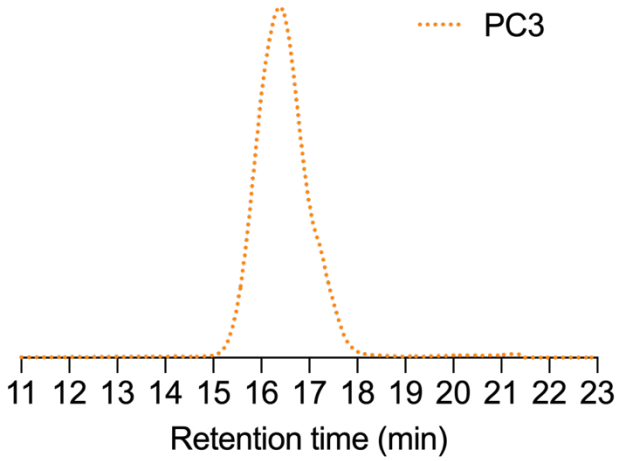

Figure S31. SEC chromatogram of purified **PC3** (in $CHCl_3$).

Poly(*oxo*-carbonate)s degradation

PC1 degradation kinetic

The percentage of polymer degraded was calculated by the equation 2:

$$P_{deg} = \left(1 - \frac{n_P}{n_{Pi}}\right) \times 100 \qquad (Eq.2)$$

P_{deg} = Polymer degradation (%).

n_P = number of mol of repeating unit of polymer at certain time*.

n_{Pi} = number of mol of repeating unit of initial polymer*.

*The number of mol were determined by integrating the peak at 2.13 ppm of the polymer in relation to the one of the standard TMB at 3.71 ppm.

Mole and the yield of product **1a** were calculated following the equations 3 and 4:

$$n_{1a} = \frac{\left(\frac{I_1}{N_{H,1}}\right) \times n_{TMB}}{\frac{I_{TMB}}{N_{H,TMB}}} \qquad (Eq.3)$$

$$Yield\ (1a) = \frac{n_1}{n_{Pi}} \times 100 \qquad (Eq.4)$$

n_1 = number of mol of product **1a**.

I_1 = Integral peak of product **1a**.

$N_{H,1}$ = Number of protons associated to the integrated peak of product **1a**.

n_{TMB} = number of mol of internal standard TMB.

I_{TMB} = Integral peak of TMB.

$N_{H,TMB}$ = Number of protons associated to the integrated peak of TMB.

Same calculation has been made for the other degradation products.

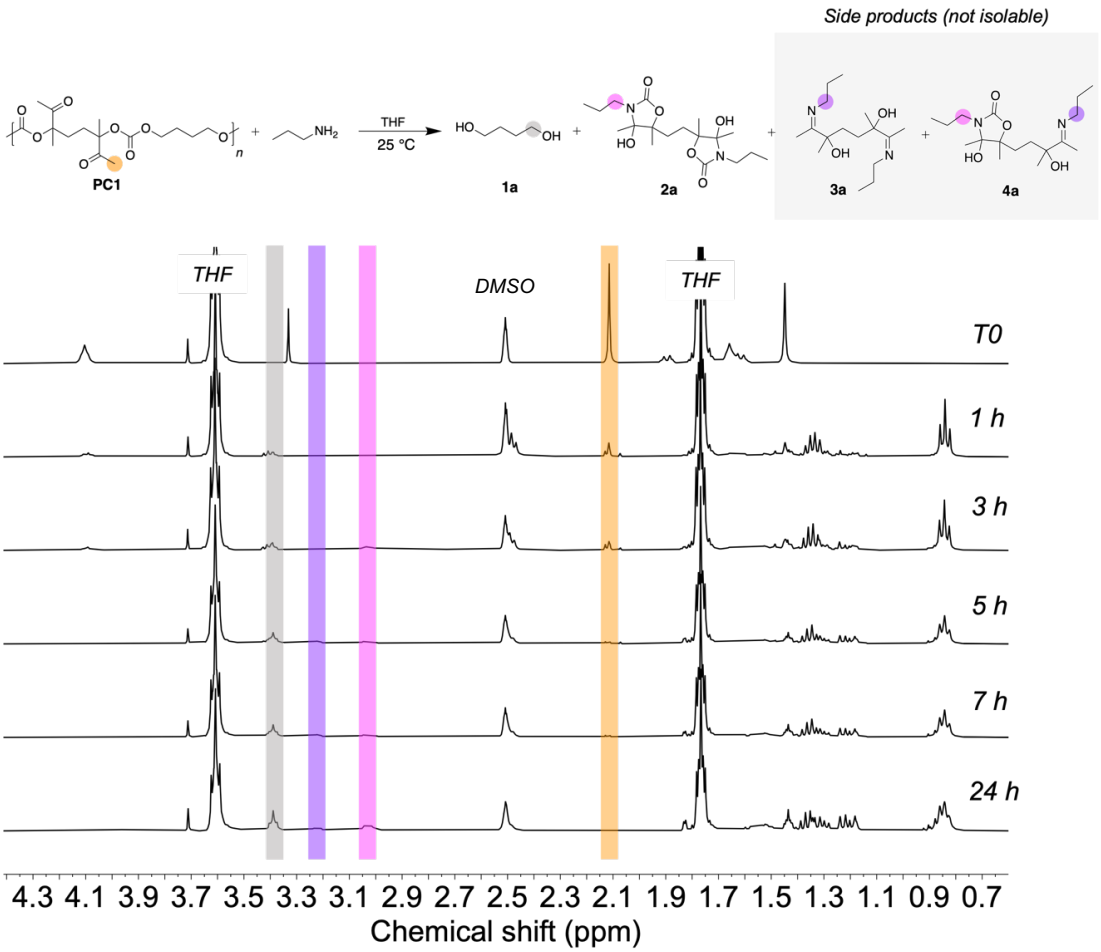

Figure S32. Overlay spectra of **PC1** aminolysis kinetic with **A1** followed by ^{1}H-NMR (in DMSO-d_6).

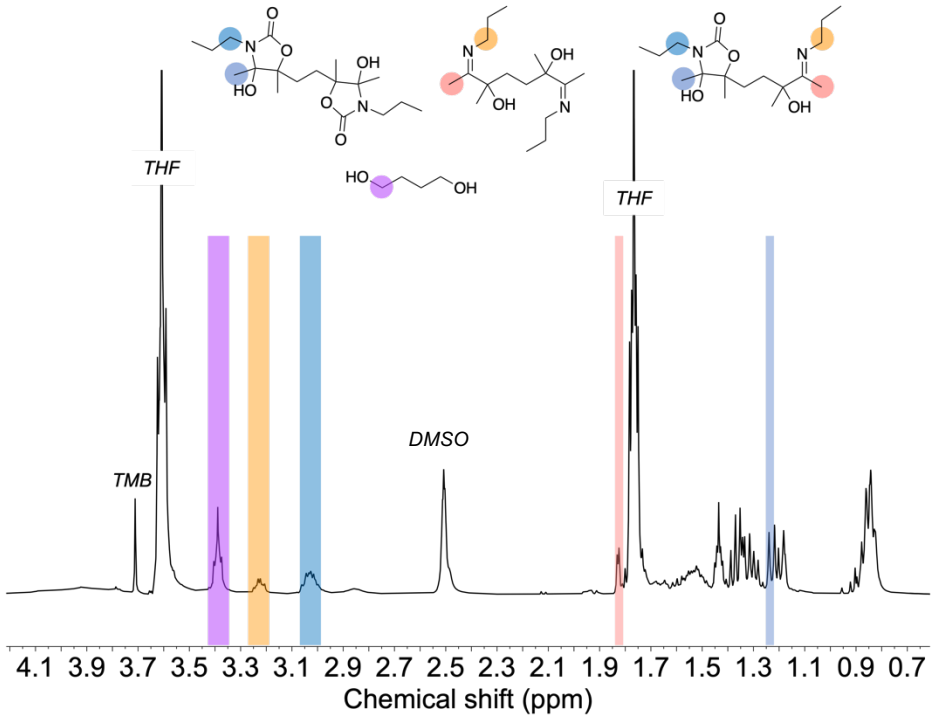

Figure S33. ^{1}H-NMR (in DMSO-d_6) spectrum of **PC1** aminolysis with **A1** after 24 h and products identification.

Characterization of 5,5'-(ethane-1,2-diyl)bis(4-hydroxy-4,5-dimethyl-3-propyloxazolidin-2-one)(2a)

^{1}H NMR (400 MHz, DMSO-d_6): δ = 5.99 ppm (s, 2H), δ = 3.03 ppm (m, 4H), δ = 1.66-1.46 ppm (m, 4H), δ = 1.34-1.24 ppm (m, 4H), δ = 1.28 ppm (s, 6H), δ = 1.27 ppm (s, 6H), δ = 0.85 ppm (m, 6H).

^{13}C NMR (400 MHz, DMSO-d_6): δ = 156.9 ppm, δ = 90.0 ppm, δ = 85.9 ppm, δ = 41.6 ppm, δ = 31.1 ppm, δ = 23.0 ppm, δ = 18.2 ppm, δ = 11.8 ppm.

ESIHRMS m/z calcd for $C_{18}H_{32}N_2O_6$ $[M+H]^+$ 372,2265, found 373,2265.

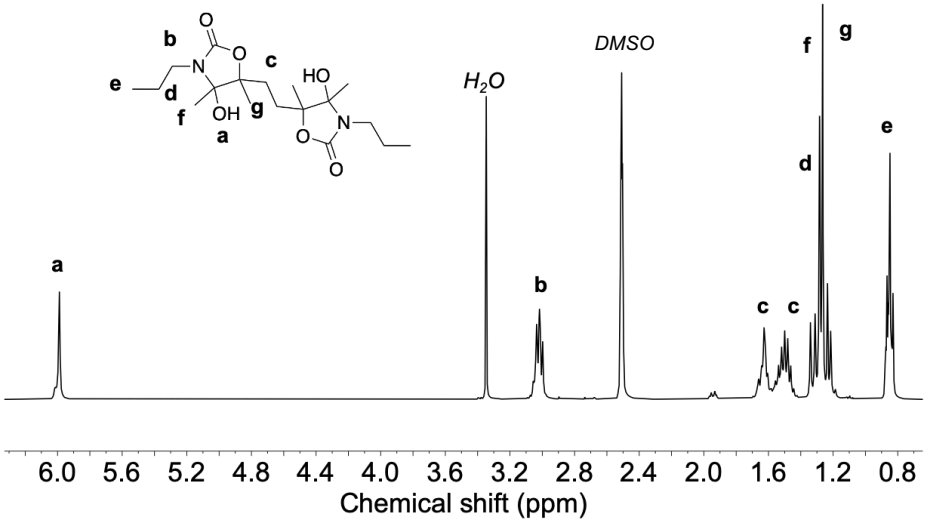

Figure S34. ^{1}H-NMR (in DMSO-d_6) of purified 5,5'-(ethane-1,2-diyl)bis(4-hydroxy-4,5-dimethyl-3-propyloxazolidin-2-one) (**2a**).

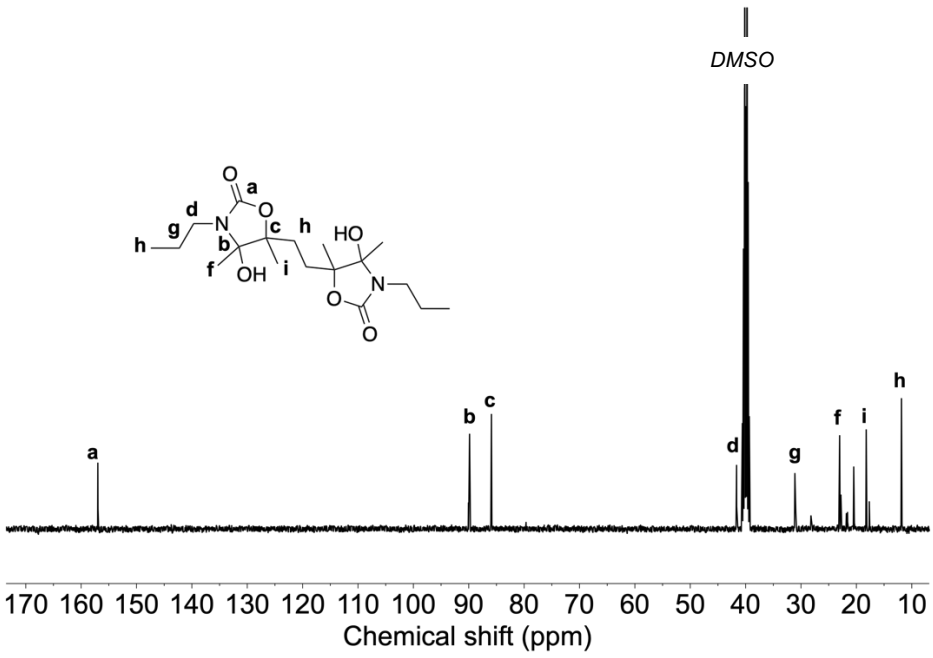

Figure S35. ^{13}C-NMR (in DMSO-d_6) of purified 5,5'-(ethane-1,2-diyl)bis(4-hydroxy-4,5-dimethyl-3-propyloxazolidin-2-one) (**2a**).

PC1 aminolysis with A1 at 6 °C and using lower amount of amine (at 25 °C)

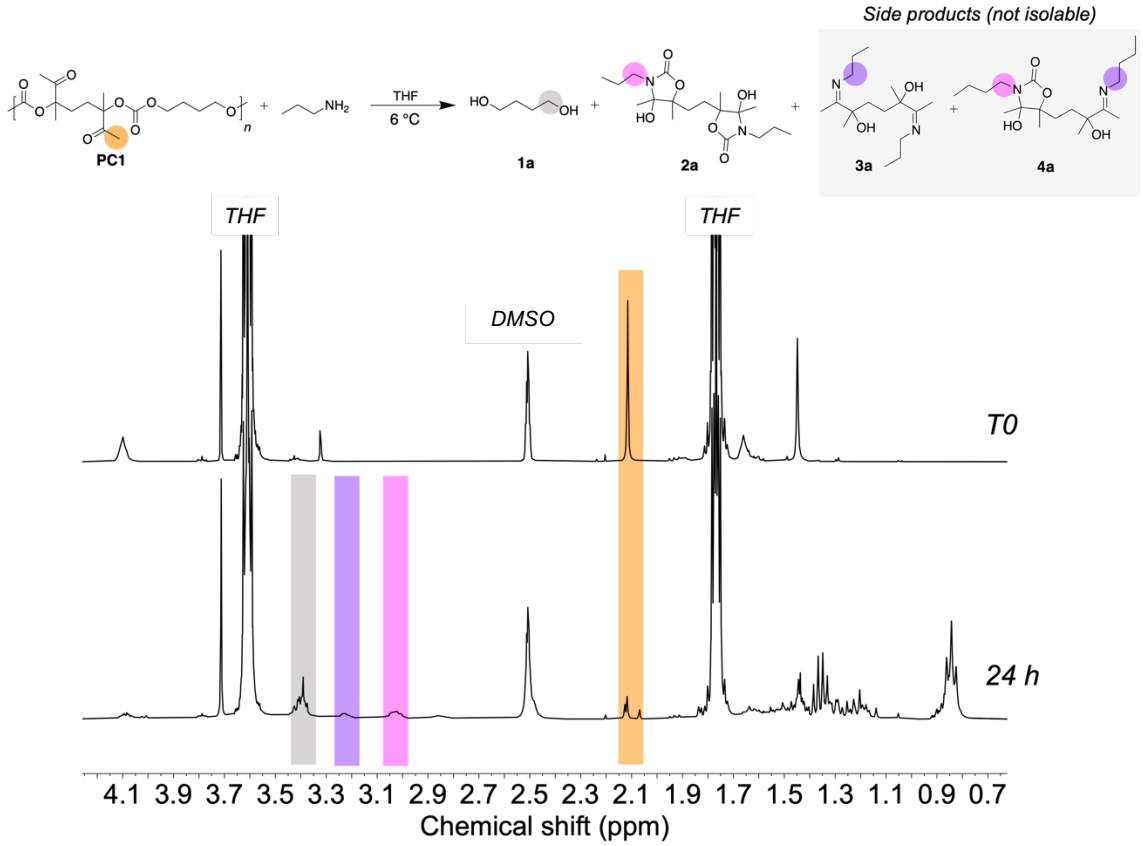

Figure S36. Overlay spectra of **PC1** aminolysis at T0 and after 24 h, carried out at 6 °C, with **A1** followed by ^{1}H-NMR (in DMSO-d_6).

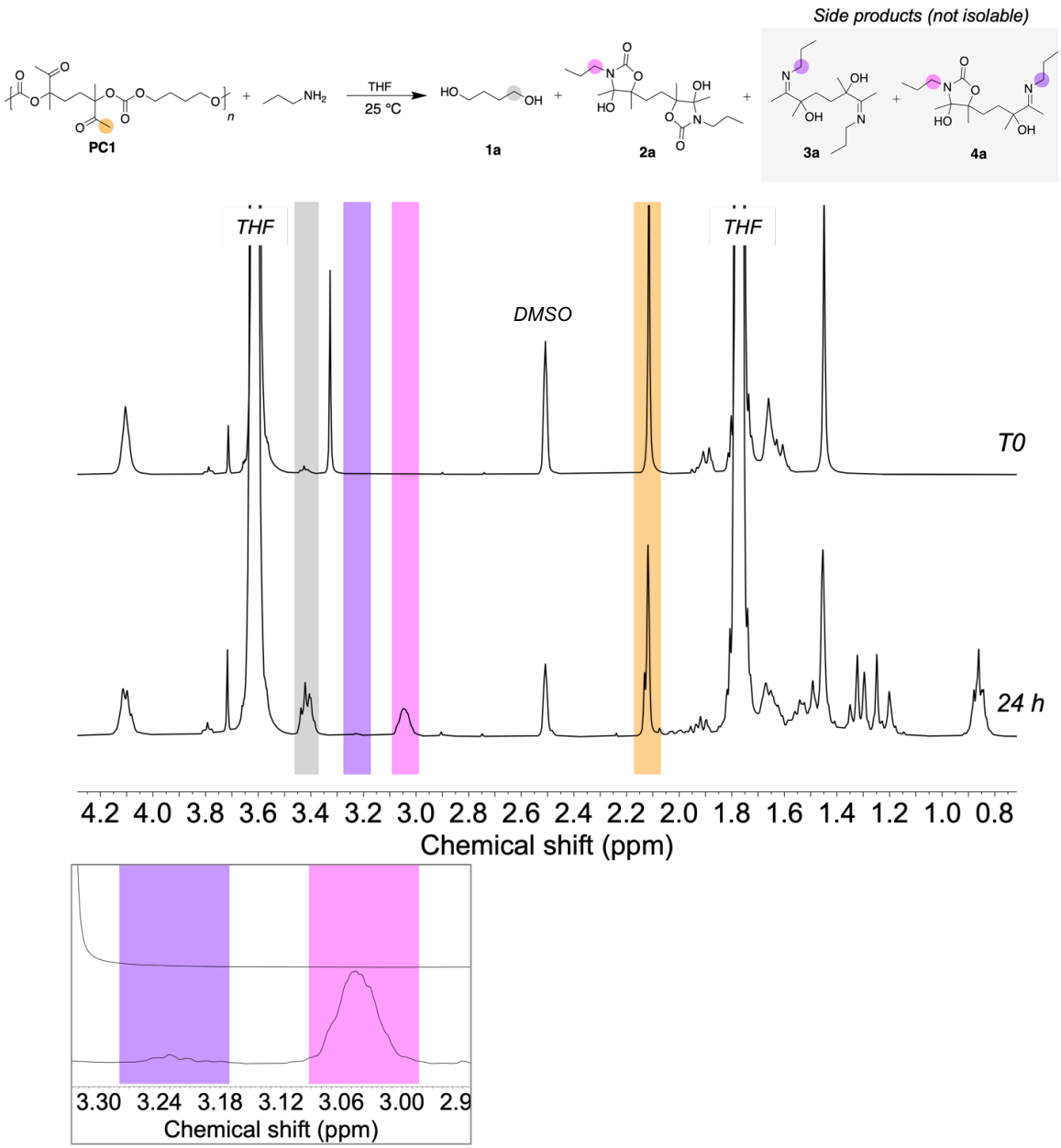

Figure S37. ^{1}H-NMR (in DMSO-d_6) overlay spectra of **PC1** aminolysis at T0 and after 24 h, with **A1** (2 eq. *vs* each ketone moiety of the polymeric repeating unit) and magnification of imine and hydroxy-oxazolidinone moieties.

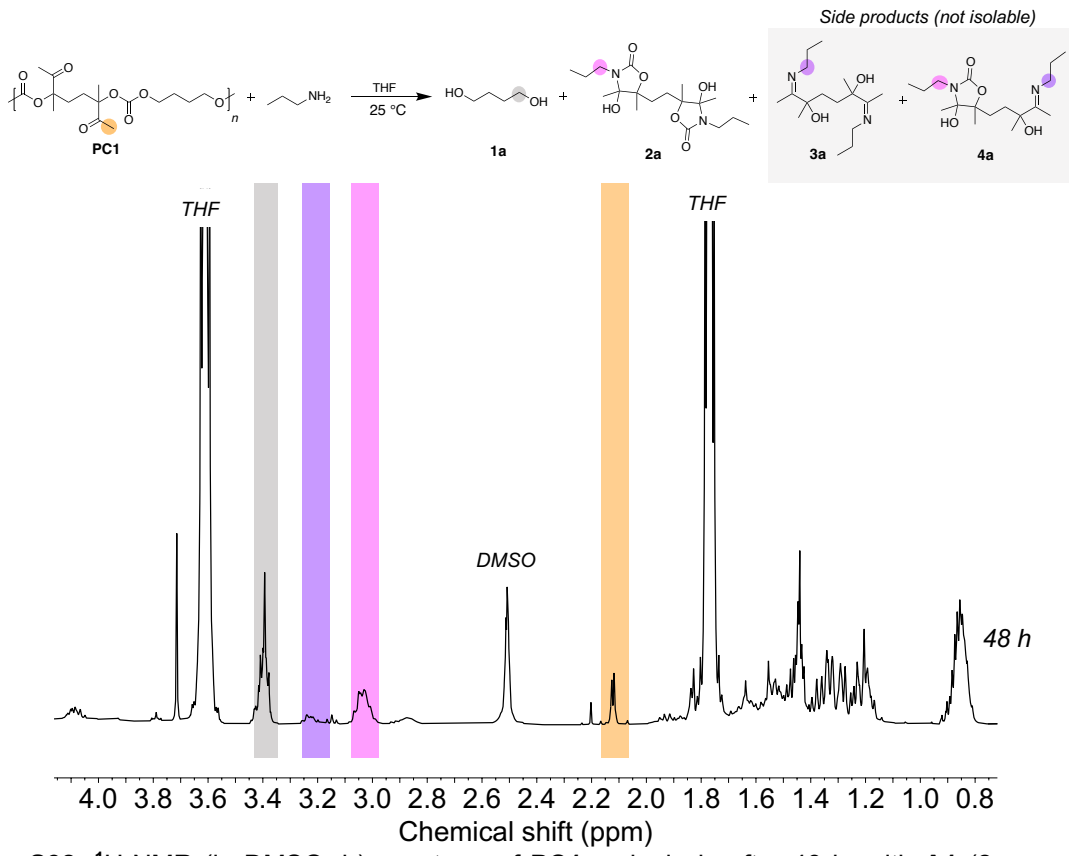

Figure S38. ^{1}H-NMR (in DMSO-d_6) spectrum of **PC1** aminolysis after 48 h, with **A1** (2 eq. *vs* each ketone moiety of the polymeric repeating unit)

Polymer degradation using amine as solvent

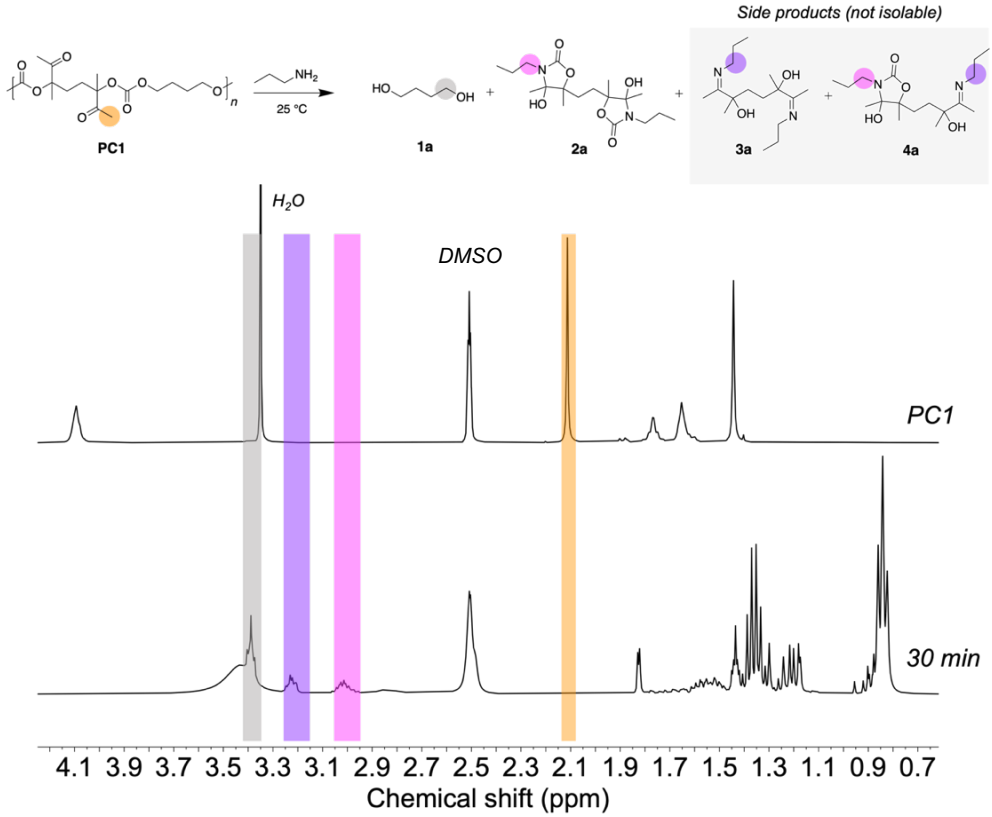

Figure S39. ^{1}H-NMR (in DMSO-d_6) overlay spectra of pure **PC1** and of **PC1** aminolysis with **A1** (as solvent) after 30 min.

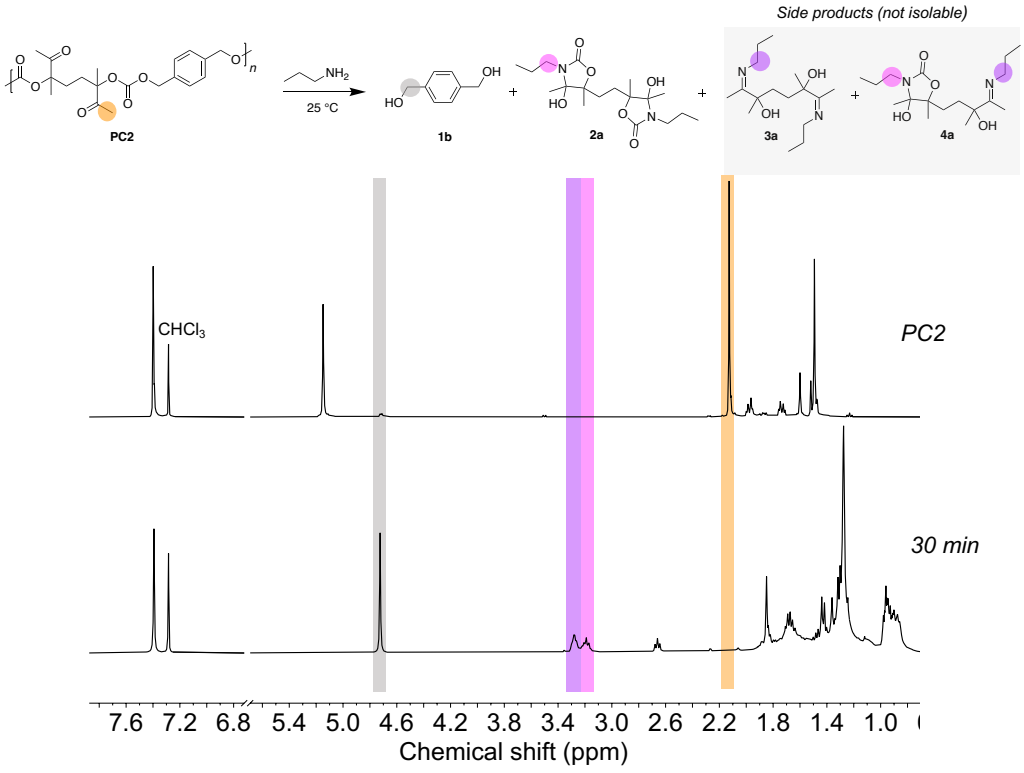

Figure S40. ^{1}H-NMR (in $CDCl_3$) overlay spectra of pure **PC2** and of **PC2** aminolysis with **A1** (as solvent) after 30 min.

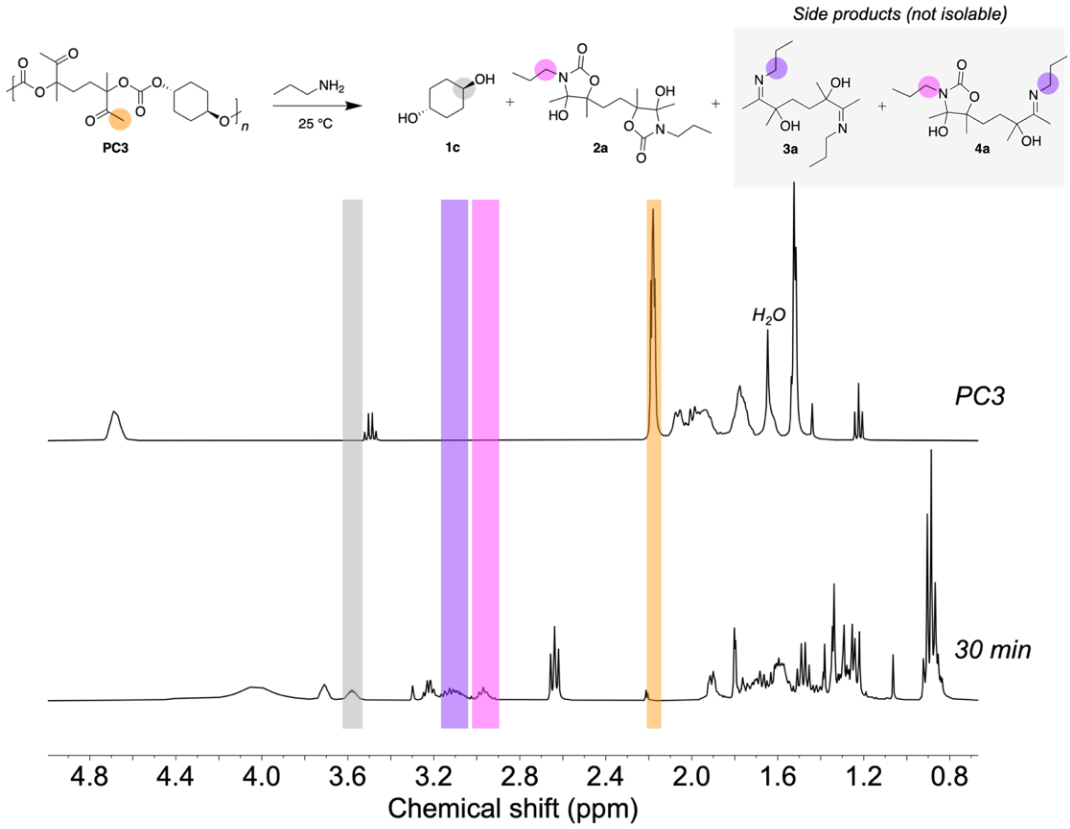

Figure S41. ^{1}H-NMR (in $CDCl_3$) overlay spectra of pure **PC3** and of **PC3** aminolysis with **A1** (as solvent) after 30 min.

Depolymerization using propanolamine A4

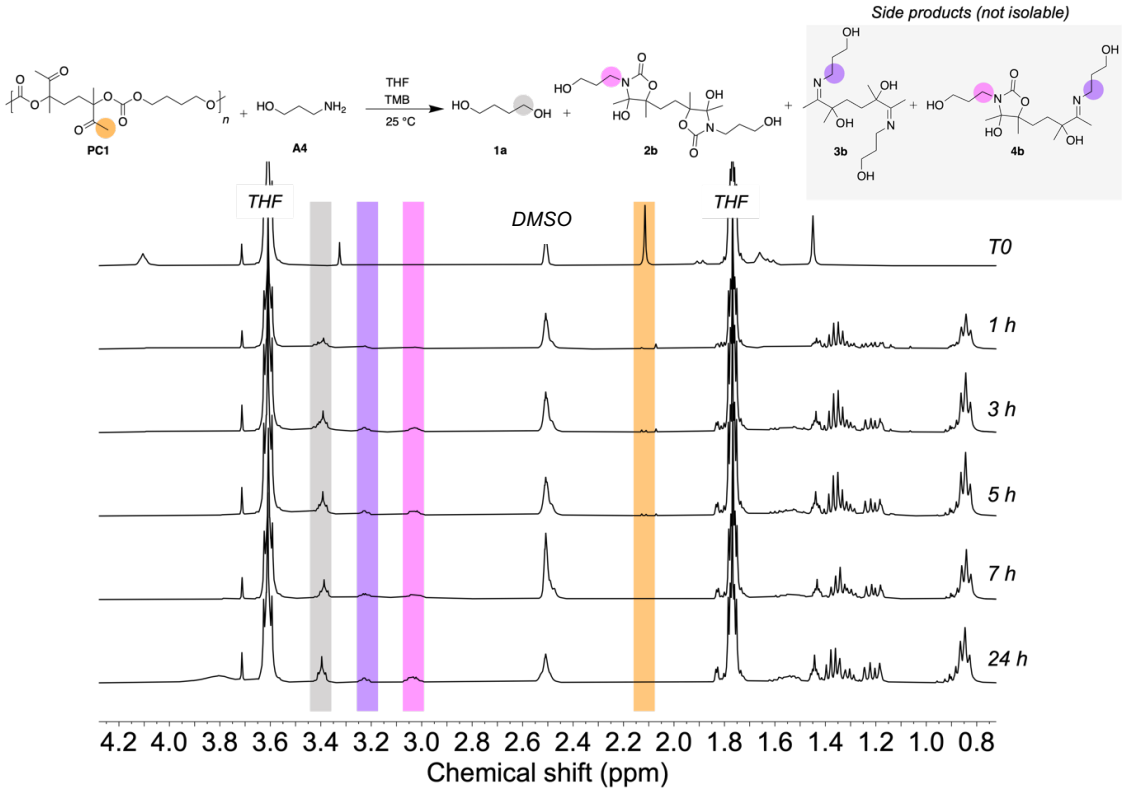

Figure S42. Overlay spectra of **PC1** aminolysis kinetic with propanol amine followed by ^{1}H-NMR (in DMSO-d_6).

Characterization of 5,5'-(ethane-1,2-diyl)bis(4-hydroxy-3-(3-hydroxypropyl)-4,5-dimethyloxazolidin-2-one) (2b)

^{1}H NMR (400 MHz, DMSO-d_6): δ = 6.03-6.01 ppm (m, 2H), δ = 4.46 ppm (m, 2H), δ = 3.42 ppm (m, 4H), δ = 3.13 ppm (m, 4H), δ = 1.26 ppm (s, 3H), δ = 1.93 ppm (m, 2H), δ = 1.69-1.62 ppm (m, 6H), δ = 1.34 ppm (s, 3H), δ = 1.29 ppm (s, 3H), δ = 1.26 ppm (s, 3H), δ = 1.21ppm (s, 3H).

^{13}C NMR (400 MHz, DMSO-d_6): δ = 156.9 ppm, δ = 90.0 ppm, δ = 86.0 ppm, δ = 59.9 ppm, δ = 37.2 ppm, δ = 32.8 ppm, δ = 28.2 ppm, δ = 21.8 ppm, δ = 18.2 ppm.

ESIHRMS m/z calcd for $C_{18}H_{32}N_2O_8$ $[M+H]^+$ 404,2165, found 405,2236.

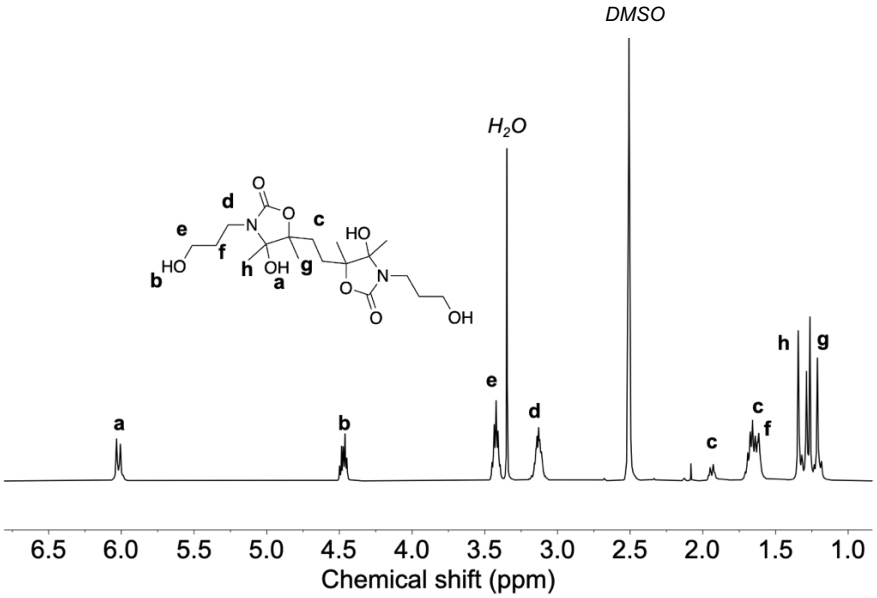

Figure S43. ^{1}H-NMR (in DMSO-d_6) of purified 5,5'-(ethane-1,2-diyl)bis(4-hydroxy-4,5-dimethyl-3-propyloxazolidin-2-one) (**2b**).

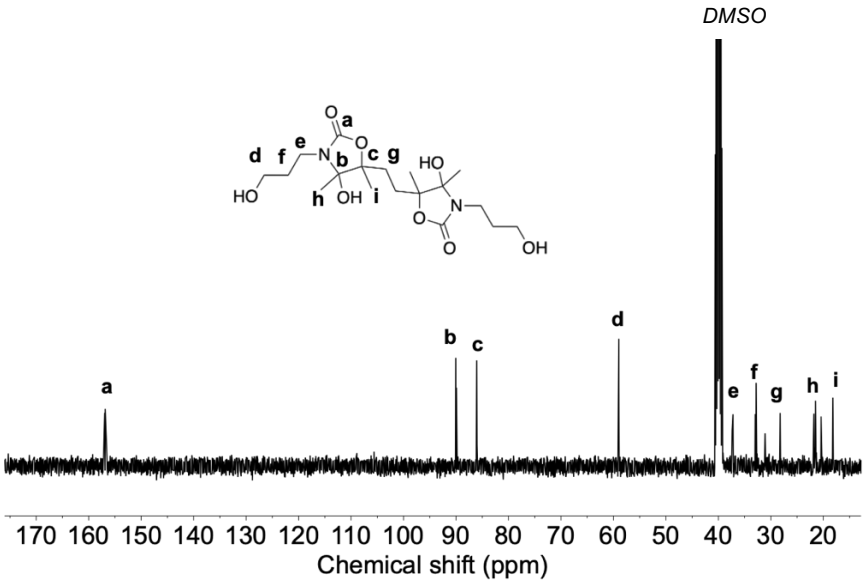

Figure S44. ^{13}C-NMR (in DMSO-d_6) of purified 5,5'-(ethane-1,2-diyl)bis(4-hydroxy-4,5-dimethyl-3-propyloxazolidin-2-one) (**2b**).

Poly(*oxo*-carbonate)-*co*-(hydroxy-oxazolidinone) PC4

^{1}H NMR (400 MHz, DMSO-d_6): δ = 6.06 ppm (m, 2H), δ = 4.11 ppm (m, 4H), δ = 3.17 ppm (m, 4H), δ = 2.12 ppm (s, 6H), δ = 1.86-1.61 ppm (m, 12H), δ = 1.44 ppm (s, 6H), δ = 1.34-1.19 ppm (m, 12H).

^{13}C NMR (400 MHz, DMSO-d_6): δ = 206.3 ppm, δ = 156.9 ppm, δ = 153.6 ppm, δ = 90.1 ppm, δ = 86.7 ppm, δ = 66.4 ppm, δ = 36.7 ppm, δ = 29.1 ppm, δ = 28.6 ppm, δ = 28.3 ppm, δ = 24.6 ppm, δ = 21.7 ppm, δ = 20.4 ppm, δ = 17.9 ppm.

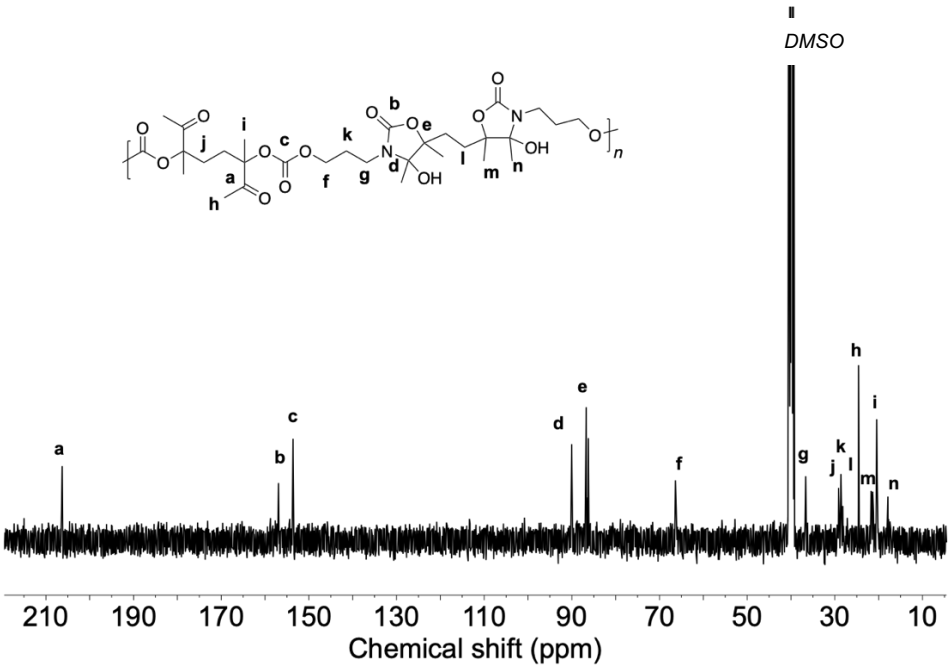

Figure S45. ^{13}C-NMR (in DMSO-d_6) of purified **PC4**.

Degradation poly(oxo-carbonate)-co-(hydroxy-oxazolidinone) PC4

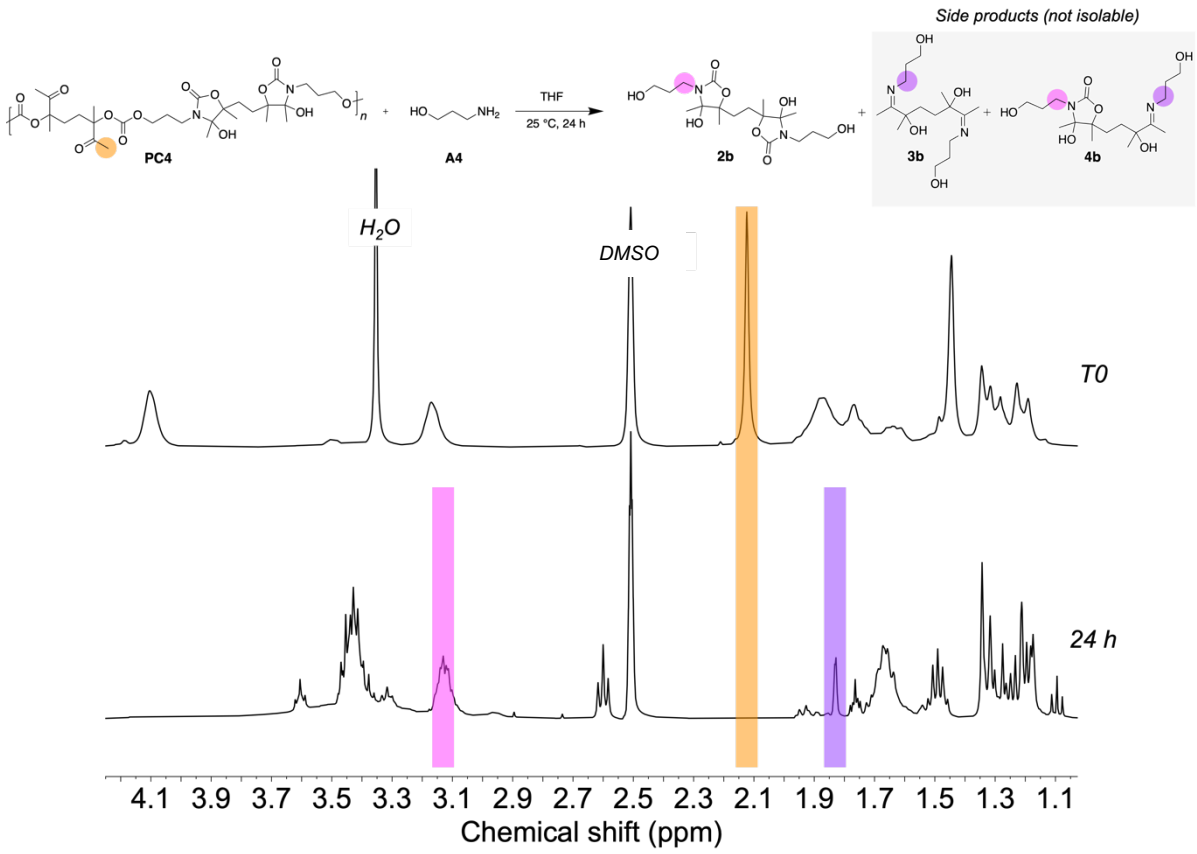

Figure S46. ^{1}H-NMR (in DMSO-d_6) overlay spectra of **PC4** aminolysis with **A4** at T0 and after 24 h. Note that, before to analyze the sample by ^{1}H-NMR, it was necessary to remove a big part of THF in order to identify the peak at 1.84 ppm.

References

(1) Álvarez-Moreno, M.; de Graaf, C.; López, N.; Maseras, F.; Poblet, J. M.; Bo, C. Managing the Computational Chemistry Big Data Problem: The IoChem-BD Platform. *Journal of Chemical Information and Modeling* **2015**, *55*, 95–103. https://doi.org/10.1021/ci500593j.

(2) Stewart, J. J. P. Optimization of Parameters for Semiempirical Methods VI: More Modifications to the NDDO Approximations and Re-Optimization of Parameters. *Journal of Molecular Modeling* **2013**, *19*, 1–32. https://doi.org/10.1007/s00894-012-1667-x.

(3) Stewart, J. J. P. MOPAC2016. Colorado Springs, CO, USA 2016.

(4) Frisch, M. J.; Trucks, G. W.; Schlegel, H. B.; Scuseria, G. E.; Robb, M. A.; Cheeseman, J. R.; Scalmani, G.; Barone, V.; Petersson, G. A.; Nakatsuji, H.; Li, X.; Caricato, M.; Marenich, A. v; Bloino, J.; Janesko, B. G.; Gomperts, R.; Mennucci, B.; Hratchian, H. P. Gaussian 16. *Gaussian, Inc.* Wallingford CT 2016.

(5) Chai, J.-D.; Head-Gordon, M. Long-Range Corrected Hybrid Density Functionals with Damped Atom–Atom Dispersion Corrections. *Physical Chemistry Chemical Physics* **2008**, *10*, 6615–6620. https://doi.org/10.1039/B810189B.

(6) Siragusa, F.; van den Broeck, E.; Ocando, C.; Müller, A. J.; de Smet, G.; Maes, B. U. W.; de Winter, J.; van Speybroeck, V.; Grignard, B.; Detrembleur, C. Access to Biorenewable and CO2-Based Polycarbonates from Exovinylene Cyclic Carbonates. *ACS Sustainable Chemistry and Engineering* **2021**, *9*, 1714–1728. https://doi.org/10.1021/acssuschemeng.0c07683.

Chapter IV

Unifying step-growth polymerization and on-demand cascade ring-closure depolymerization via polymers skeletal editing

*Fabiana Siragusa, Jeremy Demarteau, Thomas Habets, Ion Olazabal, Koen Robeyns, Gwilherm Evano, Raphael Mereau, Thierry Tassaing, Bruno Grignard, * Haritz Sardon, Christophe Detrembleur **

Reference: *Macromolecules 2022, 55,11, 4637–4646*.

https://doi.org/10.1021/acs.macromol.2c00696

Author contributions: F.S., T.H., C.D., B.G., J.D., H.S. and G.E. designed and planned the project. F.S. synthesized and characterized all polymers and carried out all the model reactions. J.D., I.O. and H.S. designed and synthesized plastics-derived monomers. T.T. and R.M. carried out DFT modelling. K.R. carried out XRD analysis. F.S. wrote the manuscript with contributions from all co-authors.

ABSTRACT

The inherent skeletal and thermal features to forge polymers by step-growth polymerization are conflicting with any depolymerization strategies via cascade back-biting reactions that necessitate adequate ceiling temperature, spacers and functionalities to create cyclic compounds. Here, we report the edition of step-growth poly(carbonate-urea)s and poly(carbonate-amide)s that are depolymerized on demand into their native precursor or added-value offspring oxazolidinones, together with a hemiacetal cyclic carbonate. The unprotected in-chain secondary amide or urea functionalities of the polymers trigger their degradation via cascade ring-closing events upon a thermal switch (from 25 to 80 °C) in the presence of an organic base as catalyst. Although most studies are realized in solution for understanding the deconstruction process, the polymers are also fully degraded in 2 h in the neat without any catalyst at 150 °C. At 80 °C, the organic base is required to accelerate the process. On the road to sustainability and circularity, we validate the concept by exploiting monomers designed from waste CO_2 and upcycled commodity plastics. Ultimately, these polymers are selectively depolymerized from plastic mixtures composed of commodity polyethylene terephthalate and polycaprolactone, offering new options for recycling plastics waste mixtures while delivering high value-added chemicals.

Introduction

Over the last century, commodity to engineered plastics have totally reshaped our modern life. Their every-day overgrowing utilization coupled to the lack of viable end-of-life scenario, their finite fossil origin and their long-term persistence in marine ecosystems and nature are now causing a major environmental crisis.[1,2] This pushes scientists to fundamentally reinvent the way to fabricate, use and recycle, ideally on-demand, these materials in a circular, sustainable and economic manner.[3–22] Circular economy of plastics is better achieved through chemical recycling, where the polymer chain is depolymerized into the pristine monomer or new value added chemicals. In this context, heteroatom-linked step-growth polymers such as polyesters, polyurethanes and polycarbonates can play a pivotal role to tackle the plastic pollution problem. The presence of in-chain C-O or C-N labile bonds offers various chemical depolymerization opportunities via solvolysis, producing either the initial monomers that are reemployed in closed-loop system or, new added-value chemicals via an open-loop upcycling approach.[8,10] Developing creative and energy efficient deconstruction strategies, beyond solvolysis, to enlarge and diversify the scope of accessible chemicals from step-growth polymers represents an exciting but rather unexplored research area.

Ring-closing depolymerization is a powerful method to transform polymer backbones into cyclic products, yet being virtually applicable to all polyesters and polycarbonates made by ring-opening (co)polymerization (RO(CO)P).[9,23–30] The almost ergoneutral polymerization energetics ($\Delta G_p \approx 0$) of these RO(CO)P polymers enable chain growth below their ceiling temperature (T_c) and the (catalytic) reversion of the materials into the native 3-, 5- or 6-membered cyclic precursors by activated chain-end unzipping above T_c.[11,31–37] Mimicking this concept with step-growth polymers is far from trivial. Impediments to the construction of step-growth materials with ring-closing degradative ability lie in the inherent incompatibility between both chain growth and deconstruction manifolds. The inadequate microstructural polymer features also prevents the formation of well-defined cyclic molecules upon back-biting reactions in most cases. This is exemplified for polycarbonates (PC).[38] The carbonylation of vicinal diols provides exclusively the corresponding 5-membered cyclic carbonates while oligomers (minor product) coexist with 6-membered trimethylene carbonates (major product) when 1,3-diols are used as templates.[28,39,40] Only 1,x-diols (with $x > 3$) deliver polycarbonates with decent molar masses by step-growth copolymerization, generally at high temperature to tackle the low reactivity of the comonomers and/or to eliminate the condensate (in polycondensations). However, the enlargement of the alkylene spacer between both hydroxyl units of the diols is detrimental for deconstructing the PCs via activated chain-end back-biting as the formation of 7-membered (if $x = 4$) or even larger rings is unfavored. Their depolymerization into macrocyclic carbonates is now possible by transesterification (i.e. not by

back-biting reaction) at elevated temperature (235-280 °C) under vacuum distillation.[41] The chemical foundations to design PCs by step-growth polymerization with ring-closing degradative ability imposes the utilization of monomers with adequate ethylene or propylene spacers between the reactive groups but also processing conditions and adequate ceiling temperature that favor their enchainment into polymers instead of the cyclic scaffolds formation. Self-immolative polymers represent an elegant solution to this issue as they can be delivered by step-growth polymerization while being prone to spontaneous disassembly via a domino fashion upon removal of a triggering moiety by an appropriate stimulus.[42–54] While interesting but rarely illustrated with polycarbonates, this class of materials suffers from 1) the utilization of protected monomers, generally not easily accessible and not sustainable, and/or 2) the stabilization of the growing chains by fast trapping of the reactive terminus to prevent reversion, limiting the molar mass to short chains, which is detrimental for the thermo-mechanical performances of the materials.[55]

Herein, we report an original and facile methodology to fabricate polycarbonate-type polymers with cascade ring-closing depolymerization ability via an activated chain-end mechanism, delivering upon deconstruction new cyclic scaffolds. Capitalizing on our recent approach furnishing regioregular polycarbonates by room temperature step-growth copolymerization of exovinylene biscyclic carbonates and diols,[56–58] we envisioned that a smart skeletal editing of these PCs should solve the conflict between step-growth copolymerization and ring-closing depolymerization. Thus, we explore the introduction of additional unprotected in-chain secondary functionalities, non-reactive at room temperature but activated on-demand upon catalytic thermal switch (Scheme 1). The concept was validated with monomers designed from CO_2 and upcycled waste plastics, creating a sustainable and circular scenario answering the requirements of our modern society.

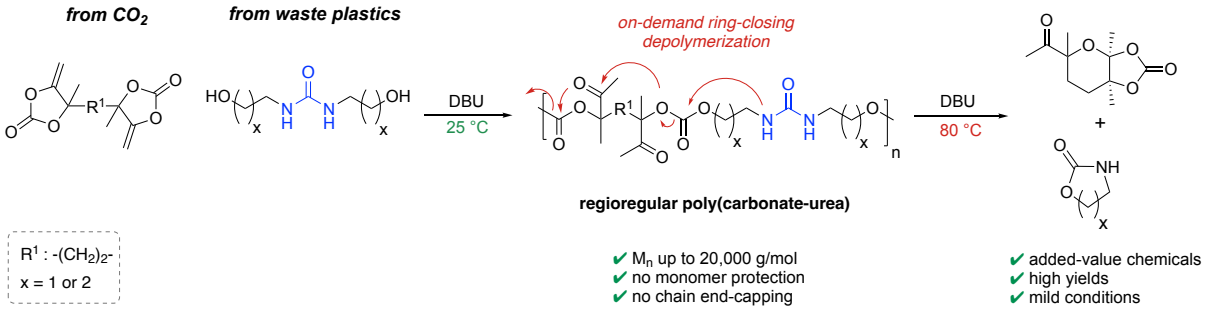

Scheme 1. Fabrication of step-growth poly(carbonate-urea)s with back-biting ring-closing depolymerization ability.

Results and discussion

Design of regioregular poly(carbonate-amide) and poly(carbonate-urea)s. Forging step-growth polycarbonates with ring-closing degradative ability requires engineering and unifying monomers with dual functionalities that can be activated on demand to drive selectively divergent catalytic polymerization and depolymerization pathways. To be applicable and guarantee the success of our methodology, the fine control of the polymer microstructure is capital. Errors in the enchainment of the monomers could create termination nodes stopping the depolymerization, further providing mixture of ill-defined products. To do so, series of polycarbonate-type polymers are synthesized by the room temperature DBU-catalyzed step-growth copolymerization of CO_2-sourced bisαCC (**C1**) with waste plastics-sourced diols containing in-chain unprotected secondary amide or urea moieties (**P1**-**3**, Scheme 2, Figures S1-S6).[59] After 24 h, polymers **C1P1**, **C1P2** and **C1P3** are obtained with a weight-average molar mass (M_w) of 27,500 g/mol, 17,000 g/mol, 29,900 g/mol, respectively (Scheme 2, Tables S1-S3 and Figures S7-S9). The ^1H and ^{13}C nuclear magnetic resonance (NMR) characterizations of the three polymers (Figure S10) attest for the regioregular nature of the chains. Moreover, all resonances are in agreement with the expected copolymers microstructure with intact in-chain amide or urea linkages and pendant ketones – functionalities that are also crucial for the ring-closing deconstruction of PCs, as it will be illustrated later, and no sign of degradation products. All polymers are isolated and display thermal stabilities with decomposition temperature at 10% weight loss ($T_{deg10\%}$) up to 162 °C, 170 °C and 164 °C, for **C1P1**, **C1P2** and **C1P3**, respectively (Table 1, Figures S11-S13). All polymers are found amorphous by differential scanning calorimetry (DSC) (Scheme 2, Figures S14-S16). **C1P1** displays a glass transition temperature (T_g) of 43 °C while, by shifting from terephthalamide segment to a less rigid urea, the T_g value decreases to 17 °C (**C1P2**). The low T_g value of 0 °C of **C1P3** reflects its more flexible nature compared to **C1P2** due to the extension of the ethylene (in **P2**) to a propylene spacer in the structure of **P3**.

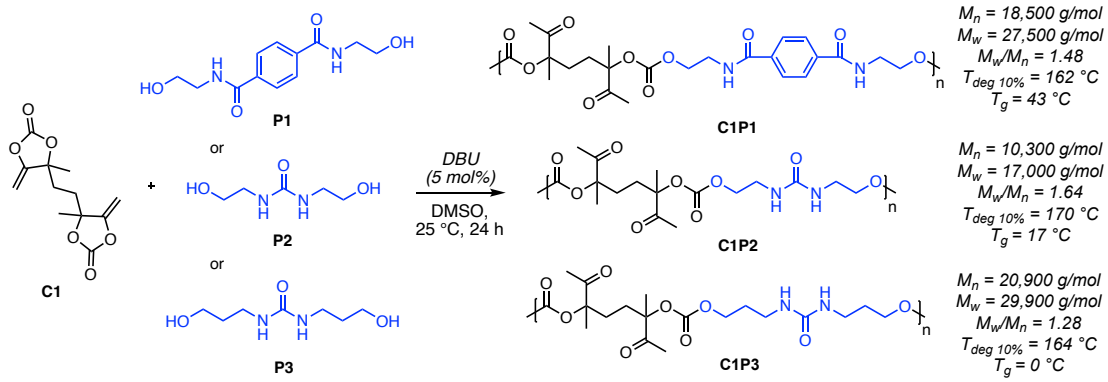

Scheme 2. Synthesis and macromolecular characteristics of **C1P1**, **C1P2** and **C1P3**. Reaction conditions: [C1]/[P1 or P2 or P3] = 1, [C1] = 0.78 M; M_n, M_w and M_w/M_n were determined by SEC in DMF/LiBr. Conversion > 99% in all cases.

Ring-closing depolymerization of poly(carbonate-amide) and poly(carbonate-urea). **C1P1** is then subjected to deconstruction using 10 mol% of DBU (compared to the polymer repeating unit). Unlike Hammond's postulate[60] specifying that the optimal ring-closing depolymerization catalyst has to differ from the one that serves in the chain construction, we have capitalized on the "master key" nature of DBU and postulated that this organobase should be also efficient for the depolymerization of our materials upon a thermal switch. This hypothesis was inspired from the DBU-promoted some side reactions that were observed when polycarbonates were prepared by copolymerizing **C1** with unfunctional diols (e.g. 1,4-benzenedimethanol) at 80 °C.[56] Some unexpected cyclic carbonate linkages were formed, together with the decrease of the polymer molar mass. To verify this assumption, the depolymerization of **C1P1** (containing amide linkages into the skeletal editing) is monitored by ^{1}H-NMR spectroscopy, using an internal standard, to identify and quantify the degradation products, and to determine the content of decomposed polymer (Figure 1A and Figure S17). These analyses correlate with the time evolution of the SEC of the polymer highlighting degradation profile (Figure 1B and Figure S18). At 80 °C, 20% of **C1P1** was degraded after 1 h, with a M_n that significantly dropped from 18,500 g/mol to 4,000 g/mol (Figure 1B), suggesting that chain scissions events rapidly split the polymer. After 24 h, ~70% of the polymer is disassembled with some remaining oligomers of M_n = 1,800 g/mol. Then, two main products were isolated and identified as the native N1,N4-bis(2-hydroxyethyl)terephthalamide **P1** (yield of 40%) and an elusive bicyclic compound **1** (yield 40%, white solid), consisting of a tetrasubstituted 5-membered ethylene carbonate fused to an acetyl-substituted tetrahydropyran (Figures S19-S20 and S21-S22). X-Ray Diffraction of the latter scaffold highlights the orientation of two methyl groups in an exclusive syn configuration, suggesting a stereoselective depolymerization process (Figure 1C, Figure S23 and Table S4). To make the deconstruction of **C1P1** more expeditious, the depolymerization is reproduced at higher temperature (Figure 1D and Figures S24-S25). At 100 °C, 95% of **C1P1** is depolymerized in 24 h and the remaining oligomers display a M_n of 1,400 g/mol while at 150 °C, a total polymer degradation is observed within only 3 h. After 24 h, the yield of the bicyclic compound **1** significantly increases from 40% at 80 °C to 53% at 100 °C and 83% at 150 °C, confirming the beneficial effect of the temperature on the depolymerization rate. However, increasing the temperature also provides a mixture of additional cyclic co-products identified by ^{1}H-NMR as N-acylated oxazolidinone and N-(2-hydroxyethyl)benzamide fragments. It suggests that beside **1** and **P1**, other products like 3,3'-terephthaloylbis(oxazolidin-2-one) **P1a** and N-(2-hydroxyethyl)-4-(2-oxoxazolidine-3-carbonyl)benzamide **P1b** might be concomitantly formed after complete chain unzipping (Figure S24). It has to be noted that since the ^{1}H-NMR signals fall in the same chemical shift, it is impossible to quantify the yield of each compound and the exact composition of the mixture (Figure S24). Every attempt to separate and isolate the various scaffolds were unsuccessful.

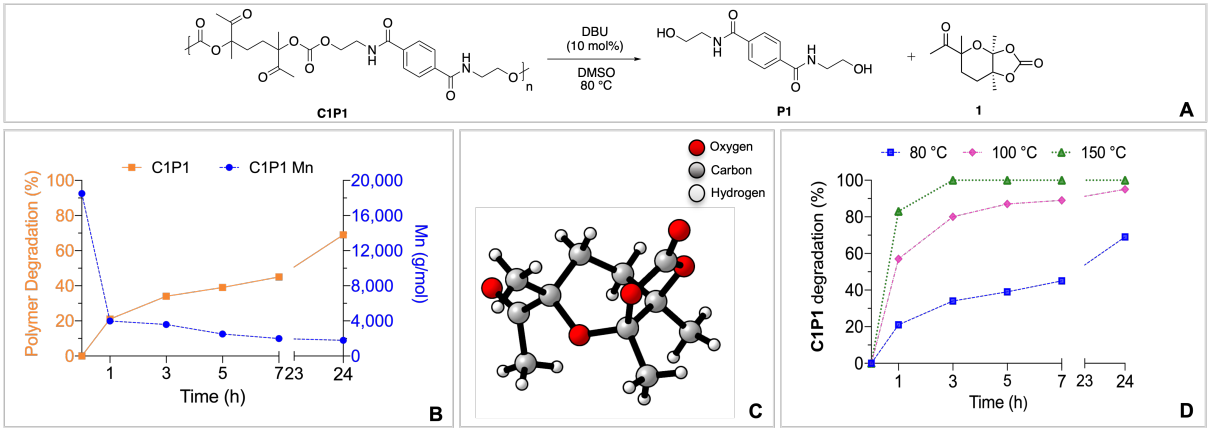

Figure 1. A) Degradation scheme for **C1P1** and main degradation products; B) time evolution of the **C1P1** M_n upon deconstruction at 80 °C; C) ORTEP representation of 5-acetyl-3a,5,7a-trimethyltetrahydro-5H-[1,3]dioxolo[4,5-b]pyran-2-oneand D) time evolution of the **C1P1** degradation at 80 °C, 100 °C and 150 °C. The reactions were in presence of DBU (10 mol% *vs* polymer repeating unit), using 1,3,5-trimethoxybenzene (TMB) as internal standard.

If the **C1P1** case validates our concept and the methodology, it furnishes a mixture of cyclic and acyclic scaffolds. This suggests that the secondary amides are not the ideal candidates to build ring-closing degradable step-growth polymers. Capitalizing on the lability of C-N linkages and the symmetry of the chemical group, we postulated that secondary ureas would provide perfect substitutes to amides and would totally decompose into oxazolidinones via a domino scenario (Scheme 3), pushing away the boundaries encountered with **C1P1**.

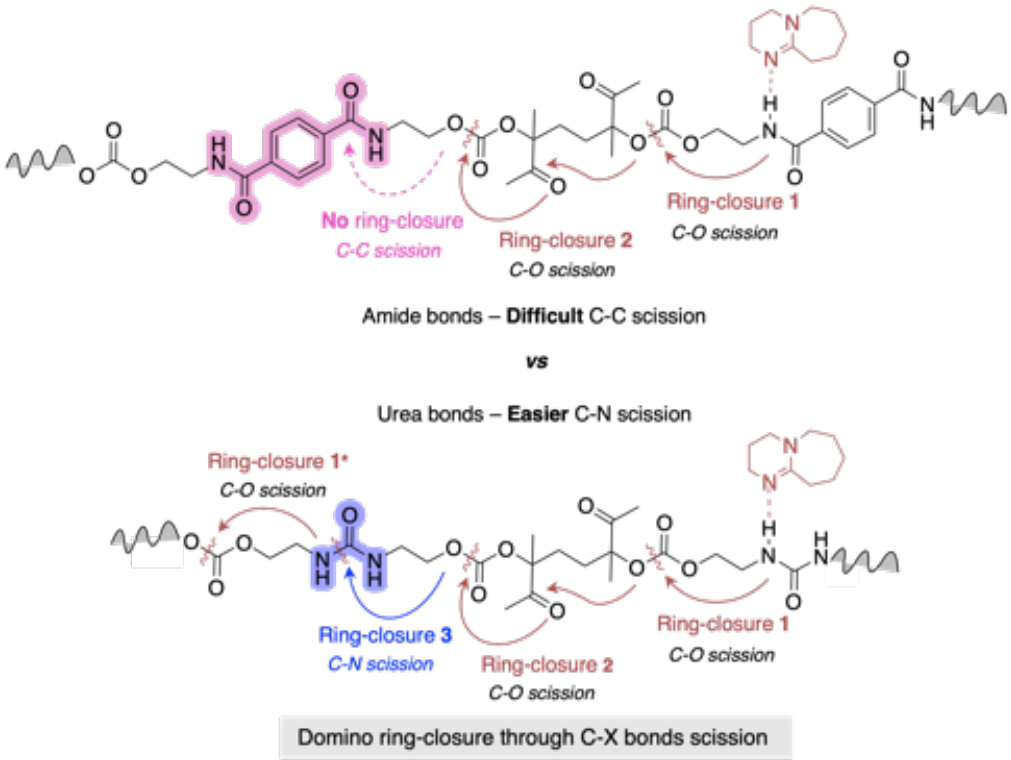

Scheme 3. Effect of the polymer structure for ring-closure depolymerization.

By applying analogous depolymerization protocol and characterization methodology as **C1P1**, 40% of the **C1P2** is already degraded after 1 h at 80 °C with a M_n that strongly decreases from 10,300 to 2,100 g/mol, and further reduces over time. After 24 h, ~93% of the polymer is deconstructed (Figure 2A-B, Figures S26-S28) furnishing the expected bicyclic compound **1** and the 5-membered 2-oxazolidinone **2** (Figures S29-S30) with respective yields of 63% and 59% (Figure 2C). In the absence of DBU, only 13% of the polymer is degraded at 80 °C after 24 h, with M_n that dropped from 9,800 to 2,900 g/mol (Figures S31-S32). This illustrates that DBU is needed for accelerating the polymer deconstruction at this temperature.

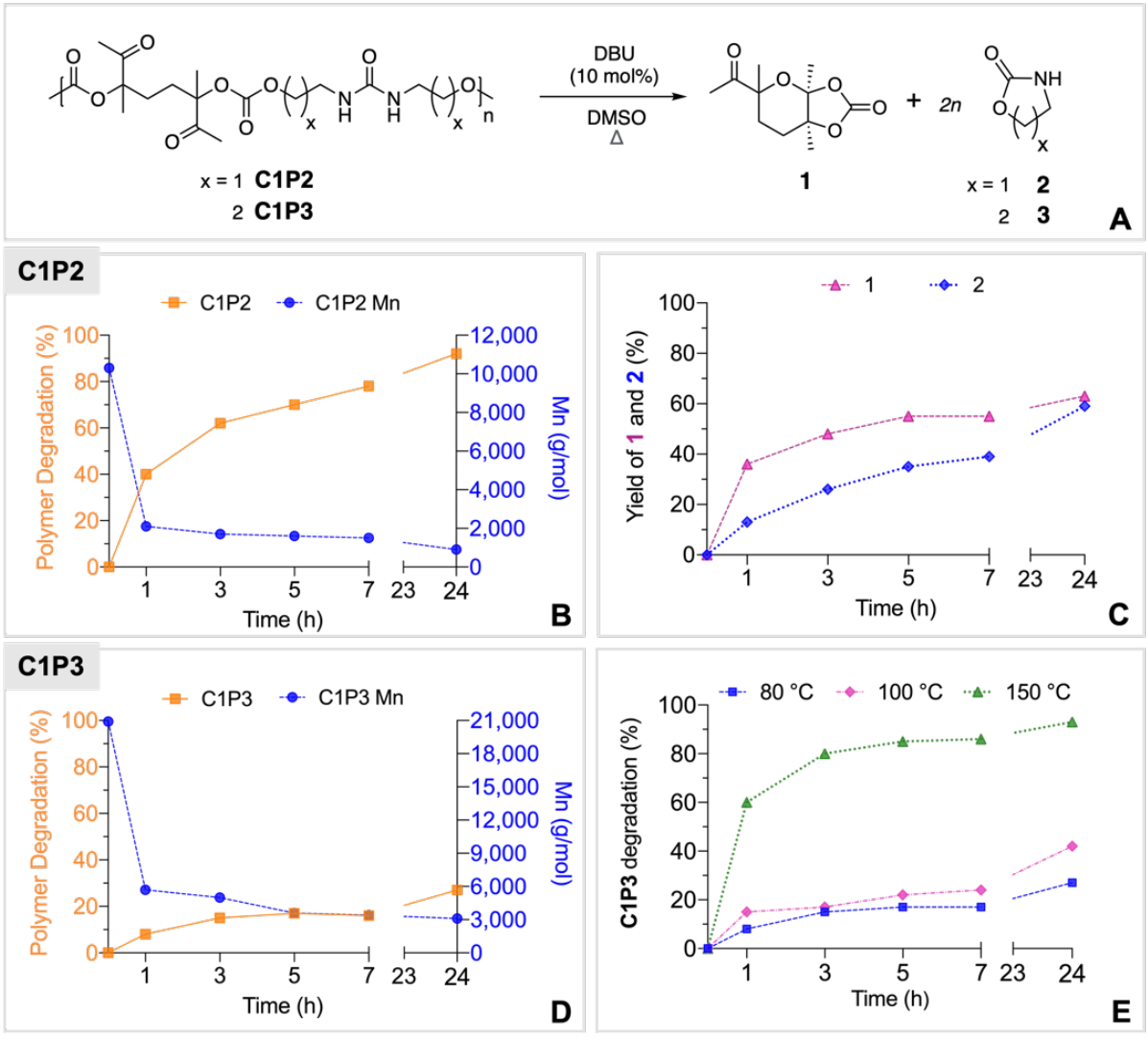

Figure 2. A) Degradation scheme for **C1P2** and **C1P3**; B) evolution of polymer degradation and M_n of **C1P2** with the reaction time at 80 °C; C) Time evolution of the **C1P2** products yields at 80 °C; D) time evolution of the **C1P3** M_n upon deconstruction at 80 °C; E) time evolution of the **C1P3** degradation at 80 °C, 100 °C and 150 °C; The reactions were conducted in presence of DBU (10 mol% *vs* polymer repeating unit), using 1,3,5-trimethoxybenzene (TMB) as internal standard.

Then, we challenged our system with **C1P3** (Figure 2A, Figure 2D and Figure S33). The presence of a propylene spacer within the polymer microstructure would affect the ring-closure

steps as the formation of the 6-membered 1,3-oxazinan-2-one 3 is kinetically less favorable than the 5-membered one **2** from **C1P2**. As expected, during the first hours at 80 °C, the significant drop of M_n from 20,900 to 3,000-5,000 g/mol (Figure 2D and Figure S34) coupled to trace formation of the bicyclic scaffold **1** and the barely detectable **3** translates a polymer fragmentation by chain scission events mainly. After 24 h, the **C1P3** degradation only reaches 27% and cyclic scaffolds **1** and **3** are produced with respective low yields of 15% and 6% (Figures S35-S36). Increasing the degradation temperature to 100 °C and 150 °C is beneficial and favors the formation of the cyclic scaffolds **1** and **3** by ring closure (Figure 2E and Figures S37-S39). The **C1P3** degradation increases from 27% at 80 °C to 42% at 100 °C, and 93% at 150 °C after 24 h of reaction (Figure 2E, Figure S37). Concomitantly, the evolution of the SEC chromatograms towards higher elution times after 24 h (Figure S38) suggests the formation of oligomers of M_n ~ 2,200 g/mol at 100 °C or a "residue" with a M_n that could not be determined (out of calibration) at 150 °C as **C1P3** was almost completely deconstructed into the six-membered cyclic carbamate **3** (35% yield) and the bicyclic carbonate **1** (81% yield) (Figure S39).

We then evaluated the degradation of the most easily degradable polymer (i.e. **C1P2**) under various conditions to illustrate the robustness of the process. Dried DMSO was initially used as solvent for our degradation studies as it is a good solvent of the polymers, and interference with water is avoided. However, in practical use, solvents always contain some water. To fit at best realistic scenarios, some water (5 wt%) is added to the reaction medium carried out at 80 °C in the presence of DBU. Similarly to the reaction performed under anhydrous conditions, **C1P2** was almost fully degraded (97% *vs* 93%) and produced the biscyclic compound **1** in similar yield (64% *vs* 63%). The oxazolidinone **2** was also obtained, however in lower yield (25.3% *vs* 59%), together with some hydrolyzed product, monomer **P2** (20.7% *vs* 0%) (Figure S40) **P2** is the starting monomer that may be reused in a closed-loop scenario for preparing **C1P2**. The degradation is thus operative under non anhydrous conditions, however is less selective for product **2**.

If removing a high boiling point solvent (here, DMSO) is not straightforward and renders the practicability of the recycling process difficult, the degradation can also be carried out in low boiling points solvents (e.g. THF) that are easy to remove by distillation and to recycle. Although **C1P2** is insoluble in THF, 90% of the polymer is deconstructed at 80 °C after 24 h in the presence of DBU. The selectivity is however affected with a yield in **1** of 51% (*vs* 63% in DMSO) and 10% in **2** (*vs* 59% in DMSO), and more unidentified side products (Figure S41).

Lastly, we decided to evaluate the depolymerization of both **C1P1** and **C1P2** under neat (without solvent) and catalyst-free conditions. After 2 h at 150 °C, **C1P1** is fully degraded into product **1** (with a yield of 63 %) and a mixture of **P1**, **P1a** and **P1b** (Figure S42), however the composition of this mixture is impossible to assess as previously discussed. Under these

operating conditions, **C1P2** totally depolymerized as well, leading to products **1** and **2** with a yield of 76 % and 67%, respectively (Figure S43). At this temperature, the depolymerizations are thus fast under attractive solvent- and catalyst-free conditions. These experiments suggest that the low degradation temperature $T_{deg10\%}$ noted for the polymers (Scheme 2) is due to their spontaneous depolymerization at this temperature. When the polymer degradation has to be realized at rather low temperature (e.g. 80°C), the use of the catalyst (DBU) is however absolutely needed.

Mechanistic insights of the poly(carbonate-urea) formation and depolymerization. To shed light on the depolymerization mechanism (Scheme 4) and their energetics, DFT calculations have been realized at the M062X/ 6–311G(d,p) level of theory and correlated with in-depth NMR characterizations and titrations. To alleviate the computational simulations and facilitate the structural elucidation of the transition states, intermediates and final products formed during the depolymerization, all calculations have been performed on model fragments of **C1P2** mimicking the monomers, the repetitive units of the polymer and/or the chain ends/intermediates formed upon chain scission and ring closure. A detailed discussion of the mechanisms involved for each of the DBU-catalyzed model reactions, their energy profile (in terms of Gibbs free energy) as well as schematic structures of the reactants, transition states, reaction intermediates and products are given in Supplementary Information. The **C1P2** formation follows a three-step mechanism from which the tautomerization of the enol - created upon ring-opening of the exovinylidene carbonate by the alcohol moiety of **P2** - into the corresponding ketone represents the rate-determining step with an energetic penalty of 26.6 kcal·mol^{-1} (Figure S44). This value is only 1.5 kcal·mol^{-1} lower in energy than the chain scission event (Scheme 4, step 1), underlying the facile fragmentation of the polymer correlating with the rapid experimental decrease of the **C1P2** molar mass upon deconstruction. This is reflected in the barrier energy of the intramolecular nucleophilic addition of the urea NH onto the adjacent carbonate linkage (ΔG = 28.1 kcal·mol^{-1}) (Scheme 4, step 1, and Figure S45) that furnishes two polymeric fragments, one terminated by a *N*-carbamoyl-oxazolidinone, the second by a hydroxyketone. Both the DFT modelling and NMR titration confirm the role of DBU in the activation of the NH groups to make them sufficiently reactive (Figures S45-S46 and related discussion). The suggested chain termini created upon scission were further detected by ^{1}H- and ^{1}H-^{1}H-COSY NMR spectroscopy of the crude reaction mixture (Figures S47-S49), with the two correlated methylene protons at δ= 3.89 ppm and δ= 4.37 ppm (triplets) of the five-membered *N*-acylated moiety and the methyl signal at δ= 2.19 ppm (singlet) of the terminal hydroxyketone. This latest, which terminal OH moiety is also activated by the organobase, initiates a double cascade cyclization furnishing the bicyclic compound **1** (Figures S50 and S51). This reaction proceeds via the creation of a 6-membered cyclic hemiacetal-type

intermediate formed by the attack of the activated tertiary -OH moiety onto a neighboring ketone of the polymer skeleton that is further fused into an ethylene carbonate via a second ring-closure reaction with the adjacent carbonate linkage (Scheme 4, step 2). This double cyclization is accompanied by the concomitant release of a new polymer fragment end-capped with a primary alcohol. This correlates with the presence of two NMR signals at δ= 3.05 ppm and 3.35 ppm analogue to the signals of the 2-hydroxyethyl spacer in **P2** (Figures S47-S49). The reaction is low in energy, illustrating the ease of formation of the bicyclic structure **1**, with a rate determining step associated to an energy barrier of only 8.6 kcal·mol^{-1} corresponding to the release of a hydroxyl-terminated PC. Finally, the polymer chain deconstruction delivers two 2-oxazolidinones **2** in a domino fashion (Figure S52). The back-biting reaction of the primary alcohol (activated by DBU) onto the carbonyl moiety of the urea linkage creates a first cyclic carbamate scaffold (Scheme 4, step 3). The vicinal off-cycle nitrogen atom is then involved in a second 2-oxazolidinone formation by a rather facile cyclization with the adjacent carbonate unit of the polymer skeleton (Scheme 4, step 3). Concomitantly, cyclization is accompanied by the release of a hydroxyketone end-capped chain that re-enters the ring-closing depolymerization loop. Due to the higher bond dissociation energy of the C-N linkages compared to the C-O ones, the oxazolidinone rings formation faces the most elevated energy barrier of 33.8 kcal·mol^{-1} and represents the rate limiting step of the overall ring-closing depolymerization process. Such a difficulty is reflected by the experimental yields in **1** and **2** that slightly deviate from the expected theoretical value of 1/2. Ultimately, the *N*-carbamoyl-oxazolidinone chain terminus derived from the initial chain scission event is decomposed to release a last 2-oxazolidinone ring, further ensuring the total polymer deconstruction.

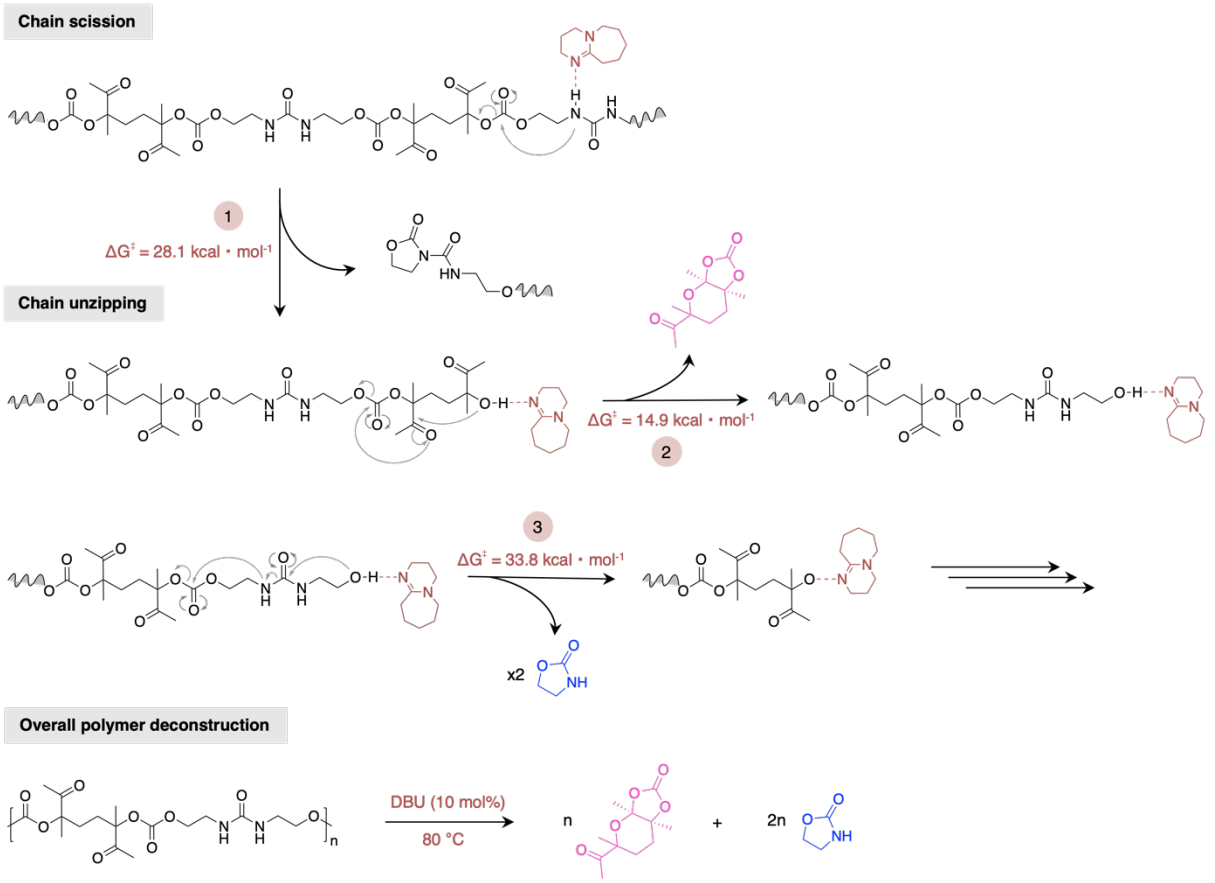

Scheme 4. General ring-closing depolymerization mechanism of **C1P2** initiated by chain scission and unzipping events.

Selective depolymerization of plastic mixtures. The (de)polymerization chemistry we have engineered offers the opportunity to program the selective degradation of mixed plastics of different nature.[16,22] To validate this rarely addressed concept, **C1P2** is mixed with two polyesters selected for their cleavable C-O bonds, i.e. either polycaprolactone (PCL), a ROP polymer prone to ring-closing depolymerization into macrocycles, solvolysis or biodegradation in living environment, or waste polyethylene terephthalate (PET) from water bottles, a polycondensation polymer degradable by solvolysis.[11,59,61,62] Both **C1P2**/PCL and **C1P2**/PET mixed polymer formulations are then subjected to depolymerization applying the previous protocol for deconstructing pure **C1P2** (10 mol% of DBU vs polymer repeating unit, 80 °C, in DMSO) (Figure 3). With the **C1P2**/PCL mix, 88% of **C1P2** was degraded in 24 h, furnishing **1** and **2** with respective yields of 85% and 63%, while 85% of the PCL is recovered with no visible sign of degradation (Figure 3 and Figures S53-S56). The missing 15% were lost during the purification procedure (combined dialysis and precipitation). Remarkably, PCL does not interfere in the depolymerization of **C1P2**, while the multiple intermediates with reactive -OH and -NH_2 termini created upon **C1P2** degradation do not induce transesterification or amidation of PCL.

Extension to the **C1P2**/PET case provides the same trend under same conditions. 95% of **C1P2** was deconstructed yielding **1** and **2** at 89% and 83% respectively, without any degradation of PET that is quantitatively recovered after the separation and purification process (Figure 3, and Figures S57).

Despite unknown, the building block **1** is obtained in a fully diastereoselective manner and possesses various handles for post-functionalization. For instance, its hydroxylated tetrahydropyran core closely resembles natural products such as merulinol A.[63] Moreover, recent patents introduced the use of such type of cyclic compound with a hemiacetal cyclic carbonate template as novel electrolytes for Li-ion batteries.[64–66] Oxazolidinone **2** is of interest for drugs fabrication.[67–74]

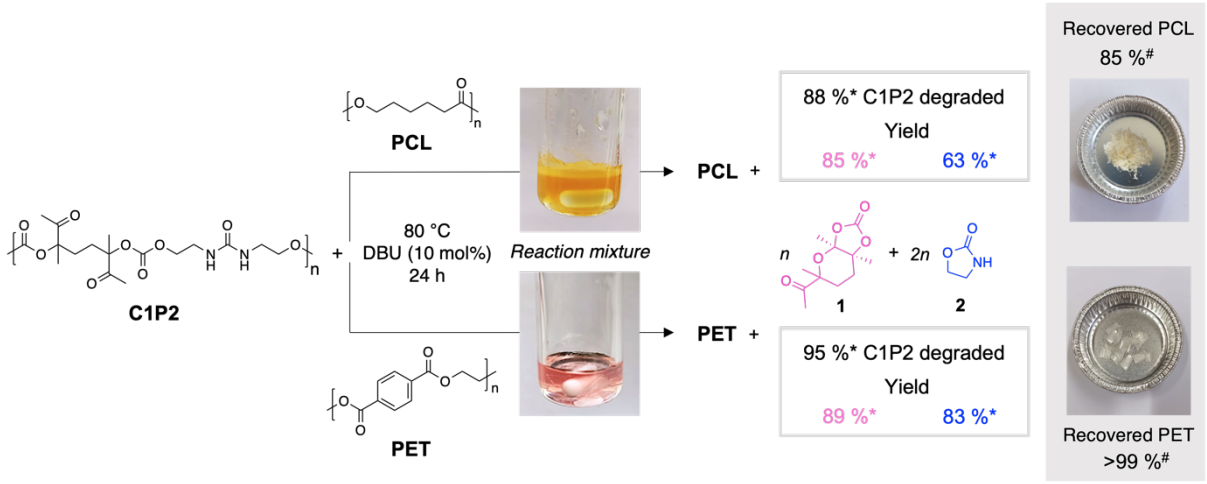

Figure 3. Selective depolymerization of **C1P2** in the presence of PCL pellets Capa® 6800 or PET flakes from water bottles.

*Determined by ^{1}H-NMR spectroscopy on the crude product after 24 h.

#Determined by weight after purification.

Reaction's conditions: 0.25 g of C1P2, 1.25 mL of DMSO, DBU (10 mol% compared to repeating unit of polymer) and 1,3,5-Trimethoxybenzene (TMB). The reactions were realized at 80 °C.

Conclusion

Herein, we have described how step-growth plastics can be edited to be easily depolymerized by cascade ring-closing approaches, offering them an attractive end-of-life scenario. Regioregular poly(carbonate-amide) and poly(carbonate-urea)s were prepared by the DBU-catalyzed step-growth copolymerization of bis-exovinylene cyclic carbonates (made from CO_2) with diols bearing unprotected secondary amide or urea linkages (made from upcycled commodity plastics) at room temperature. Upon activation by thermal switch (from 25 to 80 °C) in the presence of DBU, these groups initiated the polymer disassembly via a chain scission followed by domino ring-closing events in DMSO. The degradation of poly(carbonate-amide) provided the native diol **P1** and a hemiacetal cyclic carbonate **1**. The depolymerization was

slow at 80 °C, whereas fast and complete in few hours at 150 °C. Substituting amide by urea was found beneficial, with the quasi-total depolymerization into high yields cyclic molecules, i.e. product **1** and the oxazolidinones **2** or **3**, even at 80 °C. The process is tolerant to water and can be performed in low boiling point solvents that are easier to recycle (e.g. THF). Interestingly, fast and complete depolymerizations were achieved in solvent- and catalyst-free conditions at 150 °C. Lastly, the poly(carbonate-urea) mixed to a common polyester (PCL or PET) was totally and selectively depolymerized into **1** and **2**, leaving intact the polyesters, further suppressing the plastics sorting prior recycling. Computational modelling performed on model compounds aligns with the experimental observations, and supports that the polymerization occurred without competitive depolymerization, and that the polymer deconstruction proceeded by chain scission first, followed by unzipping via an activated chain-end mechanism.

As the polymers present a low degradation temperature (160-170 °C), they can be processed and used below this temperature. However, many products fulfil these requirements, e.g. many coatings and foams. Their potential exploitation might thus be as polyols in polyurethane formulations in order to impart to PU materials attractive degradation abilities.

Experimental section

Materials

4.4'-(ethane-1.2-diyl)bis(4-methyl-5-methylene-1.3-dioxolan-2-one (C1), tetrabutylammonium phenolate and the TDB:MSA salt were synthesized as reported elsewhere by our groups.[1,2] 1,8-diazabicyclo[5.4.0]undec-7-ene (DBU, 99%) was purchased from TCI. 1,2-Ethanolamine, 1,3-Propanolamine were purchased from Aldrich. Polycaprolactone Capa 6800 was supplied by Perstop. All the reactions were performed under inert atmosphere of N_2 and DMSO was dried under molecular sieves 3Å prior used. Dialyses were carried out with a Spectra/Por dialysis membrane (pretreated RC tubing 1 kDa).

Characterization methods

Nuclear magnetic resonance (NMR) spectroscopy. NMR analyses were performed on Bruker 400 MHz spectrometers in DMSO-d_6 at 25 °C in the Fourier transform mode. 16 or 64 scans for a ^{1}H spectra and 512 or 2048 scans for ^{13}C spectra were recorded.

Size exclusion chromatography (SEC). Number-average and weight-average molecular weights and molecular weight dispersity (M_w/M_n) values of polymers were determined by size exclusion chromatography (SEC) in i) dimethylformamide (DMF) containing LiBr (0.025 M) at 55 °C (flow rate: 1 mL/min) with a Waters chromatograph equipped with three columns (Waters Styragel PSS gram 1000 Å (×2), 30 Å), dual λ absorbance detector (Waters 2487) and a

refractive index detector (Waters 2414) or ii) in THF at 45 °C at a flow rate of 1 mL/min with a Viscotek 305 TDA liquid chromatograph equipped with two PSS SDV linear M columns calibrated with poly(methylmethacrylate) standards and a refractive index detector.

High Resolution Mass Spectrometry (HRMS). High-resolution mass spectra in positive mode were recorded using a 6520 series quadrupole time-of-flight (Q-TOF) mass spectrometer (Agilent) fitted with a multimode ion source.

X-Ray Diffraction (XRD). Diffraction data were recorded on an MAR345 image plate, using Mo Kα radiation (λ= 0.71073 Å) generated by an Incoatec microfocus source (Montel optics). Data integration and reduction was performed by CrysAlisPRO Software System[3,4], Version 1.171.37.35. Rigaku Oxford Diffraction and the implemented absorption correction was applied. The structure was solved by SHELXT and refined by least-squares against F2 by shelxt2018/3. All non-hydrogen atoms were refined anisotropically and hydrogens were placed at calculated positions and refined in riding mode with temperature factors set at 1.2 Ueq of the parent atoms (1.5 for methyl groups). The methylcarbonyl fragment was found to be disordered and refined in two discrete parts in a 55/45 ratio.

Thermogravimetric analysis (TGA) in the polymers were performed on a TGA2 instrument from Mettler Toledo. Around 5 mg of sample was heated at 20 °C/min until 600 °C under N_2 atmosphere (20 mL/min).

Differential scanning calorimetry (DSC) analyses were performed on a DSC 250 differential calorimeter (TA Instruments). All the experiments were performed under ultrapure nitrogen flow. Samples of 2–5 mg were used and placed in sealed aluminum pans. The samples were first heated at a rate of 10 °C min^{-1} from 25 °C to 100 °C. Then, after an isotherm of 5 min at 100 °C, the samples were cooled down to -80 °C at a rate of 10 °C min^{-1}, followed by an isotherm of 2 min at -80 °C. Subsequently, the samples were heated to 100 °C at 10 °C min^{-1}. The last heating cycle was used for the determination of the T_g.

Associated content

Accession Codes

CCDC 2129745 contains the supplementary crystallographic data for this paper. These data can be obtained free of charge from The Cambridge Crystallographic Data Centre via www.ccdc.cam.ac.uk/structures.

References

(1) Garcia, J. M.; Robertson, M. L. The Future of Plastics Recycling. *Science (1979)* 2017, *358*, 870–872. https://doi.org/10.1126/science.aaq0324.

(2) Zheng, J.; Suh, S. Strategies to Reduce the Global Carbon Footprint of Plastics. *Nature Climate Change* 2019, *9*, 374–378. https://doi.org/10.1038/s41558-019-0459-z.

(3) Saxon, D. J.; Gormong, E. A.; Shah, V. M.; Reineke, T. M. Rapid Synthesis of Chemically Recyclable Polycarbonates from Renewable Feedstocks. *ACS Macro Letters* 2021, *10*, 98–103. https://doi.org/10.1021/acsmacrolett.0c00747.

(4) Fagnani, D. E.; Tami, J. L.; Copley, G.; Clemons, M. N.; Getzler, Y. D. Y. L.; McNeil, A. J. 100th Anniversary of Macromolecular Science Viewpoint: Redefining Sustainable Polymers. *ACS Macro Letters* 2021, *10*, 41–53. https://doi.org/10.1021/acsmacrolett.0c00789.

(5) Roy, P. S.; Garnier, G.; Allais, F.; Saito, K. Strategic Approach Towards Plastic Waste Valorization: Challenges and Promising Chemical Upcycling Possibilities. *ChemSusChem* 2021, *14*, 1–22. https://doi.org/10.1002/cssc.202100904.

(6) Zhao, X.; Boruah, B.; Chin, K. F.; Đokić, M.; Modak, J. M.; Soo, H. S. Upcycling to Sustainably Reuse Plastics. *Advanced Materials* 2021, *2100843*, 2100843. https://doi.org/10.1002/adma.202100843.

(7) Hou, Q.; Zhen, M.; Qian, H.; Nie, Y.; Bai, X.; Xia, T.; Laiq Ur Rehman, M.; Li, Q.; Ju, M. Upcycling and Catalytic Degradation of Plastic Wastes. *Cell Reports Physical Science* 2021, *2*, 100514. https://doi.org/10.1016/j.xcrp.2021.100514.

(8) Worch, J. C.; Dove, A. P. 100th Anniversary of Macromolecular Science Viewpoint: Toward Catalytic Chemical Recycling of Waste (and Future) Plastics. *ACS Macro Letters* 2020, *9*, 1494–1506. https://doi.org/10.1021/acsmacrolett.0c00582.

(9) Jehanno, C.; Pérez-Madrigal, M. M.; Demarteau, J.; Sardon, H.; Dove, A. P. Organocatalysis for Depolymerisation. *Polymer Chemistry* 2019, *10*, 172–186. https://doi.org/10.1039/c8py01284a.

(10) Ellis, L. D.; Rorrer, N. A.; Sullivan, K. P.; Otto, M.; McGeehan, J. E.; Román-Leshkov, Y.; Wierckx, N.; Beckham, G. T. Chemical and Biological Catalysis for Plastics Recycling and Upcycling. *Nature Catalysis* 2021, *4*, 539–556. https://doi.org/10.1038/s41929-021-00648-4.

(11) Coates, G. W.; Getzler, Y. D. Y. L. Chemical Recycling to Monomer for an Ideal, Circular Polymer Economy. *Nature Reviews Materials* 2020, *5*, 501–516. https://doi.org/10.1038/s41578-020-0190-4.

(12) Chen, H.; Wan, K.; Zhang, Y.; Wang, Y. Waste to Wealth: Chemical Recycling and Chemical Upcycling of Waste Plastics for a Great Future. *ChemSusChem* 2021, *14*, 4123–4136. https://doi.org/10.1002/cssc.202100652.

(13) Shieh, P.; Zhang, W.; Husted, K. E. L.; Kristufek, S. L.; Xiong, B.; Lundberg, D. J.; Lem, J.; Veysset, D.; Sun, Y.; Nelson, K. A.; Plata, D. L.; Johnson, J. A. Cleavable Comonomers Enable Degradable, Recyclable Thermoset Plastics. *Nature* 2020, *583*, 542–547. https://doi.org/10.1038/s41586-020-2495-2.

(14) Shieh, P.; Nguyen, H. V. T.; Johnson, J. A. Tailored Silyl Ether Monomers Enable Backbone-Degradable Polynorbornene-Based Linear, Bottlebrush and Star Copolymers through ROMP. *Nature Chemistry* 2019, *11*, 1124–1132. https://doi.org/10.1038/s41557-019-0352-4.

(15) Zhu, J. B.; Watson, E. M.; Tang, J.; Chen, E. Y. X. A Synthetic Polymer System with Repeatable Chemical Recyclability. *Science (1979)* 2018, *360*, 398–403. https://doi.org/10.1126/science.aar5498.

(16) Christensen, P. R.; Scheuermann, A. M.; Loeffler, K. E.; Helms, B. A. Closed-Loop Recycling of Plastics Enabled by Dynamic Covalent Diketoenamine Bonds. *Nature Chemistry* 2019, *11*, 442–448. https://doi.org/10.1038/s41557-019-0249-2.

(17) Vora, N.; Christensen, P. R.; Demarteau, J.; Baral, N. R.; Keasling, J. D.; Helms, B. A.; Scown, C. D. Leveling the Cost and Carbon Footprint of Circular Polymers That Are Chemically Recycled to Monomer. *Science Advances* 2021, *7*, 1–12. https://doi.org/10.1126/SCIADV.ABF0187.

(18) Vollmer, I.; Jenks, M. J. F.; Roelands, M. C. P.; White, R. J.; van Harmelen, T.; de Wild, P.; van der Laan, G. P.; Meirer, F.; Keurentjes, J. T. F.; Weckhuysen, B. M. Beyond Mechanical Recycling: Giving New Life to Plastic Waste. *Angewandte Chemie - International Edition* 2020, *59*, 15402–15423. https://doi.org/10.1002/anie.201915651.

(19) Rahimi, A. R.; Garciá, J. M. Chemical Recycling of Waste Plastics for New Materials Production. *Nature Reviews Chemistry* 2017, *1*, 1–11. https://doi.org/10.1038/s41570-017-0046.

(20) Sardon, H.; Dove, A. P. Plastics Recycling with a Difference: A Novel Plastic with Useful Properties Can Easily Be Recycled Again and Again. *Science (1979)* 2018, *360*, 380–381. https://doi.org/10.1126/science.aat4997.

(21) Hong, M.; Chen, E. Y. X. Chemically Recyclable Polymers: A Circular Economy Approach to Sustainability. *Green Chemistry* 2017, *19*, 3692–3706. https://doi.org/10.1039/c7gc01496a.

(22) Jehanno, C.; Demarteau, J.; Mantione, D.; Arno, M. C.; Ruipérez, F.; Hedrick, J. L.; Dove, A. P.; Sardon, H. Selective Chemical Upcycling of Mixed Plastics Guided by a Thermally Stable Organocatalyst. *Angewandte Chemie - International Edition* 2021, *60*, 6710–6717. https://doi.org/10.1002/anie.202014860.

(23) Shi, C.; Li, Z. C.; Caporaso, L.; Cavallo, L.; Falivene, L.; Chen, E. Y. X. Hybrid Monomer Design for Unifying Conflicting Polymerizability, Recyclability, and Performance Properties. *Chem* 2021, *7*, 670–685. https://doi.org/10.1016/j.chempr.2021.02.003.

(24) Xiong, W.; Chang, W.; Shi, D.; Yang, L.; Tian, Z.; Wang, H.; Zhang, Z.; Zhou, X.; Chen, E. Q.; Lu, H. Geminal Dimethyl Substitution Enables Controlled Polymerization of Penicillamine-Derived β-Thiolactones and Reversed Depolymerization. *Chem* 2020, *6*, 1831–1843. https://doi.org/10.1016/j.chempr.2020.06.003.

(25) Lu, X. B.; Liu, Y.; Zhou, H. Learning Nature: Recyclable Monomers and Polymers. *Chemistry - A European Journal* 2018, *24*, 11255–11266. https://doi.org/10.1002/chem.201704461.

(26) Darensbourg, D. J.; Wei, S. H.; Yeung, A. D.; Ellis, W. C. An Efficient Method of Depolymerization of Poly(Cyclopentene Carbonate) to Its Comonomers: Cyclopentene Oxide and Carbon Dioxide. *Macromolecules* 2013, *46*, 5850–5855. https://doi.org/10.1021/ma401286x.

(27) Deacy, A. C.; Gregory, G. L.; Sulley, G. S.; Chen, T. T. D.; Williams, C. K. Sequence Control from Mixtures: Switchable Polymerization Catalysis and Future Materials Applications. *Journal of the American Chemical Society* 2021, *143*, 10021–10040. https://doi.org/10.1021/jacs.1c03250.

(28) Grignard, B.; Gennen, S.; Jérôme, C.; Kleij, A. W.; Detrembleur, C. Advances in the Use of CO2 as a Renewable Feedstock for the Synthesis of Polymers. *Chemical Society Reviews* 2019, *48*, 4466–4514. https://doi.org/10.1039/c9cs00047j.

(29) Yuan, J.; Xiong, W.; Zhou, X.; Zhang, Y.; Shi, D.; Li, Z.; Lu, H. 4-Hydroxyproline-Derived Sustainable Polythioesters: Controlled Ring-Opening Polymerization, Complete Recyclability, and Facile Functionalization. *Journal of the American Chemical Society* 2019, *141*, 4928–4935. https://doi.org/10.1021/jacs.9b00031.

(30) Xu, G.; Wang, Q. Chemically Recyclable Polymer Materials: Polymerization and Depolymerization Cycles. *Green Chemistry* 2022, *24*, 2321–2346. https://doi.org/10.1039/d1gc03901f.

(31) Endo, T.; Kakimoto, K.; Ochiai, B.; Nagai, D. Synthesis and Chemical Recycling of a Polycarbonate Obtained by Anionic Ring-Opening Polymerization of a Bifunctional Cyclic Carbonate. *Macromolecules* 2005, *38*, 8177–8182. https://doi.org/10.1021/ma050791v.

(32) Yu, Y.; Fang, L. M.; Liu, Y.; Lu, X. B. Chemical Synthesis of CO2-Based Polymers with Enhanced Thermal Stability and Unexpected Recyclability from Biosourced Monomers. *ACS Catalysis* 2021, *11*, 8349–8357. https://doi.org/10.1021/acscatal.1c01376.

(33) Carrodeguas, L. P.; Chen, T. T. D.; Gregory, G. L.; Sulley, G. S.; Williams, C. K. High Elasticity, Chemically Recyclable, Thermoplastics from Bio-Based Monomers: Carbon Dioxide, Limonene Oxide and ϵ-Decalactone. *Green Chemistry* 2020, *22*, 8298–8307. https://doi.org/10.1039/d0gc02295k.

(34) Li, C.; Sablong, R. J.; van Benthem, R. A. T. M.; Koning, C. E. Unique Base-Initiated Depolymerization of Limonene-Derived Polycarbonates. *ACS Macro Letters* 2017, *6*, 684–688. https://doi.org/10.1021/acsmacrolett.7b00310.

(35) Fahnhorst, G. W.; Hoye, T. R. A Carbomethoxylated Polyvalerolactone from Malic Acid: Synthesis and Divergent Chemical Recycling. *ACS Macro Letters* 2018, *7*, 143–147. https://doi.org/10.1021/acsmacrolett.7b00889.

(36) Kaitz, J. A.; Lee, O. P.; Moore, J. S. Depolymerizable Polymers: Preparation, Applications, and Future Outlook. *MRS Communications* 2015, *5*, 191–204. https://doi.org/10.1557/mrc.2015.28.

(37) Zhang, J.; Wang, L.; Liu, S.; Li, Z. Synthesis of Diverse Polycarbonates by Organocatalytic Copolymerization of CO2 and Epoxides: From High Pressure and Temperature to Ambient Conditions. *Angewandte Chemie - International Edition* 2021, e202111197. https://doi.org/10.1002/anie.202111197.

(38) Olsén, P.; Odelius, K.; Albertsson, A. C. Ring-Closing Depolymerization: A Powerful Tool for Synthesizing the Allyloxy-Functionalized Six-Membered Aliphatic Carbonate Monomer 2-Allyloxymethyl-2-Ethyltrimethylene Carbonate. *Macromolecules* 2014, *47*, 6189–6195. https://doi.org/10.1021/ma5012304.

(39) Honda, M.; Tamura, M.; Nakao, K.; Suzuki, K.; Nakagawa, Y.; Tomishige, K. Direct Cyclic Carbonate Synthesis from CO2 and Diol over Carboxylation/Hydration Cascade Catalyst of CeO2 with 2-Cyanopyridine. *ACS Catalysis* 2014, *4*, 1893–1896. https://doi.org/10.1021/cs500301d.

(40) Kindermann, N.; Jose, T.; Kleij, A. W. Synthesis of Carbonates from Alcohols and CO2. *Topics in Current Chemistry* 2017, *375*, 1–28. https://doi.org/10.1007/s41061-016-0101-8.

(41) Huang, J.; Olsén, P.; Svensson Grape, E.; Inge, A. K.; Odelius, K. Simple Approach to Macrocyclic Carbonates with Fast Polymerization Rates and Their Polymer-to-Monomer Regeneration. *Macromolecules* 2022, *55*, 608–614. https://doi.org/10.1021/acs.macromol.1c02225.

(42) Baker, M. S.; Kim, H.; Olah, M. G.; Lewis, G. G.; Phillips, S. T. Depolymerizable Poly(Benzyl Ether)-Based Materials for Selective Room Temperature Recycling. *Green Chemistry* 2015, *17*, 4541–4545. https://doi.org/10.1039/c5gc01090j.

(43) Mejia, J. S.; Gillies, E. R. Triggered Degradation of Poly(Ester Amide)s via Cyclization of Pendant Functional Groups of Amino Acid Monomers. *Polymer Chemistry* 2013, *4*, 1969–1982. https://doi.org/10.1039/c3py21094d.

(44) Dahlhauser, S. D.; Escamilla, P. R.; Vandewalle, A. N.; York, J. T.; Rapagnani, R. M.; Shei, J. S.; Glass, S. A.; Coronado, J. N.; Moor, S. R.; Saunders, D. P.; Anslyn, E. v. Sequencing of Sequence-Defined Oligourethanes via Controlled Self-Immolation. *Journal of the American Chemical Society* 2020, *142*, 2744–2749. https://doi.org/10.1021/jacs.9b12818.

(45) Yardley, R. E.; Kenaree, A. R.; Gillies, E. R. Triggering Depolymerization: Progress and Opportunities for Self-Immolative Polymers. *Macromolecules* 2019, *52*, 6342–6360. https://doi.org/10.1021/acs.macromol.9b00965.

(46) Sagi, A.; Weinstain, R.; Karton, N.; Shabat, D. Self-Immolative Polymers. *Journal of the American Chemical Society* 2008, *8*, 5434–5435.

(47) Sirianni, Q. E. A.; Gillies, E. R. The Architectural Evolution of Self-Immolative Polymers. *Polymer* 2020, *202*, 122638. https://doi.org/10.1016/j.polymer.2020.122638.

(48) Kim, H.; Brooks, A. D.; Dilauro, A. M.; Phillips, S. T. Poly(Carboxypyrrole)s That Depolymerize from Head to Tail in the Solid State in Response to Specific Applied Signals. *Journal of the American Chemical Society* 2020, *142*, 9447–9452. https://doi.org/10.1021/jacs.0c02774.

(49) Peterson, G. I.; Larsen, M. B.; Boydston, A. J. Controlled Depolymerization: Stimuli-Responsive Self-Immolative Polymers. *Macromolecules* 2012, *45*, 7317–7328. https://doi.org/10.1021/ma300817v.

(50) Pal, S.; Sommerfeldt, A.; Davidsen, M. B.; Hinge, M.; Pedersen, S. U.; Daasbjerg, K. Synthesis and Closed-Loop Recycling of Self-Immolative Poly(Dithiothreitol). *Macromolecules* 2020, *53*, 4685–4691. https://doi.org/10.1021/acs.macromol.0c00861.

(51) DeWit, M. A.; Gillies, E. R. A Cascade Biodegradable Polymer Based on Alternating Cyclization and Elimination Reactions. *Journal of the American Chemical Society* 2009, *131*, 18327–18334. https://doi.org/10.1021/ja905343x.

(52) Addy, P. S.; Shivrayan, M.; Cencer, M.; Zhuang, J.; Moore, J. S.; Thayumanavan, S. Polymer with Competing Depolymerization Pathways: Chain Unzipping versus Chain Scission. *ACS Macro Letters* 2020, *9*, 855–859. https://doi.org/10.1021/acsmacrolett.0c00250.

(53) Dahlhauser, S. D.; Moor, S. R.; Vera, M. S.; York, J. T.; Ngo, P.; Boley, A. J.; Coronado, J. N.; Simpson, Z. B.; Anslyn, E. v. Efficient Molecular Encoding in Multifunctional Self-Immolative Urethanes. *Cell Reports Physical Science* 2021, *4*, 100393. https://doi.org/10.1016/j.xcrp.2021.100393.

(54) Maschmeyer, P. G.; Liang, X.; Hung, A.; Ahmadzai, O.; Kenny, A. L.; Luong, Y. C.; Forder, T. N.; Zeng, H.; Gillies, E. R.; Roberts, D. A. Post-Polymerization 'Click' End-Capping of Polyglyoxylate Self-Immolative Polymers. *Polymer Chemistry* 2021, *12*, 6824–6831. https://doi.org/10.1039/d1py01169c.

(55) Addy, P. S.; Shivrayan, M.; Cencer, M.; Zhuang, J.; Moore, S.; Thayumanavan, S. Polymer with Competing Depolymerization Pathways: Chain Unzipping versus Chain Scission. *ACS Macro Letters* 2020, *9*, 855–859. https://doi.org/10.1021/acsmacrolett.0c00250.

(56) Siragusa, F.; van den Broeck, E.; Ocando, C.; Müller, A. J.; de Smet, G.; Maes, B. U. W.; de Winter, J.; van Speybroeck, V.; Grignard, B.; Detrembleur, C. Access to Biorenewable and CO2-Based Polycarbonates from Exovinylene Cyclic Carbonates. *ACS Sustainable Chemistry and Engineering* 2021, *9*, 1714–1728. https://doi.org/10.1021/acssuschemeng.0c07683.

(57) Gennen, S.; Grignard, B.; Tassaing, T.; Jérôme, C.; Detrembleur, C. CO2 -Sourced α-Alkylidene Cyclic Carbonates: A Step Forward in the Quest for Functional Regioregular Poly(Urethane)s and Poly(Carbonate)s. *Angewandte Chemie International Edition* 2017, *56*, 10394–10398. https://doi.org/10.1002/anie.201704467.

(58) Ngassam Tounzoua, C.; Grignard, B.; Detrembleur, C. Exovinylene Cyclic Carbonates: Multifaceted CO2-Based Building Blocks for Modern Chemistry and Polymer Science. *Angewandte Chemie International Edition* 2022, e202116066. https://doi.org/10.1002/anie.202116066.

(59) Demarteau, J.; Olazabal, I.; Jehanno, C.; Sardon, H. Aminolytic Upcycling of Poly(Ethylene Terephthalate) Wastes Using a Thermally-Stable Organocatalyst. *Polymer Chemistry* 2020, *11*, 4875–4882. https://doi.org/10.1039/d0py00067a.

(60) Hammond George S. A Correlation of Reaction Rates. *Journal of the American Chemical Society* 1955, *77*, 334–338.

(61) Jehanno, C.; Pérez-Madrigal, M. M.; Demarteau, J.; Sardon, H.; Dove, A. P. Organocatalysis for Depolymerisation. *Polymer Chemistry* 2019, *10*, 172–186. https://doi.org/10.1039/c8py01284a.

(62) Tang, X.; Chen, E. Y. X. Toward Infinitely Recyclable Plastics Derived from Renewable Cyclic Esters. *Chem* 2019, *5*, 284–312. https://doi.org/10.1016/j.chempr.2018.10.011.

(63) Choodej, S.; Teerawatananond, T.; Mitsunaga, T.; Pudhom, K. Chamigrane Sesquiterpenes from a Basidiomycetous Endophytic Fungus XG8D Associated with Thai Mangrove Xylocarpus Granatum. *Marine Drugs* 2016, *14*, 132. https://doi.org/10.3390/md14070132.

(64) Buisine, O.; Jaunzems, J.; Kim, Y.-J.; Kasubke, M. New Components for Electrolyte Compositions. WO 2020025502 A1, 2020.

(65) Hidaka, T.; Yamazaki, S.; Tani, A.; Kuwajima, Y. Electrolyte Solution, Electrochemical Device, Lithium Ion Secondary Battery, and Module. WO 2021235358 A1, 2020.

(66) Kuwajima, Y.; Hidaka, T.; Kinoshita, M.; Suzuki, Y.; Shimooka, T.; Nakamura, H.; Yamada, T.; Yamazaki, S.; Yamauchi, A.; Hayashi, K.; Yamamoto, Y.; Takahashi, K. Electrolyte, Electrochemical Device, Lithium-Ion Secondary Battery, and Module. WO 2019220764 A1, 2019.

(67) Qiu, Y.-L.; Kass, J.; Suh, B.-C.; Cao, H.; Li, W.; Peng, X.; Gao, X.; Or, Y. S. Hepatitis B Antiviral Agents. WO 2019113175 A1, 2019.

(68) Flynn, D. L.; Ahn, Y. M.; Caldwell, T.; Vogeti, L. Preparation of (Phenylamino)Pyrimidine Compounds as Autophagy Inhibitors for Treating Cancers. US 20200354352 A1, 2020.

(69) Sherman, D.; Cardozo, T. J. Indazole Derivatives as CaMKK2 Inhibitors and Their Preparation, Pharmaceutical Compositions and Use in the Treatment of Diseases. US 20200369656 A1, 2020.

(70) Bennett, F.; Imbriglio, J. E.; Kerekes, A. D.; Khan, T.; Lankin, C.; Li, D.; Wu, Z.; Xiong, Y.; Youm, H.; Yu, Y.; Kurissery, A. T.; Komanduri, V.; Ye, F. Preparation of 5,6,7,8-Tetrahydroacridine-2-

Carboxamide Derivatives as Natriuretic Peptide Receptor A Agonists Useful for the Treatment of Cardiometabolic Diseases, Kidney Disease, and Diabetes. WO 2020236690, 2020.

(71) Nieman, J.; Hena, M.; Bai, B.; Kandadai, A. S.; Belovodskiy, A. Pyridopyrazine Derivatives as Inhibitors of Human Herpesviruses and Their Preparation. WO 2021174355 A1, 2021.

(72) Benz, J.; Grether, U.; Hornsperger, B.; Kroll, C.; Kuhn, B.; O'Hara, F.; Richter, H. Preparation of Hexahydro-1H-Pyrido[1,2-a]Pyrazin-2-Yl Methanone Derivatives as Monoacylglycerol Lipase Inhibitors. WO 2021001330 A1, 2021.

(73) Boisnard, S.; El-Ahmad, Y.; Fett, E.; Halley, F.; Nicolai, E.; Tabart, M.; Terrier, C.; Vivet, B. Preparation of Novel Substituted 6,7-Dihydro-5H-Benzo[7]Annulene Compounds as Inhibitors and Degraders of Estrogen Receptors. WO 2021063967 A1, 2021.

(74) Kaldor, S. W.; Kanouni, T.; Tyhonas, J.; Murphy, E. A. N-Heteroarylphenyl Heterocyclecarboxamides as Inhibitors of RAF Kinases and Their Preparation. WO 2021081375 A1, 2021.

Supporting Informations

Synthesis and characterization of *N1,N4*-bis(2-hydroxyethyl)terephthalamide (P1) from waste PET

PET samples (0.5 g, 2.6 mmol), TBD:MSA salt (0.061g, 0.26 mmol) and ethanolamine (3.18 g, 51.04 mmol) were loaded in a 50 ml Schlenk tube with an oval magnetic stirrer. The solution was degassed during 30 min with N_2 under agitation. The Schlenk is then poured in a pre-heated bath at 180 °C and depolymerisation is started. After 10 min, the mixture is completely clear and all PET pellets disappeared. The mixture was then cooled to rt and added with 10 ml of DMSO to afford a homogeneous mixture that was further precipitated in DCM. After the white precipitate was filtrated and washed with DCM, bis(2-hydroxyethyl) terephthalamide **P1** (0.57 g, 2.42 mmol, yield = 87 %) was obtained as a fine white powder.

^{1}H NMR (400 MHz, DMSO-d_6): δ = 8.55 ppm (m, 2H), δ = 7.92 ppm (s, 4H), δ = 4.75 ppm (m, 2H), δ = 3.52 ppm (m, 4H), δ = 3.34 ppm (m, 4H).

^{13}C NMR (400 MHz, DMSO-d_6): δ = 166.2 ppm, δ = 137.1 ppm, δ = 127.6 ppm, δ = 60.1 ppm, δ = 42.7 ppm.

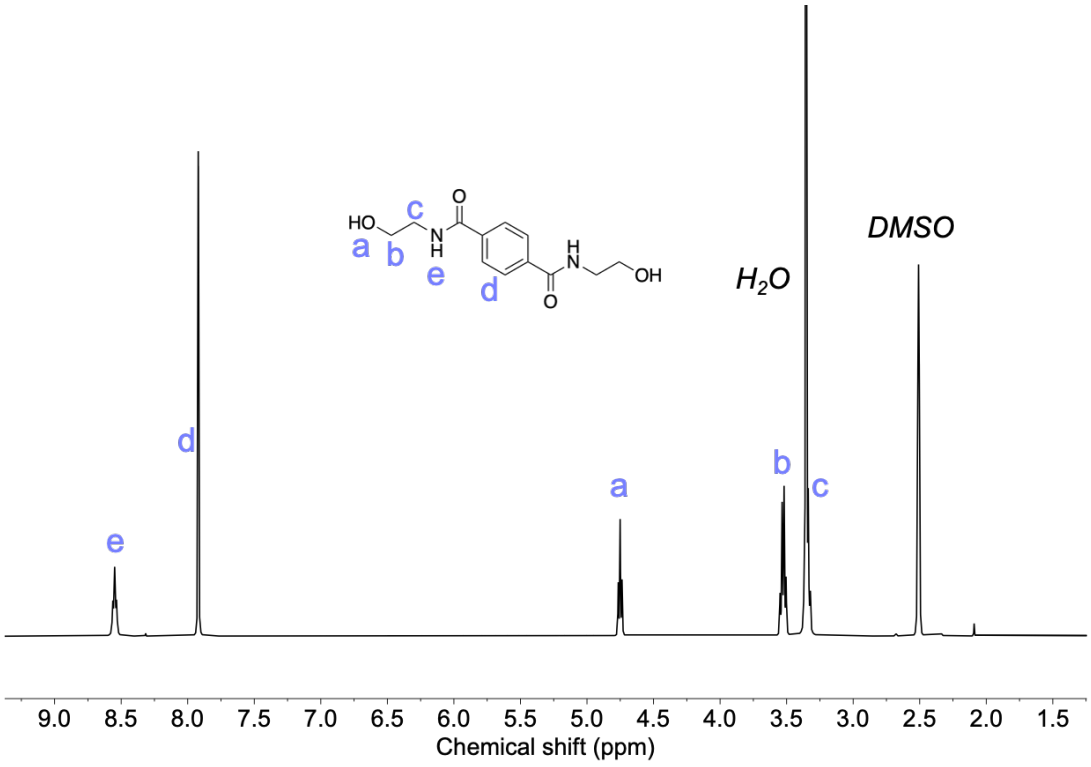

Figure S1. ^{1}H-NMR (in DMSO-d_6) of N1,N4-bis(2-hydroxyethyl)terephthalamide (BHETA) (P1).

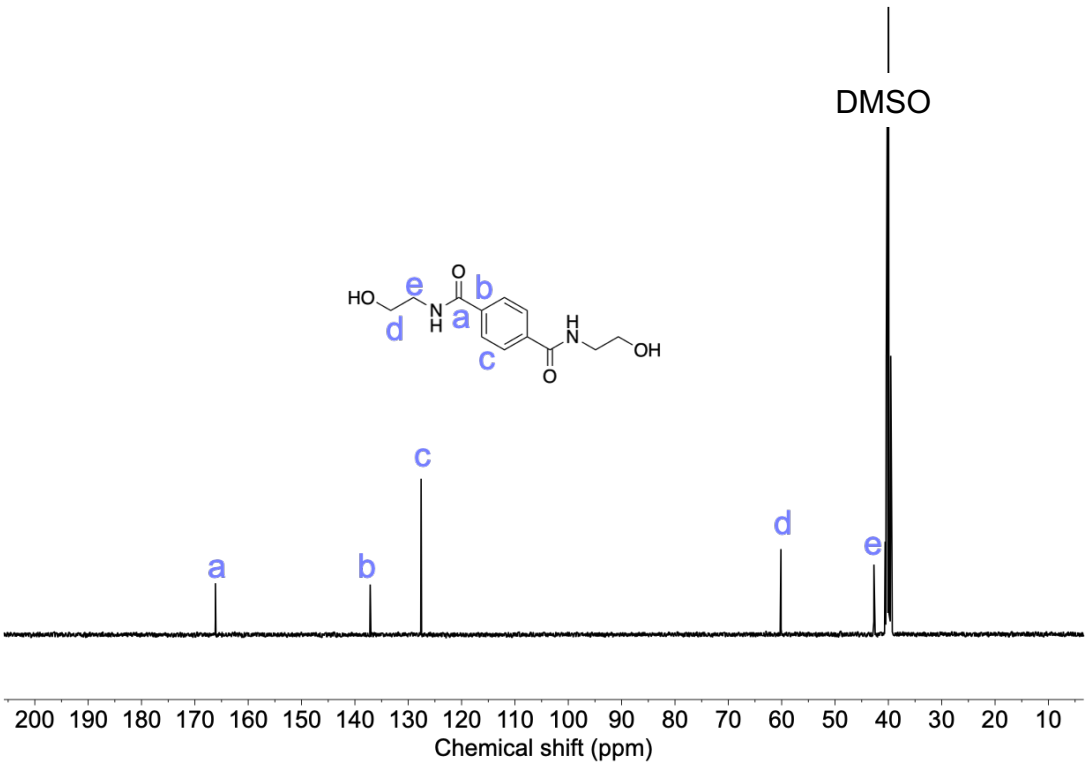

Figure S2. ^{13}C-NMR (in DMSO-d_6) of N1,N4-bis(2-hydroxyethyl)terephthalamide (BHETA) (P1).

Synthesis and characterization of 1,3-bis(2-hydroxyethyl) urea (P2) from bisphenol A Polycarbonate

BPA-PC commercial pellets (5 g, 19.69 mmol, 1eq), TBD:MSA salt (0.694g, 2.95 mmol, 0.15 eq) and Ethanolamine (8.42 g, 137 mmol, 7 eq.) were loaded in a 50 ml Schlenk tube with an magnetic stirrer. The solution was degassed during 30 min with N_2 under agitation. The Schlenk is then poured in a pre-heated bath at 130 °C and the depolymerization is started. After 40 min, the transparent mixture is clear yellow and all BPA-PC pieces disappeared. Then, the solution was cooled to rt, diluted in acetone. The product was recovered by precipitation in ethyl acetate and left overnight at 5 ºC. White crystals were collected by filtration corresponding the 1,3-bis(2-hydroxyethyl) urea (2.03 g, isolated yield = 70 %).

^{1}H NMR (400 MHz, DMSO-d_6): δ = 5.98 ppm (m, 2H), δ = 4.65 ppm (m, 2H), δ = 3.35 ppm (m, 4H), δ = 3.05 ppm (m, 4H).

^{13}C NMR (400 MHz, DMSO-d_6): δ = 158.9 ppm, δ = 61.3 ppm, δ = 42.5 ppm.

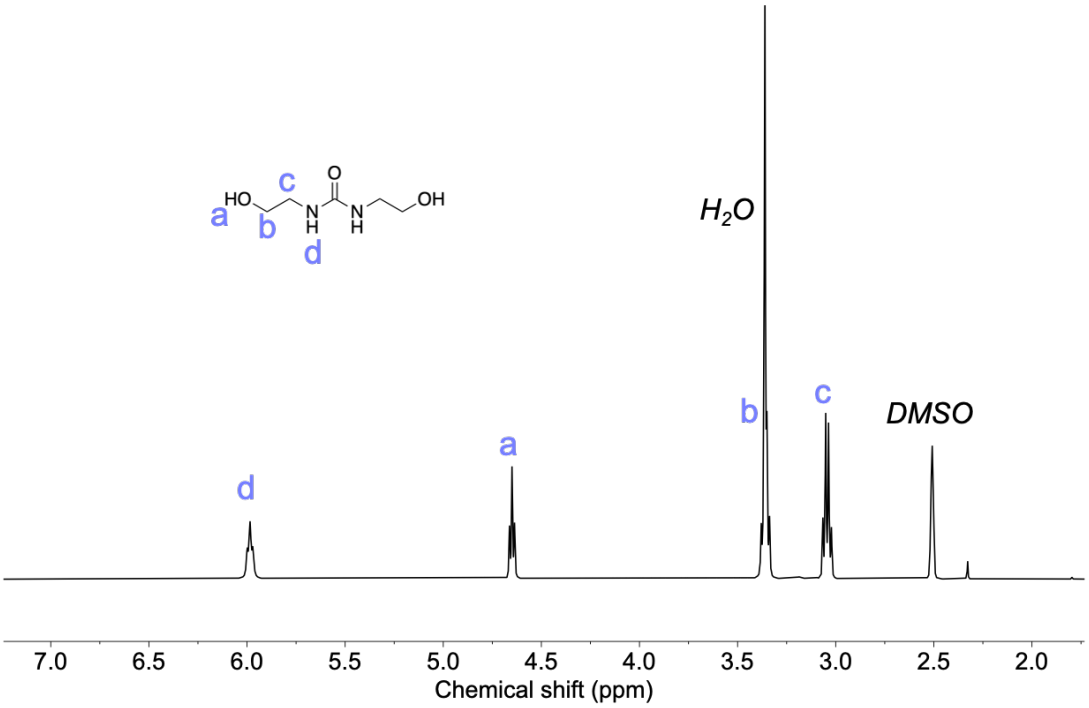

Figure S3. ^{1}H-NMR (in DMSO-d_6) of 1,3-bis(2-hydroxyethyl) urea (P2).

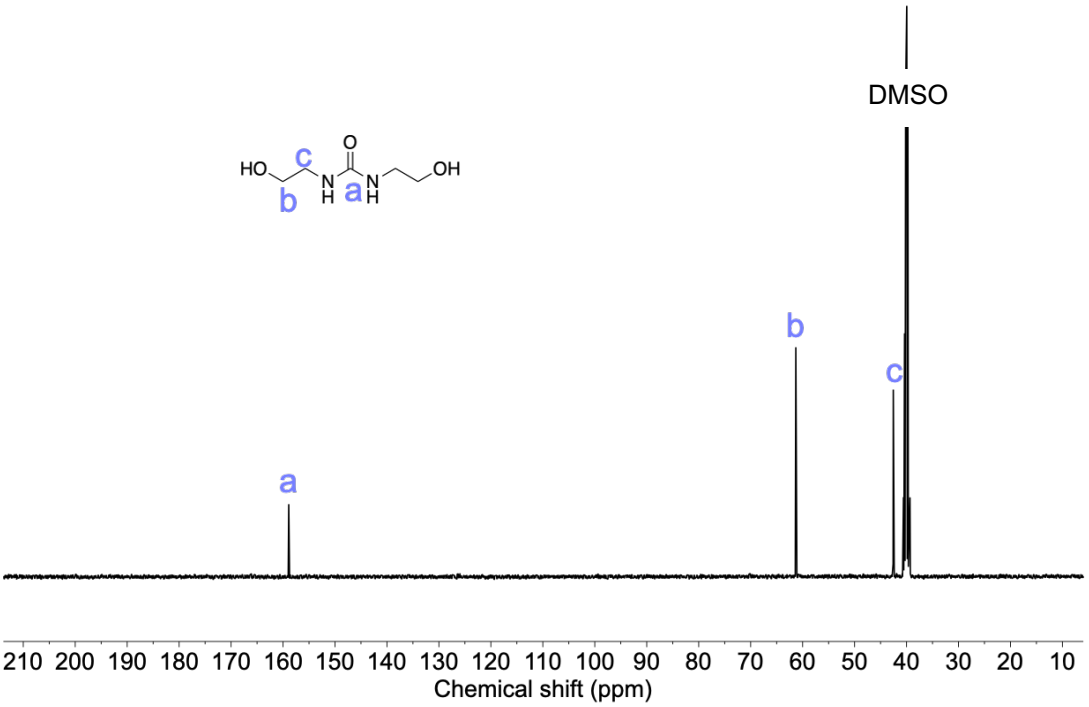

Figure S4. ^{13}C-NMR (in DMSO-d_6) of 1,3-bis(2-hydroxyethyl) urea (P2).

Synthesis and characterization of 1,3-bis(2-hydroxypropyl) urea (P3) from bisphenol A Polycarbonate

BPA-PC commercial pellets (5 g, 19.69 mmol, 1 eq), TBD:MSA salt (0.694 g, 2.95 mmol, 0.15 eq) and 3-aminopropanol (10.352 g, 137 mmol, 7 eq.) were loaded in a 50 ml Schlenk tube with an oval magnetic stirrer. The solution was degassed during 30 min with N_2 under agitation. The Schlenk is then poured in a pre-heated bath at 130 °C and the depolymerization is started. After 40 min, the transparent mixture is clear yellow and all BPA-PC pieces disappeared. Then, the solution was cooled to rt, diluted in acetone. The product was recovered by precipitation in ethyl acetate and left overnight at 5 ºC. White crystals were collected by filtration corresponding the 1,3-bis(2-hydroxypropyl) urea (2.60 g, isolated yield = 73 %).

^{1}H NMR (400 MHz, DMSO-d_6): δ = 5.82 ppm (m, 2H), δ = 4.45 ppm (m, 2H), δ = 3.39 ppm (m, 4H), δ = 3.04 ppm (m, 4H), δ = 1.50 ppm (m, 4H).

^{13}C NMR (400 MHz, DMSO-d_6): δ = 158.9 ppm, δ = 58.9 ppm, δ = 36.8 ppm, δ = 33.7 ppm.

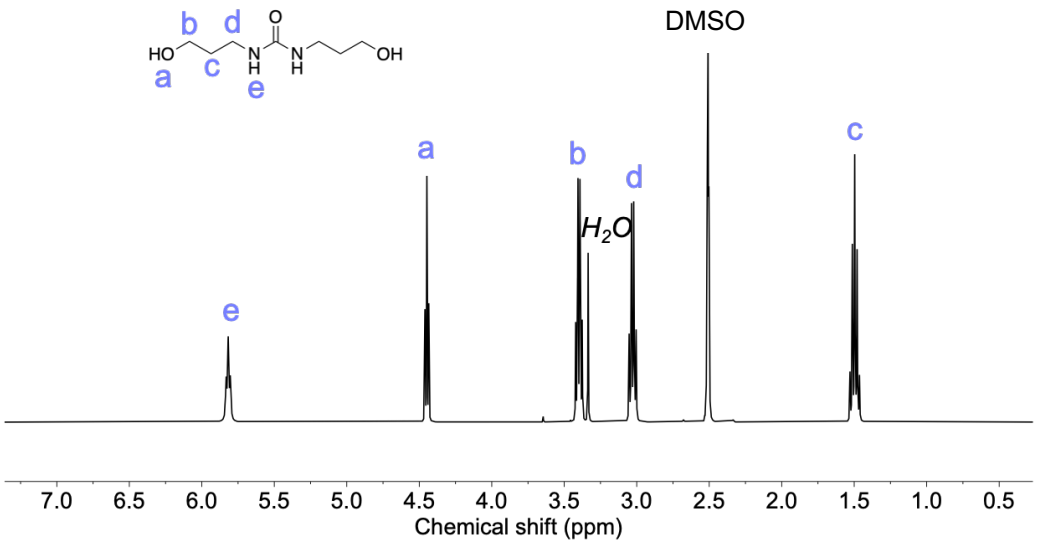

Figure S5. ^{1}H-NMR (in DMSO-d_6) of 1,3-bis(2-hydroxypropyl) urea (P3).

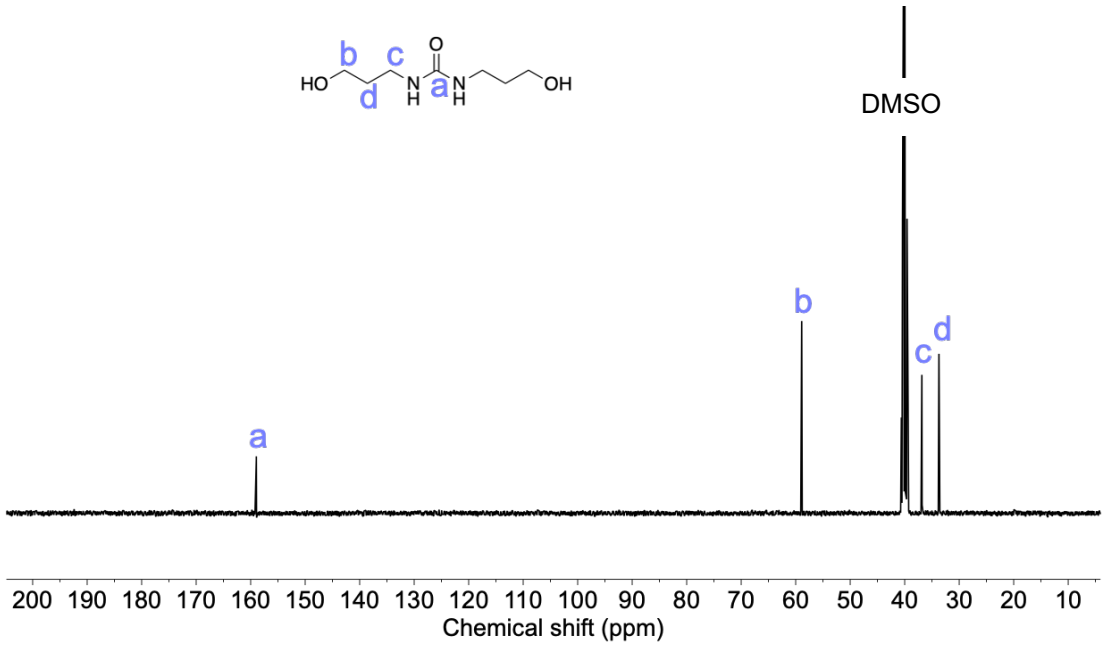

Figure S6. ^{13}C-NMR (in DMSO-d_6) of 1,3-bis(2-hydroxypropyl) urea (P3).

Synthesis and characterization of poly(carbonate-amide) and poly(carbonate-urea)s via step-growth copolymerization

Standard procedure for the synthesis of **C1P1-3**: BisαCC **C1** (3.93 mmol, 1 g), *N1,N4*-bis(2-hydroxyethyl)terephthalamide (3.93 mmol, 0.990 g), dry DMSO (5 mL) and DBU (0.196 mmol, 0.03 mL) were added in a flask under nitrogen at room temperature (25 °C). The reaction medium was then stirred at 25 °C for 24 h. At the end of the reaction, an aliquot was withdrawn to determine the conversion of the monomers by ^{1}H-NMR spectroscopy. The polymer was purified by dialysis in chloroform for 24 h. The solvent was then removed by rotavapor and the polymer further vacuum dried before analysis by ^{1}H- and ^{13}C-NMR spectroscopy and SEC. The same procedure was carried out for all other polymers.

Size exclusion chromatography (SEC) analyses

Polymer C1P1

Table S1. Synthesis and SEC analysis in DMF of purified **C1P1**.

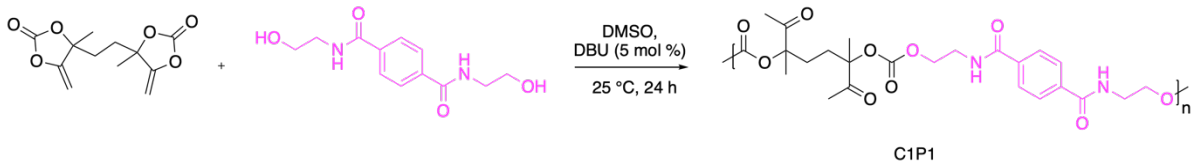

Entry	Polymer	M_n (g/mol)[a]	M_w (g/mol)[a]	$Đ$[a]
1	C1P1	18,500	27,500	1.48

Conditions: [bisαCC]/[diol] = 1, [bisαCC] = 0.78 M, DBU (5 mol%). [a]Determined by SEC in DMF/LiBr.

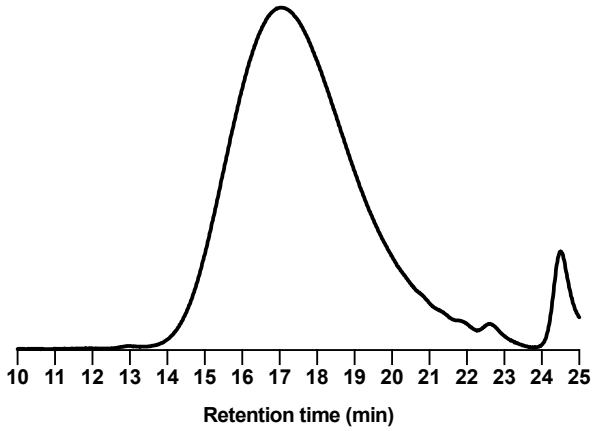

Figure S7. SEC chromatogram in DMF of purified **C1P1**.

Polymer C1P2

Table S2. Synthesis and SEC analysis in DMF of purified **C1P2**.

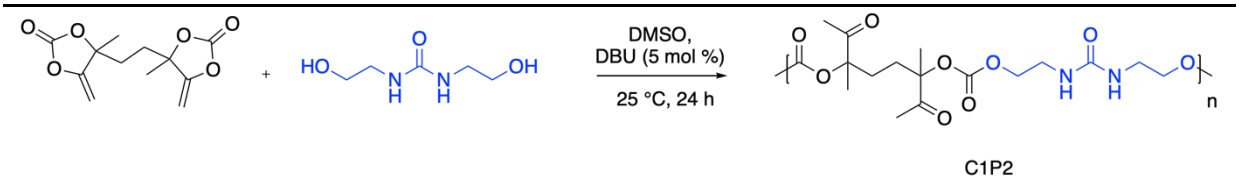

Entry	Polymer	M_n (g/mol)[a]	M_w (g/mol)[a]	$Đ$[a]
1	C1P2	10,300	17,000	1.64

Conditions: [bisαCC]/[diol] = 1, [bisαCC] = 0.78 M, DBU (5 mol%). [a]Determined by SEC in DMF/LiBr.

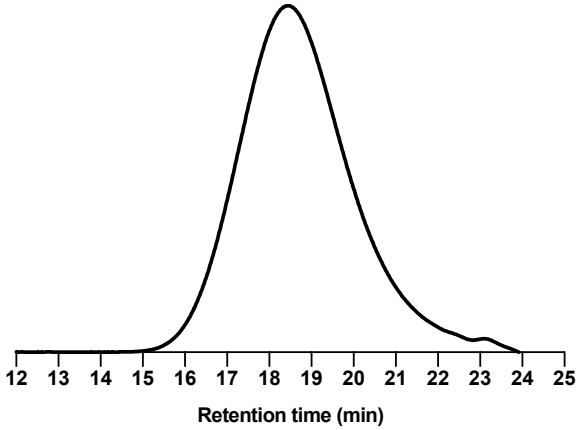

Figure S8. SEC chromatogram in DMF of purified **C1P2**.

Polymer C1P3

Table S3. Synthesis and SEC analysis in DMF of purified **C1P3**.

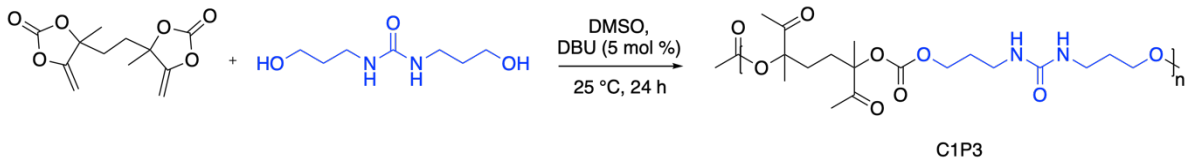

C1P3

Entry	Polymer	M_n (g/mol)[a]	M_w (g/mol)[a]	$Đ$[a]
1	C1P3	20,900	29,900	1.57

Conditions: [bisαCC]/[diol] = 1, [bisαCC] = 0.78 M, DBU (5 mol%). [a]Determined by SEC in DMF/LiBr.

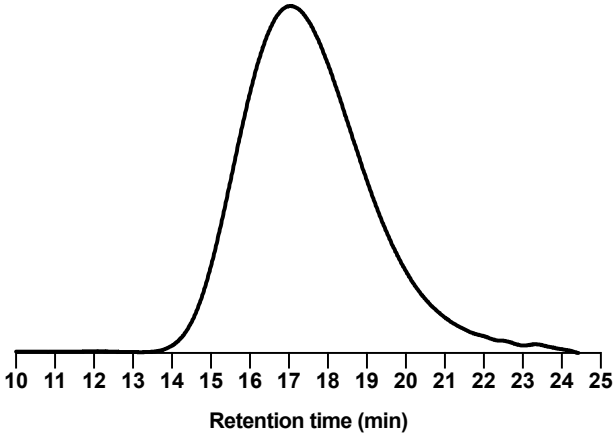

Figure S9. SEC chromatogram in DMF of purified **C1P3**.

^{1}H and ^{13}C nuclear magnetic resonance (NMR) analyses

C1P1: ^{1}H NMR (400 MHz, DMSO-d_6): δ = 8.78 ppm (m, 2H), δ = 7.90 ppm (s, 4H), δ = 4.22 ppm (m, 4H), δ = 3.53 ppm (m, 4H), δ = 2.06 ppm (s, 6H), δ = 1.85-1.61 ppm (m, 4H), δ = 1.40 ppm (s, 6H).

^{13}C NMR (400 MHz, DMSO-d_6): δ = 205.9 ppm, δ = 166.1 ppm, δ = 153.4 ppm, δ = 136.6 ppm, δ = 127.4 ppm, δ = 86.6 ppm, δ = 65.5 ppm, δ = 29.1 ppm, δ = 24.3 ppm, δ = 20.1 ppm.

C1P2: ^{1}H NMR (400 MHz, DMSO-d_6): δ = 6.17 ppm (m, 2H), δ = 4.03 ppm (m, 4H), δ = 3.26 ppm (m, 4H), δ = 2.12 ppm (s, 6H), δ = 1.90 -1.61 ppm (m, 4H), δ = 1.45 ppm (s, 6H).

^{13}C NMR (400 MHz, DMSO-d_6): δ = 205.7 ppm, δ = 157.8 ppm, δ = 153.1 ppm, δ = 86.3 ppm, δ = 67.5 ppm, δ = 28.9 ppm, δ = 24.1 ppm, δ = 20.0 ppm.

C1P3: ^{1}H NMR (400 MHz, DMSO-d_6): δ = 5.93 ppm (m, 2H), δ = 4.07 ppm (m, 4H), δ = 3.04 ppm (m, 4H), δ = 2.12 ppm (s, 6H), δ = 1.88 -1.60 ppm (m, 4H), δ = 1.60 ppm (m, 4H), δ = 1.44 ppm (s, 6H).

^{13}C NMR (400 MHz, DMSO-d_6): δ = 205.9 ppm, δ = 158.2 ppm, δ = 153.4 ppm, δ = 86.4 ppm, δ =66.0 ppm, δ = 40.3 ppm, δ = 36.0 ppm, δ = 29.5 ppm, δ = 24.3 ppm, δ = 20.0 ppm.

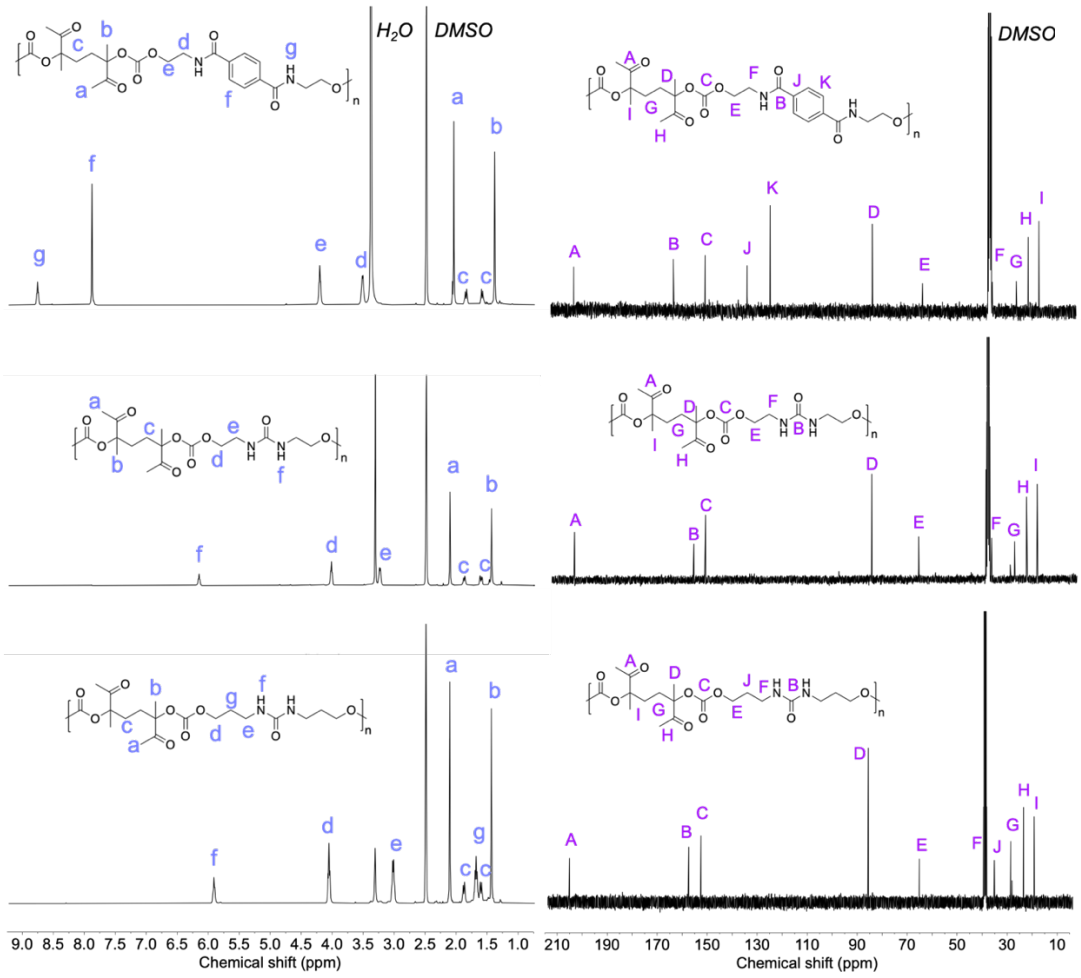

Figure S10. H-NMR and ^{13}C-NMR spectra of **C1P1**, **C1P2** and **C1P3** in DMSO-d_6.

Thermal analyses

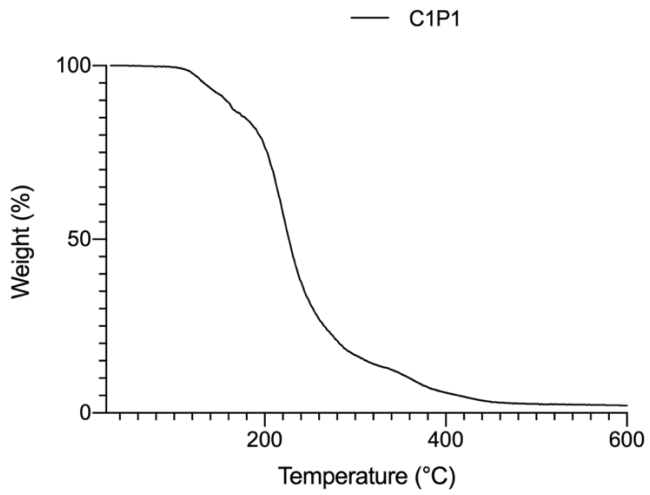

Figure S11. Thermal degradation of purified **C1P1**.

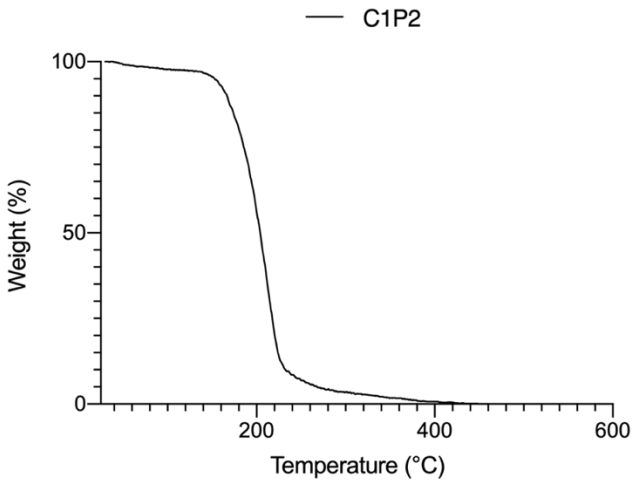

Figure S12. Thermal degradation of purified **C1P2**.

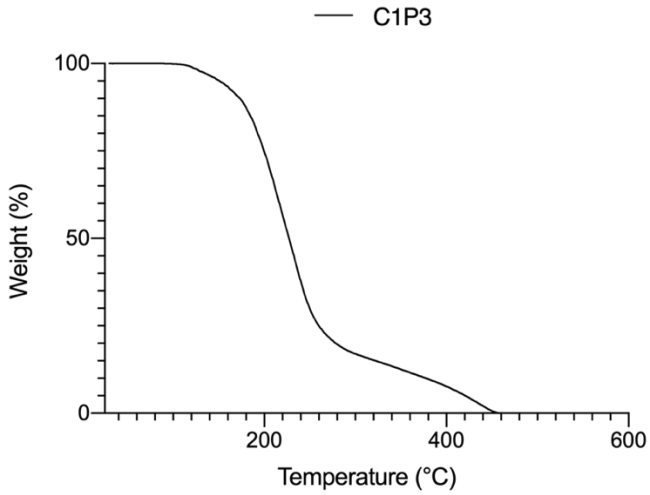

Figure S13. Thermal degradation of purified **C1P3**.

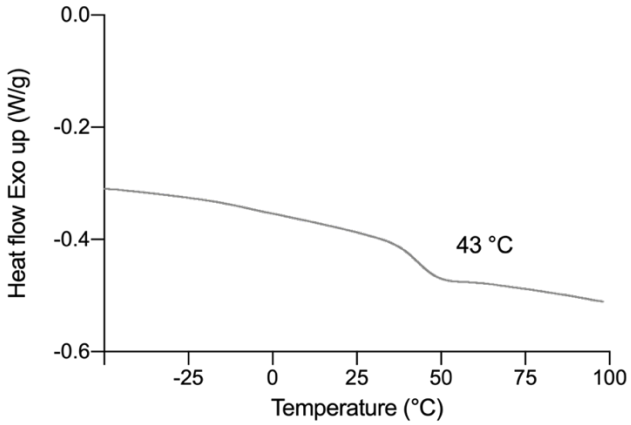

Figure S14. DSC characterization of purified **C1P1**.

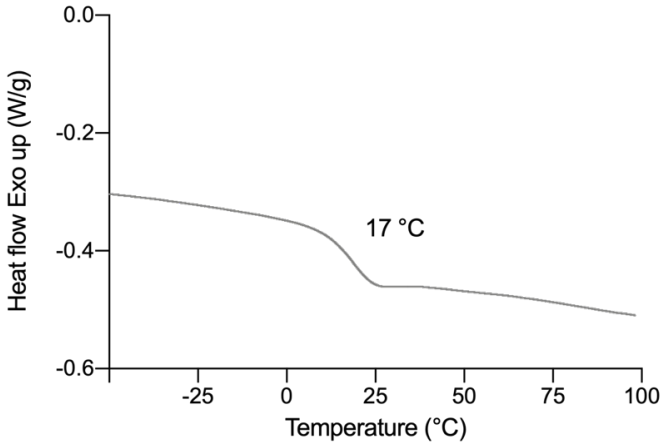

Figure S15. DSC characterization of purified **C1P2**.

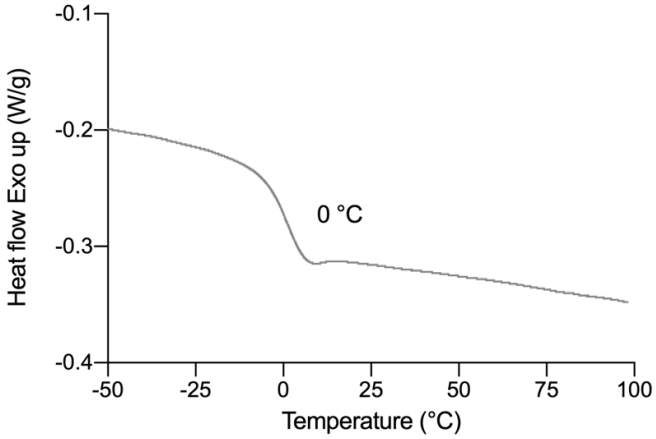

Figure S16. DSC characterization of purified **C1P3**.

Ring-closing depolymerization of step-growth poly(carbonate-amide) and poly(carbonate-urea)s

Standard procedure for the **C1P1-3** deconstruction: 0.2 g of **C1P1** were dissolved in 1 ml of dry DMSO. The solution was then degassed by bubbling of N_2 for 5 min followed by the addition of dry DBU (6 mg, 0.0395 mmol, 10 mol% compared repeating unit of polymer) and 25 mg of 1,3,5-Trimethoxybenzene (TMB) as an internal standard. The depolymerization kinetic was realized at 80 °C and monitored by ^{1}H NMR spectroscopy and by SEC analysis. The same procedure was carried out for the other polymers.

The polymer degradation was calculated following the equation:

$$P_{deg} = (1 - \frac{n_P}{n_{Pi}}) \times 100$$

P_{deg} = Polymer degradation (%).

n_P = number of mol of repeating unit of polymer at certain time*.

n_{Pi} = number of mol of repeating unit of initial polymer*.

*The number of mol were determined by integrating the peak at 2.13 ppm of the polymer in relation to the one of the standard TMB at 3.71 ppm.

Mole and the yield of product **1** were calculated following the equations:

$$n_1 = \frac{\left(\frac{I_1}{N_{H,1}}\right) \times n_{\mathrm{TMB}}}{\frac{I_{TMB}}{N_{H,TMB}}}$$

$$Yield\ (1) = \frac{n_1}{n_{Pi}} \times 100$$

n_1 = number of mol of product **1**.

I_1 = Integral peak of product **1**.

$N_{H,1}$ = Number of protons associated to the integrated peak of product **1**.

n_{TMB} = number of mol of internal standard TMB.

I_{TMB} = Integral peak of TMB.

$N_{H,TMB}$ = Number of protons associated to the integrated peak of TMB.

Same calculation was made for the other degradation products.

Purification and Characterization of depolymerization products 1-3

The degradation products were purified and recovered by flash chromatography on silica directly from the crude depolymerization mixtures.

Products **1**, **P1** and **2** produced by depolymerization of **C1P1** or **C1P2** were separated and collected using petroleum ether/ethyl acetate (7:3), then CH_2Cl_2/MeOH (1:1) eluents for **C1P1** and **C1P2** products

Products **1** and **3** produced by depolymerization of **C1P3** were separated and collected using petroleum ether/ ethyl acetate (7:3) as eluent followed by acetonitrile.

C1P1 ring-closing depolymerization and products characterization

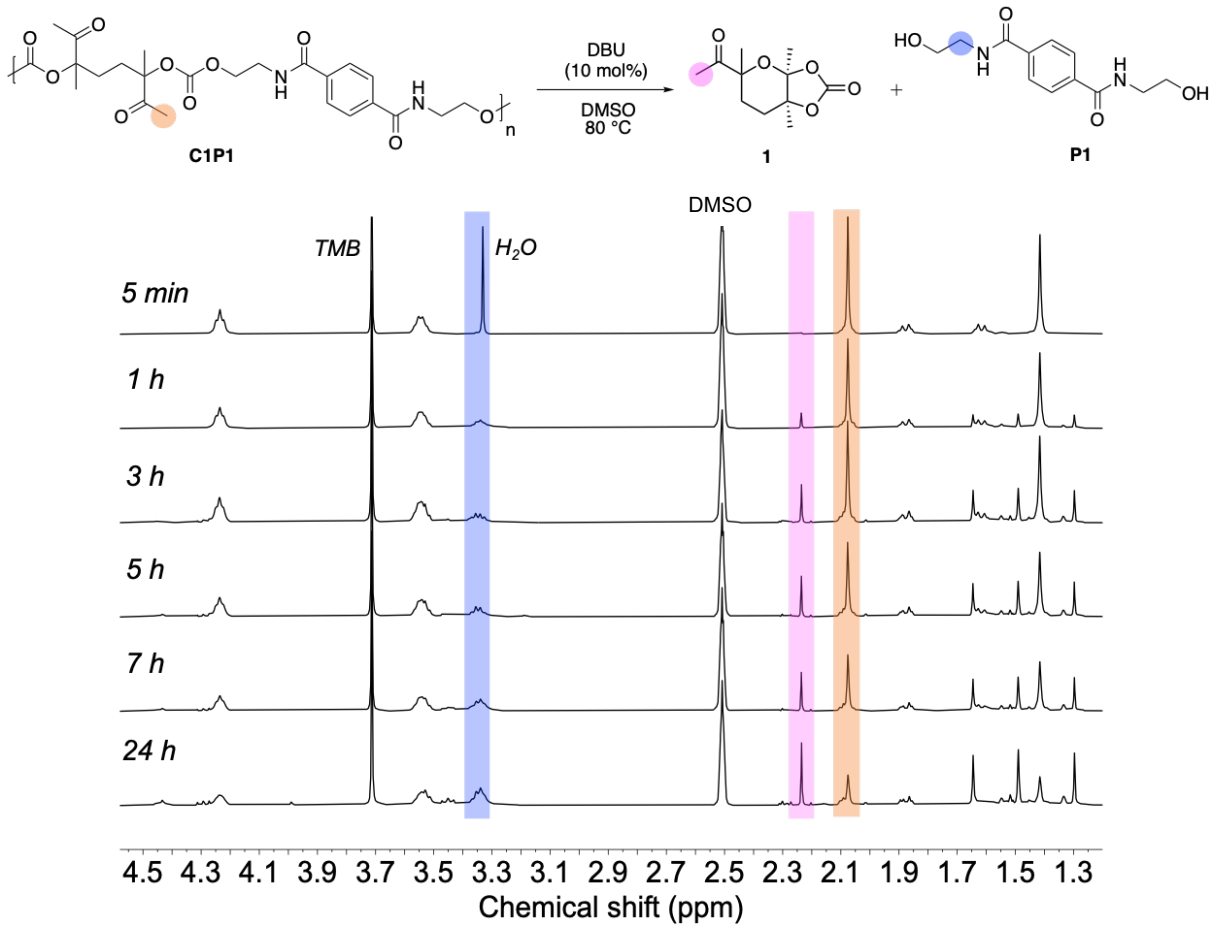

Figure S17. Kinetics of degradation of **C1P1** followed by ^{1}H-NMR (in DMSO-d_6). The reaction was conducted at 80 °C in presence of DBU (10 mol% *vs* polymer repeating unit), using 1,3,5-trimethoxybenzene (TMB) as internal standard.

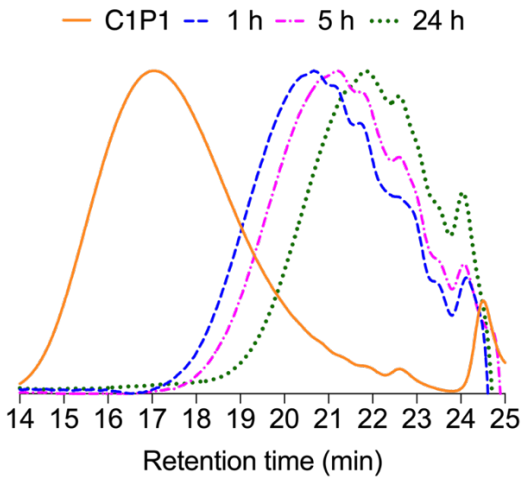

Figure S18. Time evolution of the SEC of **C1P1** upon deconstruction (recorded in DMF/LiBr). The reaction was conducted at 80 °C in presence of DBU (10 mol% *vs* polymer repeating unit), using 1,3,5-trimethoxybenzene (TMB) as internal standard.

Characterization of N1,N4-bis(2-hydroxyethyl)terephthalamide (monomer P1)

^{1}H NMR (400 MHz, DMSO-d_6): δ = 8.55 ppm (m, 2H), δ = 7.92 ppm (s, 4H), δ = 4.74 ppm (m, 2H), δ = 3.52 ppm (s, 4H), δ = 3.33 ppm (m, 4H).

^{13}C NMR (400 MHz, DMSO-d_6): δ = 166.1 ppm, δ = 137.1 ppm, δ = 127.6 ppm, δ = 60.1 ppm, δ = 42.7 ppm.

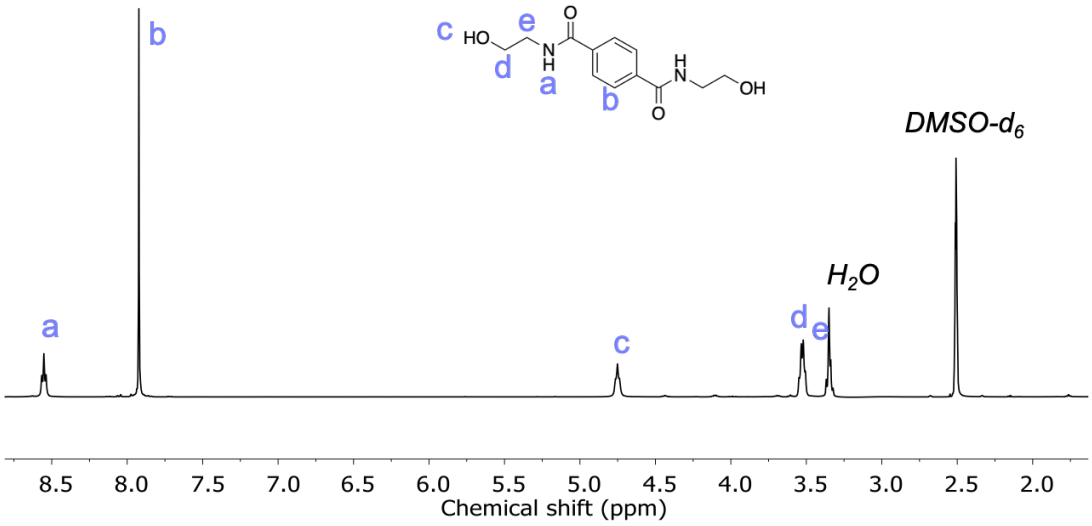

Figure S19. ^{1}H-NMR (in DMSO-d_6) spectrum of purified N1,N4-bis(2-hydroxyethyl)terephthalamide.

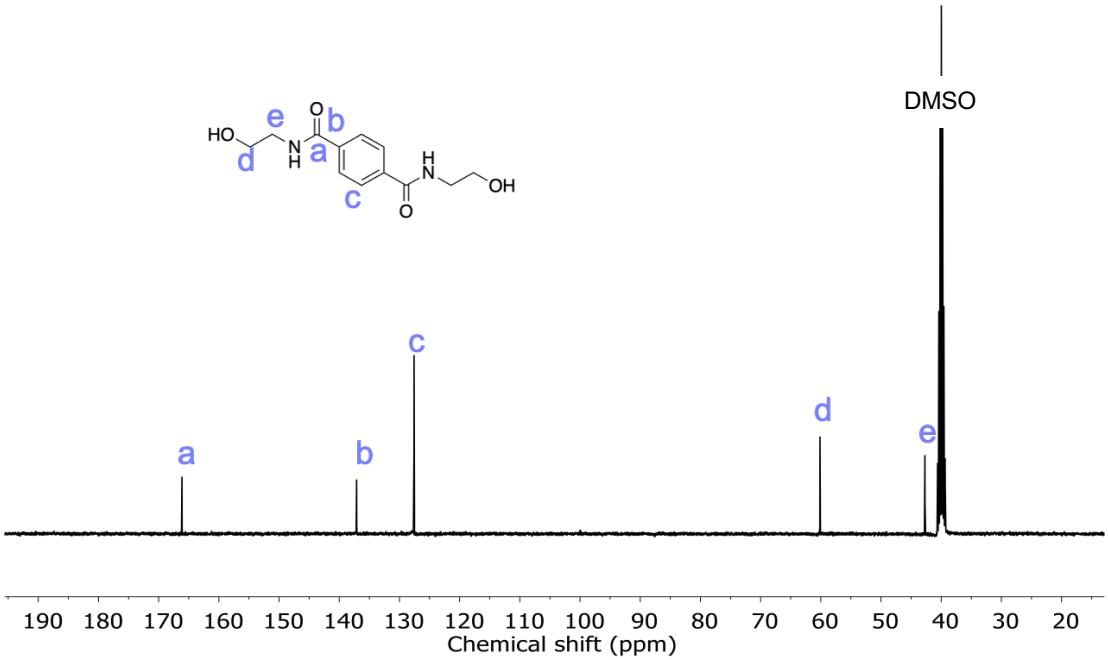

Figure S20. ^{13}C-NMR (in DMSO-d_6) spectrum of purified N1,N4-bis(2-hydroxyethyl)terephthalamide.

Characterizations of 5-acetyl-3a,5,7a-trimethyltetrahydro-5H-[1,3]dioxolo[4,5-b]pyran-2- one (product 1)

^{1}H NMR (400 MHz, DMSO-d_6): δ = 2.30 ppm (m, 1H), δ = 2.24 ppm (s, 3H), δ = 1.87 ppm (m, 1H), δ = 1.65 ppm (s, 3H), δ = 1.52 ppm (m, 2H), δ = 1.48 ppm (s, 3H), δ = 1.30 ppm (s, 3H).
^{13}C NMR (400 MHz, DMSO-d_6): δ = 210.3 ppm, δ = 151.8 ppm, δ = 108.2 ppm, δ = 83.4 ppm, δ = 82.4 ppm, δ = 29.5 ppm, δ = 26.9 ppm, δ = 25.9 ppm, δ = 25.7 ppm, δ = 23.5 ppm, δ = 22.29 ppm.
ESIHRMS m/z calcd for $C_{11}H_{16}O_5$ $[M+H]^+$ 229,1082, found 229,1071.

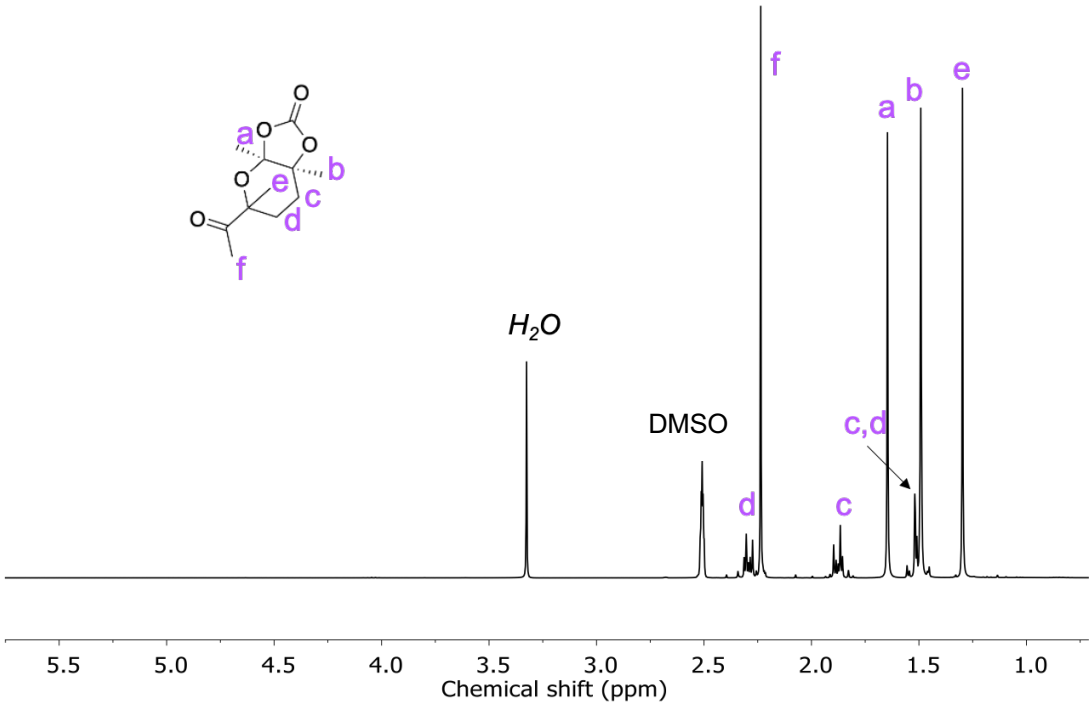

Figure S21. ^{1}H-NMR (in DMSO-d_6) spectrum of purified 5-acetyl-3a,5,7a-trimethyltetrahydro-5H-[1,3]dioxolo[4,5-b]pyran-2-one.

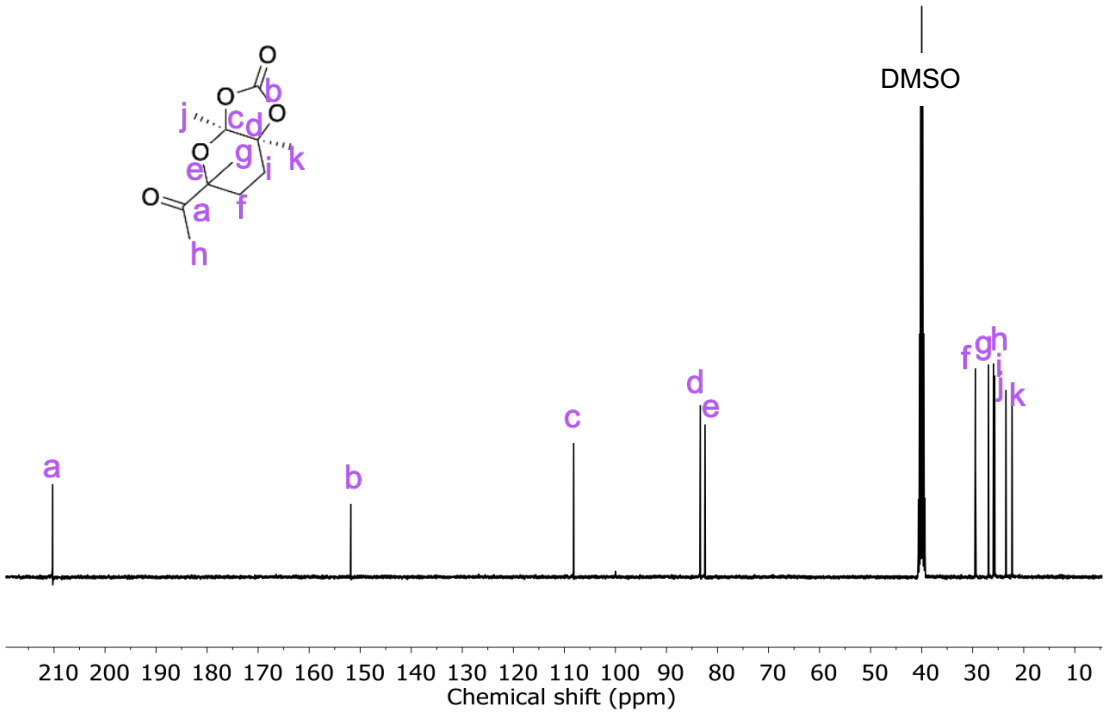

Figure S22. ^{13}C-NMR (in DMSO-d_6) spectrum of purified 5-acetyl-3a,5,7a-trimethyltetrahydro-5H-[1,3]dioxolo[4,5-b]pyran-2- one.

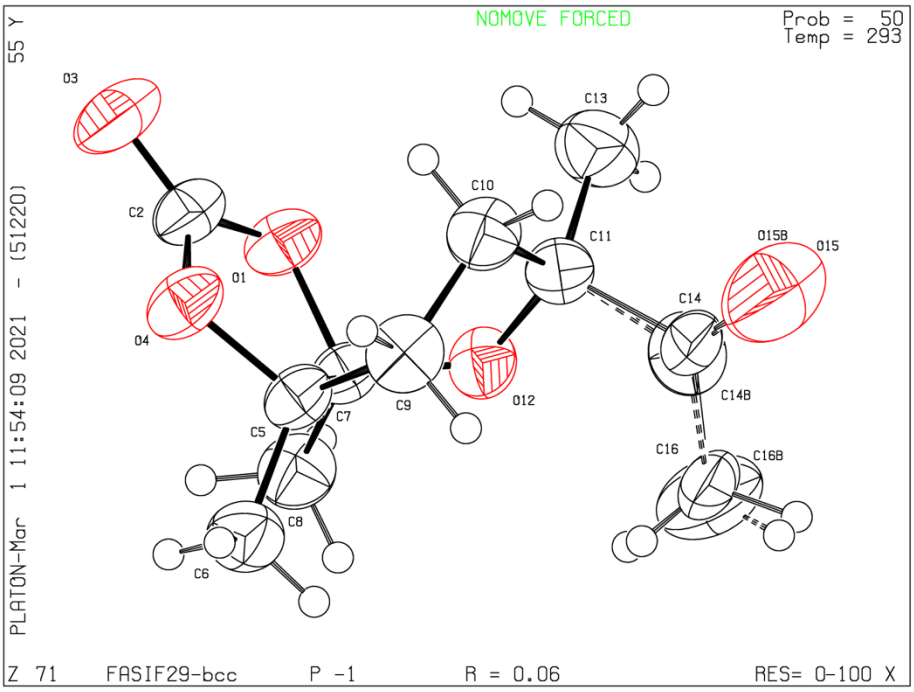

Figure S23. ORTEP representation of 5-acetyl-3a,5,7a-trimethyltetrahydro-5H-[1,3]dioxolo[4,5-b]pyran-2- one.

Table S4. Crystal data and structure refinement for 5-acetyl-3a,5,7a-trimethyltetrahydro-5H-[1,3]dioxolo[4,5-b]pyran-2- one.

Empirical formula	C_{11} H_{16} O_5
Formula weight	228.24
Temperature	293(2) K
Wavelength λ	0.71073 Å
Crystal system	Triclinic
Space group	*P*-1
Unit cell dimensions	a = 6.3526(5) Å
	b = 6.7275(17) Å
	c = 14.855(3) Å
	α= 84.455(19)°.
	β= 79.022(14)°.
	γ = 69.228(18).
Volume	582.4(2) $Å^3$
Z	2
Density (calculated)	1.301 g/cm^3
Absorption coefficient	0.103 mm^{-1}
F(000)	244
Crystal size	0.50 x 0.25 x 0.15 mm^3
Theta range for data collection	3.488 to 26.054°.
Reflections collected	8899
Independent reflections	2272 [$R_{(int)}$ = 0.0463]
Completeness to θ = 25.242°	98.7 %
Max. and min. transmission	1.00000 and 0.75288
Refinement method	Full-matrix least-squares on F^2
Data / restraints / parameters	2272 / 22 / 178
Goodness-of-fit on F^2	1.087
Final R indices [I>2σ(I)]	R_1 = 0.0616, wR_2 = 0.1388
R indices (all data)	R_1 = 0.0673, wR_2 = 0.1423
Largest diff. peak and hole	0.287 and -0.169 e.$Å^{-3}$

Influence of temperature

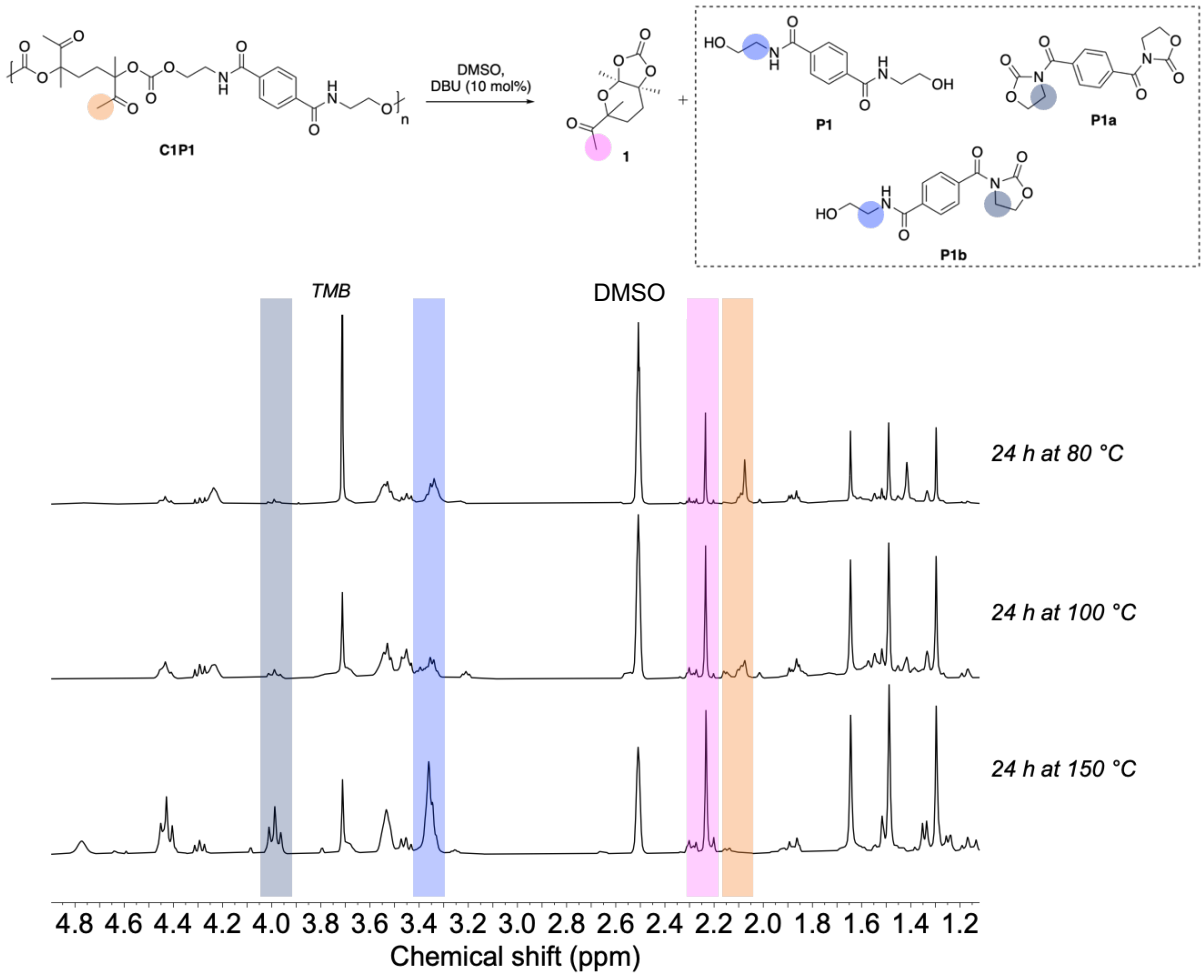

Figure S24. Influence of the temperature on the degradation of **C1P1:** overlay of the ^{1}H-NMR spectra (in DMSO-d_6) recorded after 24 h on the crude sample for experiments conducted at 80 °C, 100 °C and 150 °C

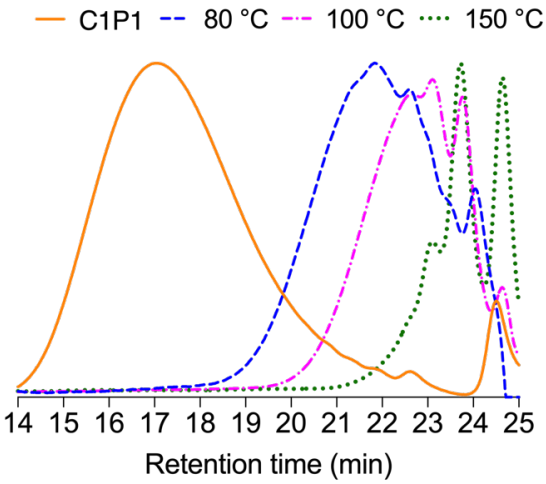

Figure S25. SEC overlays in DMF/LiBr of **C1P1** degradation at different temperatures: 80 °C, 100 °C and 150 °C.

C1P2 ring-closing depolymerization and product characterization

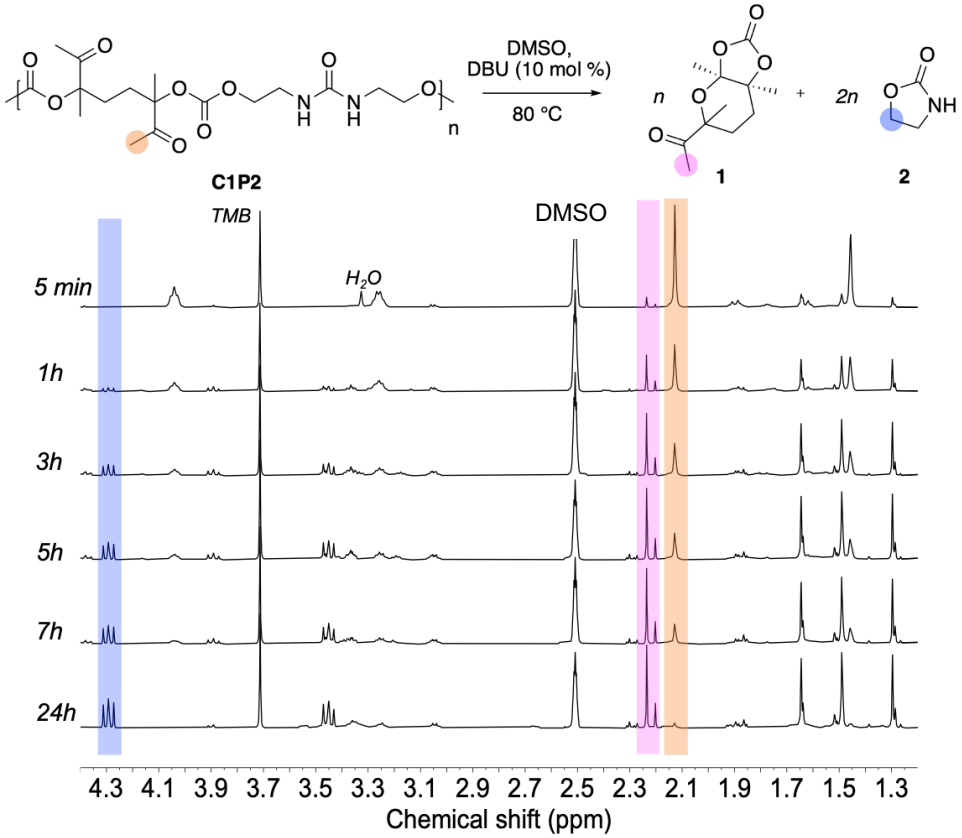

Figure S26. Kinetics of degradation of **C1P2** followed by ^{1}H-NMR (in DMSO-d_6). The reaction was conducted at 80 °C in the presence of DBU (10 mol% *vs* polymer repeating unit), using 1,3,5-trimethoxybenzene (TMB) as internal standard.

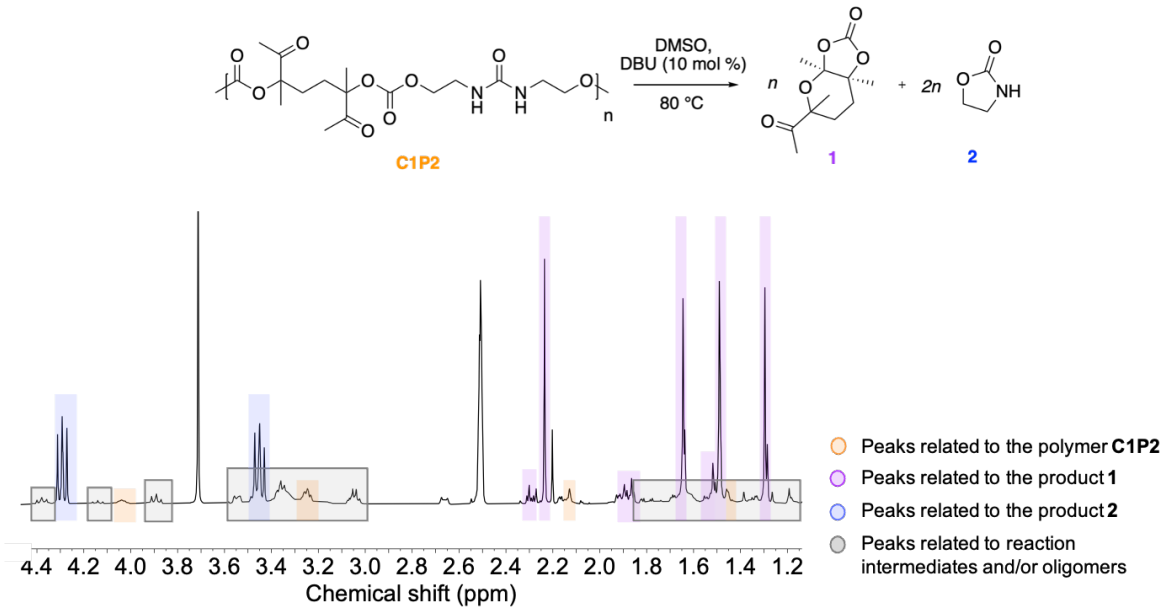

Figure S27. Crude ^{1}H-NMR spectrum (in DMSO-d_6) recorded after 24 h.

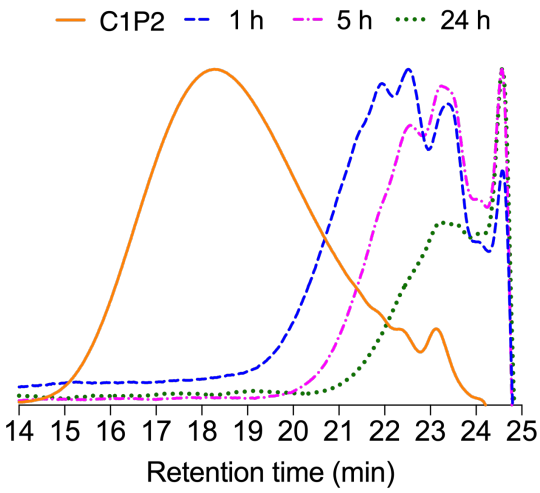

Figure S28. SEC overlays of C1P2 degradation at 80 °C for various reaction times.

Characterizations of 2-Oxazolidinone (product 2)

^{1}H NMR (400 MHz, DMSO): δ = 7.47 ppm (s, 1H), δ = 4.28 ppm (m, J=8 Hz, 2H), δ = 3.44 ppm (m, J=8 Hz, 2H).

^{13}C NMR (400 MHz, DMSO): δ = 160.0 ppm, δ = 64.6 ppm, δ = 40.3 ppm.

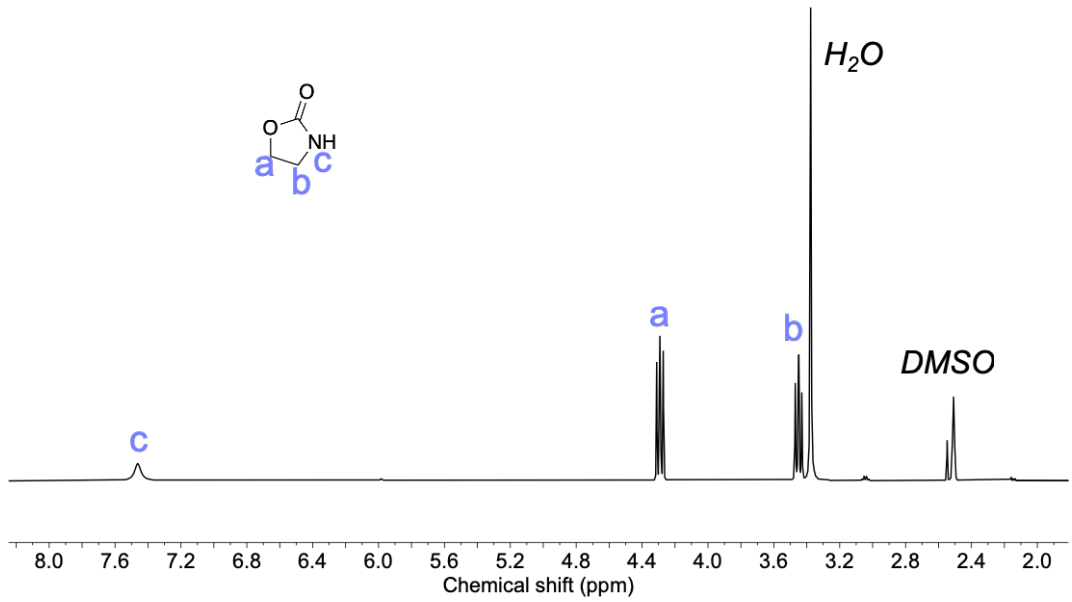

Figure S29. ^{1}H-NMR (in DMSO-d_6) spectrum of purified oxazolidin-2-one.

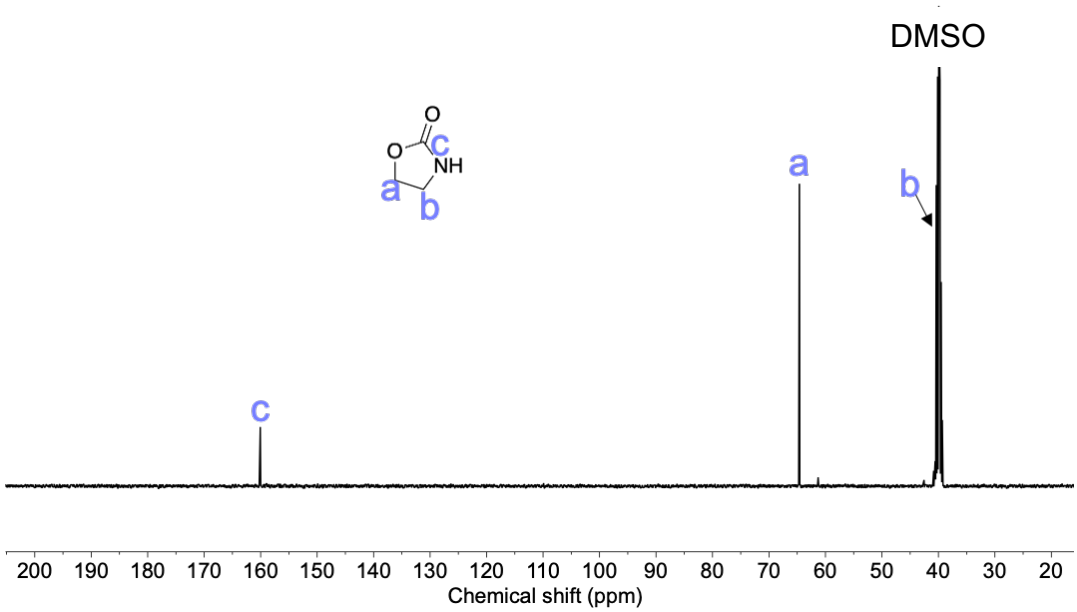

Figure S30. ^{13}C-NMR (in DMSO-d_6) spectrum of purified oxazolidin-2-one.

C1P2 ring-closing depolymerization under catalyst-free condition

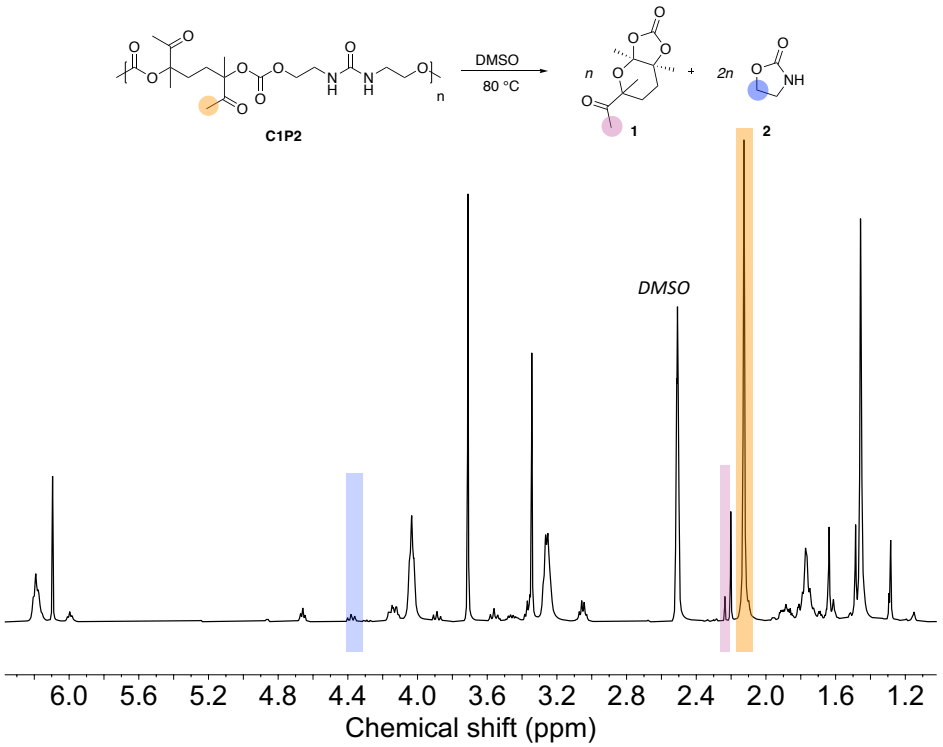

Figure S31. ^{1}H-NMR (in DMSO-d_6) spectrum of **C1P2** degradation after 24 h. The reaction was conducted at 80 °C, without catalyst, using 1,3,5-trimethoxybenzene (TMB) as internal standard.

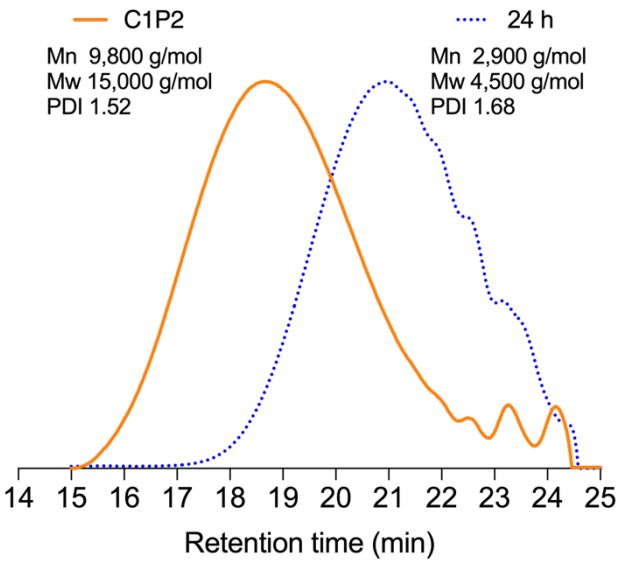

Figure S32. SEC overlays of **C1P2** at T0 and after 24 h at 80 °C, without catalyst.

C1P3 ring-closing depolymerization and product characterization

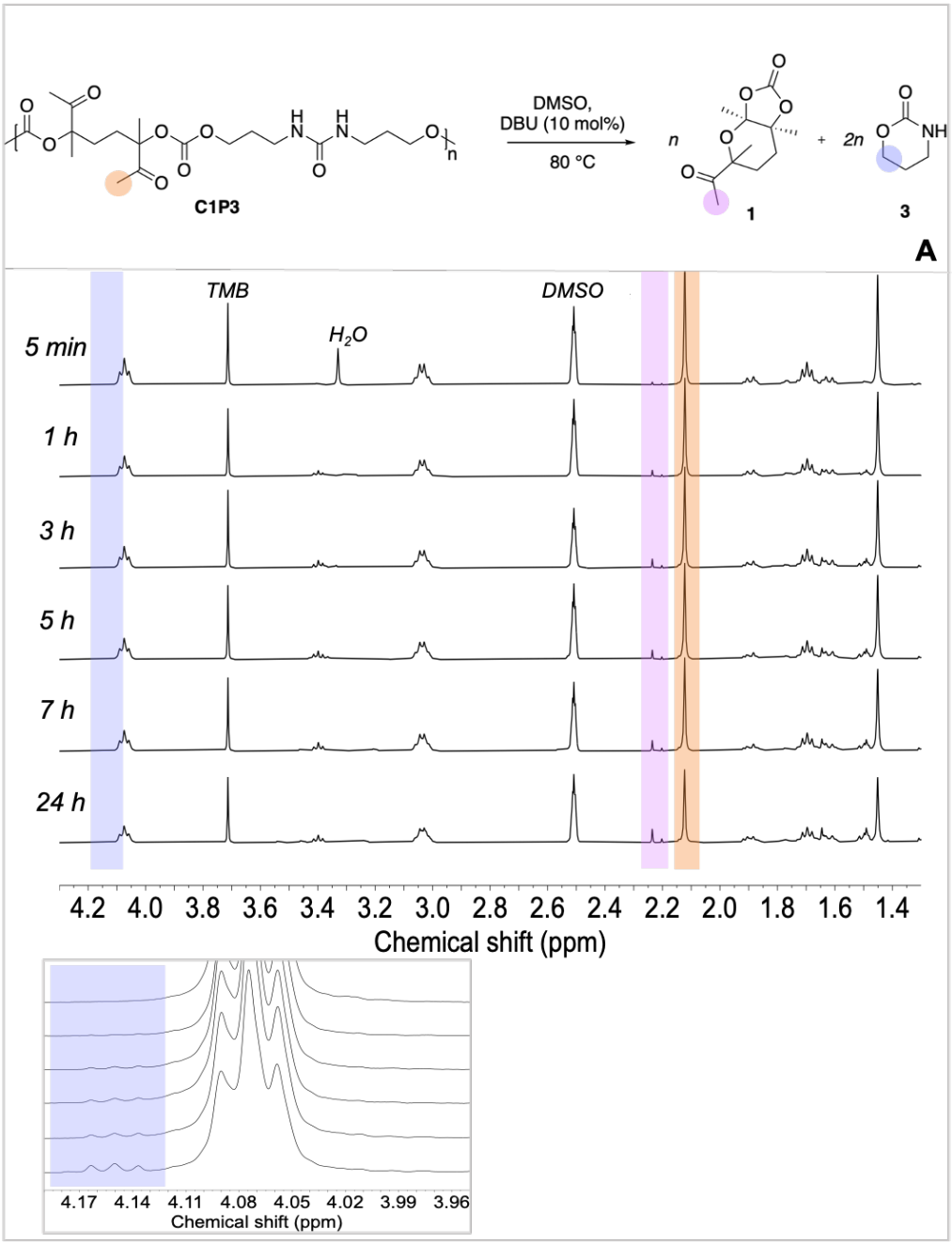

Figure S33. Kinetics of degradation of **C1P3** followed by ^{1}H-NMR (in DMSO-d_6) and magnification of the peak at 4.15 ppm relative to the formation of compound **3**. The reaction was conducted at 80 °C in presence of DBU (10 mol% *vs* polymer repeating unit), using 1,3,5-trimethoxybenzene (TMB) as internal standard.

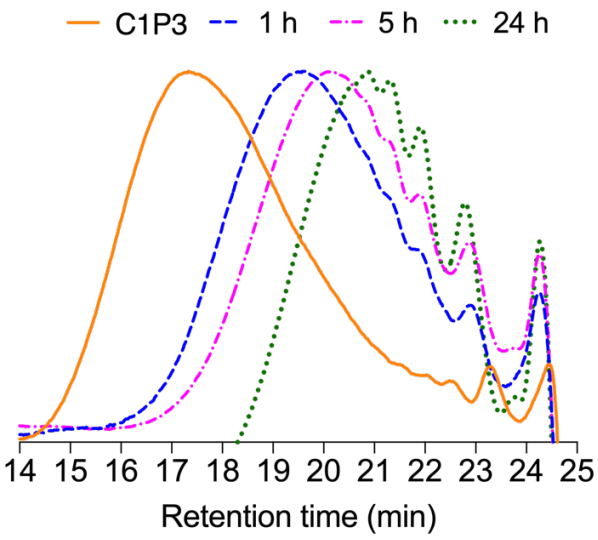

Figure S34. Time evolution of the SEC of **C1P3** upon deconstruction (recorded in DMF/LiBr). The reaction was conducted at 80 °C in the presence of DBU (10 mol% *vs* polymer repeating unit), using 1,3,5-trimethoxybenzene (TMB) as internal standard.

Characterizations of 1,3-oxazinan-2-one (product 3)

^{1}H NMR (400 MHz, DMSO-d_6): δ = 7.14 ppm (s, 1H), δ = 4.18 ppm (t, J= 4 Hz, 2H), δ = 3.15 ppm (td, J= 8, 4 Hz, 2H), δ = 1.83 ppm (m, J= 4 Hz, 2H).

^{13}C NMR (400 MHz, DMSO-d_6): δ = 153.8 ppm, δ = 66.6 ppm, δ = 21.4 ppm.

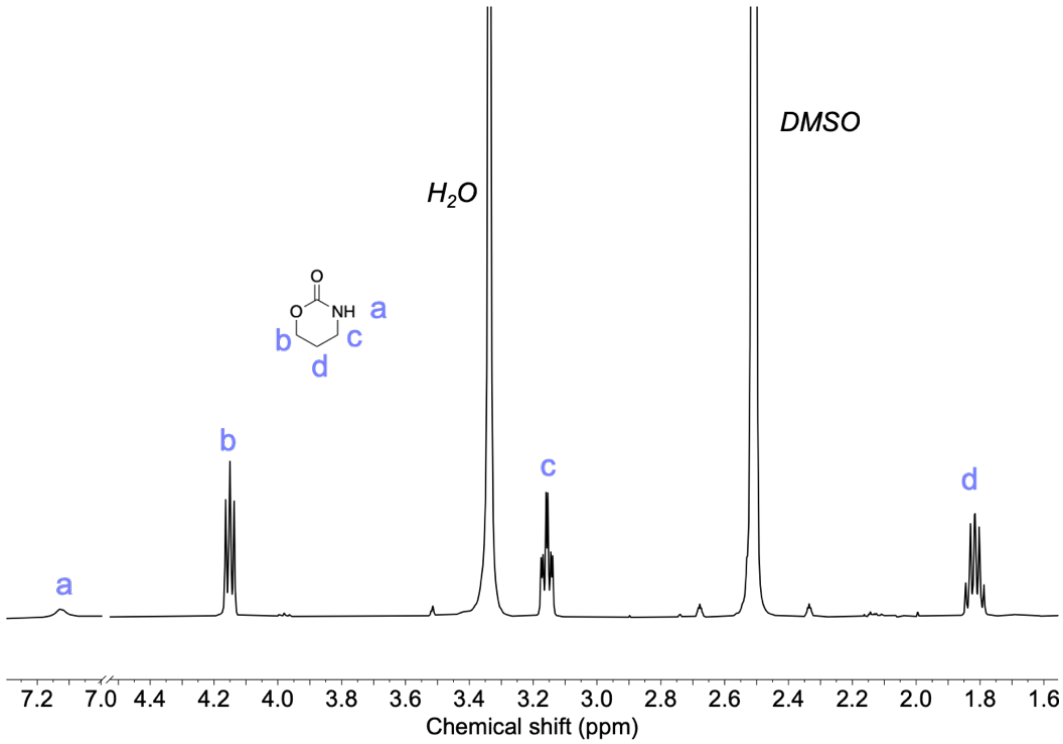

Figure S35. ^{1}H-NMR (in DMSO-d_6) spectrum of purified 1,3-oxazinan-2-one.

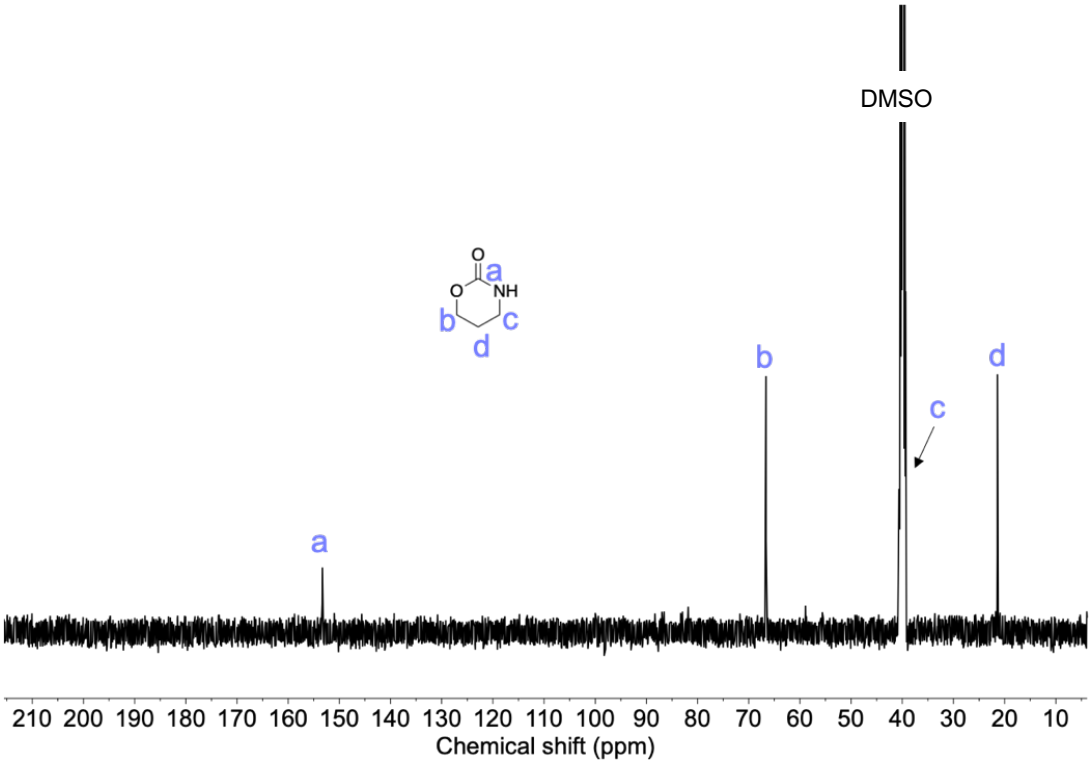

Figure S36. ^{13}C-NMR (in DMSO-d_6) spectrum of purified 1,3-oxazinan-2-one.

Influence of temperature

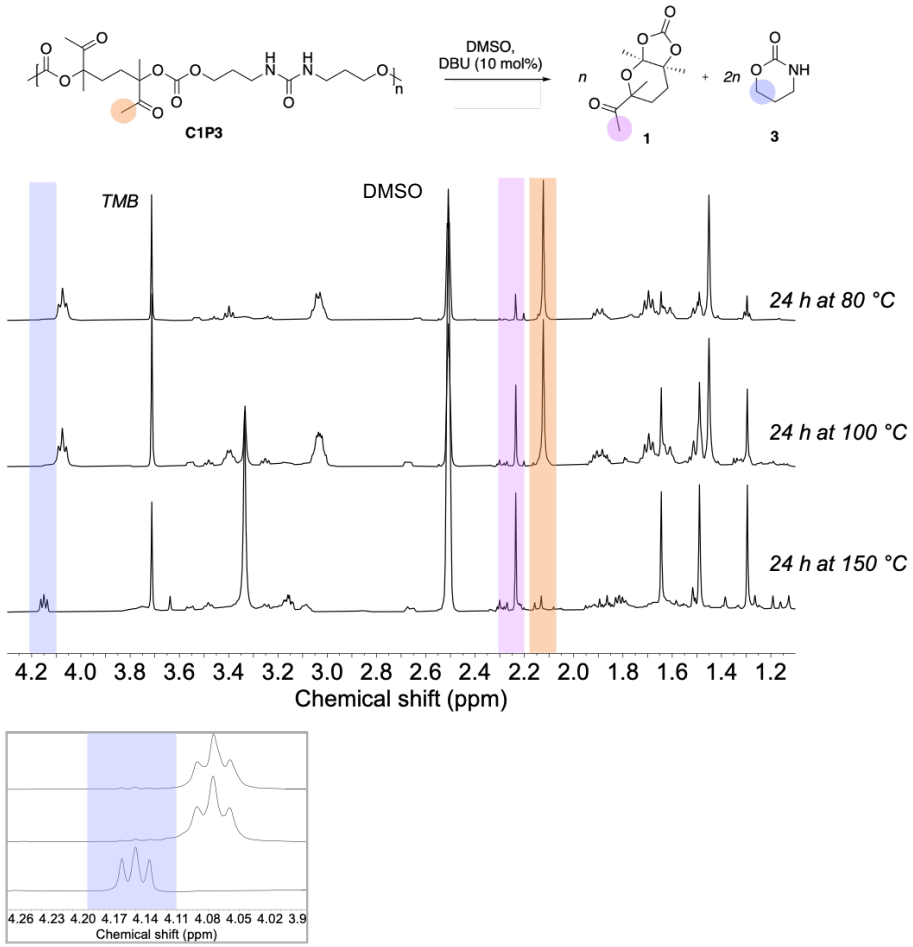

Figure S37. Depolymerization of **C1P3** at 80 °C, 100 °C and 150 °C for 24 h: Overlay of the crude ^{1}H-NMR spectra (in DMSO-d_6) and magnification of the peak at 4.15 ppm relative to the formation of compound **3**. The reaction was conducted in the presence of DBU (10 mol% *vs* polymer repeating unit), using 1,3,5-trimethoxybenzene (TMB) as internal standard.

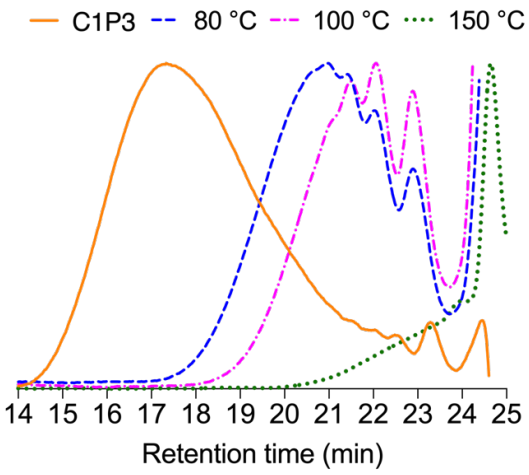

Figure S38. SEC overlays in DMF/LiBr of **C1P3** degradation at different temperatures after 24 h. The reaction was conducted in the presence of DBU (10 mol% *vs* polymer repeating unit), using 1,3,5-trimethoxybenzene (TMB) as internal standard.

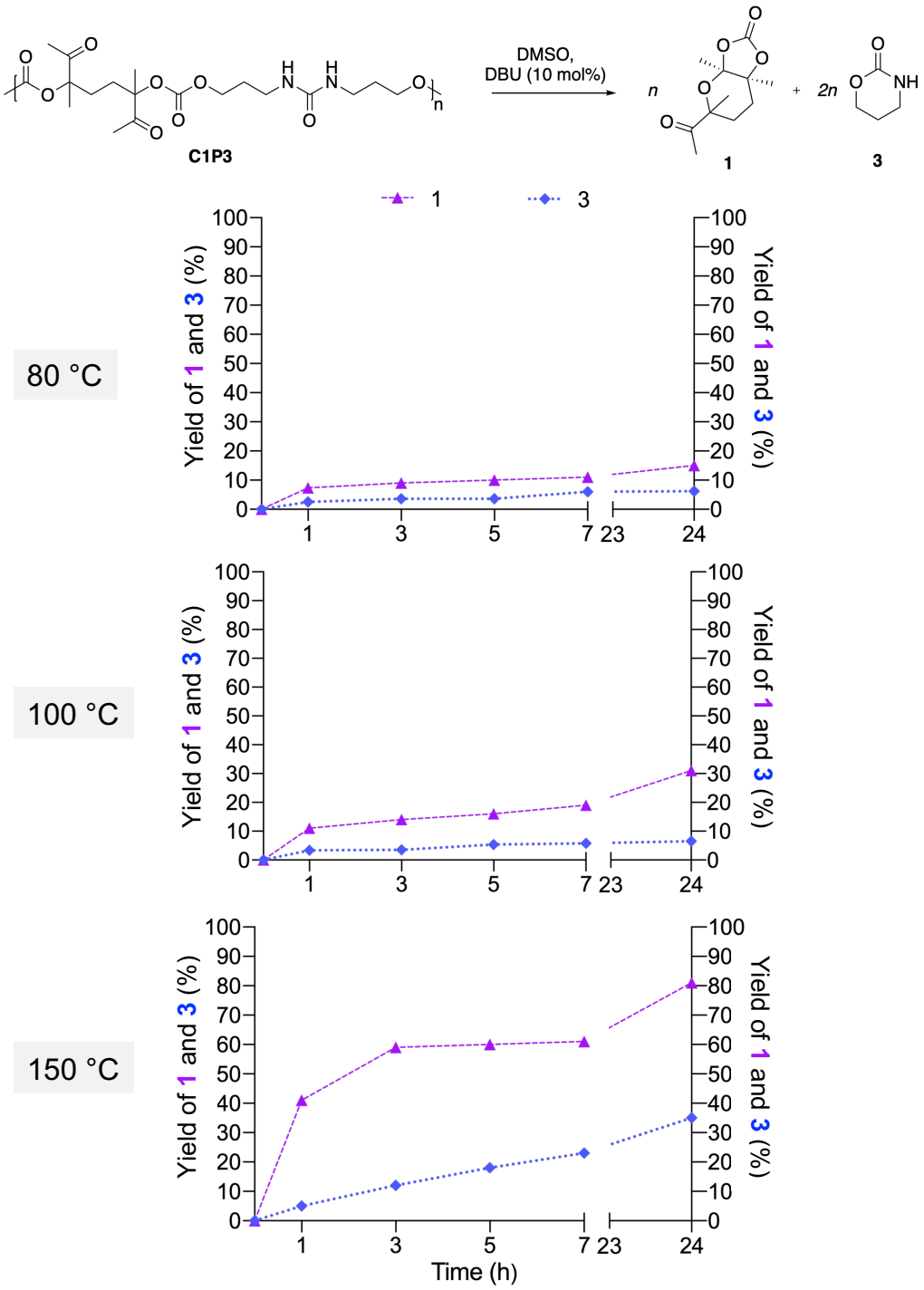

Figure S39. Temperature dependence on the yields of formation of products **1** and **3** for the **C1P3** deconstruction at 80 °C, 100 °C and 150 °C.

Ring-closing depolymerization under other conditions

-Depolymerization in presence of water

The polymer degradation was carried out following the same procedure described above and adding water (5 wt% compared DMSO) in the reaction medium.

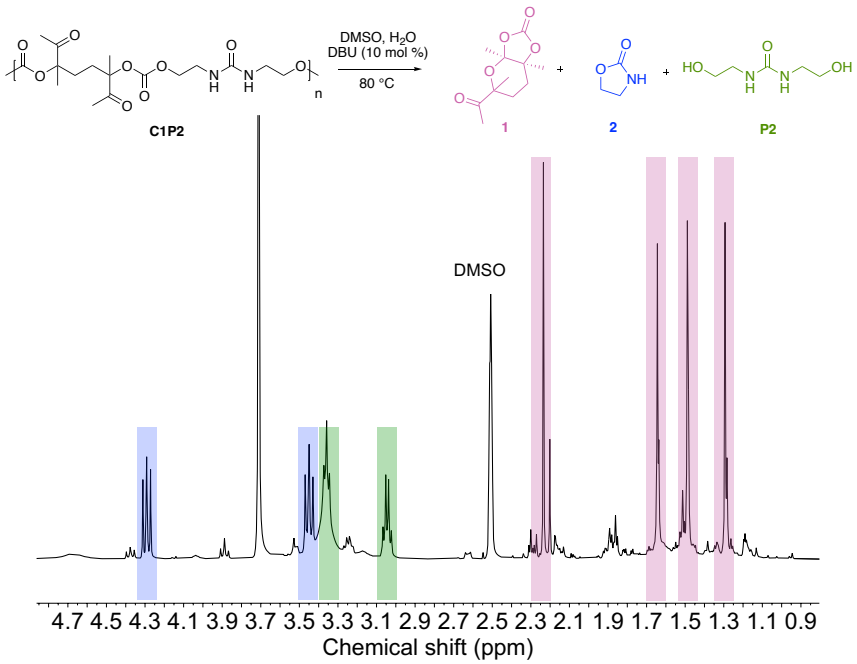

Figure S40. ^{1}H-NMR (in DMSO-d_6) spectrum of **C1P2** degradation after 24 h in presence of water. The reaction was conducted at 80 °C, with DBU (10 mol% *vs* polymer repeating unit), using 1,3,5-trimethoxybenzene (TMB) as internal standard and by adding water (5 % in volume compared DMSO).

-Depolymerization in THF

The polymer degradation was carried out following the same procedure described above by replacing DMSO with THF in the reaction medium. The polymer is insoluble in THF and, in order to determine the percentage of polymer degraded, 100 µL of the suspension was withdrawn and diluted in 700 µL of DMSO-d_6, obtaining a homogeneous solution.

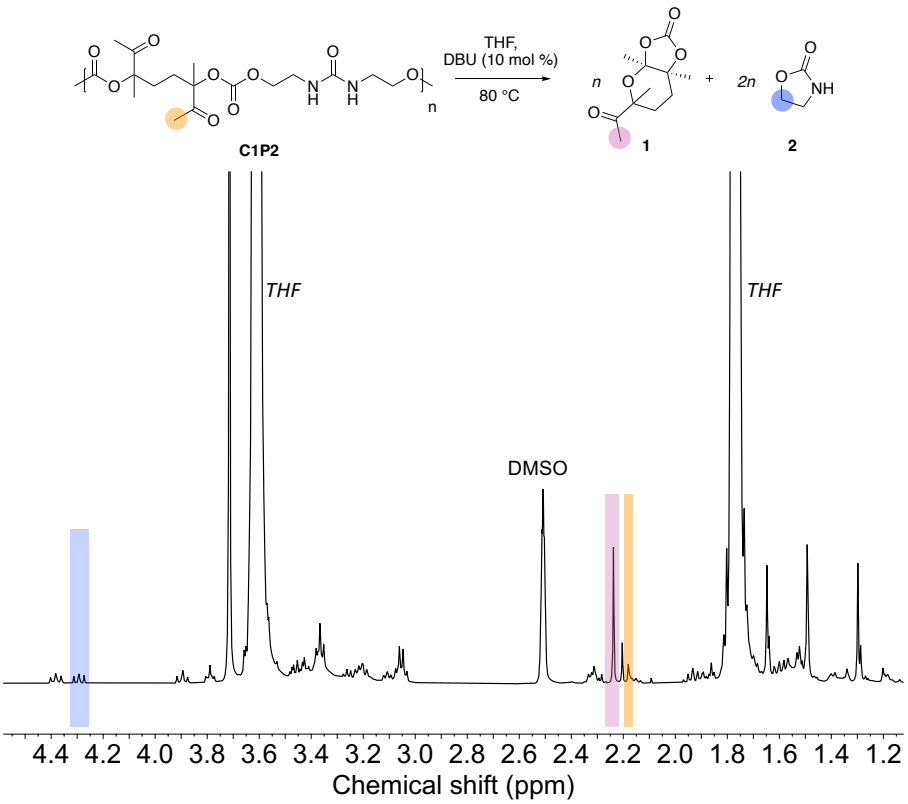

Figure S41. ^{1}H-NMR (in DMSO-d_6) spectrum of **C1P2** degradation after 24 h in THF. The reaction was conducted at 80 °C, with DBU (10 mol% *vs* polymer repeating unit), using 1,3,5-trimethoxybenzene (TMB) as internal standard.

-Depolymerization under neat and catalyst-free condition

The polymer degradation was carried out by adding the 10 mg of polymer in a sealed pot and let to react for 2 h, under neat condition, at 150 °C. The polymer degradation and the yields were calculated by using TMB as standard.

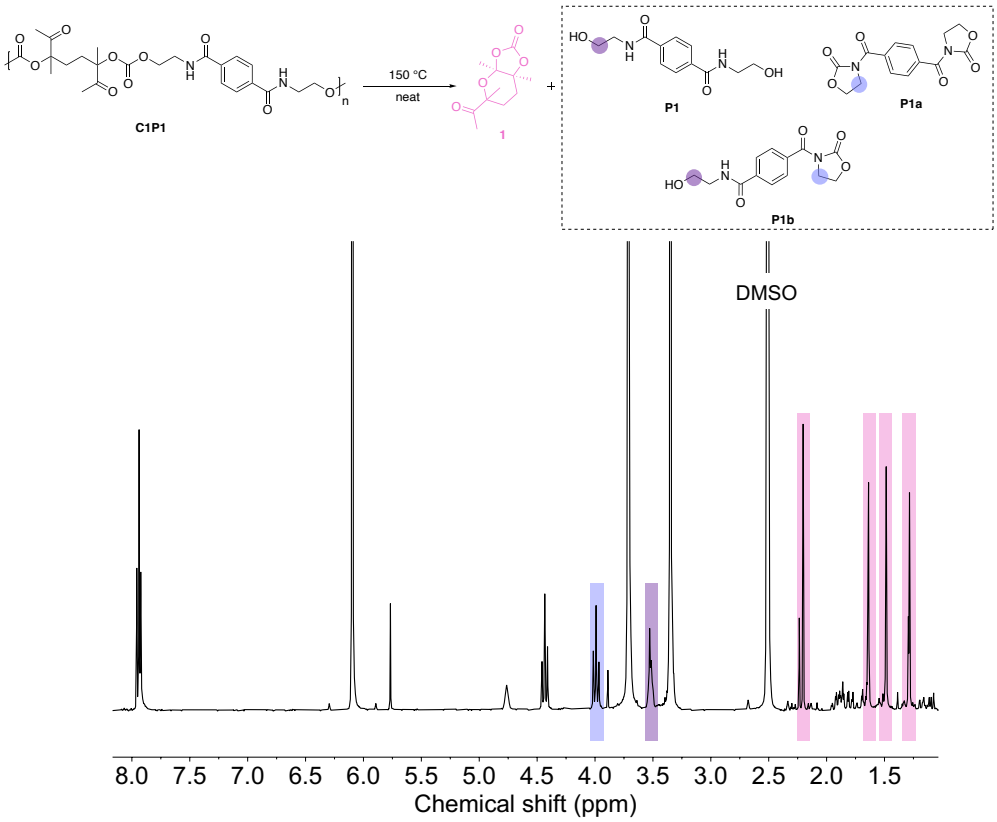

Figure S42. ^{1}H-NMR (in DMSO-d_6) spectrum of **C1P1** degradation after 2 h. The reaction was conducted at 150 °C, without catalyst, under neat condition.

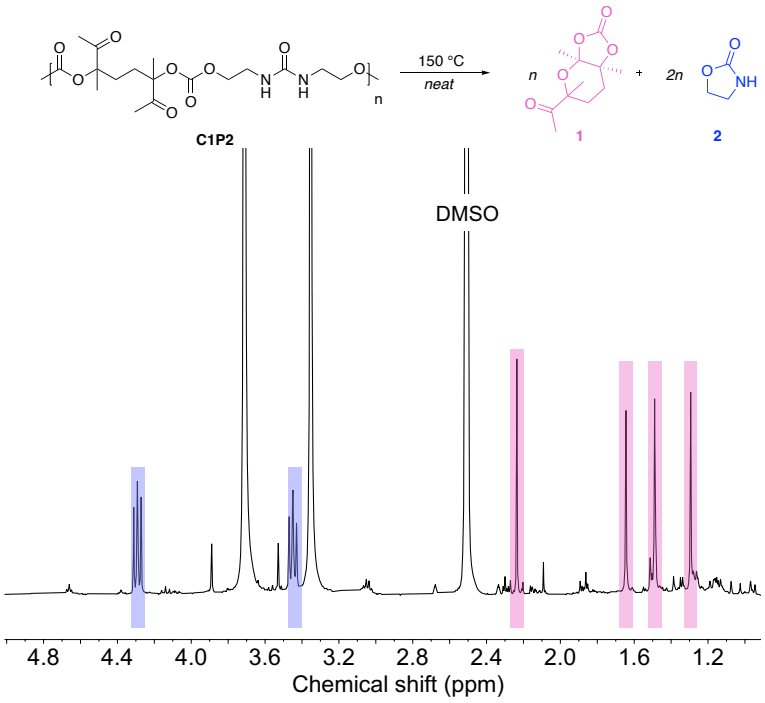

Figure S43. ^{1}H-NMR (in DMSO-d_6) spectrum of **C1P2** degradation after 2 h. The reaction was conducted at 150 °C, without catalyst, under neat condition.

Mechanistic insight of the DBU-catalyzed model reactions mimicking the C1P2 formation and its ring-closing depolymerization processes.

Computational details

Preliminary calculations of equilibrium structures were performed using a semi-empirical model (AM1-D3H4)[5,6] to determine the most stable conformations. These semi-empirical calculations were performed using the AMPAC software.[7] The CHAIN algorithm[8] was used for locating intermediates and transition states along the reaction path. The lowest energy structures obtained at the AM1-D3H4 level were further investigated using the Density Functional Theory method (DFT) implemented in the Gaussian 16 package.[9] DFT calculations of geometries, energies, and vibrational frequencies reported in this paper were carried out with the M06-2X functional[10] using the 6-311G(d,p) basis set. All frequencies of each structure have also been calculated to verify the presence of a single imaginary frequency for transition states and the absence of imaginary frequency for ground states. The intrinsic reaction coordinate (IRC) method has been used to verify that the obtained transition states were effectively connected to the desired minima. For all catalysts, a wide range of possible configurations and interactions have been modelled and the more stable of them are
Figures S44-S45 and S50 and S52 depict the Gibbs free energy profile for the different model reactions investigated and the Gibbs free energy of each structure is relative to the sum of the individual Gibbs free energies of the reactants for each pathway. For the sake of comparisons between the different systems, the starting point energies for all systems coincide with zero energy.

Polymerization

As shown on the Figure S44, starting from a 5-membered cyclic carbonate (5CC), i.e. 4,4-dimethyl-5-methylidene-1,3-dioxolan-2-one, and 1-(2-hydroxyethyl)-3-methylurea in the presence of DBU as catalyst, the overall reaction proceeds in 3 distinct steps. The first one associated with a barrier height of 10.1 kcal·mol^{-1} sees the attack of the oxygen atom of the alcohol group of the urea molecule on the 5CC's carbon of the carbonate group while the H atom of the alcohol is abstracted by the DBU to produce the intermediate I1 (which appears to be not very stable as it's just 0.1 kcal·mol^{-1} below the TS1). This step is accompanying by hydrogen-bonds between the hydrogen atoms linked to the nitrogen atoms of the urea linkage with the oxygen atom of the carbonate group of 5CC. Secondly, with a barrier height of 4.8 kcal·mol^{-1}, is occurring a ring opening between the C of the former carbonyl and the O adjacent to the C=C of the former 5CC while this O atom recovered the proton of $DBUH^+$ to produce a stable enolate form (I2, -4.9 kcal·mol^{-1}) of the final product. Finally, a costly tautomerization takes place helped by DBU to form the ketone form of the polymer (-12.1 kcal·mol^{-1}). This last

step is the rate determining step of the polymerization process with a barrier height of 26.6 kcal·mol^{-1}.

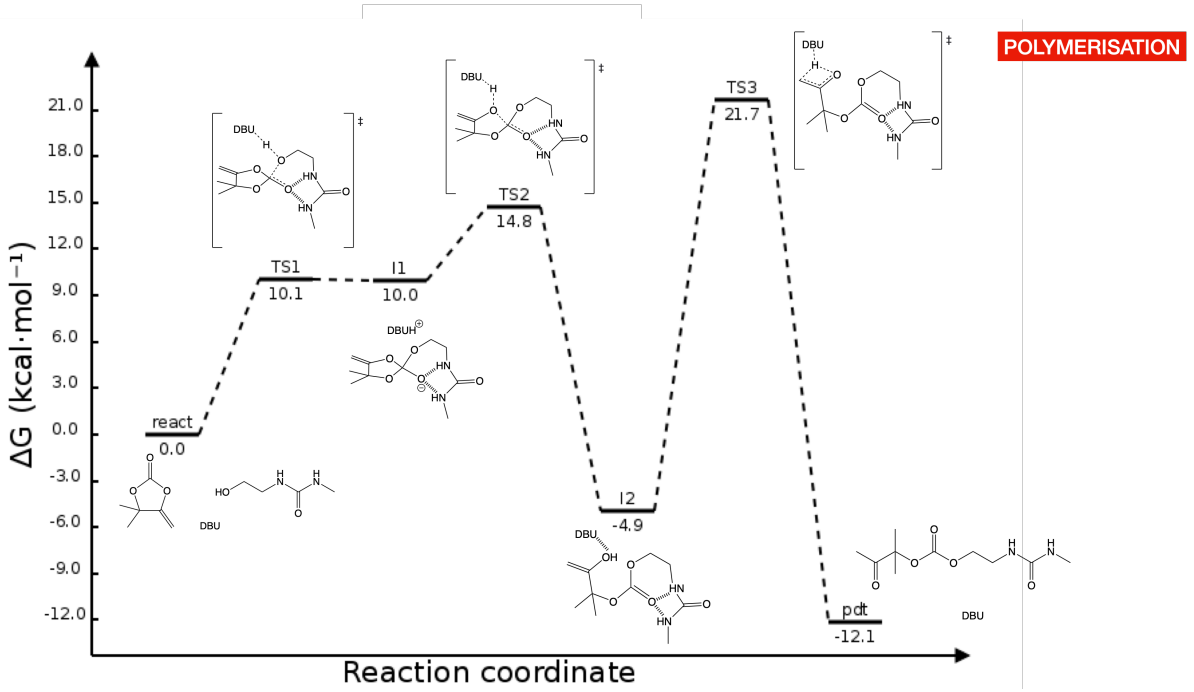

Figure S44. M062X/6-311G(d,p) Gibbs free energy profile for the model reaction of the polymerization process with DBU as catalyst.

Depolymerization

Chain Scission

The polymer degradation is initiated by a chain scission as depicted on Figure S45 on a model polymer. It proceeds in 2 steps. First, for a cost of 28.1 kcal·mol^{-1}, there is attack of the terminal N atom on the carbon atom of the carbonate group while its H atom is transferred to DBU to produce I1 (+8.3 kcal·mol^{-1}). Then, via TS2 (barrier height of 17.3 kcal·mol^{-1}), the system sees the departure of the leaving group ($CH_3C(=O)C(CH_3)_2O^-$) which recovers the proton of $DBUH^+$ to form an N- carbamoyl-oxazolidinone-like fragment as well as a hydroxyl-terminated moiety (-7.5 kcal/mol).

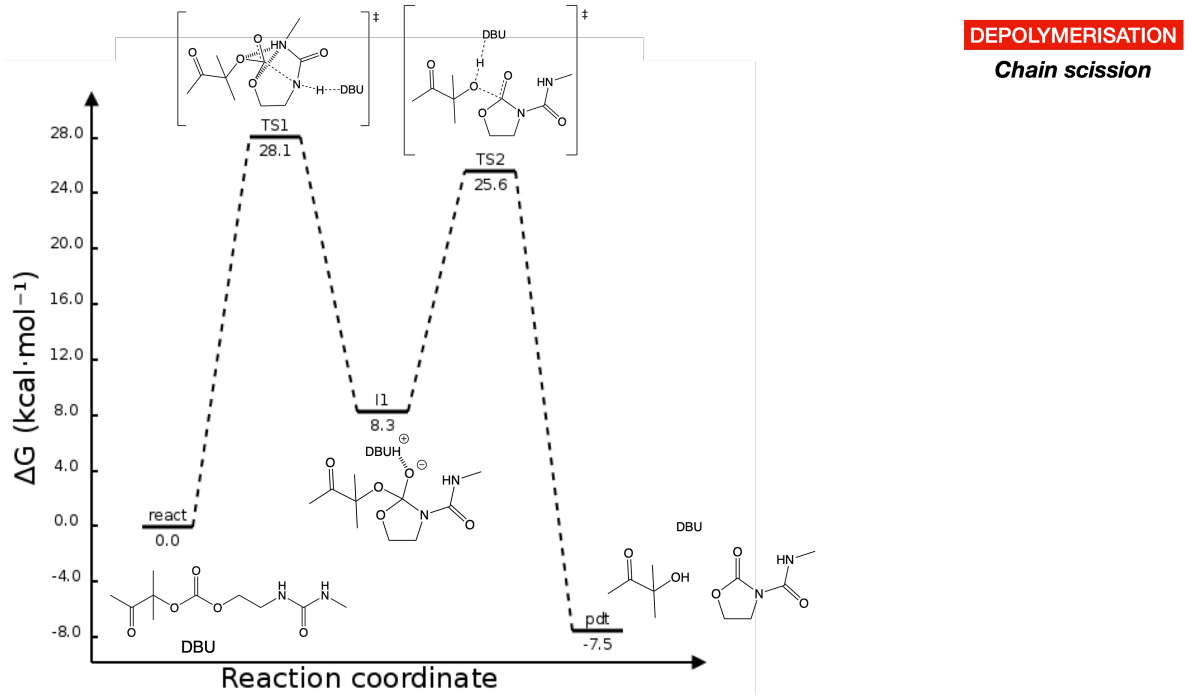

Figure S45. M062X/6-311G(d,p) Gibbs free energy profile for the model reaction of the chain scission with DBU as catalyst.

Monitoring of the DBU-urea interaction

We studied how DBU triggered the polymer degradation and more particularly the first step of the process (i.e. the chain scission) by activating the secondary NH groups of urea. To probe this interaction, a ^{1}H-NMR titration was carried out on a mixture consisting of DBU and a model urea, diethylurea (DeU). Figure S46 shows that the chemical shift of NH group increased with the content of DBU, demonstrating the hydrogen-bonding interaction between the urea moieties and DBU, and supporting the DBU-promoted activation of urea for the nucleophilic attack.

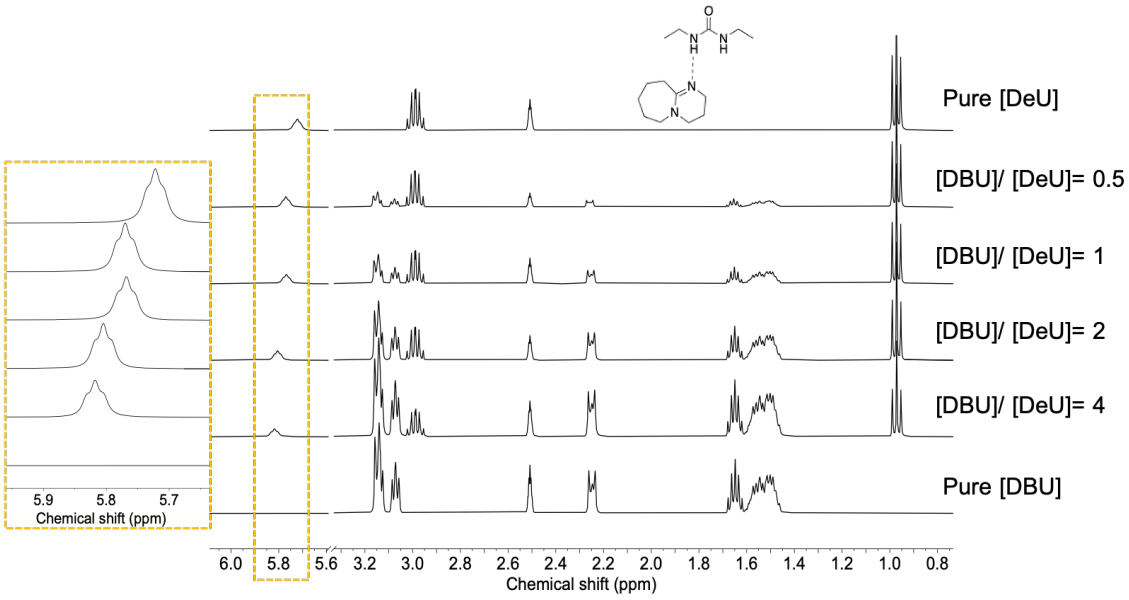

Figure S46. ^{1}H-NMR (in DMSO-d$_6$) titration of diethylurea (DeU) by DBU.

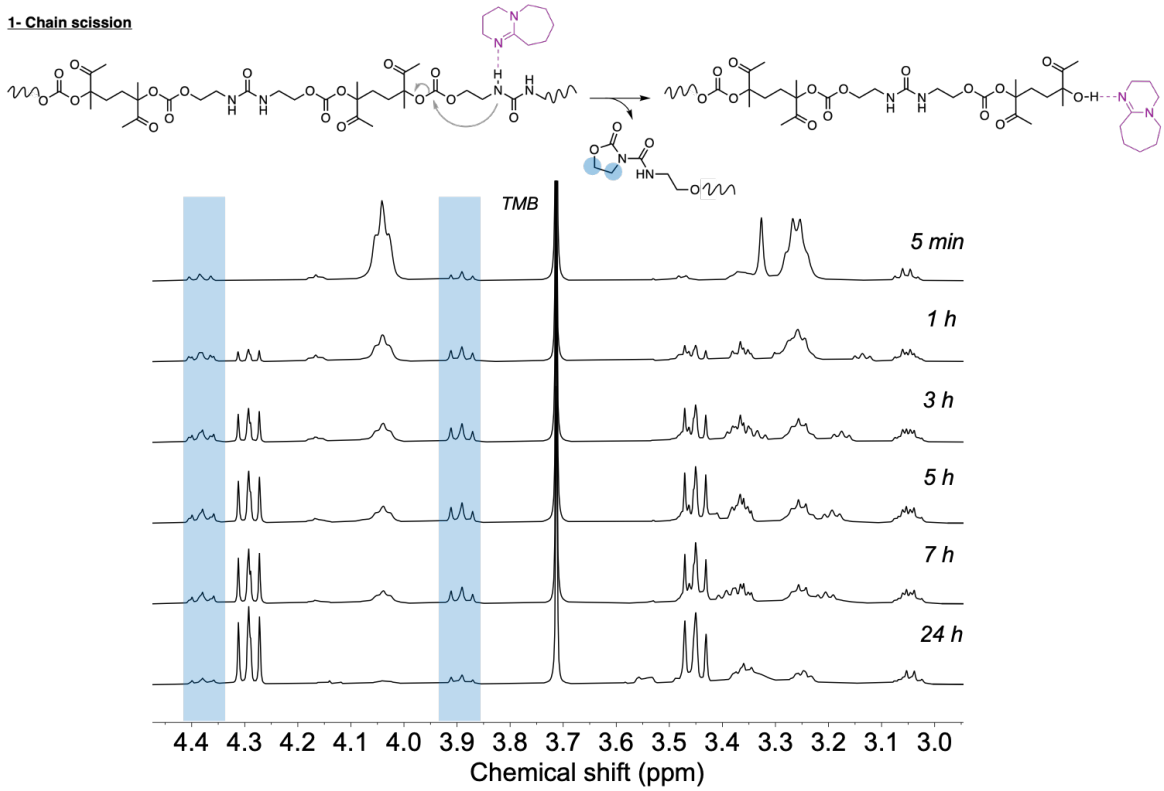

Figure S47. Highlights of the *N*-carbamoyl-oxazolidinone chain end created after scission of **C1P2** via ^{1}H-NMR (in DMSO-d$_6$, blue peaks).

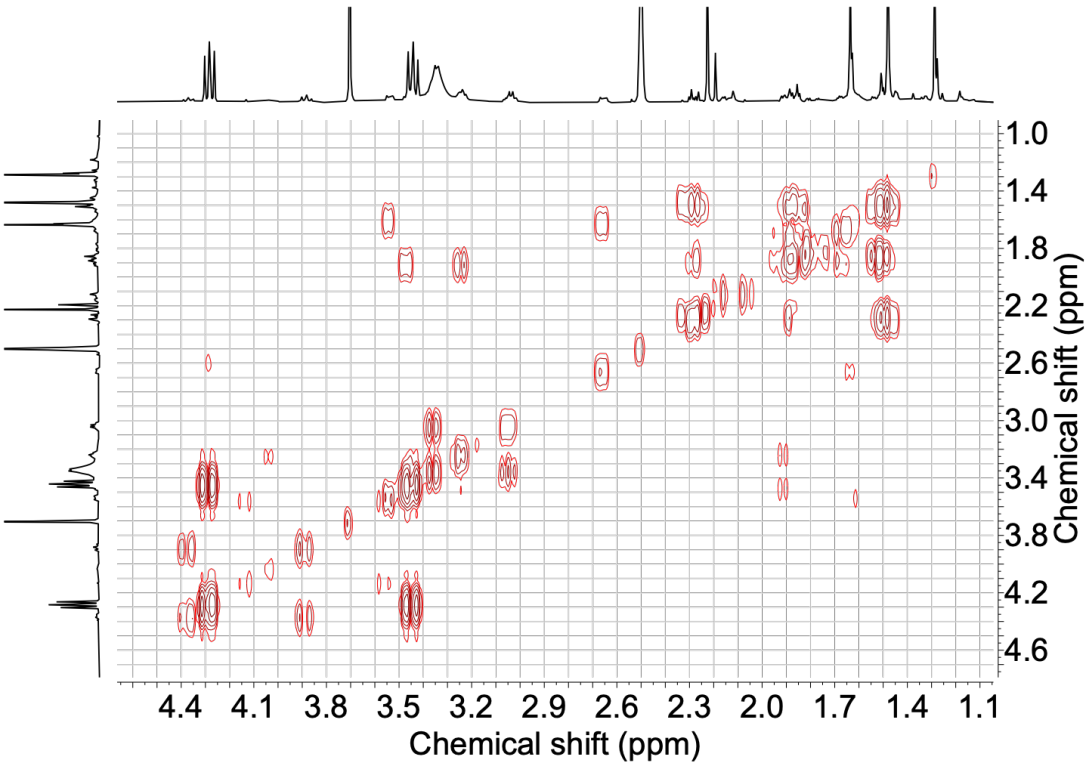

Figure S48. ^{1}H-^{1}H-COSY NMR (in DMSO-d_6) of **C1P2** degradation.

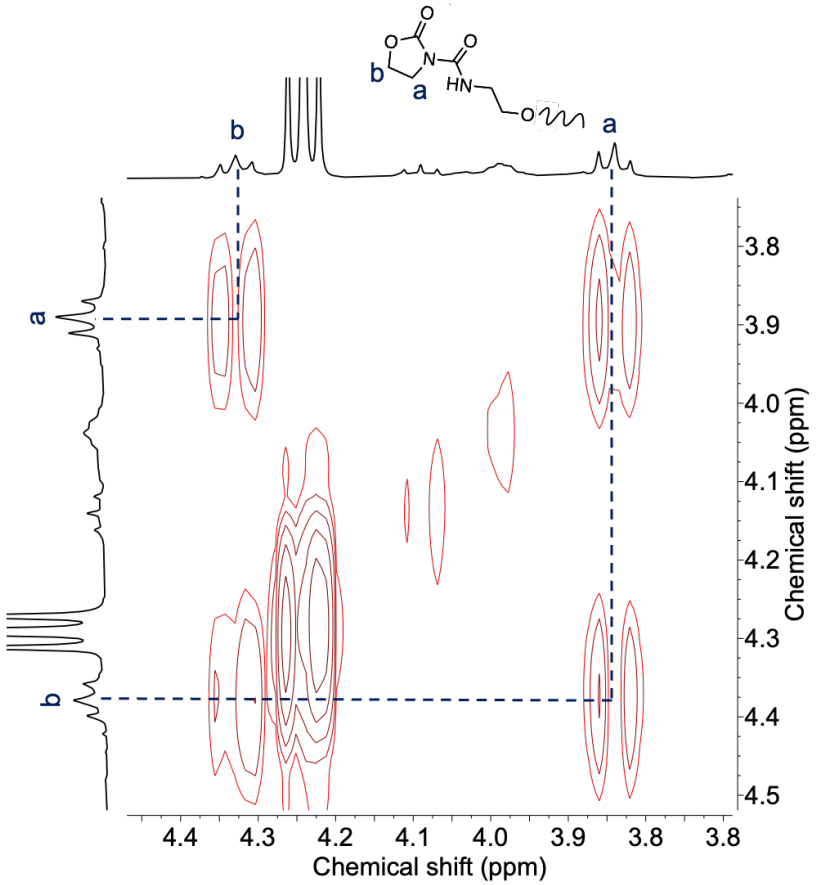

Figure S49. Highlights of the N-carbamoyl-oxazolidinone chain end created after scission of **C1P2** via ^{1}H-^{1}H-COSY NMR (in DMSO-d_6) reported in Figure S48. Magnification of the correlation of *N*-carbamoyl-oxazolidinone protons.

*Chain unzipping - formation of the bicyclic compound **1**.*

The hydroxyl-terminated polymer moiety resulting from chain scission degradation undergoes further deconstruction by a chain unzipping process which was mimicked on a model system shown in Figure S50. First, there is a formation of the 6-membered cycle via TS1 (8.3 kcal·mol^{-1}) (Figure S51-A) which sees a H-abstraction of the alcohol group by DBU accompanied by the attack of the O atom on the carbon atom of the carbonyl group. The produced intermediate I1 (+8.0 kcal·mol^{-1}) undergoes a rapid transformation via TS2 (Figure S51-B) associated with a barrier height of 0.7 kcal.mol^{-1} where takes place a ring closure of the 5- membered cycle by attack of the alkoxide on the carbon atom of the carbonate group to form the intermediate I2 (+6.3 kcal·mol^{-1}). The third and final step (Figure S51-C) (barrier height of 8.6 kcal·mol^{-1}) is the departure of the ethoxy group linked to the carbon atom of the carbonate coupled with a H-transfer from DBUH^{+} to form ethanol and the bicyclic carbonate.

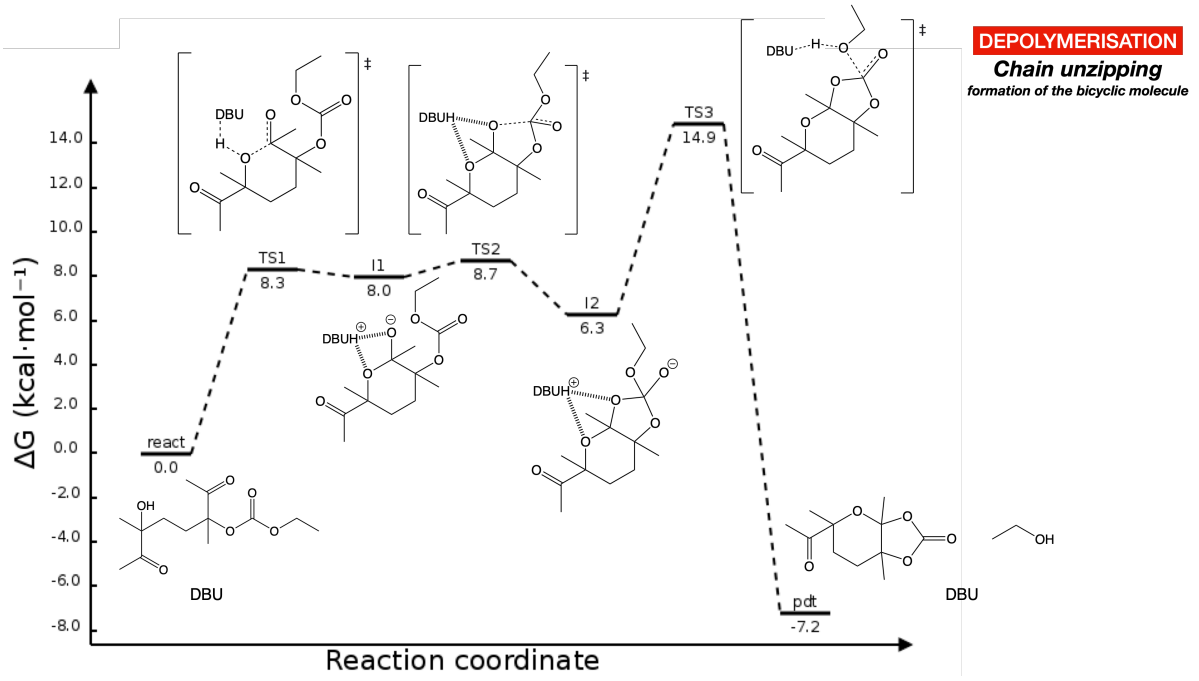

Figure S50. M062X/6-311G(d,p) Gibbs free energy profile for the model reaction of the chain unzipping (formation of the bicyclic compound) with DBU as catalyst.

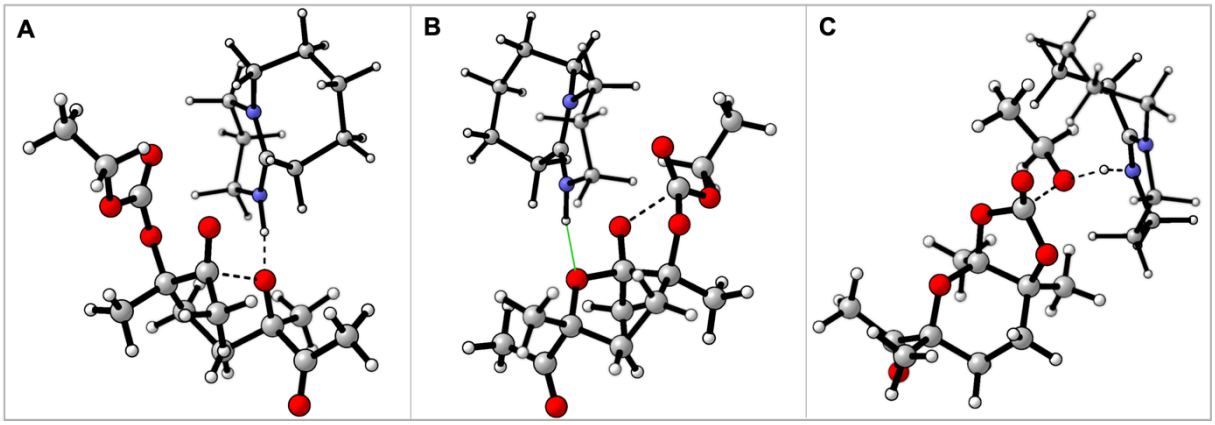

Figure S51. Geometries of (A) the transition state **TS 1**, (B) the transition state **TS 2** and (C) the transition state **TS 3**.

*Chain unzipping - formation of 2-Oxazolidinone **2***

After the release of the bicyclic compound, the resulting polymer chain is endowed with a primary alcohol termination which attacks the urea linkage as depicted in Figure S52 to form a cyclic reaction intermediate I1 (+15.7 kcal·mol^{-1}). This first step exhibits a significant barrier height of 33.8 kcal·mol^{-1}. In a second time and with a barrier height of 18.5 kcal.mol^{-1}, the intermediate I1 undergoes a second cyclization where the off-cycle nitrogen atom reacts with the carbon of the carbonate group while the DBU tears the hydrogen from the hydroxyl group carried by the first 5-membered cycle. It leads to the reaction intermediate I2 (+14.7 kcal·mol^{-1}) where an oxazolidinone interacts by double H-bonding with the 5-membered cycle termination of the remaining chain. The last step is the departure of the hydroxy ketone which recovers the proton from DBUH^{+} (barrier height of 1.8 kcal·mol^{-1}) to produce a new oxazolidinone.

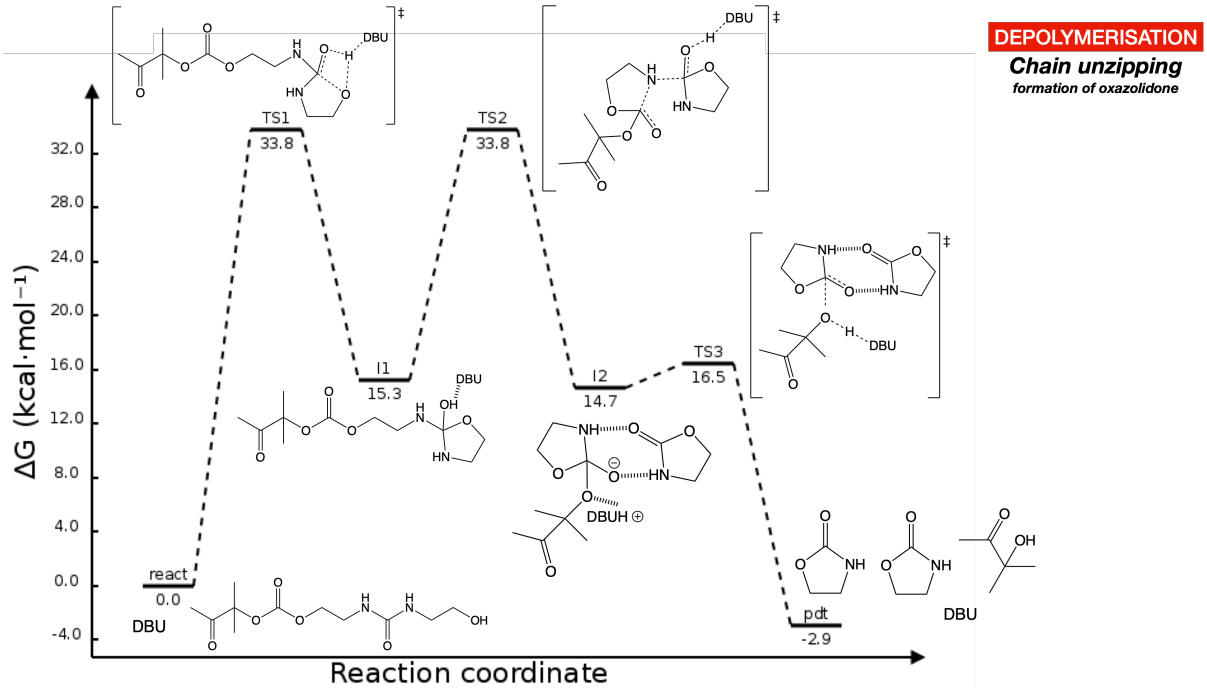

Figure S52. M062X/6-311G(d,p) Gibbs free energy profile for the model reaction of the chain unzipping (formation of oxazolidinone) with DBU as catalyst.

For the Optimized Cartesian Coordinates, please, refer back to the article:

Macromolecules 2022, 55,11, 4637–4646.

Selective degradation of polymer mixtures

C1P2 (250 mg, 0.621 mmol), polycaprolactone (PCL) pellets (M_n of 36,300 g/mol, M_w 73,300 g/mol, PDI 2, determined by SEC in THF, with -OH chain ends groups) (70 mg, 0.621 mmol), dry DMSO (1.25 mL), 1,3,5-Trimethoxybenzene (TMB) (25 mg) and DBU (10 mol% vs polymer repeating unit, 9.5 µL) were added in a flask under nitrogen at 80 °C, for 24 h. At the end of the reaction, an aliquot was withdrawn to determine the polymer degradation by ^{1}H-NMR spectroscopy in DMSO-d_6. It has to be noted that, while at 80 °C the reaction medium was homogeneous, PCL is not soluble in cold DMSO. Then it was necessary to analyze the crude of the reaction in $CDCl_3$. The PCL was purified by dialysis in chloroform for 24 h. The solvent was then removed by rotavapor and the polymer further vacuum dried before analysis by ^{1}H-NMR spectroscopy and SEC in THF. The selective degradation using PET instead of PCL was carried out using the same reaction condition reported for PCL. At the end of the reaction, an aliquot was withdrawn to determine the polymer degradation by ^{1}H-NMR spectroscopy in DMSO-d_6. The PET was recovered by filtration, washed with methanol and dried under vacuum.

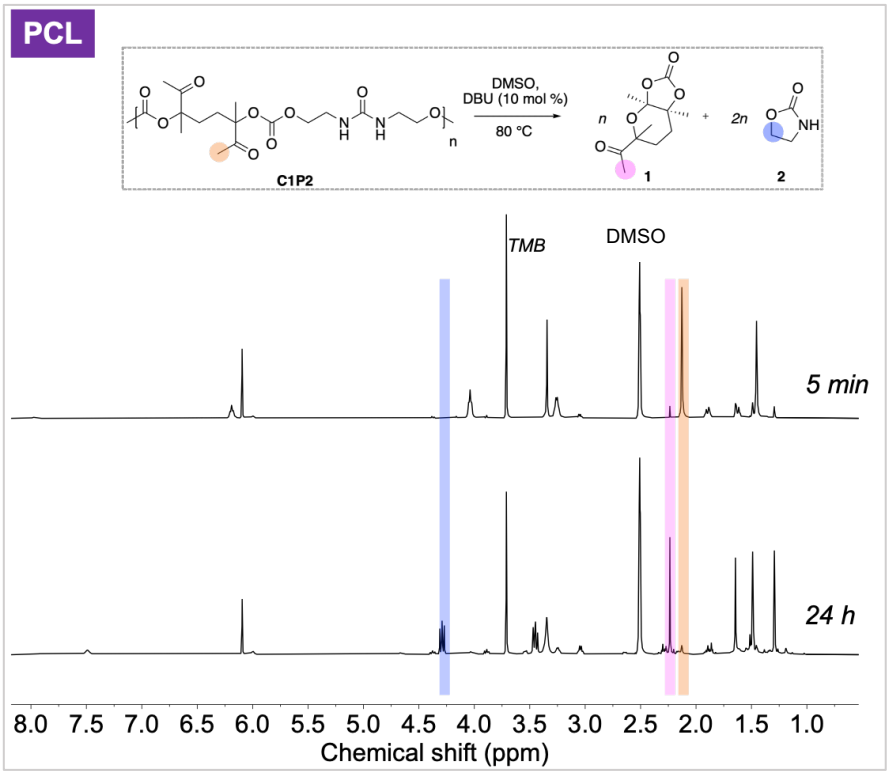

Figure S53. ^{1}H NMR spectra overlay of selective depolymerization of **C1P2** with PCL Capa® 6800 pellets (in DMSO-d_6), after 5 min and 24 h. Note that PCL is insoluble in the reaction media.

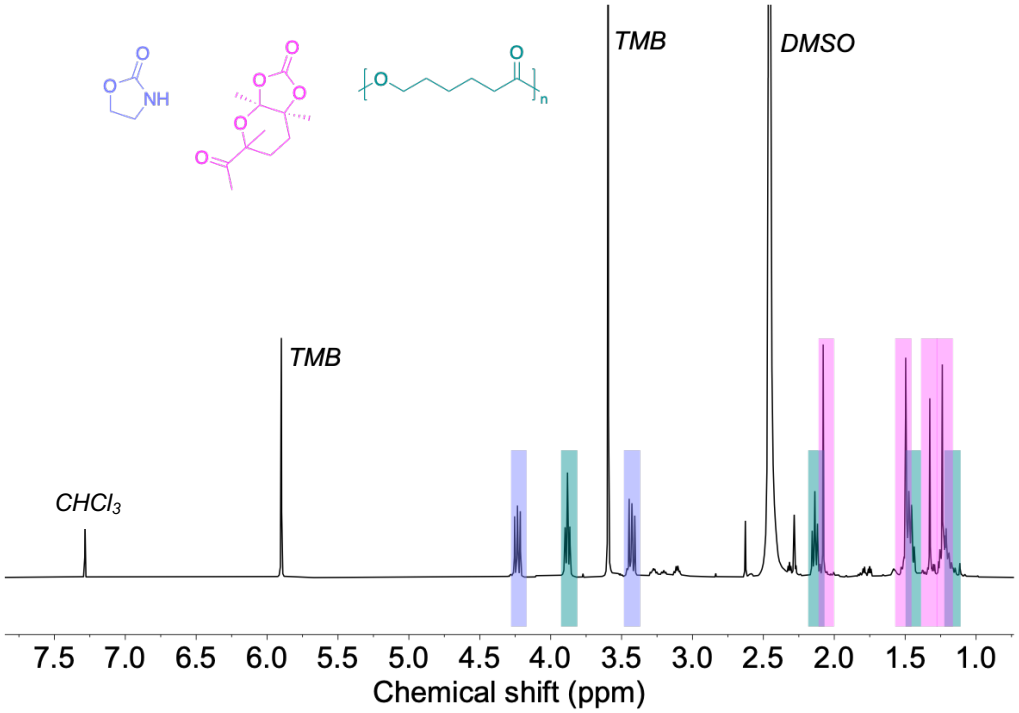

Figure S54. ^{1}H-NMR spectrum of the crude mixture of selective depolymerization of **C1P2** with PCL Capa® 6800 pellets (in $CDCl_3$), after 24 h. Note that PCL chemical shifts are slightly displaced due to the solvent effect between $CDCl_3$ and DMSO.

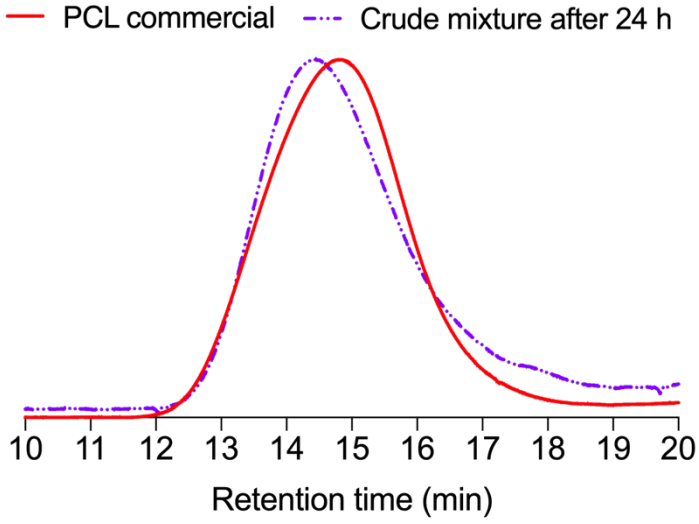

Figure S55. SEC chromatogram overlay in THF of PCL commercial (red line) (M_n 36,300 g/mol, M_w 73,300 g/mol, PDI 2) and of PCL in the selective depolymerization crude mixture, after 24 h, (purple dotted line) (M_n 36,300 g/mol, M_w 72,300 g/mol, PDI 1.98).

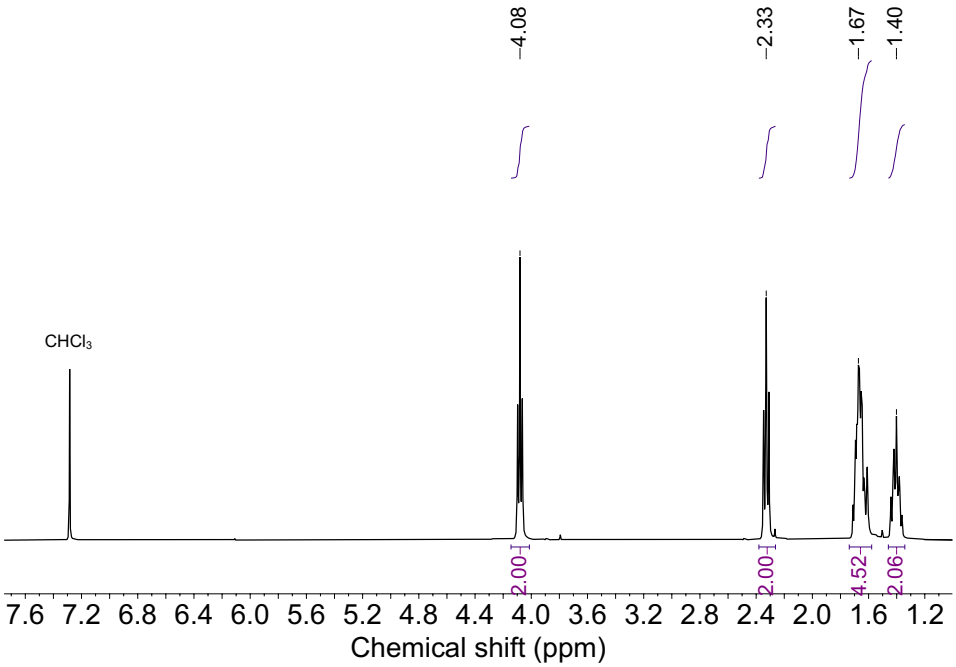

Figure S56. ^{1}H NMR spectrum of purified PCL in $CDCl_3$.

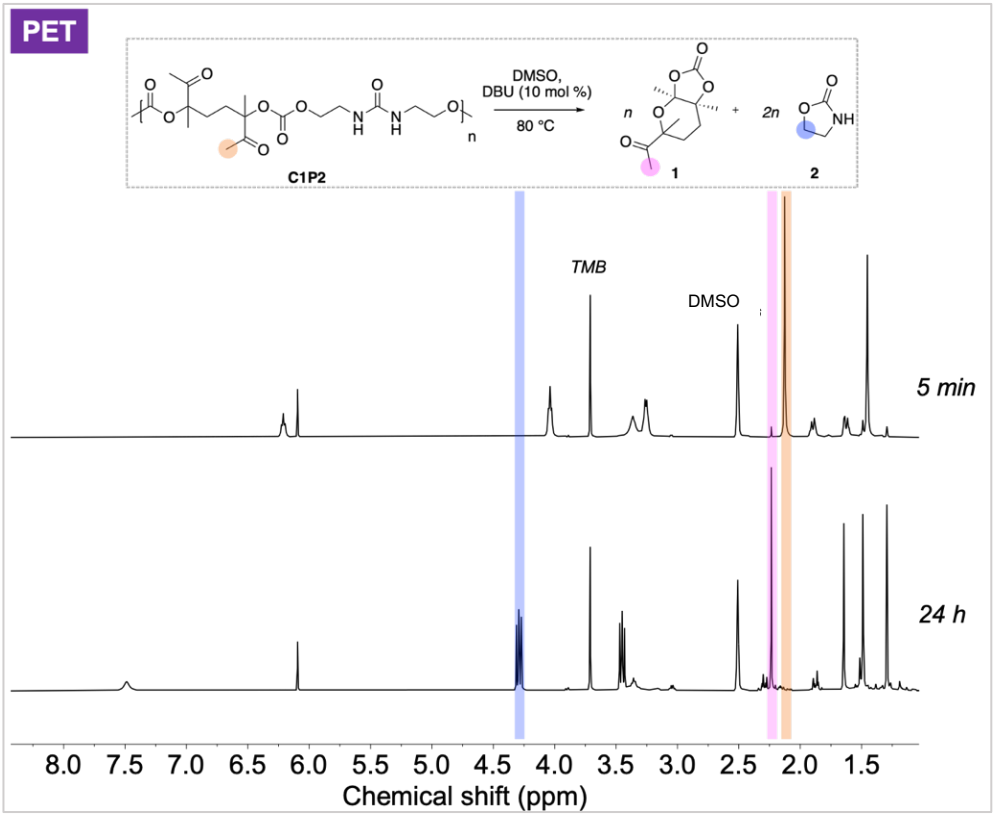

Figure S57. ^{1}H-NMR spectra overlay of selective depolymerization of **C1P2** with PET bottle flakes (in DMSO-d_6), after 5 min and 24 h.

References

(1) Siragusa, F.; van den Broeck, E.; Ocando, C.; Müller, A. J.; de Smet, G.; Maes, B. U. W.; de Winter, J.; van Speybroeck, V.; Grignard, B.; Detrembleur, C. Access to Biorenewable and CO2-Based Polycarbonates from Exovinylene Cyclic Carbonates. *ACS Sustainable Chemistry and Engineering* **2021**, *9*, 1714–1728. https://doi.org/10.1021/acssuschemeng.0c07683.

(2) Jehanno, C.; Demarteau, J.; Mantione, D.; Arno, M. C.; Ruipérez, F.; Hedrick, J. L.; Dove, A. P.; Sardon, H. Synthesis of Functionalized Cyclic Carbonates through Commodity Polymer Upcycling. *ACS Macro Letters* **2020**, *9*, 443–447. https://doi.org/10.1021/acsmacrolett.0c00164.

(3) Sheldrick, G. M. SHELXT - Integrated Space-Group and Crystal-Structure Determination. *Acta Crystallographica Section A: Foundations of Crystallography* **2015**, *71*, 3–8. https://doi.org/10.1107/S2053273314026370.

(4) Sheldrick, G. M. Crystal Structure Refinement with SHELXL. *Acta Crystallographica Section C: Structural Chemistry* **2015**, *71*, 3–8. https://doi.org/10.1107/S2053229614024218.

(5) Dewar, M. J. S.; Zoebisch, E. G.; Healy, E. F.; Stewart, J. J. P. Development and Use of Quantum Mechanical Molecular Models. 76. AM1: A New General Purpose Quantum Mechanical Molecular Model. *Journal of the American Chemical Society* **1985**, *107*, 3902–3909. https://doi.org/10.1021/ja00299a024.

(6) Řezáč, J.; Hobza, P. Advanced Corrections of Hydrogen Bonding and Dispersion for Semiempirical Quantum Mechanical Methods. *Journal of Chemical Theory and Computation* **2012**, *8*, 141–151. https://doi.org/10.1021/ct200751e.

(7) AMPAC 10, © 1992–2013 Semichem, Inc. PO Box 1649, Shawnee, KS 66222. © 1992–2013 Semichem, Inc.: Shawnee.

(8) Liotard, D. A. Algorithmic Tools in the Study of Semiempirical Potential Surfaces. *International Journal of Quantum Chemistry* **1992**, *44* (5), 723–741. https://doi.org/https://doi.org/10.1002/qua.560440505.

(9) Frisch, M. J.; Trucks, G. W.; Schlegel, H. B.; Scuseria, G. E.; Robb, M. A.; Cheeseman, J. R.; Scalmani, G.; Barone, V.; Petersson, G. A.; Nakatsuji, H.; Li, X.; Caricato, M.; Marenich, A. v; Bloino, J.; Janesko, B. G.; Gomperts, R.; Mennucci, B.; Hratchian, H. P. Gaussian 16. *Gaussian, Inc.* Wallingford CT 2016.

(10) Zhao, Y.; Truhlar, D. G. The M06 Suite of Density Functionals for Main Group Thermochemistry, Thermochemical Kinetics, Noncovalent Interactions, Excited States, and Transition Elements: Two New Functionals and Systematic Testing of Four M06-Class Functionals and 12 Other Functionals. *Theoretical Chemistry Accounts* **2008**, *120*, 215–241. https://doi.org/10.1007/s00214-007-0310-x.

Chapter V

Advancing the synthesis of isocyanate-free poly(oxazolidinones)s: scope and limitations

*Thomas Habets, Fabiana Siragusa, Bruno Grignard, Christophe Detrembleur[a]**

Reference: *Macromolecules 2020, 53, 15, 6396–6408.*

https://doi.org/10.1021/acs.macromol.0c01231

Author contributions: T.H., F.S. C.D. and B.G. designed and planned the project. T.H. synthesized and characterized all polymers and carried out all the model reactions. T.H. wrote the manuscript with contributions from all co-authors.

ABSTRACT

Poly(oxazolidone) is an emerging class of polyurethanes (PUs) that is easily accessible by an isocyanate-free pathway via the step-growth copolymerization of CO_2-based monomers (bis(α-alkylidene cyclic carbonate)s) with primary diamines at room temperature. Here, we explore the scope and limitation of this process by investigating the influence of the diamine and the reaction conditions on the structure and macromolecular parameters of the polymer. Less hindered diamines (aliphatic and benzylic) provide selectively poly(hydroxy-oxazolidone)s, whereas the bulkier ones (cycloaliphatic) furnish polymer chains bearing two types of linkages, *oxo*-urethane and hydroxy-oxazolidinone ones. The increase of the reaction temperature or the addition of DBU as a catalyst enables to accelerate the polymerizations. The quantitative polymer dehydration is also achieved by refluxing in acetic acid, providing a new class of unsaturated poly(oxazolidone)s composed of α-alkylidene oxazolidone linkages (for hindered polymers) or a mixture of α- and β-alkylidene oxazolidone linkages (for the less hindered ones). These unsaturated poly(oxazolidone)s present a high glass transition temperature (90 °C ≤ T_g ≤ 130 °C) and a remarkable thermal stability (T_d > 360 °C), rendering these polymers attractive for applications requiring high temperatures. This work is therefore opening an avenue to novel functional isocyanate-free PUs, with the pendant hydroxyl or olefin groups that are expected to be easily derivatized.

Introduction

Polyurethanes (PUs) account for 8 % of the total plastic demand, which corresponds to a production of 16 millions of tons for the world market[1,2]. The industrial production of PUs is based on the polyaddition of diisocyanates with diols,[3,4] with the advantage that many different types of diols (petro- and/or bio-sourced) are accessible at low cost, giving access to cost-effective PUs with a diversified palette of properties[5]. Many types of products can therefore be synthesized by exploiting this chemistry such as thermoplastic elastomers[6,7], foams[8,9] for thermal insulation or comfort, adhesives[10,11] and coatings[12,13] to cite only the most important ones.

Among the PU family, poly(oxazolidinone)s (POxa) that are characterized by 5-membered cyclic carbamate (urethane) linkages have received attention. Their unique chemical inertness, high thermal stability and high glass transition temperature make them ideal candidates for applications as materials requiring high thermal and chemical resistance.[14–20] Unlike conventional PUs, POxa are more challenging to prepare and many of them are found insoluble in common organic solvents, rendering difficult their characterization. As illustrated in Scheme 1a, the most relevant pathway for POxa consists in the polyaddition of diisocyanates with diepoxides at temperature >150-200°C.[21] Under these harsh conditions, the chain propagation was accompanied by major side-reactions causing difficulties to design high molar mass linear polymer chains. These include the thermally favored trimerization of isocyanates into isocyanurates, leading to a deviation of stoichiometry of the reagents and the formation of a cross-linked network.[22] The reactions of isocyanates with some solvents such as DMF to form amidine end-capped POxa chains, or with the catalyst also limited the scope of chemicals that could be used together with the comonomers.[23,24] POxa with ether linkage defects within their microstructure were formed by two or more consecutive chain enchainments involving the epoxide monomers. It should be noted that the reaction furnished two types of oxazolidinone linkages, i.e. 4- and 5-substituted ring, due to the regio-irregular ring-forming step.[24] To surpass these hurdles, Buchmeiser's group developed recently new cooperative catalysts based on a N-heterocyclic carbene and a metal halide to prepare POxa of high molar mass (M_n = 30-50 kg/mol) in sulfolane.[24] However, the process still required high polymerization temperatures (T > 200 °C) and the use of toxic isocyanates. Alternative routes to deliver POxa free of defects under less demanding conditions and without using isocyanates are highly desired. Only few relevant examples can be cited, such as the polycondensation of diurethanes with diepoxides at 90 °C using a tertiary amine as catalyst (Scheme 1b),[14,25] or the copper-catalyzed 4-components reaction between a dialkyne, a diamine, an aldehyde and carbon dioxide at 75-80 °C (Scheme 1c).[26–28] Recently, we reported a novel methodology to fabricate POxa by the facile polyaddition of CO_2-sourced bis(α-alkylidene cyclic carbonate)s

(bisαCCs) with a primary diamine (1,8-octanediamine) (Scheme 1d).[29,30] As the α-alkylidene cyclic carbonate group is highly reactive towards aminolysis, the polymerizations occurred at room temperature under catalyst-free conditions, furnishing unprecedented defect-free and regioregular POxa bearing additional pendant hydroxyl groups, named poly(hydroxy-oxazolidinone)s. Although the proof of concept was validated on a single non-hindered aliphatic primary diamine (1,8-octanediamine), the large diversity of diamines that can potentially be used and the presence of the hydroxyl groups on the polymer backbone easily transformable by chemical modification are offering many unexplored possibilities for the construction of functional poly(oxazolidinone)s under mild experimental conditions. Moreover, as the oxazolidinone linkage originates from a two-step process, i.e. the regioselective aminolysis of the α-alkylidene cyclic carbonate group into the *oxo*-urethane function followed by the spontaneous intramolecular cyclization (Scheme 2), we hypothesized that the structure of the polymer might be tuned by selecting the reaction conditions and the chemical structure of the comonomers. For instance, the cyclization might be slowed down by the use of sterically hindered diamines, leading to POxa bearing both oxazolidinone and *oxo*-urethane linkages.
This work aims at establishing a roadmap of the polymerization features and the structural characteristics of the poly(oxazolidinone)s regarding the nature of the diamines and the reaction conditions. This will open the access to a library of new regioregular isocyanate-free polyurethanes with hydroxyl functionality and/or pendent ketones under mild reaction conditions. Then, the dehydration of the poly(hydroxy-oxazolidinone)s will be investigated to afford a novel class of poly(oxazolidinone)s with exocyclic vinylene functionality, i.e. poly(alkylidene oxazolidinone)s, with remarkable thermal stability. This work clearly highlights the potential of this simple chemistry for the construction of hydroxyl- or olefinic-functional poly(oxazolidinone)s under mild operating conditions.

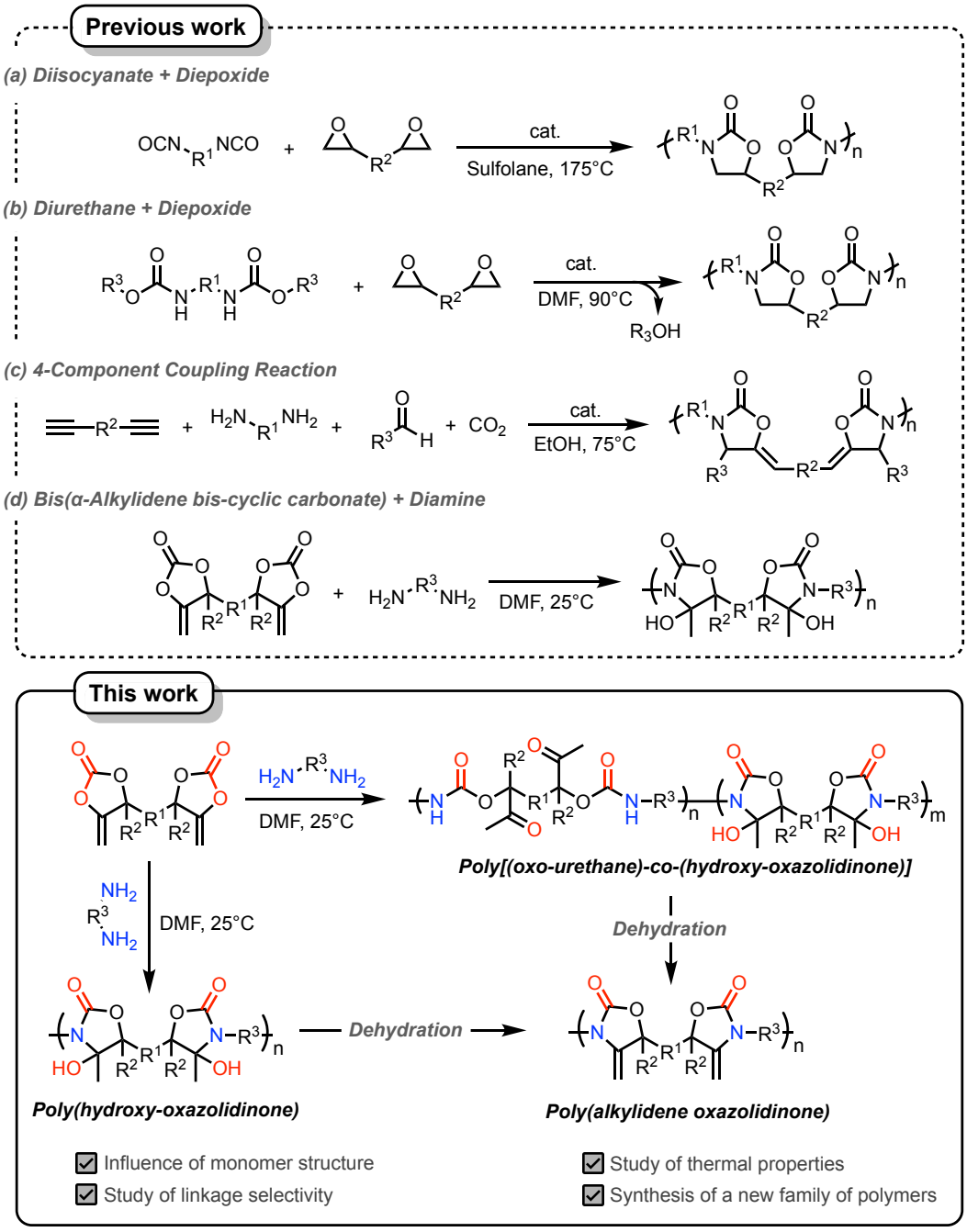

Scheme 1. Main routes towards poly(oxazolidinone)s and scope of this work.

Results and discussion.

In our initial communication highlighting the proof of concept, we introduced the synthesis of poly(hydroxy-oxazolidinone)s from a bis(αCC) (**αCC1**, Scheme 2) and a single primary diamine, the aliphatic primary 1,8-octanediamine (**AA1**), at room temperature for 24 h. To enlarge the scope of the process and get further insights into the microstructural and thermal characteristics of the polymers, we extended the step-growth copolymerization to two bis(αCC)s (**αCC1** and **αCC2**, Scheme 2) with (cyclo)aliphatic and aromatic diamines of different steric hindrance and nucleophilicity such as 1,8-octanediamine **AA1** (as the reference diamine), 1,2-bis(2-aminoethoxy)ethane (Jeffamine EDR-148, **AA2**), 3,3′-Diamino-N-methyldipropylamine (**AA3**), various cyclohexane diamine stereoisomers (**AA4**, **AA5**, and **AA6**) and m-xylylene diamine (**AA7**) (Scheme 2). The cyclohexane diamines stereoisomers and m-xylylene diamine have been selected due to their different stereo-electronic characters, but also because of their possible biorenewable supply from lignin-fractionation and derivatization.[32,33] To understand how the amine may influence the aminolysis rate of α-alkylidene cyclic carbonate and the subsequent cyclization step, model reactions were first investigated on monofunctional organic molecules before implementing the optimal conditions to the polymerization (Scheme 2).

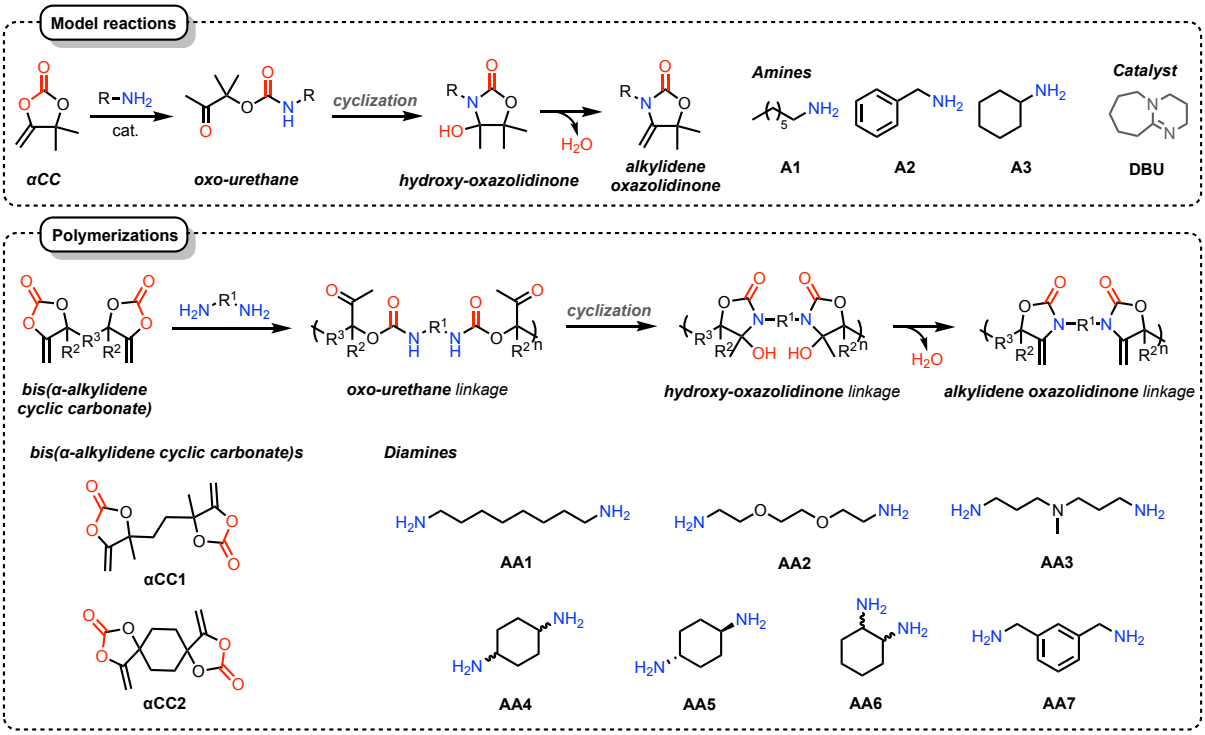

Scheme 2. Substrate scope for the model reaction of **αCC** with several amines and for the polyaddition of bis(α-alkylidene cyclic carbonate)s to diamines.

Model reactions

The DBU-catalyzed aminolysis of the model α-alkylidene cyclic carbonate, 4,4-dimethyl-5-methylene-1,3-dioxolan-2-one (**αCC**), by heptylamine **A1** (as the reference amine), benzylamine **A2** and cyclohexylamine **A3** was first investigated (Scheme 2). The reagents were used in stoichiometric conditions (in order to mimic the polymerization conditions) in DMF (C = 3.90 M) at 25 °C. It should be noted that experiments involving the aromatic amine **A2** were studied in a twice more diluted medium (C = 1.95 M) since the obtained product presented a low solubility in DMF. For a fair comparison of the different amines, this model reaction was also achieved under identical reaction conditions for heptylamine **A1**. The kinetics of the model reactions were monitored by ^{1}H-NMR spectroscopy. All aliquots were quenched by the addition of one drop of acid to protonate the amine before storage at -20 °C.

Figure 1 summarizes both the **αCC** conversion and selectivity for the *oxo*-urethane **1** and the hydroxy-oxazolidinone **2** regarding the amine scope (**A1**-**3**).

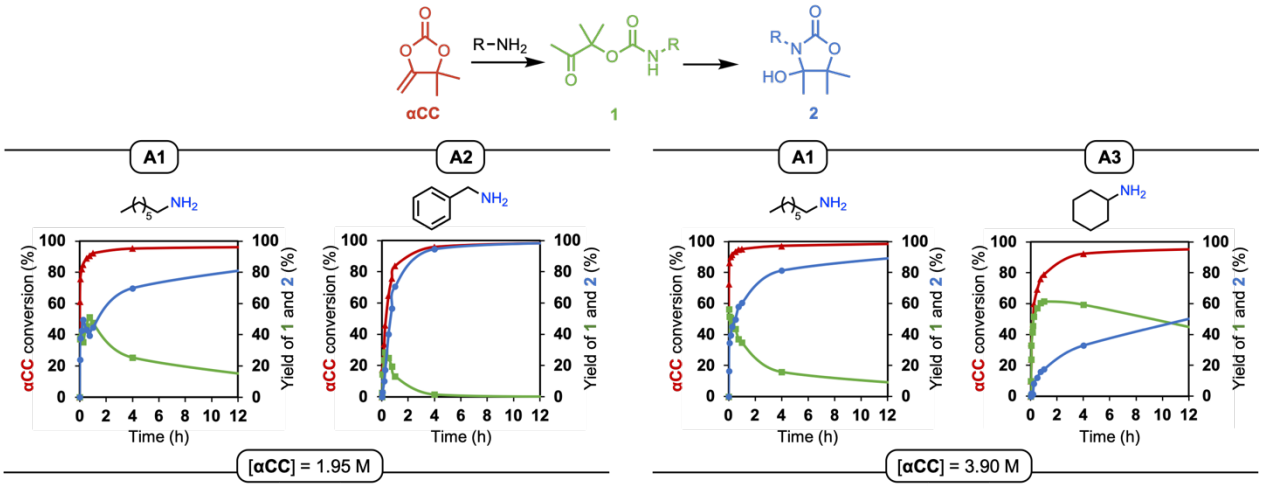

Figure 1. Time evolution of the **αCC** conversion and yields in *oxo*-urethane **1** and hydroxy-oxazolidinone **2**. Left: aminolysis of **αCC** with heptylamine (**A1**) or benzylamine (**A2**) in DMF (C = 1.95 M). Right: aminolysis of αCC with heptylamine (**A1**) or cyclohexylamine (**A3**) in DMF (C = 3.90 M). Conditions: [αCC]/[NH_2] = 1, 25 °C, no catalyst.

At 25 °C under catalyst-free conditions, the three amines ring-opened **αCC** with an almost quantitative conversion after 24 h (Table 1). The primary aliphatic amine **A1** was the most reactive, as expected from its more flexible chemical structure, while the cycloaliphatic one **A3** presented the lowest reactivity, probably due to an increased steric hindrance (Figure 1). Indeed, 92 % of **αCC** were converted by reaction with **A1** after only 15 min compared to 60 % with **A3** at identical concentration (C = 3.90 M) (Table 1, entries 1 and 7). The aromatic amine **A2** was less reactive than **A1** affording a moderate conversion of 46 % after 15 min at C = 1.95 M compared to 85 % with **A1** under identical experimental conditions (Table 1, entries 3 and 5).

Table 1. Selected kinetic data for the model reaction between **αCC** and the amines **A1**, **A2**, **A3**.

Entry	Amine	[C] (M)	Time	Conversion of αCC (%)	Yield for 1 (%)	Yield for 2 (%)	Selectivity for 1 (%)	Selectivity for 2 (%)
1	A1	3.90	15 min	92	47	45	51	49
2			24 h	> 99	2	98	2	98
3		1.95	15 min	85	35	50	41	59
4			24 h	97	3	94	3	97
5	A2	1.95	15 min	46	27	17	61	39
6			24 h	> 99	0	>99	0	100
7	A3	3.90	15 min	60	52	8	87	13
8			24 h	97	97	23	24	76

Conditions: [aCC]/[NH_2] = 1, 25 °C, solvent =DMF, no catalyst.

All amine/**αCC** model reactions delivered after 15 min a mixture *oxo*-urethane **1** and oxazolidinone **2**. The **αCC** conversion increased with the reaction time to reach almost completion after 12 h of reaction for **A1** and **A2** (Figure 1). Reaction was slower with **A3** but almost complete after 24 h (Table 1). Importantly, the product selectivity progressively evolved with time in all cases (Figure 1), as the consequence of the spontaneous intramolecular cyclization of **1** into **2**, to afford the corresponding oxazolidinones with a selectivity of 76 % for **A3**, 98% for **A1** and 100 % for **A2** after 24 h (Table 1).

The careful interpretation of the kinetic studies demonstrated that the oxazolidinone ring formation followed a trend in opposition with the **αCC** ring opening upon the nucleophilic attack of the selected amines. Indeed, the ring closure of the *oxo*-urethane into product **2** was faster using benzyl amine **A2** (Figure 1). The cyclohexylamine **A3** presented the lowest reactivity for both the ring-opening of **αCC** and the cyclization towards the formation of **2** (Figure 1). These studies highlight that both the electronic effects and the hindered structure of the amine had a strong influence on the rates of the aminolysis and the intramolecular cyclization of the *oxo*-carbonate intermediate into the oxazolidinone.

The effect of the addition of an organobase (DBU) (at a loading of 5 mol%) on the **αCC** conversion and the product selectivity was then evaluated for reactions carried out for 24 h at 25 °C. DBU was selected as it facilitated the ring-opening of **αCC** by amines[29], alcohols[29] and thiols[31]. In order to evaluate the influence of DBU on the rate of formation of the *oxo*-urethane

1 and the hydroxy-oxazolidinone **2**, the reactions were followed by ^{1}H-NMR spectroscopy for 2 h and the results are collected in Figure 2.

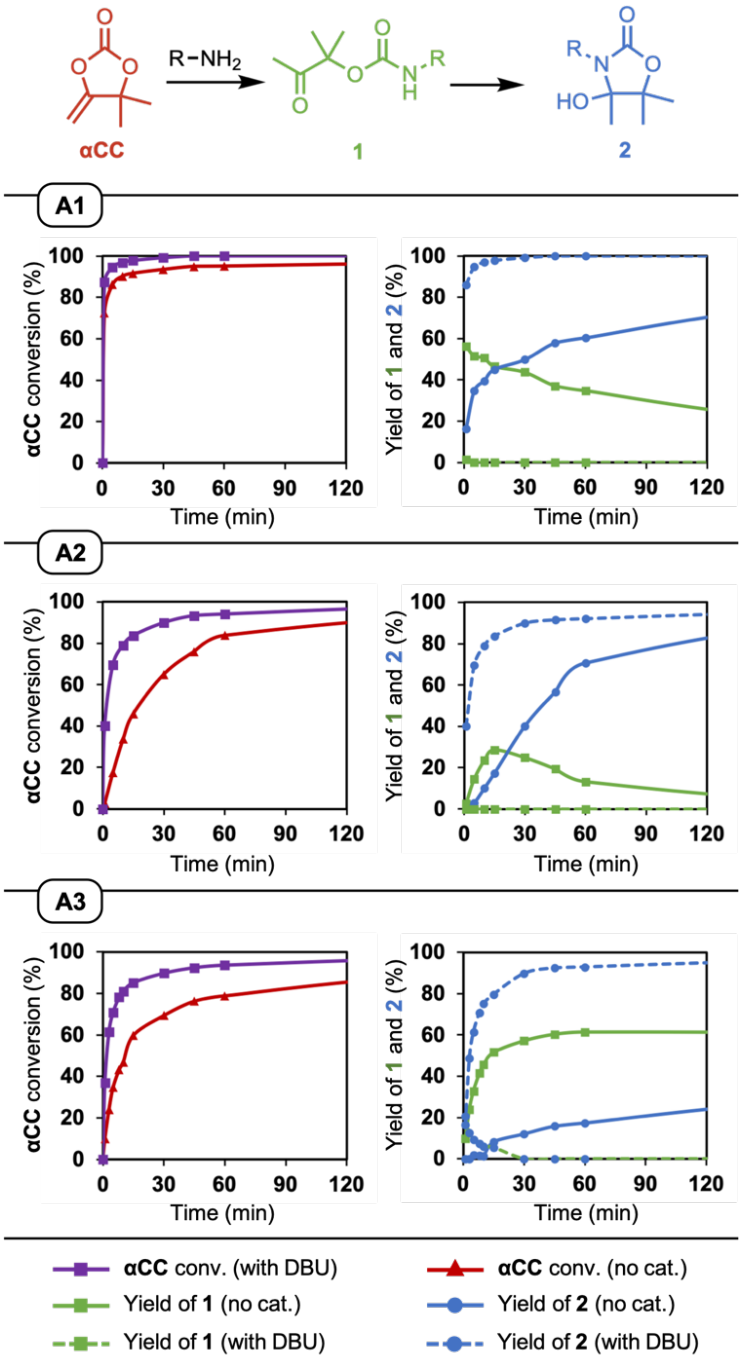

Figure 2. Benchmarking of the time evolution of the αCC conversion and yields in *oxo*-urethane **1** and hydroxy-oxazolidinone **2** for the aminolysis of **αCC** with the amines **A1**-**A3** under catalyst-free or DBU driven reactions at 25 °C. *Conditions: [αCC]/[NH$_2$] =1, [αCC] =3.90 M with A1 and A3, or [αCC] = 1.95 M with A2; DMF, 25°C, 5 mol% DBU compared to αCC.*

In all cases, the addition of DBU strongly accelerated both steps of the cascade reactions (Figure 2). For instance, **αCC** was fully reacted with **A1** in only 45 min in the presence of DBU (compared to 24 h in the absence of DBU). The catalytic effect of the organobase was much

more marked for the less reactive amines **A2** and **A3** with **αCC** conversions of 85% or 82% being reached after 15 min with **A3** or **A2**, respectively (compared to 60% or 46% without catalyst). Besides the organocatalyst had a remarkable catalytic activity on the intramolecular ring formation step and improved the product selectivity. As illustrated in Figure 2, the *oxo*-urethane **1** was indeed nearly not observed in the presence of the catalyst even at the early stage of the reaction and for the three different amines, which is in sharp contrast to the reactions carried out in the absence of catalyst. Overall, the reactions of **αCC** with the different amines (**A1**, **A2**, **A3**) illustrate the versatility and applicability of the methodology that is able to deliver oxazolidinones with a yield close to 100% in less than 2 h.

Dehydration of hydroxy-oxazolidinones

The presence of a tertiary alcohol in the chemical structure of the hydroxy-oxazolidinones makes these latest suitable candidates to deliver oxazolidinones with exocyclic vinylene functionality by dehydration. The optimization of the reaction on model compounds is a then prelude to the fabrication of functional poly(α-alkylidene-oxazolidinone)s by dehydration of the parent poly(hydroxy-oxazolidinone)s. The substrate scope was first enlarged by synthesizing, isolating and purifying three hydroxy-oxazolidinones **2a**, **2b**, and **2c** (Scheme S5) by the reaction between **αCC** and **A1**, **A2** or **A3** following procedures discussed above (see experimental section 1).

Inspired by the literature,[34] the dehydration of the hydroxy-oxazolidinones **2a-c** was realized in refluxing glacial acetic acid (HAc), a cheap, non-toxic, readily available and biorenewable reagent. The dehydration of **2** into the corresponding α-alkylidene oxazolidinone **3** (Scheme 3) was monitored by ^{1}H-NMR spectroscopy (see ESI). Excellent dehydration yields of 92 to 100% were obtained for all substrates, including the more sterically hindered product **2c**, with the selective formation of the corresponding α-alkylidene oxazolidinone **3**.

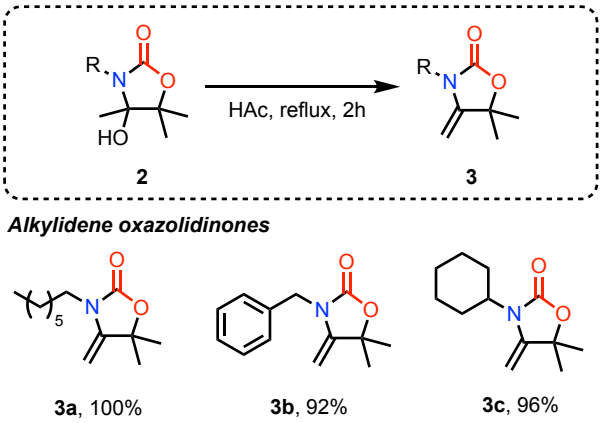

Scheme 3. Substrate scope of hydroxy-oxazolidinones dehydration into α-alkylidene oxazolidinones. *Conditions: [O]=0.22 M in glacial acetic acid, 120 °C, 2 h.*

Synthesis of poly(hydroxy-oxazolidinone)s

The polyaddition of two CO_2-sourced bis(α-alkylidene cyclic carbonate)s (bisαCCs; **αCC1** and **αCC2**) with 7 different diamines (**AA1** – **AA7**) was then considered (Scheme 2) with the aim to elucidate the influence of the comonomer structures on the polymerization course. This facile polyaddition approach was expected to provide a library of new polyurethanes. It has to be noted that alike poly(oxazolidinone)s made from diisocyanates and diepoxides, some of our poly(hydroxy-oxazolidinone)s displayed poor or no solubility in common organic solvents. Therefore, for insoluble polymers, their molecular parameters (M_n, M_w/M_n) could not be determined by size-exclusion chromatography (SEC). Their microstructural characterization was also difficult and could be elucidated by ^{13}C-solid state NMR spectroscopy only.

Polymerizations under ambient and catalyst-free conditions. Polymerizations were first carried out at 25 °C in DMF for 24 h without any catalyst. Table 2 summarizes the conversion of the bisαCCs, determined by ^1H-NMR spectroscopy and the selectivity for the *oxo*-urethane and oxazolidinone linkages. The macromolecular parameters of the chains are also included and were determined by SEC on the crude reaction medium to avoid any fractionation of the polymers during precipitation.

The bisαCCs conversions were high (> 99 %) in all cases, except for the polymerization carried out with the cycloaliphatic vicinal diamine **AA6** (Table 2, entry 6). In this latter case, the conversion could not be accurately measured due to some peak overlapping. With **αCC1**, the polymerization medium remained homogeneous all along the span of the reaction, except for **P(CC1-AA5)** synthesis with a polymer that precipitated during its formation. With **αCC2**, the polymer chains precipitated during their formation and were insoluble in common solvents for SEC analysis (THF or DMF/LiBr) or other common organic solvents (DMF, DMSO, DMAc, THF, chloroform, sulfolane, etc.). Only **P(CC2-AA2)** displayed solubility in DMSO which allowed its characterization by liquid-state NMR. The reference polymer, **P(CC1-AA1)**, and the tertiary amine functionalized one, **P(CC1-AA3)**, displayed similar molecular characteristics with relative number average molar masses (M_n) around 20,000 to 25,000 g/mol and a dispersity of 1.8 (Table 2). Figure 3 shows the SEC chromatograms evolution for samples taken at different reaction times (1 min, 1 h and 24 h) for these two polymerizations. In both cases, SEC chromatograms shifted towards the lower elution time and thus higher molar masses with the polymerization time, as expected for a step-growth type process. Molecular characteristics (M_n, M_w, dispersity D) of the different samples are summarized in Table 3. All other polymers made from **αCC1** presented lower M_n values (Table 3). However, because the molar masses were determined based on a PS calibration and the hydrodynamic volume of

the polymers are expected to be different to each other, the molar masses given by SEC analysis are relative and the values cannot be compared.

Table 2. Conversions, molecular characteristics and linkages selectivity for polymers obtained by the polyaddition of bisαCCs with diamines after 24 h at 25 °C in DMF (the structure of the monomers is illustrated in Scheme 2).

bis(α-alkylidene cyclic carbonate)s

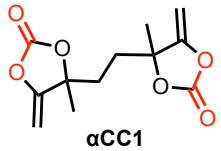

αCC1

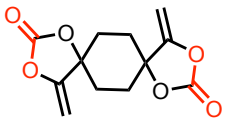

αCC2

Diamines

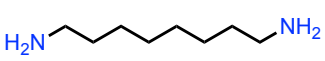

AA1

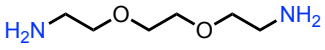

AA2

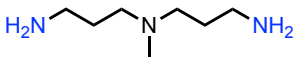

AA3

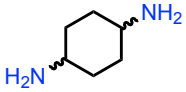

AA4

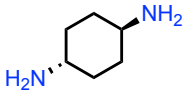

AA5

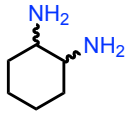

AA6

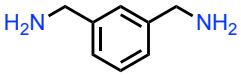

AA7

Entry	Polymer	Conv. (%)[a]	Polymer characteristics				
			M_n (g/mol)[b]	M_w (g/mol)[b]	D[b]	*Oxo*-urethane linkage (%)	Oxazolidinone linkage (%)
1	P(CC1-AA1)		24,900	44,800	1.8	/	100
2	P(CC1-AA2)		4,200	8,400	2.0	/	100
3	P(CC1-AA3)	> 99	20,400	36,100	1.8	/	100
4	P(CC1-AA4)		3,000	4,700	1.6	32	68
5	P(CC1-AA5)		--[c]	--[c]	--[c]	N.Q.[d]	N.Q.[d]
6	P(CC1-AA6)	N.d.	500	400	1.4	14	86
7	P(CC1-AA7)	> 99	4,000	7,600	1.9	/	100
8	P(CC2-AA1)		--[c]	--[c]	--[c]	/	100
9	P(CC2-AA2)	> 99	--[c]	--[c]	--[c]	/	100
10	P(CC2-AA5)		--[c]	--[c]	--[c]	N.Q.[d]	N.Q.[d]
11	P(CC2-AA6)	N.d.	--[c]	--[c]	--[c]	/	100
12	P(CC2-AA7)	> 99	--[c]	--[c]	--[c]	/	100

Conditions: [BisαCC] = 0.67 M in DMF, 25 °C, 24 h, no catalyst.

[a]conversion in cyclic carbonate determined by ^{1}H-NMR in DMSO-d_6. N.d. not determined.

[b]determined on the crude product by SEC in DMF/LiBr by using a PS calibration.

[c]not determined due to polymer insolubility in DMF/LiBr and THF.

[d] N.Q.: not quantified. For P(CC1-AA5) and P(CC2-AA5), the solid-state ^{13}C-NMR-spectrum evidenced the presence of the two types of linkages but they could not be quantified.

We have also to note that the dispersities were rather low for a step-growth polymerization process (they should be around 2), especially for sample **P(CC1-AA6)** which is due to its oligomeric structure constituted of dimers and trimers (Figure S42). The low M_n obtained for **P(CC1-AA6)** was assumed to be the consequence of a low monomer conversion originating from the high steric hindrance that had to be overcome to increase the polymer chain length or to some side reactions occurring during the process. Further experiments would be required for drawing more conclusions regarding this specific case.

Table 3. Temporal evolution of molecular characteristics during polymerization for **P(CC1-AA1)** and **P(CC1-AA3)**.

Entry	Polymer	Time	M_n (g/mol)[b]	M_w (g/mol)[b]	D[b]
1	P(CC1-AA1)	1 min	4,200	5,600	1.3
2		1 h	11,700	19,800	1.7
3		24 h	24,900	44,800	1.8
4	P(CC1-AA3)	1 min	2,700	5,100	1.8
5		1 h	11,600	17,900	1.5
6		24 h	20,400	36,100	1.8

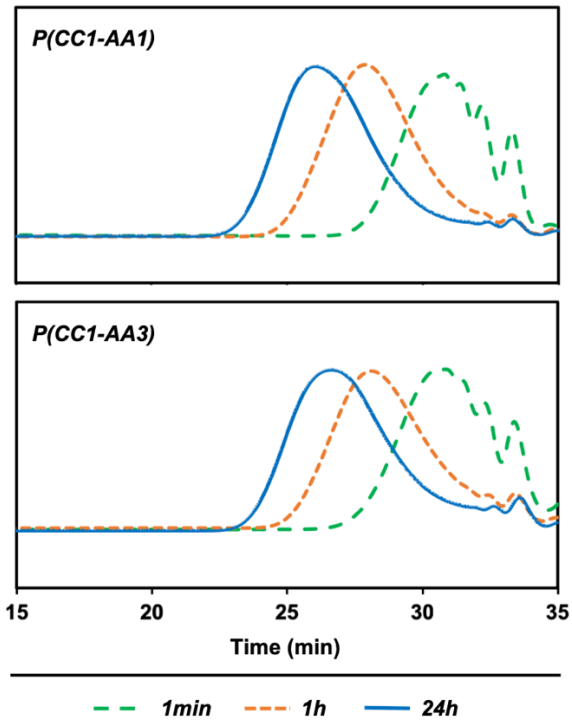

Figure 3. Temporal evolution of SEC chromatograms during the formation of **P(CC1-AA1)** and **P(CC1-AA3)**.

The structure of all polymers prepared from **αCC1** was elucidated by ^{1}H- and ^{13}C-NMR spectroscopies on purified products. As expected from the model reactions, the microstructure of polymers synthesized from the primary aliphatic or aromatic diamines **AA1**, **AA2**, **AA3** and **AA7** contained exclusively hydroxy-oxazolidinone linkages as highlighted by the presence of the typical signal of the alcohol pendant group (δ = 6-6.25 ppm) (Figure 4). All the other signals were also characteristic of the targeted polymer structure. ^{13}C-NMR spectra confirmed the formation of poly(hydroxy-oxazolidinone)s by the typical carbonyl resonance of oxazolidinone linkage (δ = 157 ppm) and the two quaternary carbon atoms from the ring structure (δ = 87 and 91 ppm) (Figure 5). All peaks assignments were confirmed by HSQC and HMBC analyses (Figures S16-S18 for **P(CC1-AA1)**, Figures S19-S21 for **P(CC1-AA2)**, Figures S22-S24 for **P(CC1-AA3)**, Figures S29-S30 for **P(CC1-AA6)**, Figures S31-S32 for **P(CC1-AA7)**).

Importantly, it was found that hydroxy-oxazolidinones and *oxo*-urethane linkages coexisted within the skeleton of the polymers prepared from vicinal and 1,4-cyclohexanediamine isomers (**AA4**, **AA5**, **AA6**) (Figure 4-d for **P(CC1-AA4)**, Figure 5-d for **P(CC1-AA5)**, Figure 4-e for **P(CC1-AA6)**). The hydroxy-oxazolidinones/*oxo*-urethane selectivity in each polymer was determined by ^{1}H-NMR spectroscopy. The selectivity toward each moiety was not determined for **P(CC1-AA5)** due to its lack of solubility. The polymer **P(CC1-AA4)** was constituted by 68 mol% of the hydroxy-oxazolidinone moiety and 32 mol% of the *oxo*-urethane unit. Polymer **P(CC1-AA6)** found to contain 14 mol% of *oxo*-urethane linkage. The presence of the oxo-urethane linkages was due to the cyclization step (transformation of *oxo*-urethane into oxazolidinone) that was slower when sterically hindered amines were used, in line with the model reactions (aminolysis of **αCC** with cyclohexylamine **A3**, Figure 1). The structural identification of insoluble polymers prepared from **αCC2** was realized by solid-state ^{13}C-NMR spectroscopy (Figure 6). At the exception of **P(CC2-AA5)**, all polymers displayed only 100% of oxazolidinone-type linkages, at least within the detection limit of the solid ^{13}C-NMR spectroscopy. The characteristic carbonyl resonances of the oxazolidinone group (δ = 155-160 ppm) and the two quaternary carbon atoms of the hydroxy-oxazolidinone ring structure (δ = 80-87 ppm and 87-95 ppm) were clearly observed in all samples, as well as all other carbon atoms, in line with the proposed structures. The *oxo*-urethane linkage content was very low or close to zero since no signal characteristic of a ketone group at 210 ppm was observed in solid state ^{13}C-NMR. As previously observed for the polymers prepared from **αCC1**, the polymer prepared from **αCC2** and the 1,4-cyclohexanediamine isomer **AA4** was characterized by hydroxy-oxazolidinones and *oxo*-urethane linkages, resulting from a partial intramolecular cyclization of *oxo*-urethane moieties. It was however not possible to quantify the amount of each moiety in the polymer structure since the solid-state ^{13}C NMR technique does not allow a quantitative analysis.

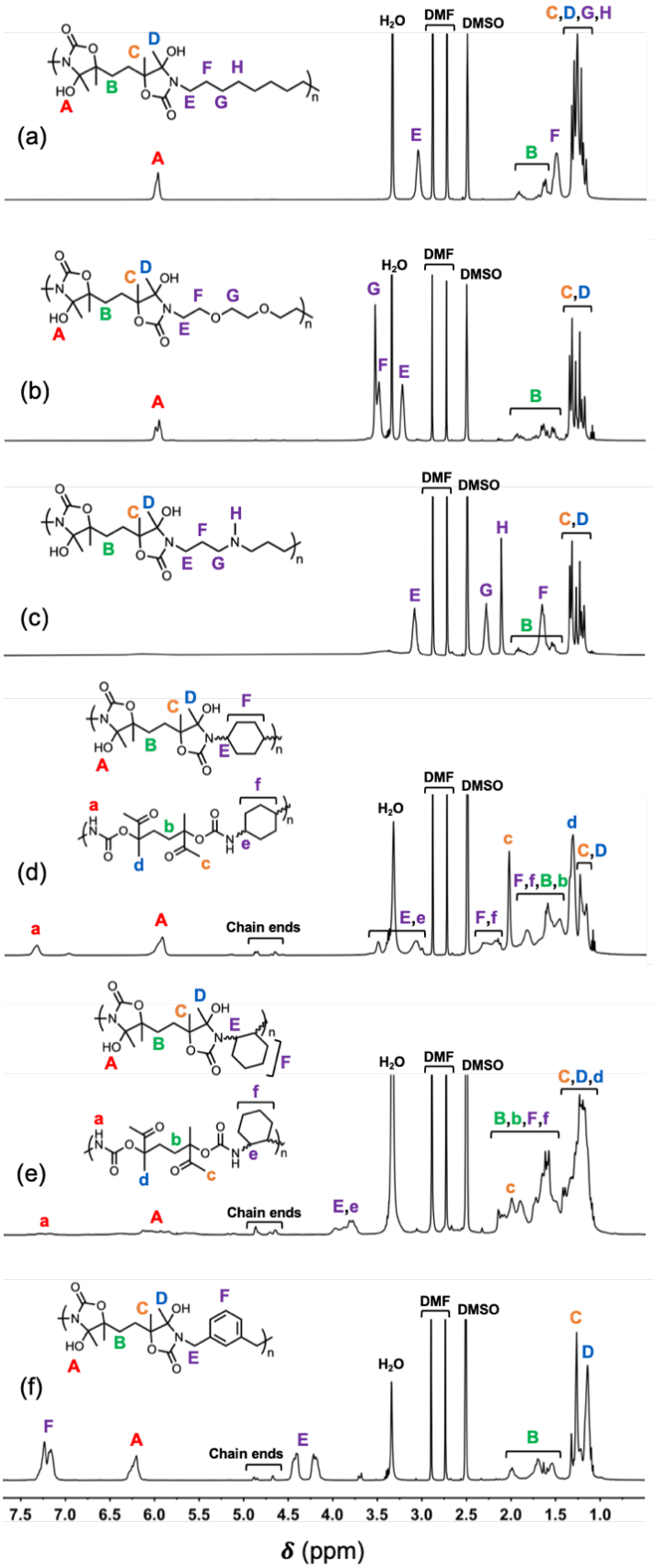
(a)
(b)
(c)
(d)
(e)
(f)
H2O
DMF
DMSO
Chain ends
7.5 7.0 6.5 6.0 5.5 5.0 4.5 4.0 3.5 3.0 2.5 2.0 1.5 1.0
δ (ppm)

Figure 4. Stacked ^{1}H-NMR spectra of (a) **P(CC1-AA1)** (Table 2, entry 1), (b) **P(CC1-AA2)** (Table 2, entry 2), (c) **P(CC1-AA3)** (Table 2, entry 3), (d) **P(CC1-AA4)** (Table 2, entry 4), (e) **P(CC1-AA6)** (Table 2, entry 6) and (f) **P(CC1-AA7)** (Table 2, entry 7) in DMSO-d_6 (after purification).

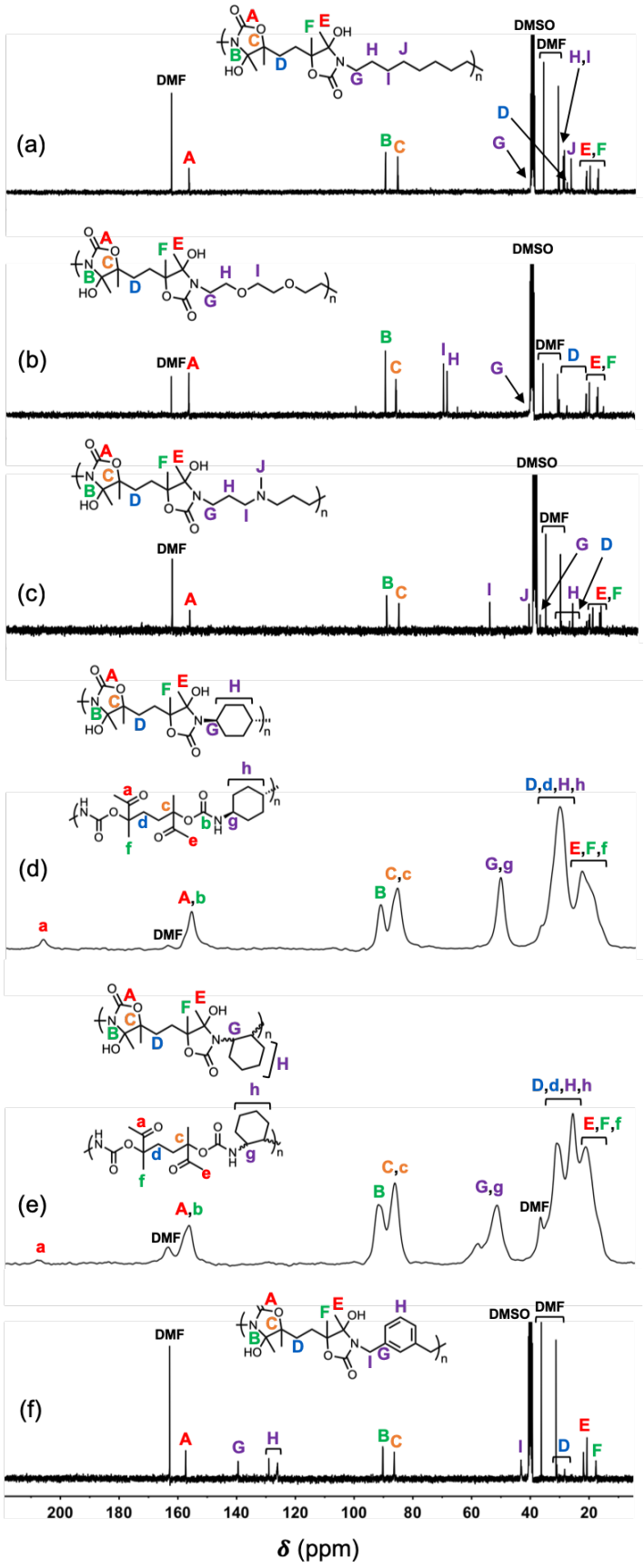

Figure 5. Stacked ^{13}C-NMR and solid-state ^{13}C-NMR spectra of (a) **P(CC1-AA1)** (Table 2, entry 1), (b) **P(CC1-AA2)** (Table 2, entry 2), (c) **P(CC1-AA3)** (Table 2, entry 3), (d) **P(CC1-AA5)** (Table 2, entry 5), (e) **P(CC1-AA6)** (Table 2, entry 6) and (f) **P(CC1-AA7)** (Table 2, entry 7) in DMSO-d_6 (after purification).

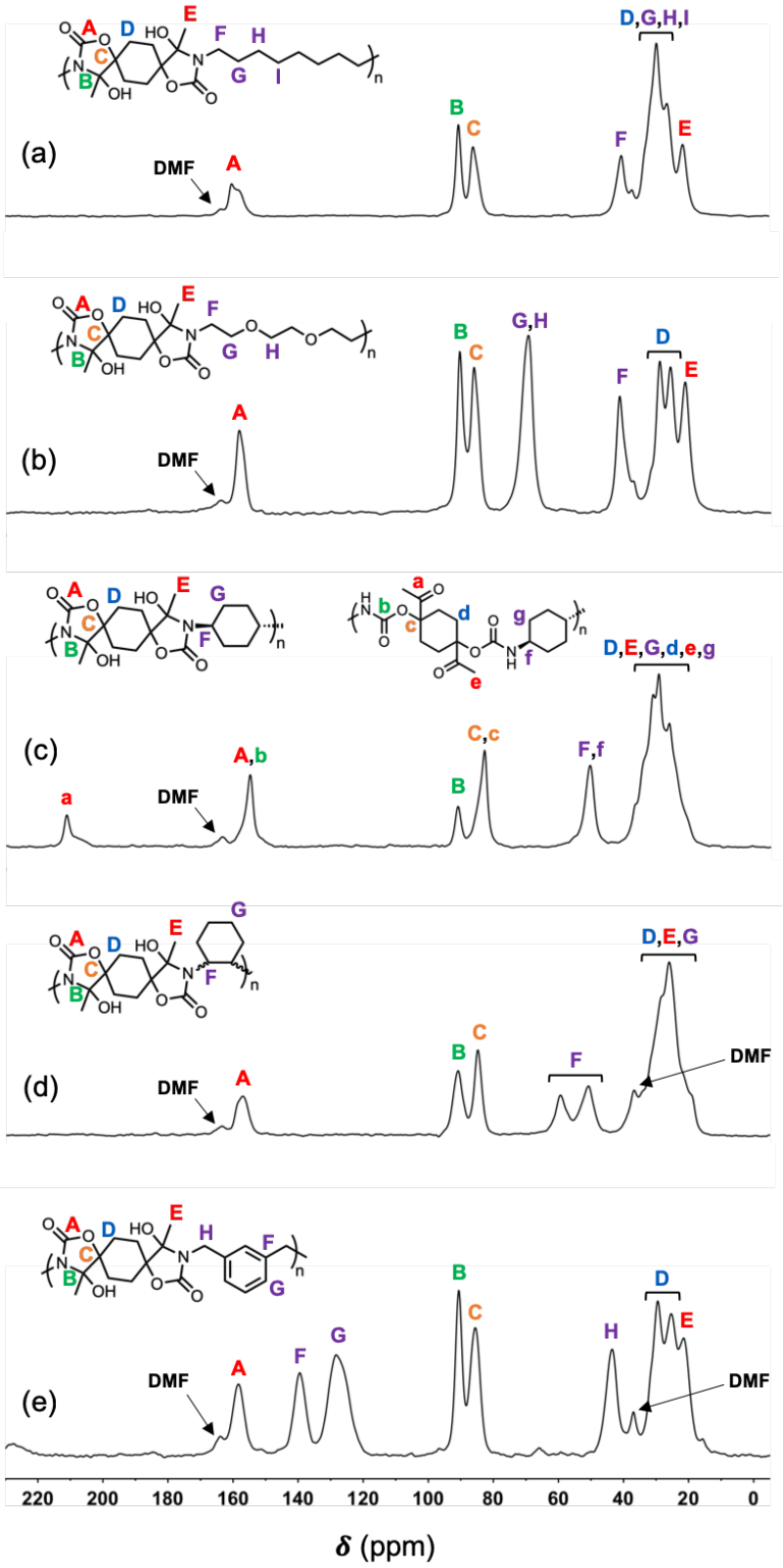

Figure 6. Stacked solid-state ^{13}C NMR spectra of (a) **P(CC2-AA1)**, (b) **P(CC2-AA2)**, (c) **P(CC2-AA5)**, (d) **P(CC2-AA6)**, (e) **P(CC2-AA7)** (after purification).

Polymerizations using a catalyst and/or at higher temperatures. We then evaluated the impact of the DBU catalyst or the temperature (T = 25 or 80 °C) on the polymerization of bisαCC with the diamines on the macromolecular characteristics of the polymers. Since the polymers synthesized from **αCC2** were insoluble in all tested organic solvents, this study was conducted with **αCC1** only and with some of the amines **AA2**, **AA4** and **AA7** that provided soluble polymers at high yield. Results for the polymerizations carried out for 24 h are summarized in Table 4.

Table 4. Conversions and molar masses of polymers prepared by copolymerization of **αCC1** with various diamines with or without DBU and at different temperatures.

Entry	BisαCC	Diamine	T (°C)	Catalyst	Conv. (%)[a]	M_n (g/mol)[b]	M_w (g/mol)[b]	D^b
1	αCC1	AA2	25	--	> 99	4,200	8,400	2.0
2			80	--		7,500	17,200	2.2
3			25	DBU		15,500	25,500	1.7
4		AA4	25	--	> 99	3,000	4,700	1.6
5			80	--		--[c]	--[c]	--[c]
6			25	DBU		--[c]	--[c]	--[c]
7		AA7	25	--	> 99	4,000	7,600	1.9
8			80	--		--[c]	--[c]	--[c]
9			25	DBU		--[c]	--[c]	--[c]

Conditions: [αCC1] = 0.67 M in DMF, 24 h, no catalyst or DBU (5 mol%).
[a]conversion in cyclic carbonate determined by ^{1}H NMR in DMSO-d_6. N.d. not determined.
[b]determined on crude products by SEC in DMF/LiBr and by using a PS calibration.
[c]not determined due to polymer insolubility in DMF/LiBr and THF.

By increasing the temperature from 25 to 80 °C, the molar mass of the polymer formed from **AA2** was almost doubled with a molar mass of 7,500 g/mol (compared to 4,200 g/mol at 25 °C) (Table 4, entries 1-2). The use of DBU (5 mol%) at 25 °C had a huge influence on the polymer molar mass that was strongly increased to 15,500 g/mol (Table 4, entry 3). It seemed that the use of a catalyst was the best option for accelerating the growth of the polymer chains, and thus for providing longer polymer chains.

When **AA4** and **AA7** were concerned, the addition of DBU or the increase of the temperature furnished polymers that precipitated during the polymerization and that were insoluble in the solvent used for SEC analysis. This was in sharp contrast to the same polymerizations carried

out without DBU at rt that yielded soluble polymers in the reaction medium. These observations suggested that the molar mass of the polymer prepared in the presence of DBU at 25 °C or at 80 °C without DBU were higher than that noted at 25 °C without DBU, and exceeded the solubility limit of the product in DMF (Table 4, entries 5-6 and 8-9). In order to give any clue to this hypothesis and that a possible modification of the chemical structure of the polymer was not responsible for this lack of solubility, we analyzed the polymer **P(CC1-AA7)** prepared under the different reaction conditions (rt without catalyst, rt with DBU, and 80 °C without DBU) by solid-state ^{13}C-NMR spectroscopy under identical conditions. (Note here that solid state NMR was required because the polymers prepared with DBU or at higher temperature were insoluble in many organic solvents). Figure S41 confirmed that increasing the temperature or adding a catalyst had no impact on the polymer microstructure, the NMR spectra being identical. The difference of solubility of the polymers synthesized under the different conditions was therefore assigned to a higher molar mass when DBU or a higher temperature was employed for their synthesis, and is not due to a different chemical structure.

Dehydration of poly(hydroxy-oxazolidinone)s

The dehydration of poly(hydroxy-oxazolidinone)s was tested on polymers soluble in common organic solvents, thus on **P(CC1-AA1)**, **P(CC1-AA2)**, **P(CC1-AA4)** and **P(CC1-AA7)**. Polymers were dispersed in glacial acetic acid and the mixture was refluxed at 120 °C for 2 h.

Table 5. Dehydration of poly(hydroxy-oxazolidinone)s into poly(alkylidene oxazolidinone)s. Macromolecular parameters of the polymers before and after dehydration, and selectivity for the two linkages **D1** and **D2** of the dehydrated polymers.

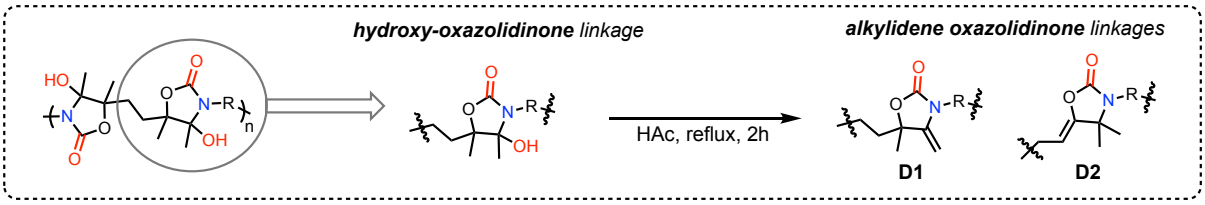

Entry	Polymer	R	M_n (g/mol)[b]	M_w (g/mol)[b]	D[b]	Polymer linkages
1	P(CC1-AA1)	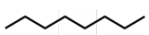	79,200	157,900	2.0	
2	P(CC1-AA1)D		36,700	68,300	1.9	D1/D2:58/42
3	P(CC1-AA2)	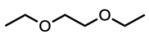	15,900	26,200	1.6	
4	P(CC1-AA2)D		4,600	8,700	1.9	D1/D2:50/50
5	P(CC1-AA4)		3,000	5,200	1.7	
6	P(CC1-AA4)D		2,400	4,100	1.7	D1/D2:100/0
7	P(CC1-AA7)	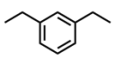	7,200	18,500	2.6	
8	P(CC1-AA7)D		4,300	9,000	2.1	D1/D2:100/0

The structure of the novel polymers was elucidated by ^{1}H- and ^{13}C-NMR spectroscopies on the purified products (Figures 7-8). The less sterically hindered poly(hydroxy-oxazolidinone)s, **P(CC1-AA1)** and **P(CC1-AA2)**, were completely dehydrated into the unsaturated poly(oxazolidinone) with the formation of the expected α-alkylidene oxazolidinone linkage **D1** but also a second linkage **D2** (β-alkylidene oxazolidinone) (Table 5). Typical signals for the unsaturated poly(oxazolidinone) were indeed identified by the two non-equivalent olefinic protons (δ = 4.10-4.30 ppm) for the linkage **D1** and the olefinic proton associated to **D2** (δ = 4.50-4.70 ppm), in accordance with the chemical shift of similar structures studied in a previous study on small molecules[35]. The complete disappearance of the hydroxy-oxazolidinone alcohol group (δ = 6 ppm) attested for the completeness of the reaction. ^{13}C-NMR spectrum also showed the appearance of the typical olefinic signals (δ = 82 ppm and 148 ppm for **D1**, δ = 100 ppm and 141 ppm for **D2**) (Figure 8). All these assignments were confirmed by HSQC and HMBC analyses (Figure S33-S40). This **D2** linkage was observed in large amount after dehydrating the sterically unhindered polymers **P(CC1-AA1)** (D1/D2 = 58/42) and **P(CC1-AA2)** (D1/D2 = 50/50). The dehydration of the bulkier poly(hydroxy-oxazolidinone)s **P(CC1-AA3)** and **P(CC1-AA6)** was also successful and complete. Importantly, the exclusive formation of α-alkylidene oxazolidinone linkages **D1** was observed in these two cases.

It is suggested that the **D2** linkage resulted from the carbocation 1,2-Wagner-Meerwein-type rearrangement to yield a more substituted alkene (Scheme 4). This rearrangement was not observed in the model reactions where both alkenes would have the same substitution number. The spontaneous methyl shift might thus be promoted for polymers made up from sterically unhindered diamines. Although further investigations are needed, the presence of a bulky group (such as cycloaliphatic or aromatic group) seemed to prevent this methyl shift.

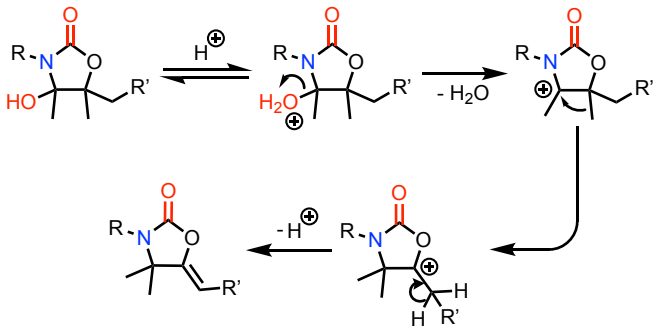

Scheme 4. Proposed mechanism for the dehydration of hydroxy-oxazolidinones through a Wagner-Meerwein rearrangement.

The molecular parameters of the polymers before and after dehydration are collected in Table 5. The dehydrated polymers had lower apparent M_n than the starting poly(hydroxy-oxazolidinone)s. However, the chemical structure of the polymers was different and these relative molar masses values could not be compared as the hydrodynamic volume of the

polymers was expected to be different in the solvent used for SEC analysis. Note here that the M_n of the starting products (poly(hydroxy-oxazolidinone)s) were higher than those reported in Table 2 because the polymers were purified by precipitation before performing the dehydration reaction (in Table 2, crude polymers were analyzed). Some fractionation was thus occurring during purification, explaining the higher M_n observed.

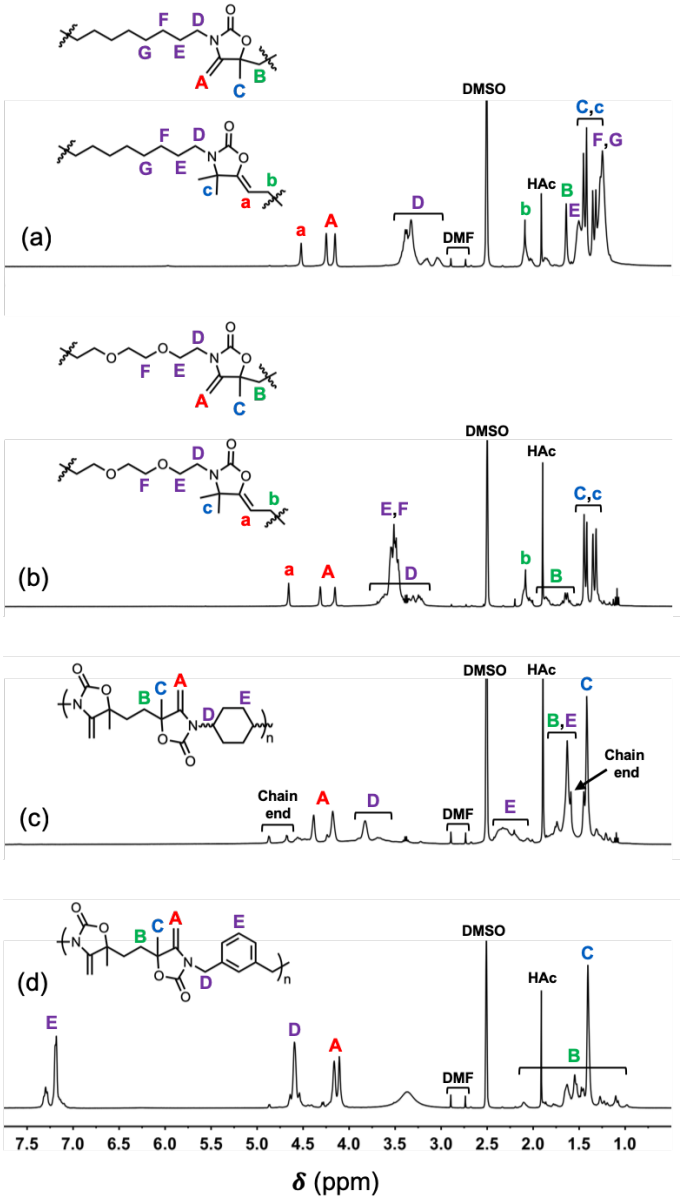

Figure 7. Stacked ^{1}H-NMR spectra of (a) **P(CC1-AA1)D** (Table 5, entry 2), (b) **P(CC1-AA2)D** (Table 5, entry 4), (c) **P(CC1-AA4)D** (Table 5, entry 6) and (d) **P(CC1-AA7)D** (Table 5, entry 8) in DMSO-d_6 (after purification).

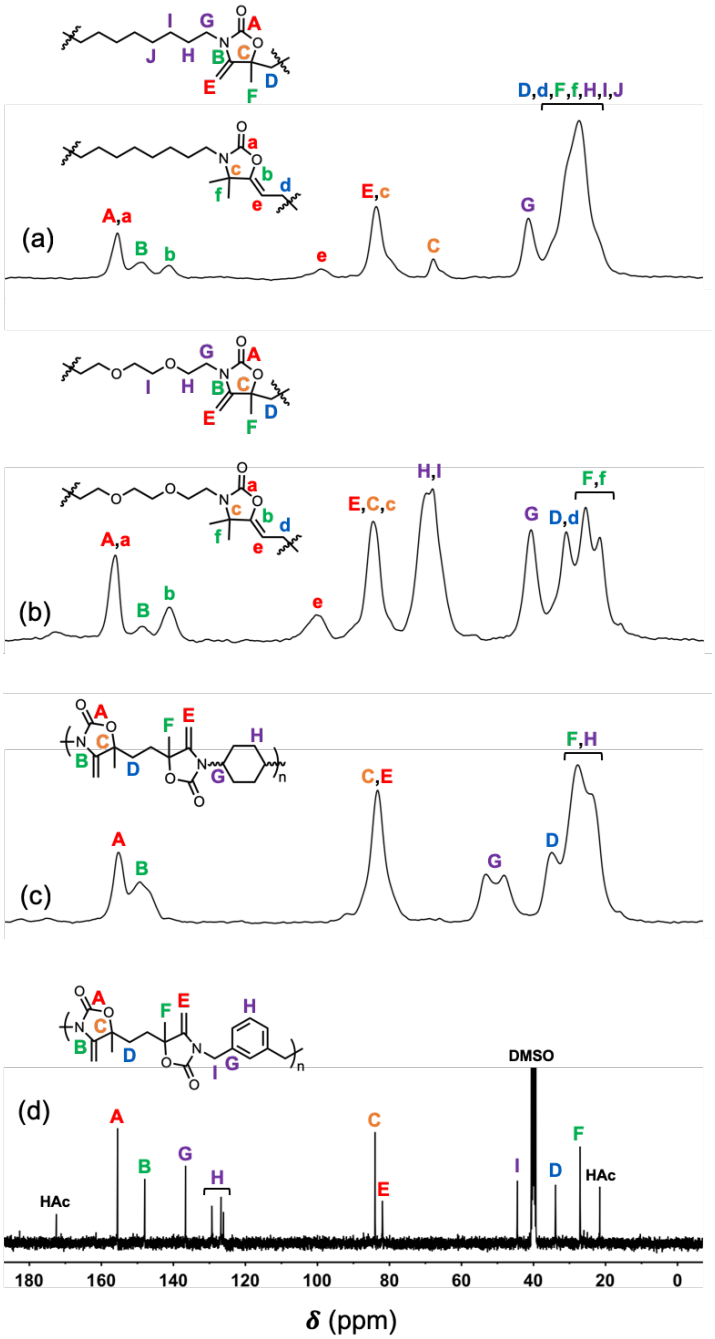

Figure 8. Stacked ^{13}C-NMR and solid-state ^{13}C-NMR spectra of (a) **P(CC1-AA1)D** (Table 5, entry 2), (b) **P(CC1-AA2)D** (Table 5, entry 4), (c) **P(CC1-AA4)D** (Table 5, entry 6) and (d) **P(CC1-AA7)D** (Table 5, entry 8) in DMSO-d_6 (after purification).

Thermal properties of the polymers

The thermal degradation temperature at 10 wt% loss ($T_{d,10\%}$) of the polymers was evaluated by thermogravimetric analysis (TGA) and all data are summarized in Table 6. A multistep degradation pattern was observed for all studied poly(hydroxy-oxazolidinones)s (Figure 9). The first mass loss at around 150 °C was the result of the evaporation of residual DMF that was impossible to completely remove after polymer synthesis and purification. The second

main degradation appeared at around 275 °C for all polymers and was followed by a more important degradation at around 400 °C.

Importantly, TGA analyses of the dehydrated polymers, the poly(alkylidene oxazolidinone)s, presented a single degradation pattern at high temperature ($T_{d,10\%}$ = 370-400 °C) (the small mass loss at around 150 °C corresponded to the evaporation of residual acetic acid), highlighting the high thermal stability of the polymer. This $T_{d,10\%}$ was similar to that measured for the final degradation pattern of the parent poly(hydroxy-oxazolidinone)s. Although additional experiments would be required, this suggests that the first degradation step of poly(hydroxy-oxazolidinone) corresponded to the dehydration of the polymer with the formation of the poly(alkylidene oxazolidinone). Additionally, the poly(hydroxy-oxazolidinone) **P(CC1-AA7)** and poly(alkylidene oxazolidinone) **P(CC1-AA7)D** prepared from m-xylylene diamine provided some char at 600 °C, 13.5 and 12.6 wt% respectively (after subtracting the content of residual solvent trapped in the polymer).

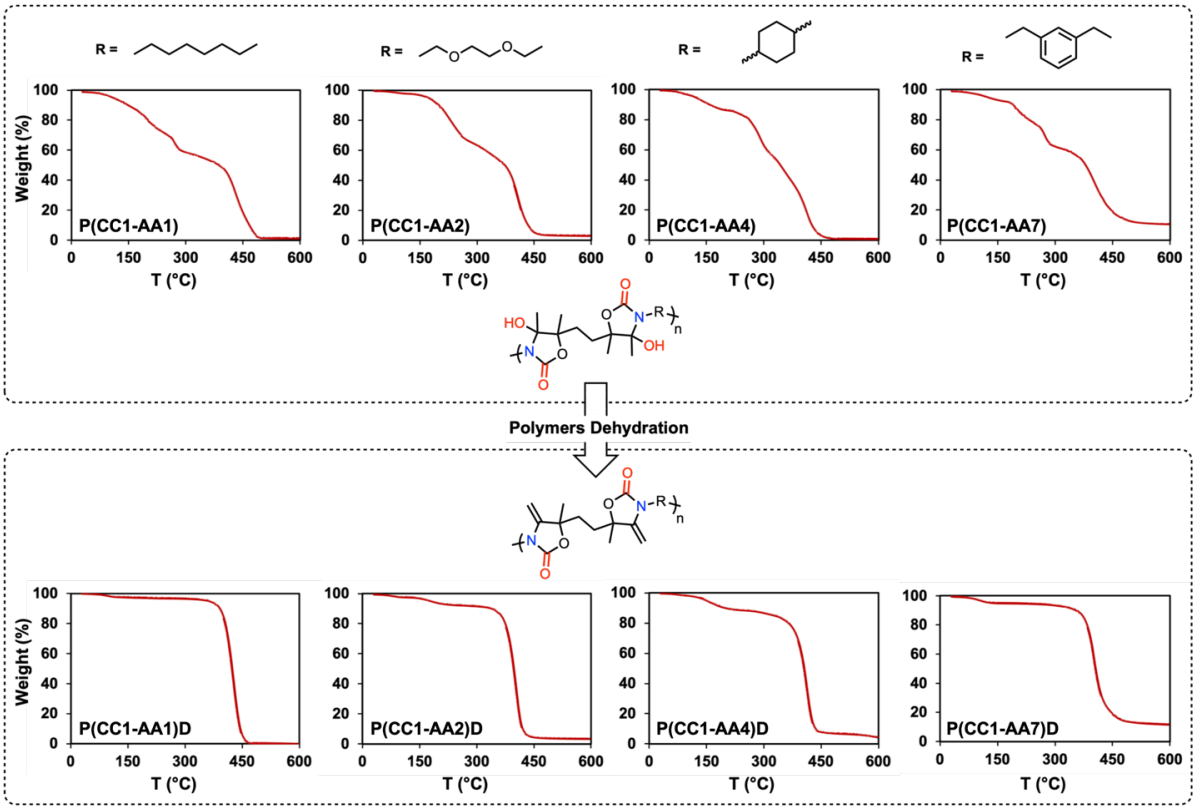

Figure 9. TGA curves for the polymers P(CC1-AA1), P(CC1-AA2), P(CC1-AA4) and P(CC1-AA7) (top) and their respective dehydrated product (bottom).

We then analyzed the polymers by dynamic scanning calorimetry (DSC) to evaluate the glass transition temperature (T_g) of the polymers. Due to solvent evaporation and probably the thermal-induced dehydration of the poly(hydroxy-oxazolidinone)s, we were not able to determine their T_g. However T_g values were obtained for the dehydrated polymers **P(CC1-**

AA1)D (T_g = 89 °C) and **P(CC1-AA7)D** (T_g = 130 °C) (Table 6). The highest T_g was measured for the polymer prepared from m-xylylene diamine **AA7**. No melting temperature was observed under the investigated conditions. Despite their clean TGA pattern, polymers **P(CC1-AA2)D** and **P(CC1-AA4)D** did not provide exploitable data by DSC and no glass transition or melting temperatures were determined for these polymers.

Table 6. Degradation temperature and glass transition temperature determined by TGA and DSC analyses for the dehydrated polymers.

Entry	Polymer	$T_{d,10\%}$ (°C)	T_g (°C)
1	P(CC1-AA1)D	397	89
2	P(CC1-AA2)D	370	N.d.
3	P(CC1-AA4)D	367	N.d.
4	P(CC1-AA7)D	375	130

N.d. could not be determined.

Conclusions

This work described the synthesis and the characterization of novel poly(oxazolidinone)s by polyaddition of CO_2-sourced bis(α-alkylidene cyclic carbonate)s (bisαCCs) with various di-primary amines, with the objective to study the influence of the reaction conditions on the structure and macromolecular parameters of the polymers. Model reactions on small molecules were first performed in order to understand the impact of the structure of the amine on the rate, yield and selectivity of the reactions. The amine structure showed to have an influence on the rates of reaction for both the ring-opening of the cyclic carbonate and the intramolecular cyclization of the *oxo*-urethane intermediate into the hydroxy-oxazolidinone. Aliphatic and benzylic amines provided mainly the hydroxy-oxazolidinone, thus the intramolecular cyclization of the *oxo*-urethane was fast. Cycloaliphatic amines however afforded both the *oxo*-urethane and the hydroxy-oxazolidinone products, the steric hindrance of these amines was assumed to be responsible for slowing down the cyclization step. This step was however accelerated by the addition of DBU as catalyst.

Various poly(hydroxy-oxazolidinone)s were then synthesized by polyaddition of bisαCCs with the diamines. In line with model reactions, the more sterically hindered cycloaliphatic diamines yielded polymers containing both *oxo*-urethane and hydroxy-oxazolidinone linkages. The addition of DBU favored the formation of polymers of higher molar masses. Aliphatic and benzylic diamines provided exclusively poly(hydroxy-oxazolidinone)s. Some of the polymers, mainly those produced from a bisαCC bearing a cyclohexyl group between the two cyclic

carbonate moieties were precipitating during the polymerization and were insoluble in many organic solvents.

We also succeeded in quantitatively dehydrating the different poly(hydroxy-oxazolidinone)s by refluxing in glacial acetic acid, yielding poly(alkylidene oxazolidinone)s. Importantly, two types of oxazolidinone linkages with exocyclic olefin moieties were observed depending on the steric hindrance of the poly(hydroxy-oxazolidinone). For sterically hindered ones, α-alkylidene oxazolidinone linkages were selectively formed while a mixture of α- and β-alkylidene oxazolidinone linkages (almost in equimolar amounts) were noted for the less bulky ones.

Although the T_g of the poly(hydroxy-oxazolidinone)s could not be measured due to low polymer degradation temperature, the unsaturated poly(oxazolidinone)s presented a high thermal degradation temperature (T_d > 370 °C) with a high T_g (90-130 °C). This novel family of polymers is highly appealing for applications requiring high temperatures. Future works in our laboratory are to exploit the olefins to modify the polymers and to enlarge the scope of this unexplored polymer family. As the reactivity of the two alkylidene oxazolidinone linkages are expected to be different, selective modifications should be feasible which should give access to novel functional poly(oxazolidinone)s.

Experimental section

Materials

Potassium hydroxide (85 %) and Sulfuric acid were purchased from Acros Organics. 1,2-Diaminocyclohexane (mixture of isomers, 99 %) and Triethylamine (> 99 %) were purchased from Alfa Aesar. 1,4-Cyclohexanedione (98 %), Cyclohexane-1,4-diamine (mixture of isomers, 99 %), trans-1,4-Diaminocyclohexane (99%) and Zinc iodide (≥ 99 %) were purchased from Fluorochem. 1,8-Diazabicyclo(5.4.0)undec-7-ene (DBU) (99 %) was purchased from Fluka. 1,8-Diaminooctane (98 %), 2,5-Hexanedione (≥ 98 %), 3-Methyl-3-butyn-2-ol (98 %), 3,3′-Diamino-N-methyldipropylamine (96 %), Aniline (≥ 99.5 %), Benzylamine (≥ 99 %), Copper iodide (≥ 98 %), Cyclohexylamine (> 99 %), Ethynylmagnesium bromide solution (0.5 M in THF), Heptylamine (99%), m-Xylylenediamine (99 %), Phenol (≥ 99 %), Tetrabutylammonium bromide (≥ 98 %) were purchased from Sigma-Aldrich. Hydrochloric acid was purchased from Labotech. 1,2-Bis(2-aminoethoxy)ethane (> 98 %) was purchased from TCI. Glacial acetic acid and ammonium chloride (≥ 99.5 %) were purchased from VWR. Copper iodide was dispersed in acetic acid glacial overnight, filtered, washed with methanol under nitrogen flow, and dried under vacuum.

4,4-dimethyl-5-methylene-1,3-dioxolan-2-one (αCC) was synthesized according to the protocol described elsewhere[29]. The two bis(αCC)s monomers, 4,4'-(ethane-1,2-diyl)bis(4-methyl-5-methylene-1,3-dioxolan-2-one) (αCC1) and 4,12-dimethylene-1,3,9,11-

tetraoxadispiro[4.2.48.25]tetradecane-2,10-dione (αCC2) were synthesized according to a procedure described elsewhere.[31]

Characterization methods

Nuclear magnetic resonance (NMR) spectroscopy. ^{1}H-NMR analyses were performed on a Bruker 400 MHz spectrometer at 25 °C in the Fourier transform mode. 16 scans for ^{1}H spectra and 512 scans for ^{13}C spectra were recorded. Cross-polarization magic angle spinning (CP-MAS) solid state ^{13}C-NMR spectra were collected using a Bruker Avance DSX-400 instrument. Samples were packed in 4 mm zirconia rotors and spun at 10 kHz.

Size exclusion chromatography (SEC). Number-average molecular weight (M_n) and dispersity (D) of the polymers were determined by size exclusion chromatography (SEC) in dimethylformamide (DMF) containing LiBr (0.025 M) at 55 °C (flow rate: 1 mL/min) with a Waters chromatograph equipped with three columns (PSS gram 1000Å (x2), 30 Å) and a precolumn, a dual absorbance detector (Waters 2487) and a refractive index detector (Waters 2414).

Thermogravimetric analysis (TGA). TGA analysis was performed on a TGA2 instrument from Mettler Toledo. Around 10 mg of sample was flushed with nitrogen (20 mL/min) for 10 min at 25 °C. The sample was then heated at 20 °C/min until 600 °C under nitrogen atmosphere (20 mL/min).

Dynamic scanning calorimetry (DSC). DSC analysis was performed on a DSC Q2000 differential calorimeter (TA Instruments). All the experiments were performed under ultrapure nitrogen flow. Samples of 5–8 mg were used and placed in sealed aluminum pans. The samples were first heated at a rate of 10 °C min-1 from 25 °C to 150 °C. Subsequently, the samples were cooled down to -80 °C at a rate of 10 °C/min and then heated to 250 °C at 10 °C/min. The last heating cycle was used for the determination of the T_g.

General procedure for the synthesis of hydroxy-oxazolidinones by aminolysis of model αCC.

Synthesis protocol for 3-heptyl-4-hydroxy-4,5,5-trimethyloxazolidin-2-one (2a) and 3-benzyl-4-hydroxy-4,5,5-trimethyloxazolidin-2-one (2b). αCC (2 g, 15.6 mmol, 1 eq.) was added to a reaction tube containing dichloromethane (4 mL) and the amine (A1 or A2) (15.6 mmol, 1 eq.). The mixture was stirred at 50 °C for 24 h. The product was purified by chromatography onto silica (eluent: dichloromethane then dichloromethane/methanol (50:50)) and collected by evaporation of the solvent under reduced pressure at room temperature for 24 h. ^{1}H- and ^{13}C-NMR and ATR-IR spectra are provided in supporting information (Figures S1-S3, S4-S6).

Synthesis of 3-cyclohexyl-4-hydroxy-4,5,5-trimethyloxazolidin-2-one (2c). αCC (2 g, 15.6 mmol, 1 eq.) was added to a reaction tube containing DMF (4 mL) and the amine A3 (15.6 mmol, 1 eq.). The mixture was stirred at 25 °C for 48 h. The solvent was evaporated and the

obtained solid was washed with water on a Buchner apparatus, and dried under reduced pressure at room temperature for 24 h. ^{1}H- and ^{13}C-NMR and ATR-IR spectra are provided in supporting information (Figures S7-S9).

General procedure for the synthesis of poly(hydroxy-oxazolidinone)s.

The bis(α-alkylidene cyclic carbonate) (αCC1 or αCC2; 0.79 mmol, 1 eq.) was added to a reaction tube containing dry DMF (1.2 mL). The diamine (AA1-AA7; 1 eq.) was added and the tube was stirred at the specified temperature. After 24 h, an aliquot of the crude product was taken out for SEC and ^{1}H-NMR characterizations. The polymer was purified by precipitation in diethyl ether before filtration and vacuum drying at room temperature overnight.

The structure of the purified polymers was obtained by ^{1}H- and ^{13}C-NMR characterizations. Insoluble polymers were characterized by solid-state ^{13}C-NMR. All NMR characterizations are provided in the supporting information section.

General procedure for the dehydration of poly(hydroxy-oxazolidinone)s.

The polymer (500 mg) was added to a round bottom flask containing glacial acetic acid (5 mL). The mixture was stirred and refluxed for 2 h at 120 °C. Then, the dehydrated polymer was collected by precipitation in diethyl ether at -20 °C for 24 h before filtration and vacuum drying for 24 h at room temperature. All NMR characterizations are provided in supporting information.

References

(1) PlasticsEurope. The Facts 2019. *PlasticsEurope*. 2019.

(2) PlasticsInsight. Polyurethane Production, Pricing and Market Demand.

(3) Wegener, G.; Brandt, M.; Duda, L.; Hofmann, J.; Klesczewski, B.; Koch, D.; Kumpf, R.-J.; Orzesek, H.; Pirkl, H.-G.; Six, C.; Steinlein, C.; Weisbeck, M. Trends in Industrial Catalysis in the Polyurethane Industry. *Appl. Catal. A Gen.* 2001, *221* (1), 303–335. https://doi.org/https://doi.org/10.1016/S0926-860X(01)00910-3.

(4) Delebecq, E.; Pascault, J.-P.; Boutevin, B.; Ganachaud, F. On the Versatility of Urethane/Urea Bonds: Reversibility, Blocked Isocyanate, and Non-Isocyanate Polyurethane. *Chem. Rev.* 2013, *113* (1), 80–118. https://doi.org/10.1021/cr300195n.

(5) Engels, H.-W.; Pirkl, H.-G.; Albers, R.; Albach, R. W.; Krause, J.; Hoffmann, A.; Casselmann, H.; Dormish, J. Polyurethanes: Versatile Materials and Sustainable Problem Solvers for Today's Challenges. *Angew. Chemie Int. Ed.* 2013, *52* (36), 9422–9441. https://doi.org/10.1002/anie.201302766.

(6) Hepburn, C. *Polyurethane Elastomers*; Springer Netherlands, 2012.

(7) Qi, H. J.; Boyce, M. C. Stress-Strain Behavior of Thermoplastic Polyurethanes. *Mech. Mater.* 2005, *37* (8), 817–839. https://doi.org/https://doi.org/10.1016/j.mechmat.2004.08.001.

(8) Guo, A.; Javni, I.; Petrovic, Z. Rigid Polyurethane Foams Based on Soybean Oil. *J. Appl. Polym. Sci.* 2000, *77* (2), 467–473. https://doi.org/10.1002/(SICI)1097-4628(20000711)77:2<467::AID-APP25>3.0.CO;2-F.

(9) Cinelli, P.; Anguillesi, I.; Lazzeri, A. Green Synthesis of Flexible Polyurethane Foams from Liquefied Lignin. *Eur. Polym. J.* 2013, *49* (6), 1174–1184. https://doi.org/https://doi.org/10.1016/j.eurpolymj.2013.04.005.

(10) Panchireddy, S.; Grignard, B.; Thomassin, J.-M.; Jerome, C.; Detrembleur, C. Catechol Containing Polyhydroxyurethanes as High-Performance Coatings and Adhesives. *ACS Sustain. Chem. Eng.* 2018, *6* (11), 14936–14944. https://doi.org/10.1021/acssuschemeng.8b03429.

(11) Desai, S. D.; Patel, J. V; Sinha, V. K. Polyurethane Adhesive System from Biomaterial-Based Polyol for Bonding Wood. *Int. J. Adhes. Adhes.* 2003, *23* (5), 393–399. https://doi.org/https://doi.org/10.1016/S0143-7496(03)00070-8.

(12) Deka, H.; Karak, N. Bio-Based Hyperbranched Polyurethanes for Surface Coating Applications. *Prog. Org. Coatings* 2009, *66* (3), 192–198. https://doi.org/https://doi.org/10.1016/j.porgcoat.2009.07.005.

(13) Jena, K. K.; Raju, K. V. S. N. Synthesis and Characterization of Hyperbranched Polyurethane-Urea/Silica Based Hybrid Coatings. *Ind. Eng. Chem. Res.* 2007, *46* (20), 6408–6416. https://doi.org/10.1021/ie0703181.

(14) Pankratov, V. A.; Frenkel', T. M.; Fainleib, A. M. 2-Oxazolidinones. *Russ. Chem. Rev.* 1983, *52* (6), 576–593. https://doi.org/10.1070/rc1983v052n06abeh002864.

(15) Sandler, S. R. Poly-2-Oxazolidones as Cryogenic Adhesives. *J. Appl. Polym. Sci.* 1969, *13* (12), 2699–2703. https://doi.org/10.1002/app.1969.070131217.

(16) Kinjo, N.; Numata, S.-I.; Koyama, T.; Narahara, T. Synthesis and Viscoelastic Properties of New Thermosetting Resins Having Isocyanurate and Oxazolidone Rings in Their Molecular Structures. *J. Appl. Polym. Sci.* 1983, *28* (5), 1729–1741. https://doi.org/10.1002/app.1983.070280516.

(17) Sendijarevic, V.; Sendijarevic, A.; Lekovic, H.; Lekovic, H.; Frisch, K. C. Polyoxazolidones for High Temperature Applications. *J. Elastomers Plast.* 1996, *28* (1), 63–83. https://doi.org/10.1177/009524439602800104.

(18) Kitayama, M.; Isda, Y.; Odaka, F.; Anzai, S.; Irako, K. Synthesis and Properties of Polyoxazolidone Elastomers from Diepoxides and Diisocyanates. *Rubber Chem. Technol.* 1980, *53* (1), 1–13. https://doi.org/10.5254/1.3535029.

(19) Sendijarevic, V.; Sendijarevic, A.; Frisch, K. C.; Reulen, P. Novel Isocyanate-Based Matrix Resins for High Temperature Composite Applications. *Polym. Compos.* 1996, *17* (2), 180–186. https://doi.org/10.1002/pc.10603.

(20) Pelzer, T.; Eling, B.; Thomas, H.-J.; Luinstra, G. A. Toward Polymers with Oxazolidin-2-One Building Blocks through Tetra-n-Butyl-Ammonium Halides (Cl, Br, I) Catalyzed Coupling of Epoxides with Isocyanates. *Eur. Polym. J.* 2018, *107*, 1–8. https://doi.org/https://doi.org/10.1016/j.eurpolymj.2018.07.039.

(21) Speranza, G. P.; Peppel, W. J. Preparation of Substituted 2-Oxazolidones from 1,2-Epoxides and Isocyanates. *J. Org. Chem.* 1958, *23* (12), 1922–1924. https://doi.org/10.1021/jo01106a027.

(22) Prokofyeva, A.; Laurenzen, H.; Dijkstra, D. J.; Frick, E.; Schmidt, A. M.; Guertler, C.; Koopmans, C.; Wolf, A. Poly-2-Oxazolidones with Tailored Physical Properties Synthesized by Catalyzed Polyaddition of 2,4-Toluene Diisocyanate and Different Bisphenol-Based Diepoxides. *Polym. Int.* 2017, *66* (3), 399–404. https://doi.org/10.1002/pi.5279.

(23) Herweh, J. E.; Whitmore, W. Y. Poly-2-Oxazolidones: Preparation and Characterization. *J. Polym. Sci. Part A-1 Polym. Chem.* 1970, *8* (10), 2759–2773. https://doi.org/10.1002/pol.1970.150081004.

(24) Altmann, H. J.; Clauss, M.; König, S.; Frick-Delaittre, E.; Koopmans, C.; Wolf, A.; Guertler, C.; Naumann, S.; Buchmeiser, M. R. Synthesis of Linear Poly(Oxazolidin-2-One)s by Cooperative Catalysis Based on N-Heterocyclic Carbenes and Simple Lewis Acids. *Macromolecules* 2019, *52* (2), 487–494. https://doi.org/10.1021/acs.macromol.8b02403.

(25) Iwakura, Y.; Izawa, S.-I.; Hayano, F. Polyoxazolidones Prepared from Bisurethans and Bisepoxides. *J. Polym. Sci. Part A-1 Polym. Chem.* 1966, *4* (4), 751–760. https://doi.org/10.1002/pol.1966.150040402.

(26) Yoo, W.-J.; Li, C.-J. Copper-Catalyzed Four-Component Coupling between Aldehydes, Amines, Alkynes, and Carbon Dioxide. *Adv. Synth. Catal.* 2008, *350* (10), 1503–1506. https://doi.org/10.1002/adsc.200800232.

(27) Teffahi, D.; Li, S. H.; Chao-Jun. Synthesis of Oxazolidinones, Dioxazolidinone and Polyoxazolidinone (A New Polyurethane) Via A Multi Component-Coupling of Aldehyde, Diamine Dihydrochloride, Terminal Alkyne and CO2. *Letters in Organic Chemistry*. 2012, pp 585–593. https://doi.org/http://dx.doi.org/10.2174/157017812802850221.

(28) Wu, Q.; Chen, J.; Guo, X.; Xu, Y. Copper(I)-Catalyzed Four-Component Coupling Using Renewable Building Blocks of CO2 and Biomass-Based Aldehydes. *European J. Org. Chem.* 2018, *2018* (24), 3105–3113. https://doi.org/10.1002/ejoc.201800461.

(29) Gennen, S.; Grignard, B.; Tassaing, T.; Jérôme, C.; Detrembleur, C. CO2-Sourced α-Alkylidene Cyclic Carbonates: A Step Forward in the Quest for Functional Regioregular Poly(Urethane)s and Poly(Carbonate)S. *Angew. Chemie Int. Ed.* 2017, *56* (35), 10394–10398. https://doi.org/10.1002/anie.201704467.

(30) Grignard, B.; Gennen, S.; Jérôme, C.; Kleij, A. W.; Detrembleur, C. Advances in the Use of CO2 as a Renewable Feedstock for the Synthesis of Polymers. *Chem. Soc. Rev.* 2019, *48* (16), 4466–4514. https://doi.org/10.1039/C9CS00047J.

(31) Ouhib, F.; Grignard, B.; Van Den Broeck, E.; Luxen, A.; Robeyns, K.; Van Speybroeck, V.; Jerome, C.; Detrembleur, C. A Switchable Domino Process for the Construction of Novel CO2-Sourced Sulfur-Containing Building Blocks and Polymers. *Angew. Chemie Int. Ed.* 2019, *58* (34), 11768–11773. https://doi.org/10.1002/anie.201905969.

(32) Delidovich, I.; Hausoul, P. J. C.; Deng, L.; Pfützenreuter, R.; Rose, M.; Palkovits, R. Alternative Monomers Based on Lignocellulose and Their Use for Polymer Production. *Chem. Rev.* 2016, *116* (3), 1540–1599. https://doi.org/10.1021/acs.chemrev.5b00354.

(33) Upton, B. M.; Kasko, A. M. Strategies for the Conversion of Lignin to High-Value Polymeric Materials: Review and Perspective. *Chem. Rev.* 2016, *116* (4), 2275–2306. https://doi.org/10.1021/acs.chemrev.5b00345.

(34) Francis, T.; Thorne, M. P. Carbamates and 2-Oxazolidinones from Tertiary Alcohols and Isocyanates. *Can. J. Chem.* 1976, *54* (1), 24–30. https://doi.org/10.1139/v76-006.

(35) Hase, S.; Kayaki, Y.; Ikariya, T. Mechanistic Aspects of the Carboxylative Cyclization of Propargylamines and Carbon Dioxide Catalyzed by Gold(I) Complexes Bearing an N-Heterocyclic Carbene Ligand. *ACS Catal.* 2015, *5* (9), 5135–5140. https://doi.org/10.1021/acscatal.5b01335.

Supporting Informations

Synthesis of model hydroxy-oxazolidinones 2a-2c.

*Synthesis of 3-heptyl-4-hydroxy-4,5,5-trimethyloxazolidin-2-one (**2a**)*

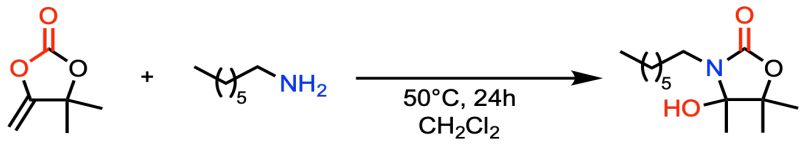

Scheme S1. Synthetic route for **2a**.

αCC (2 g, 15.6 mmol, 1 eq.) was added to a reaction tube containing dichloromethane (4 mL) and **A1** (2.31 ml, 15.6 mmol, 1 eq.). The mixture was stirred at 50 °C for 24 h. The product was purified by chromatography onto silica (eluent: dichloromethane then dichloromethane / methanol (50:50)). An orange solid was collected after evaporation of the solvent (3.05 g, isolated yield = 80%).

^{1}H NMR (DMSO-d$_6$, 400 MHz): (s, 1H), 3.06 (m, 2H), 1.51 (q, 2H, J=7Hz), 1.18 (m, 17H), 0.87 (t, 3H) ppm.

^{13}C NMR (DMSO-d$_6$, 400 MHz): 156.89, 89.65, 84.39, 39.88, 31.72, 29.58, 28.89, 26.84, 24.99, 22.52, 20.95, 20.91, 14.36 ppm.

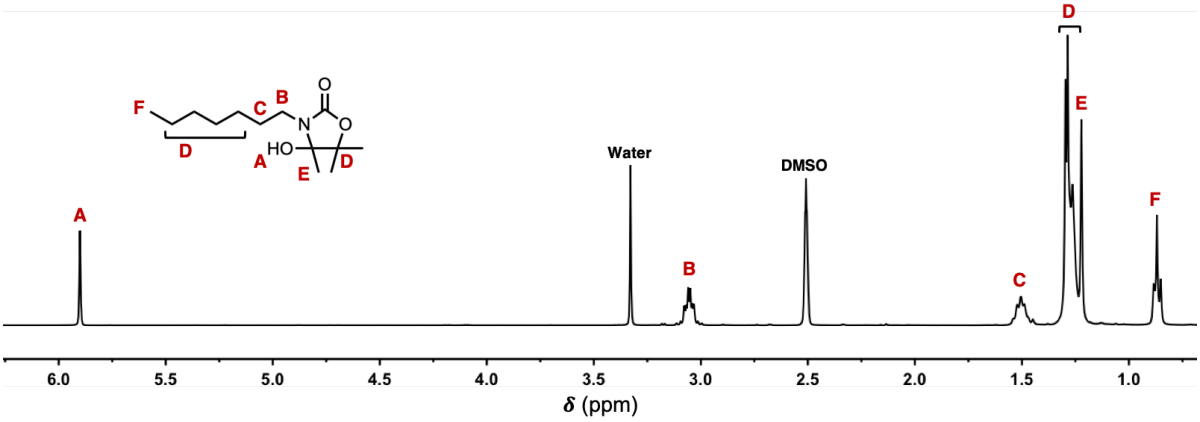

Figure S1. ^{1}H-NMR spectrum (400 MHz, DMSO-d$_6$) of **2a**.

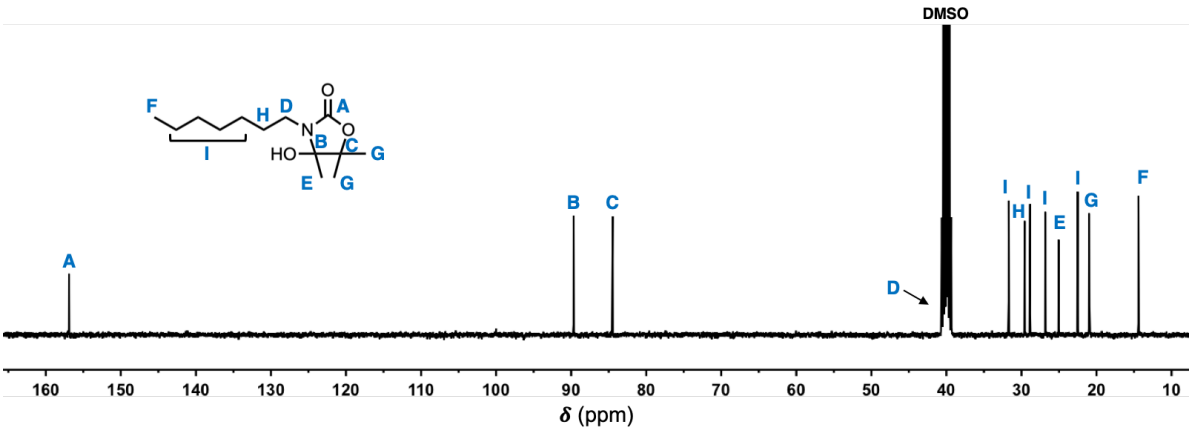

Figure S2. ^{13}C-NMR spectrum (400 MHz, DMSO-d_6) of **2a**.

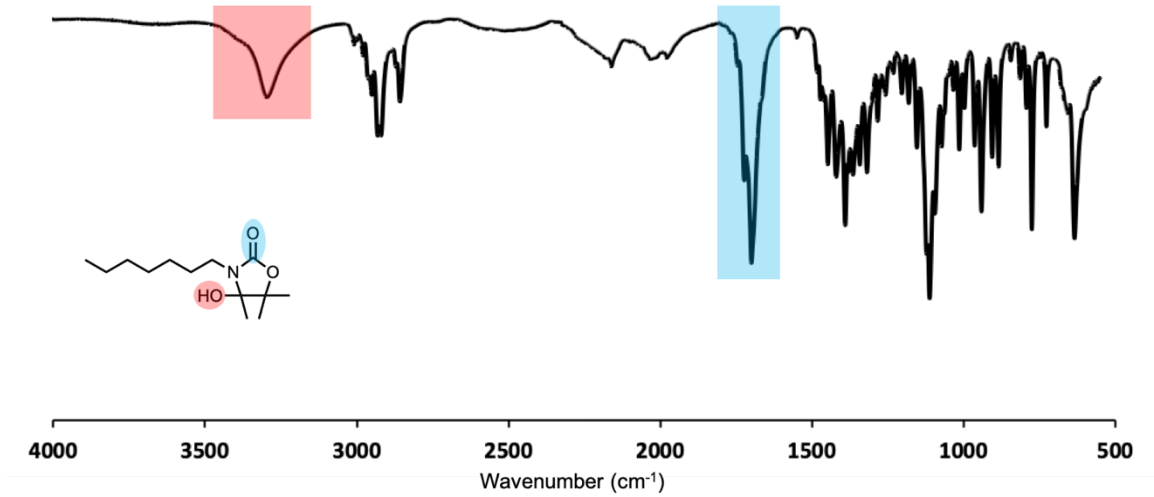

Figure S3. ATR-IR spectrum of **2a**.

*Synthesis of 3-benzyl-4-hydroxy-4,5,5-trimethyloxazolidin-2-one (**2b**)*

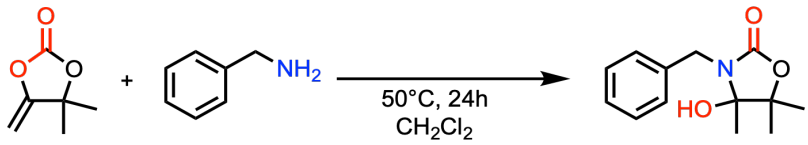

Scheme S2. Synthetic route for **2b**.

αCC (2 g, 15.6 mmol, 1 eq.) was added to a reaction tube in 4 ml of dichloromethane with **A2** (1.70 ml, 15.6 mmol, 1 eq.). The mixture was stirred at 50 °C for 24 h. The product was purified via chromatography onto silica (eluent: dichloromethane then dichloromethane / methanol (50:50)). A white solid was collected after evaporation of the solvent (3.50 g, isolated yield = 95%).

^{1}H NMR (DMSO-d_6, 400 MHz): 7.38 (m, 5H), 6.15 (s, 1H), 4.44 (d, 1H, J=16Hz), 4.20 (d, 1H, J=16 Hz), 1.33 (s, 3H), 1.26 (s, 3H), 1.13 (s, 3H) ppm.

^{13}C NMR (DMSO-d_6, 400 MHz): 157.45, 139.39, 128.84, 127.33, 89.84, 84.93, 43.09, 25.19, 21.19, 20.98 ppm.

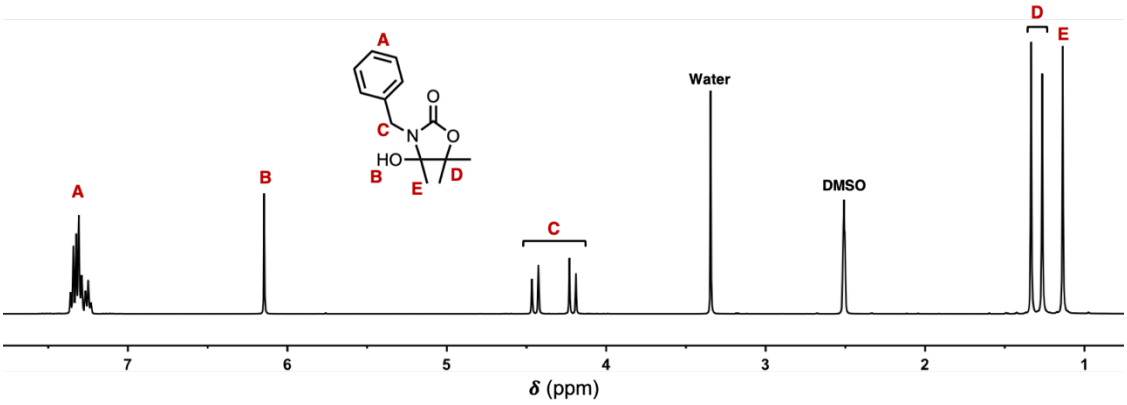

Figure S4. ^{1}H NMR spectrum (400 MHz, DMSO-d_6) of **2b**.

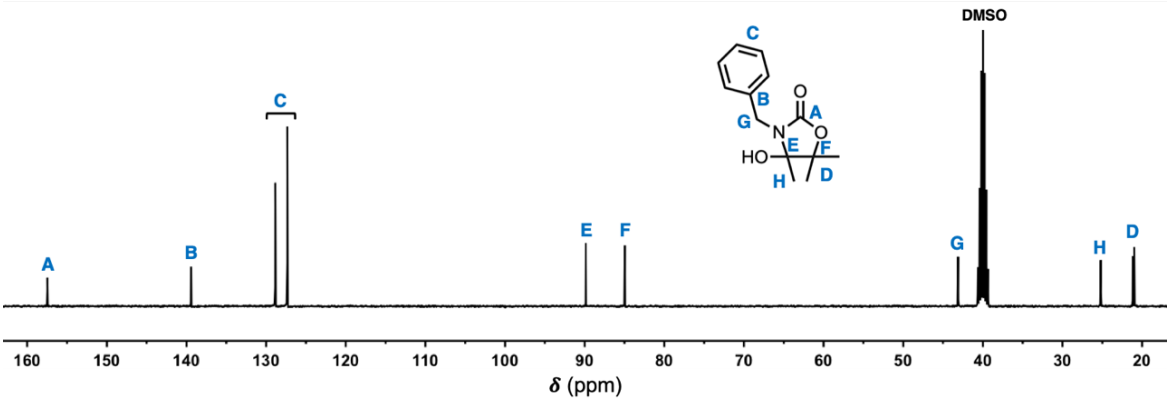

Figure S5. ^{13}C NMR spectrum (400 MHz, DMSO-d_6) of **2b**.

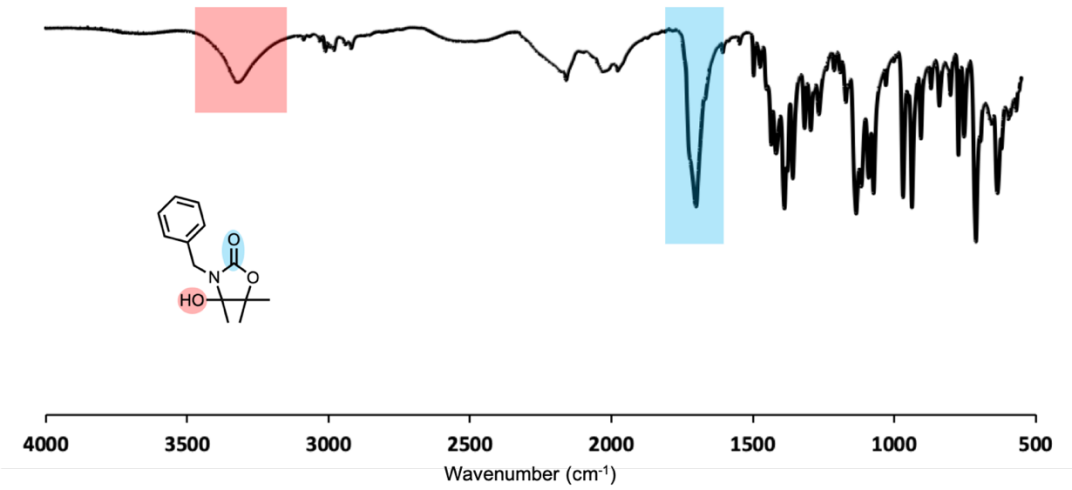

Figure S6. ATR-IR spectrum of **2b**.

*Synthesis of 3-cyclohexyl-4-hydroxy-4,5,5-trimethyloxazolidin-2-one (**2c**)*

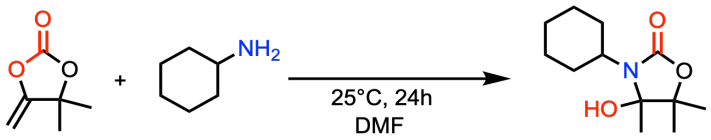

Scheme S3. Synthetic route for **2c**.

αCC (2 g, 15.6 mmol, 1 eq.) was added to a reaction tube in 4 ml of DMF with **A3** (1.78 ml, 15.6 mmol, 1 eq.). The mixture was stirred at 25°C for 48h. The solvent was evaporated and the obtained white solid was washed with water on a Buchner apparatus, and dried under vacuum at room temperature for 24h (1.2 g, isolated yield = 34%).

^{1}H NMR (DMSO-d$_6$, 400 MHz): 6.86 (s, 1H), 3.05 (tt, 1H), 1.84-2.11 (m, 2H), 1.53-1.78 (m, 5H), 1.30 (s, 3H), 1.26 (s, 3H), 1.20 (s, 3H), 1.17-1.35 (m, 2H), 1-1.14 (m, 1H) ppm.

^{13}C NMR (DMSO-d$_6$, 400 MHz): 155.10, 90.44, 83.81, 51.44, 30.66, 30.47, 26.22, 26.15, 25.50, 24.95, 21.19, 21.04 ppm.

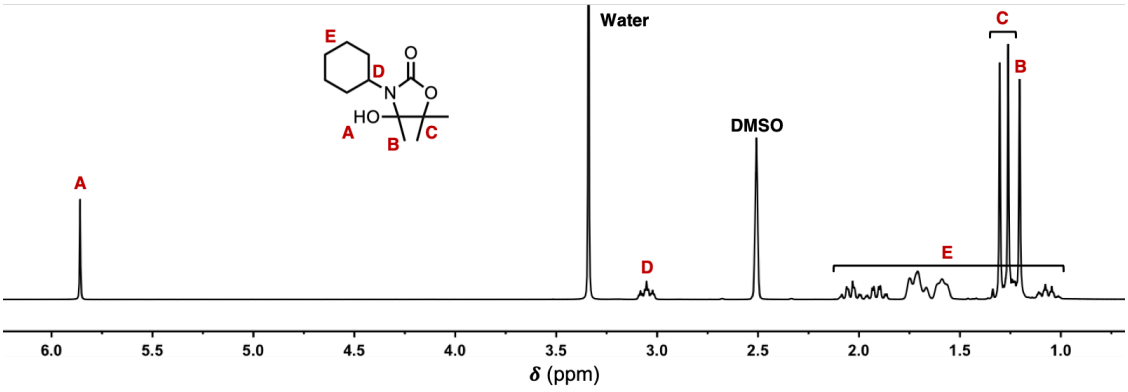

Figure S7. ^{1}H NMR spectrum (400 MHz, DMSO-d$_6$) of **2c**.

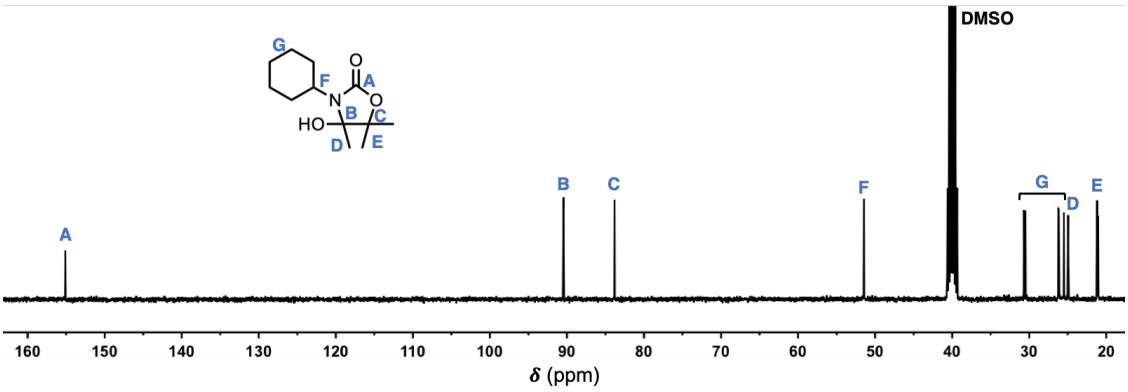

Figure S8. ^{13}C NMR spectrum (400 MHz, DMSO-d$_6$) of **2c**

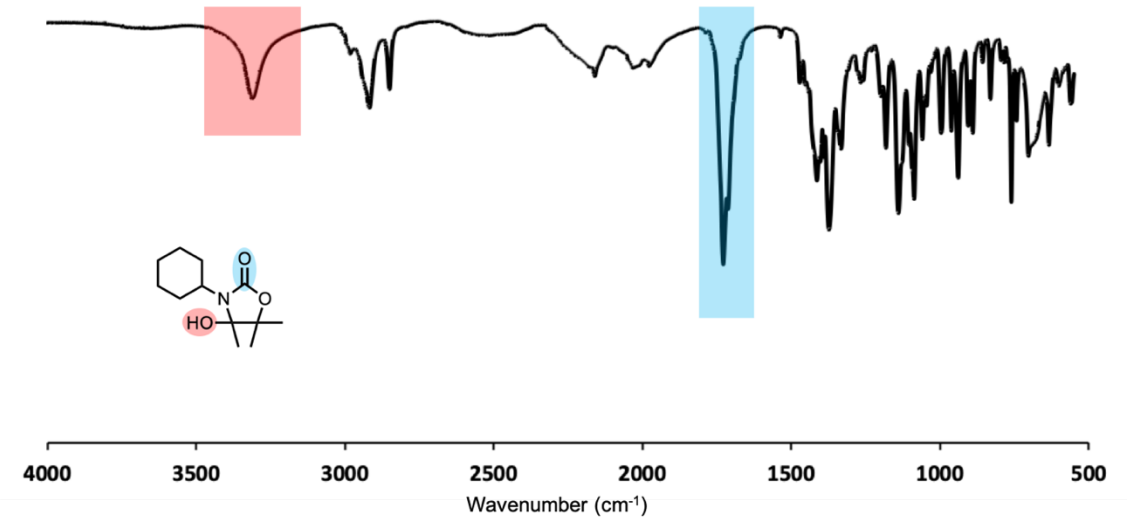

Figure S9. ATR-IR spectrum of **2c**.

Aminolysis of αCC with model amines

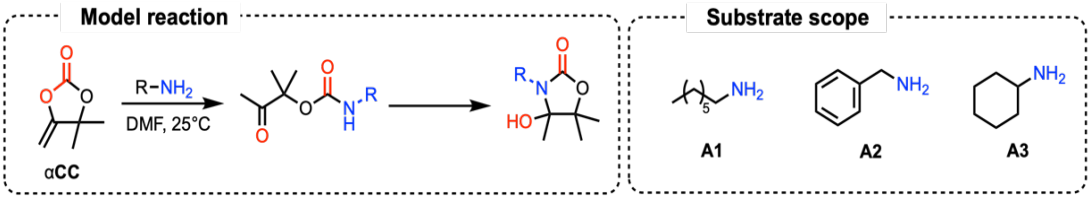

Scheme S4. Aminolysis of **αCC** by a primary amine and substrate scope.

Model reactions between **αCC** and the different monofunctional amines (**A1**, **A2**, **A3**) have been carried out under different conditions. The kinetics were monitored by ^{1}H NMR spectroscopy by sampling over time. The conversion of **αCC** and the selectivity toward the different products were then calculated by comparison of the relative intensities of the resonance of the olefinic protons of **αCC** at 4.77 (or 4.37) ppm and the resonance associated to the hydroxy-oxazolidinone as it will be described below.

General procedure

αCC (0.5g, 3.91mmol, 1 eq.) was added to a reaction tube and dissolved in a volume of solvent (DMF or DMSO) at a specified temperature under stirring. If used, DBU (29.85 mL, 0.2 mmol, 0.05 eq.) was added to the mixture. The reaction was then carried out by adding the amine (**A1**, **A2** or **A3**; 1eq.) to the reaction medium under stirring.

The NMR samples were prepared by mixing 7-8 drops of the reaction medium, one drop of acid (HCl or acetic acid depending on the amine) to quench the reaction, and 700 µL of $CDCl_3$. The tube was then stored at -20°C until NMR analysis.

Aminolysis of αCC by **A1**

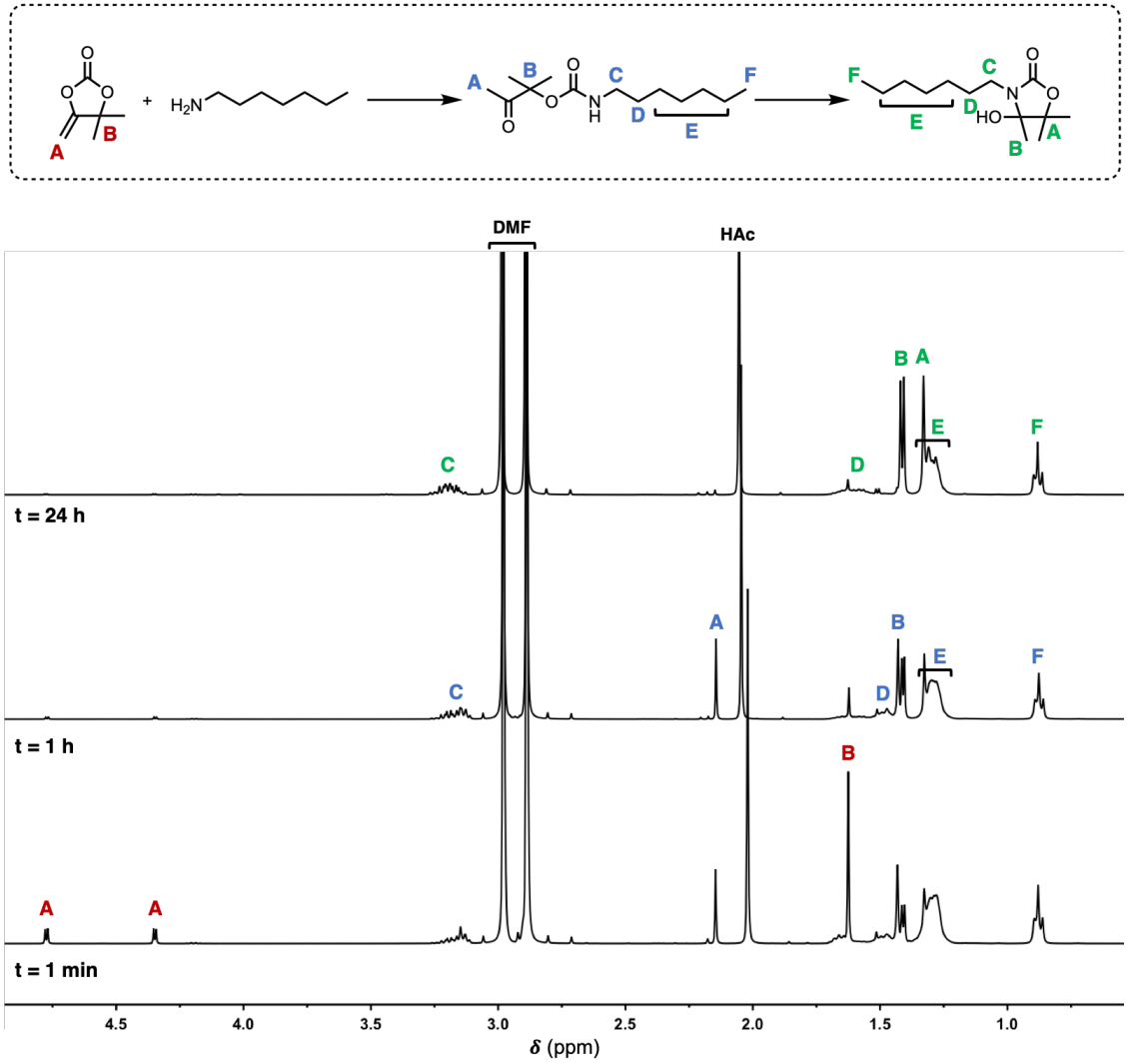

Figure S10. Kinetic study of the aminolysis of αCC by heptylamine **A1**.

For each compound of the reaction, a peak was selected and integrated: 4.77 ppm for αCC (1H), 2.15 ppm for the linear intermediate (3H), and two peaks from 1.4 to 1.43 ppm for the oxazolidinone (6H).

$$Conv. = 1 - \left(\frac{I(4.77)}{I(4.77) + \frac{I(2.15)}{3} + \frac{I(1.42)}{6}}\right)$$

Aminolysis of αCC by **A2**

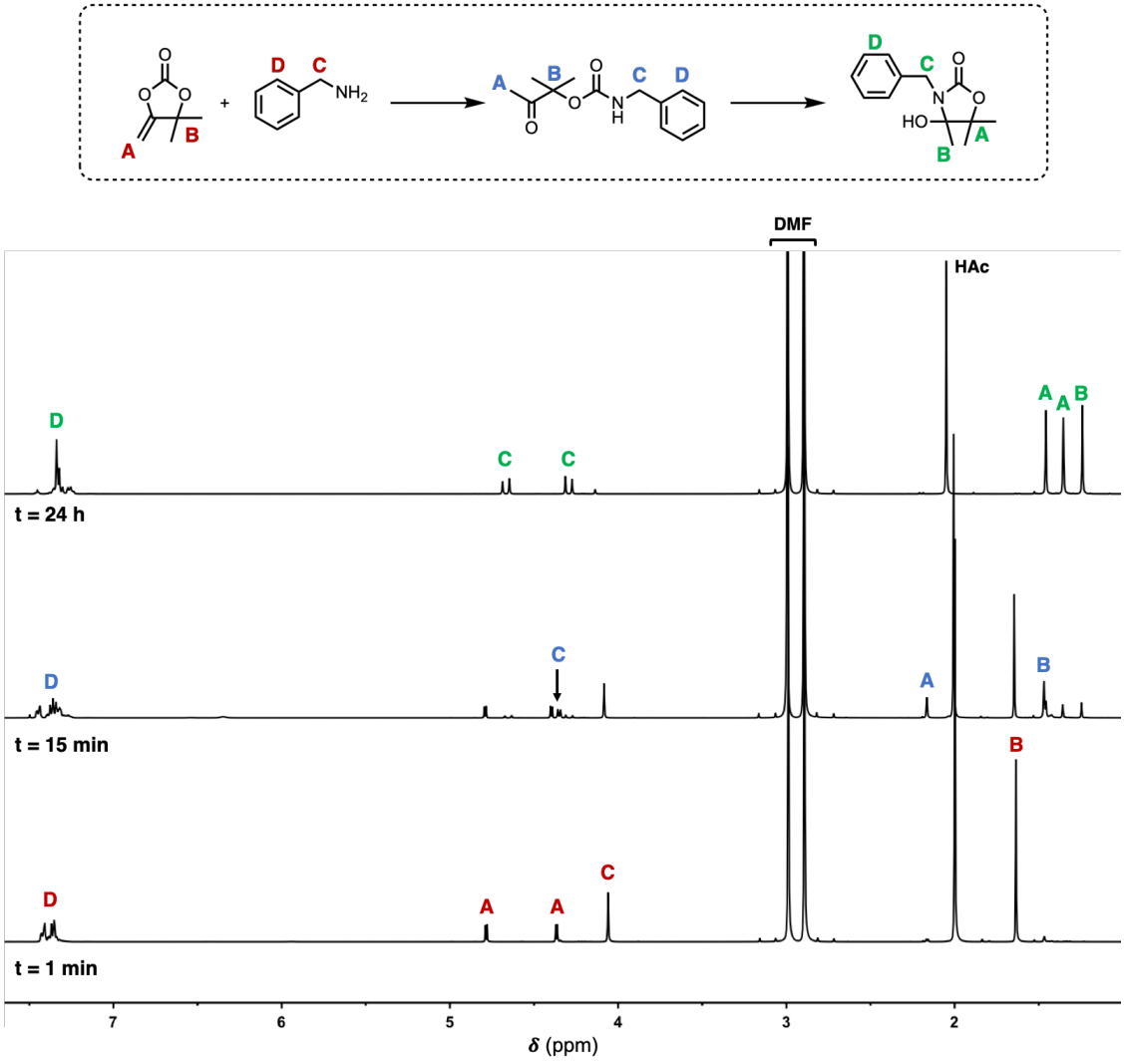

Figure S11. Kinetic study of the aminolysis of **αCC** by benzylamine **A2**.

For each compound of the reaction, a peak was selected and integrated: 4.77 ppm for **αCC** (1H), 2.14 ppm for the linear intermediate (3H), and 1.22 ppm for the oxazolidinone (3H).

$$Conv. = 1 - \left(\frac{I(4.77)}{I(4.77) + \frac{I(2.14)}{3} + \frac{I(1.22)}{3}}\right)$$

Aminolysis of αCC by A3

Since some α-alkylidene oxazolidinone was formed by the acid-catalyzed dehydration reaction when quenching with HCl, the selectivity for this α-alkylidene oxazolidinone was included in the selectivity of the hydroxy-oxazolidinone product. A kinetics without quench has been achieved to check the absence of the dehydrated product.

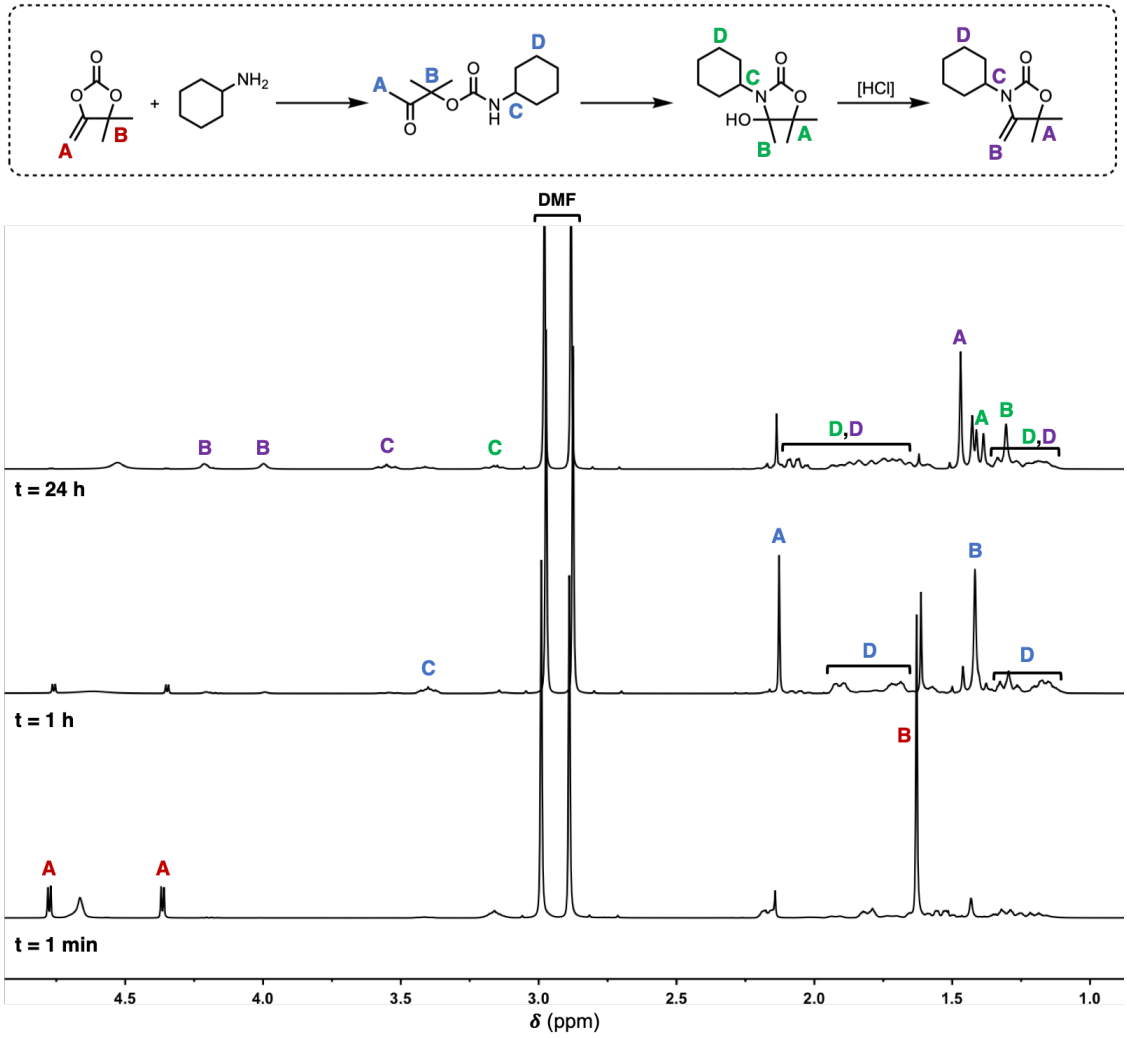

Figure S12. Kinetic study of the aminolysis of **αCC** by cyclohexylamine **A3**.

For each compound of the reaction, a peak was selected and integrated: 4.37 ppm for **αCC** (1H), 3.42 ppm for the linear intermediate (1H), 1.39 ppm for the oxazolidinone (3H), and 3.55 ppm for the dehydrated oxazolidinone (1H).

$$Conv. = 1 - \left(\frac{I(4.37)}{I(4.37) + \frac{I(3.42)}{1} + \frac{I(1.39)}{3} + \frac{I(3.55)}{1}}\right)$$

Dehydration of hydroxy-oxazolidinones

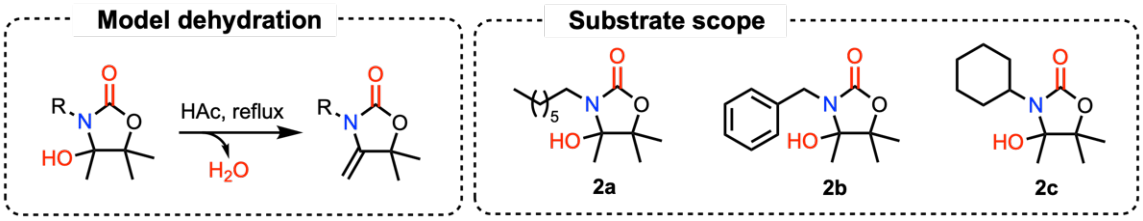

Scheme S5. Dehydration of hydroxy-oxazolidinones **2a**, **2b** and **2c** into α-alkylidene oxazolidinones.

Dehydration of the model hydroxy-oxazolidinones (**2a**, **2b**, **2c**) have been carried out under reflux in acetic acid as solvent. Hydroxy-oxazolidinone conversions were determined by ^{1}H-NMR spectroscopy. Results are collected in Scheme 3.

General procedure for the dehydration in acetic acid.

The hydroxy-oxazolidinone (**2a**, **2b** or **2c**) (2.2 mmol, 1 eq.) was added to a round-bottom flask with 10 mL of acetic acid. The reaction mixture was stirred for 2h under reflux (120°C). The solvent was then evaporated under vacuum and the product was characterized by ^{1}H-NMR spectroscopy in DMSO-d_6.

For **2a** dehydration: the product was quantitatively formed.

For **2b** dehydration: For each compound of the reaction, a peak was selected and integrated: 4.62 ppm for the dehydrated oxazolidinone (2H) and 1.13 ppm for **2b** (3H).

$$Conv. = 1 - \left(\frac{\frac{I(1.13)}{3}}{\frac{I(1.13)}{3} + \frac{I(4.62)}{2}}\right)$$

For **2c** dehydration: For each compound of the reaction, a peak was selected and integrated: 3.54 ppm for the dehydrated oxazolidinone (1H) and 3.05 ppm for **2c** (1H).

$$Conv. = 1 - \left(\frac{\frac{I(1.13)}{3}}{\frac{I(1.13)}{3} + \frac{I(4.62)}{2}}\right)$$

2a dehydration into 3-heptyl-5,5-dimethyl-4-methyleneoxazolidin-2-one (**3a**)

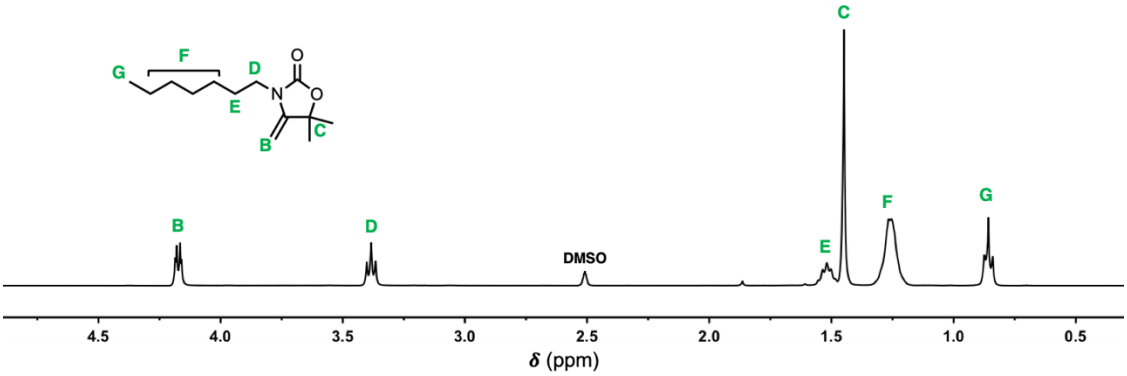

Figure S13. ^{1}H-NMR spectrum (400 MHz, DMSO-d_6) of the dehydrated **2a.**

2b dehydration into 3-benzyl-5,5-dimethyl-4-methyleneoxazolidin-2-one (**3b**)

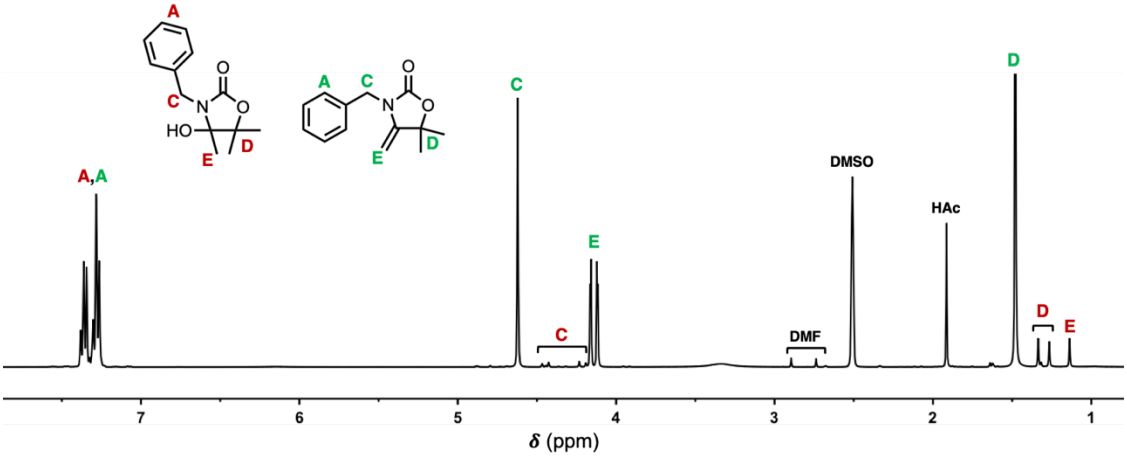

Figure S14. ^{1}H-NMR spectrum (400 MHz, DMSO-d_6) of the dehydrated **2b**.

2c dehydration into 3-cyclohexyl-5,5-dimethyl-4-methyleneoxazolidin-2-one (**3c**)

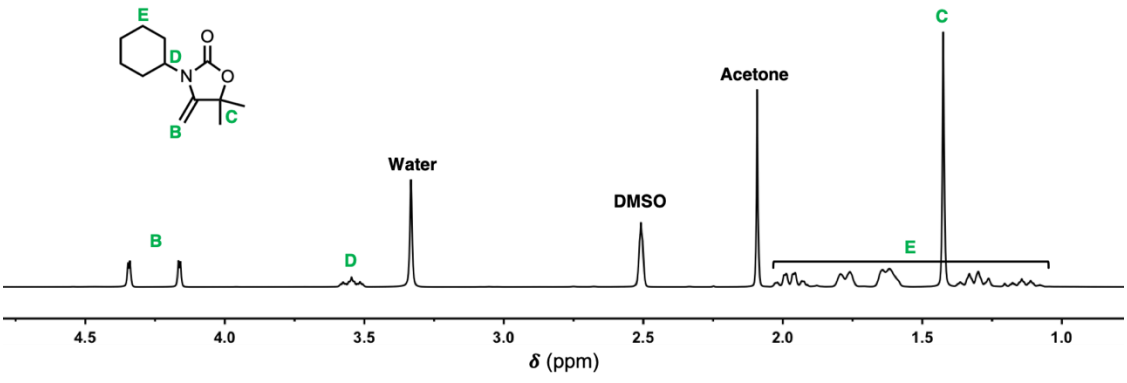

Figure S15. ^{1}H NMR spectrum (400 MHz, DMSO-d_6) of the dehydrated **2c**.

COSY, HSQC and HMBC NMR characterizations of the polymers

P(CC1-AA1)

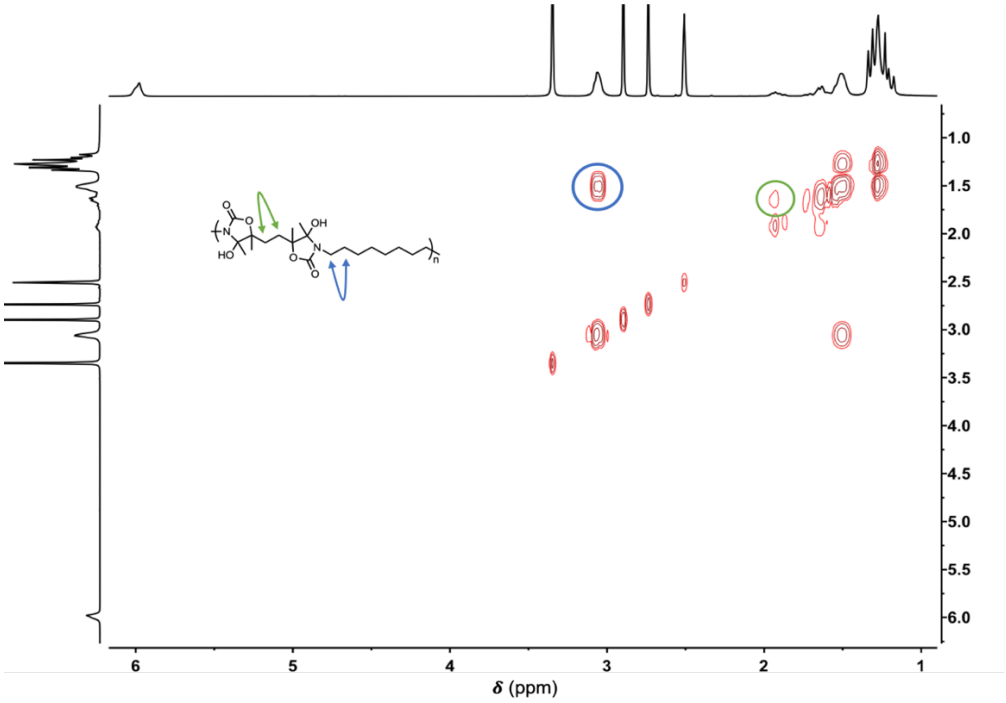

Figure S16. COSY NMR spectrum (400 MHz, DMSO-d_6) of **P(CC1-AA1)**.

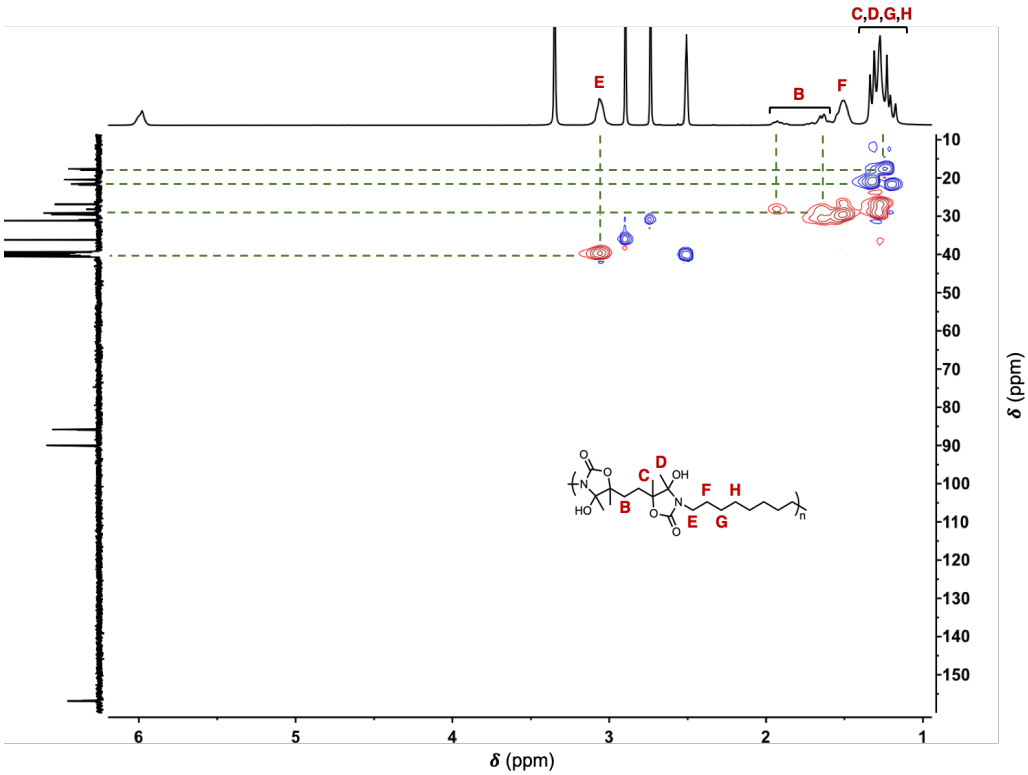

Figure S17. HSQC NMR spectrum (400 MHz, DMSO-d_6) of **P(CC1-AA1)**.

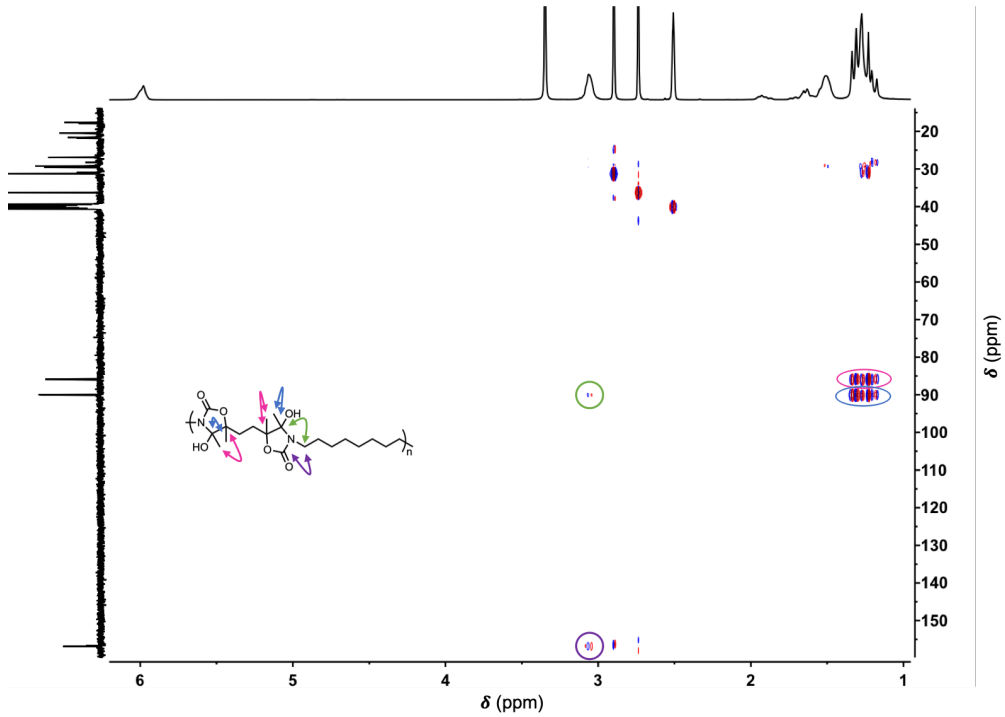

Figure S18. HMBC NMR spectrum (400 MHz, DMSO-d_6) of **P(CC1-AA1)**.

P(CC1-AA2)

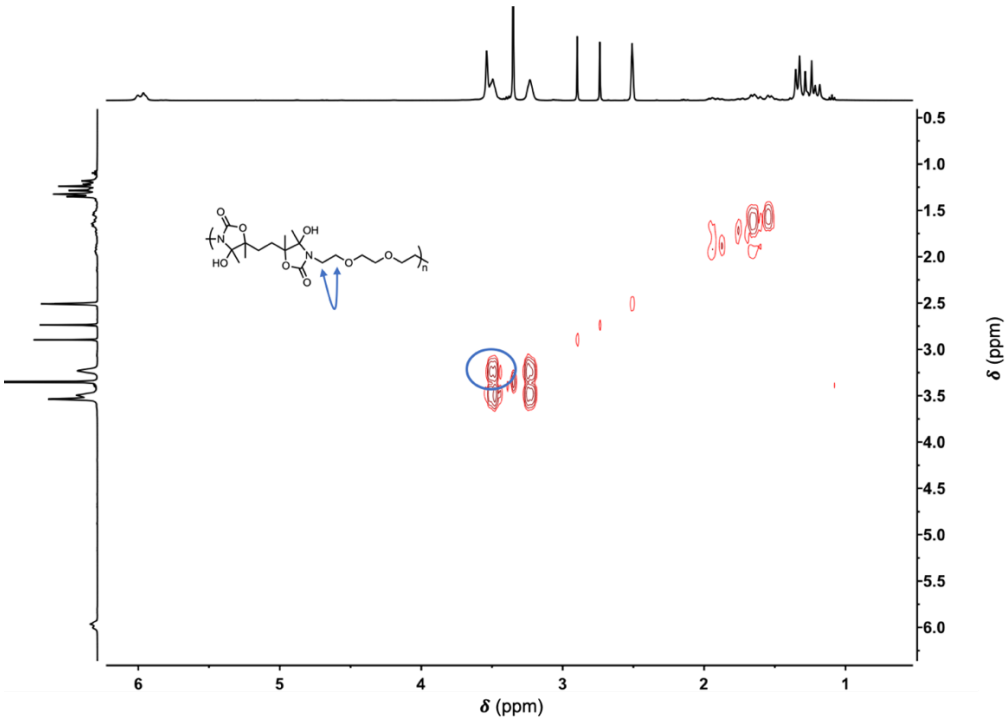

Figure S19. COSY NMR spectrum (400 MHz, DMSO-d_6) of **P(CC1-AA2)**.

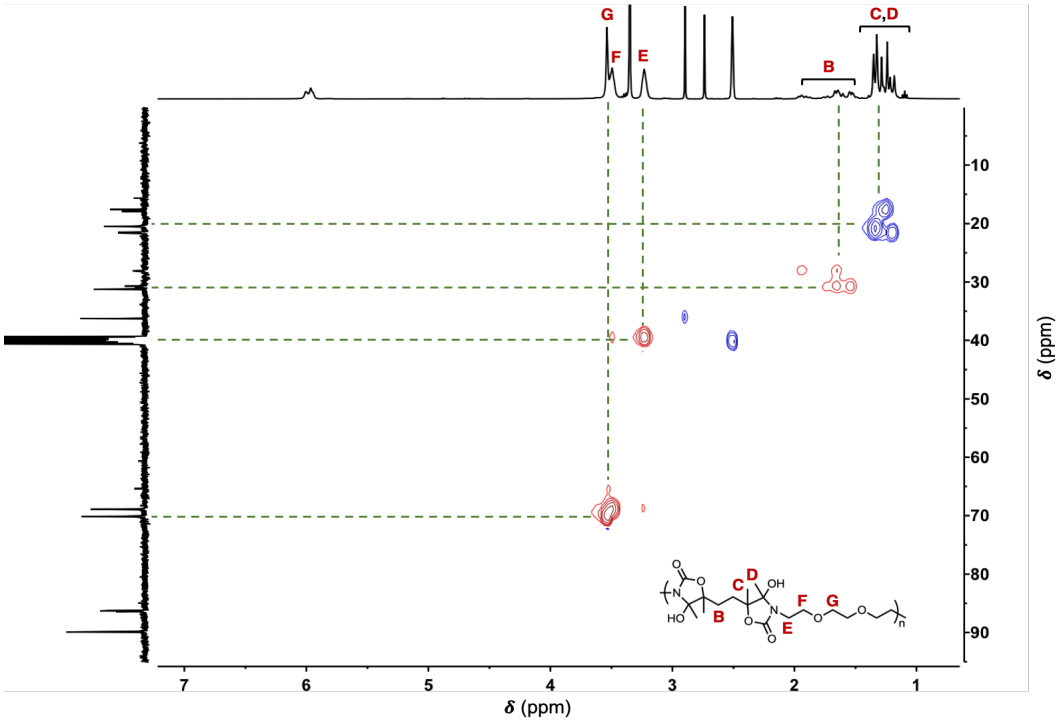

Figure S20. HSQC NMR spectrum (400 MHz, DMSO-d_6) of **P(CC1-AA2)**.

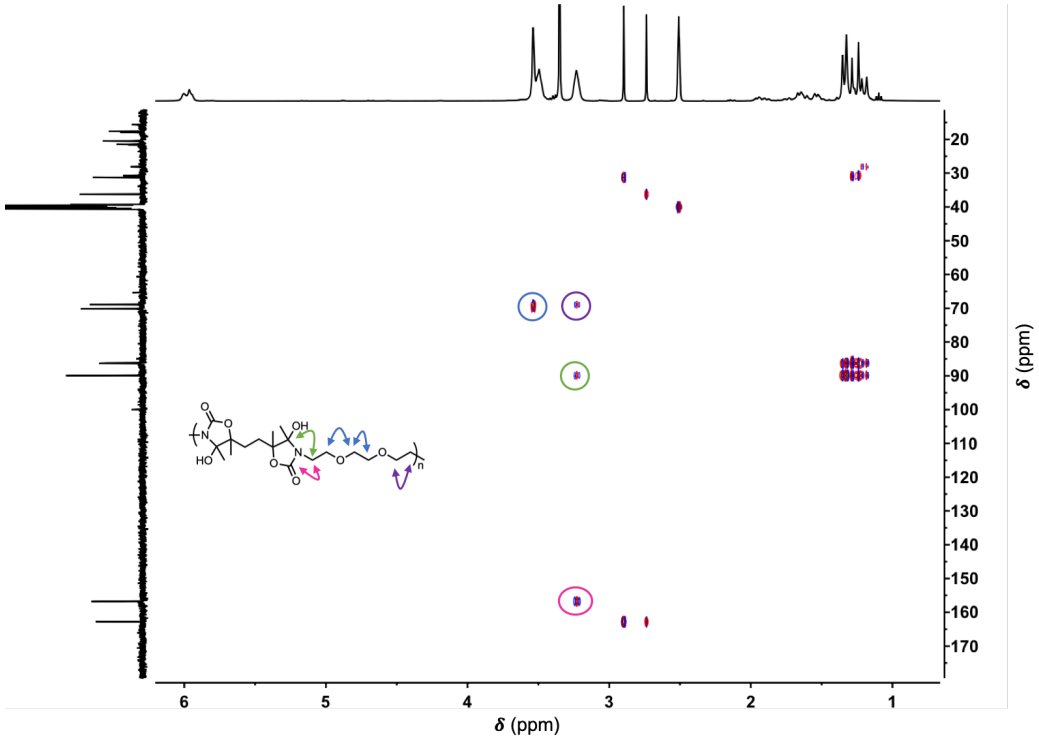

Figure S21. HMBC NMR spectrum (400 MHz, DMSO-d_6) of **P(CC1-AA2)**.

P(CC1-AA3)

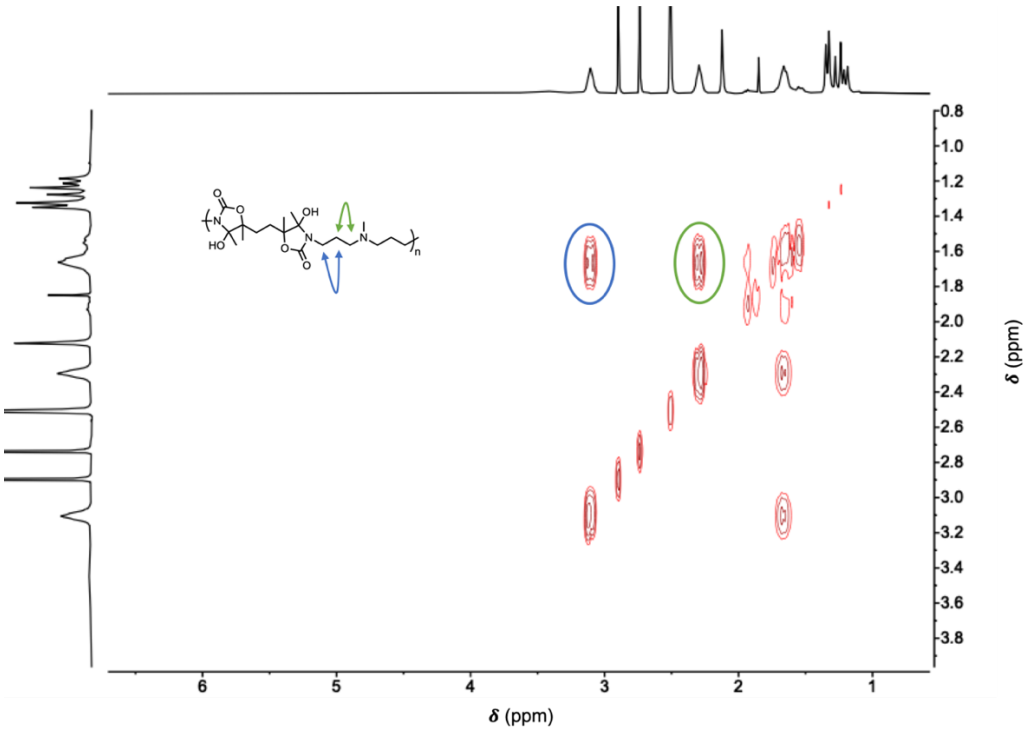

Figure S22. COSY NMR spectrum (400 MHz, DMSO-d_6) of **P(CC1-AA3)**.

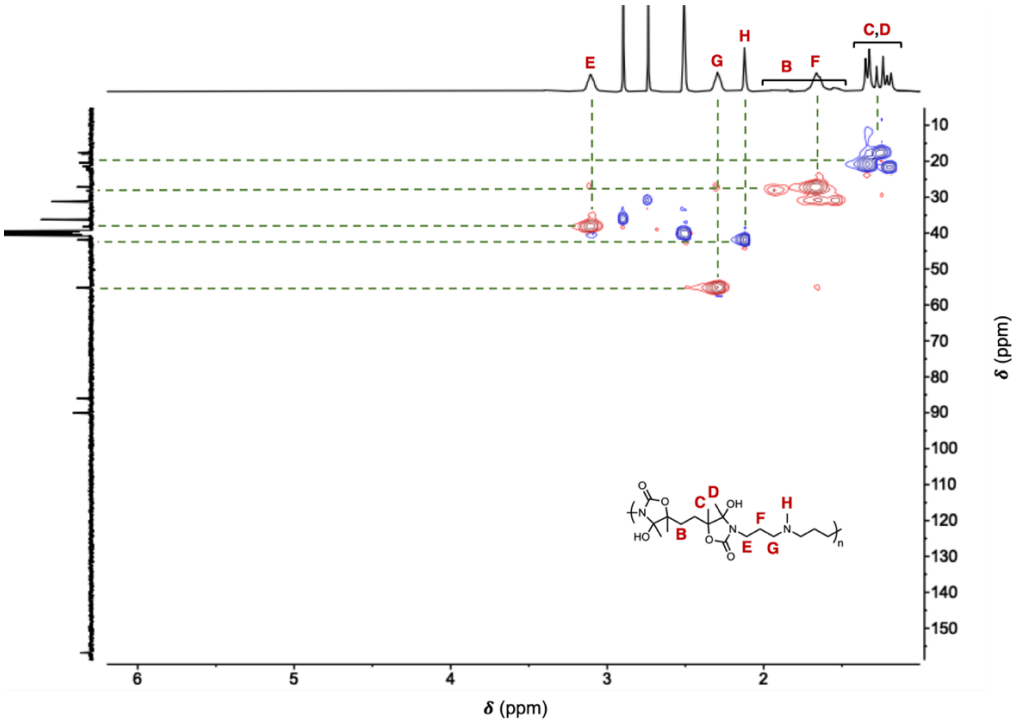

Figure S23. HSQC NMR spectrum (400 MHz, DMSO-d_6) of **P(CC1-AA3)**.

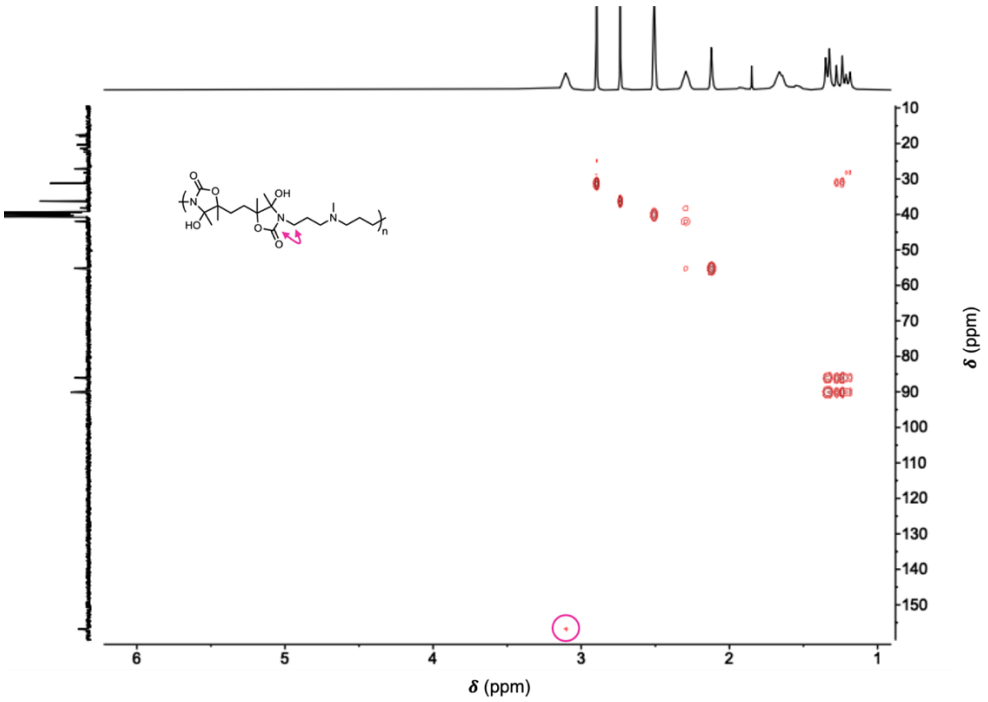

Figure S24. HMBC NMR spectrum (400 MHz, DMSO-d_6) of **P(CC1-AA3)**.

P(CC1-AA4)

Despite the decent solubility of the polymer **P(CC1-AA4)** in DMSO-d_6, ^{13}C NMR analyses gave a very low signal and the spectrum can't thus be interpreted. A solid state ^{13}C NMR analysis was then be conducted in order to achieve the attribution.

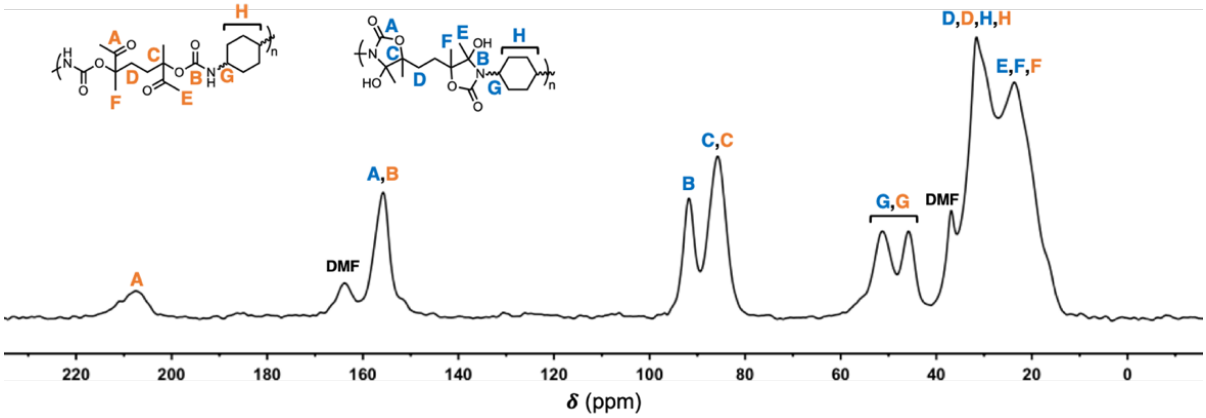

Figure S25. Solid-state ^{13}C NMR spectrum (400 MHz) of **P(CC1-AA4)**.

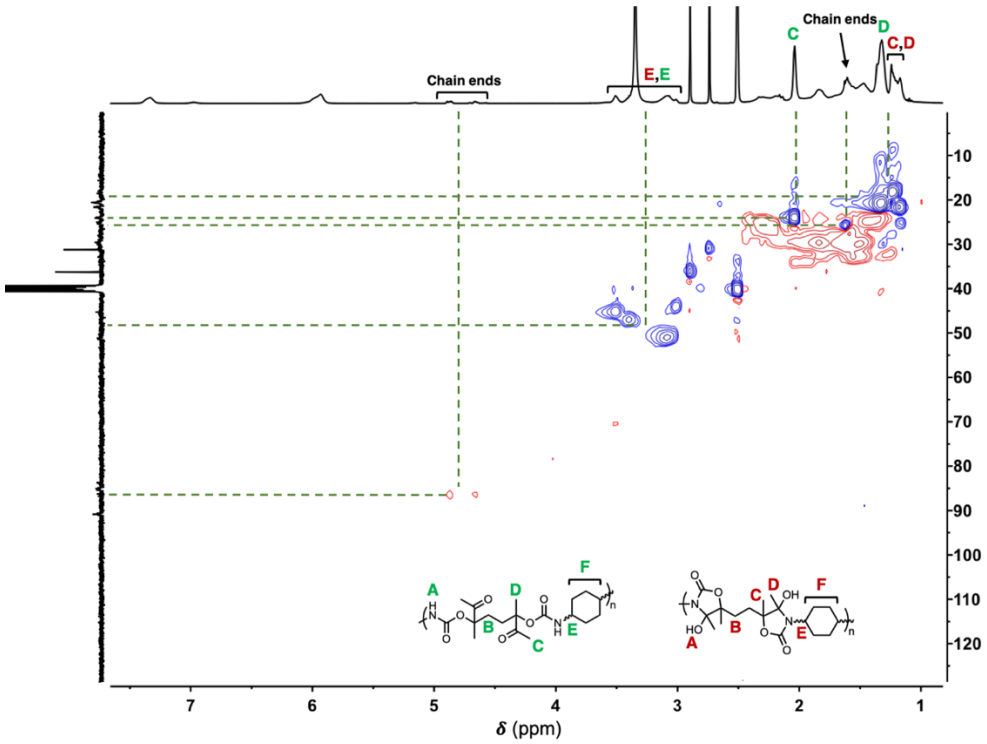

Figure S26. HSQC NMR spectrum (400 MHz, DMSO-d_6) of **P(CC1-AA4)**.

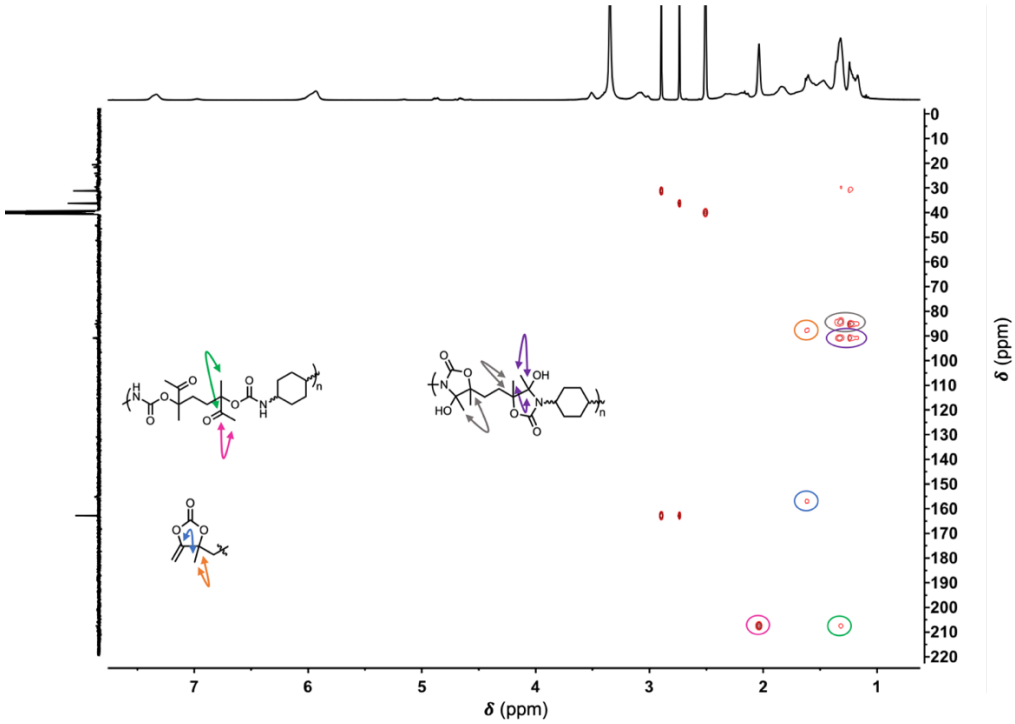

Figure S27. HMBC NMR spectrum (400 MHz, DMSO-d_6) of **P(CC1-AA4)**.

P(CC1-AA6)

Despite the decent solubility of the polymer **P(CC1-AA6)** in DMSO-d_6, ^{13}C NMR analyses gave a very low signal and the spectrum can't thus be interpreted. A solid state ^{13}C NMR analysis was then be conducted in order to achieve the attribution.

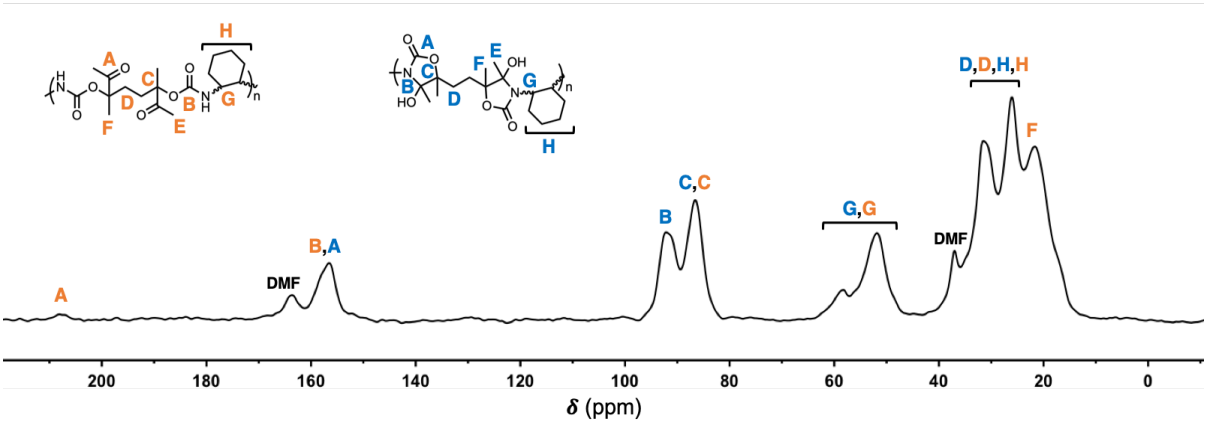

Figure S28. Solid-state ^{13}C NMR spectrum (400 MHz) of **P(CC1-AA6)**.

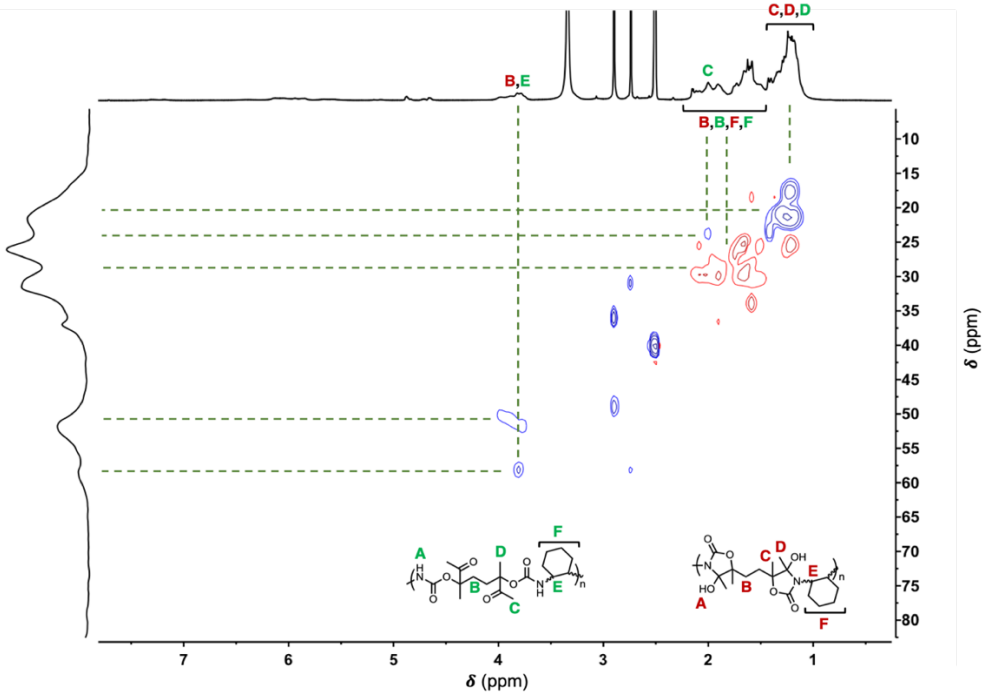

Figure S29. HSQC NMR spectrum (400 MHz, DMSO-d_6) of **P(CC1-AA6)**.

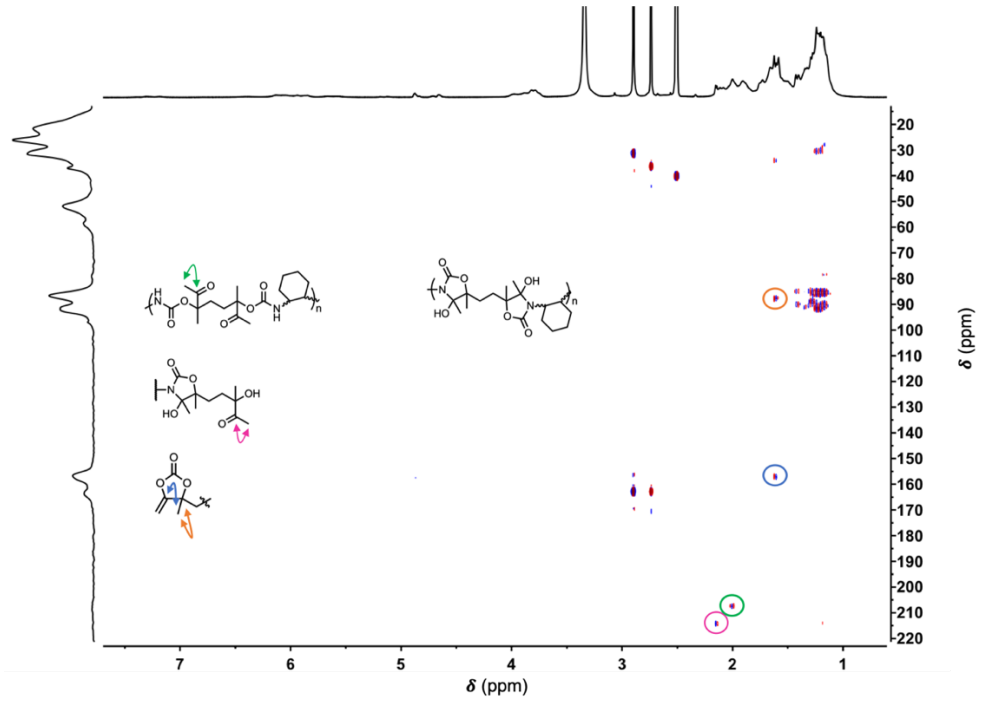

Figure S30. HMBC NMR spectrum (400 MHz, DMSO-d_6) of **P(CC1-AA6)**.

P(CC1-AA7)

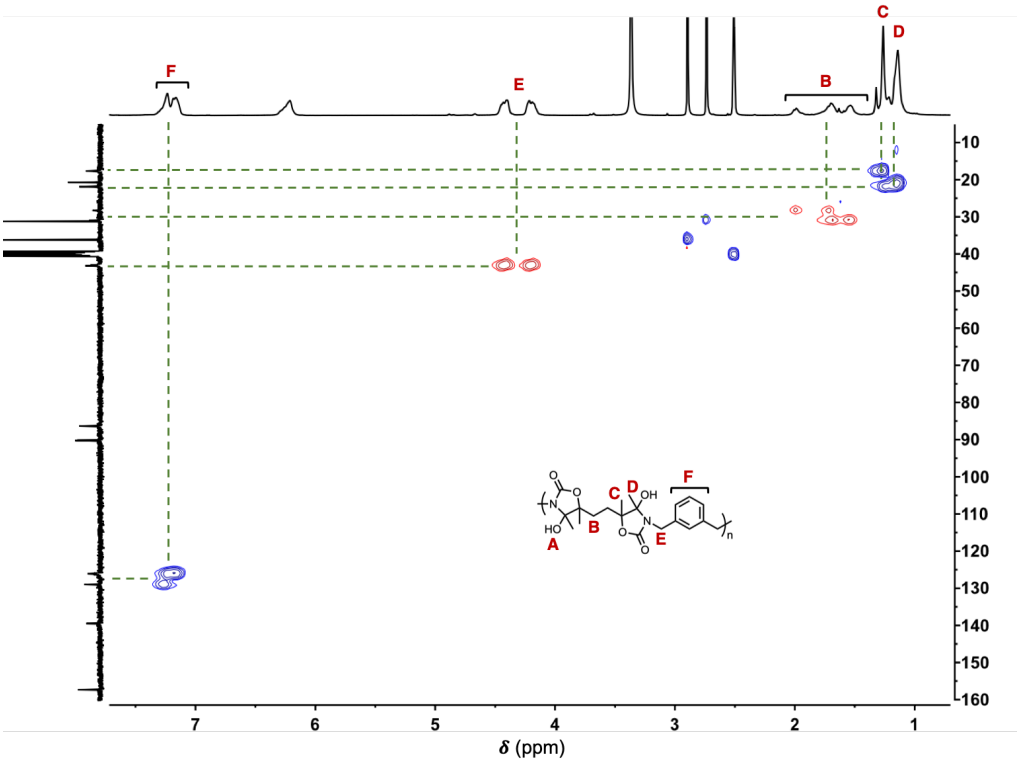

Figure S31. HSQC NMR spectrum (400 MHz, DMSO-d_6) of **P(CC1-AA7)**.

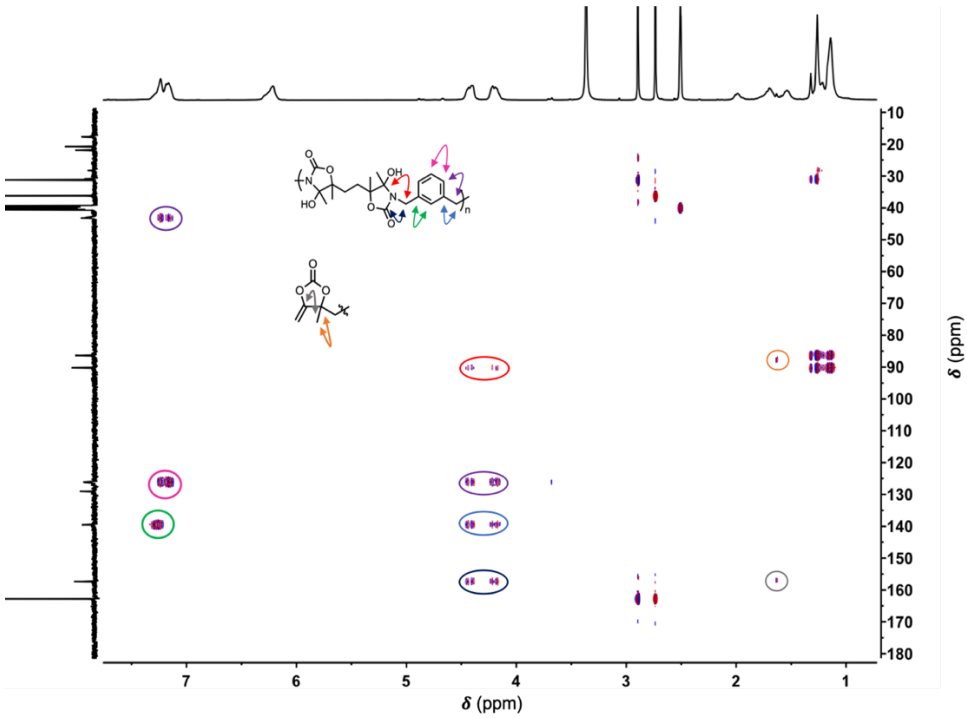

Figure S32. HMBC NMR spectrum (400 MHz, DMSO-d_6) of **P(CC1-AA7)**.

P(CC1-AA1)D

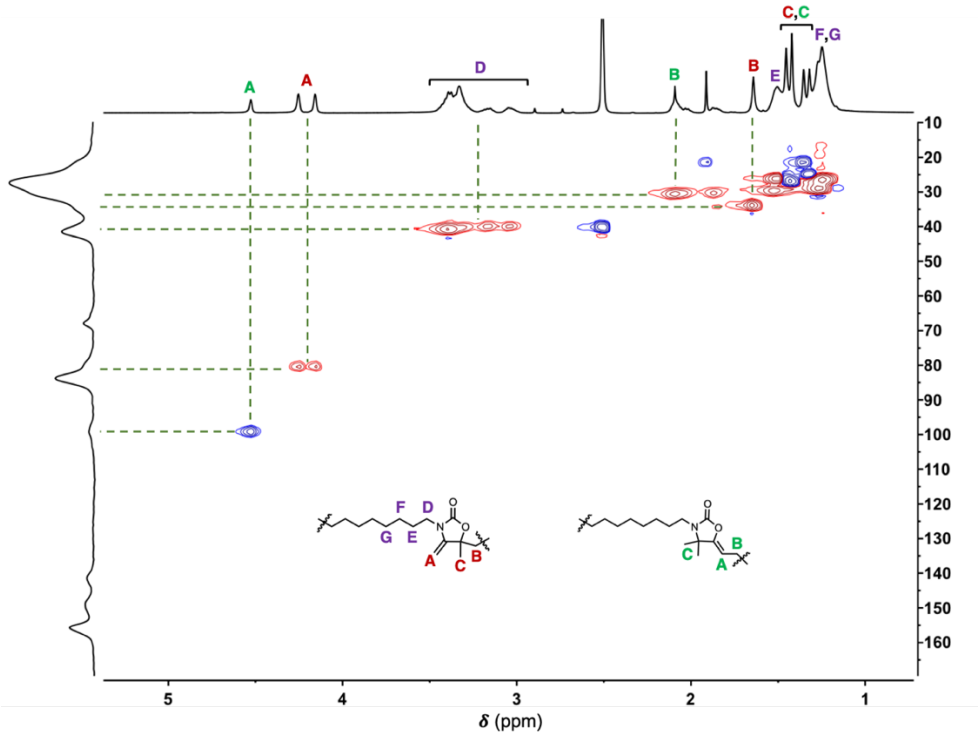

Figure S33. HSQC NMR spectrum (400 MHz, DMSO-d_6) of **P(CC1-AA1)D**.

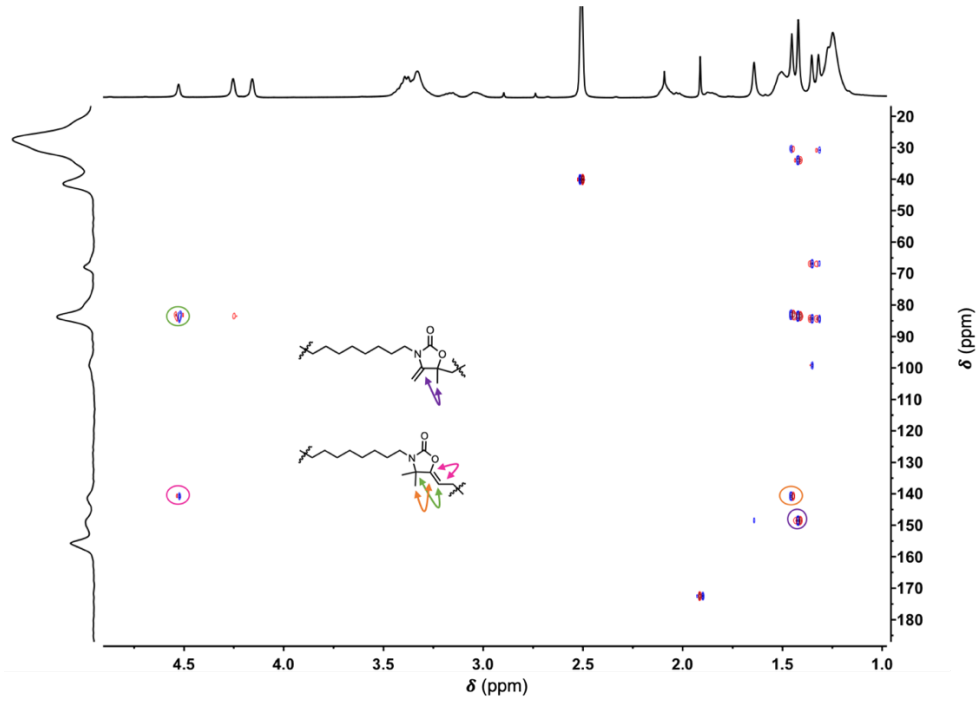

Figure S34. HMBC NMR spectrum (400 MHz, DMSO-d_6) of **P(CC1-AA1)D**.

P(CC1-AA2)D

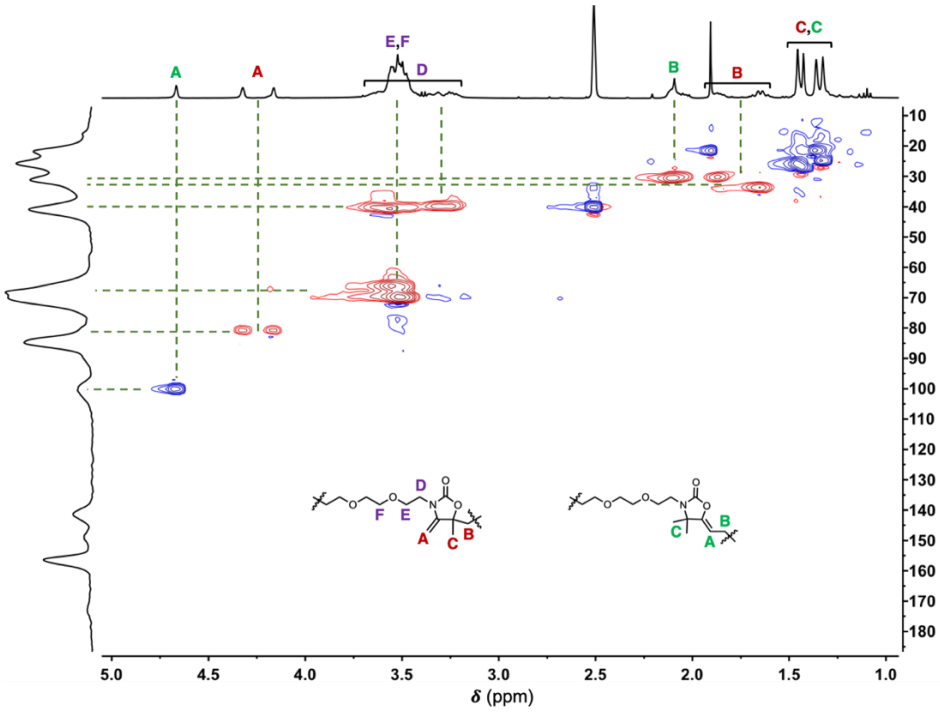

Figure S35. HSQC NMR spectrum (400 MHz, DMSO-d_6) of **P(CC1-AA2)D**.

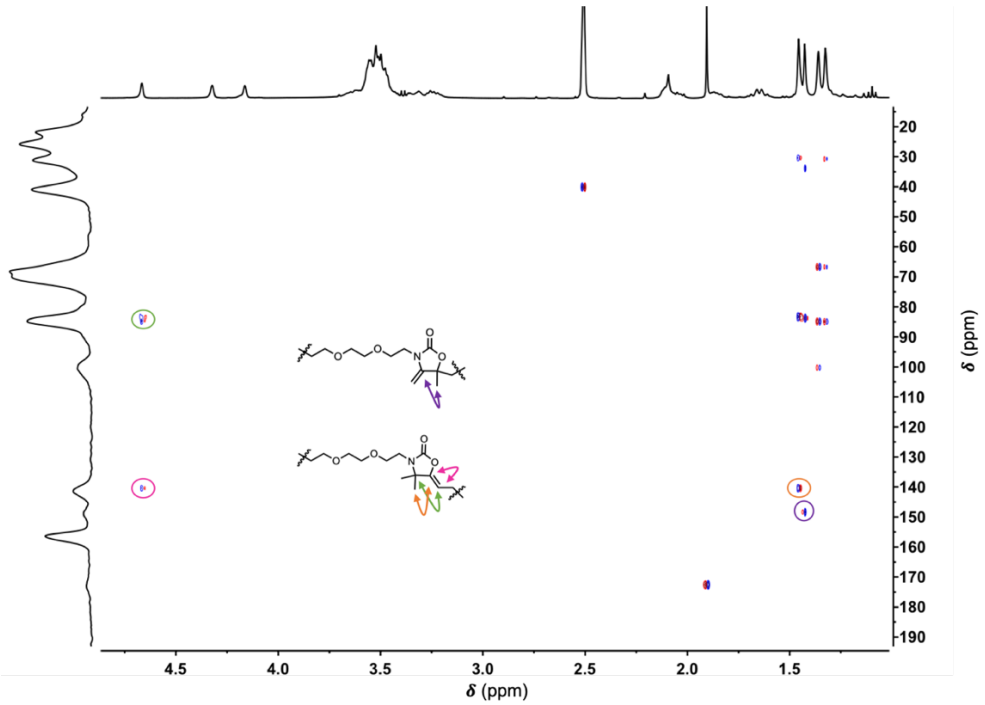

Figure S36. HMBC NMR spectrum (400 MHz, DMSO-d_6) of **P(CC1-AA2)D**.

P(CC1-AA4)D

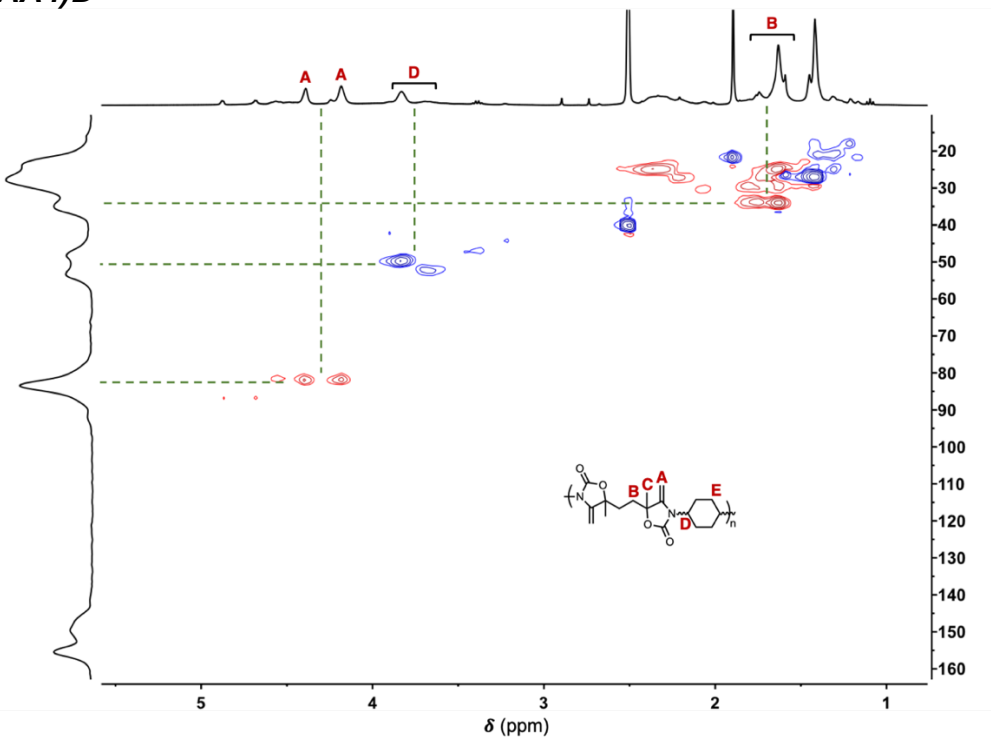

Figure S37. HSQC NMR spectrum (400 MHz, DMSO-d_6) of **P(CC1-AA4)D**.

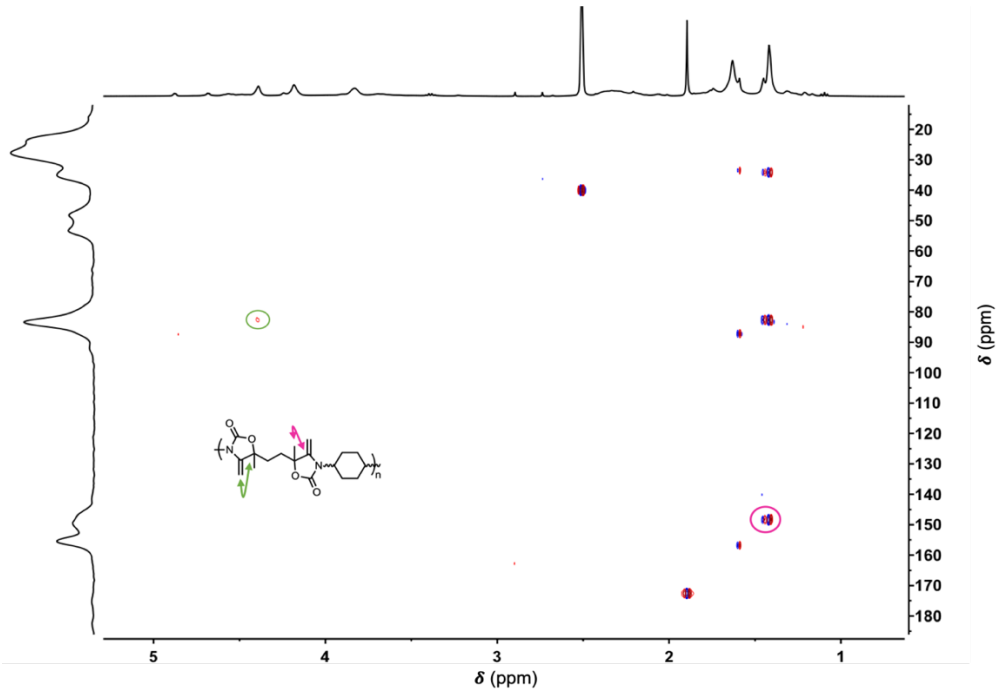

Figure S38. HMBC NMR spectrum (400 MHz, DMSO-d_6) of **P(CC1-AA4)D**.

P(CC1-AA7)D

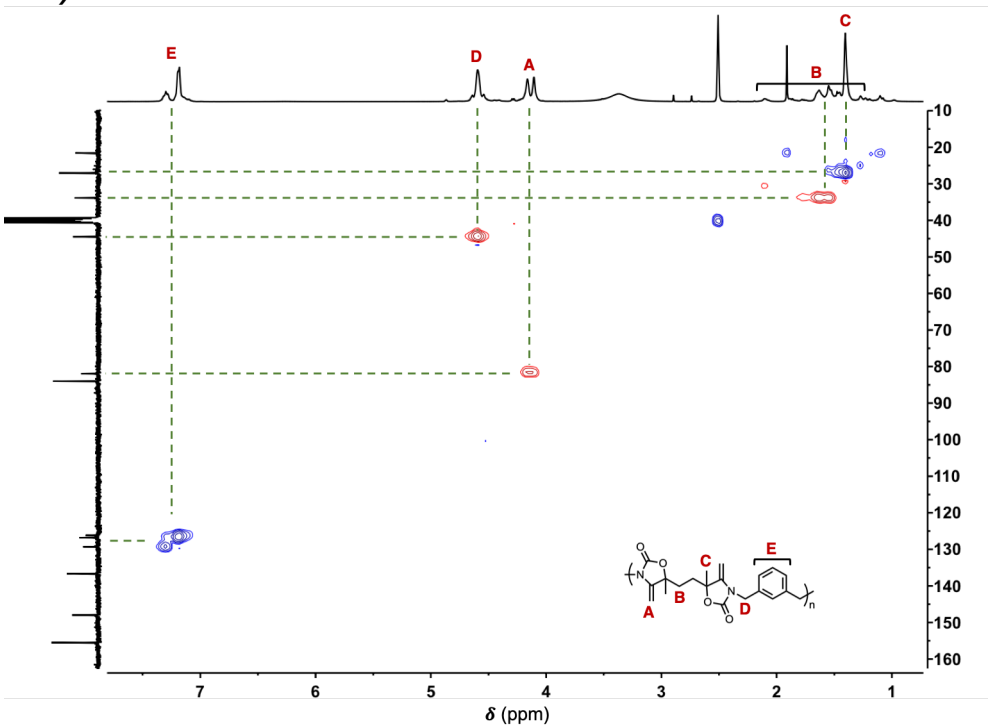

Figure S39. HSQC NMR spectrum (400 MHz, DMSO-d_6) of **P(CC1-AA7)D**.

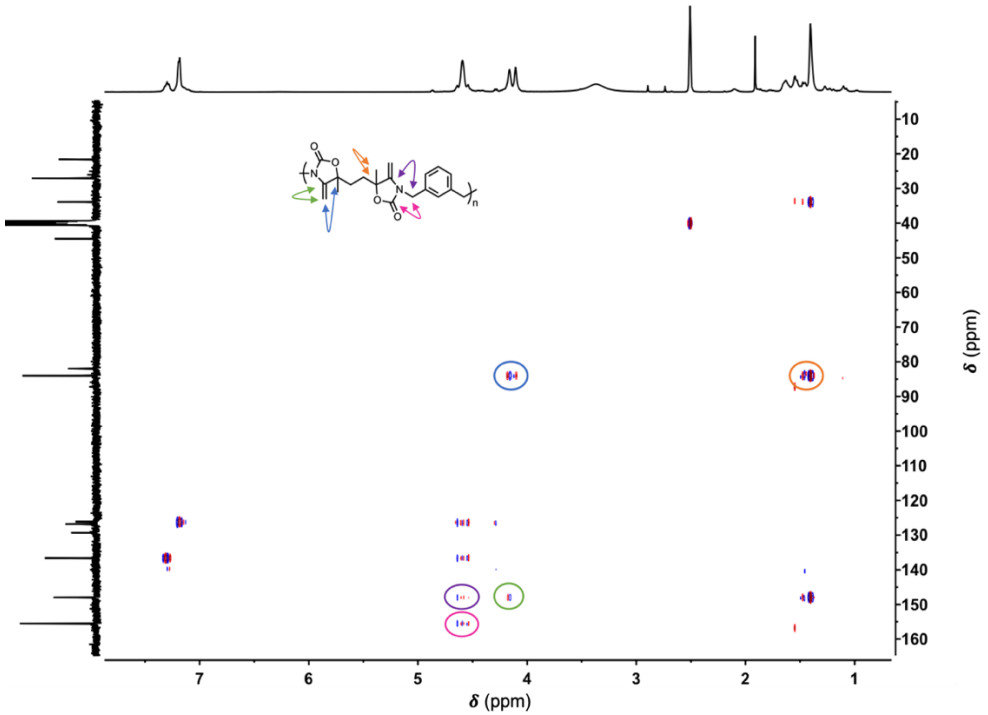

Figure S40. HMBC NMR spectrum (400 MHz, DMSO-d_6) of **P(CC1-AA7)D**.

Solid-state ^{13}C NMR spectra of P(CC1-AA7) prepared under different conditions

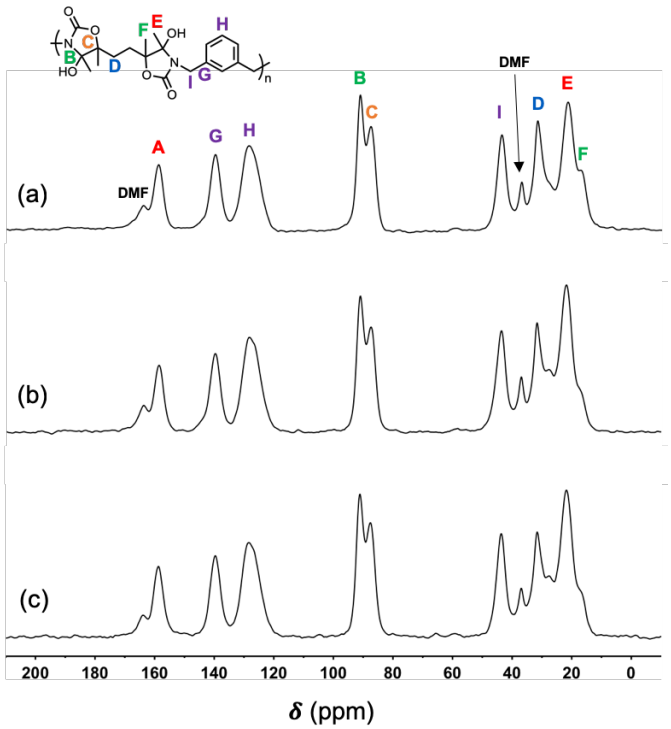

Figure S41. Stacked solid-state 13C-NMR spectra of **P(CC1-AA7)** prepared (a) at 25 °C without DBU, (b) at 25 °C with DBU (5 mol%) and (c) at 80 °C without DBU (after purification).

SEC characterizations of the polymers

Typical SEC chromatograms are shown in Figure S38 for polymers synthesized in mild conditions (25°C in DMF, no catalyst).

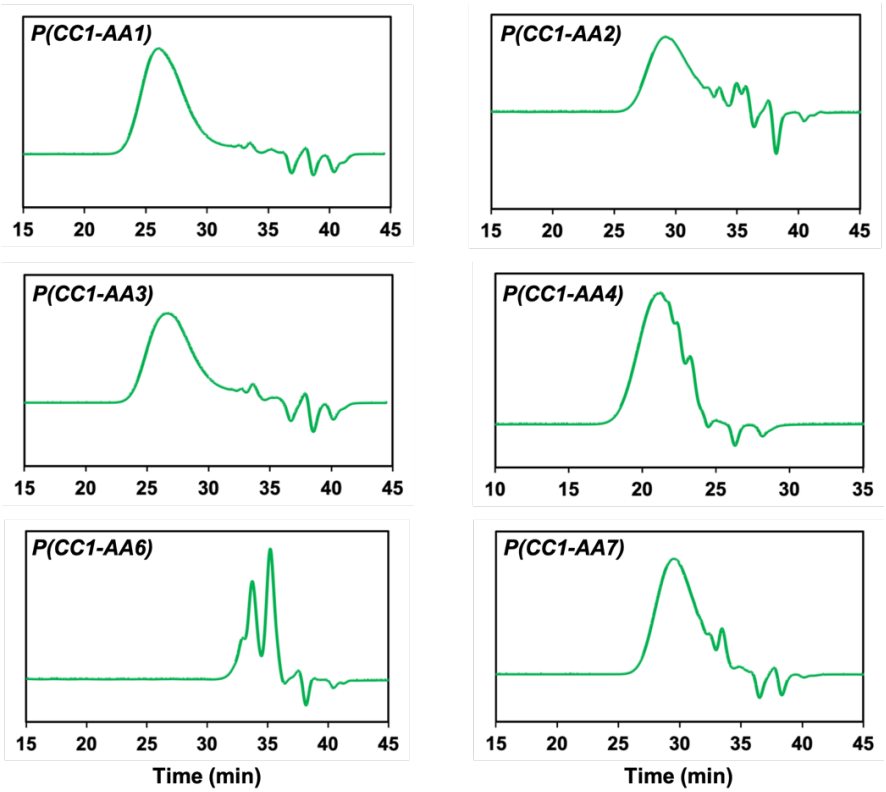

Figure S42. SEC chromatograms (before purification) of polymers **P(CC1-AA1)**, **P(CC1-AA2)**, **P(CC1-AA3)**, **P(CC1-AA4)**, **P(CC1-AA6)** and **P(CC1-AA7)** synthesized at 25°C in DMF without catalyst (Table 3).

Thermal properties of the polymers

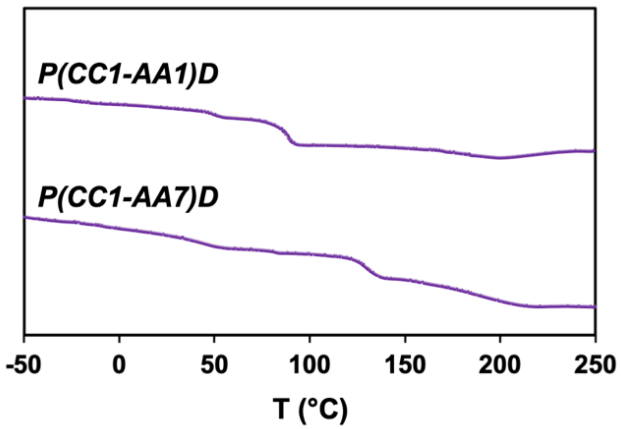

Figure S43. DSC curves for polymers **P(CC1-AA1)D** and **P(CC1-AA7)D**.

Conclusions and Perspectives

Conclusions

The emergence of CO_2-sourced bis(exovinylene cyclic carbonate)s (bisαCCs) in polymer science prompted us to investigate the scope and limitations of their organocatalyzed step-growth copolymerization with diols and diamines into poly(*oxo*-carbonate)s and non-isocyanate-based polyurethanes (poly(hydroxy-oxazolidinone)s), respectively. A significant attention was also devoted to the chemical degradation of poly(*oxo*-carbonate)s by aminolysis or by introducing functionalities within the polymeric-chain that are capable to initiate on demand the polymer degradation.

As described in Chapter II, we investigated the facile synthesis of novel poly(*oxo*-carbonate)s by step-growth copolymerization of various sugar- or lignin-based diols with bisαCCs under mild reaction conditions (Scheme 1). After a first study on model reactions to understand the structural influence of the alcohols and the temperature (25 or 80 °C) on both the polymerization rate and product selectivity, a series of regioregular poly(*oxo*-carbonate)s of different structures and reasonable molar masses (M_w up to 26,700 g/mol) were prepared at 25 °C. By performing the polymerizations at 80 °C, structural defects were however introduced within the chains which limited the polymer molar mass for long reaction times. These structural defects originated from two side reactions: a transcarbonation reaction and the formation of a cyclic carbonate linkage induced by the organocatalyzed nucleophilic attack of an alcohol to the pending ketone of the polymer.

Finally, the thermal properties of the poly(*oxo*-carbonate)s designed at 25 °C were evaluated. A degradation temperature of poly(*oxo*-carbonate)s between 216 °C and 271 °C was noted. With the exception of one poly(*oxo*-carbonate) made from isosorbide that was amorphous, all the other polycarbonates were semi-crystalline with a melting temperature (T_m) ranging from 60 to 343 °C.

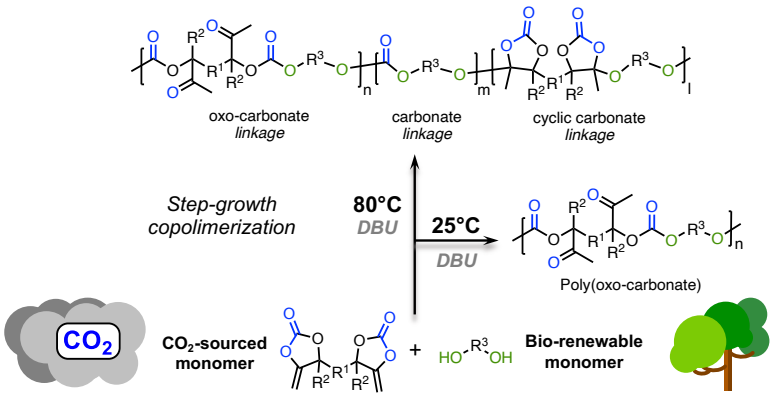

Scheme 1. Synthesis of CO_2- and bio-based poly(*oxo*-carbonate)s. Effect of the polymerization temperature on the microstructure features.

In Chapter III we exploited the unique microstructural features of the poly(*oxo*-carbonate)s for their rapid and complete deconstruction by aminolysis at room temperature without any catalyst (Scheme 2). Model reactions were carried out to understand the influence of the amine on the efficiency of the aminolysis and the selectivity of the reaction. DFT calculations evidenced the preferential attack of the amine to the more electrophilic ketone rather than to the carbonate. The cyclization of an hemiaminal intermediate lead to the oxazolidinone scaffold after the release of an alcohol. Impressively, the polymers were rapidly (< 30 min) and totally deconstructed into the parent diol and a bis(oxazolidinone) by catalyst-free aminolysis at 25 °C. By suitably choosing the amine (e.g. propanolamine), the facile and complete PC deconstruction was reached at rt after 24 h, yielding the starting diol and a bis(oxazolidinone) bearing two primary alcohols. This latter could be utilized to re-construct new polymeric materials by copolymerization with bisαCCs at rt, furnishing a polymer alternating oxazolidinone and carbonate linkages. This polymer could also be fully degraded into the starting monomer by aminolysis with propanolamine, offering a close-loop recycling scenario to this product.

Capitalizing on the synthetic method to produce PCs described in Chapter II, we described in Chapter IV the skeletal-editing of polycarbonates by introducing amide or urea functions within the diols that could polymerize by step-growth copolymerization with bisαCCs producing poly(carbonate-amide)s and poly(carbonate-urea)s (Scheme 2). To do so, upcycled commodity plastics derived-diols were employed and the in-chain secondary amides or ureas functionalities, in the presence of a base catalyst and a thermal switch (from 25 to 80 °C), triggered the polymers depolymerization on-demand *via* chain scission followed by domino ring-closure unzipping. This method permits to put an end to inextricable conflict between step-growth copolymerization and ring closing depolymerization, without protecting the reactive groups, and creating new value-added organic scaffolds such as a hemiacetal cyclic

carbonate and the native diol, or oxazolidinones. Interestingly, fast and complete depolymerizations were also achieved in solvent- and catalyst- free conditions at 150 °C. Finally, these polymers were selectively depolymerized from plastic mixtures composed of PCL or PET, offering new options for recycling plastics waste mixtures.

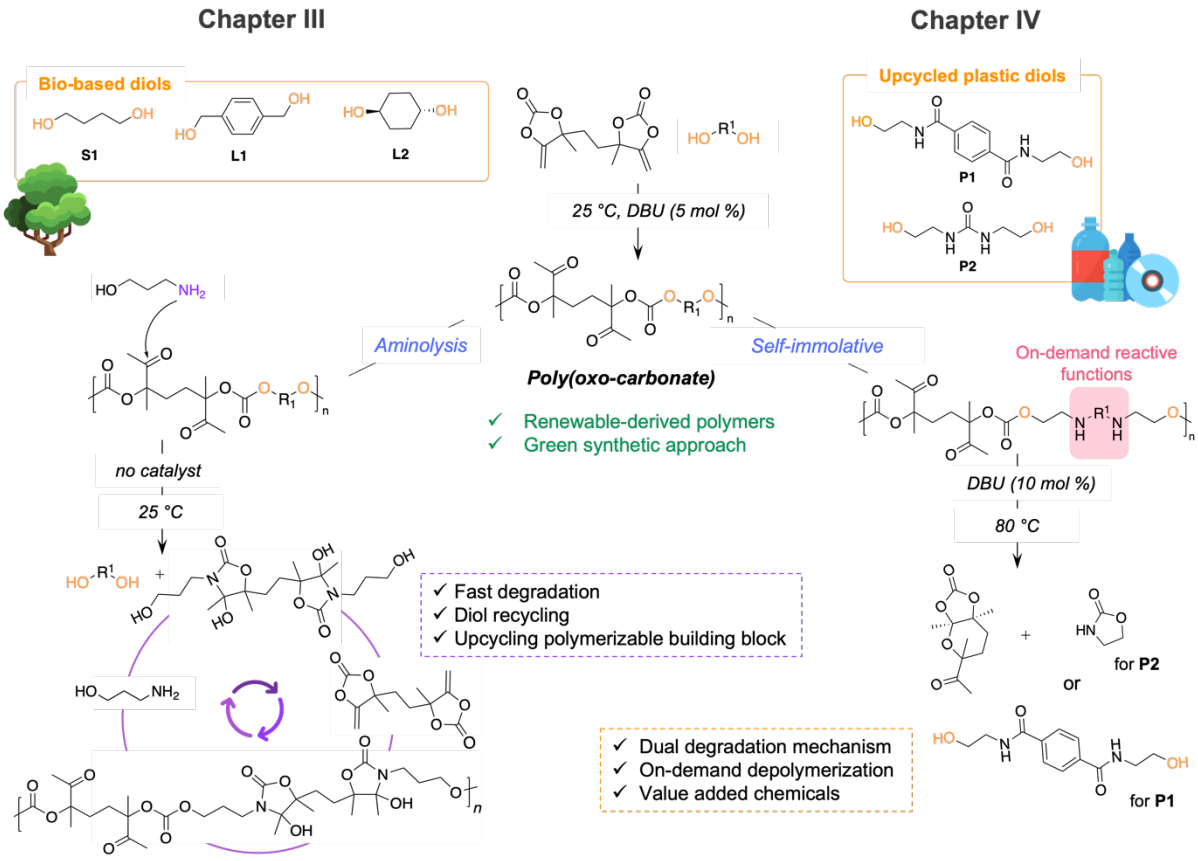

Scheme 2. Degradation of bio- and CO_2-sourced poly(*oxo*-carbonate)s (Chapter III) or specifically edited polymers issued from plastics wastes and CO_2 (Chapter IV).

In the last chapter we discussed the synthesis of an emerging class of non-isocyanate polyurethanes (poly(hydroxy-oxazolidinone)s) that is easily formed *via* the step-growth copolymerization of bis(α-alkylidene cyclic carbonate)s with bio-based primary diamines at room temperature (Scheme 3). Model reactions on small molecules were first performed in order to understand the impact of the structure of the amine on the rate, yield and selectivity of the reactions. The amine was shown to have an influence on the rates of reaction for both the ring-opening of the cyclic carbonate and the intramolecular cyclization of the *oxo*-urethane intermediate into the hydroxy-oxazolidinone. Various poly(hydroxy-oxazolidinone)s were then synthesized by polyaddition of bisαCCs with the diamines. In line with model reactions, the more sterically hindered cycloaliphatic diamines yielded polymers containing both *oxo*-urethane and hydroxy-oxazolidinone linkages, while the less sterically hindered ones provided hydroxy-oxazolidinone ones exclusively. Dehydrated poly(hydroxy-oxazolidinone)s were

successfully obtained by refluxing in glacial acetic acid, providing a new class of unsaturated poly(oxazolidinone)s composed of α-alkylidene oxazolidinone linkages (for hindered polymers) or a mixture of α- and β-alkylidene oxazolidinone linkages (for the less hindered ones). Remarkably, these unsaturated poly(oxazolidinone)s presented a high glass transition temperature (up to 130 °C) and an important thermal stability (T_d > 360 °C), making this novel family of polymers attractive for applications requiring high temperatures.

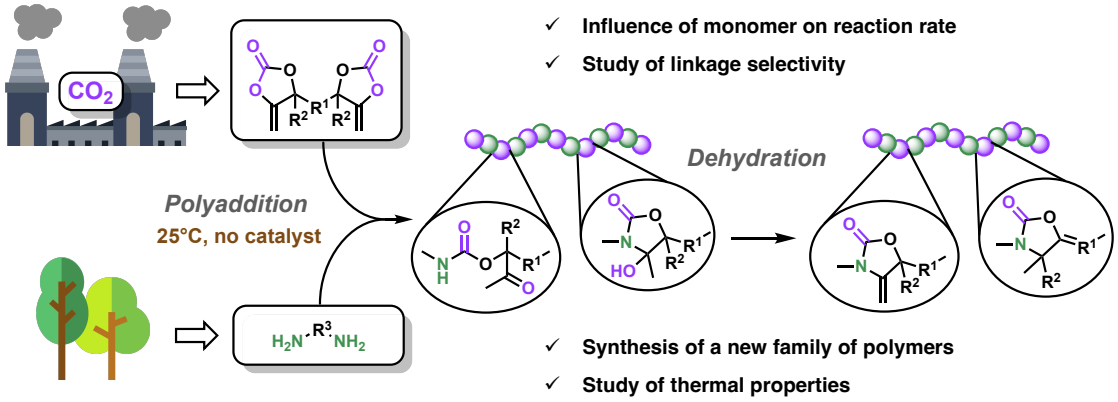

Scheme 3. Synthetic route toward the formation of CO_2- and bio-based poly(hydroxy-oxazolidinone)s and poly(alkylidene oxazolidinone)s.

Perspectives

The work realized in the frame of my PhD thesis lays the foundations for the exovinylene cyclic carbonate utilization in the area of polymer sciences. Further deployment of this chemistry will necessitate new research outputs the resolve some of the limitations that have been identified regarding the bisαCCs monomers, the polymerization process, the scope of applications and the end-of-life scenario of these new materials.

BisαCCs monomers are produced by carboxylative coupling of CO_2 with diacetylenic alcohol precursors. These latest are not commercial. They are typically made from hazardous and expensive diketones and Grignard's reagent (i.e. ethynylmagnesium bromide) under dry conditions. Therefore, developing new experimental protocols exploiting cheap calcium carbide as substitute to the organomagnesium bromide reagent may strongly reduce the production cost of the BisαCCs. Besides, the scope of BisαCCs is now limited to two molecules of high melting temperature and low solubility in polar solvents such as toxic DMF or DMSO that are difficult to remove. This causes diverse difficulties for the solvent-free construction of polymers but also to adjust their microstructure for answering specific properties/needs (solubility, glass transition temperature, melting temperature, melt viscosity, thermal stability…) dictated by the envisioned applications. In this context, developing new low melting temperature or even liquid versions of BisαCCs, ideally from biobased raw

chemicals, would strongly facilitate the synthesis of polymers by solvent free and/or continuous approaches, e.g. via reactive extrusion or flow chemistry. This latest concept is now ongoing in our group in the frame of the CO_2Fluidics project dealing with the carbon dioxide transformation for the sustainable production of valued-added organics and polymers. Finally, developing efficient and facile strategies to convert monopropargylic alcohols available at large scale and low cost by BASF into BisαCCs might be considered.

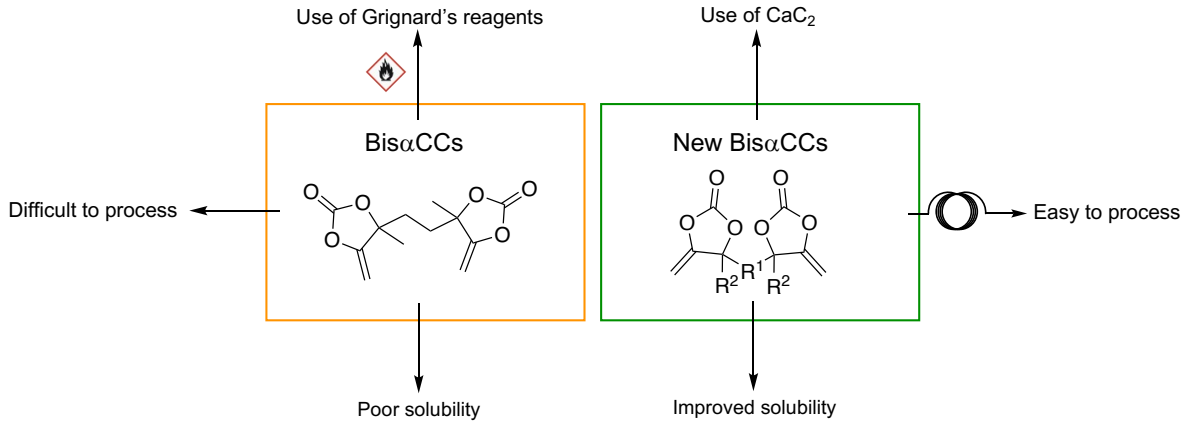

Scheme 4. CO_2-sourced BisαCCs monomers.

Unlike commodity PCs derived from bisphenol A (BPA-PC), poly(*oxo*-carbonate)s display insufficient resistance and thermal stability for considering packaging applications. To date, only aliphatic polymers have been utilized to design solid electrolytes for Li-ion batteries. To broaden the scope of utilization of this family of PCs, yet providing a competitive alternative to conventional BPA-PC, new aromatic BisαCCs, ideally with internal exocyclic olefins, should be designed. By polymerization of these monomers, one expects that the insertion of the *oxo* moieties within the main polymer skeleton - instead of pending acetyl groups with external exovinylene cyclic carbonates - combined to the presence of aromatic groups will strongly improve the thermo-mechanical properties of the materials. Finally, one also underlines the possible engineering and valorization of the aliphatic poly(*oxo*-carbonate)s for biomedical purposes such as drug loaded degradable implants. In this context, knowing the biocompatibility, the biodegradability and cytotoxicity of these materials is a prerequisite.

Finally, on the path to circularity, other depolymerization methods should be investigated to enlarge the library of recoverable from these materials. The hydrolysis of the carbonate linkages should trigger the formation of diols with bis-hydroxy ketone. Depending on the operative conditions and the pH, the alcoholysis of the chains may provide two depolymerization scenarios. Alike aminolysis (Chapter III), alcoholysis of the chains at high pH will occur via the pending acetyl moieties, yet forming a hemiacetal intermediate involved in a cascade intramolecular ring-closure reaction to deliver the 5-membered biscyclic

carbonates and diols. One believes that low pH values will favor the alcoholysis of the chains via attack on the carbonate linkages, providing mixtures of diols, (a)cyclic carbonates and bis-hydroxyketones. As third option, the selective hydrogenation of the acetyl groups of the chains by the use of appropriate reductant should transform the poly(*oxo*-carbonate)s into diols and 5-membered biscyclic carbonates that might be used to prepare other polymers of interest. For instance, five-membered biscyclic carbonates are particularly relevant monomers largely exploited for the construction of isocyanate-free poly(hydroxy-urethane)s by step-growth copolymerization with di- or poly-amines.

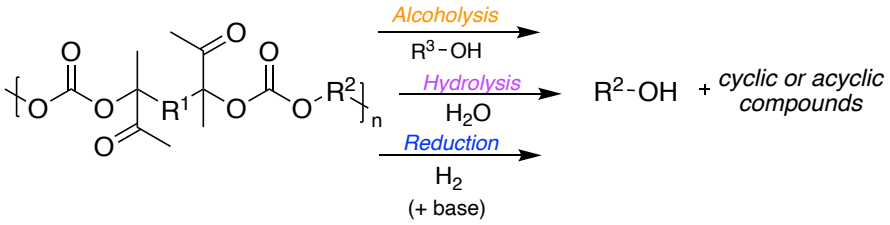

Scheme 5. Other degradation methods of poly(*oxo*-carbonate)s.

Thanks to their high reactivity, even under ambient conditions, the BASF company has recently qualified BisαCCs as the most promising alternatives to isocyanates for constructing polyurethanes. But, for large scale utilization and design of poly(oxazolidinone)s, as described in the last chapter, similar hurdles as the ones identified for poly(*oxo*-carbonate)s regarding the monomer design and polymer processing have to be surpassed. Such polymers should also be evaluated for key relevant applications e.g. as adhesives, coatings, or foams and their performances benchmarked with the ones of conventional polyurethanes. Finally, poly(oxazolidinone)s have shown remarkable high thermal and chemical stability making them highly appealing for applications in unfriendly environments. Ongoing works in our group ("CO2 switch" project funded by the FNRS) are now exploiting the pending C=C double bonds of the dehydrated version of the polymers (i.e. poly(alkylidene oxazolidinone)s) for the easy post-modification of the chains and for enlarging their utility/functionality/thermo-mechanical properties. However, poly(hydroxy-oxazolidinone)s are highly stable materials making their chemical degradation very challenging. Therefore, finding viable recycling options of these new materials is absolutely necessary to respond to the sustainability and circular objectives imposed by the European Commission. In this context, new projects are focused on the chemical degradation of non-isocyanate polyurethanes in the frame of the on-going NIPU European Joint Doctorate training network from the Marie Curie action.

List of publications

1) Thomas Habets, Fabiana Siragusa, Bruno Grignard, Christophe Detrembleur. *Macromolecules* ***2020****, 53, 6396–6408.*

2) Fabiana Siragusa, Elias Van Den Broeck, Connie Ocando, Alejandro J. Müller, Gilles De Smet, Bert U.W. Maes, Julien De Winter, Veronique Van Speybroeck,Bruno Grignard, Christophe Detrembleur. *ACS Sustainable Chem. Eng.* ***2021****, 9, 1714–1728*

3) Thomas Habets, Fabiana Siragusa, Alejandro J. Müller, Quentin Grossman, Davide Ruffoni, Bruno Grignard, Christophe Detrembleur. *Polym. Chem*. **2022**, 13, 3076–3090.

4) Fabiana Siragusa, Thomas Habets, Raphael Mereau, Gwilherm Evano, Bruno Grignard, Christophe Detrembleur. *ACS Sustainable Chem. Eng.* ***2022****, 10,* 8863–8875*.*

5) Fabiana Siragusa, Jeremy Demarteau, Thomas Habets, Ion Olazabal, Koen Robeyns, Gwilherm Evano, Raphael Mereau, Thierry Tassaing, Bruno Grignard, Haritz Sardon, Christophe Detrembleur. *Macromolecules* ***2022****, 55, 4637–4646.*